R-08-36

Safety assessment for a KBS-3H spent nuclear fuel repository at Olkiluoto

Process report

Peter Gribi, S+R Consult

Lawrence Johnson, Nagra

Daniel Suter, Science Solutions

Paul Smith, Safety Assessment Management Ltd

Barbara Pastina, Margit Snellman
Saanio & Riekkola Oy

January 2008

Svensk Kärnbränslehantering AB
Swedish Nuclear Fuel
and Waste Management Co
Box 250, SE-101 24 Stockholm
Tel +46 8 459 84 00

ISSN 1402-3091
SKB Rapport R-08-36

Safety assessment for a KBS-3H spent nuclear fuel repository at Olkiluoto

Process report

Peter Gribi, S+R Consult

Lawrence Johnson, Nagra

Daniel Suter, Science Solutions

Paul Smith, Safety Assessment Management Ltd

Barbara Pastina, Margit Snellman
Saanio & Riekkola Oy

January 2008

Keywords: KBS-3H, Safety case, Safety assessment, Long-term safety, Processes, Spent fuel, Nuclear waste, Disposal, Crystalline bedrock.

Abstract

The KBS-3 method, based on multiple barriers, is the proposed spent fuel disposal method both in Sweden and Finland. KBS-3H and KBS-3V are the two design alternatives of the KBS-3 spent fuel disposal method. Posiva and SKB have conducted a joint research, demonstration and development (RD&D) programme in 2002–2007 with the overall aim of establishing whether KBS-3H represents a feasible alternative to the reference alternative KBS-3V. The overall objectives of the present phase covering the period 2004–2007 have been to demonstrate that the horizontal deposition alternative is technically feasible and to demonstrate that it fulfils the same long-term safety requirements as KBS-3V. The safety studies conducted as part of this programme include a safety assessment of a preliminary design of a KBS-3H repository for spent nuclear fuel located about 400 m underground at the Olkiluoto site, which is the proposed site for a spent fuel repository in Finland. In the KBS-3H design alternative, each canister, with a surrounding layer of bentonite clay, is placed in a perforated steel cylinder prior to emplacement; the entire assembly is called the supercontainer. Several supercontainers are positioned along parallel, 100–300 m long deposition drifts, which are sealed following waste emplacement using drift end plugs. Bentonite distance blocks separate the supercontainers, one from another, along the drift. Steel compartment plugs can be used to seal off drift sections with higher inflow, thus isolating the different compartments within the drift.

The present report describes the main processes potentially affecting the long-term safety of the system, covering radiation-related, thermal, hydraulic, mechanical, chemical (including microbiological) and radionuclide transport-related processes. The process descriptions deal sequentially with the main sub-systems: fuel/cavity in canister, cast iron insert and copper canister, buffer and other bentonite components, supercontainer shell and other steel structural materials, repository sealing and backfilling, and geosphere. The process description is based on a “difference analysis” approach comparing processes in KBS-3V and KBS-3H. The focus mostly on internal processes relevant to a single deposition drift and its immediate environment (near-field rock, drift end plugs), but also include the impact of important external factors such as glaciation and post-glacial faulting.

The issues that were evaluated in detail are the following: i) piping and erosion during the operational phase; ii) displacements of the supercontainers and the distance blocks due to hydraulic pressure differences in the drift; iii) rupturing of the supercontainer due to buffer swelling; iv) impact of gas generation from the corrosion of steel components in the drift; v) iron-bentonite interaction due to the presence of the supercontainer steel shell; vi) cement-bentonite interaction; and vii) water ingress followed by radionuclide expulsion from an initially penetrated canister. Except issues ii, iii, iv, the others are in common with KBS-3V.

Piping/erosion, along with the potential displacement of the supercontainer and distance blocks are viewed as processes that can be avoided or minimised with further developments of the KBS-3H design. Rupturing of the supercontainer due to buffer swelling was considered because it may result in corrosion products in direct contact with the rock hence having a negative effect on the canister lifetime and radionuclide transport. Gas generation from the corrosion of the steel supercontainer shell (and other steel components in the drift) will last approximately 4,500–5,000 years, based on the steel components’ thickness and a steel corrosion rate of 1 micrometre/year. The potential consequences are transient high gas pressures and delayed resaturation but no impacts on long-term safety have been identified. The interaction between iron and bentonite was considered because of the close proximity of the steel shell with the buffer inside the supercontainer leading to mineral transformations possibly affecting the buffer transport properties. A background study on the iron/bentonite interaction for KBS-3H suggests that the perturbation zone in the outer region of bentonite is spatially limited (a few cm deep the bentonite ring). Piping/erosion and iron/bentonite interaction have been identified as issues relevant also to KBS-3V and warranting further studies.

This report is a result of a joint project between Posiva and SKB. This report will also be printed as a Posiva report, POSIVA 2007-09.

Foreword

This study was coordinated by Margit Snellman (Saanio & Riekkola Oy) on behalf of Posiva Oy. The progress of the study was supervised by the KBS-3H Review Group consisting of Aimo Hautojärvi (Posiva), Jukka-Pekka Salo (Posiva), Marjut Vähänen (Posiva), Barbara Pastina (Saanio & Riekkola Oy), Margit Snellman (Saanio & Riekkola Oy), Jorma Autio (Saanio & Riekkola Oy), Stig Pettersson (SKB), Erik Thurner (SKB), Börje Torstenfelt (Swedpower), Lennart Börgesson (Clay Technology) and Lawrence Johnson (Nagra). This Process Report was largely written by Peter Gribi (S+R Consult), Lawrence Johnson (Nagra), Daniel Suter (Science Solutions), Paul Smith (SAM), Barbara Pastina (Saanio & Riekkola Oy) and Margit Snellman (Saanio & Riekkola Oy) with contributions from Paul Wersin (Nagra), Paul Marschall (Nagra), Bill Lanyon (Fracture Systems) and other members of the KBS-3H Review Group.

Jorma Autio provided material related to the KBS-3H design and characterisation of the excavation-damaged zone. Erik Johansson (Saanio & Riekkola Oy) and Aleksis Lehtonen (Saanio & Riekkola Oy) provided input on rock mechanics processes. Important contributions on scientific understanding of the behaviour of the buffer material stem from Lennart Börgesson, Torbjörn Sandén and co-workers (Clay Technology), by way of laboratory tests, modelling and scenario analysis.

The effects of cement on bentonite were summarised by Barbara Pastina (Saanio & Riekkola Oy), the modelling of cement-bentonite interaction was done by Jarmo Lehikoinen (VTT at the time of writing), Ari Luukkonen (VTT) and Henrik Nordman (VTT), and the grout take estimates were performed by Ursula Sievänen (Saanio & Riekkola Oy). Christine Bircher (Nagra), Aline Playfair (Nagra), Heini Laine (Saanio & Riekkola Oy) and Päivikki Mäntylä (Saanio & Riekkola Oy) provided editorial support.

The interdisciplinary effort required the contributions of many individual scientists representing different areas of research. The flow of information was ensured by project meetings, reference reports and reviews by scientists in their respective fields of expertise. A companion report (Evolution Report) was written by Paul Smith, Lawrence Johnson, Margit Snellman, Barbara Pastina and Peter Gribi. In the course of the project, the two companion reports were cross-checked in several steps (outline, draft versions, final version) to ensure consistency.

The report was reviewed in draft form by the following individuals: Jordi Bruno (Enviros Spain LS, Spain), Roland Pusch (Geodevelopment International AB, Sweden), John Hudson (Rock Engineering Consultants, UK), Tom Doe (Golder Associates, USA), Raymond Munier for Sections 7.5 and 7.6 (SKB, Sweden), Johan Andersson (Streamflow AB, Sweden), Pirjo Hellä (Pöyry Environment, Finland), Nuria Marcos (Saanio & Riekkola Oy, Finland), Christer Svemar (SKB, Sweden) and Jan-Olof Selroos (SKB, Sweden).

Contents

1 Introduction

1.1 KBS-3H long-term safety studies

The KBS-3 method, based on multiple barriers, is the proposed spent fuel disposal method in both Sweden and Finland. There are two design alternatives for the KBS-3 method: KBS-3V, in which the canisters are emplaced in individual vertical deposition holes and KBS-3H, in which several canisters are emplaced in horizontal deposition drifts (see Figure 1-1). The reference alternative for the implementing organisations, SKB in Sweden and Posiva in Finland, is KBS-3V. SKB and Posiva have also conducted a Research, Development and Demonstration (RD&D) programme over the period 2002–2007 with the overall aim of establishing whether KBS-3H represents a feasible alternative to KBS-3V on which to base construction license applications for spent fuel repositories in Finland and Sweden.

In KBS-3H, multiple canisters containing spent fuel are emplaced in parallel, up to 300 m long, slightly inclined horizontal deposition drifts. The canisters, each with a surrounding layer of bentonite clay, are placed in steel supercontainer shells prior to deposition in the drifts. In KBS-3V, canisters are emplaced vertically in individual deposition holes, as shown in Figure 1-1.

There are currently a number of design variants under consideration for a KBS-3H repository, as well as differences between the fuel types, the characteristics and inventories of the canisters, and the proposed repository site for a spent fuel repository in Finland (Olkiluoto, in the municipality of Eurajoki) and the sites still under consideration in Sweden. In order to focus the KBS-3H long-term safety studies, however, these are applied to the Olkiluoto site

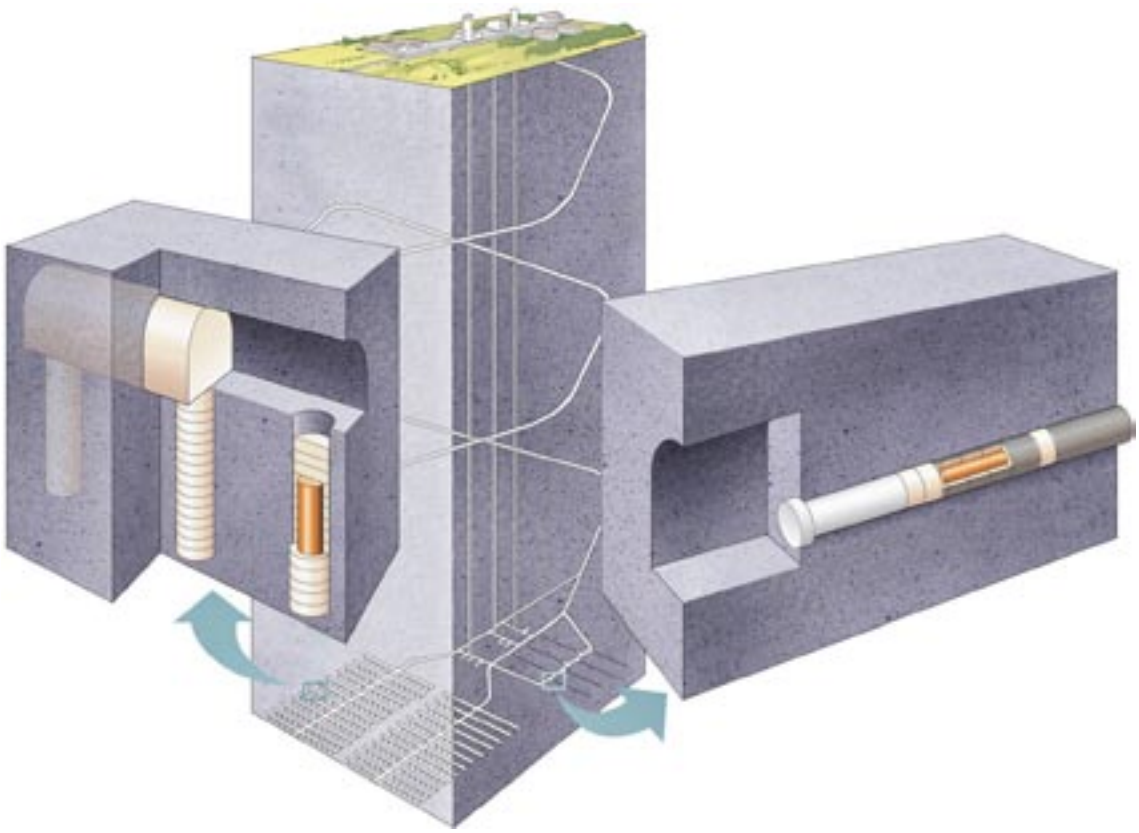

Figure 1-1. *The KBS-3V (left) and KBS-3H (right) alternatives of the KBS-3 spent fuel disposal method.*

and the reference fuel is the Finnish BWR fuel from Olkiluoto 1 and 2 reactors. The reference design used in the KBS-3H safety assessement is the Basic Design as described in the Design Description 2006 /Autio et al. 2007/. At the time of selection of the reference KBS-3H design for the long-term safety studies, no major differences between the Basic Design and the design alternative, termed DAWE (Drainage Artificial Watering and air Evacuation), had been identified that were relevant to long-term safety. The Basic Design is the outcome of several years of studies of different design options for the drift. DAWE was introduced at a later stage in the programme to address some uncertainties regarding the feasibility of implementing the Basic Design in less favourable locations along the drifts. At the time of selection, however, both designs were judged to be potentially feasible, and the Basic Design was selected for the safety assessment. Releases of radionuclides from the repository are also compared with Finnish regulatory guidelines, with only brief comments about the Swedish regulatory context.

Specific high-level questions addressed by the KBS-3H long-term safety studies are:

- are there safety issues specific to KBS-3H with the potential to lead to unacceptable radiological consequences?; and
- is KBS-3H promising at a site with the broad characteristics of Olkiluoto from the long-term safety point of view?

Due to the limitations in the scope of the KBS-3H long-term safety studies, the following questions are not currently addressed:

- is KBS-3H more or less favourable than KBS-3V from a long-term safety point of view?; and
- does the specific realisation of the KBS-3H design considered in the long-term safety studies satisfy all relevant regulatory guidelines?

A detailed comparative study of favourable and less favourable features in KBS-3H vs. KBS-3V is beyond the scope of the long-term safety studies carried out so far. Regarding the second question, although the performance of a KBS-3H repository has been analysed in a number of cases representing alternative evolutions of the repository and its environment and the results compared with Finnish regulatory guidelines, the analyses have a number of limitations, as described in the KBS-3H Radionuclide Transport Report /Smith et al. 2007a/. These limitations would have to be addressed before it could be judged whether all relevant regulatory guidelines are satisfied. Differences between the fuel, canisters and repository sites under consideration in Sweden and Finland will have to be considered in transferring the detailed findings of the current long-term safety studies to a Swedish context.

Safety studies refer to long-term or post-emplacement safety, i.e. safety from the time of emplacement of the first canisters in the repository. Construction and operation of the repository drifts will continue over several decades following emplacement of the first canisters, and long-term safety studies consider evolution and performance in this period, as well as in the period subsequent to repository closure. The safety of the workforce and the public during construction, operation and closure of the repository (operational safety) is not included in the long-term safety studies and will be addressed in the upcoming Design Description 2007 /Autio et al. 2008/. Throughout this report, the terms “safety studies” and “KBS-3H safety studies” refer to the KBS-3H long-term safety studies described here.

Long-term safety studies specific to KBS-3H are complemented by detailed studies of:

- the function of the bentonite buffer;
- repository design and layout adaptation to the Olkiluoto site in Finland;
- deposition equipment;
- the retrievability of the canister in KBS-3H; and
- the comparative costs of the KBS-3H and KBS-3V alternatives.

The long-term safety studies are intended to be sufficiently comprehensive that they can be used, along with the technical demonstration, environmental and cost studies, as a technical basis for a decision at the beginning of 2008 on whether or not to continue the development of the KBS-3H. The main conclusions from these KBS-3H studies and answers to the high-level questions above will be presented in the KBS-3H summary report for the years 2004–2007 /SKB/Posiva 2008/.

1.2 Reporting of KBS-3H long-term safety studies

The several reports that document and support the long-term safety studies of a KBS-3H repository at Olkiluoto are shown in Figure 1-2 (although some are common to the KBS-3H and KBS-3V and will be developed in the context of Posiva's KBS-3V programme). The reporting structure of the KBS-3H safety studies is based on Posiva's safety case plan /Vieno and Ikonen 2005/.

The overall outcome of the KBS-3H long-term safety studies is documented in the "Safety assessment for a KBS-3H spent nuclear fuel repository at Olkiluoto" report (referred to as **summary report** in Figure 1-2). /Smith et al. 2007b/. The summary report is supported by a number of further high-level reports (those shown in Figure 1-2), one of which is this **Process Report**[1].

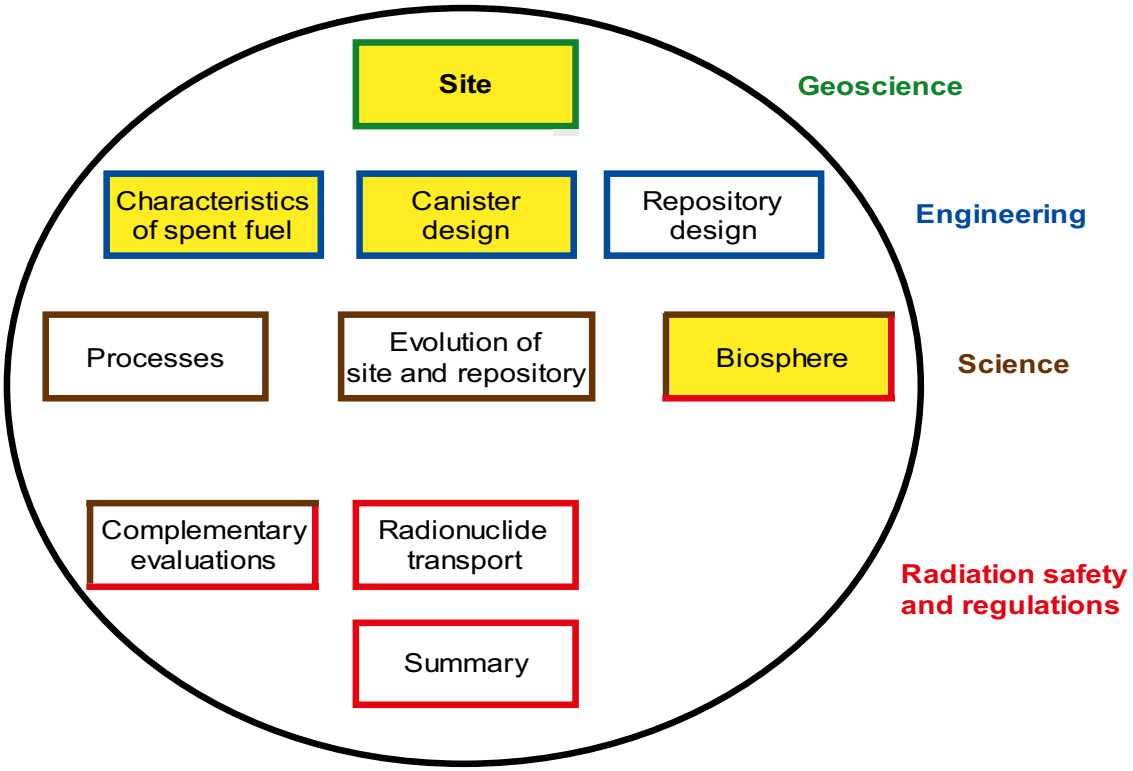

Figure 1-2. *The reporting structure for KBS-3H long-term safety studies. The colours of the boxes indicate the areas covered by the reports (as listed on the right-hand side of the figure). Yellow filling indicates reports common to the KBS-3H and -3V safety studies. All the other boxes represent reports produced within the KBS-3H safety studies or design studies. The safety assessment for a KBS-3H spent nuclear fuel repository at Olkiluoto is presented in the Summary report. For details see the main text.*

[1] Unless stated otherwise, the term Process Report refers to the present KBS-3H Process Report.

The geoscientific basis of the long-term safety studies is provided in Olkiluoto **site reports** /Posiva 2003, 2005, Andersson et al. 2007/, including the present situation at, and past evolution of, the Olkiluoto site, and disturbances caused by ONKALO[2]. Data from the most recent Olkiluoto Site Description 2006 /Andersson et al. 2007/ are used whenever possible in this report, although further work is required to incorporate these data fully in future safety assessments.

The engineering basis is provided by the reports on the **characteristics of spent fuel** /Anttila 2005a/, **canister design** /Raiko 2005/, and **repository design** /Autio 2007, Autio et al. 2007/. The preliminary "reference design" analysed in the present safety assessment is presented in the repository design report titled "Design Description 2006" /Autio et al. 2007/. The reference design for the KBS-3H safety studies (termed Basic Design) was frozen at the beginning of 2007. The KBS-3H repository design is still ongoing and subsequent design developments are presented in the Design Description 2007 report /Autio et al. 2008/. The repository design report also discusses long-term safety features, together with manufacturing and installation aspects of the buffer and backfill for KBS-3H.

The present **Process Report** provides a description of the main processes potentially affecting the long-term safety of the system. The processes discussed in the Process Report are selected based on the comparison with the KBS-3V processes discussed in the SR-Can safety assessment /SKB 2006a/, according to a "difference analysis" approach (see Section 1.5.1). The **Evolution Report** /Smith et al. 2007c/ provides a detailed description of the evolution of the repository in different time frames, based on the scientific information on processes documented in the present report. The Evolution Report describes the same processes as in the present report, but in broadly chronological order, highlighting the interactions between the processes whenever possible, starting from repository construction and continuing up to one million years from the beginning of repository operations.[3] The Evolution Report also discusses the implications of the evolution of the KBS-3H repository for radionuclide release and transport, providing a list of cases for evaluation in the safety assessment.

The Process and Evolution Reports provide the basis for the selection of the assessment cases calculated in the **Radionuclide Transport Report** /Smith et al. 2007a/. A **Complementary Evaluations of Safety Report** /Neall et al. 2007/ provides additional arguments, mostly non quantitative, on the long-term safety aspects of a KBS-3H repository located at the Olkiluoto site. A **Biosphere Analysis Report** /Broed et al. 2007/ was produced in parallel to the above-mentioned reports using input from the KBS-3H radionuclide transport report and the main conclusions on the ensuing releases to the biosphere are summarised in the safety assessment summary report /Smith et al. 2007b/.

These high-level reports are further supported by more detailed technical reports compiled in support of KBS-3H long-term safety studies, including reports on thermal analyses /Ikonen 2003, 2005/, thermo-mechanical analyses /Lönnqvist and Hökmark 2007/, layout studies based on data from the Olkiluoto site /Hellä et al. 2006/, discrete fracture network modelling of the site /Lanyon and Marschall 2006/, analyses of hydro-mechanical, chemical, gaseous and microbiological (HMCGB) processes related to the steel components /Johnson et al. 2005/, experimental and modelling studies on the interaction of iron and bentonite /Carlson et al. 2006, Wersin et al. 2007/, and solubility estimation in support of radionuclide release and transport calculations /Grivé et al. 2007/.

---

[2] ONKALO is the Olkiluoto Underground Rock Characterisation facility for site-specific underground investigations. ONKALO has been under construction since mid-2004 and will serve as an access route to the repository and the first disposal tunnels are planned to be adjacent to ONKALO`s main characterization level.

[3] A certain degree of overlap between the Process and the Evolution Reports is unavoidable and deemed beneficial if the reports are read separately. However, the authors recognise that it is preferable to read both the Evolution and Process Reports together to fully grasp the couplings and relative importance of processes in such a complex system.

1.3 Purpose and scope of this report

This report provides a description of the processes in a preliminary design of a KBS-3H repository constructed underground at a depth of about 400–500 m at the Olkiluoto site in Finland.

Considerable weight is put on demonstrating that the features, events and processes (FEPs) described, analysed and discussed in this report allow a description of the system and its evolution to be developed to the stage that is sufficient for the purposes of safety assessment, even if the data to parameterise all processes, for example, are not available. The report also identifies some of the current uncertainties affecting the process understanding and how these are handled in the safety assessment.

1.4 The regulatory context

The present safety assessment addresses the long-term safety of a KBS-3H repository for Finnish spent fuel located at the Olkiluoto site in Finland. It is therefore appropriate to base the assessment on Finnish regulatory requirements[4]. The regulatory requirements for a spent fuel repository at Olkiluoto are set forth in the Government Decision on the safety of the disposal of spent nuclear fuel /STUK 1999/ and, in more detail, in Guide YVL 8.4 issued by the Finnish regulator /STUK 2001/. These requirements are, however, currently under revision. A detailed discussion of regulatory requirements related to the safety case, including dose and radionuclide release constraints in different time frames, is given in Posiva's TKS-2006 report describing the programme for research, development and technical design /Posiva 2006/. Some key points relevant to the present report are summarised below.

Finnish regulations distinguish between the "environmentally predictable future" (lasting "several thousand years"), during which conservative estimates of dose must be made, and the "era of large-scale climate changes" when periods of permafrost and glaciations are expected, and radiation protection criteria are based on constraints on nuclide-specific activity fluxes from the geosphere ("geo-bio flux" constraints). Posiva's interpretation of the duration of the "environmentally predictable future" is typically 10,000 years. The annual effective dose constraint for the most exposed members of the public applicable over this time frame is 10^{-4} Sv per year, while the average annual effective doses to other members of the public should, according to the regulations, remain insignificantly low. It is also stated in YVL 8.4 that the radiation exposure of flora and fauna shall remain clearly below the levels that would cause decline in biodiversity or other significant detriment to any living population on the basis of the best available scientific knowledge. Moreover, rare animals and plants as well as domestic animals shall not be exposed detrimentally as individuals.

Regarding the characteristic and performance of the engineered barrier system, YVL 8.4 requires that:

The barriers shall effectively hinder the release of disposed radioactive substances into the host rock for several thousands of years.

The importance to long-term safety of unlikely disruptive events shall, according to regulations, be assessed. According to STUK, these events are to include at least:

- boring a deep water well at the disposal site;
- core drilling hitting a spent fuel canister; and
- a substantial rock movement occurring in the environs of the repository.

[4] The differences between the Swedish and Finnish regulatory systems are discussed in Appendix C of the Complementary Evaluations of Safety Report /Neall et al. 2007/.

The likelihood and consequence of the first two events is not considered to differ significantly between KBS-3V and KBS-3H repositories (although some differences in the probability of a vertical borehole intersecting vertically emplaced canister exist compared with horizontally emplaced canisters) and these are not discussed in the present report. The impact of substantial rock movement occurring in the environs of the repository is, however, discussed in the context of post-glacial earthquakes.

In the very long term, after at least several hundred thousand years, no rigorous quantitative safety assessment is required by the regulator, but the judgement of safety can be based on more qualitative considerations.

1.5 Structure and basis for process descriptions

1.5.1 A difference analysis approach

In order to judge the feasibility of implementing the KBS-3H alternative from a long-term safety point of view, relevant safety issues must be understood as well for KBS-3H as they are for KBS-3V. There is a broad scientific and technical foundation that is common to both alternatives, and much of the work carried out by both Posiva and SKB in the context of KBS-3V is also directly applicable to KBS-3H. Thus, there is comparatively much more limited documentation that has been developed specifically relating to KBS-3H, and this documentation focuses primarily on the differences identified between the two alternatives in a systematic "difference analysis" approach.

Consistent with this approach, at the onset of the KBS-3H long-term safety studies, a decision was taken to follow the approach in SKB's most recent safety assessment, SR-Can /SKB 2006a/, for process selection and to accept the understanding and modelling basis presented in SR-Can in areas in which KBS-3H and KBS-3V are very similar, in particular in modelling canister processes and fuel processes. The reason for this is that major efforts would have to be made to advance the models (e.g. fuel dissolution model, copper corrosion model) beyond what was presented in SR-Can, and such advances were not part of the KBS-3H programme mandate. Such developments may, however, be considered in future project stages for both the KBS-3H and -3V alternatives.

Given the limited scope of the KBS-3H long-term safety studies, the documentation in this report is not exhaustive from a scientific point of view but it is sufficiently detailed to motivate, by arguments founded on scientific understanding, the treatment of relevant scenarios in the Radionuclide Transport Report /Smith et al. 2007a/. The purpose is further to determine how to handle each process in the safety assessment at an appropriate degree of detail, and to demonstrate how uncertainties are handled in the safety assessment. In the course of the project, the difficulties in quantifying uncertainties in some areas led to more detailed studies (e.g. iron-bentonite interactions) that helped to establish the significance of such processes and how they should be evaluated in radionuclide transport calculations.

1.5.2 Focus on early evolution and on the near field

Early in the evolution of the repository, mass and energy fluxes occur as a result of the various gradients created by repository construction and emplacement of the spent fuel. In both alternatives, the system evolves from the initial state through an early, transient phase towards a quasi-steady state, in which key safety-relevant physical and chemical characteristics (e.g. temperature, buffer density and swelling pressure) are subject to much slower changes than in the transient phase. It is in the early, transient phase that most of the significant differences in evolution between KBS-3H and KBS-3V arise, although there are also some differences at later times (for example, in the impact of post-glacial faulting and in the gas-induced release of dissolved radionuclides in the case of a defective canister). Thus, processes occurring during the early, transient evolution of the repository and, in particular, processes influencing the

development of full saturation in the KBS-3H buffer and associated with the corrosion of the steel supercontainer shell receive particular attention in this report (Chapters 4 and 5).

This Process Report focuses also mostly on internal processes relevant to a single drift and its immediate environment (near-field rock, drift end plugs) at the Olkiluoto site. The discussions of geosphere processes are thus restricted to aspects related to the performance of the near-field rock in the presence of a KBS-3H deposition drift. Site properties and aspects of system evolution common to the two alternatives are described in more detail in the Olkiluoto Site Description 2006 /Andersson et al. 2007/ and in the evolution report for a KBS-3V repository at Olkiluoto /Pastina and Hellä 2006/.

1.5.3 Input data

Because of a project decision not to prepare a separate data report (in contrast to the case of SR-Can), all data used in this report and in other reports of the KBS-3H long-term safety studies are reported in Appendix A. Furthermore, in certain sections of the present report, additional data are derived as a result of modelling calculations as no other sources exist for the data and models, which was not the case for SR-Can. Data used in this report are based on the information available at the time of report writing (2006–2007). Input data were selected on the basis of the preliminary design information presented in the KBS-3H Design Description 2006 /Autio et al. 2007/, laboratory data, field data, modelling, calculations, and in some cases, expert judgment. The bases for data selection and assumptions used have been reported as much as possible in Appendix A. The models, datasets and computer codes used in the radionuclide release and transport calculations are described in detail in the Radionuclide Transport Report /Smith et al. 2007a/. A more complete data report for both KBS-3H and -3V will be published by Posiva at a later date.

1.5.4 Structure of this report

The initial model and basis for the structure of this Process Report was SKB's SR 97 Process Report for a KBS-3V repository /SKB 1999/, which was applied to the Finnish repository site, Olkiluoto, by /Rasilainen 2004/. When the main report of the SR-Can safety assessment /SKB 2006a/ and its related process reports for the fuel and canister /SKB 2006c/, buffer and backfill /SKB 2006d/ and for the geosphere /SKB 2006e/ were published, they provided further input for the content and structure of the present report.

The aim of this Process Report is not, therefore, to reproduce these previous process reports in the context of the KBS-3H. The focus instead is mostly on processes that differ between KBS-3V and -3H (i.e. a difference analysis approach) and evaluating their impacts on repository evolution and safety functions. The available information on similar/identical processes is referenced.

This Process Report is therefore organised in a similar manner to the SR-Can process reports and the first Posiva KBS-3V Process report /Rasilainen 2004/.[5] Separate chapters are dedicated to the nested subsystems spent fuel, canister, buffer and distance block, supercontainer shell and other steel structural materials, drift end plug, backfill and geosphere (Figure 1-3).

The SR-Can FEP report /SKB 2006b/ classifies FEPs into *internal processes, initial state* and *external factors*. A list of internal processes is defined for each component of the repository system (including the geosphere). Initial state FEPs refer to the initial conditions for the evolution of the repository system. Relevant FEPs occurring outside the system boundary are classified as external factors (e.g. climatic processes and effects, tectonics, seismic activity, future human actions, etc).

[5] A new Posiva's KBS-3V Process Report was published at the end of 2007 /Miller and Marcos 2007/.

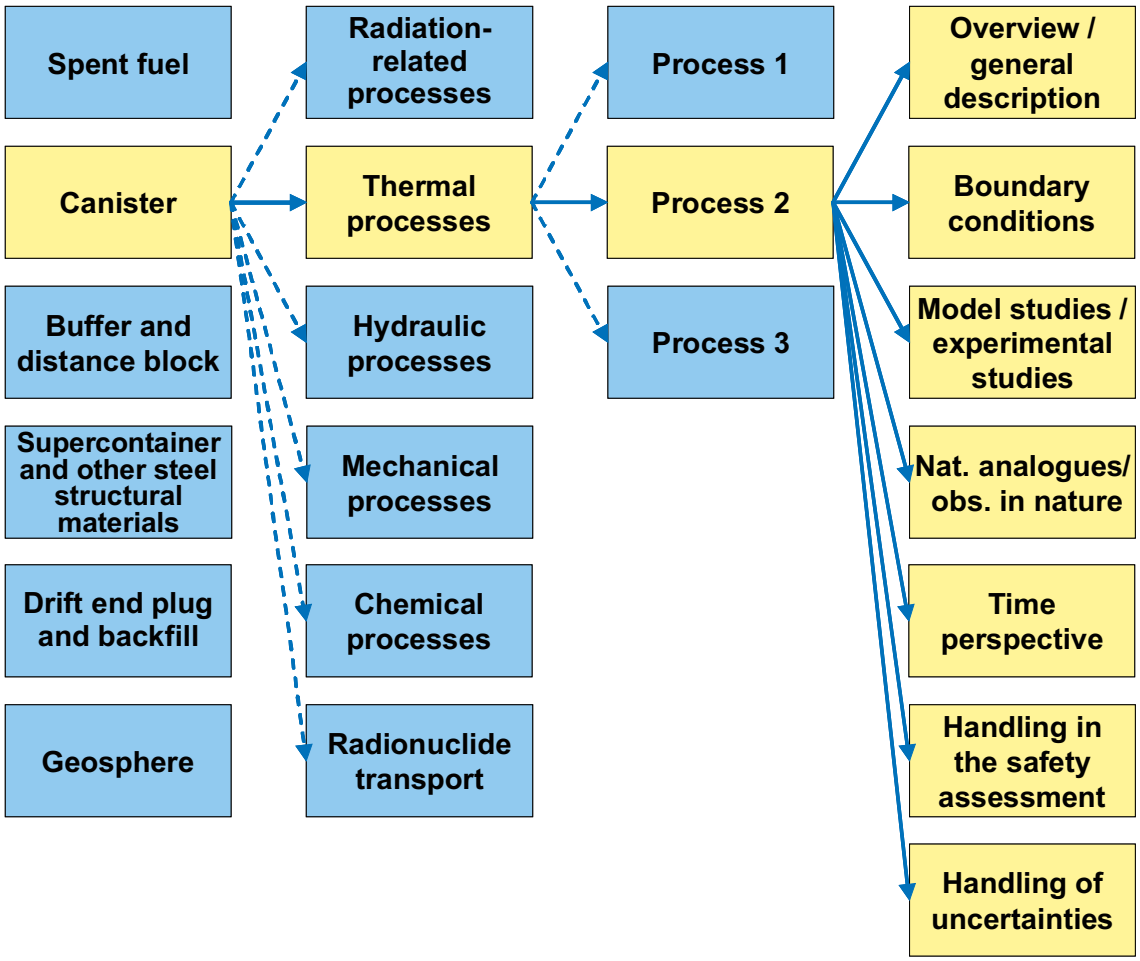

Figure 1-3. *Organisation of the KBS-3H Process Report.*

Initial conditions and external factors are discussed in detail in the Evolution Report for KBS-3H /Smith et al. 2007c/. The initial conditions in the deposition drift are summarised in Section 1.7 of the present report. The impacts of external factors on internal processes are considered where relevant. For example, the impact of glaciations and post-glacial faulting on canister integrity is discussed in the context of mechanical processes in the subsystems canister and geosphere.

The repository-bedrock system is divided into six nested subsystems (first column). For each subsystem the processes are grouped into six process categories (second column). In each process category all identified processes are discussed that are specifically relevant to KBS-3H (third column). Whenever there is a difference with KBS-3V, the relevant process is discussed according to the same logic (fourth column). As an example, the yellow boxes present the full description of process 2 belonging to the thermal group of processes relevant to the canister.

Relevant processes are selected based on the screening against the relevant lists of processes for the various system components which is in turn based on the FEPs Analysis Report /SKB 2006b/ that was used in the SR-Can Main Report /SKB 2006a/. In Appendix B, the methodology to adapt the list of processes from SR-Can to KBS-3H is described. The relevant processes are summarised in tabular form under the heading "Summary of handling in the safety assessment" for each system component. Only those processes that are identified as being specifically relevant for KBS-3H are discussed according to the structure defined in SKB's SR-Can process reports (see Figure 1-3 derived from /SKB 2006 cde/), as follows:

Overview/general description

Under this heading, a general description of the available knowledge regarding the process is given. For KBS-3V, the information basis is provided by the Process Reports for SR 97 /SKB 1999/ and SR-Can /SKB 2006 cde/ and by Posiva's localisation of the SR 97 Process Report to Olkiluoto /Rasilainen 2004/. For KBS-3H, the available information is provided by a number of different reports, including the report on KBS-3H hydro-mechanical-chemical-biological-gas-(HMCBG-) related processes /Johnson et al. 2005/, the report on buffer behaviour /Börgesson et al. 2005/, thermal dimensioning analyses /Ikonen 2003, 2005/ and many others.

For each process, a table documents the inter-dependence of the processes and the specified set of variables in the relevant system component (similar to Tables 2-4, 2-5, 2-6 etc in /Rasilainen 2004/).

Boundary conditions

The boundary conditions for each process are discussed, referring to the relevant boundaries of the system component. For example, for the buffer the relevant boundaries are the buffer interfaces with the canister, the supercontainer and (after swelling through the holes of the supercontainer) the walls of the deposition drift.

Model studies/experimental studies

Model and experimental studies of the process are summarised. This documentation is the major source of information for many of the processes relevant to KBS-3H.

Natural analogues/observations in nature

If relevant, natural/archaeological analogues and/or observations from nature regarding the process are documented under this heading.

Time perspective

The relevant time scales for the process are indicated.

Handling in the safety assessment for KBS-3H

The analyses presented principally provide insights regarding processes that occur in one single drift and its environment within the disposal system. These insights provide much of the basis for indicating which processes might lead to changes significant enough to influence the safety functions of the canister, buffer and host rock. In some cases processes are further explored to provide recommendations for assessment cases that could quantify radionuclide release and transport processes, as described in the Radionuclide Transport Report /Smith et al. 2007a/.

Following SR-Can, a process is either

- omitted from models on the basis of the information under the previous headings (which leads to a conclusion of negligible impact or that it is conservative to omit the process),
- omitted from models provided that a certain condition is fulfilled (e.g. that the buffer density is within a certain range), or
- included by means of modelling or scoping/bounding calculations.

The following aspects are covered: Time perspective, boundary conditions, interactions with other processes, special cases (e.g. failed canisters).

Handling of uncertainties

Given the adopted handling of processes in the safety assessment calculations for KBS-3H as described above, the handling of different types of uncertainties associated with the processes are summarised.

- Uncertainties in mechanistic understanding: The uncertainty in the general understanding of the process is discussed based on the available documentation and with the aim of answering the question: Are the basic mechanisms governing the process understood to a level necessary for the suggested handling?
- Model simplification uncertainties: In most cases, the quantitative representation of a process will contain simplifications. These may result in a significant source of uncertainty in the interpretation of calculational results.
- Input data and data uncertainties: The set of input data necessary to quantify the process for the suggested handling is documented and the relevant uncertainties discussed. The list of input data with references is in Appendix A.

1.6 Repository design

1.6.1 General description

In KBS-3H and in KBS-3V, the spent fuel is encapsulated in copper canisters with cast iron inserts, which have a design lifetime of at least 100,000 years (see Section 3.1.1 for details). The copper canister and its contents are assumed to be the same as in the KBS-3V. The reference fuel is the Finnish BWR fuel from the Olkiluoto 1 and 2 reactors. The canisters, each with a surrounding layer of bentonite clay (the reference bentonite for this report is MX-80), are placed in perforated steel shells prior to emplacement in the drifts. The entire assembly is called a supercontainer. The supercontainers are deposited coaxially in the drifts, supported on steel feet to leave an annular gap to the drift wall (about 4 cm). Adjacent supercontainers in the drift are separated from each other by bentonite distance blocks One supercontainer and one distance block are referred to as a "supercontainer unit". A section of drift with two supercontainers and one distance block is shown in Figure 1-4 and the entire drift is shown in Figure 1-5. Void spaces around the supercontainers and distance blocks will become filled with bentonite as the drift saturates and the bentonite swells, although the rate at which this occurs may vary considerably along the drift due to the heterogeneity of the rock and the spatial variability of water inflow, as discussed in Chapter 4.

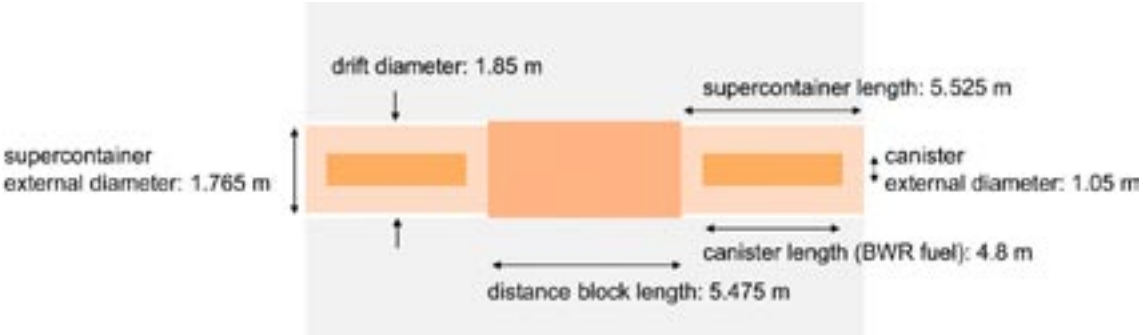

Figure 1-4. *Illustration of a section of a KBS-3H deposition drift with two supercontainers separated by a distance block (for references see Appendix A). The 5.475 m distance block length is for the reference fuel for the present safety studies (BWR spent fuel from the Olkiluoto 1 and 2 reactors).*

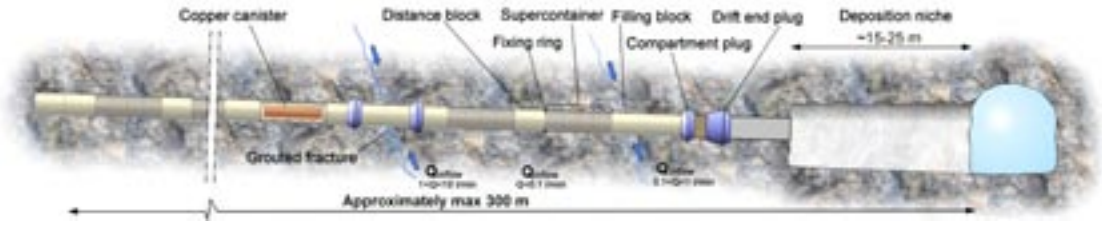

Figure 1-5. *Illustration of a generic KBS-3H drift showing one canister in copper colour for better visualisation. At one end of the drift, a wider area (deposition niche) hosts the deposition equipment while the other end of the drift is closed off. The different components are described in Section 1.6.4.*

The bentonite inside the supercontainers and the bentonite distance blocks are jointly termed the "buffer" in contrast to the KBS-3V terminology in which the term buffer refers only to the bentonite surrounding the canister.

A tunnel section in front of each drift (before the drift end plug) a 15-metre long, wider section of the drift (with a 50 m^2 cross section) hosts the deposition equipment for supercontainers and distance blocks. This section is called "deposition niche" and is considered part of the drift for material inventory purposes. The maximum length of the drifts is 300 m, the estimated minimum length is 100 m and the average length is about 272 m, based on site-specific features /Autio et al. 2007/. In the current design, the drifts are dead-ended, i.e. there is no access tunnel on the other end.

A preliminary layout for a one-storey facility based on the current bedrock model and the hydraulic, thermal and mechanical considerations described above is given in /Johansson et al. 2007/. In this preliminary layout, which is illustrated in Figure 2-2, the repository is constructed in a single layer at a depth in the range 400 to 420 m below ground (note that the drifts are slightly inclined to the horizontal to facilitate drainage during construction and operation – see Figure 1-5). This preliminary layout uses about 95% of the currently well-characterised and available bedrock resource[6] at Olkiluoto, which takes into account the major fracture zones, respect distances to investigation boreholes, the access tunnel to the ONKALO, the shoreline of Olkiluoto Island, and the boundaries of the current investigation area. Although the margin for uncertainties is therefore small in this layout, it would, if necessary, be possible to increase this margin by extending the current investigation area or constructing the repository in multiple layers.

1.6.2 Design options under consideration

Localised water inflow along the drift may potentially give rise to large hydraulic pressure differences along the drift between the void spaces around neighbouring supercontainers. A key consideration in the development of the present reference and alternative designs is to minimise the possibility that these pressure differences develop rapidly, before the bentonite of the distance blocks swells and contacts the drift walls and a high swelling pressure and bentonite density develop at this interface. The concern is that, if high pressure differences develop too rapidly, this could result in movement of the distance blocks and supercontainers, or transient water flows ("piping") along the interface, which could in turn lead to erosion and loss of bentonite mass in some supercontainer sections, and possibly an increase in mass in others.

[6] For comparison, the current reference KBS-3V layout at Olkiluoto uses about 80% of the available bedrock resource /Johansson et al. 2007/.

Two broad design options are currently being developed in parallel. The Basic Design is the current reference design chosen for long-term safety studies reports (including the present report) and is described below (some alternative realisations of the Basic Design are described in Appendix K of /Autio et al. 2007/. The Drainage, Artificial Watering and air Evacuation (DAWE) design variant is summarised in Appendix D and described in more detail in the Design Description 2006 /Autio et al. 2007/. Each option has a number of open design issues (e.g. physical dimensions of some components) that are still under consideration, thus both options are considered to be preliminary. After the main design features become fixed, development will concentrate on the dimensioning of components and confirmation that they will perform their intended design functions.

In all design options, the copper canisters are fully retrievable, as will be described in the Design Description 2007 /Autio et al. 2008/. An SKB report evaluating canister retrievability techniques for both KBS-3H and KBS-3V /Kalbantner and Sjöblom 2000/ concluded that canister retrieval feasibility is equivalent for both alternatives.

1.6.3 Groundwater control and compartmentalisation of the drifts

Groundwater control measures in the form of pre- or post-grouting to reduce inflow to the drifts will be implemented for reasons of engineering practicality and operational safety. Currently, the possibility of using a large-scale post-grouting device (called Mega-Packer-type, see /Autio et al. 2007/ to inject Silica Sol into transmissive fractures is being investigated. In spite of such measures (and in particular because they cannot be relied upon for the purposes of long-term safety assessment), highly transmissive fractures intersecting the drift may render particular sections unsuitable for the emplacement of supercontainers and distance blocks.

In this report (and other reports of the KBS-3H safety studies), it is assumed that drift sections having an inflow higher than 0.1 litres per minute (summed over discrete inflow points within an approx. 10 m long drift section) will be excluded as distance block or supercontainer emplacement locations. The 0.1 litre per minute inflow criterion is roughly equivalent to a maximum fracture transmissivity $T = 3 \times 10^{-9}$ m^2 s^{-1} assumption if most of the inflow to a drift section is conveyed by a single fracture (see Section 7.1.4 and Appendix B.2 of /Smith et al. 2007c/).

In the current reference design, additional "filling blocks" will be emplaced along drift sections where inflows exceed about 0.1 litres per minute but do not exceed about 1 litre per minute after grouting. The maximum allowable inflow in the case of filling blocks is currently 1 litre per minute, higher that that allowed for distance blocks. This is because of the different functions of these two components. The distance blocks should prevent significant water flow by piping between adjacent supercontainer drift sections during saturation of the drift, which could otherwise lead to buffer erosion. The filling blocks, on the other hand, are not used to separate adjacent supercontainers and so the prevention of piping is not a primary consideration in deciding where they can be emplaced. There is, however, a requirement to avoid erosion of these blocks by water flowing around the drift through intersecting transmissive fractures and erosion (Section 5.5.6 and Appendix L of /Autio et al. 2007/). The relevant inflow criterion for filling blocks is expected to be higher, although the present choice of 1 liter per minute is preliminary and somewhat arbitrary value that may be updated in view of future studies and possible design changes. Steel compartment plugs will be used to seal off drift sections where inflows are higher than 1 litre per minute (after grouting), thus dividing the drift into compartments (Figure 1-5).

According to the discrete fracture network modelling carried out by /Lanyon and Marschall 2006/ and the hydrogeological considerations about the Olkiluoto site, a 300 m-long KBS-3H drift contains, on average, 17–18 supercontainers for the reference fuel type (BWR from OL1-2) or 22–23 supercontainers (in average) for all fuel types, one drift section (30 m long) with unfavourable hydraulic features, which is isolated from the rest of the drift by compartment plugs and 3–4 filling blocks (10 m each). On average, 17% of the drift is unusable due to water inflow exceeding the 0.1 L/m criterion. A higher figure of 25% is tentatively and conservatively assumed in the layout adaptation (/Johansson et al. 2007/ see also Section 2.2.7 of the KBS-3H

Evolution Report /Smith et al. 2007c/). This figure is based on a drift separation of 25 m, and consideration of all different Finnish fuel types under consideration (canister pitch ranging from 9.1 to 11 m). This also takes into account the possibility that some relatively tight fractures, which have the potential to undergo shear movements sufficiently large to damage the canisters, are identified and avoided (Section 7.6.2).

1.6.4 Key components specific to KBS-3H in the Basic Design

Key engineered system components specific to KBS-3H, as realised in the Basic Design, are the supercontainer, the buffer inside the supercontainer, the distance blocks, the filling blocks, the fixing rings, the compartment plugs, the filling within and between and adjacent to the compartment plugs, the spray and drip shields, the drift end plug, and the backfill and seals of other repository cavities (see Figure 1-5). A list of parameters and references for these components can be found in Appendix A. These components are described individually in the following sections.

(i) The supercontainers

The supercontainers are 1.765 m in diameter. Their lengths will vary according to fuel type that they contain. They are, for example, 5.525 m long for BWR fuel from the Olkiluoto 1-2 reactors. The buffer inside each supercontainer is comprised of a set of bentonite ring blocks surrounding the canister and two end blocks (Figure 1-6). The cylindrical steel shell that contains the buffer and canister is 8 mm thick and perforated with 100 mm diameter holes covering 62% of the cylindrical surface (Figure 1-7). The buffer inside the supercontainers will swell through these perforations as it saturates. The surfaces of the end plates are unperforated to favour a good contact between the supercontainers and the adjacent distance blocks. The canister is described in Section 3.1.

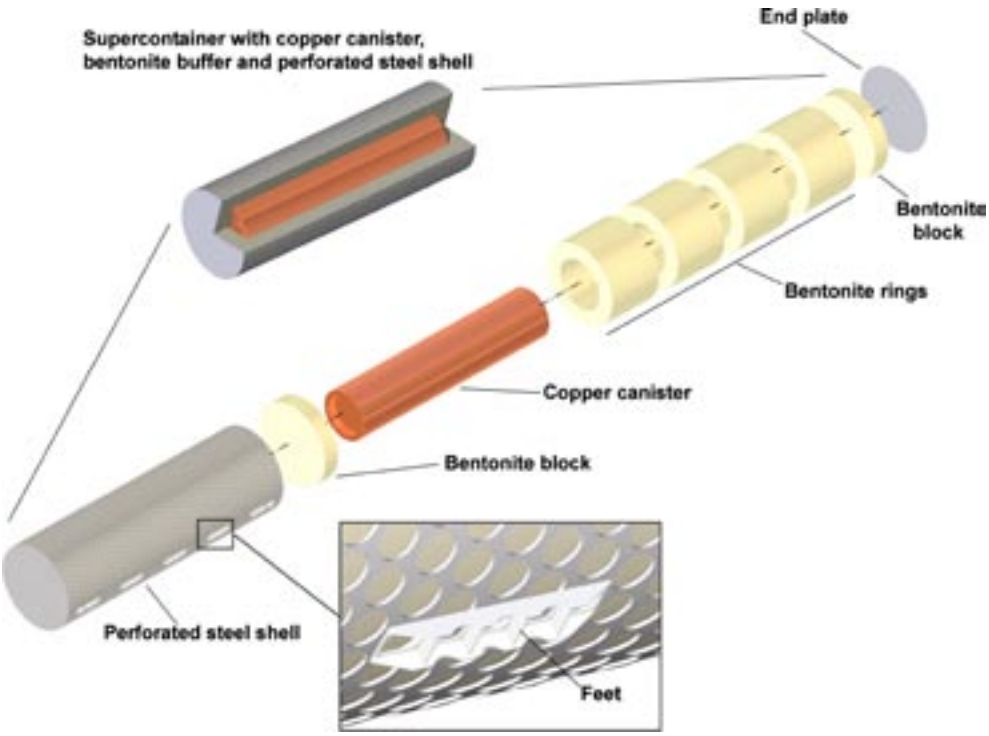

Figure 1-6. *The supercontainer with buffer and copper canister.*

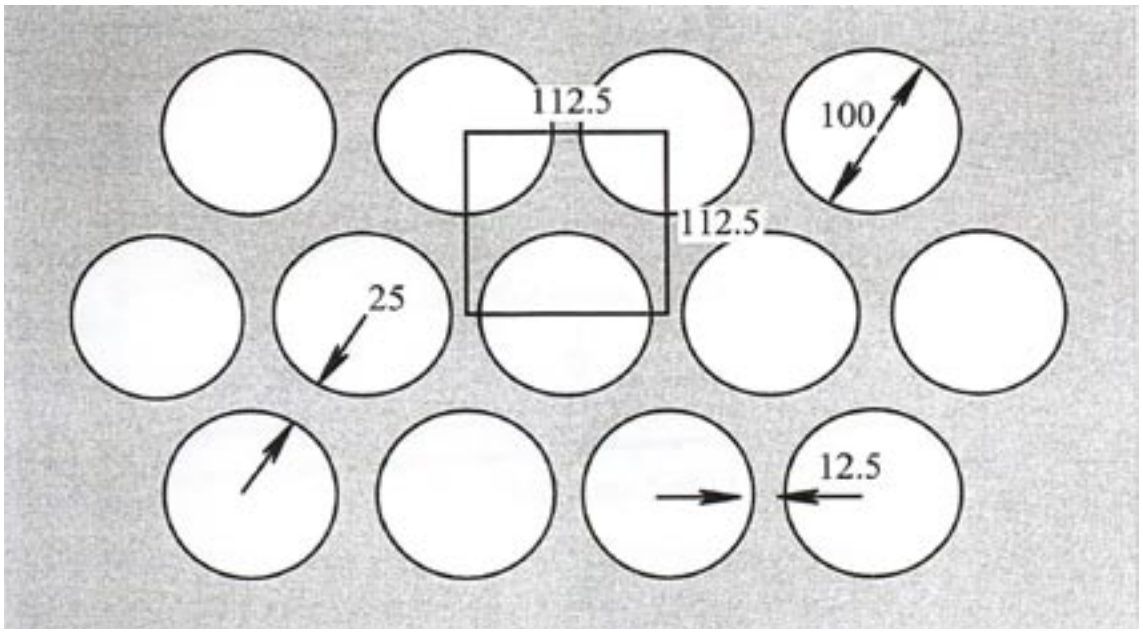

Figure 1-7. *Section of supercontainer shell surface showing dimensions [mm] of the perforations.*

(ii) The buffer contained within the supercontainers

The reference bentonite material considered in this report is sodium-bentonite (MX-80); other bentonite clays that are under consideration for KBS-3V (e.g. calcium-bentonites) have not been addressed. The buffer inside the supercontainers comprises a set of MX-80 bentonite ring blocks surrounding the canister and two end blocks (Figure 1-6).

The ring blocks have 10% initial water content and a dry density of 1,885 kg m^{-3}. The end blocks also have 10% initial water content, but have a lower dry density (1,753 kg m^{-3}). The design density and porosity of these buffer components following saturation and swelling into the gap around the supercontainer are 2,000 kg m^{-3} and 0.44, respectively.[7] Some differences in buffer density are, however, likely to occur, especially between the saturated buffer inside and outside the supercontainer. These differences may persist indefinitely because friction may limit buffer homogenisation (Section 4.6.1).

(iii) The distance blocks

The distance blocks, which hydraulically separate the supercontainers one from another, are also composed of MX-80 bentonite. In the Basic Design, the reference distance block design uses two different bentonite components in series: a "tight" block and a "loose" block as shown in Figure 1-8. The gap between the distance block and the drift wall is made small (a few mm in the case of the "tight" blocks and up to a maximum of 15 mm in the case of the "loose blocks") to favour rapid closing and sealing /Autio et al. 2007/. In the DAWE design alternative, the distance blocks are all of uniform dimensions with a 40 mm gap (see Appendix D). Buffer and design development studies have been performed /Börgesson et al. 2005, Sandén et al. 2007/ Appendix L in /Autio et al. 2007/ and are still ongoing to verify that the sealing ability of the proposed design is adequate (see Appendix D).

[7] In the various scoping calculations presented in this report and in the Evolution Report /Smith et al. 2007a/, the porosity of the saturated buffer is taken to be 0.44, which is also the value given in the Design Description 2006 /Autio et al. 2007/. For the purposes of radionuclide transport calculations, the decision was taken to use near-field data from the SR-Can safety assessment, where this is not affected by the specific characteristics of the Olkiluoto site and the KBS-3H concept. These near-field data include a slightly lower saturated buffer porosity of 0.43.

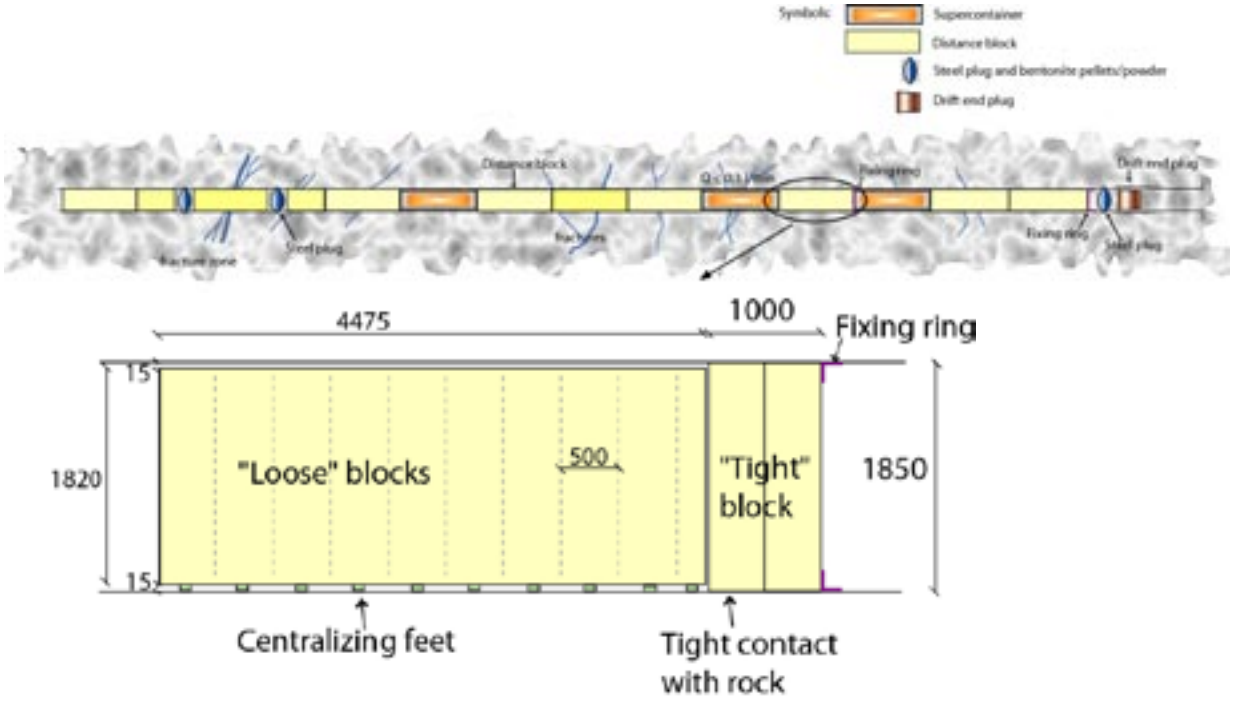

Figure 1-8. *Drift view (above) and detail (below) of "tight" and "loose" components of the distance block in the Basic Design (after Figure 5-2 of /Autio et al. 2007/).*

In the Basic Design option, the vertical gaps between distance blocks and supercontainer are also minimised in order to prevent the possibility of exposing the entire vertical face of a distance block to full hydrostatic pressure during saturation of the drift, which could otherwise lead to the possibility of pressure-induced movement of distance blocks and supercontainers. If the gap is small (a few millimetres), the full hydrostatic pressure is expected to be exerted only around the periphery of the face (see the discussion of fixing rings and compartment plugs, below) thus the overall force on the face is smaller. The small size of the gap between the distance block and the supercontainer makes the Basic Design difficult to implement (see Appendix D). In the case of DAWE the size of the gap is not so critical because the gaps are saturated during the operational phase and therefore there is no possibility for pressure-induced movements of distance blocks.

The length of the distance blocks is determined by the thermal management requirements of the spent fuel. The distance blocks for Posiva BWR fuel canisters from the Olkiluoto 1-2 reactors are, for example, 5.475 m long (Figure 1-4 and Figure 1-8).

In the Basic Design, the "loose and "tight" distance blocks both have a 24% initial water content, The "loose" blocks have an initial dry density of 1,610 kg m^{-3}, and the "tight" blocks an initial dry density of 1,559 kg m^{-3}. The design saturated density and porosity are 2,000 kg m^{-3} and 0.44, respectively, for both the "loose" and the "tight" blocks. The initial dry density and water content is different for DAWE compared with the Basic Design (see Appendix D) but the final saturated density and porosity are the same.

(iv) Filling blocks

Although the details have not been specified in the Design Description 2006, the MX-80 bentonite filling blocks are expected to be similar in design to the distance block units. Filling blocks for the Basic Design are expected to be different for the DAWE design. Their use is illustrated in Figure 1-9.

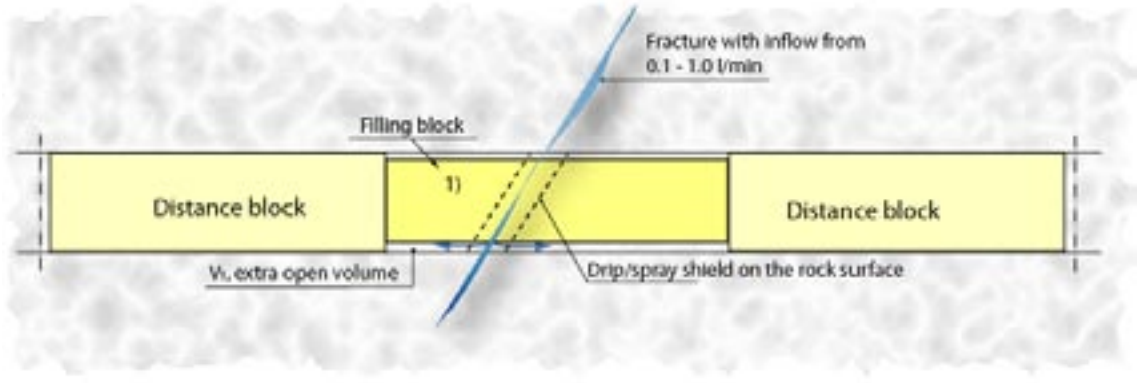

Figure 1-9. *Filling block similar to distance block emplaced in positions where water inflow is higher than 0.1 l/min (after Figure 5-15 in /Autio 2007/).*

(v) Fixing rings

As noted in Section 4.6, large pressure differences may develop along the drift during and after operation due to localised water inflow. A distance block separating drift sections in which the gaps become rapidly water filled from a tighter drift section may experience full hydrostatic pressure ($P_{hydrostatic}$ in Figure 1-10) around the periphery of one vertical face, while the pressure on the opposite vertical face remains low. A measure that will be implemented, where necessary, to avoid displacement of the distance blocks is the use of steel fixing rings, as described in Section 5.2.3 of /Autio et al. 2007/ and illustrated in Figure 1-10.

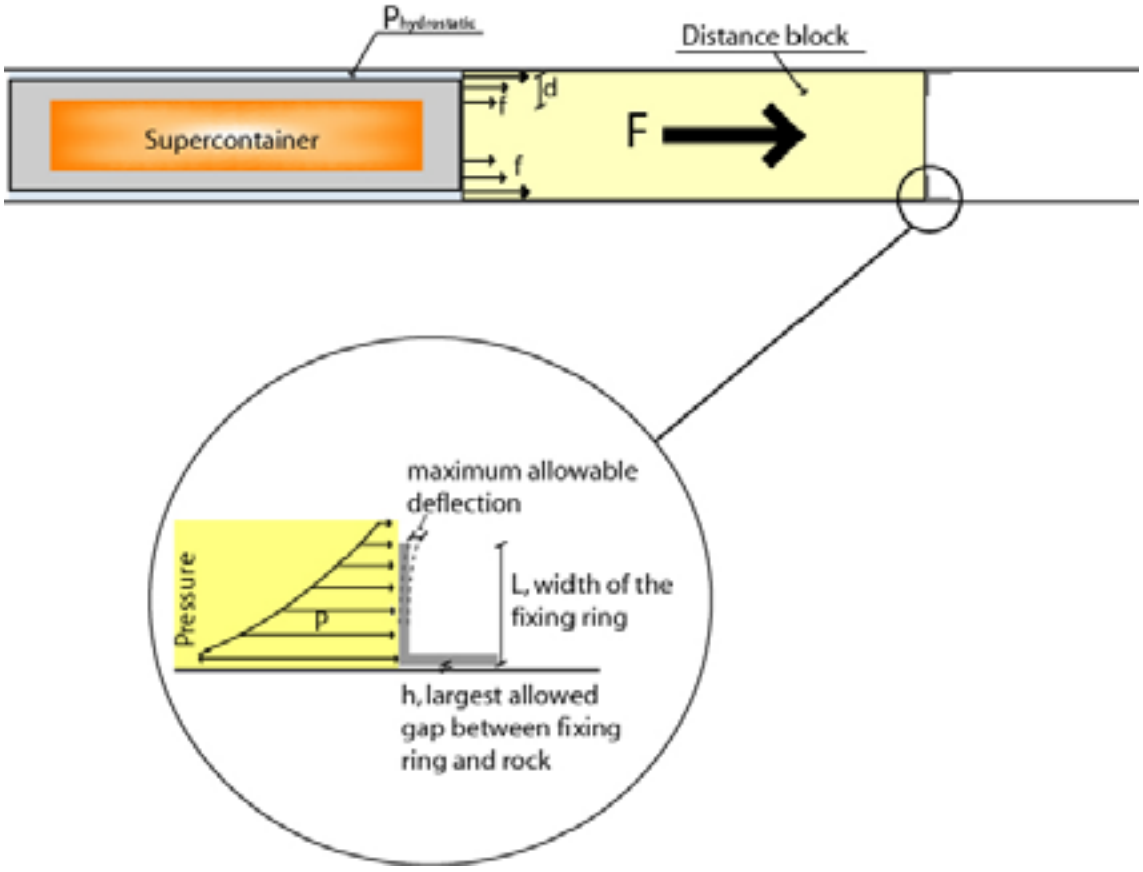

Figure 1-10. *The principle of using fixing rings in the Basic Design to prevent displacement of a distance block during drift operation (after Figure 5-8 of /Autio et al. 2007/).*

The fixing ring consists of a 10 mm-thick steel plate, supported by a steel collar grouted and bolted into the rock, as described in Section 5.2.3 of /Autio et al. 2007/. In the current reference design (Basic Design), fixing rings are installed in every position where the inflow to a supercontainer unit exceeds 0.01 litres per minute. This tentative criterion will, however, need to be confirmed by further studies. An average of 4–5 fixing rings per drift is expected /Hagros 2007a/. No fixing rings will be used in the DAWE design alternative (see Appendix D).

(vi) Compartment plugs

Steel compartment plugs will be used to seal off drift sections where inflows are higher than 1litre per minute (after grouting). The compartment plugs are steel structures and are described in detail in Section 4.3 of /Autio et al. 2007/. At each location where a plug is required, a steel collar structure will be attached to the drift surface before drift operation starts and sealed using concrete. The centre part of the plug, which takes the form of one or two dome-shaped caps attached to a flange (Figure 1-11 shows the variant with two caps) will then be installed rapidly during drift operation, following emplacement of the supercontainers and distance blocks in a compartment. The plugs are designed to withstand the full hydrostatic pressure exerted on the convex side of the cap. If the hydrostatic pressure is exerted on both sides, the double-capped version of the plug is used, as shown in Figure 1-11. The design of the compartment plug is still under development and demonstration tests are planned to be performed at the Äspö Hard Rock Laboratory.

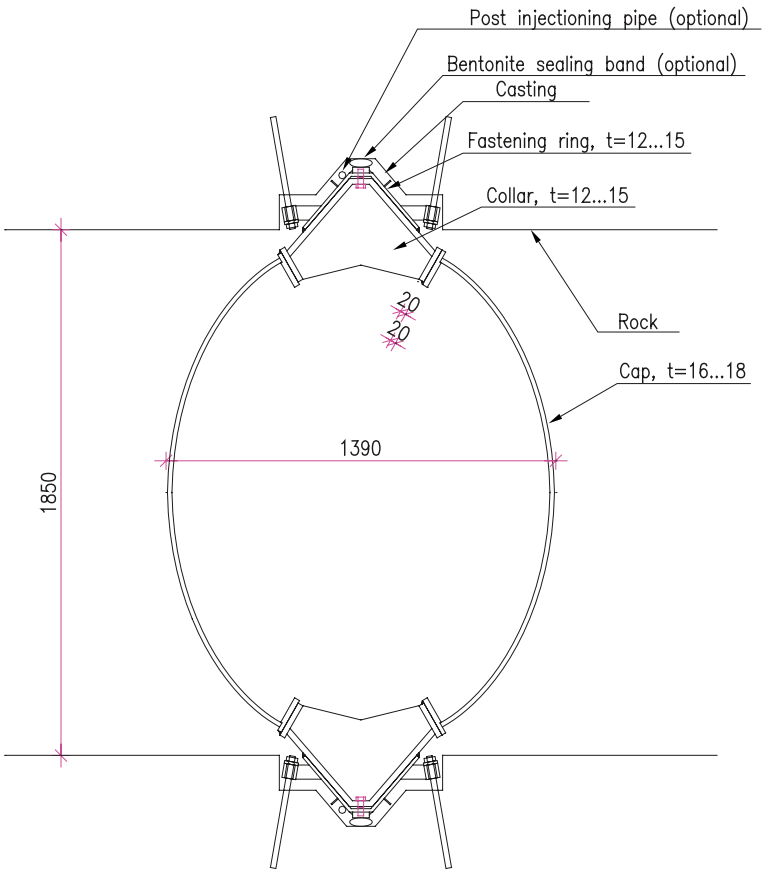

Figure 1-11. *Cross-section of the steel compartment plug (after Figure 4-12 of /Autio et al. 2007/). The figure shows the double-capped version of the plug. The plug design has not yet been finalised.*

(vii) Filling adjacent to, within and between compartment plugs

Void spaces within and around the compartment plugs will be filled to avoid the presence of large void spaces within the drift that could eventually lead to a loss in buffer density. Spaces to be filled are:

- the space between the compartment plugs and the adjacent distance blocks;
- the space between the concave surfaces of the compartment plugs (Figure 1-11); and
- the drift section unsuitable for distance blocks and supercontainer emplacement that is sealed off by compartment plugs.

In the current reference design, cylindrical transition blocks are placed between the compartment plugs and the adjacent distance blocks. The transition blocks are similar to the "loose" component of the distance blocks. The remaining void space next to the convex surfaces of the plugs will be filled with MX-80 bentonite pellets or sand (Figure 1-12). The space between the concave surfaces of the compartment plugs will be filled with sand, according to preliminary considerations.

The drift section sealed off by compartment plugs will be backfilled and drained during operation until the emplacement of supercontainers and distance blocks continues in the next compartment. No detailed design has as yet been developed for the backfill between the plugs in the sealed off section. One tentative possibility is illustrated in Figure 1-13.

In this possible design, the inflow zone is filled with a permeable material, such as crushed rock, which is graded to prevent the bentonite used to fill the "no-flow zone" and the "through-flow zone" from swelling into interstitial spaces. It should be noted that, in the term "through-flow zone", "through-flow" refers to flow along the floor of the drift prior to installation of the plug nearest to the entrance to the drift. Once the plug is installed and the bentonite saturates, the only long-term flow will be into and out of the inflow zone of the fracture zone.

(viii) Spray and drip shields

The possibility of erosion of bentonite due to the spraying, dripping and squirting of water from the drift walls onto the distance blocks and supercontainers will be prevented by placing thin steel spray shields over inflow points (Section 4.2.2 of /Autio et al. 2007/). It is anticipated that four to five drip and spray shields will be used in each drift. These shields will be left in place after plugging the drift.

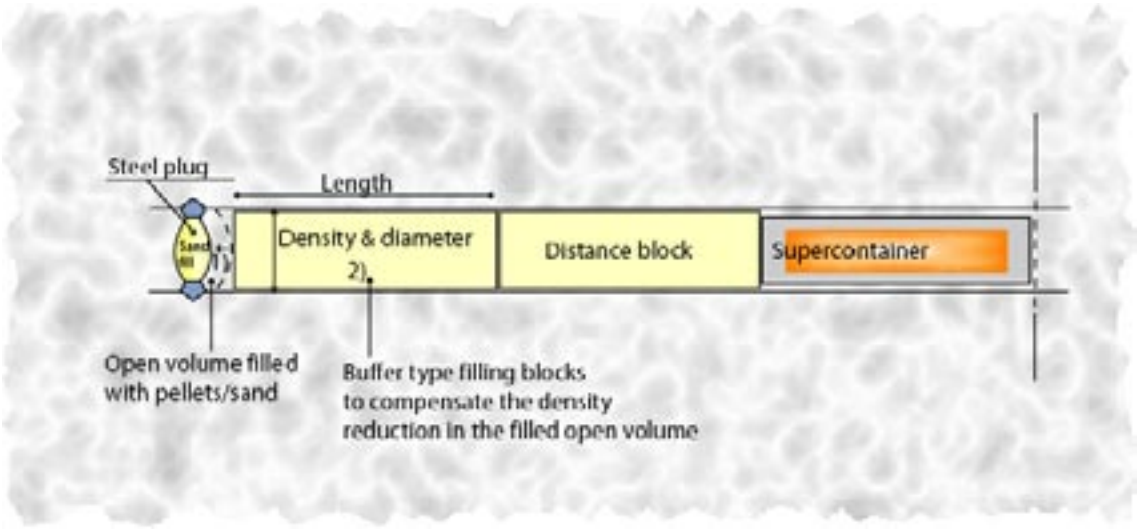

Figure 1-12. *Filling adjacent to and within compartment plugs (after Figure 5-12 of /Autio et al. 2007/).*

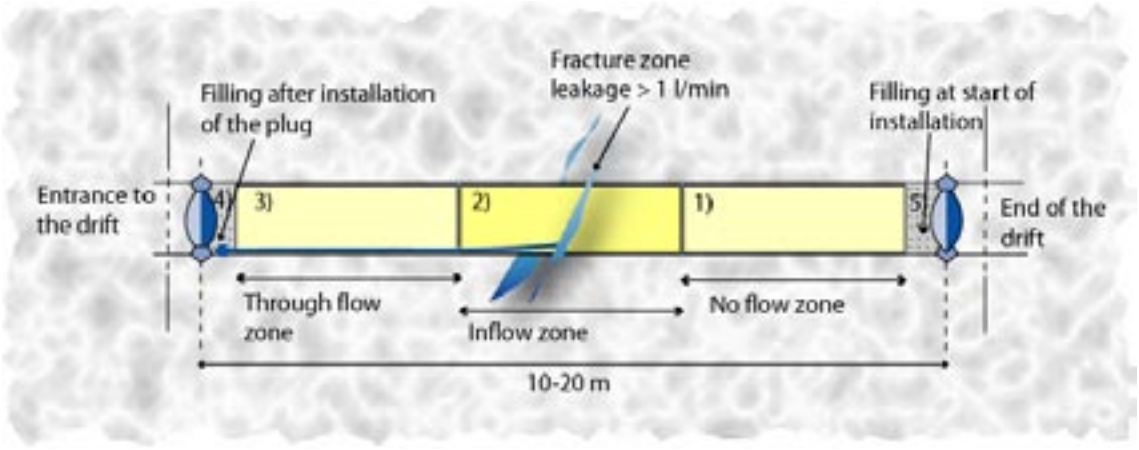

Figure 1-13. *Filling between steel compartment plugs (after Figure 5-14 of /Autio et al. 2007/). The design of filling components between the steel plugs is presented in the Design Description 2007 /Autio et al. 2008/.*

(ix) Drift end plugs

Drift end plugs are placed at the ends of the drifts at their intersection with the deposition niche. The reference design for the drift end plugs is a steel-reinforced low-pH concrete bulkhead positioned in a notch (Figure 4-6 of /Autio et al. 2007/).

A steel plug (similar to a single-cap compartment plug) are installed first, where necessary, to provide rapid sealing while the concrete structure is emplaced and hardens. It is also likely that one or more filling blocks is/are installed in the drift adjacent to the drift end plugs, to isolate the canisters and their surrounding buffer from any leachates from the concrete bulkhead (see Section 6.1). The detailed composition of the concrete is yet to be developed, but one example of a possible composition is given in Appendix A and in Table 4-3 of /Autio et al. 2007/.

(x) The backfill and seals of other repository cavities

The backfilling and sealing of other repository cavities (e.g. deposition niche, access and central tunnels, shafts) with impermeable material is required to prevent the formation of water-conductive flow paths. It is also required to keep the drift end plug in place once the backfill has reached the desired swelling pressure and to allow the release of repository-generated gases. Backfilling and sealing materials and methods are likely to be similar to those envisioned for KBS-3V, as outlined below.

The current candidate backfill materials are Friedland clay and a mixture of bentonite (MX-80) and crushed rock (30% bentonite and 70% crushed rock or 15% bentonite 85% crushed rock, depending on the backfill location). Friedland clay and bentonite/ crushed rock mixtures both carry impurities into the repository, such as organic carbon, pyrite and gypsum. These impurities could have a long-term safety effect because they may accelerate either directly or indirectly (e.g. by impairing the buffer effectiveness) the canister corrosion rate /Pastina and Hellä 2006/.

The design of plugs for sealing boreholes and other access to the surface is ongoing for KBS-3V. The current plan is to employ a combination of bentonite and cementitious material for the different types of plugs to be emplaced at different places (e.g. characterisation bore-holes, shafts). The same type of plugs are expected to be used in KBS-3H.

1.6.5 Use of cement and other construction materials

Cement and other construction materials are being used in the construction of ONKALO and will be used in the construction and operation of the repository, whether the KBS-3V or the KBS-3H. The purposes of such materials are to limit the groundwater inflow (grouting), to stabilise the rock (shotcrete, castings of rock bolts), to construct plugs and seals (e.g. drift end plugs, compartment plugs), to fill, for example, anchoring holes and for operational safety purposes (floors, supporting walls etc). Concrete will also be used for temporary construction elements (walls, intermediate floors, doors). Most of the cementitious materials will be removed before the final closure of the repository but, according to the estimates of residual materials in the KBS-3H repository, between 1,200,000 and 1,800,000 kg[8] of cement will be left in the entire repository (including ONKALO). Of these, an average of 2,600 to 3,900 kg of cement will be located in each drift /Hagros 2007a/.

Cementitious grout or other water inflow-controlling materials will be needed during repository construction to ensure operational safety and possibly to reduce inflows for sufficient time to prevent piping and erosion of buffer. Depending on the type of material used, these materials may include small amounts of organic materials, silica and chlorides. Therefore, their composition, amount and removal efficiency are relevant to long-term safety.

Three grouting materials are considered for both KBS-3H and KBS-3V in various parts of the repository:

- ordinary cement;
- low-pH cement; and
- colloidal silica.

These alternatives may require additives, such as accelerators (i.e. inorganic salts) and superplasticisers (i.e. organic substances). Detailed material descriptions and inventories are presented in /Hagros 2007ab/. It is assumed that the inventory of residual materials will be the same for KBS-3H as for -3V. High alkalinity materials, such as ordinary portland cement, are not envisaged in the deposition drift itself. The most likely options are therefore low-pH cement and colloidal silica. The compositions of the low-pH cement and Silica Sol (colloidal silica) used for grouting in the reference design are given in Appendix A.

Shotcreting is not envisaged in the deposition drifts because the quality of the rock and inflow rate should be adequate for drift constructability by design. However other parts of the repository, including the deposition niche (see Figure 1-5), may require supporting by shotcreting /Hagros 2007ab/. As in the KBS-3V case, ordinary and low-pH cement are both considered as shotcreting materials. Shotcrete will be removed to the maximum extent practical before closure. The detailed composition of shotcrete in both alternatives is described in /Hagros 2007a/.

1.6.6 Use of steel

A key difference between KBS-3V and KBS-3H is the use, in KBS-3H, of additional steel components (in particular the supercontainers) that will corrode and generate gases. As part of the safety case, the overall effect of the steel components thus needs to be evaluated with respect to corrosion, gas formation, gas generation rate and the potential for the creation of gas overpressures, and the chemical interaction and consequences for bentonite. Quantities and details regarding dimensions of steel components are given in Section 5.1.

1.6.7 Operational procedure for implementing the Basic Design

Assuming that a drift is divided into two compartments of similar length, the period required to emplace supercontainers, distance blocks and a compartment plug in the first compartment is in the order of 10–14 days, depending on the length and capacity of the compartment and, to some

[8] Estimates depend on the alternatives for design, rock support, grouting, backfill and drift end plug.

extent, on the requirement for fixing rings, as described in the Design Description 2005 /Autio et al. 2007/. After the filling of this compartment, it may be necessary to interrupt operations and monitor the development of groundwater pressure for, say, a further week before proceeding with the installation of filling material and a second compartment plug to isolate the drift section considered unsuitable for supercontainer and distance block (or filling block) emplacement. This is likely to require in the order of another week. Finally another 10–14 days will be required to emplace supercontainers, distance blocks and a drift end plug in the second compartment, giving an overall operational period for a drift in the order of about 6 weeks (the drift end plug will require time to harden, but, as noted in Section 1.6.4, there is a steel plug next to the end plug to enable rapid sealing if needed). The operational procedure for the DAWE alternative design is described in Appendix D. Operational risks, such as fires, rock falling, sudden water inflow during the operational period are being addressed in the Design Description 2007 report /Autio et al. 2008/.

1.7 Initial state of the deposition drift

Excavation damage

The excavation-damaged zones (EDZs) adjacent to the surfaces of repository drifts may affect both resaturation and the transport of repository-generated gas. A description of the EDZ for a KBS-3H drift is given in Section 7.6.3. Although the information presented suggests that the hydraulic significance of the EDZ is small, its properties are subject to considerable uncertainties, being dependent on the rock properties and a variety of site-specific factors as well as on the repository layout and engineering techniques applied. Furthermore, the data used in analyses so far are based on measurements made on a limited number of samples taken from the VLJ Research Tunnel at Olkiluoto and these may not correspond fully to the properties at repository depth (see Appendix A). In particular, measurements of intrinsic gas permeability were based on unfractured samples. Samples containing fractures or microfractures were rejected. Thus, on average, the EDZ is likely to have a higher intrinsic permeability than that suggested by the measured values.

Drift temperature

The air temperature in open deposition drift sections will be controlled during operations. Following the sealing of a drift compartment, however, the heat generated by the fuel, the heat-transfer properties of the system components and the ambient rock temperature will determine subsequent temperature evolution. The ambient rock temperatures at depths of 400 m and 500 m are 10.5°C and 12°C, respectively /Anttila et al. 1999/.

Air humidity

The humidity in the deposition drifts is expected to be close to 100% at the start of operations due to evaporation from the drift walls, although this may be reduced as bentonite is emplaced in the drifts and starts to take up moisture from the air. The rate of uptake of humidity by bentonite in an open drift is affected by significant uncertainties. Furthermore, although evaporation from wet surfaces within the drift will tend to maintain high levels of humidity in the drift, air humidity will also be affected during the operational period by design issues such as the possible use of spray and drip shields, which would cover such surfaces.

Forced ventilation will be assured during the drift characterization period, for operational safety reasons. However, the drift will not be ventilated during the period in which the deposition vehicle is used to emplace the supercontainers and distance blocks. There will be some exchange of air because of the movement of transportation equipment, however the leakages and water cushion system will keep the air humid.

Water inflow

Some water inflow to the drifts will occur at discrete locations due to intersections with transmissive fractures (or channels within those fractures), while some may be more dispersed by fractures in the excavation disturbed zone (EDZ) surrounding the drifts.

Based on analysis of available geohydrological (borehole) data in /Hellä et al. 2006/, flow conditions in a repository drift have been estimated as follows:

- the total leakage into a compartment may be up to 10 litres per minute[9],
- the average frequency with which fractures with transmissivities greater than 10^{-9} m^2 s^{-1} intersect a drift is 4 per 100 m (10^{-9} m^2 s^{-1} is the detection limit – fractures of this transmissivity would be expected to give rise to a flow of about 0.04 litres per minute into the drift),
- the flow into 5 m drift intervals (corresponding to the length of a KBS-3H supercontainer) is less than 0.1 litres per minute over more than 90% percent of the drift length,
- the flow into 10 m drift intervals (corresponding to the length of a KBS-3H "supercontainer unit" comprising one supercontainer and one distance block) is less than 0.1 litres per minute over about 85% percent of the drift length, and
- there are long sections (100 m or more) of the drift that are intersected by no highly transmissive fractures (transmissivities greater than 10^{-8} m^2 s^{-1}).

In order to provide drainage during the operational period, the drifts will have a shallow dip (1.5–2 degrees) towards the main tunnels from which they are excavated. Spray and drip shields may be used to avoid the possibility of dripping water, which could damage the engineered barrier system by causing erosion of bentonite /Autio 2007/. The possibility of controlling water inflow, for example by injecting Silica Sol or low-pH cement into more transmissive fractures is currently under investigation.

Engineered barrier system

The initial state of the fuel, canister, buffer and distance block, supercontainer and drift end plugs are discussed in the introduction of the corresponding main chapters and, in more detail, in the KBS-3H Evolution Report /Smith et al. 2007c/.

1.8 Definition of system variables

The system variables are physical variables that allow an adequate description of the evolution of the various components in the safety assessment.

A list of system variables will be suggested for each system component, based on the SR-Can Process Reports, but adapted to the needs of KBS-3H. These lists will be introduced at the beginning of each main chapter. For example, Table 2-1 summarises the system variables for fuel and fuel cavity in the canister, Table 3-2 those for the cast iron insert and copper canister, etc.

1.9 Safety functions in KBS-3H and how they are provided

The canister, the buffer (i.e. the bentonite material originally inside the supercontainers, together with the distance blocks) and the host rock are the main KBS-3H system components that together ensure isolation of the spent fuel and containment of radionuclides according to the

[9] The total leakage can be inferred from Figures 16 and 17 in /Hellä et al. 2006/. It has been observed at Äspö and in the interim storage facilities for low-level waste at Loviisa and Olkiluoto (VLJ repositories) that inflows have a tendency to decrease over time, possibly due to precipitation of solids in fractures (see, e.g. /Hagros and Öhberg 2007/).

KBS-3 safety concept. Other system components, including the filling blocks, the compartment and drift end plugs, the steel supercontainer shells, fixing rings and other structural materials, have not been assigned safety functions. They are, however, designed to be compatible with, and support the safety functions of the canister, the buffer and the host rock.

The safety function on the canister is the same as in KBS-3V. The main safety function of the canisters is to ensure a prolonged period of complete containment of the spent fuel. As long as its copper shell is not breached, a canister will provide complete containment of radionuclides, and the spent fuel will interact with the environment only by means of heat generation and low level gamma and neutron radiation penetrating through the canister walls.

Safety functions of the buffer are (a), protection of the canisters, and (b), retardation of radionuclide releases in the event of canister failure. These safety functions are the same in KBS-3V and KBS-3H. The current KBS-3H design includes the use of steel components external to the canister, which will corrode over time and give rise to potentially[10] porous or fractured corrosion products. These may interact chemically with adjacent bentonite and the slow formation of an altered zone with perturbed mass-transport properties at the bentonite/rock interface at supercontainer locations cannot be excluded (Section 4.7). A final safety function of the KBS-3H buffer (or, more specifically, the distance blocks) is, therefore, (c), to separate the supercontainers hydraulically one from another, thus preventing the possibility of preferential pathways for flow and advective transport within the drifts through the corrosion products or altered buffer.

The safety functions of the host rock are the same in KBS-3V and KBS-3H. They are (a), to isolate the spent fuel from the biosphere, (b), to provide favourable and predictable mechanical, geochemical and hydrogeological conditions for the engineered barriers and to protect them from potentially detrimental processes taking place above and near the ground surface and (c), to limit and retard both the inflow of harmful substances[11] to the engineered barrier system and the release of radionuclides to the biosphere.

Design requirements to support the safety functions of the canister, buffer and host rock are discussed in Section 2.4 of the KBS-3H Evolution Report /Smith et al. 2007c/.

1.10 Use of safety function indicators and criteria in safety assessment

To assess the performance and safety of a KBS-3H or KBS-3V repository, it is necessary to determine the conditions under which the identified safety functions will operate as intended, and the conditions under which they will fail, or operate with reduced effectiveness. Following the methodology adopted in the Swedish SR-Can safety assessment /SKB 2006a/, KBS-3H safety studies make use of the concept of safety function indicators and associated criteria. One or more safety function indicators are assigned to each safety function. If the safety function indicators fulfil certain criteria, then the safety functions can be assumed to be provided. If, however, plausible situations can be identified where the criteria for one or more safety function indicators are not fulfilled, then the consequences of loss or degraded performance of the cor-

[10] Magnetite, the most likely corrosion product, can form a thin but protective layer against corrosion with little or no connected porosity when produced under high pressure and temperature. In the repository, steel components external to the canister will be converted to magnetite under a high buffer swelling pressure, although the temperature will not be high. The porosity and hydraulic conductivity of the magnetite formed under these conditions are uncertain. Furthermore, it may also be fractured and the possibility of it forming a hydraulically conductive layer at the buffer-rock interface cannot currently be excluded. In addition, other corrosion products may also be formed.

[11] Including the chemically toxic components of spent fuel, as discussed in the Complementary Evaluations of Safety Report /Neall et al. 2007/.

responding safety function should be evaluated in the safety assessment. The process analyses presented in Chapters 2 to 7 related to the various repository subsystems (Figure 1-3) evaluate how various phenomena occurring in the repository system influence the safety functions, using the behaviour in relation to criteria as guidance for how the subsystem components and their associated processes should be treated in safety analyses.

It is important to distinguish design requirements (as discussed in Section 2.4.2 of the Evolution Report /Smith et al. 2007c/ from the criteria for safety function indicators. In general, design requirements refer to attributes that the repository is ensured to have by design at the time of emplacement of the first canister, or during the early evolution of the repository in the period leading up to saturation, although some design requirements also affect the long-term evolution of the system. Repository design also aims to ensure that the criteria for the safety function indicators are fulfilled over the required time frames, but this is seen as a target, rather than as a design requirement.

Adherence to design requirements and fulfilment of safety function indicator criteria are both considered and if necessary quantitatively evaluated as part of the safety case, although the former largely concerns initial conditions and early evolution, whereas the latter concerns the overall timeframe addressed by the safety case. It is emphasised that if there are plausible situations where one or more of the criteria for safety function indicators are not satisfied, this does not imply that the system as a whole is unsafe. Such situations must, however, be carefully analysed, for example by means of radionuclide release and transport calculations, as described in the KBS-3H Radionuclide Transport Report /Smith et al. 2007a/. Safety function indicators and criteria for the canisters, buffer and host rock are discussed at the beginning of the relevant chapters.

1.11 Summary of handling in safety assessment

In each main chapter of this report, a summary of the handling of processes in the KBS-3H safety assessment is provided in table form (“Process Tables”). For example, Table 2-1 summarises the handling in the safety assessment of processes occurring in the fuel/ cavity in the canister. Whenever relevant to the KBS-3H case, detailed information on the handling is given in the various sections containing the process descriptions, under the heading

Handling in the safety assessment for KBS-3H

The assessment cases calculated in the KBS-3H Radionuclide Transport Report /Smith et al. 2007a/ are based on the scientific information on processes documented in the present report and on the description of the evolution of the repository in different time frames presented in the Evolution Report /Smith et al. 2007c/. The Evolution Report also discusses the implications of the evolution of the KBS-3H repository for radionuclide release and transport and significant uncertainties. The assessment cases calculated in the Radionuclide Transport Report are structured according to the three fundamental modes that may, in principle, lead to failure of a single or several canisters: i) initial, penetrating defects, ii) failure due to corrosion of copper shell and insert, and iii) rupture due to rock shear and the transfer of shear stresses from the rock via the buffer to the canister (in particular, in the event of post-glacial earthquake). Appendix G contains two tables summarizing the link between the Process and Evolution reports and the assessment cases in the Radionuclide Transport report.

A detailed comparison of the approach to safety assessment and key assumptions of SR-Can, TILA-99 and the KBS-3H safety assessment is provided in the KBS-3H Complementary Evaluations Report /Neall et al. 2007/. This includes a comparison of assessment cases, models and databases.

2 Fuel and fuel cavity in the canister

2.1 Description of fuel and fuel cavity in the canister

The fuel and fuel cavity in the canister are the same as in the KBS-3V case. No fuel process specific to KBS-3H has been identified. The purpose of the data provided below is to provide some overall background information to this report.

2.1.1 The spent fuel inventory

For the present safety studies, the working hypothesis is that a Finnish repository for spent fuel will need to accommodate approximately 5,500 tU of fuel, encapsulated in approximately 3,000 canisters /Pastina and Hellä 2006/. This comprises fuel from the following facilities:

- Loviisa 1-2: 700 canisters containing 1,020 tU of spent fuel
- Olkiluoto 1-2: 1,210 canisters containing 2,530 tU of spent fuel
- Olkiluoto 3: 930 canisters containing 1,980 tU of spent fuel
- Total: 2,840 canisters and 5,530 tU from the spent fuel

The reference spent fuel in this report is the BWR fuel from Olkiluoto 1 and 2 (OL1-2). The Finnish fuel has an average burnup of 37–39 MWd/kgU and a maximum burnup of 45 MWd/kgU for Loviisa and 50 MWd/kgU for Olkiluoto. Spent fuel inventory estimates are based on maximum discharge burnup of 45 and 50 MWd/kgU. These estimates may change in the future along with the development of reactor load factors, fuel designs and burnup. For comparison purposes, SKB's safety assessment SR-Can assumes a total of 6,000 canisters corresponding to 12,000 tU. The average burnup for Swedish nuclear fuel estimated in 2003 was 33 MWd/kgU but the average burnup is gradually increasing and will be in the range 40–50 MWd/kgU for newer fuel /SKB 2006c/.

2.1.2 Overview of variables

For the safety assessment, the fuel is described by means of a set of variables, which together characterise the fuel in a suitable way for the assessment, see Table 2-1. The description applies not only to the fuel itself, but also to the cavities in the canister, into which water can penetrate in the event of a defect in the copper overpack of the canister (see Section 2.5). Processes will then take place in the cavity, such as fuel dissolution and corrosion of the cast iron insert. The cavity could thus be included in either the fuel or the canister part of the system, and has been included in the fuel here.

The variables listed in Table 2-1 for KBS-3H are identical to the variables defined for KBS-3V (Table 2-3 in /Rasilainen 2004/).

2.1.3 Safety function indicators

For the fuel/cavity in the canister, no safety function indicators and criteria are defined.

Table 2-1. Variables in the fuel and fuel cavity in the canister.

Variable	Explanation
Geometry	Geometric dimensions of all components of the fuel assembly, such as fuel pellets and Zircaloy cladding. Also includes the detailed geometry, including cracking, of fuel pellets.
Radiation intensity	Intensity of α-, β-, γ-, and neutron radiation as a function of time and space in the fuel assembly.
Temperature	Temperature as a function of time and space in the fuel assembly.
Hydrovariables	Flows and pressures of water and gas as functions of time and space in the cavities in the fuel and the canister.
Stress state	Stress conditions as a function of time and space in the fuel assembly.
Radionuclide inventory	Occurrence of radionuclides as a function of time and space in the different parts of the fuel assembly. The distribution of the radionuclides in the pellets between matrix and surface is also described here.
Material composition	The materials of which the different components in the fuel assembly are composed, excluding radionuclides.
Water composition	Composition of water (including any radionuclides and dissolved gases) in the cavities in the fuel and canister.
Gas composition	Composition of gas (including any radionuclides) in the cavities in the fuel and canister.

2.1.4 Summary of handling in safety assessment

Table 2-2 summarises the handling of processes in the fuel/cavity in the canister in the safety assessment for KBS-3H, as suggested in the following sections of Chapter 2. In the table, the process is either "mapped" to a model by which it will be quantified or associated with a brief verbal description of how it will be handled. The cases of intact and defective canisters are discussed separately. In the case of intact canisters, the term "quantified in modelling" means that supporting thermal calculations are performed; in the case of failed canisters, quantified in modelling means that analyses relevant to radionuclide transport calculations are performed.

In Table 2-2, the term "REPCOM" refers to a compartment model that was used in the previous radionuclide release and transport calculations /Vieno and Nordman 1999/ and is used in the current KBS-3H Radionuclide Transport Report /Smith et al. 2007b/.

2.2 Overview of processes

Based on the FEP analysis for KBS-3V /SKB 2006b/, a list of processes for the fuel/ cavity in the canister has been derived in the Main Report of the SR-Can /SKB 2006a/. Following the methodology in Appendix B, this list of processes is considered appropriate for KBS-3H because the fuel and the fuel cavity in the canister are the same in both alternatives.

The processes are structured into radiation-related, thermal, hydraulic, mechanical and chemical process categories. Radionuclide transport and related processes are discussed separately. In the introductory part of each of the following chapters, the processes pertinent to the process category are tabulated.

Table 2-2. Process table for the fuel/cavity in the canister describing how processes are handled for intact canisters and in the special cases of failed canisters. Green fields denote processes that are omitted or irrelevant for the time period of concern. Red fields denote processes that are quantified by modelling in the safety assessment of KBS-3H. Orange fields denote processes that are omitted subject to a specified condition. Motives for handling are given in the relevant sections of Chapter 2. The handling of processes in the KBS-3H safety assessment and the handling of uncertainties are discussed only in certain cases specific to KBS-3H (as noted in the table). If not mentioned, the handling of other processes and uncertainties are assumed to be handled in the same way as for KBS-3V and are not discussed in this report.

Process type	Internal process	Intact canister	Failed canister	Notes/*Section in KBS-3H Process Report*
Radiation-related processes	F1. Radioactive decay	Thermal process model /Ikonen 2003, 2005/.	REPCOM (a compartment model used for radionuclide release and transport calculations).	Radioactive decay is considered in all safety assessment calculations. *Section 2.3*
	F2. Radiation attenuation/ heat generation	Thermal process model /Ikonen 2003, 2005/.	No specific analysis for KBS-3H. SR-Can: Omitted as long-term releases occur after period of elevated temperatures.	*Section 2.3*
	F3. Induced fission (criticality)	Omitted since there will be insufficient amounts of moderator inside the canister prior to failure.	Omitted since the probability is negligibly small if credit is taken for the burnup of the fuel.	Effective neutron multiplication factor (K_{eff}) may be affected by canister orientation (more affected in KBS-3V due to accumulation of fissile material at the bottom of fuel channels). *The handling of the process in the safety assessment for KBS-3H is also discussed in Section 2.3.*
Thermal processes	F4. Heat transport	Thermal process model /Ikonen 2003, 2005/	No specific analysis for KBS-3H. SR-Can: Omitted as long-term releases occur after period of elevated temperatures.	Temperature field similar in KBS-3V and 3H. *Section 2.4*
Hydraulic processes	F5. Water and gas transport in canister cavity, boiling/ condensation	Not relevant	Analysis of HMG processes for defective canisters.	In the Radionuclide Transport report, a postulated initial penetrated defect scenario is considered. A base case (PD-BC) and several variant cases are calculated. Specific variant case for KBS-3H: Gas-induced displacement of contaminated water through defect into buffer (PD-EXPELL). *The handling of the process in the safety assessment for KBS-3H and the handling of uncertainties are also discussed.* *Section 2.5*

Process type	Internal process	Intact canister	Failed canister	Notes/*Section in KBS-3H Process Report*
Mechanical processes	F6. Cladding failure	Not relevant	No credit taken for barrier function (pessimistic assumption; as in SR-Can)	*Section 2.6*
	F7. Structural evolution of fuel matrix	Not relevant	Omitted SR-Can: Omitted since burnup is sufficiently low for all fuel types and burnups (up to 60 MWd/kgU) relevant for the Swedish repository.	The Finnish fuel has an average burnup of 37–39 MWd/kgU and a maximum burnup of 45 MWd/kgU for Loviisa and 50 MWd/kgU for Olkiluoto. The process can thus be neglected in the safety assessment. *Section 2.6*
Chemical processes	F8. Advection and diffusion	Not relevant	Analysis of HMG processes for defective canisters.	See F5 *Section 2.7*
	F9. Residual gas radiolysis/ acid formation	Omitted since negligible amounts of corrosive agents are produced (as in SR-Can)	Not relevant	*Section 2.7*
	F10. Water radiolysis	Omitted (as in SR-Can)	No specific analysis for KBS-3H. (SR-Can: Omitted except for fuel dissolution, see that process.)	SR-Can: Initial water consumed by nitric acid formation or cast iron corrosion. *Section 2.7*
	F11. Metal corrosion	Not relevant	Same approach as in TILA-99 – congruent release with pessimistically chosen corrosion rates. (Pessimistic handling in SR-Can: a) no barrier function, all radionuclides instantaneously released upon water contact, b) 1,000 years for complete corrosion if advective conditions in the buffer).	*Section 2.7*
	F12. Fuel dissolution	Not relevant	Modelled as constant, pessimistic dissolution rate (as in SR-Can).	Fuel dissolution rates from SR-Can are used in safety assessment for KBS-3H. The handling of the uncertainty in fuel dissolution rate in the safety assessment is discussed. *Section 2.7*
	F13. Dissolution of gap inventory	Not relevant	Pessimistic, instantaneous (as in SR-Can).	Instant release rates mostly based on SR-Can are used in KBS-3H Radionuclide Transport Report /Smith et al. 2007b/. Partitioning between the fuel matrix and the IRF is based on Table A-4 of the SR-Can data report /SKB 2006f/ – realistic, central values). This is justified by the similarity in the fuels and burnups in the Swedish and Finnish cases, also given the likely future increases in fuel burnup expected in Finland. *Section 2.7*

Process type	Internal process	Intact canister	Failed canister	Notes/*Section in KBS-3H Process Report*
Radionuclide transport-related processes	F14. Speciation of radionuclides, colloid formation	Not relevant	REPCOM	Solubility limits from /Grivé et al. 2007/ are used in safety assessment for KBS-3H. *Section 2.7*
	F15. Helium production	Omitted since the amount of helium produced will not significantly increase the pressure inside the canister.	Not relevant	*Section 2.7*
	F16. Radionuclide transport		REPCOM Bounding calculations for volatile radionuclides.	Integrated modelling of release and transport of radionuclides, considering fuel dissolution, precipitation/ dissolution, chain decay, pinhole release and transport through buffer (similar as in SR-Can). Specific variant case for KBS-3H: Gas-induced displacement of contaminated water through defect into buffer. Radionuclide transport in the gas phase (e.g. volatile C-14) handled by bounding calculations. Colloid-facilitated transport is neglected, provided the buffer completely surrounds the canister. *The handling of the process in the safety assessment for KBS-3H is also discussed.* *Section 2.8*

2.3 Radiation-related processes

An overview of radiation-related processes in the fuel/cavity in the canister is shown in Table 2-3. Radiation-related processes, such as radioactive decay and radiation attenuation/heat generation, are independent of the specific geometry and conditions in KBS-3H. An exception is the possible accumulation of fissile material at the bottom of the fuel channels as a result of degradation of fuel assemblies, which depends on the orientation of the canister in the gravity field (see discussion below). No other issue has been identified for KBS-3H that is additional to those presented in the relevant Process Reports for KBS-3V /Rasilainen 2004, SKB 2006c/. Thermal effects arising from radioactive decay are evaluated in Section 2.4.

2.3.1 Induced fission (criticality)

Overview/general description

The possibility of nuclear criticality, i.e. the risk of a spontaneous and sustained nuclear chain reaction, has been discussed in a number of studies; see e.g. /SKB 2006a/ and /Nagra 2002/. Recent calculations by /Agrenius 2002/ and /Nagra 2002/ show that, based on state-of-the-art methods and a reasonable assessment of the uncertainties, burn-up credit[12] is a possible way to demonstrate control of the reactivity in the canisters. /Anttila 2005a/ performed criticality analyses in the case of Olkiluoto spent fuel and concluded that the spent fuel inside the container will remain subcritical even if the canister becomes filled with water.

There seems to be a possibility of re-distribution of fissile material inside the canister through mechanical degradation of fuel rods leading to fuel pieces falling along the fuel channel. Different situations are conceivable, depending on the orientation of the emplaced canisters. For vertically emplaced canisters, fissile material may accumulate in the restricted space at the lower ends of the vertically oriented fuel channels. The effects of such a situation need to be assessed in the context of a defective canister, i.e. when water comes into contact with the re-distributed fissile material. In contrast, for horizontally emplaced canisters, degraded fuel material may accumulate all along the bottom of the horizontally oriented fuel channels. In such a situation, the re-distributed amount of fissile material per unit channel length would not change compared with the initial fuel configuration. It seems, therefore, unlikely that the effective neutron multiplication factor (k_{eff}) would be significantly different for disintegrated fuel assemblies as compared with intact fuel assemblies in the horizontal orientation. Induced fission is thus likely to be of more concern in KBS-3V compared with KBS-3H.

Table 2-3. The inter-dependence of radiation-related processes and identified variables in fuel/cavity in the canister.

Radiation-related processes	Variables in fuel/cavity in the canister								
	Radiation intensity	Temperature	Hydrovariables (pressure and flows)	Geometry (incl. dimensions)	Stress state	Radionuclide inventory	Material composition	Water composition	Gas composition
Radioactive decay	×	×				×		×	×
Radiation attenuation/heat generation	×	×	×	×	×	×	×		
Induced fission (criticality)	×	×	×	×	×	×	×	×	×

[12] Burnup credit means taking credit for the reduction in reactivity due to irradiation of nuclear fuel (i.e. fuel burnup), thereby allowing the fuel to be disposed of more efficiently and economically while maintaining safety.

The potential for criticality as a result of re-distribution of fissile material at various locations outside the canister have been analysed by /Behrenz and Hannerz 1978/ and /Oversby 1996, 1998/, the latter studies being based on observations from the natural reactor at Oklo. In both cases the conclusions were that criticality outside the canister has a vanishingly small probability, requiring several highly improbable events to occur simultaneously.

Handling in the safety assessment for KBS-3H

Prior to canister failure, induced fission is irrelevant and thus omitted because there will be insufficient amounts of moderator inside the canister. In the case of a defective canister, the process is also omitted because the probability of occurrence is negligibly small if credit is taken for the burnup of the fuel. The effective neutron multiplication factor (K_{eff}) may be affected by canister orientation. However, determining whether a KBS-3H canister is more or less prone to criticality compared to a KBS-3V canister is speculative because of assumptions concerning the physical state of the corrosion products arising from corrosion of the cast iron insert and whether the orientation and spacing of fuel rods are maintained. The current assumption, based on calculations in /Agrenius 2002/ and /Anttila 2005a/ is that in both the KBS-3H and KBS-3V cases the fuel will remain subcritical because burnup credit can be assumed and because the geometry is likely to be basically maintained despite corrosion.

2.4 Thermal processes

An overview of thermal processes in the subsystem fuel/cavity in the canister is shown in Table 2-4. The absolute temperature in the fuel and the cavity inside the canister will be affected by the entire heat transport pathway from fuel through the engineered and geological barriers into the biosphere, the latter being the ultimate heat sink of the system.

The amount of spent fuel deposited in the repository and the total heat generation as a function of time are shown in Figure 2-1. The total heat generation is at its highest – approx. 2.5 MW – at the closure of the repository. Assuming that the total cross-sectional area of the repository (incl. areas between deposition panels) is approx. 1.6 km^2, the averaged heat generation is approximately 1.6 W m^{-2} at the closure of the repository. Due to the slow radioactive decay of some actinides, the disposed spent fuel produces heat for long time periods: The total thermal output is reduced to about 5 kW after 10^5 years and to about 2 kW after 10^6 years /Anttila 2005a/, depending slightly on the type of fuel and on burnup.

Table 2-4. The inter-dependence of thermal processes and identified variables in fuel/ cavity in the canister.

Thermal processes	Variables in fuel/cavity in the canister								
	Radiation intensity	Temperature	Hydrovariables (pressure and flows)	Geometry (incl. dimensions)	Stress state	Radionuclide inventory	Material composition	Water composition	Gas composition
Heat transport		×	×	×	×		×		×

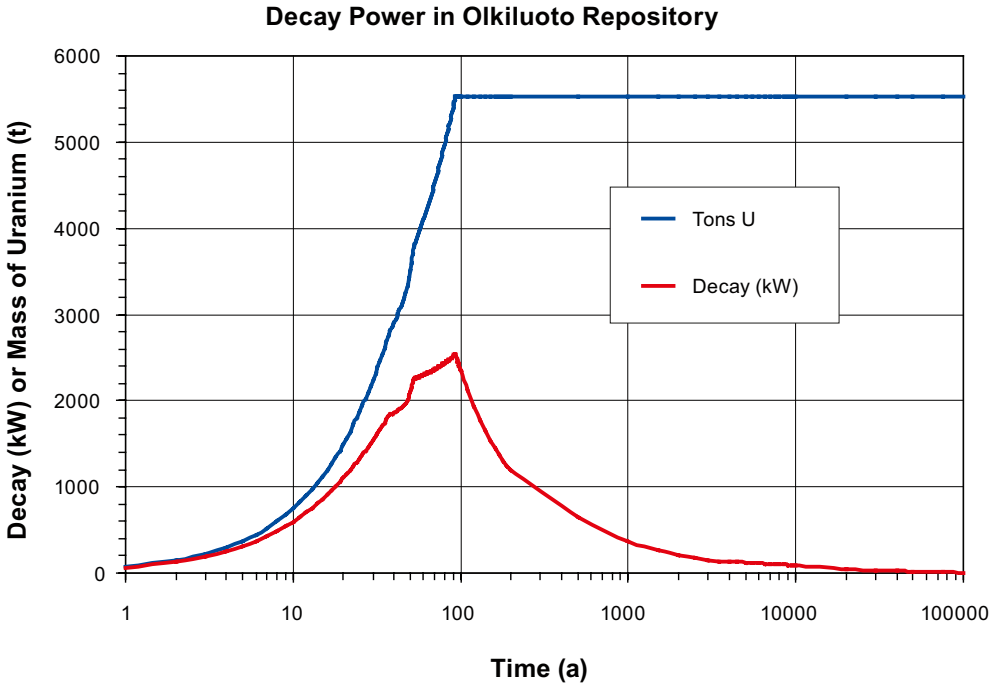

Figure 2-1. *Amount of spent fuel deposited in the repository and total heat generation as a function of time. From /Löfman 2005/, based on data of /Saanio et al. 2004/ and /Raiko 2005/.*

Thermal processes in the fuel/cavity in the canister do not depend significantly on the specific conditions in KBS-3H (identical fuel and canister as in KBS-3V). No other issue has been identified for KBS-3H that is additional to those presented in the relevant Process Reports for KBS-3V /Rasilainen 2004, SKB 2006c/.

Differences arise only due to the specific geometry and conditions outside the canister. As concluded by /Ikonen 2003/ based on model studies, the overall thermal evolution in KBS-3V and 3H are very similar. Furthermore, the analysis of the thermal evolution during the operational phase demonstrated that the maximal temperature is only marginally affected by the rate of canister emplacement /Ikonen 2005/. The details of these model studies and their implications for the safety assessment are discussed in the context of the buffer and distance block, see Section 4.4.

2.5 Hydraulic processes

An overview of hydraulic processes in the fuel/cavity in the canister is shown in Table 2-5. The generation of gases, mainly by anaerobic corrosion of the cast iron insert, leads to a build-up of pressure in the cavity of the canister. This chapter deals with inflow/ outflow of water, vapour and gases through a hole present in the hypothetical case of an initially defective canister (see Table 2-2).

Table 2-5. The inter-dependence of hydraulic processes and identified variables in fuel/ cavity in the canister.

Hydraulic processes	Variables in fuel/cavity in the canister								
	Radiation intensity	Temperature	Hydrovariables (pressure and flows)	Geometry (incl. dimensions)	Stress state	Radionuclide inventory	Material composition	Water composition	Gas composition
Water and gas transport in canister cavity, boiling/ condensation		×	×		×			×	×

2.5.1 Water and gas transport in canister cavity, boiling/condensation

Overview/general description

The fate of water/vapour/gas depends to some extent on the location of a possible defect in the canister, as well as on the orientation of the canister (the hole size, contact surfaces, the corrosion rate, etc). This affects the level of the water/gas interface inside the canister, water/gas transport into and out of the canister (possibly including gas-induced porewater displacement) and radionuclide transport. The water ingress – gas generation – water expulsion scenario is more likely to occur in KBS-3H. This is because the defect is most likely in the weld region located at the top of the canister. Thus, in KBS-3V, wherever the defect occurs along the weld, it will be located near the top of the canister, whereas, in KBS-3H, defects will occur with similar probabilities at the underside and upper side of the canister.

The effects of boiling/condensation in the canister cavity /Rasilainen 2004, SKB 2006c/ are similar in KBS-3V and 3H and will not be discussed in the following.

Boundary conditions

The boundary conditions for the processes summarised above are set internally by the fuel surfaces and on the outside by the internal surface of the canister insert, the defect through the canister wall and the bentonite buffer. Temperature effects are not considered in the present analysis, i.e. isothermal conditions are assumed. Internal volume changes due to corrosion are assumed not to affect the available pore space. Vapour transport in the canister interior is included implicitly in the argumentation, but not explicitly taken into account in the model calculations.

Model studies/experimental studies

The complex behaviour of the water/vapour/gas system in a defective copper-iron canister has been discussed in various reports /Vieno et al. 1992, Wikramaratna et al. 1993, Bond et al. 1997, Vieno and Nordman 1999, Rasilainen 2004/.

The following simplified calculations aim at elucidating the conditions under which gas-induced displacement of contaminated water from the canister interior through the defect occurs. They are not, however, intended to model gas flow through saturated bentonite (although gas flow through the bentonite is briefly discussed). The relevant processes governing the pressure evolution and water/gas migration into and out of a defect at the underside of a canister are summarised in the following paragraphs and illustrated in Figure 2-2.

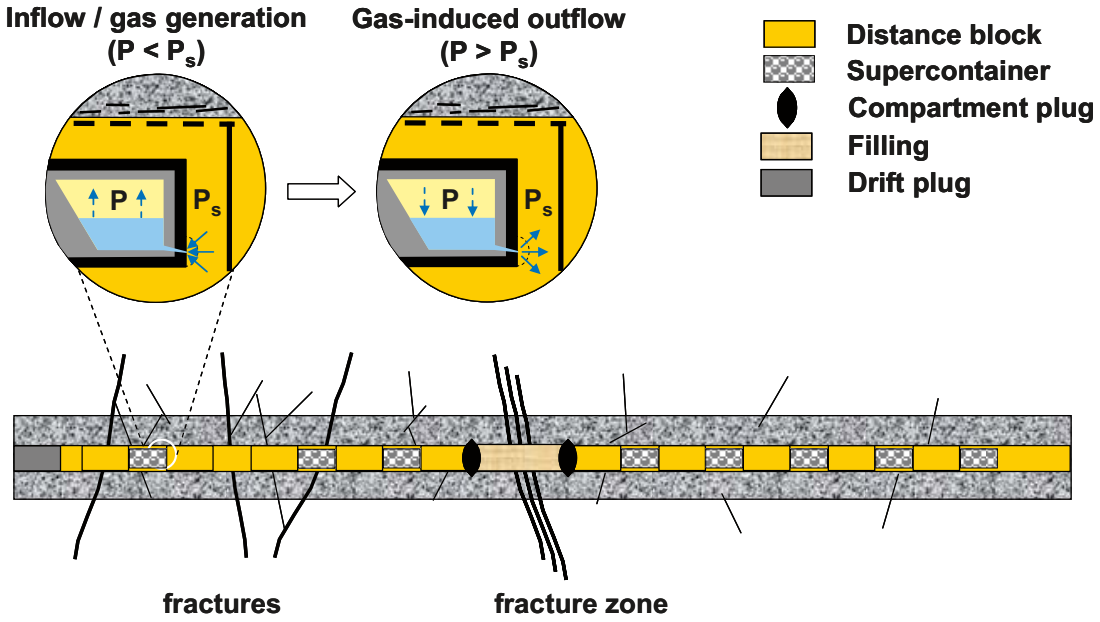

Figure 2-2. *Conceptual model for transport of water and gas into and out of a defective spent fuel canister. The amount of free gas within the canister is affected by a number of different processes (gas generation, advection and diffusion of dissolved gases, dissolution/degassing; these processes are not shown in the figure but are discussed in the text).*

Water flow into defective canister

Following the failure of copper shell and cast iron insert in the form of a small penetrating defect due to corrosion, some time (at least 1,000 years /SKB 2006a/) will elapse before a continuous hydraulic path between the fuel and the canister exterior is established. While the gas pressure within the canister is below the hydrostatic pressure at repository depth, slow inflow of water occurs from the buffer through the defect into the canister interior. If flow in the buffer is assumed to be governed by Darcy's Law, and assuming that the hole is small and that the buffer can be approximated as a semi-infinite medium, the hydraulic head, h [m], within the buffer adjacent to the hole is given by a solution to the 1-D Laplace's equation:

$$\frac{d}{dr}\left(r^2 \frac{dh}{dr}\right) = 0 \qquad \text{(Eq. 2-1)}$$

where the r-coordinate has its origin at the defect. If the hole is approximated by a hemispherical uniform-head surface of radius a, this has the solution:

$$h = \frac{a}{r}\frac{P - P_s}{\rho_w g} + \frac{P_s}{\rho_w g} \qquad \text{(Eq. 2-2)}$$

where

P pressure within the canister [Pa]

P_s hydrostatic pressure at repository depth [Pa]

a radius of the hole [m]

ρ_w density of water [kg m^{-3}]

g gravitational acceleration [m s^{-2}]

The flow through any hemispherical surface centred on the defect (including the defect itself) is then:

$$Q_W = 2\pi r^2 K \frac{dh}{dr} = 2\pi a K \frac{P - P_s}{\rho_w g} \qquad \text{(Eq. 2-3)}$$

where

Q_w water flow rate through hole (inflow for $P–P_s<0$, outflow for $P–P_s>0$) [$m^3\ s^{-1}$]
K hydraulic conductivity of saturated bentonite at the mouth of the hole [$m\ s^{-1}$]

The buffer is, in reality, not semi-infinite. However, the impact of the hole on hydraulic head is limited to small distances around the hole. From the above equation for head:

$$h \approx \frac{P_s}{\rho_w g} \quad \text{if} \quad a << r \qquad \text{(Eq. 2-4)}$$

i.e. the hydraulic head within the buffer is unaffected by a 1 mm hole at the outer boundary of the buffer, which lies at a minimum distance from the hole of 40 cm.

Note that in Equation 2-3, the bentonite is modelled as a semi-infinite medium – i.e. the curvature of the canister surface and the limited thickness of the bentonite layer are assumed to have negligible effects on the water flow rate. Also, the impact of hydraulic heterogeneity of the rock on the rate of inflow to the hole via the buffer has not been considered. Assuming that the radius of the hole is 0.5 mm, the hydraulic conductivity of the bentonite at the mouth of the hole is 10^{-13} to 10^{-12} m s^{-1} and that the pressure difference across the buffer is 4.2 MPa (corresponding to the hydrostatic pressure at the depth of 420 m, the lower end of the inclined drift), the water flow rate into the canister is in the order of 0.004 and 0.04 litres per year. At such a rate, the canister with an internal void of roughly 950 litres (see Table 3-1) would thus be filled with water in approximately 20,000 to 200,000 years. Plugging of the hole with bentonite or corrosion products and the decrease of the hydraulic gradient over time due to gas pressure buildup will reduce the rate of water inflow into the canister.

In addition to liquid water, water vapour may be transported through a partially saturated defect into the canister interior, as long as a gradient of relative humidity persists. Air will be trapped in the cavity between the fuel and the inner walls of the cast iron insert as well as between the insert and the copper shell.

Gas generation

After sealing the canister, decay gases (helium) will accumulate within the cavity. The generation rate of decay gases is known to be very low and does not lead to a noticeable increase of gas pressure within the intact canister /SKB 1999/.

Upon contact with liquid water or vapour entering a defective canister, anaerobic corrosion of the cast iron insert and of the Zircaloy fuel cladding starts, thereby consuming water and generating hydrogen gas. The rate of gas generation is determined largely by the corrosion rate of the cast iron insert because the corrosion rate for Zircaloy is much lower (see Section 2.7). Different corrosion rates for the cast iron insert are considered: 1 µm a^{-1} (base case) and 10 µm a^{-1}/0.1 µm a^{-1} (values for sensitivity analysis). In laboratory tests conducted by /Smart et al. 2004, 2006/, the corrosion rate of steel was measured in direct contact with compacted bentonite. For these conditions, a steel corrosion rate of 1–2 µm a^{-1} was measured, although the measured values still decreased at the end of the measurements (see Section 5.7.1). In contrast /SKB 2006a/ uses corrosion rates for the cast iron insert in the order of 0.1 µm a^{-1}, based on

earlier measurements by /Smart et al. 2002ab/ conducted without direct contact of steel with bentonite. The rates under such conditions were observed to be consistently lower than in direct contact with bentonite.

Corrosion rates in the order of 10 μm a^{-1} are measured only in short-term experiments, but there is no experimental evidence for such high corrosion rates in the longer term. This value is thus only used to test the robustness of the system with regard to steel corrosion. The large range was used because inflow/outflow is very sensitive to the corrosion rate. Because the outflow could include dissolved radionuclides, it is particularly relevant to consider a wide range, even if the entire range of values is not considered likely. As is later discussed, the calculations of inflow and outflow show that it is the lowest corrosion rate that leads to the highest water outflow, thus using a low corrosion rate (0.1 μm a^{-1}) is the most conservative scenario. Corrosion of the supercontainer and other structural materials is discussed in Section 5.7.1.

As mentioned above, the water intruding into the canister is consumed by the corrosion of iron. Based on the corrosion reaction producing hydrogen and magnetite ($3Fe + 4\ H_2O \rightarrow Fe_3O_4 + 4\ H_2$), 0.75 moles of iron are consumed per mole of water. The intruding water, estimated above as 0.004 to 0.04 litres per year could hypothetically corrode about 0.01 to 0.1 kg of iron per year. Averaged over the total inner surface of the cast iron insert (about 34 m^2 for BWR canisters), this would necessitate a corrosion rate of about 0.04 to 0.4 μm a^{-1} (rounded values). The rate of hydrogen gas generation may thus be limited by the availability of water within the canister (see also Figure 2-3). The gas generation rate is calculated from:

$$\dot{n}_p = \begin{cases} \dot{n}_{p,\max} & V_w > 0 \\ \min(-Q_w \frac{\rho_w}{M_w}, \dot{n}_{p,\max}) & V_w = 0 \end{cases} \qquad n_p(t_0) = n_0 \qquad \text{(Eq. 2-5)}$$

$$\dot{n}_{p,\max} = \frac{4}{3} R F_0 \frac{\rho_{Fe}}{M_{Fe}} \qquad \text{(Eq. 2-6)}$$

where

$\dot{n}_p$	gas generation rate within the canister (the dot signifies time derivative) [mol s^{-1}]
$\dot{n}_{p,max}$	maximum gas generation rate (for unlimited water supply) [mol s^{-1}]
Vw	water volume inside canister [m^3]
R	steel corrosion rate [m s^{-1}]
F0	total inner surface of cast iron insert [m^2]
ρ_w, ρ_{Fe}	density of water and iron [kg m^{-3}]
M_w, M_{Fe}	molar weight of water and iron [kg mol^{-1}]

In Equation 2-5 it is implicitly assumed that in the presence of liquid water in the voids, the entire inner surface of the cast iron insert undergoes corrosion at the maximum rate, whether or not it is in contact with liquid water. This is because the water vapour pressure is sufficient to maintain a thin water film on steel surfaces not contacting liquid water. Furthermore, it is assumed in Equation 2-5 that hydrogen gas generation stops when the inflow of water ceases. In reality, the generation of hydrogen gas continues even after the inflow of water has stopped, because further water will be supplied by vapour transport. This latter process has not been modelled in the present investigations.

It is assumed that the inventory of activation products in Zircaloy and other metal parts is released congruently with the corrosion of the metal (a more pessimistic approach is taken in SR-Can, where no credit is taken for the delay due to the limited rate of metal corrosion). The other metal parts are mostly stainless steel (53 kg/tU) and Inconel (2.9 kg/tU), which have significant Nb-94 and C-14 inventories /Anttila 2005/. The low corrosion rates of the Zircaloy

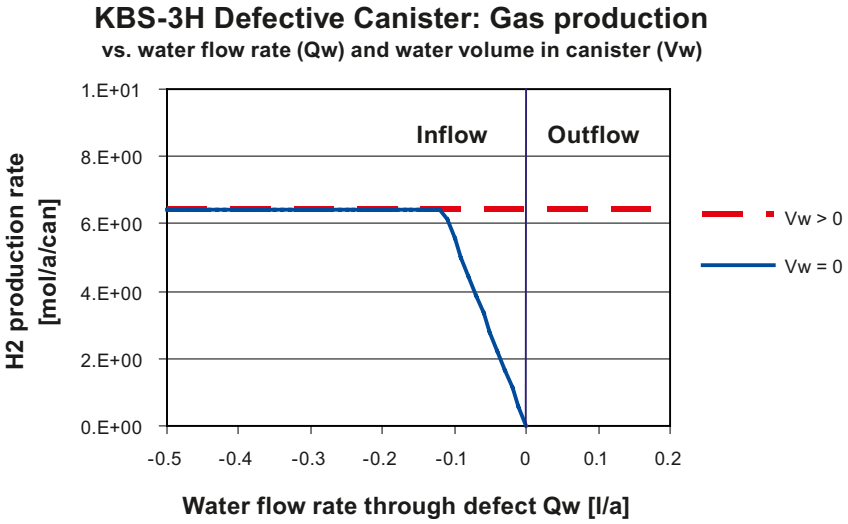

Figure 2-3. *Gas production rate in cavity of cast iron insert for a steel corrosion rate of 1 µm a^{-1} and a total inner surface of the cast iron insert of 34 m^2. In reality, the gas production continues even after water inflow has stopped ($Q_w > 0$) and after all liquid water within the cavity has been consumed ($V_w = 0$), because some water is supplied by vapour transport through the hole.*

and other metal parts, may, in reality, mean that some radionuclides, including potentially significant amounts of Nb-94 and C-14, are retained within these components beyond the period of gas expulsion. In TILA-99, it was assumed that the fractional corrosion rate of all other metal parts (cast iron, stainless steel, Inconel) was 10^{-3} per year and that of Zircaloy was 10^{-4} per year (p. 101 of /Vieno and Nordman 1999/). In reality, the corrosion rate of stainless steel is less than that of cast iron and, as cast iron is lower in the galvanic series than stainless steel, the stainless steel will be protected against corrosion for as long as cast iron is present. The assumed fractional corrosion rate of Zircaloy of 10^{-4} per year), is also somewhat higher that the expected rate of corrosion /see Johnson and McGinnes 2002/, and is conservative, since it will lead to higher than expected radionuclide release rates. This high corrosion rate leads to an inconsistency, in that sustaining it would require more water than will enter through a defect of the postulated size. The corrosion of the approximately 5,000 moles of Zircaloy in a canister at a rate of 10^{-4} per year will produce ~1 mole of H_2 per year (one mole of Zircaloy produces two moles of H_2), consuming 1 mole of water. However, it is also shown that the water flow rate into a canister with a one millimetre diameter defect is only in the order of 0.004 and 0.04 litres per year, or 0.2 to 2 mols per year, based on a hydraulic conductivity of the bentonite at the mouth of the hole of 10^{-13} to 10^{-12} m s^{-1} and a pressure difference across the buffer is 4.2 MPa (corresponding to the hydrostatic pressure at the depth of 420 m, the lower end of the inclined drift). Furthermore, plugging of the hole with bentonite or corrosion products and the decrease of the hydraulic gradient over time due to gas pressure buildup will reduce the rate of water inflow into the canister. In spite of this inconsistency, the decision has been taken to use the conservative Zircaloy corrosion rate from TILA-99 for calculating radionuclide release rates in the present safety assessment, although the possibility of using a more realistic corrosion rate may be considered in future studies.

Degassing, dissolution and diffusion of gas

The inflowing water may contain some dissolved hydrogen gas previously generated by corrosion of the supercontainer and other structural materials in the emplacement drift as well as some dissolved natural gases from the host rock (mainly methane and hydrogen). The natural hydrogen concentration at Olkiluoto is far from its solubility limit under repository conditions /Rasilainen 2004/ and is not taken into account in the present calculations. Although the natural

methane concentration is relatively close to its solubility limit in the deep saline groundwater, it is not taken into account, because there is no significant interaction with hydrogen gas.

Due to the initially lower pressure inside the canister, degassing of hydrogen may occur and – as a result of the lowered dissolved gas concentration – dissolved hydrogen gas may diffuse from the buffer into the canister. As the pressure increases, hydrogen gas may again dissolve in the liquid phase and – as a result of the increased dissolved gas concentration – dissolved hydrogen gas may diffuse from the canister outwards into the buffer.

It is shown in Chapter 5 that hydrogen dissolution/diffusion is not sufficient to balance the generation of hydrogen gas produced by the corrosion of the steel supercontainers. By similar arguments and by considering the transport resistance of the hole (bottleneck), the total rate of hydrogen transported by these processes can be shown to be several orders of magnitudes smaller than the rate of hydrogen generated by corrosion of the cast iron insert. These processes are thus neglected in the model calculations.

Saturation of cavity and water displacement by gas pressure buildup

Any gases trapped/generated within the canister or transported into the canister will accumulate and will be compressed within the cavity. The volume of gas may, however, change due to the supply of water through the hole and due to water consumption by steel corrosion:

$$\dot{V}_g = Q_w + \dot{V}_{consumed}; \qquad V_g(t_0) = V_0; \quad V_g(t) = V_0 - V_w(t) \qquad \text{(Eq. 2-7)}$$

$$\dot{V}_{consumed} = \begin{cases} Q_{crit} & V_w > 0 \\ \min(-Q_w; Q_{crit}) & V_w = 0 \end{cases} \qquad \text{(Eq. 2-8)}$$

$$Q_{crit} = \frac{4}{3} R F_0 \frac{M_w \rho_{Fe}}{M_{Fe} \rho_w} = \dot{n}_{p,\max} \frac{M_w}{\rho_w} \qquad \text{(Eq. 2-9)}$$

where

$\dot{V}_g$ rate of change of gas volume inside canister [$m^3\ s^{-1}$]
V_0 void volume within the canister insert [m^3]
V_w water volume inside canister [m^3]
$\dot{V}_{consumed}$ rate of water consumption by steel corrosion [$m^3\ s^{-1}$]
Q_{crit} maximal water consumption rate by steel corrosion [$m^3\ s^{-1}$]

In Equation 2-7 it has been implicitly assumed that the available void space in the canister does not change with time. In reality, it may become filled with corrosion products. The effect of this simplifying assumption is considered to be small, because in the time period of interest (a few thousand years) only a minor amount of corrosion products will be produced.

The maximal water consumption rate by steel corrosion is about 0.1 litres per year for a steel corrosion rate of 1 μm a^{-1} and a total inner surface of the cast iron insert of 34 m^2. From the ideal[13] gas law, the fluid pressure P (for gas/water) within the cavity is derived:

[13] $H_2(g)$ is assumed to behave as an ideal gas at the pressures considered, around 10 MPa. At these pressures, H_2 is 5–10% less compressible than what is calculated, which is within the uncertainty range.

$$P = \frac{n_p}{V_g} R_0 T_0 = \frac{n_0 + \int_{t0}^{t} \dot{n}_p(\tau)\, d\tau}{V_0 + \int_{t0}^{t} \dot{V}_g(\tau)\, d\tau} R_0 T_0 \qquad P(t_0) = P_0$$

(Eq. 2-10)

P_0 atmospheric pressure [Pa]

R_0 ideal gas constant [J K^{-1} mol^{-1}]

T_0 temperature within the canister cavity [K] (about 10°C after several thousand years, assumed to be time-independent – note the ambient rock temperature at depth of 400 m is 10.5°C, see Appendix A, Table A-1)

With respect to saturation of the cavity within the canister insert, two limiting cases are of interest for radionuclide release from the canister:

i) The inflow rate of liquid water exceeds the maximal consumption rate of water by anaerobic steel corrosion. In this case, liquid water slowly accumulates within the cavity until the gas pressure is in equilibrium with the pressure outside the canister (P_s). Due to ongoing gas generation, the pressure inside the canister may further rise. As a consequence, for certain hole locations, any contaminated water previously accumulated within the canister is slowly squeezed outwards through the hole (Figure 2-2).

ii) The inflow rate of liquid water is smaller than the maximal consumption rate of water by anaerobic steel corrosion. In this case the cavity remains fully gas saturated.

In both cases, the generation of gas continues even for internal pressures exceeding the outer pressure P_s due to slow transport of water vapour through the hole. The gas pressure further rises until the pressure is high enough for gas to break through the saturated buffer (threshold pressure). At this point in time, release of volatile radionuclides in the gas phase may take place (mainly C-14).

Gas flow through bentonite

Gas flow through saturated bentonite is treated in this section because it is linked to the water and gas transport processes arising from water in contact with the fuel and insert. Gas flow through bentonite is treated as in SR-Can. Detailed description of assumptions and simplifications are discussed in detail in /Harrington and Horseman 2003/ and /SKB 2006d/ and are only summarised here. For constant volume boundary condition, gas breakthrough pressure through saturated bentonite occurs when the gas pressure P_g attains a value:

$$P_g = T + 2\sigma_{eff} + P_w \qquad \text{(Eq. 2-11)}$$

P_g gas breakthrough pressure in saturated bentonite [Pa]

T tensile strength of bentonite [Pa]

σ_{eff} isotropic effective stress outside the region of stress concentration [Pa]

P_w pore water pressure in saturated bentonite [Pa]

At such pressures, gas pathways are formed from the defect through the bentonite to the rock walls around the emplacement drifts, resulting in gas flow. There is clear evidence that little water is expelled by gas flow within dense saturated bentonite /Harrington and Horseman 2003/. Once the gas pathways are formed, the bentonite has lost its tensile strength and the gas pathways remain open as long as gas generation is sufficient to maintain a pressure within the pathways above the "shut-in pressure":

$$P_g = \sigma = \sigma_{eff} + P_w \qquad \text{(Eq. 2-12)}$$

When the gas generation ceases, or if the gas generation rates are low enough, the transport pathways are expected to close. This will occur when the pressure falls below the "shut-in pressure". When the pathways close, gas migrates solely by diffusion. Note that in saturated bentonite, the isotropic effective stress is roughly equal to the swelling pressure. On the other hand, the gas pressure cannot fall below the sum of the capillary pressure and externally applied water pressure, providing a lower bound for the "shut-in pressure":

$$P_g > P_c + P_s \qquad \text{(Eq. 2-13)}$$

P_c capillary pressure [Pa]
P_s externally applied water pressure (equal to hydrostatic pressure) [Pa]

The sequence of processes described above may be repeated. /Rasilainen 2004/ argues that this scenario of combined gas and water flows, where all gases generated are trapped inside the canister cavity, is neither the only conceivable nor the most likely scenario. As a matter of fact, the water ingress – gas expulsion scenario is considered to be rather unlikely because it is based on a number of pessimistic conceptual assumptions (see discussion below).

Model results

Figure 2-4 shows the results of the simplified gas calculations based on Equation 2-3 to 2-10. Only 1 out of 6 investigated cases represents the limiting case (i) above: For the expulsion of dissolved radionuclides by gas to occur, a relatively high hydraulic conductivity of 10^{-12} m s^{-1} for saturated bentonite[14] has been assumed, combined with a low steel corrosion rate of 0.1 μm a^{-1}. As discussed above, a low corrosion rate is conservative because it leads to a greater initial water inflow into the canister. For this rather unlikely case, a maximal water saturation of about 3% (0.03 m^3 water in 1 m^3 void space) and a maximal water pressure of about 6 MPa within the canister interior are calculated. In the time period from 2,800 to 4,100 years, water is expelled through the hole at a maximal rate of 0.02 litres per year. This water flux may convey dissolved radionuclides, mainly from the instant release fraction of spent fuel (assuming that the fuel cladding has ruptured, and water has access to fuel surfaces).

All other investigated cases are representatives of the limiting case (ii): the inflowing water is completely consumed by steel corrosion. The gas pressure does not significantly exceed the water pressure outside the canister (assumed to be equal to the hydrostatic pressure of 4.2 MPa) and there is no gas-induced displacement of contaminated water through the hole into the saturated bentonite. In reality, the hydrogen gas generation continues even after the inflow of water has stopped, because further water will be supplied by vapour transport. As a result, the gas pressure continues to rise until the breakthrough pressure for gas flow through bentonite is reached. These processes have not been modelled in the present investigations.

On the basis of the modelling results, the more likely situation is that inflowing water will be completely consumed by steel corrosion (situation (ii), above), and there will be no gas-induced displacement of contaminated water through the hole into the saturated bentonite.

Water volume in the cavity within the cast iron insert (upper figure), water flow rates through the hole in the canister (middle figure) and gas pressure in the cavity within the cast iron insert (lower figure).

[14] Note that in Figure 4-8 of the SR-Can Main Report /SKB 2006a/, the range of hydraulic conductivities for bentonite exposed to solutions of variable NaCl concentrations is between 10^{-12} and 10^{-14} m s^{-1}, for bentonite dry densities of about 1,200 to 1,600 kg m^{-3}.

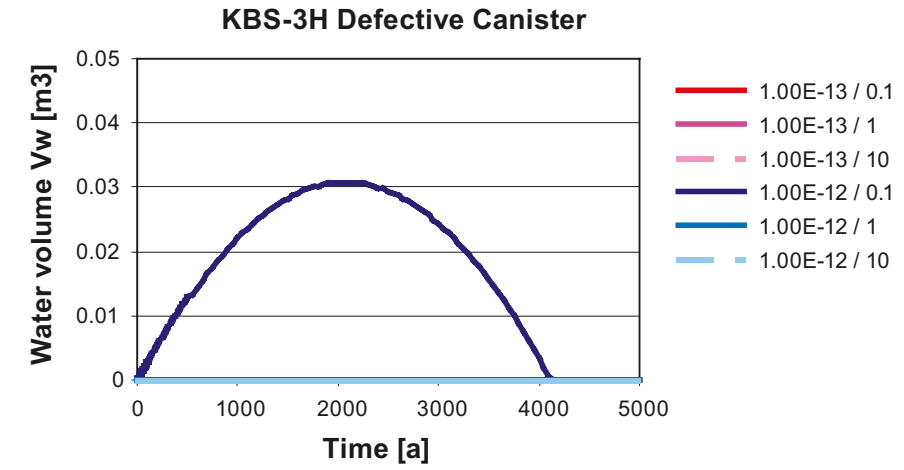

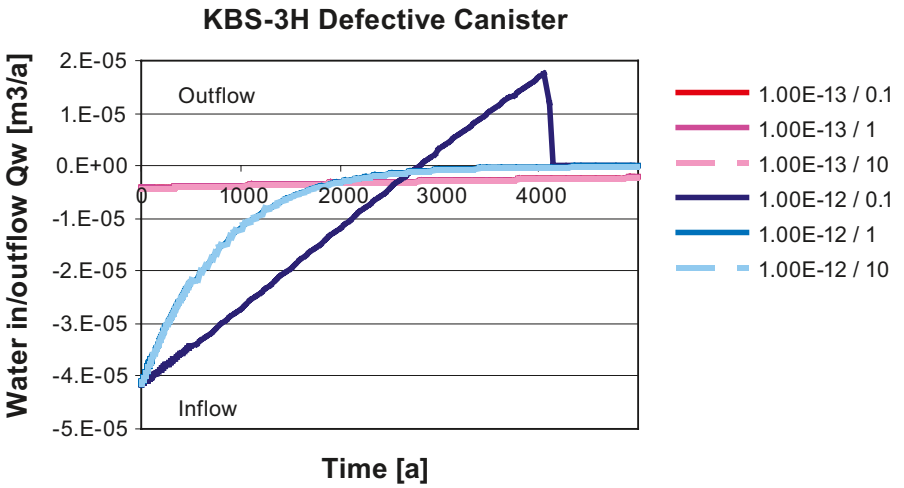

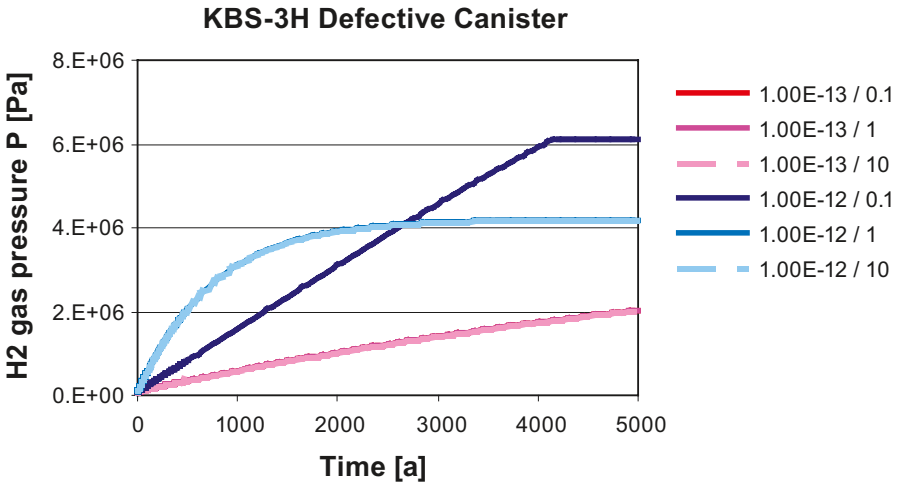

Figure 2-4. *Results of simplified gas calculations for various hydraulic conductivities (left numbers in m s^{-1}) of saturated bentonite and steel corrosion rates (right numbers in µm a^{-1}).*

Natural analogues/observations in nature

Not applicable.

Time perspective

The relevant time scale for the above processes is in the order of several thousand years. However, the time required to fully corrode the canister insert may be some tens to hundreds of thousands of years, depending on the rate of steel corrosion under the expected repository conditions.

Handling in the safety assessment for KBS-3H

KBS-3H Radionuclide Transport Report /Smith et al. 2007b/ describes radionuclide release and transport analyses in the case of a canister with an initial penetrating defect in a KBS-3H repository (assessment case called PD-BC). In the majority of the investigated cases, no gas-induced displacement of contaminated water takes place through the hole of a defective canister. The assessment case called PD-EXPELL addresses uncertainties regarding the possibility of gas-induced displacement of contaminated porewater from the cavity of the iron insert through the hole (located at the canister underside) into the saturated bentonite (see Section 2.8). In KBS-3H this variant case has a higher probability of occurrence compared with KBS-3V, due to the similar probability of a defect being located in the lower and upper part of the canister.

Some other significant uncertainties are acknowledged in the detailed modelling of hydraulic and gas-related processes associated with a penetrating defect in a canister. Two assessment cases (PD-VOL-1, PD-VOL-2) are associated with a scenario in which C-14 is transported in volatile form by corrosion-generated gas at two different rates of steel corrosion (1 μm a^{-1} and 0.1 μm a^{-1}) For additional information on assessment cases, see Appendix G.

Handling of uncertainties

The evolution of a canister defect and the processes leading to subsequent radionuclide release are complex and depend on a number of uncertain factors. The hydro-mechanical behaviour of the water/vapour/gas system in a defective canister is governed by several coupled processes (including water and gas transport through the buffer, steel corrosion) and parameters (including permeability of the buffer, steel corrosion rate, gas breakthrough pressure and sizes, locations and growth/closure rates of defects and other voids in the two-layer canister). There exist significant uncertainties related to the mechanistic understanding, system modelling and data, among which the following may deserve special attention:

- The rate of steel corrosion under repository conditions is still uncertain. In the present investigations, a reference value of 1 μm a^{-1} has been assumed. To address data uncertainty, a large range of corrosion rates from 0.1 to 10 μm a^{-1} have also been investigated. In /SKB 2006a/, a corrosion rate for cast iron of 0.1 μm a^{-1} is used for bentonite-conditioned pore water.
- There is a lack of detailed mechanistic understanding of the evolution of a small initial weld defect to a large defect of the canister. In the present investigation, simple pessimistic assumptions have been adopted (hole radius of 0.5 mm, hydraulic breakthrough occurring at 1,000 years, etc). The Base Case for radionuclide release through a growing pinhole failure, as defined in Chapter 10.5 in /SKB 2006a/ for KBS-3V, is considered adequate for the Finnish Safety Case for KBS-3H. Moreover, no substantial differences are expected regarding the timing and rates of radionuclide release in the horizontal and vertical disposal alternatives.

- The possibility of accelerated radionuclide release from a defective canister arising from hydrogen gas production due to corrosion of internal surfaces of the cast iron insert and consequent expulsion of contaminated water is considered to be rather unlikely. In reality, the defect may not be located at the underside of the canister and the water inflows may be much reduced due to sealing of the hole by bentonite and corrosion products. In both situations, no gas-induced displacement of contaminated porewater would take place. In the KBS-3H Radionuclide Transport Report /Smith et al. 2007b/ three variant cases (PD-EXPELL, PD-VOL-1, PD-VOL-2) have been defined to address the possibility of gas-induced release of contaminated water from the canister interior.

2.6 Mechanical processes

An overview of mechanical processes in the fuel/cavity in the canister is shown in Table 2-6. Structural evolution of the fuel matrix and mechanical cladding failure are not considered to depend significantly on the specific conditions in KBS-3H. Also, the structural evolution of the fuel matrix is negligible if the burnup is lower than the 45–50 GWd/t range (specific to fuel type), where the fission gas release and instant release fraction of BWR fuel starts to increase /Johnson and McGinnes 2002/. This burnup range is relevant to all types of Finnish and Swedish fuel types (see Section 2.1.1). For PWR fuel for the new EPR Olkiluoto reactor (OL-3), the design burnup is near the upper limit (47 GWd/t), but EPR fuel fission gas release and instant release fraction values are generally lower in this burnup region compared with that for BWR fuel.

The partitioning between the fuel matrix and the IRF used in the safety assessment is based on Table A-4 of the SR-Can data report (/SKB 2006f/ – realistic, central values). This is justified by the similarity in the fuels and burnups in the Swedish and Finnish cases, also given the likely future increases in fuel burnup expected in Finland.

Structural evolution of the fuel matrix can, therefore, be neglected in the safety assessment. Cladding failure is handled pessimistically in the safety assessment in that no credit for a barrier function is taken, i.e. the fuel cladding fails at the time of canister failure. The handling of these processes in the KBS-3H safety studies is summarized in Table 2-2.

Table 2-6. The inter-dependence of mechanical processes and identified variables in fuel/cavity in the canister.

Mechanical processes	Variables in fuel/cavity in the canister								
	Radiation intensity	Temperature	Hydrovariables (pressure and flows)	Geometry (incl. dimensions)	Stress state	Radionuclide inventory	Material composition	Water composition	Gas composition
Structural evolution of fuel matrix	×					×			
Cladding failure		×			×	×	×		

2.7 Chemical processes

An overview of chemical processes in the fuel/cavity in the canister is shown in Table 2-7. None of these processes is considered to significantly depend on the specific conditions in KBS-3H, except for advection, which is treated in Section 2.5. There are no additions or comments to the discussions in the relevant Process Reports for KBS-3V /Rasilainen 2004, SKB 2006c/. The handling of these processes in the KBS-3H safety studies is summarized in Table 2-2.

The fuel dissolution model adopted in SR-Can has been utilised here without further evaluation. The assumed fractional corrosion rate used in the Radionuclide Transport Report /Smith et al. 2007b/ of the Zircaloy of the fuel cladding is 10^{-4} per year based on the value used in TILA-99 (p. 101 of /Vieno and Nordman 1999/). This corrosion rate is somewhat higher than the expected rate of corrosion /see Johnson and McGinnes 2002/, and is conservative, since it will lead to higher than expected radionuclide release rates. This high corrosion rate leads to an inconsistency, in that sustaining it would require more water than will enter through a defect of the postulated size. The corrosion of the approximately 5,000 moles of Zircaloy in a canister at a rate of 10^{-4} per year will produce ~1 mole of H_2 per year (one mole of Zircaloy produces two moles of H_2), consuming 1 mole of water. However, as shown in Section 2.5.1, the water flow rate into a canister with a one millimetre diameter defect is only in the order of 0.004 and 0.04 litres per year, or 0.2 to 2 mols per year, based on a hydraulic conductivity of the bentonite at the mouth of the hole of 10^{-13} to 10^{-12} m s^{-1} and a pressure difference across the buffer is 4.2 MPa. Furthermore, the plugging of the hole with bentonite or corrosion products and the decrease of the hydraulic gradient over time due to gas pressure buildup will reduce the rate of water inflow into the canister. In spite of this inconsistency, the decision has been taken to use the conservative Zircaloy corrosion rate from TILA-99 in the Radionuclide Transport Report, although the possibility of using a more realistic corrosion rate may be considered in future studies.

There remain considerable uncertainty regarding the validity of various proposed models for fuel dissolution, thus this remains an important area for further studies common to KBS-3H and KBS-3V.

Table 2-7. The inter-dependence of chemical processes and identified variables in fuel/cavity in the canister.

Chemical processes	Variables in fuel/cavity in the canister								
	Radiation intensity	Temperature	Hydrovariables (pressure and flows)	Geometry (incl. dimensions)	Stress state	Radionuclide inventory	Material composition	Water composition	Gas composition
Advection and diffusion		×	×	×		×		×	×
Residual gas radiolysis/acid formation	×		×					×	×
Water radiolysis	×	×	×					×	×
Metal corrosion	×	×	×		×	×	×	×	
Fuel dissolution	×	×	×	×		×	×	×	×
Dissolution of gap inventory		×	×	×		×	×	×	×
Speciation of radionuclides, colloid formation		×	×	×			×	×	×
Helium production	×				×	×			×

In the Radionuclide Transport Report, it is also assumed that the inventory of activation products in Zircaloy and other metal parts is released congruently with the corrosion of the metal (a more pessimistic approach is taken in SR-Can, where no credit is taken for the delay due to the limited rate of metal corrosion).

2.8 Radionuclide transport processes

Overview/general description

An overview of processes related to radionuclide transport in the fuel/cavity in the canister is shown in Table 2-8. These processes have been identified in /SKB 1999/ and /Rasilainen 2004/ to be relevant for the fuel/cavity in the canister in KBS-3V. None of these processes is considered to significantly depend on the specific conditions in KBS-3H. An exception is gas-induced porewater displacement from the canister interior through a hole at the underside of a canister conveying dissolved radionuclides (see discussion in Section 2.5). There are no additions or comments related to process understanding in the relevant Process Reports for KBS-3V /Rasilainen 2004, SKB 2006c/. The handling of these processes in the KBS-3H safety studies is summarized in Table 2-2.

Handling in the safety assessment for KBS-3H

In the KBS-3H Radionuclide Transport Report /Smith et al. 2007b/, the base case for an initial penetrating defect of size is 1 mm (radius 0.5 mm) and it is assumed that radionuclides are transported entirely as dissolved species. Gaseous radionuclides (e.g. Rn-222), as well as radionuclides such as C-14 that can form volatile species, are considered in separate release and transport cases (PD-VOL-1 and PD-VOL-2), which consider high and low rates of repository gas generation, respectively. Such radionuclides are assumed to mix with gas generated in the interior of the canister and be transported with this gas through the buffer to the geosphere.

Table 2-8. The inter-dependence of radionuclide transport and identified variables in fuel/cavity in the canister.

Radionuclide transport	Variables in fuel/cavity in thecanister								
	Radiation intensity	Temperature	Hydrovariables (pressure and flows)	Geometry (incl. dimensions)	Stress state	Radionuclide inventory	Material composition	Water composition	Gas composition
Radionuclide transport:		×	×			×		×	×
- advection									
- diffusion									
- sorption									
- colloid transport									
- gas phase transport									
- radioactive decay									

As in the case of SR-Can /SKB 2006a/, it is assumed that 1,000 years (fixed value) will elapse before a continuous transport pathway between the fuel and the canister exterior is established, allowing radionuclide transport to take place. The further development of the small defect is assumed to eventually lead to a large failure of the copper canister. This may occur at any time between 0 and 100,000 years after the onset of a continuous transport pathway (triangular distribution between 0–100,000 years, with a maximum at 100,000 years). For the purpose of stylised calculations, it is, however, assumed that the large defect in the single canister considered occurs 10,000 years after deposition, i.e. 9,000 years after the defect becomes a transport pathway. After that time, any residual transport resistance of the remaining canister is pessimistically neglected.

For KBS-3H, a new variant case (PD-EXPELL) is defined to cover uncertainties regarding the possibility of gas-induced displacement of contaminated porewater from the cavity of the iron insert through the hole into the saturated bentonite. The following assumptions are proposed, based on the modelling results from Section 2.5.1:

The water pulse through a hole in a single canister:

- starts at 2,500 years after deposition and lasts for 2,000 years,
- occurs at a constant rate of 0.02 litres per year,
- conveys the entire instant release fraction as dissolved radionuclides,
- leads to advective/dispersive transport of radionuclides through the buffer, considering sorption, solubility limitation and decay,
- followed by release of radionuclides into the relevant transport paths in near field and geosphere.

The formation of colloids inside the canister would need to be considered if there were plausible situations in which the buffer no longer enveloped a defective canister, for example, due to a massive earthquake-related rock shear displacement. Fracture zones with a potential to leading to such massive shear deformations will be avoided in the repository layout. As long as the buffer of highly compacted bentonite around the canister has a sufficient density ($> 1{,}650$ kg m^{-3}), it effectively hinders the transport of inorganic colloids formed inside the canister. The process is omitted in the KBS-3H Radionuclide Transport Report /Smith et al. 2007b/.

In addition to the base case for an initially penetrated defect (PD-BC), the Radionuclide Transport Report /Smith et al. 2007b/ addresses the following variabilities or uncertainties in its assessment cases:

- Variability in the case of different fuel types, VVER (PD-VVER) and EPR (PD-EPR).
- Uncertainty due to the expulsion of contaminated water by gas build-up (PD-EXPELL).
- Uncertainties in the redox conditions affecting near-field solubility values (PD-NFSLV).
- Uncertainties in the instant release fraction (PD-IRF).
- Uncertainties in the fuel dissolution rates in the case of a penetrated canister, high dissolution rate (PD-HIFDR) and low dissolution rate (PD-LOFDR).
- Uncertainties in the fuel dissolution rates in the case of canister failure by corrosion (CC-HIFDR and CC-LOFDR).

For additional information on assessment cases in the Radionuclide Transport report, see Appendix G.

3 Cast iron insert and copper canister

3.1 Description of cast iron insert and copper canister

3.1.1 General

The canister is the same for KBS-3H and KBS-3V. The design and dimensioning analyses of the copper-iron canister for spent fuel are presented in /Raiko 2005/. The canister structure consists of a massive cast iron insert covered by a 50 mm thick copper shell. There are three versions of the canister, one for each reactor type in Finland (Figures 3-1 and 3-2). The spent fuel is sealed in the canisters as whole fuel assemblies including the flow channel outside the VVER-440 and BWR fuel bundles.

The insert is made of nodular graphite cast iron. The lid of the insert is made of structural steel. The material of the overpack is oxygen-free high conductivity copper (Cu-OF) with an addition of 30 to 70 ppm phosphorus. The microalloying is made to improve the creep strain properties of Cu-OF at a high temperature (200 to 300°C). The total weight of the tight, long-living and strong vessel with the fuel bundles is 20–25 tonnes depending on the canister type. The contents and physical properties of the canister materials are presented in /Raiko 2005/.

Figure 3-1. *Copper-iron canisters for the spent fuel from the Loviisa 1-2 (VVER-440), Olkiluoto 1-2 (BWR) and Olkiluoto 3(EPR) reactors (from left to right; figure taken from /Raiko 2005/).*

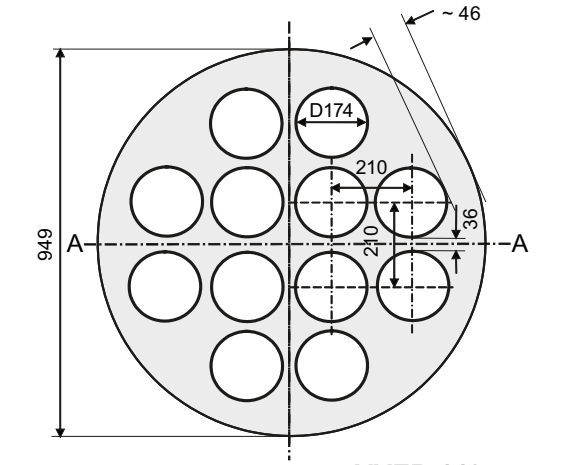

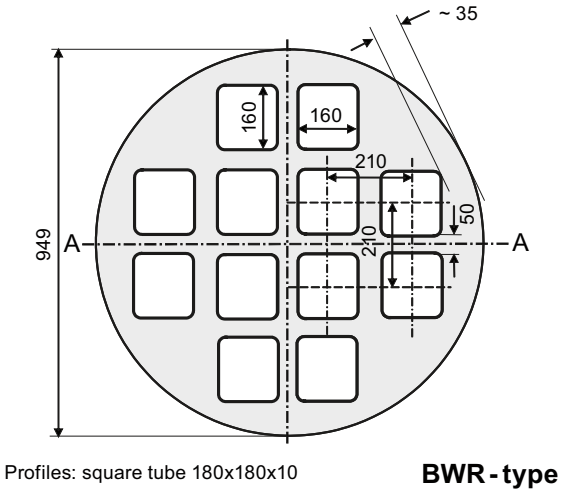

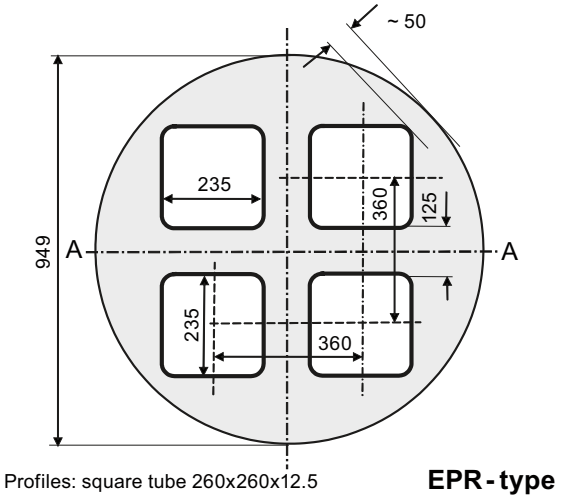

Figure 3-2. *Cross-sections of the cast iron inserts for the three types of spent fuel (from /Raiko 2005/).*

The VVER type insert is shorter and the openings are circle shaped (diameter 174 mm) instead of the square openings of the BWR type (160 × 160 mm) and EPR type (235 × 235 mm). The insert of the canister is an integrated block made by casting. The insert acts as a load-carrying component, a rack for the fuel bundles, a radiation protection wall, a thermal conductor, a separator to form a sub-critical geometry and filler of the empty space in the canister. The lid of the insert is fixed centrally with a screw and there is a gasket between the lid edge and the insert body.

Posiva and SKB are carrying out a joint programme to develop methods to manufacture, seal and inspect copper-iron canisters for spent fuel. Canister manufacturing, fuel encapsulation, canister sealing, and inspection are described in /Posiva 2006, SKB 2004a, Andersson et al. 2004, Raiko 2005/.

Due to the great similarity of Posiva's and SKB's canister design, the main physical properties affecting the long-term behaviour are similar and even identical in some instances. There are, however, some slight differences between Posiva's and SKB's canister design and welding techniques:

- Posiva's lid is welded at the end face of the copper shell, whereas SKB's lid is welded on the circumference of the copper shell;
- Posiva plans to seal the lid of the copper overpack with electron beam welding (friction stir welding is being investigated as an alternative); SKB's reference welding technique is friction stir welding;
- Electron beam welding will be performed in a vacuum, whereas friction stir welding will be performed in open air;
- Different heights/dimensions of the lid (e.g. SKB's lid height is larger due to the different reference welding technique);
- Different dimensions and shape of fuel assemblies, canisters and iron insert. The main dimensions and masses of the canisters are presented in Table 3-1. All versions of the canister have the same outer diameter of 1.05 metres. (Posiva's dimensions are described in detail in /Raiko 2005/ and SKB's dimensions in /SKB 2006c/).

Table 3-1. Main dimensions and masses of the canisters for the different types of spent fuel /from Raiko 2005/. The reference fuel/canister is that for Olkiluoto 1-2 BWR fuel.

	Loviisa 1-2 (VVER-440)	Olkiluoto 1-2 (BWR)	Olkiluoto 3 (EPR)
Outer diameter (m)	1.05	1.05	1.05
Height (m)	3.60	4.80	5.25
Thickness of copper cylinder (mm)	48	48	48
Thickness of copper lid and bottom (mm)	50	50	50
Total volume (m^3)	3.0	4.1	4.5
Fuel assemblies	12	12	4
Amount of spent fuel (tU)	1.4	2.2	2.1
Void space (m^3)	0.61	0.95	0.67
Mass of fuel assemblies (ton)	2.6	3.6	3.1
Mass of iron and steel (ton)	10.4	13.4	18.0
Mass of copper (ton)	5.7	7.4	8.0
Total mass (ton)	18.6	24.3	29.1

A quality assurance and quality control programme for canister manufacturing, conditioning, and sealing is being developed as described in /Posiva 2006, SKB 2004a/ and in /Andersson et al. 2004/.

In the Finnish and Swedish safety concepts, the canister containment function plays a central role. The canisters are designed for long-term integrity, i.e. gas and water-tightness, and have a design lifetime of at least 100,000 years. This canister design lifetime means that the canisters are designed to maintain their integrity taking into account the processes and events that are considered likely to take place in the repository over a design basis period of 100,000 years. It does not exclude the possibility that canister integrity will be retained significantly beyond the design basis period, nor that less likely, extreme conditions will give rise to earlier canister failures, and these possibilities must be considered in safety assessment. The terminology is similar to that used in the reactor safety area: a design basis is defined to reflect the most likely conditions for the system but safety assessment must address less likely situations as well.

In order to achieve their minimum design lifetime, canisters are required to have:

1. a low probability of occurrence of initial penetrating defects;
2. corrosion resistance; and
3. mechanical strength.

The minimum design lifetime also implies a number of design requirements on repository layout (avoidance of fractures that may undergo shear movements that could damage the canisters – see Section 3.6 below) and on the buffer. The probability of occurrence of initial penetrating defects is still under investigation. In the current design, corrosion resistance is provided by the copper canister shell, and mechanical strength primarily by the cast iron insert. If the copper shell is breached, then a canister is considered to have failed, even though it may continue to offer some resistance to the ingress of water and the release of radionuclides for a significant period thereafter (see Section 2.8).

The breaching time for the copper shell (i.e. when the copper thickness is zero somewhere on the surface of the shell) is inversely proportional to the minimum initial thickness of the copper shell. The number and timing of initial defects in canisters are thus crucial parameters for the safety assessment (see Section 2.8). Corrosion of the copper shell takes place initially due to oxygen entrapped at the time of deposition, and in the longer-term, due principally to sulphide present in the buffer and in the groundwater. Given the expected low long-term corrosion rate, corrosion of the canisters leading to failure will not occur within, say, one million year time frame, unless locally much reduced initial copper thicknesses are present as a result of defects. In principle, such defects could occur anywhere in the copper shell, but they are most likely to occur along welds and, in particular, at the seal of the canister top lid.

SKB has conducted a demonstration series of 20 canister lids welded by friction stir welding under production-like conditions /Ronneteg et al. 2006/. After the lids were welded, each weld was examined using the Non Destructive Testing (NDT) methods available at the SKB Canister Laboratory to find defects in the welds. After NDT, the welds were further analysed using destructive methods to determine the exact size and, for some welds, the material composition in the defects. The maximum defect sizes obtained for this demonstration series were then used to predict the expected maximum defect size for the total production series using extreme value statistics, i.e. by fitting the measured defect sizes to a generalised extreme value distribution /SKB 2006f/. SKB's conclusion on the reliability of the friction stir welding method is that "the welding process produces reproducible results which satisfy stipulated requirements on minimum copper thickness with very good margins" /Ronneteg et al. 2006/. SKB conclusion on the proposed NDT methods is that they are suitable to indicate the weld quality /Müller et al. 2006/.

According to SKB, based on the results of the demonstration series, the best estimate of the maximum defect size (i.e. the depth to which the defect extends) in a set of 4,500 canisters is 4.8 mm with 95% confidence limit at 7.8 mm /SKB 2006f/. In addition to the modelled data, measurement errors from the NDT testing are added resulting in an estimate of the maximum defect size of 10 mm. For the purpose of the SR-Can safety assessment, the defect distribution is assumed to be as follows (see Table 4-1 in /SKB 2006f/):

- 99% of all canisters have a defect smaller than 10 mm
- 1% of all canisters have a defect smaller than 15 mm.

The differences in Posiva's and SKB's canister designs, including the chosen reference welding technique, are not expected to have any significant impact on the probability of an initial canister defect. In both methods, the seal location is on, or within a few centimetres of, the end-face of the canister, so that no differences can be identified between electron beam welding and friction stir welding from the long-term safety point of view if an initial penetrating defect is assumed to be present.On the other hand, in Finland, the quality assurance program for NDT techniques is still in an early phase of development. A non-destructive examination method for canister component manufacture and sealing will only be selected by the end of 2008. A qualification programme for the applicable examination procedures will be made by the end of 2009 and executed by the end of 2012, before the application of the encapsulation plant construction license is submitted. Thus, Posiva is not yet taking any position on the likelihood of occurrence of canisters with initial penetrating defects.

In the Radionuclide Transport Report /Smith et al. 2007a/, a scenario in which a canister has an initial penetration is used to illustrate the impact of a range of uncertainties affecting release and transport processes in the event of canister failure, whatever the cause or the timing the failure event. In SR-Can, although no initial penetrating defects are expected, evolution in case of a growing pinhole failure is described and its consequences evaluated (Section 10.5 of SR-Can Main report /SKB 2006a/).

3.1.2 Overview of variables

The canister insert and overpack geometry is described in Section 3.1.1. Other variables that are relevant to the subsystem canister are radiation intensity, temperature, stress state, material composition, and water composition (Table 3-2).

3.1.3 Safety function indicators

Following SR-Can's approach, four fundamental modes have been identified by which, in principle, one or more canisters could fail to provide their safety function of complete containment of the spent fuel and associated radionuclides /SKB 2006a/: i) initial, penetrating defects, ii) failure due to corrosion of copper shell, iii) rupture due to rock shear and the transfer of shear stresses from the rock via the buffer to the canister (in particular, in the event of a large earthquake), and iv) collapse due to isostatic loading. The probability of initial penetrating defects for the Finnish and Swedish canister designs is discussed above in Section 3.1.1. The mechanical strength of the canisters, which must be such as to allow them to withstand that isostatic pressures and shear stresses to which they will be exposed over time, is discussed in /Raiko 2005/.

Safety function indicators for the canister are (i), minimum copper thickness – failure occurs if this is zero at any point on the canister surface, due to the presence of an initial defect that penetrates the entire thickness of the shell or due to localised and general corrosion processes leading to the gradual thinning of the shell, (ii), the isostatic pressure on the canister – failure occurs if this exceeds the isostatic pressure for collapse, and (iii), the shear stress on the canister – failure occurs if this exceeds the rupture limit. The canister safety function indicators and associated criteria, as presented in SR-Can /SKB 2006a/, are summarised in Table 3-3.

Table 3-2. Variables in the cast iron insert and copper canister.

Variable	Explanation
Geometry	Geometric dimensions for the canister components. This also includes a description of any fabrication defects in welds, etc.
Radiation intensity	Intensity of α-, β-, γ-, and neutron radiation as a function of time and space in the canister components.
Temperature	Temperature as a function of time and space in the canister components.
Stress state	Stress conditions as a function of time and space in the canister components.
Material composition	Material composition of the canister components.
Groundwater composition	Groundwater composition may affect the canister lifetime.

Table 3-3. Safety function indicators and criteria for the canister (after Figure 7-2 of /SKB 2006a/).

Safety function indicator	Criterion	Rationale
Minimum copper thickness	> 0 mm	Zero copper thickness anywhere on the copper surface would allow relatively rapid water ingress to the canister interior and radionuclide release
Isostatic pressure on canister	< pressure for isostatic collapse (varies between canisters, but probability of collapse at 44 MPa is vanishingly small)	An isostatic pressure on the canister greater than 44 MPa would imply a more significant possibility of failure due to isostatic collapse
Shear stress on canister	< rupture limit	A shear stress on the canister greater than the rupture limit would imply failure due to rupture

3.1.4 Summary of handling in safety assessment

Table 3-4 summarises the handling of processes in the subsystem “cast iron insert and copper canister” in the safety assessment for KBS-3H, as suggested in the following sections of Chapter 3. In the table, the process is either “mapped” to a model by which it will be quantified or associated with a brief verbal description of how it will be handled. The cases of intact and defective canisters are discussed separately.

3.2 Overview of processes

Based on the FEP analysis for KBS-3V, a list of processes for the cast iron insert and copper canister has been derived in /SKB 2006b/. Following the methodology in Appendix B, this list of processes is considered appropriate for KBS-3H.

The processes are structured into radiation-related, thermal, hydraulic, mechanical and chemical process categories, see Figure 1-3. In addition, radionuclide transport is discussed separately. In the introductory part of each of the following chapters, the processes pertinent to the process category are tabulated.

Table 3-4. Process table for the cast iron insert and the copper canister describing how processes are handled for intact canisters and in the special cases of failed canisters. Green fields denote processes that are omitted or irrelevant for the time period of concern. Red fields denote processes that are quantified by modelling in the safety assessment. Orange fields denote processes that are neglected subject to a specified condition. Motives for handling are given in the relevant sections of Chapter 3. The handling of processes in the KBS-3H safety assessment and the handling of uncertainties are discussed only in certain cases specific to KBS-3H (as noted in the table). If not mentioned, the handling of other processes and uncertainties are assumed to be handled in the same way as for KBS-3V and are not discussed in this report.

Process type	Internal process	Intact canister	Failed canister	Notes/*Section in KBS-3H Process Report*
Radiation-related processes	C1. Radiation attenuation/ heat generation	Thermal process model /Ikonen 2003, 2005/.	No specific analysis for KBS-3H. SR-Can: Neglected as long as releases occur after period of elevated temperatures.	*The handling in the safety assessment for KBS-3H is discussed.* *Section 3.3*
Thermal processes	C2. Heat transport	Thermal process model /Ikonen 2003, 2005/.	No specific analysis for KBS-3H. SR-Can: Omitted as long releases occur after period of elevated temperatures.	Temperature field similar in KBS-3V and 3H. *Section 3.4*
Mechanical processes	C3. Deformation of cast iron insert	Specific analysis for KBS-3H: Estimate of probability of intersection of canisters with shear horizons. Treatment in SR-Can: Isostatic: Comparison of external pressure with probabilistically calculated isostatic collapse load. Uneven swelling: Neglected based on pessimistically simplified calculations and model calculations. Tectonic events: Criterion for canister failure provided. Creep for all above cases: not included. (Creep testing of the insert ongoing.)	Not relevant	Probability of intersection of canisters with shear horizons is slightly lower in KBS-3H than in 3V. KBS-3V is more sensitive to subhorizontal fracture zones and KBS-3H is more sensitive to subvertical fracture zones. *Section 3.6*
	C4. Deformation of copper canister from external pressure	No specific analysis for KBS-3H. (Treatment in SR-Can: Initial creep due to buffer swelling pressure until gap closed. Otherwise, deformation according to that of cast iron insert considering also creep.)	Not relevant	Handling of shear deformations, see C3. *The handling in the safety assessment for KBS-3H and the handling of uncertainties are also discussed.* *Section 3.6*

Process type	Internal process	Intact canister	Failed canister	Notes/*Section in KBS-3H Process Report*
	C5. Thermal expansion (both cast iron insert and copper canister)	Omitted since the thermal expansion will cause negligible strains in the materials (as in SR-Can).	Not relevant	*Section 3.6*
	C6. Copper deformation from internal corrosion products	Not relevant	No specific analysis for KBS-3H. (Description in SR-Can Main report, integrated with other relevant processes.)	*Section 3.6*
Chemical Processes	C7. Corrosion of cast iron insert	Not relevant	No specific analysis for KBS-3H. (Description in SR-Can Main report, integrated with other relevant processes.)	*Section 3.7*
	C8. Galvanic corrosion	Not relevant	No specific analysis for KBS-3H. Description in SR-Can Main report, integrated with other relevant processes.	*Section 3.7*
	C9. Stress corrosion cracking of cast iron insert	Omitted since stress corrosion cracking is considered unlikely and even if it occurred it would have no consequences for stability of the insert (as in SR-Can).	Not relevant since the canister has already failed.	*Section 3.7*
	C10. Radiation effects	Omitted since its effects on the mechanical and chemical properties of the insert would be negligibly low (as in SR-Can).	Not relevant since the canister has already failed.	*Section 3.7*

Process type	Internal process	Intact canister	Failed canister	Notes/*Section in KBS-3H Process Report*
	C11. Corrosion of copper canister	Specific analysis for KBS-3H: Estimate of enhanced sulphide transport and copper corrosion through buffer altered by iron/ bentonite interactions. (SR-Can: Sulphide in buffer and backfill modelled.) Microbially generated sulphide in buffer neglected if buffer density sufficiently high, otherwise possibly pessimistically modelled as "sulphate corrosion" (strictly a buffer process). Initial oxygen in buffer (strictly a buffer process): Remaining oxygen in buffer pores is consumed by iron minerals and copper. Oxygen in the gap between the supercontainer and rock is consumed by the steel and microbial processes. Potentially intruding oxygen: Integrated handling of rock and buffer conditions. Pitting (oxygen corrosion): Described as uneven general corrosion. Nitric acid corrosion: Omitted since only negligible quantities will be produced. Chloride corrosion: Omitted since it requires very low pH and high temperatures to proceed under reducing conditions.	Not relevant since the canister has already failed.	At Olkiluoto the sulphate rich groundwater coming in contact with the deep-seated methane saline waters might give rise to relatively high levels of sulphide close to the repository. Recent model calculations indicate that the sulphate rich brackish waters are very likely at repository depth within 1,000´s of years. This is, however, not specific to KBS-3H, but is described in the KBS-3V Evolution Report /Pastina and Hellä 2006/. After emplacement, there are similar amounts of oxygen present in the pores of the buffer in KBS-3V and 3H. *Section 3.7*
	C12. Stress corrosion cracking, copper canister	Negligible if concentrations of SCC promoting agents (e.g. nitrite, ammonia, acetate, etc) are sufficiently low. (SR-Can: Omitted due to the combined effect of very low, if any, concentrations of SCC promoting agents and the insufficient availability of oxidants.)	Not relevant since the canister has already failed.	Small amounts of nitrite and ammonia could result from human activity during construction (residual materials /Hagros 2007b, Pastina and Hellä 2006/. *Section 3.7*
	C13. Earth currents – Stray current corrosion	Omitted due to e.g. the high polarisation resistance of copper under reducing conditions (as in SR-Can).	Not relevant since the canister has already failed.	*Section 3.7*
	C14. Deposition of salts on canister surface	Process exists, but consequences negligible (as in SR-Can).	Not relevant since the canister has already failed.	*Section 3.7*
Radionuclide transport-related processes	C15. Radionuclide transport	Not relevant	REPCOM (a compartment model used for radionuclide release and transport calculations).	see F16

3.3 Radiation-related processes

Radiation attenuation/heat generation is the only radiation-related process relevant to the canister. The inter-dependence between this process and the variables in the cast iron insert and copper canister is shown in Table 3-5.

3.3.1 Radiation attenuation/heat generation

The decay heat estimates for Finnish spent nuclear fuels are presented in /Raiko and Salo 1999/, the radiation shielding calculations are presented in /Anttila 1998/ and the criticality safety calculations are presented in /Anttila 1999/. Thermal effects are evaluated in the Section 3.4. There are no additional comments to the discussions in the relevant Process Reports for KBS-3V /Rasilainen 2004, SKB 2006c/. The handling of these processes in the KBS-3H safety studies is summarized in Table 3-4.

Handling in the safety assessment for KBS-3H

Prior to canister failure, the process is considered in the thermal modelling (see Section 3.4). In the case of a defective canister, the process is neglected provided the radionuclide releases occur after the period of elevated temperatures.

3.4 Thermal processes

Heat transport is the only thermal process relevant to the canister. The inter-dependence between this process and the variables in the cast iron insert and copper canister is shown in Table 3-6. The absolute temperature in the canister will be affected by the entire heat transport pathway from fuel through the engineered and geological barriers into the biosphere, the latter being the ultimate heat sink of the system. Thermal processes in the subsystem cast iron insert and copper canister do not depend significantly on the specific conditions in KBS-3H (identical fuel and canister as in KBS-3V).

Table 3-5. The inter-dependence of radiation-related processes and identified variables in the cast iron insert and copper canister.

Radiation-related processes	Variables in cast iron insert and copper canister				
	Radiation intensity	Temperature	Canister geometry	Material composition	Stress state
Radiation attenuation/heat generation	×	×	×	×	

Table 3-6. The inter-dependence of thermal processes and identified variables in the cast iron insert and copper canister.

Thermal processes	Variables in cast iron insert and copper canister				
	Radiation intensity	Temperature	Canister geometry	Material composition	Stress state
Heat transport		×	×	×	×

Differences arise only due to the specific geometry and conditions outside the canister. As concluded by /Ikonen 2003/ based on model studies, the overall thermal evolution in KBS-3V and 3H are very similar. The details of these model studies are discussed in the context of the buffer and distance block, see Section 4.4. As discussed in SR-Can Fuel and Canister Process Report /SKB 2006c/, radiation intensity has no impact on heat transport.

3.5 Hydraulic processes

The specifics of hydraulic processes within the canister due to gas generation are discussed in the context of the subsystem fuel /cavity inside canister (see Section 2.5). The handling of these processes in the KBS-3H safety studies is summarized in Table 3-4.

3.6 Mechanical processes

An overview of mechanical processes in the subsystem cast iron insert and copper canister is shown in Table 3-7. The deformation of canister cast iron insert and copper canister by external loads depends on the relative orientation of the canister in the stress field. For this reason, some differences are expected between the behaviour in KBS-3V and KBS-3H. All other processes do not significantly depend on the specific conditions in KBS-3H. Therefore, no additional comments to the discussions in the relevant Process Reports for KBS-3V are presented for these processes /Rasilainen 2004, SKB 2006c/. The handling of these processes in the KBS-3H safety studies is summarized in Table 3-4.

3.6.1 Deformation of cast iron insert and of copper canister from external pressures

Overview/general description

During the saturation and swelling of the bentonite buffer, the mechanical load on the canister is expected to be uneven. The impact of these uneven loads on the canister or the weld has been demonstrated to be negligible already in earlier studies of KBS-3V /SKB 1999/ and in light of more recent experimental and modelling results as reported in Posiva's canister design report /Raiko 2005/ as well as according to SKB's recent weld test results reported in the FUD programme description /SKB 2007/.

Table 3-7. The inter-dependence of mechanical processes and identified variables in the cast iron insert and copper canister.

Mechanical processes	Variables in cast iron insert and copper canister				
	Radiation intensity	Temperature	Canister geometry	Material composition	Stress state
Deformation of cast iron insert		×	×	×	×
Deformation of copper canister from external pressure		×	×	×	×
Thermal expansion (both cast iron insert and copper canister)		×	×	×	×
Deformation from internal corrosion products			×	×	×
Radiation effects	×	×		×	

Posiva's canister design report /Raiko 2005/ contains a number of conservatively selected load cases that describe the load conditions caused by non-uniform wetting. The iron insert is shown to be strong enough to withstand the postulated loads. The swelling pressure causes displacement-controlled load that, in turn, causes secondary stresses. Secondary stresses are not expected to compromise canister integrity, because, even in case of yielding, the strains do not increase significantly. Furthermore, the secondary stresses will decrease and eventually vanish due to elastic and plastic deformation.

According to the strength analyses in the canister design report /Raiko 2005/, the strains in the cast iron insert are usually low in all cases considered. They are usually elastic, but some plastic deformation is also observed in the highest strain cases. The elastic modulus of copper is only half of that of iron. Thus, the stresses in the copper liner around the iron insert are only about half the stresses in iron. The plastic ductility of copper is much higher than that of iron. Therefore, there is no risk for copper cracking or tearing in the kinds of load conditions postulated.

As for the voids in copper welds acting as crack initiation nuclei in yielding or creeping condition, the creep tests carried out by SKB on copper weld material yielded to cracking or tearing only under high strain conditions (20–30% in the case of electron beam welding and >40% for friction stir welding) according to /SKB 2007/.

The conclusions for the KBS-3V case are also likely to hold for KBS-3H, although, as discussed in Chapter 4, partially saturated conditions may persist for several hundred to a few thousand years and the time to complete resaturation may be substantially longer (some thousands of years) for the latter in tight drift sections, due to the impact of gas generated by the corrosion of the supercontainers.

Following saturation, the stress on the canister is expected to be approximately isostatic (i.e. equally large over the entire canister surface area) with a value of 11–12 MPa, which is the sum of:

- the groundwater pressure at repository depth – about 4 MPa at a depth of 400 m (or 5 MPa at a depth of 500 m); and
- the swelling pressure of the bentonite – 7 to 8 MPa (affected to some extent by the volume expansion of the supercontainer by corrosion – see Section 4.6.1) and to some degree by variability and uncertainty in groundwater salinity;

The maximum swelling pressure of bentonite can be higher due to the possibility of bentonite redistribution (see Chapter 4). In /SKB 2006c/, a maximal bentonite swelling pressure of 13 MPa is assumed, leading to a maximal load on the canister of 17–18 MPa. The bentonite counteracts part of the in situ rock stress with its swelling pressure. Stresses due to small rock movements (<10 cm) will be largely absorbed by the bentonite.

Glacial loading will affect pore pressure in the rock and in the saturated buffer and the isostatic load exerted on the canisters. As stated earlier, at Olkiluoto the maximum expected isostatic load on the canister in the absence of an ice sheet is about 11–12 MPa. The maximum ice thickness over Olkiluoto is estimated to have been about 2 km during the last glacial maximum /Lambeck et al. 1998/. A 2 km-thick ice sheet will increase the load on the canisters by about 18 MPa and a 3 km thick ice sheet by about 27 MPa (/SKB 1999, Rasilainen 2004/ assuming an average ice density of 900 kg m^{-3}).

The expected minimum pressure giving rise to total collapse of an intact canister is significantly higher than this (80–114 MPa – see, e.g. Section 4.3.1 of /Pastina and Hellä 2006/), so no failure of canisters is expected by this mechanism without prior weakening of the insert by corrosion (which could occur, for example, in the case of a canister with an initial penetrating defect).

A more localised failure may be possible at lower pressures. /Dillström 2005/ has carried out a probabilistic analysis in which two failure modes are considered:

- local plastic collapse of the insert; and
- crack growth from an assumed initial defect in the insert.

The results of the analysis showed that in all cases where crack growth occurred to a significant extent, local plastic collapse occurred at a smaller load. For a base case pressure of 44 MPa, the probability of failure by either mode is insignificant ($\sim 2 \times 10^{-9}$), although the probability of local plastic collapse was found to be strongly dependent on the outer corner radius of the fuel channels and the eccentricity of the steel section cassette. In the base case, it was assumed that the cassette was centred and the outer corner radius was 20 mm.

Creep movements due to the glacial loading are neglected in KBS-3V because the additional stresses are not sufficiently high /SKB 2006e, Rasilainen 2004/. This conclusion is also expected to hold for KBS-3H.

Shear movement on fractures intersecting the deposition drifts may also give rise to mechanical forces on the canisters. There are a number of potential causes for such displacements, including /SKB 2006a/:

- rock excavation in other parts of the repository;
- heat load;
- tectonic seismicity; and
- direct mechanical response to the glacial load (and deglaciation).

Among these, post-glacial earthquakes, which are expected to occur during or shortly after any future deglaciation, have the potential to give rise to the largest displacements and are of greatest concern.

The canisters are protected from damaging shear displacements by:

- avoiding placing canisters in drift sections intersected by fractures that could potentially undergo shear displacements large enough to damage the integrity of the canisters; and
- surrounding the canisters by a plastic bentonite buffer to reduce the shear stresses exerted on the canisters by shear displacements in the rock.

Assuming that the buffer behaves as expected, issues that then arise are:

- how large do shear displacements on fractures have to be to cause damage?
- which are the fractures that could potentially undergo such displacements?
- how does the buffer evolve from a rather virgin, plastic clay to a possibly chemically altered buffer due to the presence of iron, silica precipitation, and residual materials?

Processes that could have a detrimental effect on the mechanical protection of the canisters afforded by the buffer also have to be considered. In particular, protection could potentially be compromised if:

- the maximum buffer density around the canisters increases above about 2,050 kg m^{-3} (safety function indicator, see Section 7.3.2 in /SKB 2006a/);
- the canisters sink through the buffer under their own weight, especially if they come into direct contact with the drift walls; or
- if chemical alteration processes result in a significant reduction in buffer plasticity.

These factors are discussed in more detail in the following sections, with particular emphasis on aspects that have a different significance for, or potential impact on, KBS-3H compared with KBS-3V.

Boundary conditions

The outer boundary conditions are determined by the mechanical properties of the buffer and the rock surrounding the deposition drift, in particular the properties of fractures that may undergo shear displacements in the future.

Model studies/experimental studies

Impact of rock shear on canisters

The impact of rock shear on canisters is influenced by a number of factors, including:

- the magnitude of the shear displacement;
- the rate at which the displacement occurs;
- the location and orientation of the shear plane with respect to the canister; and
- the density and plasticity of the buffer.

Numerical investigations have been carried out by /Börgesson 1992/ to assess how much rock shear can take place without damaging the integrity of canisters surrounded by bentonite buffer. These formed the basis of the 0.1 m failure criterion on rock shear movement used in SR-97 /SKB 1999/. More recently /Börgesson et al. 2004/ performed a series of scale laboratory tests and numerical modelling studies that indicated that this criterion might be conservative, but it is nevertheless retained in ongoing studies by SKB. The studies by /Börgesson et al. 2004/ and /Börgesson and Hernelind 2006b/ also addressed sensitivity to some of the other factors mentioned above, and identified, for example, a strong sensitivity to buffer density and shear plane location.

The various studies, and the resulting failure criterion, make no assumptions regarding vertical or horizontal canister orientation, and should be equally applicable to KBS-3V and KBS-3H.

Fractures that could give rise to damaging rock shear

The amount of shear movement that will actually occur on fractures intersecting the repository drift as a result of future post-glacial earthquakes is uncertain. The potential of a fracture to undergo shear movements is related to its size, as well as its distance from the earthquake, and orientation effects /Munier and Hökmark 2004, Fälth and Hökmark 2006/. The quantification of the size of fractures from observations at the drift wall is, however, subject to significant uncertainties. In the case of KBS-3V, fractures with the potential to undergo shear movements of 0.1 m or greater are of greater concern /SKB 2006a/. The probability that these fractures will, in practice, be detected and avoided has not yet been evaluated but efforts are underway.

An issue for future study is thus the impact of multiple small (< 0.1 m) rock movements on the safety functions of the buffer and canister. It should be noted, however, that the potential of shear displacements to damage a canister is a function not only of the total shear displacement, but also of the shear velocity, with a higher shear velocity being more likely to result in canister damage /Börgesson and Hernelind 2006b/. The average shear velocity in the event of multiple small displacements is likely to be significantly less than in the event of a single displacement of the same magnitude resulting from a single earthquake. The potential to cause canister damage is therefore expected to be less.

Major deformation zones capable of accommodating significant slip should be readily identified and KBS-3H drifts will not be constructed within, or in the immediate vicinity of such zones. An earthquake occurring on a major deformation zone may, however, give rise to stress changes in the rock that trigger the reactivation of smaller-scale fractures that cannot be avoided when constructing the drifts.

Due to the higher stiffness of canisters in the longitudinal direction, shear displacements on reactivated flat (subhorizontal) fractures across the deposition holes are most relevant for KBS-3V, whereas in KBS-3H canisters are likely to be more vulnerable to shear displacements on steep (subvertical) fractures perpendicular to the axis of the deposition drift. In principle, if its size and the shear movement it underwent were sufficiently large, a single subhorizontal fracture could affect multiple KBS-3H canisters (Figure 3-3). It is, however, considered likely that any such fracture would be readily detected and that portion of the drift affected by it would be excluded for canister emplacement. Thus, the main concern for KBS-3H remains movement on subvertical fractures.

The amount of movement on such fractures is a function of a number of factors including:

- the change on shear stress acting on the plane of the deformation zone on which the earthquake occurs;
- the distance of the reactivated fracture from the epicentre of the earthquake;
- size and orientation of the reactivated fractures;
- the density of reactivated fractures; and
- friction on the fracture surfaces.

For a discussion of these factors, see Section 7.6.2. For the fracture conditions at Olkiluoto it is likely to be impossible to locate deposition drifts free of fractures having the possibility of shear displacements greater than 0.1 m. This is not a problem as long as these fractures do not intersect any canisters. The potential impact of such displacements on distance blocks or sealed drift sections between compartments, however, is shown to be limited (see Section 4.6.1).

Effects of buffer density variations

Studies reported in /Börgesson et al. 2004/ indicate that buffer density is a sensitive parameter in determining the impact of a given rock shear movement on the canister, with higher buffer densities affording less protection of the canisters (see e.g. Figure 6.2 in /Börgesson et al. 2004/).

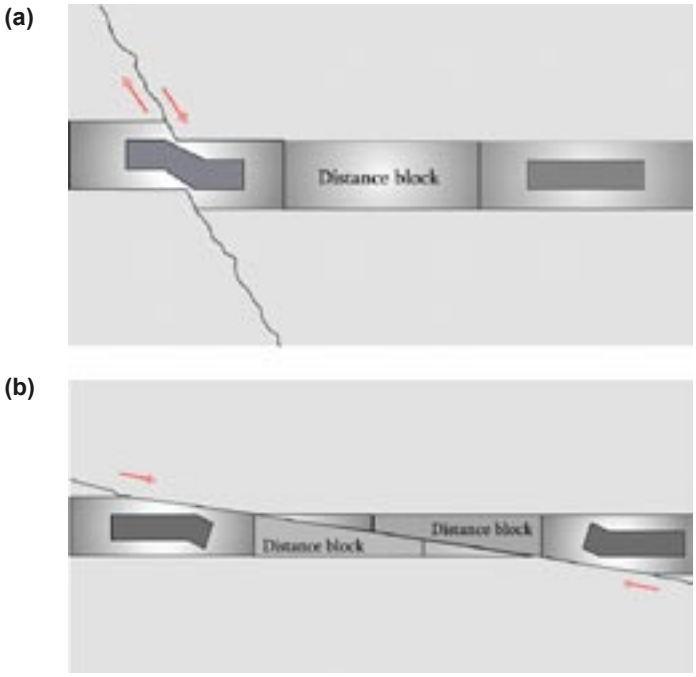

Figure 3-3. *Shear displacements on (a), a subvertical and (b), a subhorizontal fracture intersecting a KBS-3H drift.*

A criterion for buffer density has been derived that (assuming no loss of buffer plasticity due to chemical effects – see below) should ensure protection of the canisters in the case of rock shear displacements of less than 0.1 m. This criterion is that the buffer density should not exceed 2,050 kg m^{-3}.

Processes with a different significance for, or potential impact on, KBS-3H compared with KBS-3V that could give rise to increases in buffer density over time are discussed in Section 4.6.1. These include:

- Axial displacements of distance blocks and supercontainers caused by differential saturation and swelling along the deposition drift. Depending on the nature and rates of changes of the mechanical stresses, displacements may occur in line with the relatively slow swelling process, or in a more abrupt manner due to hydraulic forces leading to the abrupt sliding of entire supercontainer units.
- Piping along the bentonite/rock interface, which may occur if the inflow rate from the rock exceeds 0.1 litres min–1, the pressure increases at rates above 0.1 MPa hour–1 and the total applied pressure difference between "less tight" and "tighter"[15] units is above 2 MPa. This may lead to significant water flows between "less tight" and "tight" supercontainer units that cause erosion of bentonite in some parts of the drift and possibly deposition (an increase in buffer density) in others.
- Bentonite compaction due to volume changes by formation of steel corrosion products (mainly magnetite, but also some iron sulphide and siderite).

The scoping calculations presented in Section 4.6.1 indicate that only corrosion of the canister insert in a defective canister would lead to the density criterion being slightly exceeded. Assuming pessimistically that only the buffer originally inside the supercontainer and the void space inside the canister take up the increased volume, and that the insert is completely converted to magnetite, a scoping calculation in Appendix B.4 of the KBS-3H Evolution Report /Smith et al. 2007c/ indicates an increase in buffer density around the canister to 2,160 kg m^{-3}. This does not satisfy the criteria for the safety function indicators for the buffer, which give a maximum buffer density of 2,050 kg m^{-3} (Table 2-3 in the 3H Evolution Report). The calculation is, however, conservative. In reality, there is likely to be some relaxation of the increased density by buffer creep along the drift, although internal friction will mean that some locally increased density around the failed canister is likely to remain.

Canister sinking

The canister would be more vulnerable to mechanical damage by rock shear or other rock displacements if it were to sink through the buffer under its own weight, especially if it were to come into direct contact with the drift wall because of the advective flow that would be generated. The possibility of canister sinking through the buffer is discussed in the context of KBS-3V in /Börgesson and Hernelind 2006a/, where it is argued to lead to insignificant vertical displacements of the canister. For a given buffer density, if canister sinking is of little concern for KBS-3V, then it is even less a concern for KBS-3H, since the pressure exerted by the KBS-3H canister on the bentonite that supports it is less than in the case of KBS-3V due to the weight of the KBS-3H canister being distributed over a larger horizontal area. Canister sinking could conceivably occur if there was a significant decrease in buffer density. The scoping calculations described in Section 4.6.1, however, indicate that none of the identified processes that have a different significance for, or potential impact on, KBS-3H compared with KBS-3V have the potential to cause a significant buffer density decrease.

[15] The expressions "less tight" and "tight" drift sections stand for drift sections in which the hydraulic conductivity (K) of the surrounding rock is greater or smaller than about 10^{-12} m s^{-1}, respectively (see Section 4.5.1).

Effects of chemical perturbations on buffer plasticity

The plasticity of the bentonite buffer provides mechanical protection to the canisters. If there is some loss of plasticity, either through an increase in density (above) or through long-term mineralogical change, then this protection could potentially be compromised. The supercontainers used in KBS-3H will corrode over a period of several thousand years. In the still longer term, these corrosion products will interact with the bentonite buffer, and may convert smectite into non-swelling clays. A simple mass balance estimate presented in Section 4.7 indicates that substantial amounts of montmorillonite (10–30%) would be transformed if all the iron from the SC would react with it and produce a non-swelling Fe clay. The process is expected to be slow, and more realistic reactive transport calculations show that the outermost few cm could be changed to a non-swelling clay within some hundreds of thousands of years /Wersin et al. 2007/.

If the conversion to non-swelling clay results in a significant change in the overall plasticity of the bentonite buffer and a significant proportion of the buffer is affected, then the 0.1 m failure criterion for shear movement discussed above may no longer be conservative in the long term (more than 10^5 years, say) and may need to be revised. Although this is not expected, the evolution of the buffer including drying/wetting, impact of Fe-saturation, silica precipitation and the inhomogeneity of bentonite at the buffer/rock interface caused by the rupture and subsequent deformation of the supercontainer shell needs thorough investigation.

Natural analogues/observations in nature

Not applicable.

Time perspective

The initial transient phase of bentonite saturation and swelling may last up to several thousand years in “tight” drift sections, but will be substantially faster in drift sections intersected by transmissive fractures. During this period, the mechanical load on the canisters is expected to be uneven, but does not have the potential to compromise canister integrity.

Following saturation, the load on the canister is expected to be approximately isostatic. This isostatic load may be increased during glacial periods, but will remain well below the isostatic load required to cause collapse.

Small shear displacements on fractures intersecting the deposition drifts may occur at any time, but the most significant displacements are likely to be those due to post-glacial earthquakes occurring during or shortly after any future glaciation (at least 70,000 years AP, according to the Weichselian-R scenario, see the Evolution Report /Smith et al. 2007c/.

Handling in the safety assessment for KBS-3H

The canisters are protected from damaging shear displacements by:

1. Avoiding placing canisters in drift sections intersected by fractures that could potentially undergo shear displacements large enough to damage the integrity of the canisters.
2. Surrounding the canisters by a plastic bentonite buffer to reduce the shear stresses exerted on the canisters by shear displacements in the rock.

Shearing of fractures in the rock is one of the basic mechanisms that lead to canister failure. This process is treated in the same way as in SR-Can.

The protection afforded by the buffer could potentially be compromised if its density were to rise above 2,050 kg m^{-3}. Scoping calculations, however, indicate that only one process, that of corrosion of the canister insert in a canister with a defect and the associated volume increase, would lead to the density criterion being slightly exceeded after a very long time.

The calculation is, however, conservative and the consequence may be some damage to the rock, which is addressed implicitly in KBS-3H Radionuclide Transport Report by defining a rock shear base case assessment case (RS-BC) and a rock shear in presence of glacial meltwater[16] (RS-GMW) /Smith et al. 2007a/.

Canister sinking through the bentonite is also expected to be insignificant. The effects of buffer density increases and of the sinking of the canister can probably be neglected on the basis of the information presented above and in SR-Can.

The impact of very long-term (some hundreds of thousands of years) mineralogical changes in the bentonite on buffer plasticity due to interactions with supercontainer corrosion products still, however, requires further investigation.

Handling of uncertainties

The mechanical behaviour of a canister and the processes possibly leading to subsequent radionuclide release are complex and depend on a number of uncertain factors. The major uncertainties are:

- the magnitudes and rates of shear displacements occurring at Olkiluoto in the far future;
- the location and orientation of the shear plane with respect to the canister;
- the factors affecting the density and plasticity of the buffer;
- whether potentially damaging fractures can be detected and avoided.

The effects of these uncertainties on the safety functions of the system are taken into account considering the relevant safety function indicators for the buffer and rock (minimal and maximal values for the saturated density, maximal shear displacements in fractures intersecting the deposition drift at the position of a supercontainer, a distance block or filling block between two compartment plugs).

Work on the identification of large fracture zones at Olkiluoto is progressing. Despite these investigations, there will always be some residual uncertainty on the existence of undetected fracture zones that may undergo substantial shear during or after a future glaciation at Olkiluoto and the existence of undetected fracture zones where secondary displacements could take place. However, given the detailed geological modelling and the ability to map the deposition drifts before emplacement, the uncertainty regarding the presence of such fracture zones can be reduced to an acceptable level.

3.7 Chemical processes

An overview of chemical processes in the subsystem “cast iron insert and copper canister” is shown in Table 3-8. None of these processes is considered to significantly depend on the specific conditions in KBS-3H.

The rate of copper corrosion depends, among other factors, on the amount of oxygen and sulphide available for chemical reactions at the canister surface. After emplacement, there are similar amounts of oxygen present in the pores of the buffer in KBS-3V and -3H. However, due to the larger amounts of iron in KBS-3H, the initial oxygen will be consumed in a shorter time. At Olkiluoto, the sulphate-rich groundwater coming in contact with the deep-seated methane saline waters might give rise to relatively high levels of sulphide close to the repository. In addition to methane also the corrosion-derived hydrogen can be used by the sulphate reducing bacteria to produce sulphide. Recent model calculations indicate that the sulphate-rich brackish waters are very likely at repository depth within thousands of years.

[16] Glacial meltwater is a very dilute ice-melting water. Saline groundwater represents a water with a salinity, expressed as Total Dissolved Solids of about 20 g/l. For detailed composition of the waters used in the assessment, see Appendix D of Radionuclide Transport report.

The Fe/bentonite interaction may affect the rate of transfer of sulphide to the canister surface, and hence the rate of Cu corrosion /Wersin et al. 2007/ – see process C11 in Table 3.4. The potential impact on canister lifetime has been modelled in Appendix B of the KBS-3H Evolution Report /Smith et al. 2007c/.

Stress-corrosion cracking of copper is negligible if concentrations of SCC promoting agents (e.g. nitrogen oxides, ammonia, or certain organic compounds such as acetate) are sufficiently low and the tensile stress is below the SCC critical threshold. Small amounts of nitrogen oxides and ammonia could result from human activity during construction /Hagros 2007b/.

These aspects are, however, not specific to KBS-3H, and have been described in detail in the framework of the KBS-3V Evolution Report /Pastina and Hellä 2006/. There are no other additions or comments to the discussions in the relevant Process Reports for KBS-3V /Rasilainen 2004, SKB 2006c/. The handling of these processes in the KBS-3H safety studies is summarized in Table 3-4.

Time perspective

The copper canister will experience aerobic corrosion during the short oxic stage (a few hundred years, pessimistically). Afterwards corrosion will be very slow and canister lifetimes are expected to exceed 100,000 years /e.g. King et al. 2001/2002/.

Handling in the safety assessment for KBS-3H

The treatment of the various chemical processes in the KBS-3H safety assessment is summarized in Table 3-4. To address the uncertainties on copper corrosion due to the evolution of groundwater conditions and geosphere transport resistance discussed in the 3H Evolution Report /Smith et al. 2007c/, the following cases have been calculated in the Radionuclide Transport Report:

- CC-BC: base case for canister failure due to copper corrosion,
- CC-GMW: glacial meltwater present at repository depth,
- CC-LOGEOR: reduced geosphere transport resistance,
- CC-LOGEORG: reduced geosphere transport resistance, glacial meltwater
- CC-LOGEORS: reduced geosphere transport resistance, saline groundwater.[17]

Table 3-8. The inter-dependence of chemical processes and identified variables in the cast iron insert and copper canister.

Chemical processes	Variables in cast iron insert and copper canister				
	Radiation intensity	Temperature	Canister geometry	Material composition	Stress state
Corrosion of cast iron insert	×	×		×	×
Galvanic corrosion		×	×	×	
Stress corrosion cracking of cast iron insert	×	×		×	×
Corrosion of copper canister		×	×	×	
Stress corrosion cracking of copper canister		×		×	×
Earth currents – stray current corrosion			×	×	
Deposition of salts on canister surface		×		×	

[17] This case was selected because there is potential for local increase in the salinity at repository depth (for further details see /Smith et al. 2007a/).

Handling of uncertainties

Uncertainties in the geochemical conditions present at various times in the repository are addressed by various calculation cases in the Radionuclide Transport Report (see Appendix G).

3.8 Radionuclide transport processes

The specifics of radionuclide transport processes within the canister are discussed in the context of the subsystem fuel/cavity inside the canister (see Section 2.8). The handling of these processes in the KBS-3H safety studies is summarized in Table 3-4.

Radionuclide transport in the buffer outside the canister may be affected by the iron from the cast iron insert as Fe(II) generated by corrosion of the insert sorbs strongly onto the clay surface. This may compete with that of other radionuclides, e.g. Ni (II) and Sr(II). The process is also mentioned in Section 5.8 as it is similar to the supercontainer iron effect on the buffer. Although the iron corrosion products formed act as an efficient sink for many radionuclides (in particular for redox sensitive ones, such as uranium or selenium), the ultimate fate of the sorbed radionuclide is unknown as they could be released at a later time in the geosphere should the geochemical conditions change. This issue is also relevant to KBS-3V and requires further work.

Handling in the safety assessment for KBS-3H

In the Radionuclide Transport Report /Smith et al. 2007a/, an initially penetrated canister is the scenario with most variants because it is useful in illustrating the impact of a range of uncertainties affecting release and transport processes in the event of canister failure, whatever the cause or the timing of canister failure. Posiva is not yet taking any position on the likelihood of occurrence of canisters with initial penetrating defects. In SR-Can, although no initial penetrating defects are expected, evolution in case of a growing pinhole failure is described and its consequences evaluated (Section 10.5 of /SKB 2006a/). Therefore, in the present report, the processes due to the presence of a hypothetical initial penetrating defect are also considered.

The Radionuclide Transport report /Smith et al. 2007a/ considers the scenario of a hypothetical defective canister in the following assessment cases:

- Base case (PD-BC).
- Increase of defect size (PD-BIGHOLE).
- Increased/decreased delay until loss of defect transport resistance compared with base case (PD-HIDELAY and PD-LODELAY).
- Increased defect size plus decreased delay until loss of defect transport resistance (PD-BHLD).

For additional information about the scenarios, see Appendix G and the Radionuclide Transport Report /Smith et al. 2007a/.

4 Buffer and other bentonite components

4.1 Description of buffer and other bentonite components

The following description of processes for the buffer and other bentonite components in the reference design for the KBS-3H /Autio et al. 2007/ is based on information presented in the KBS-3V process reports for SR-Can /SKB 2006d/ and Posiva /Rasilainen 2004/ and in the KBS-3V Evolution Report /Pastina and Hellä 2006/.

4.1.1 General

In KBS-3H, each canister, with its surrounding bentonite buffer, is placed in a steel supercontainer prior to emplacement (Figure 1-7). The supercontainers are emplaced coaxially in the drifts, supported on steel feet to leave a ca 4 cm annular gap to the drift wall, and are hydraulically separated from each other by bentonite distance blocks (also considered to be part of the buffer). A section of drift with two supercontainers and one distance block is shown in Figure 1-4. The distance block for the Basic Design is composed of two different bentonite components in series: a "tight" block and a "loose" block as shown in Figure 1-8. Filling blocks of bentonite are also emplaced in drift locations (Figure 1-9) where inflow may exceed 0.1 l/min, adjacent to steel compartment plugs (Figure 1-12) and adjacent to the end plug in the drift (Figure 1-5). These do not have a long-term safety function; therefore, they are not considered part of the buffer.

In addition to the above-mentioned Basic Design (BD) alternative, a second alternative, the Drainage, Artificial Watering and Air Evacuation (DAWE) design variant, is under consideration (see Appendix D). A more detailed description of features and properties of the Basic Design and the DAWE Design can be found in /Autio 2007/ and /Autio et al. 2007/. The focus of this chapter is on the Basic Design but main differences with the DAWE alternative are also mentioned.

The buffer inside the supercontainer consists of highly compacted MX-80 bentonite rings emplaced around the canister and end blocks placed on either side of the canister. The dimensions and densities of the blocks are fixed in such a way as to yield a density after saturation and homogenisation of 2,000 kg/m^3 (with an uncertainty range of 1,950–2,050 kg/m^3). The rings and end blocks have a design diameter of 1,739 mm (whereas the diameter of the deposition drift is approx. 1,850 mm) and a length of 4 × 1,202.5 mm and 2 × 350 mm, respectively, for the canister with the reference fuel OL 1-2. The radial gaps to the canister and the supercontainer are approx. 5 mm.

The initial physical properties of the buffer are presented in Table 4-1. At the initial water content of 10%w there is initially a very high suction (negative pressure) of about –70 MPa (/SKB 2006d/, p. 39), corresponding to the relative humidity (RH) of the air in equilibrium with the bentonite. The density of clay solids is 2,750 kg/m^3. The porosity of the saturated buffer with a saturated density of 1,950–2,050 kg/m^3 is thus approx. 41–47%. The list of input data concerning the buffer and other bentonite components is in Appendix A.

Table 4-1. Initial physical properties of MX-80 buffer in the KBS-3H Basic Design. (For references, see also Table A-1.)

Parameter	Unit	Basic Design
Material	–	MX-80
Buffer dimensions: - Ring blocks - End blocks	mm	 1,739 (diameter); 4 × 1,202.5 (length)* 1,739 (diameter); 2 × 350 (length)
Distance block dimensions ("tight"/"loose" component)	mm	 1,850/1,820 (diameter); 5,475 (total length)
Initial water content (w) of the distance blocks (weight of water divided by weight of dry mass)	w-%	24
Initial dry density ("tight"/"loose" component)	kg m^{-3}	 1,559/1,610
Saturated density	kg m^{-3}	2,000 (1,950–2,050)
Saturated porosity (volume of water/total volume)	%	44

* Length of the blocks for the canister with spent fuel from OL 1-2.

Mineralogy and porewater composition

The reference buffer material for the bentonite in the supercontainers and distance blocks as well as for other bentonite components in the drift is highly compacted Na-rich MX-80 bentonite clay. Under saturated conditions the main fraction of the interstitial water is "bound" water occurring in the interlayers and at the outer surfaces of the smectite and only a small fraction is "free", i.e. not affected by the clay surface charge. The thermodynamic properties of this porewater, being thus strongly affected by the electric double layer of the negatively charged clay particles, are not fully understood.

Nevertheless, simple thermodynamic models (that largely ignore these effects) appear to describe the porewater composition adequately. This has been shown for example by modelling of bentonite – water interaction experiments performed by /Muurinen and Lehikoinen 1999/, which covered a large range of solid/liquid ratios. In fact, a modelling exercise performed by /Curti and Wersin 2002, Wersin 2003/ revealed that experimental data could be simulated by conventional ion exchange and surface complexation models /Wanner et al. 1994, Bradbury and Baeyens 1997/. Furthermore, as shown by geochemical modelling, a high acid – base buffering capacity of compacted bentonite results from the high cation exchange and proton exchange capacity and the presence of calcite.

As a consequence, the bentonite porewater chemistry is expected to remain fairly stable over long time periods under the expected conditions of relatively slow exchange of solutes with groundwater from the host rock. The main change will be induced by the exchange of Ca for Na at the clay exchanger /Wanner et al. 1992, Bruno et al. 1999/. Irreversible processes caused by temperature gradients, such as illite formation or cementation, which would reduce the swelling capacity, are expected to be insignificant below 100°C /e.g. Karnland and Birgersson 2006/. However, these are treated as a variant in the Radionuclide Transport Report addressing uncertainties in the performance of bentonite /Smith et al. 2007a/.

Similarly to SR-Can, Posiva will evaluate the evolution of the repository using two reference materials for the bentonite buffer, although not in the present KBS-3H safety studies: a natural sodium bentonite from Wyoming, United States, (MX-80), and a natural calcium bentonite from the Greek island of Milos (Deponit CA-N). An important difference between the two bentonites is the relatively large content of calcite in the Milos bentonite and larger amount of pyrite in the Milos bentonite (Table 4-2).

Table 4-2. Composition of the reference bentonite MX-80 used in this study. For comparison also the composition of Deponit CA-N bentonite, the alternative bentonite under consideration, has been included. From Table 1-2 in /SKB 2006d/. Values in weight-%, unless otherwise specified.

Component	MX-80 (wt-%)	Deponit CA-N (wt-%)	Uncertainty (± wt-%)
Calcite + Siderite	0	10	1
Quartz	3	1	0.5
Cristobalite	2	1	0.5
Pyrite	0.07	0.5	0.05
Mica	4	0	1
Gypsum + anhydrite	0.7	1.8	0.2
Albite	3	0	1
Dolomite	0	3	1
Montmorillonite	87	81	3
Na^+	72%	24%	5% units
Ca^{2+}	18%	46%	5% units
Mg^{2+}	8%	29%	5% units
K^+	2%	2%	1% units
Anorthoclase	0	2	1
CEC[1)] (meq/100 g)	75	70	2

[1)] Cation exchange capacity.

The structural formula of the montmorillonite component in MX-80 is:

$(Si_{7.86}Al_{0.14})\ (Al_{3.11}Fe^{3+}_{0.37}Mg_{0.50}Ti_{0.01})\ O_{20}(OH)_4,\ Na_{0.47}Ca_{0.05}Mg_{0.02}K_{0.01}$

and in Deponit CA-N is:

$(Si_{7.74}Al_{0.26})\ (Al_{2.90}Fe^{3+}_{0.44}Mg_{0.58}Ti_{0.08})\ O_{20}(OH)_4,\ Na_{0.18}Ca_{0.17}Mg_{0.11}K_{0.02}$

Table 4-3 shows the porewater composition for MX-80 bentonite equilibrated with the two reference groundwaters and the two alternative waters from Olkiluoto given in Chapter 7 (Table 7-1). The conventional model of / Baeyens and Bradbury 1997/, as applied by /Curti and Wersin 2002/, under the constraint of constant pCO_2 was used in this case. The assumption that pCO_2 is constrained by the rock is justified if long-term conditions are considered, because diffusion of dissolved CO_2 in bentonite is fast relative to the timescales of interest (> 10,000 years).

The results indicate that, due to cation exchange and dissolution of calcite and gypsum, some changes in composition of the buffer porewater relative to the groundwater will occur. The changes are obviously greatest in the case of the bentonite contacting the “dilute” groundwater where the equilibrium with the ion exchanger will lead to increased cation concentrations. It is important to note, however, that because of strong buffering of the clay surface and the presence of calcite, the pH conditions will remain remarkably stable. The main change predicted for long timescales is enrichment of Ca relative to Na on the exchanger.

Table 4-3. Calculated bentonite (MX-80) porewater composition for different Olkiluoto groundwater compositions. From /Wersin et al. 2007/. Concentrations in mmol l^{-1}, unless otherwise indicated.

	Reference waters Brackish type	Saline type	Limiting Saline water	Limiting Dilute water
Solution composition				
Ionic strength (meq l^{-1})	315	507	1,169	220
pH	7.82	7.66	8.03	7.39
Alkalinity	0.52	0.40	0.072	2.50
SO_4	34.9	22.6	11.9	74.2
Cl	185	386	924	15.1
Na	271	384	645	167
K	0.85	1.24	2.3	0.53
Ca	20.8	42.9	167	10.4
Mg	6.32	10.9	24.9	1.1
Surface species				
NaX	1,990	1,980	1,890	1,990
CaX2	249	247	324	248
MgX2	69.3	63.8	49.8	70.3
KX	23.4	23.0	22.1	23.5
SOH	221	234	203	250
SO^-	68.2	54.4	86.1	35.4
SOH_2^+	2.14	3.12	1.3	5.68
Eh calculation				
Fe	2.3E–3	4.2E–3	4E–03	0.04
S^{2-}tot	5.3E–3	4.8E–3	1.3E–03	–
Eh (mV)	–171 Fe_3O_4/FeS	–160 Fe_3O_4/FeS	–280 Fe_3O_4/FeS	–202 Fe_3O_4/$FeCO_3$

Redox conditions

Wyoming bentonite generally contains Fe(II) mineral impurities, such as pyrite and siderite /Müller Von-Moos and Kahr 1983/. In addition, traces of iron oxides /Baeyens and Bradbury 1997/ are present. Because of the variability in bentonite composition and possible oxidation of Fe^{2+} during processing of the raw material, the relative amounts of reactive iron phases may vary considerably. Moreover, the smectite fraction in MX-80 typically contains about 2 wt% of structural iron, most of which is Fe(III) /Vogt and Köster 1978/.

The redox conditions in the near field will change from oxic to anoxic after repository closure. Large-scale tests to evaluate oxygen consumption in bentonite have been carried out in the framework of the LOT project /Muurinen 2006/ for KBS-3V. Although there are significant uncertainties and variability between different locations within the repository, the large-scale tests indicate that the timescale for oxygen depletion from individual KBS-3V deposition holes is no more than a few hundred years at most, and could be as little as a few years /Muurinen 2006/.

Based on the discussion in Section 5.7.1, since the presence of the steel supercontainer and other steel components in KBS-3H provides an additional sink for oxygen depletion in addition to those present in and around a KBS-3V deposition hole, the timescale for initial oxygen depletion will certainly be no higher in KBS-3H than in KBS-3V (a few years to, pessimistically, a few hundred years), and could be somewhat less. Because the depletion timescale is likely to be controlled by the transport time of oxygen within the buffer rather than by reaction rates, any differences are likely to be quite limited, but they have not so far been possible to quantify.

Compacted bentonite acts as an efficient filter towards microbes. As shown by /Pusch 1999/ sulphate-reducing bacteria (SRB) are immobile in bentonite exceeding 1.9 Mg m^{-3} saturated density. Moreover, experiments performed by Pedersen /e.g. Pedersen 2000/ showed that the activity of SRB in bentonite ceases at densities higher than 1.5 Mg m^{-3}. Recent studies indicate that bacterial activity will be suppressed, and both cultivatability and viability will decrease, at swelling pressures exceeding 2 MPa /Stroes-Gascoyne et al. 2006, Masurat 2006/. It is likely that microbes are barely active under these conditions (although this is an issue that is still under investigation). Below about 2 MPa, however, significant microbial activity cannot be excluded. Studies performed by /JNC 2000/ confirmed that SRB introduced into compacted bentonite surrounding steel samples had no effect on corrosion rates and were not cultivatable after the test. In SR-Can, a minimal swelling pressure of 2 MPa is considered sufficient to exclude significant microbial activity in the buffer (see also safety function indicator criteria in Table 4-5). As a consequence, it is not expected that microbially mediated sulphate reduction will occur in the main part of the buffer away from the rock wall. However, due to reduced density in the buffer region between the supercontainer and rock wall, and also the possible contact of the supercontainer and its corrosion products with the drift wall, microbial activity at or near the interface with the rock cannot be excluded.

4.1.2 Overview of variables

The geometry of the buffer is described in Section 4.1.1. The buffer is characterised thermally by the temperature field and with respect to radiation by the radiation intensity, mainly γ and neutron radiation. The hydraulic state is determined by the saturation (content), pressure and flows of water and gas. Mechanically, the buffer is characterised by its mechanical state.

The chemical state of the buffer is characterised by the composition of bentonite, which includes montmorillonite and impurities. It is also defined by the porewater composition and by the possible existence of structural and residual materials.

The variables for the buffer are summarised in Table 4-4.

Table 4-4. Variables for the buffer.

Variable	Explanation
Geometry	Geometric dimensions for the buffer. A description of e.g. interfaces to other system components.
Pore geometry	Pore geometry as a function of time and space in the buffer. The porosity, i.e. the fraction of the volume that is not occupied by solid material is given.
Radiation intensity	Intensity of α-, β-, γ-, and neutron radiation as a function of time and space in the buffer.
Temperature	Temperature as a function of time and space in the buffer.
Water content	Water content as a function of time and space in the buffer.
Gas content	Gas contents (including any radionuclides) as a function of time and space in the buffer.
Hydrovariables	Flows and pressures of water and gas as a function of time and space in the buffer.
Stress state	Stress conditions as a function of time and space in the buffer.
Bentonite composition	Mineralogical/chemical composition of the bentonite (including any radionuclides) in time and space in buffer. Levels of impurities in time and space. Impurities also include minerals, other than montmorillonite.
Montmorillonite composition	Mineralogical composition and structure of the montmorillonite mineral in the bentonite. This variable also includes the charge compensating cations attached to the montmorillonite surface.
Porewater composition	Composition of porewater (including any radionuclides and dissolved gases) in time and space in the buffer.
Structural and residual materials	Chemical composition and quantity of structural and residual materials.

4.1.3 Safety function indicators

Three broad modes can be envisaged by which a bentonite buffer could conceivably cease to perform its safety functions fully: loss or redistribution of buffer mass, mineral alteration of the buffer, freezing of the buffer.

1. Loss or redistribution of buffer mass

The loss or redistribution of buffer mass due, for example, to piping and erosion by flowing water could in principle lead to:

- a loss of swelling pressure at the drift wall, which could, if sufficiently large, lead to a loss of tightness of the contact between the buffer and the rock, and, in turn, enhance the transfer of mass (dissolved corrosive agents – especially sulphide – and radionuclides) between the rock and the buffer and thus compromise or reduce the ability of the buffer to perform any of its three safety functions;
- a loss of swelling pressure at the drift wall, could also lead to enhanced thermal spalling due to reduction in confining pressure associated with time-dependent degradation of rock strength;
- a more general loss of swelling pressure, which could, if sufficiently large, lead to microbial activity within the buffer, potentially increasing the rate of canister corrosion by reducing dissolved sulphate to sulphide, and, for still larger losses in swelling pressure, the possibility of canister sinking;
- an increase in buffer hydraulic conductivity, which, if sufficiently high, could lead to advective transport of dissolved corrosive agents and radionuclides in the buffer and hence compromise the ability of the buffer to perform any of its three safety functions (note that isolated regions of higher hydraulic conductivity around the canisters would have a less significant effect);
- a reduction in buffer density, which, if sufficiently large, could lead to the possibility of colloid-facilitated radionuclide transport in the buffer and reduce the ability of the buffer to limit and retard radionuclide releases (note again that isolated regions affected in this way would have a less significant affect); and
- an increase in buffer density at some locations along the drift, which, if sufficiently large, could lead to mechanical damage of the rock, and compromise the ability of the buffer to protect the canisters from rock shear movements of less that 10 cm.

2. Mineral alteration of the buffer

Mineral alteration of the buffer due, for example, to high temperatures around the canisters or to chemical interactions between the buffer and the steel or cementitious components could in principle lead to:

- a change to a less plastic material, which, if it affects a significant proportion of the buffer between the canisters and the drift wall, could compromise the ability of the buffer to protect the canister from rock movements, including shear displacements at canister locations;
- a loss of swelling pressure, with potential consequences as described above in the context of loss or redistribution of buffer mass; and
- a loss of self-healing capacity, which could lead to fracturing of the buffer and an increase in hydraulic conductivity, again with potential consequences as described above in the context of loss or redistribution of buffer mass.

3. Freezing of the buffer

Freezing of the buffer as a result, for example, of the deep penetration of permafrost following a major climate change would, if it were to occur, detrimental changes in buffer properties that could compromise its capacity to protect the canister and to limit and retard radionuclide releases from a failed canister. As noted in Section 12.4.1 of /SKB 2006a/, it is uncertain what transport properties the buffer would have after thawing. According to present knowledge based on past glaciations, the permafrost layer is not expected to reach more than 180 metres below ground at Olkiluoto /Hartikainen 2006/ and is thus not considered as a potential cause of major loss of buffer safety functions in the present study. The possibility that conditions at Olkiluoto could in the future differ significantly from those during the past glaciations and lead to buffer freezing may, however, require further consideration in future studies.

Consideration of these three possible modes for loss or degradation of the buffer safety functions leads to the safety function indicators and associated criteria that are summarised in Table 4-5. Most are taken directly from SR-Can. It should be noted that the criterion given in Table 4-5 that there is a negligible impact on the rheological and hydraulic properties of the buffer due to mineral alteration subsumes the SR-Can criterion for a Swedish KBS-3V repository that buffer temperature remains below 100°C.

The potential chemical processes which may occur at elevated temperature are, for example, silica dissolution close to the canister followed by transport outwards by diffusion to colder parts and precipitation, as well as buffer cementation due to the dissolution, transport and precipitation of silica or aluminosilicate minerals. But neither experimental or natural analogue studies have shown that this will actually occur. The effect of buffer cementation due to silica precipitation is, however, an issue for further work. The present criterion takes account of the concern that the buffer of a KBS-3H repository may be more affected by certain chemical interactions, and particularly those between the corrosion products of steel components external to the canisters and bentonite (see Section 4.7.1), than is the case for a KBS-3V repository.

Table 4-5. Safety function indicators and criteria for the buffer. (Adapted for KBS-3H from Figure 7-2 of /SKB 2006a/).

Safety function indicator	Criterion	Rationale
Bulk hydraulic conductivity	< 10^{-12} m s^{-1}	Avoid advective transport in buffer
Swelling pressure at drift wall	> 1 MPa	Ensure tightness, self sealing
Swelling pressure in bulk of buffer	> 2 MPa	Prevent significant microbial activity
	> 0.2 MPa[1)]	Prevent canister sinking
Saturated density	> 1,650 kg m^{-3}	Prevent colloid-facilitated radionuclide transport
	< 2,050 kg m^{-3}	Ensure protection of canister against rock shear
Mineralogical composition	No changes resulting in significant perturbations to the rheological and hydraulic properties of the buffer (e.g. from iron or cement interaction or related to temperature)	See main text
Minimum buffer temperature	> –5°C	Avoid freezing

[1)] Although developed for KBS-3V, this criterion is also expected to be applicable to KBS-3H, and is likely to be more conservative for the latter since, in KBS-3H, the weight of the canister is distributed over a larger horizontal area compared with KBS-3V.

Combined with consideration of the extremes of salinity expected during the course of repository evolution, the information in Table 4-5 can be used to derive upper and lower bounds for saturated densities within which the buffer will continue to meet the criteria for the safety function indicators. This derived range is then used throughout Chapter 4 as a basis to evaluate the significance of various buffer-related processes.

The upper bound of 2,050 kg m^{-3} is taken directly from Table 4-5 and is based on the requirement on the buffer to protect the canisters in the event of rock shear movements. The lower bound of 1,890 is derived firstly from the requirement on the buffer to prevent microbial activity. The corresponding safety function indicator criterion given in Table 4-5 is a swelling pressure of 2 MPa, below which microbial activity cannot be excluded (see Section 4.1.1) This condition is met for 0.3 M NaCl solution (corresponding roughly to the present-day 10–20 g per litre total dissolved solids (TDS) at Olkiluoto) for dry densities above about 1,300 kg m^{-3} (1,830 kg m^{-3} saturated) (see Figure 4-7 of /SKB 2006a/). A conservative estimate of the maximum salinity is 30–45 g per litre which is the calculated salinity that could occur at a depth of about 550 m at Olkiluoto at future times /Pastina and Hellä 2006/. For a 1 M NaCl solution (which corresponds to about 60 g per litre TDS) a 2 MPa swelling pressure is achieved at a dry density of about 1,400 kg m^{-3} (1,890 kg m^{-3} saturated).

In the case of the lower bound, a saturated density of 1,890 kg m^{-3} will prevent colloid-facilitated radionuclide transport as well as preventing microbial activity (see Section 2.5.4 of /SKB 2006d/ for further discussion). Furthermore, since the swelling pressure will never be less than 2 MPa irrespective of salinity variations in the expected range, it will also prevent the possibility of canister sinking and ensure tightness at the drift wall and self sealing capability (Table 4-5). Finally, it will ensure diffusion-dominated transport in the buffer. Hydraulic conductivity of less than 10^{-12} m^2 s^{-1} is achieved for MX-80 bentonite in saline conditions at dry densities above about 1,200 kg m^{-3} (1,760 kg m^{-3} saturated) (see Figure 4-8 of /SKB 2006a/). Diffusion dominates over advection as a transport process at these conductivities.

4.1.4 Summary of handling in safety assessment

Table 4-6 summarises the handling of processes in the buffer in the safety assessment for KBS-3H, as suggested in the following sections of Chapter 4. In the table, the process is either "mapped" to a model by which it will be quantified or associated with a brief verbal description of how it will be handled. Since the early evolution of the repository is in many respects different from the long-term, saturated phase, the description in the table has been divided accordingly. Early evolution covers evolution in the transient phase following the emplacement of the first canister in the repository during which mass and energy fluxes occur as a result of the various gradients created by the construction of the repository and emplacement of the spent fuel. The end-point of early evolution is not well defined; many of the transient processes that occur during this period do not suddenly cease, but rather gradually diminish over time. Nevertheless, two key transient process – heat dissipation from the spent fuel and saturation of the repository external to the canisters – may take up to several thousands of years (or even longer in the case of saturation of the tightest sections) and this may be taken as the rough duration of the period covered by early evolution.

Table 4-6. Process table for the buffer and other bentonite components describing how processes are handled in different time periods. Green fields denote processes that are omitted or irrelevant for the time period of concern. Red fields denote processes that are quantified by modelling in the safety assessment. Orange fields denote processes that are omitted subject to a specified condition. Motives for handling are given in the relevant sections of Chapter 4. The handling of processes in the KBS-3H safety assessment and the handling of uncertainties are discussed only in certain cases specific to KBS-3H (as noted in the table). If not mentioned, the handling of other processes and uncertainties are assumed to be handled in the same way as for KBS-3V and are not discussed in this report.

Process type	Internal process	Early evolution of the repository	The longer term	Notes/*Section in KBS-3H Process Report*
Intact canister				
Radiation-related processes	Bu1. Radiation attenuation/ heat generation	Omitted since dose rate is too low to be of importance for the buffer (as in SR-Can).	Omitted since dose rate is too low to be of importance for the buffer (as in SR-Can).	*Section 4.3*
Thermal processes	Bu2. Heat transport	Thermal process model /Ikonen 2003, 2005/.	Thermal process model /Ikonen 2003, 2005/.	KBS-3H specific heat transport calculations show similar results as for KBS-3V. *The handling in in the safety assessment for KBS-3H and the handling of uncertainties are also discussed.* *Section 4.4*
	Bu3. Freezing	Omitted, since this requires permafrost conditions (as in SR-Can).	Omitted if buffer temperature > 0°C. SR-Can: Bounding consequence calculations are performed, should this condition not be fulfilled.	Repository temperatures remain above zero for at least 200,000 years, as indicated by permafrost depth modelling based on past history of the site (process model by /Hartikainen 2006/. The possibility that conditions at Olkiluoto could in the future differ significantly compared with those during the past glaciations and lead to buffer freezing as well as the possibility of permafrost at the Swedish sites may, however, require consideration in future studies. *The handling of the process in the safety assessment for KBS-3H is also discussed.* *Section 4.4*
Hydraulic processes	Bu4. Water uptake and transport for unsaturated conditions	Thermal-hydraulic-mechanical (THM) process model.	Not relevant by definition.	KBS-3H specific THM process model, addressing the saturation process in the buffer. *The handling of the process in the safety assessment for KBS-3H is also discussed.* *Section 4.5*
	Bu5. Water transport for saturated conditions	Not relevant by definition.	Omitted if hydraulic conductivity < 10^{-12} m/s (as in SR-Can) and no expulsion of water from canisters by gas pressurisation.	See also Bu10 *Section 4.5*
	Bu6. Gas transport/ dissolution	Gas Model (process model).	Not relevant by definition.	Storage of gas in part of buffer porosity located around super-container; dissolved gas in porewater of inner buffer (see Ge4). *Section 4.5*

Process type	Internal process	Early evolution of the repository	The longer term	Notes/*Section in KBS-3H Process Report*
	Bu7. Piping/erosion	Avoided by design – model study (scoping calculations).	Negligible, provided transient phase has no long-term impact.	The current reference design has been selected to minimise the possibility of significant piping and erosion during saturation. Piping could be an issue with the alternative designs (see Appendix D). Potential impacts (loss of buffer mass) are studied by scoping calculations, see Bu8. *The handling of the process in the safety assessment for KBS-3H is also discussed.* *Section 4.5*
Mechanical processes	Bu8. Swelling/Mass redistribution	THM process modelling including interaction buffer/near-field rock and thermal expansion. Loss of buffer mass by redistribution of bentonite is estimated by scoping calculations.	No specific analysis for KBS-3H. (Integrated evaluation of erosion, convergence, corrosion products, creep, swelling pressure changes due to ion exchange and salinity, canister sinking in SR-Can.)	The consequences of a reduced buffer density caused by mass redistribution will be evaluated by evaluating radionuclide release and transport in a case with increased solute diffusion in the buffer. *Section 4.6*
	Bu9. Liquefaction	Not relevant	Omitted, because liquefaction from a short pulse during earthquake cannot occur in a high-density bentonite due to high effective stresses (as in SR-Can).	KBS-3H is also less prone to be affected by any possible short term period of liquefaction than KBS-3V, due due to the larger canister surface area to be supported by the buffer, requiring lower effective stresses to prevent canister sinking. *Section 4.6*
Chemical processes	Bu10. Advection	No specific analysis for KBS-3H. (Simplified assumptions of mass transport of dissolved species during saturation in SR-Can).	Omitted if hydraulic conductivity < 10^{-12} m/s (as in SR-Can) and no expulsion of water from canisters by gas pressurisation.	Saturation process evaluated using scoping calculations. No advection in buffer in base case radionuclide release and transport calculations. Radionuclide release and transport in the case of a buffer with increased solute diffusion due to decreased density is analysed (Bu8). The consequences of advection in the outer part of the buffer due, for example, to Fe/bentonite interaction are also evaluated (see Bu17). *Section 4.7*
	Bu11. Diffusion	No specific analysis for KBS-3H. (Chemistry model (thermal, saturated phase; unsaturated phase disregarded) in SR-Can.)	No specific analysis for KBS-3H. (Chemistry model, system model in SR-Can.)	Diffusion in buffer is considered in all radionuclide release and transport assessment cases. Diffusion constants from SR-Can are used in the safety assessment for KBS-3H. *Section 4.7*
	Bu12. Sorption (including ion-exchange)	No specific analysis for KBS-3H. (Chemistry model (thermal, saturated phase; unsaturated phase disregarded) in SR-Can.)	No specific analysis for KBS-3H. (Chemistry model, system model in SR-Can.)	Sorption in buffer is considered in all radionuclide release and transport assessment cases. In most cases, sorption constants from SR-Can are used in safety assessment for KBS-3H. *Section 4.7*

Process type	Internal process	Early evolution of the repository	The longer term	Notes/*Section in KBS-3H Process Report*
	Bu13. Alterations of impurities	No specific analysis for KBS-3H. (Chemistry model (thermal, saturated phase; unsaturated phase disregarded) in SR-Can.)	No specific analysis for KBS-3H. (Chemistry model, system model in SR-Can.)	*Section 4.7*
	Bu14. Pore water speciation	No specific analysis for KBS-3H. (Chemistry model (thermal, saturated phase; unsaturated phase disregarded) in SR-Can.)	Analysis performed in context of Fe-bentonite interaction and solubility calculations.	*Section 4.7 and 4.8 /Wersin et al. 2007, Grivé et al. 2007/*
	Bu15. Osmosis	No specific analysis for KBS-3H. (System model (initial swelling) in SR-Can.)	No specific analysis for KBS-3H. (Evaluation through comparison with empirical data; system model in SR-Can.)	SR-Can: Handling of long-term intrusion of saline water. *Section 4.7*
	Bu16. Montmorillonite transformation	No specific analysis for KBS-3H. (Model calculations (thermal, saturated phase; unsaturated phase disregarded) in SR-Can.)	Fe/bentonite analysis and cement bentonite analysis.	*Section 4.7*
	Bu17. Iron/bentonite interaction	Specific analyses for KBS-3H (impact of supercontainer estimated by model calculations).	Specific analyses for KBS-3H (impact of supercontainer estimated by model calculations).	*The handling of the process in the safety assessment for KBS-3H and the handling of uncertainties are discussed.* Two different buffer domains with increased hydraulic conductivity are modelled in the Radionuclide Transport Report /Smith et al. 2007a/: - the inner buffer is not affected by Fe/bentonite interaction - the outer buffer (cemented buffer) and the corrosion products act as a porous medium with increased conductivity (mixing tank, leading to reduced transport resistance at buffer/rock interface). *Section 4.7*
	Bu18. Colloid release/erosion	Impact of buffer erosion estimated by scoping calculations (see Bu7/8).	Omitted if $[M^{2+}]$ > 1 mM, and provided transient phase has no long-term impact. Buffer erosion during glacial period estimated in SR-Can by scoping calculations.	Radionuclide release and transport is analysed in the case of loss of buffer mass due to the influx of dilute glacial meltwater, leading to advective conditions in the buffer and relatively rapid corrosion failure of the canister. (see also Bu8). *The handling of the process in the safety assessment for KBS-3H and the handling of uncertainties are also discussed.* *Section 4.7*
	Bu19. Radiation-induced transformations	Omitted since dose rate outside canister is too low to have any effect (as in SR-Can).	Omitted since dose rate outside canister is too low to have any effect (as in SR-Can).	*Section 4.7*
	Bu20. Radiolysis of pore water	Omitted since dose rate outside canister is too low to have any effect (as in SR-Can).	Omitted since dose rate outside canister is too low to have any effect (as in SR-Can).	*Section 4.7*

Process type	Internal process	Early evolution of the repository	The longer term	Notes/*Section in KBS-3H Process Report*
	Bu21. Microbial processes	Omitted under unsaturated conditions, since the extent of aqueous reactions is limited. For saturated conditions the treatment is the same as for "Long-term" (as in SR-Can).	Omitted if swelling pressure > 2 MPa, (otherwise quantitative estimate of sulphate reduction in SR-Can).	*Section 4.7*
	Bu22. Cement/bentonite interaction	Omitted under unsaturated conditions, because the extent of reactions is limited.	Quantitative estimates of impact.	Impacts of cement/bentonite interaction or other low-pH materials (e.g. Silica Sol). *The handling of the process in the safety assessment for KBS-3H and the handling of uncertainties are also discussed.* *Section 4.7.*
Failed canister				
Hydraulic processes	Bu6. Gas transport/dissolution	Omitted, because little water would enter the canister during the transient period. (SR-Can: Quantitative estimate based on empirical data.)	Quantitative estimate based on empirical data.	Analysis of HMG processes in defective canisters in KBS-3H (see F5 in Table 2-2). *Section 4.5*
Chemical processes	Bu18. Colloid transport	Omitted, because no radionuclide releases from the canister are expected during this period. (SR-Can: neglected if density > 1,650 kg/m^3, otherwise bounding calculations.)	Omitted if density > 1,650 kg/m^3 (otherwise bounding calculation in SR-Can).	*Section 4.7*
	Bu19. Radiation-induced transformations	Omitted since dose rate outside canister is too low to have any effect (as in SR-Can).	No specific analysis for KBS-3H. (The effect of α-radiation from nuclides from a failed canister is estimated in SR-Can.)	*Section 4.7*
Radionuclide transport-related processes	Bu23. Speciation of radionuclides	Omitted, because no radionuclide releases from the canister are expected during this period. (SR-Can: Assumptions based on empirical data.)	Modelled in radionuclide solubility calculations. (SR-Can: Assumptions based on empirical data.)	*A solubility report has been produced for the KBS-3H safety assessment /Grivé et al. 2007/.* *Section 4.8.*
	Bu24. Transport of radionuclides in water phase	Omitted, because no radionuclide releases from the canister are expected during this period. (SR-Can: COMP23, analytic calculations)	Modelled in radionuclide release and transport assessment cases.	*See Section 4.8. The handling of the process in the safety assessment for KBS-3H and the handling of uncertainties are also discussed.*
	Bu25. Transport of radionuclides in gas phase	Omitted, because no radionuclide releases from the canister are expected during this period. (SR-Can: Quantitative estimate)	Quantitative estimate – included in radionuclide release and transport assessment cases (as in SR-Can).	Fate of volatile radionuclides in gas phase somewhat different in KBS-3V/3H due to gas generation by supercontainer and other structural materials in the case of 3H (see Fu17). *Section 4.8.*

4.2 Overview of processes

Based on the FEP analysis for KBS-3V, a list of processes for the buffer has been derived in /SKB 2006b/. Following the methodology in Appendix B, this list of processes is considered appropriate for KBS-3H. The only added processes are “iron/ bentonite interactions” and “cement/bentonite interactions” (see Table 4-15).

The processes are structured into radiation-related, thermal, hydraulic, mechanical and chemical process categories see Figure 1-3. In addition, radionuclide transport is discussed separately. In the introductory part of each of the following chapters, the processes pertinent to the process category are tabulated.

A detailed discussion of processes for the buffer in KBS-3V is given in the Buffer and Backfill Process Report for the SR-Can Safety Assessment /SKB 2006d/. The present report uses much of this material. However, the detailed descriptions of various processes have been adapted to the specific conditions in KBS-3H.

4.3 Radiation-related processes

Radiation attenuation/heat generation is the only radiation-related process relevant to the bentonite. The interdependence between this process and the variables in the buffer is shown in Table 4-7. Attenuation of γ and neutron radiation will raise the temperature of the buffer, but the effect is negligible compared with other temperature-raising processes. The radiation is relevant to the chemical processes, radiation-induced transformations and radiolysis of porewater.

There are no additional comments to the discussions in the relevant Process Reports for KBS-3V /Rasilainen 2004, SKB 2006d/. Radiolytic effects outside the canister can be neglected because of the initially low gamma dose rate at the canister surface (less than 1 Gy per hour by design) and because gamma radiation, mainly due to Cs-137 decay, decreases by a factor of 1,000 within 300 years (/SKB 2006a/ Section 6.4.1). Alpha and beta radiation are shielded by the copper canister and therefore do not cause any radiolysis outside the canister. The handling of these processes in the KBS-3H safety studies is summarized in Table 4-6.

Table 4-7. The interdependence of radiation-related processes and identified variables for the buffer.

Radiation-related processes	Variables for the buffer												
	Geometry	Pore geometry	Radiation intensity	Temperature	Water content	Gas content	Hydrovariables	Stress state	Bentonite composition	Montmorillonite composition	Porewater composition	Structural and residual materials
Radiation attenuation/heat generation	×		×	×	×	×			×	×		

4.4 Thermal processes

Heat transport and freezing are the only thermal processes relevant to the buffer. Mineralogical changes related to temperature gradients (e.g. silica precipitation and buffer cementation are described in Sections 4.4.1 and 4.7). The interdependence between these processes and the variables in the buffer is shown in Table 4-8. The basic processes and the boundary conditions at the canister surface are identical in KBS-3V and KBS-3H. Differences arise only due to the specific geometry and boundary conditions outside the buffer, particularly due to the presence of the supercontainer itself and due to the properties of the interfaces (gaps) to the rock surface and to the adjacent distance blocks.

4.4.1 Heat transport

Overview/general description

Heat is generated by the radioactive decay of the spent fuel inside the canisters at a time-dependent rate. This heat is transferred continuously to the surrounding media by:

- conduction through metal components, bentonite, rock and any gas- or water-filled gaps between these media,
- radiation from surfaces, and
- convection of gas or water in gaps and voids.

The saturation process affects the evolution of temperature within the bentonite. Conversely, the saturation process will be affected by the evolution of temperature. In particular, the temperature gradients outwards from the canister surfaces will inhibit the saturation process. Heat can also affect the pore pressure due to thermal expansion of water and the viscosity of fluids. In bentonite, the thermally induced increase of pore pressure is only likely to be significant once full saturation is achieved in a hydraulically isolated part of the drift, due to the high compressibility of any trapped or repository-generated gas /Rasilainen 2004/. In the near-field rock, thermal effects tend to increase water inflows towards the drift due to increased pore pressures in the rock and decreased viscosity. Because of the declining heat output from the fuel, insignificant effects are expected in drift sections requiring more than a few hundred years to saturate. Heat output from the fuel is expected to have no significant impact on gas transport or corrosion phenomena. The timeframe for the build-up of significant gas pressures is expected to be in the order of hundreds of years or more (Section 7.5), by which time the thermal transient will be largely complete. Furthermore, long-term steel corrosion (which gives rise to repository-generated gas) shows no influence of temperature within the range of 30–85°C /Smart et al. 2001/. The solubility of gas is somewhat decreased at higher temperatures.

Table 4-8. The interdependence of thermal processes and identified variables for the buffer.

Thermal processes	Variables for the buffer											
	Geometry	Pore geometry	Radiation intensity	Temperature	Water content	Gas content	Hydrovariables	Stress state	Bentonite composition	Montmorillonite composition	Porewater composition	Structural and residual materials
Heat transport	×	×		×	×				×			×
Freezing	×	×		×	×	×	×	×	×	×	×	×

Upon emplacement of the first supercontainer, the thermal evolution of the interior of the supercontainer (which begins prior to emplacement) will continue and, in addition, heat is transferred to air within the open part of the deposition drift and to the host rock. When the first distance block is emplaced, its temperature will start to rise as a result of heat transfer from the first supercontainer, and from the next supercontainer as soon as it is emplaced, and so on until emplacement operations are complete. The thermal evolution within and around any individual supercontainer and distance block is thus, in principle, dependent on the emplacement schedule and the duration of the operational period for a deposition drift. It is also dependent on the position of a given supercontainer with respect to other supercontainers in the same drift as well as in neighbouring drifts.

The general description of these thermal processes and their interdependence with the system variables in the KBS-3H buffer is similar to KBS-3V. The buffer and backfill process report of SR-Can /SKB 2006d/ presents a comprehensive, state-of-the-art description of thermal processes in the buffer, the details of which are not repeated here.

At high temperature and unsaturated conditions the saturation of the buffer is slow, which means lower density in localised parts of the buffer. The high temperatures, in combination with a low density, may change the bentonite properties although this effect is not expected to be relevant for temperatures below 100°C /SKB 2006d/.

Compared with the buffer, the distance blocks experience somewhat delayed heating and slightly lower maximum temperatures, due to the larger distance from the heat source /Ikonen 2003/. Any thermal effects that are – from the safety point of view – judged to be acceptable for the buffer are also likely to be acceptable for the distance blocks. The effect of thermal expansion of the rock causing fractures to open or to close on the water inflow and buffer saturation time has not been evaluated.

Boundary conditions

The heat flux from the canister, determined by the characteristics of the spent fuel that it contains, sets the inner boundary condition for the buffer. The outer boundary is provided by the temperature at the rock surface of the deposition drift. Both these conditions are identical in KBS-3V and 3H. Differences arise in the specific geometry and materials used in KBS-3H, particularly the spacing between supercontainers provided by distance blocks and the spacing between drifts.

Model studies

Thermal analyses for a KBS-3H type repository at Olkiluoto have been performed by /Ikonen 2003, 2005/. Special attention has been paid to the effects of gaps (canister – buffer, buffer – supercontainer/rock) and to the thermal dimensioning of the repository.

/Ikonen 2005/ carried out an analysis of thermal evolution for BWR spent fuel during the operational phase for two limiting cases. In the first of these, the hypothetical assumption is made that an infinite row of supercontainers and distance blocks is emplaced in the drift instantaneously at time zero – i.e. the operational period is, in effect, instantaneous and all supercontainers evolve identically. This assumption is expected to lead to an over-estimate of temperatures, because the number of emplaced supercontainers is finite and because the supercontainers are not disposed of simultaneously.

Figure 4-1 (upper figure) shows the calculated temperature evolution over a 30-day period in a vertical plane normal to the drift axis and passing through the centre of a supercontainer (i.e. where temperatures are highest) at three radial distances from the drift axis, corresponding to:

- the canister surface,
- the outer surface of the bentonite buffer, and
- the rock surface.

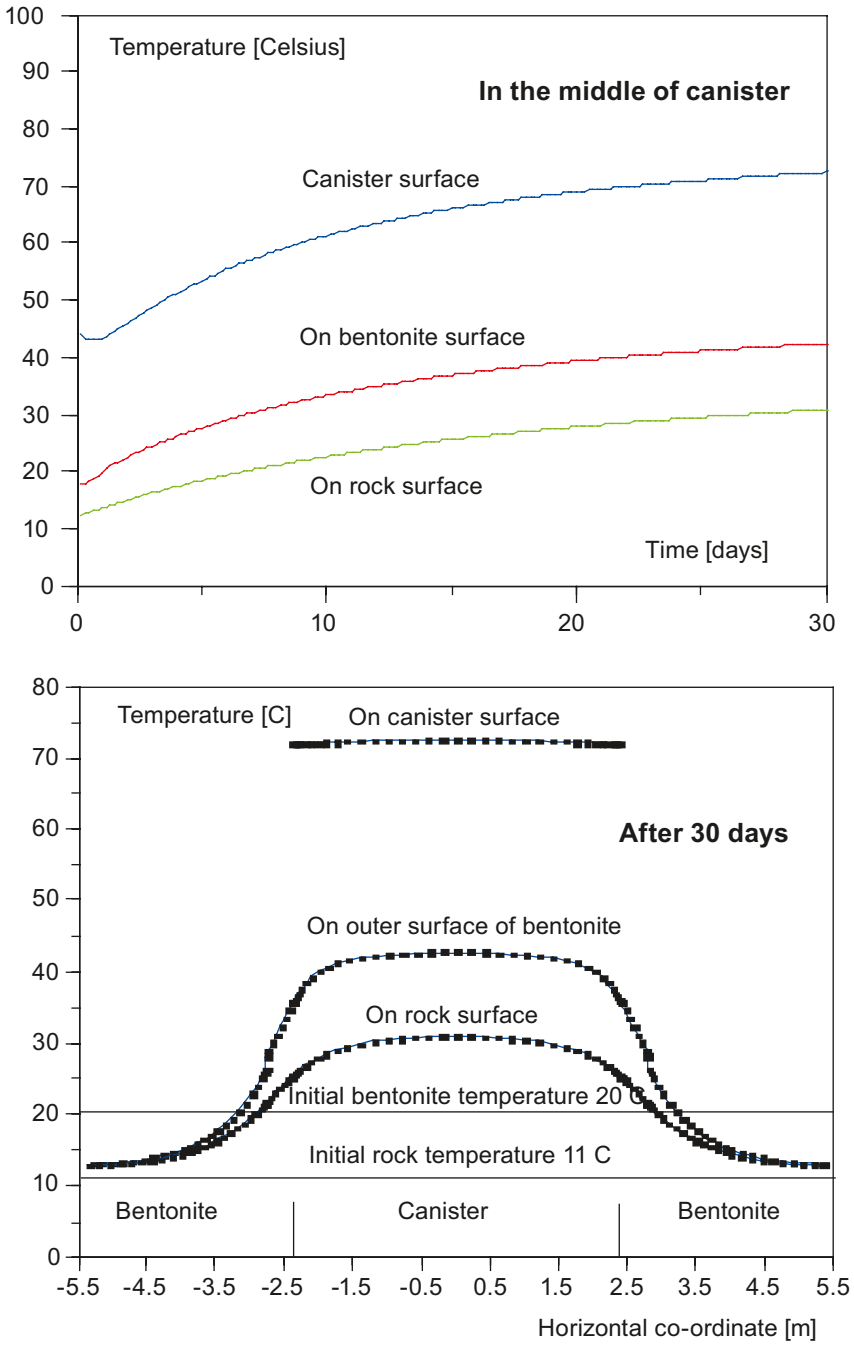

Figure 4-1. *Upper figure: The temperature evolution over a 30 day period in a vertical plane normal to the drift axis and passing through the centre of a supercontainer at three radial distances from the drift axis (from Figure 19 in /Ikonen 2005/). Bottom figure: The temperature profile parallel to the drift axis at each of the radial positions shown in the upper figure (after 30 days, from Figure 18 in /Ikonen 2005/). Note: The 46°C initial temperature at the canister surface is the estimated steady surface temperature of the canister in ventilated storage at the encapsulation plant. A decay heat of 1,700 W per canister dissipated through a canister surface area (cylinder and top lid) of 16.7 m^2 with a heat transfer coefficient at the canister surface of 4 W m^{-2} °C^{-1} gives rise to a 26°C higher temperature at the canister surface compared with ambient air temperature, which is assumed to be 20°C.*

The gap between the supercontainer and the drift surface is assumed to be filled with air for the duration of the calculated period. The degree of bias introduced into the calculated results by this assumption has not been evaluated quantitatively. The assumption will, however, tend to under-estimate the maximum rate of heat transfer from the canister to the buffer, since, in reality, the canister will be in contact with the buffer at its lowest point. This will lead to an under-estimate of maximum buffer temperature. To ensure that the bentonite temperature assessment is conservative, the bentonite temperature at all points on its inner boundary is set equal to the temperature at the copper canister surface.

The bottom figure of Figure 4-1 shows the temperature profile parallel to the drift axis at each of these radial positions. According to this analysis, the air temperature in the gap between the supercontainer and the rock midway along the canister rises to between about 30 and 40°C over 30 days. The temperature on the canister surface rises to a little over 70°C.

/Ikonen 2005/ carried out a further analysis based on an alternative limiting case in which the operational period is in effect infinite – only a single supercontainer and single distance block are present from time zero across the entire calculational period. This assumption leads to an under-estimate of temperatures. The actual evolution of temperature will follow a path somewhere between these two limiting cases. However, the maximum temperatures calculated by Ikonen – i.e. the temperatures in a vertical plane passing through the centre of a supercontainer – are similar in both cases (Figure 4-2), indicating that neither the duration of the operational period, nor the position of one supercontainer with respect to other supercontainers in a drift, are important factors influencing the evolution of temperature in this plane. Figure 4-3 shows the thermal evolution of the canister and bentonite buffer temperature in a KBS-3V repository until approximately 50,000 years, which qualitatively describes the evolution also in a KBS-3H repository.

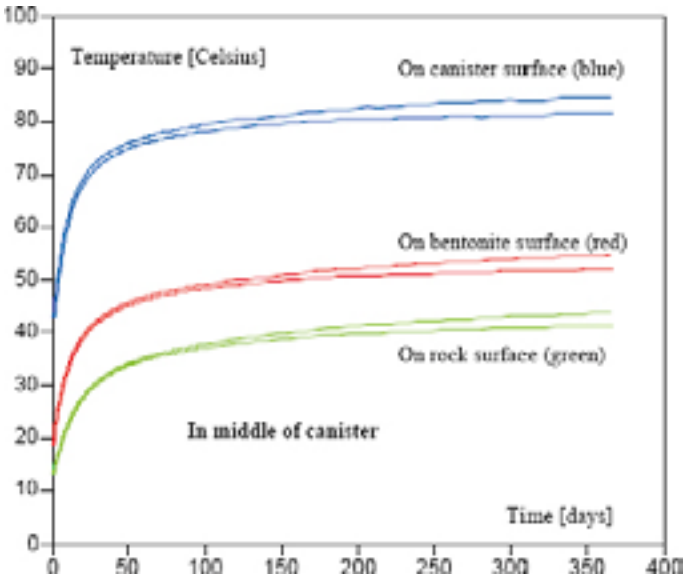

Figure 4-2. *The temperature evolution over a 365-day period in a vertical plane normal to the drift axis and passing through the centre of a supercontainer at three radial distances from the drift axis. Upper curves: Case 1 with infinite queue of supercontainers; lower curves: Case 2 with single supercontainer (from Figure 30 in /Ikonen 2005/).*

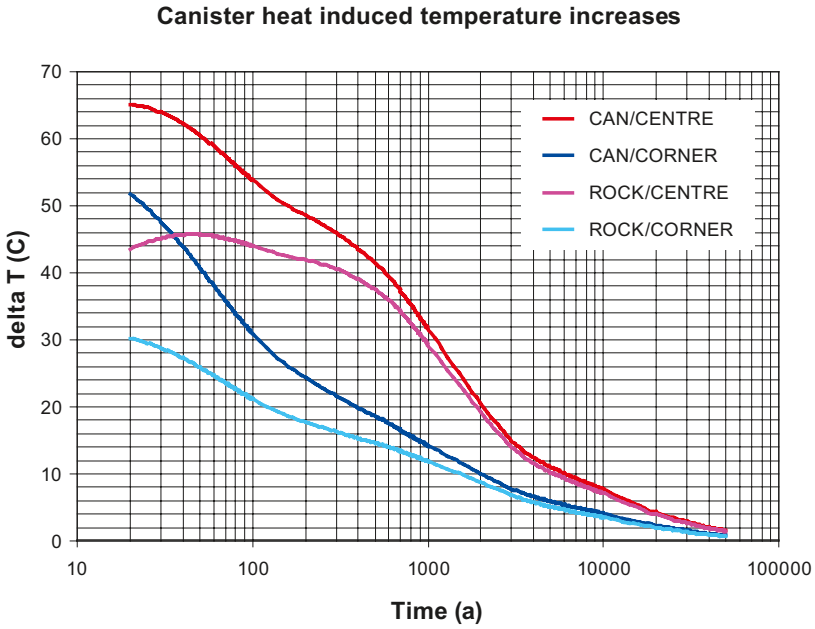

Figure 4-3. *Canister and bentonite buffer temperature increase in a KBS-3V repository after closure and before the next glaciation, i.e. until 50,000 years AP. To obtain absolute temperatures, the ambient rock temperature (10.5°C at the depth of -400 m in Olkiluoto) can be added. Further details given in /Pastina and Hellä 2006/. As the spent fuel emplacement densities are similar for KBS-3V and KBS-3H, this figure also gives an indication of the magnitude and duration of the elevated temperatures occurring within and around a KBS-3H repository.*

In the longer term, the temperature within and around the repository will peak and then start to decline due to the diminishing heat output from the spent fuel. Repository temperature will tend towards the ambient rock temperature over a few thousand years. The evolution of the temperature around a canister will not only be affected by heat output from canisters in the same drift, but also by the heat output from canisters in neighbouring drifts. /Ikonen 2003/ carried out analyses of the thermal evolution of a repository panel with different canister pitches in a drift, and with both 25 m and 40 m drift separation (Figure 4-4). The resaturation of the buffer will affect its thermal properties, and will close air-filled gaps. In the calculations, however, fixed thermal properties were assumed for the bentonite and the gaps were assumed to remain open.

In the thermal dimensioning of the repository layout, the governing constraint is that the temperature at the buffer should be less than 100°C to limit alteration of the bentonite. In the thermal analyses /Ikonen 2003, 2005/ uncertainties and variability in the thermal parameters are taken into account with a safety margin of 10°C, so that the maximum temperature at the canister surface is set as 90°C. The thermal dimensioning is done by limiting the heat power per canister and by adjusting the spacing of supercontainers and deposition drifts.

The results showed that, for a canister pitch of 11 m and a drift separation of 25 m, temperature at the canister/bentonite interface at the centre of a canister peaks at 90°C after 50 years (Finnish BWR spent fuel with 1,700 W). For a drift spacing of 40 m, the temperature maximum is slightly lower (84°C) and is reached slightly earlier (40 years). /Ikonen 2003/ also showed that the maximal temperatures obtained for KBS-3V and KBS-3H are very similar, in spite of some differences in geometry (gaps).

Natural analogues/observations in nature

Not applicable.

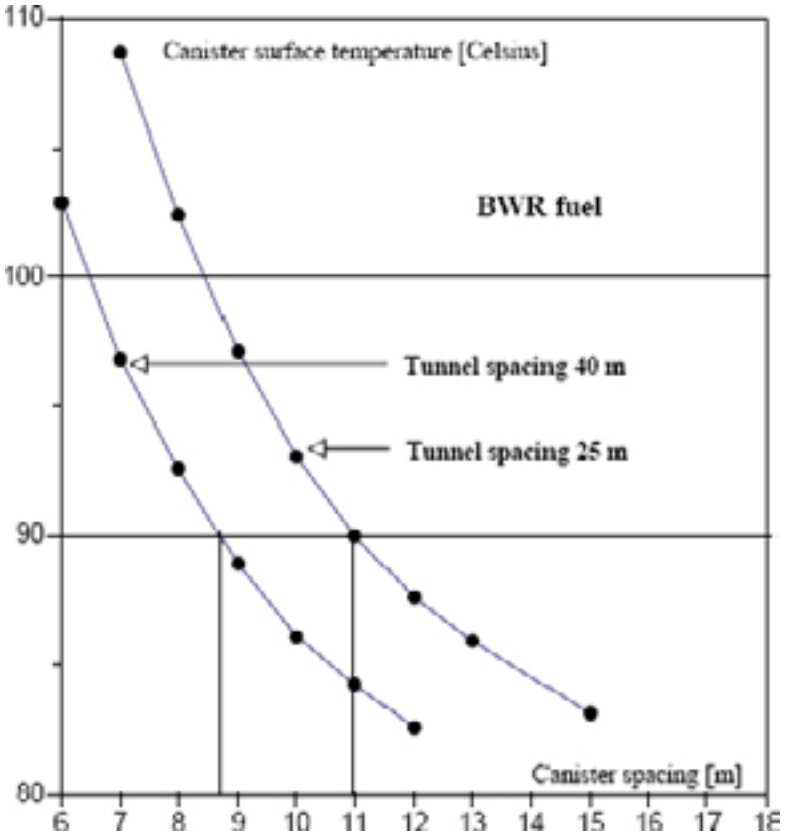

Figure 4-4. *Maximal temperatures for a repository panel containing 1,500 BWR canisters (each with 1,700 W) as a function of the spacing of supercontainers and deposition drifts (from Figure 25 in /Ikonen 2003/).*

Time perspective

The relevant time scales for the thermal evolution are governed by the time frames for heat production and for saturation. As discussed in Section 4.5.1, the time to full saturation is in the order of 10 years for drift sections in permeable rock, but may be as long as 100 years or even several thousand years in tight drift sections. After full saturation, heat transport takes place predominantly by conduction under well-defined conditions with known thermal conductivities. Before full saturation, heat transport is affected by the presence of gaps and joints.

The heat production due to radioactive decay gradually declines over time and, after a few thousand years, will be reduced by about two orders of magnitude.

Handling in the safety assessment for KBS-3H

The evaluated evolution of buffer temperature indicates that thermal effects will have no major impact on long-term safety functions of either the buffer or canister (although it may have indirect implications by affecting the early saturation process). The temperature within the buffer and at the buffer/canister interface will remain below 90°C which, according to the criteria for safety function indicators given in the SR-Can safety assessment, will ensure no thermal degradation of the buffer (according to /Pusch and Karnland 1990/ irreversible chemical changes such as illite formation and cementation, which would reduce swelling capacity, are expected to be insignificant below 100°C).

Cementation by precipitation of sulphates due to elevated temperatures around the canisters may lead to the formation of a zone in the buffer adjacent to the canisters with increased strength but reduced plasticity. When the temperature and temperature gradient decrease, it is likely that the precipitated solids will dissolve to some degree and disperse within the buffer by diffusion.

Silica in the buffer close to the canister is, on the other hand, expected to dissolve during the period of elevated temperature and be transported outwards by diffusion to colder parts where precipitation may take place. There is great uncertainty associated especially with the cementation processes as a consequence of dissolution, transport and precipitation of silica or aluminosilicate minerals, and the process has not been confirmed to take place in either experimental or natural analogue studies. The short period of elevated temperatures (a few hundred years) and the slow diffusion of silica to colder regions of the buffer may limit the extent of buffer cementation. Nevertheless, this is an issue requiring further work for both KBS-3H and KBS-3V.

Early thermal evolution has a key impact on design, in that it is a major factor determining deposition drift spacing and the spacing of canisters within a drift (i.e. the axial dimension of the distance blocks). The canister pitch of 11 m in the current KBS-3H layout for Finnish BWR spent fuel is based on the considerations of thermal evolution reported in /Ikonen 2003/.

In the Radionuclide Transport report /Smith et al. 2007a/, no failure modes that could give rise to radionuclide releases from the canister due to thermal effects have been identified. Even in the case of a canister with an initial penetrating defect, transport through the defect is expected to be so slow due to the small size of a defect that no radionuclide releases are expected during the thermal phase. The impact of heat is thus not relevant to the radionuclide release and transport calculations.

Handling of uncertainties

Well-established physical laws describe the processes controlling heat transfer from canisters to the surrounding media. Nevertheless, there are some significant uncertainties in the parameter values that are appropriate when applying these laws to a KBS-3H repository at Olkiluoto. The emissivity of copper, for example, a parameter relevant to radiative heat transfer from the canister surface, depends on the quality of the surface, which will be a function of the manufacturing process and will also vary with time as the surface oxidises (see Section 2.5 of /Ikonen 2005/). The thermal conductivity of bentonite and the presence of gaps around the peripheries of the bentonite blocks depend on the saturation state as well as on temperature and pressure, and thus heat transfer rates are affected by the various uncertainties that affect the saturation process.

In the calculations described in /Ikonen 2003, 2005/, such uncertainties are either argued to be of negligible consequence, or are handled by conservative parameter value selection (i.e. values are used that lead to an over-estimate of temperatures). Model simplifications are also made to facilitate the analyses, such as the neglect of convective heat transfer. These are again argued either to be of negligible consequence or conservative. The temperature maxima reached in reality during the operational period and in the longer-term are therefore expected to be lower than those calculated.

4.4.2 Freezing

Overview/general description

According to /SKB 2006d/, potential effects of freezing and thawing of the buffer, were this to take place, include:

- increased stress levels during freezing;
- frost heave if water and long time periods are available;
- risk of relocation of embedded objects (the canisters);

- creation of fractures and openings, which might be closed after thaw;
- changes in hydraulic conductivity after freezing and thawing;
- temperature induced consolidation effects; and
- different stress/strain relation after freezing and thawing.

Freezing of bentonite depends only indirectly on the specific conditions in KBS-3H, namely via the temperature field (see discussion in Section 4.4.1). Due to the slow radioactive decay of some actinides, the disposed spent fuel produces heat for long time periods: The total thermal output is reduced to about 5 kW after 10^5 years and to about 2 kW after 10^6 years /Anttila 2005/, depending somewhat on the type of fuel and on burnup. In addition, the freezing point is slightly lowered by the governing hydraulic pressure and salinity at repository depth at Olkiluoto.

No other issue has been identified for KBS-3H, in addition to those presented in SR-Can Process Report for KBS-3V /SKB 2006d/.

Model studies/experimental studies

No studies on freezing of buffer materials have been done so far.

Natural analogues/observations in nature

Knowledge can probably be achieved by laboratory tests with frozen bentonite and by studying permafrost areas, but no study has been performed yet.

Handling in the safety assessment for KBS-3H

The process is negligible if the near-field of the repository has a temperature which is higher than the freezing point of bentonite, which is slightly lower than 0°C due to the hydraulic pressure and salinity at repository depth. SR-Can calculations showed that freezing cannot be excluded in the case of a water-filled deposition hole in presence of eroded bentonite in Forsmark, in case of the most pessimistic climatic assumption /SKB 2006a/. However, a recent review of possible future climate scenarios for the Olkiluoto site and permafrost depth modelling based on the past history of the site indicate that permafrost is not expected to reach repository depth for at least 125,000–200,000 years (see Section 7.4). Nevertheless, the possibility that conditions at Olkiluoto could in the future differ significantly compared with those during the past glaciations and lead to buffer freezing may require further consideration in future studies.

If freezing cannot be excluded, e.g. in the more distant future, canister integrity cannot be guaranteed, based on the preliminary evaluation in /SKB 2006d/. It is noted that this would apply to all canisters in the repository simultaneously. No strategy is currently available for dealing with freezing of bentonite. A need for further analyses is identified. This issue, however, is not specific to KBS-3H.

4.5 Hydraulic processes

Water uptake and transport under unsaturated and saturated conditions, gas transport/ dissolution and piping/erosion are the only hydraulic processes relevant to the buffer. The inter-dependence between these processes and the variables in the buffer is shown in Table 4-9.

The basic processes and the boundary conditions at the canister surface are identical in KBS-3V and 3H. Differences arise, however, due to the specific geometry (including canister orientation) and the boundary conditions outside the buffer, particularly due to the presence of the supercontainer and distance block and due to the properties of the interfaces (gaps) between bentonite and rock. For example, saturation and piping/erosion are qualitatively different in KBS-3V and

Table 4-9. The interdependence of hydraulic processes and identified variables in the buffer.

Hydraulic processes	Variables for the buffer											
	Geometry	Pore geometry	Radiation intensity	Temperature	Water content	Gas content	Hydrovariables	Stress state	Bentonite composition	Montmorillonite composition	Porewater composition	Structural and residual materials
Water uptake and transport under unsaturated conditions	×	×		×	×	×	×	×	×	×	×	×
Water transport under saturated conditions	×	×		×	×	×	×		×	×	×	×
Gas transport/dissolution	×	×		×	×	×	×	×				
Piping/erosion	×	×			×		×	×	×	×	×	

3H. This is mainly due to the orientation difference, the different backfilled volumes and to the presence of large amounts of gas-generating materials in KBS-3H. On the one hand, the more permeable backfill tends to homogenise the hydraulic conditions along a KBS-3V deposition tunnel more rapidly than in the case of the KBS-3H drift. On the other hand, the generation of hydrogen by anaerobic corrosion of steel in the KBS-3H deposition drift will prolong the duration of saturation in tight drift sections.

As a consequence, hydraulic gradients and water saturation are expected to be heterogeneous for longer periods of time within a KBS-3H deposition drift.

The processes of water transport under saturated conditions and gas transport/dissolution are, however, similar in KBS-3V and 3H. This is because these processes mainly depend on bulk properties of the bentonite, which are similar or identical in KBS-3V and 3H. There are no additional comments to the discussions in the relevant Process Reports for KBS-3V /Rasilainen 2004, SKB 2006d/. The handling of these processes in the KBS-3H safety studies is summarized in Table 4-6.

The special issues related to the presence of the supercontainer and other structural materials are discussed elsewhere: The effects of gas generation, dissolution and storage are investigated in Section 5.5.1 and gas pressure build-up and transport are discussed in Section 7.5.2. Iron/bentonite interactions and the impact on transport properties of bentonite (e.g. hydraulic conductivity) are addressed separately in Section 4.7.1. Gas flow through bentonite in the case of a penetrated canister is discussed in Section 2.5.1.

4.5.1 Water transport under unsaturated conditions

Overview/general description

In general, the description of processes relevant for water transport in unsaturated bentonite given in /SKB 1999, Rasilainen 2004/ and /SKB 2006d/ presents a comprehensive state-of-the-art review of current scientific knowledge. The general description of these processes is, therefore, not repeated here.

Three typical situations with different evolutionary pathways can be distinguished in a KBS-3H deposition drift:

1. Less tight drift sections

These are defined as drift sections in which the average hydraulic conductivity (K) of the rock is about 10^{-12} m s^{-1} or more. This corresponds, for example, to a fracture spacing of ten metres and a fracture transmissivity of 10^{-11} m^2 s^{-1} or more, or 10^{-12} m^2 s^{-1} or more for one metre fracture spacing. It also corresponds to an initial inflow to a 10 m drift section of about 0.4 ml per minute or more[18]. Assuming that inflow is fairly evenly distributed along the drift, the rate of buffer saturation in these sections will not be limited by the hydraulic conductivity of the rock, but rather by the rate at which water can migrate into the buffer. Repository-generated gas can readily escape via the intersecting fractures, and thus plays no significant role in the saturation process. Such sections are expected to be the most common – note that all but one of the supercontainer sections in an example drift considered in discrete fracture network modelling for KBS-3H fall into this category /Lanyon and Marschall 2006/. Since no significant gas pressure will build up in these sections, the fluid pressure remains near the hydrostatic value (see Section 7.5.2). The minimum saturation time in these sections is about 10 years /Börgesson et al. 2005/ in accordance with the minimal saturation times calculated for KBS-3V /SKB 2006d/.

2. Tighter drift sections

These are defined as drift sections in which the average hydraulic conductivity of the rock is in the range 10^{-13} to 10^{-12} m s^{-1}. In "tighter" drift sections, the saturation times are governed by the hydraulic conductivity (K) of the rock around the drift (including the transmissivity of intersecting fractures) and by the rate of gas generation by anaerobic steel corrosion. The time needed for full saturation is estimated to be in the order of several thousand years ($K = 10^{-13}$–10^{-12} m s^{-1}) and is determined by the rates of gas generation and gas escape through the tight rock. For $K < 10^{-11}$ m s^{-1}, a sustained gas phase forms and gas pressures may rise considerably above the hydrostatic pressure as long as gas is being generated (about 5,000 years for a steel corrosion rate of 1 μm a^{-1}, Section 7.5.2).

3. Tightest drift sections

These are defined as drift sections in which the average hydraulic conductivity of the rock is less than 10^{-13} m s^{-1}. It may not, in practice, be possible to differentiate such sections from the tighter drift sections defined above, since neither may give rise to detectable initial water inflow. Nevertheless, the existence of these tightest drift sections cannot currently be excluded, and the saturation of the buffer may proceed somewhat differently in such sections due to their tightness with respect to both groundwater flow and the flow of repository generated gas. In these sections, the buffer may remain only partially saturated for up to several thousand years, as it is possible that repository-generated gas could hinder or prevent altogether the saturation of the buffer until gas generation by steel corrosion ceases and gas pressure falls (which is also expected to take up to several thousands years).

It is also possible that the rock surface may experience limited desaturation during the short time that the drift stays open (less than a month, according to /Autio et al. 2007/. This desaturation could lead to some loss of water from the buffer surface during the thermal phase. The volume

[18] Based on Darcy's law in a radial configuration (Thiem's equation; see Section 4.5.1, Equation 4-15), and using the same geometrical parameters and assumed maximum hydraulic pressure difference as described in Section 1.6.1. An inflow as low as about 1 ml per minute can be observed, e.g. by ventilation tests or, if the inflow is localised in a small number of leakage points, as damp locations on the drift wall.

of water lost from the buffer is estimated to be in the order of 10 litres per supercontainer[19], which is negligible compared with the 1,650[20] litres of water in the buffer.

Examination of the moisture retention curves of buffer and rock reported by /Börgesson and Hernelind 1999/ based on measurements at Grimsel Test Site suggests that it is not possible for the rock to draw water from the buffer during the unsaturated phase in the case of the tightest drift sections. For example, based on the above-mentioned results, the suction of the buffer exceeds that of the rock by a factor of 8 for an equivalent degree of saturation of 0.5.

The possibility of a permanent collapse of the smectite stacks that could modify the original properties of the buffer has been considered but this process is relevant only at higher temperatures than those calculated in the buffer (30–85°C, see Section 4.4), as shown by /Karnland and Birgersson 2006/. Therefore collapse of the smectite stacks can be neglected at the buffer temperature and hydrogeochemical conditions expected during the repository evolution. The consequences of hypothetical cementation and cracking of the buffer in terms of solute transport through a damaged buffer have been investigated by /Neretnieks 2006/.

Bentonite compression due to the slow gas pressure increase and subsequent increase of the critical gas entry pressure causing non-uniformities in the saturation of the buffer have also been considered. Although local compaction of bentonite is possible, with only a few centimetres of bentonite between the supercontainer and the rock and a generally lower density than the bulk of the buffer, this process seems highly improbable. Gas generation has a slightly more important effect on buffer saturation in rather dry sections, when the saturation times are of the order of gas generation times (a few thousand years). Since the bentonite has a pore size distribution, water will be drawn into the finest connected pores by capillary forces isolating the gas in some pockets but also expelling the gas through the larger connected pores. The swelling pressure is an average entity as measured; locally, it can be both larger and smaller but the average swelling pressure may be uniform nonetheless.

It is unclear, however, whether there is any long-term safety impact of a delay of saturation or local non-uniformity of saturation. Even if gas production delays the saturation such that the buffer remains only partly saturated for up to several hundred to a few thousand years, the long-term safety consequences will be negligible if the bentonite maintains its swelling capacity even in dry conditions.

4. Tight drift section adjacent to a less tight drift section

The case of a “tight” drift section neighbouring a “less tight” (permeable) drift section is characterised by relatively high gradients (saturation, water pressure, swelling pressure, etc). This may lead to flow along the EDZ or through the distance blocks, although such flows will be severely limited by the expected tightness of the EDZ and low permeability of the saturated buffer. Under certain circumstances (high inflow rate and rate of pressure build-up in the permeable drift section) it could also lead to piping at the interface between distance block and rock and possibly to some erosion of bentonite. The possibility of such circumstances arising in practice is avoided to a large extent in the current design (drift sections with high inflows are avoided when positioning supercontainers and distance block). Nevertheless, additional scoping calculations are presented below that aim at quantifying the effects of various processes on the saturation time.

---

[19] 10 litres is the approximate volume of water contained in an annular region of wall rock extending one metre from the drift wall, assuming this to be the maximum extent of desaturation during the time that the drift remains open, and with a length equal to that of the supercontainer, assuming a rock matrix porosity of 0.2%.

[20] The calculation is based on the Basic Design with a buffer volume of 7.2 m^3 and a dry density of 1,885 kg m^{-3} for ring blocks and a volume of 1.7 m^3 and a dry density of 1,753 kg m^{-3} for end blocks, assuming an initial water content of 10%w (see Appendix A). Thus, a water volume of 1,350 litres is initially contained within the ring blocks and about 300 litres of water is initially contained within the end blocks. The complete derivation is presented in Appendix B.6 of the Evolution Repor /Smith et al. 2007c/.

In the case of less tight, tighter and tightest sections, the drift section may contain just a single supercontainer, or several adjacent supercontainers and distance blocks. Section 5.5 of the Evolution Report /Smith et al. 2007c/ gives a brief account of the saturation of sections between compartment plugs, with possible deviations from the expected evolution and discusses the wider impact of the phenomena on system evolution and on safety functions.

Model studies

Figure 4-5 shows the results of finite element modelling of buffer saturation as a function of host rock hydraulic conductivity, in which the rock is treated as a homogeneous porous medium (cases 1 and 2). The model, which takes coupled thermohydraulic processes and water vapour transport into account, indicates that saturation takes at least about a decade, even in drift sections in highly conductive rock. This is in accordance with the minimum saturation times calculated for KBS-3V /SKB 2006b/. For hydraulic conductivities above about 10^{-12} m s^{-1} saturation time is controlled by the ability of the bentonite to take up water (principally by capillary flow), and is insensitive to hydraulic conductivity. At lower hydraulic conductivities, saturation time is controlled by the water supply from the host rock. This analysis, however, disregards:

- the possibility of flow along the EDZ or through the partially saturated distance blocks from saturated to unsaturated (tight) drift sections, and
- the impact of repository-generated gas (the gas phase was modelled as being fixed at atmospheric pressure).

Scoping calculations have been performed to estimate the saturation time of a relatively tight drift section (a supercontainer and distance block unit section) adjacent to a more permeable drift section. The relevant processes are sketched in Figure 4-6.

Where a tight drift section exists adjacent to a more permeable drift section (case 3 above), water flow driven by hydraulic pressure gradients along the drift axis may accelerate the saturation process. Scoping calculations of the flow along the EDZ or through the partially saturated distance blocks (and also a discussion of the potential impact of piping) have been performed to estimate the saturation time in case 3.

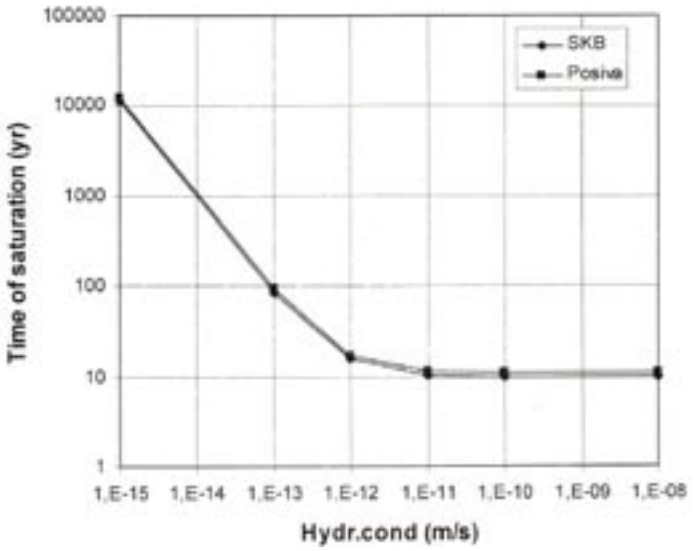

Figure 4-5. *Time to saturation of drift sections containing a supercontainer and distance block for different hydraulic conductivities. The curves are plotted according to SKB's and Posiva's different model geometry for the canister and the near field (e.g. length of the canister). (From Figure 8-14 in /Börgesson et al. 2005/.)*

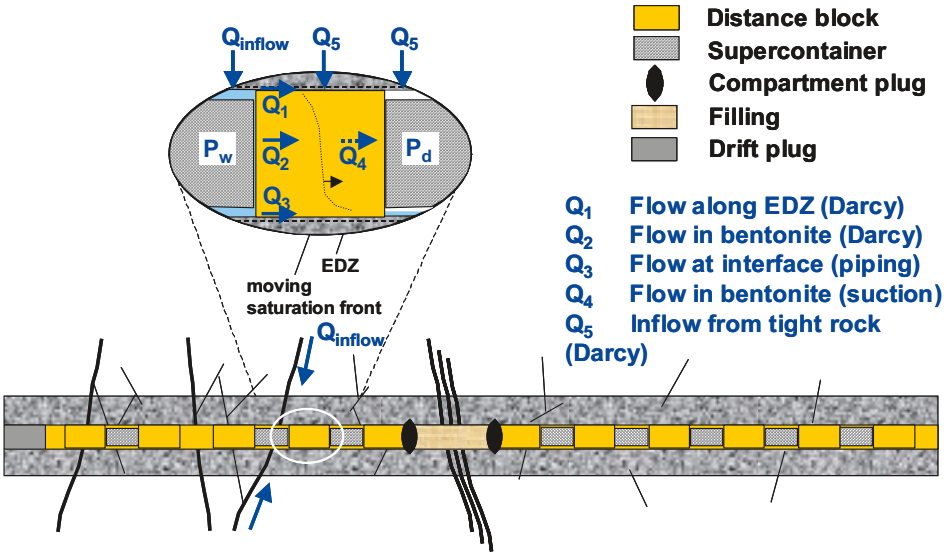

Figure 4-6. *Processes relevant for the transport of water from a permeable drift section towards a supercontainer located in a tight section of the deposition drift (case 3).*

The saturation time of the buffer is determined by the void volume to be filled with water, V [m^3], and the inflow rate of water, Q [m^3 a^{-1}]:

$$T_{sat} = \frac{V}{Q} \qquad \text{(Eq. 4-1)}$$

where

$$V = V_{void} + \varepsilon_B V_B (1 - S_{B,0}) \qquad \text{(Eq. 4-2)}$$

V_{void} void volume within and around a supercontainer (not including unsaturated buffer pores) [m^3]

V_B initial bulk volume of buffer inside a supercontainer [m^3]

ε_B initial buffer porosity [–]

$S_{B,0}$ initial buffer saturation [–]

The initial dry density and water content of the ring blocks (ρ_{rb} [kg m^{-3}] and w_{rb} [% by weight]) around the canister are different from those of the end blocks (ρ_{eb} [kg m^{-3}] and w_{eb} [% by weight]) at each end of the supercontainer.

The initial buffer porosity of the ring blocks, ε_{rb}, is given by:

$$\varepsilon_{rb} = 1 - \frac{\rho_{rb}}{\rho_s} \qquad \text{(Eq. 4-3)}$$

with:

ρ_s mineral density of bentonite [kg m^{-3}]

The initial water content of the ring blocks is related to their saturation, S_{rb}, by:

$$\frac{w_{rb}}{100} = \frac{\varepsilon_{rb} S_{rb} \rho_w}{(1-\varepsilon_{rb})\rho_s + \varepsilon_{rb} S_{rb} \rho_w} \qquad \text{(Eq. 4-4)}$$

with

ρ_w density of water [kg m^{-3}]

Similar equations apply to the end blocks.

Using these equations, Equation 4-2 can be written:

$$V = V_{void} + \pi \left(l_{rb} \left(r_B^2 - r_c^2 \right) \left[\left(1 - \frac{\rho_{rb}}{\rho_s} \right) - \frac{\rho_{rb}}{\rho_w} \left(\frac{w_{rb}}{100} \right) \right] + l_{eb} r_B^2 \left[\left(1 - \frac{\rho_{eb}}{\rho_s} \right) - \frac{\rho_{eb}}{\rho_w} \left(\frac{w_{eb}}{100} \right) \right] \right) \qquad \text{(Eq. 4-5)}$$

with:

r_c canister radius
r_B buffer block radius within a supercontainer [m]
l_{rb} combined length of buffer ring blocks within a supercontainer
l_{eb} combined length of buffer end blocks within a supercontainer

Based on the parameter values given in Appendix A, V takes a value of about 2.7 m^3 (about 1.5 m^3 of open space and an unsaturated bentonite pore volume of about 1.2 m^3). In the following, the saturation time of the buffer in a tight drift section is estimated on the basis of the alternative assumptions that it is controlled by (i), the rate of water flow from a permeable drift section via the EDZ adjacent to the distance block (Q_1 in Figure 4-6), (ii), the rate of water flow through the distance block (Q_4 in Figure 4-6 prior to distance block saturation and Q_2 after saturation), and (iii), the rate of water flow through (poorly transmissive) fractures in the host rock. The possible impact of piping on saturation times is also assessed.

A summary of the results of the scoping calculations of saturation times, described one-by-one in the following sections, is given in Figure 4-7.

Water flow along EDZ

The transport of liquid water in the EDZ surrounding a distance block separating "less tight" and "tight" drift sections, Q_1 [m^{3}a^{-1}], can be estimated using Darcy's law:

$$Q_1 = \pi \left(2r_t + t_{EDZ} \right) t_{EDZ} K_{EDZ} \frac{\Delta P}{\rho_w \, g \, p} \qquad \text{(Eq. 4-6)}$$

with:

r_t drift radius [m]
t_{EDZ} EDZ thickness [m]
K_{EDZ} maximum hydraulic conductivity of EDZ [m s^{-1}]
ΔP magnitude of the pressure difference in the EDZ between the fully saturated ("less tight") drift section and the dry ("tight") drift section [Pa]
g gravitational acceleration [m s^{-2}]
p distance block length [m]

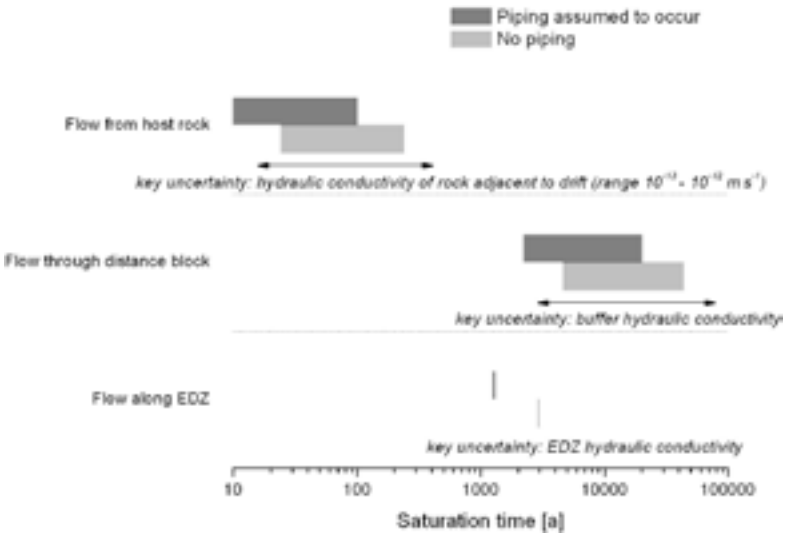

Figure 4-7. *Summary of results of scoping calculations of water saturation of a tight drift section (supercontainer and distance block unit section) adjacent to a more permeable drift section (dark grey bars: piping assumed to occur; light grey bars: no piping).*

The "less tight" section is expected to be fully water saturated within about 10 years after spent fuel emplacement and sealing of the deposition drift, due to the presence of one or more transmissive fractures (see Figure 4-5). The "tighter" section (including its EDZ) remains in an unsaturated state for some time before it is slowly filled with water. Here, it is assumed that the interface between the saturated and unsaturated parts of the EDZ coincides approximately with the interface between the distance block and the supercontainer in the "dry" section (i.e. the EDZ adjacent to the distance block is assumed to be fully saturated). Assuming that the interface is static, the water pressure in the EDZ at the interface is equal to the gas pressure minus the capillary pressure in the EDZ. This can be estimated using Young's equation. Based on the mean aperture of fractures in the EDZ of 2 μm (/Johnson et al. 2005/, Appendix C), a capillary pressure of 0.15 MPa is calculated. This means that the downstream water pressure in the EDZ is lower than the gas pressure by 0.15 MPa. The gas pressure itself is initially atmospheric and gradually increases due to the slow inflow of water and generation of hydrogen gas by anaerobic corrosion of steel.

Based on a maximal pressure difference of 4 MPa, the maximal water flow rate through the EDZ is estimated to be 1 litre a^{-1} and the corresponding minimum saturation time of the buffer is 2,800 years.

In reality, the distance block will remain partially saturated for a prolonged period of time (see below), especially in the vicinity of the "tight" drift section. During transport along the EDZ, some water may thus be sucked from the EDZ radially into the bentonite, leading to a sustained unsaturated state in the EDZ. By this process, the saturation of the distance block is speeded up and the saturation of the "tight" drift section is slowed down. This coupling of processes, which has not been taken into account in the above scoping calculations, would result in an even longer saturation time for the "tight" drift section.

Water flow through the distance block

Upon contact with water entering through the permeable fractures in the "less tight" drift section, the face of the distance block exposed to water starts to take up water by suction and swells, while the remaining part of the distance block is still in its initial (partially saturated) state. In the course of time, a saturation front moves axially through the distance block. It is well established that the dominant water movement in unsaturated bentonite takes place by transport

of vapour when the water content is low and by transport of liquid water when the water content is high. Transport of water in unsaturated bentonite may be represented as a diffusion-like process (see, e.g. /Börgesson 1985, Pusch 2000, JNC 2000/), described by:

$$\frac{\partial S}{\partial t} = \frac{D}{\varepsilon}\frac{\partial^2 S}{\partial z^2} \qquad S(0,t) = 1 \; for \; t > 0; S(z,0) = S_0 \; for \; z > 0 \qquad \text{(Eq. 4-7)}$$

with:

D an empirical coefficient [$m^2 s^{-1}$]

ε buffer porosity

S saturation of bentonite [–]

z axial distance into the distance block from its interface with the supercontainer in the permeable drift section [m]

The distance block porosity will vary slightly with time as the bentonite swells into the gaps surrounding the blocks, but this small effect is neglected here.

Applying this 1-D equation and boundary conditions to the distance block assumes that a free water phase exists across the entire wetted vertical face of the distance block. In reality, contact between the supercontainer and the distance block will restrict the flow of water to the distance block, particularly once the distance block starts to swell, and Equation 4-7 will thus tend to overestimate the rate at which water migrates into the block. It also disregards the impact on the saturation process at the boundary with the supercontainer in the permeable drift section; the impact of this simplification has not been evaluated.

The analytical solution to Equation 4-7 is:

$$S(z,t) = S_0 + (1 - S_0)\, erfc\left[\frac{z}{2\sqrt{Dt/\varepsilon}}\right] \qquad \text{(Eq. 4-8)}$$

where S_0 is the initial saturation of the distance block.

J [m^3], the amount of water that enters the distance block in time t is given by:

$$J = -\pi r_t^2 D \int_0^t \left.\frac{\partial S}{\partial z}\right|_{z=0} dt \qquad \text{(Eq. 4-9)}$$

From Equation 4-8 and Equation 4-9:

$$J = 2\pi r_t^2 (1 - S_0)\sqrt{\frac{\varepsilon D t}{\pi}} \qquad \text{(Eq. 4-10)}$$

An identical equation is obtained if the saturation process is modelled as a moving saturation front, with flow upstream of the front described by Darcy's Law, driven by a "suction pressure" p_s [Pa] given by:

$$\frac{p_s}{\rho g} = \frac{2D}{\pi K_B} \qquad \text{(Eq. 4-11)}$$

where K_B [m a^{-1}] is the hydraulic conductivity of saturated bentonite.

It can be assumed that the distance block is saturated when the amount of water that enters the distance block is equal to the initial unsaturated pore space within the distance block (or equivalently when the saturation front reaches the downstream boundary of the distance block):

$$J = 2\pi r_t^2 (1 - S_0)\sqrt{\frac{\varepsilon D t}{\pi}} = \varepsilon \pi r_t^2 (1 - S_0) p \qquad \text{(Eq. 4-12)}$$

$$t = \frac{\pi \varepsilon p^2}{4D} \qquad \text{(Eq. 4-13)}$$

with p [m] being the distance block length.

The critical parameter for this process is the effective water diffusion constant which depends on a number of variables (water content, temperature, etc). /Börgesson 1985, Pusch 2000/ provide a value of 3×10^{-10} m^2 s^{-1}. /JNC 2000/ gives effective diffusion constants of 10^{-9}–10^{-10} m^2 s^{-1}, for a range of volumetric water contents of 0.05–0.3 and for a temperature range of 25–60°C. Using an effective diffusion constant of 10^{-9} m^2 s^{-1}, Equation 4-14 gives a saturation time of about 300 years. Alternatively, the time to saturation is about 1,000 years for an effective water diffusion constant of 3×10^{-10} m^2 s^{-1}.

Once the distance block is largely saturated, water will flow through the distance block from the permeable drift section at a rate Q_2 [m^3 a^{-1}] that can be estimated using Darcy's law:

$$Q_2 = \pi r_t^2 K_B \frac{\Delta P}{\rho_w g\, p} \qquad \text{(Eq. 4-14)}$$

with:

r_t	drift radius [m]
p	distance block length [m]
K_B	hydraulic conductivity of saturated buffer [m s^{-1}]
ΔP	maximum pressure difference along the drift [Pa]
ρ_w	density of water [kg m^{-3}]
g	gravitational acceleration [m s^{-2}]

This yields an estimated water flow rate through a fully water-saturated distance block of 0.06 to 0.6 litres per year for the range of buffer hydraulic conductivities given in Table 4-2 and a saturation time of the 2.7 m^3 total void volume in a supercontainer section of 4,300 to 43,000 years, calculated from the time of distance block saturation. Adding the time of distance block saturation, gives a total saturation time in the range of above 4,600 to 44,000 years.

Inflow from tight rock

The inflow of liquid water from the tight rock directly into the "tight" section can also be estimated using Darcy's law in a radial configuration (Thiem's equation), as given by Equation 4-15, expressed in terms of the hydraulic conductivity of the rock adjacent to the drift section containing a supercontainer (K [m s^{-1}]):

$$Q_5 = 2\pi l_s K \frac{\Delta P}{\rho_w g \ln(l_h / r_t)} \qquad \text{(Eq. 4-15)}$$

with

l_s the length of a supercontainer [m]

l_h hydraulic length (from drift to nearest major fracture zone) [m]

Tighter drift sections, as defined at the beginning of Section 4.5.1, have hydraulic conductivities in the range 10^{-13} to 10^{-12} m s^{-1}. This gives water flow rates in the range 11–110 litres per year and saturation times of the buffer in the range 24 to 240 years. Where hydraulic conductivities exceed the higher end of this range, saturation times will be controlled not by fracture transmissivity, but rather by the ability of the bentonite to take up water. Thus, in accordance with the results shown in Figure 4-5, saturation will take a minimum of about 10 years.

For tighter drift sections, saturation will be hindered even more by the build-up of gas pressure due to anaerobic corrosion of steel (see Figure 5-1).

Possible impact of piping on the time to saturation

Flow of water along the bentonite/host rock interface (which is experimentally observed to occur in discrete channels and is termed piping) is described in Section 4.5.2. If piping were to occur, significant water flow (conveying some suspended bentonite) could take place through the pipes from a "less tight" drift section down gradient to a tighter section. In Section 4.5.2, it is noted that laboratory and modelling studies indicate, in the case of the current reference design (Basic Design), that transient hydraulic pressure differences along the drifts will not develop sufficiently rapidly to cause piping provided the inflow rate to a drift section including a supercontainer plus a distance block during saturation is 0.1 litres per minute or less. Whether the inflow is distributed or in a single source point does not affect piping if the inflow is below 0.1 litres per minute. If the inflow is 0.1 litres per minutes or slightly higher, distributed sources of inflow do not necessarily imply piping. This is a preliminary design criterion for supercontainer and distance block emplacement. Of course, small and evenly distributed sources of inflow (vs. one inflow point of 0.1 litres per minute) allow a quicker and more uniform buffer swelling.

Even if piping were to occur, its duration and impact would be limited. When all open voids in the "tight" section (excluding unsaturated bentonite pores) became filled with the water/bentonite suspension, the pressure gradient along the pipes would decrease, the flow through the pipes will stop and the pipes would be closed by bentonite swelling provided that the outer plug is tight. The time needed to fill all open voids within and around a supercontainer (V_{void} – about 1.5 m^3) is estimated to be several days to weeks, mainly depending on the pressure gradient and on the rate of water inflow into the "less tight" drift section. Thereafter, gradual saturation of the remaining pore volume (2.7–1.5 m^3 = 1.2 m^3) will occur by the same processes as described above (Q_1, Q_2, Q_4, Q_5, defined as in Figure 4-6):

- for saturation via a flow of 1 litre per year along the EDZ (Q_1), the minimum time to saturation is reduced from 2,900 years to 1,300 years;
- for saturation via flow of between 0.06 and 0.6 litres per year through a saturated distance block (Q_2), the time to saturation of a supercontainer section is reduced from between 4,300 and 41,000 years to between 1,900 and 19,000 years; combined with a distance block saturation time of 300 to 1,000 years (via Q_4), this gives a total saturation time in the range of above 2,200 to 20,000 years, compared with a range without piping of 4,600 to 44,000 years; and
- for saturation via inflow from the rock a rate of between 11 and 110 litres per year (Q_5), the time to saturation is reduced from between 24 and 240 years to between about 10 and 100 years; for lower hydraulic conductivities, the impact of gas is likely to extend the time to saturation to several thousand years.

In summary, heterogeneity of the near-field rock results in widely differing saturation times for different drift sections, with the tightest drift sections potentially remaining only partially saturated for up to thousands of years. Changes may occur during this time, including mechanical failure of the supercontainer. Furthermore, on a timescale of a few years, thermal spalling may occur in drift sections in which the buffer does not exert swelling pressure on the drift wall (Section 4.4). No irreversible chemical changes are, however, expected to affect the bulk of the buffer (Section 4.7), although some more localised changes due, for example, to iron-bentonite interaction, may take place (Section 4.7.1). Even in the tightest drift sections, the buffer is expected to retain its initial water content, and will eventually fully saturate, at which time it is expected to perform its full range of safety functions.

Handling in the safety assessment for KBS-3H

THM modelling is used to identify important factors affecting the resaturation of the buffer in KBS-3H. Even in the case of a canister with an initial penetrating defect, the maximum expected defect size (r = 0.5 mm) would permit very little water to enter a canister during the transient hydraulic phase, thus no continuous hydraulic pathway for transport of dissolved radionuclides would be expected to exist during this period. Therefore, the buffer is assumed to be fully saturated in all radionuclide release and transport assessment cases (see Section 2.5.1). In the Radionuclide Transport Report /Smith et al. 2007a/, three calculations cases address processes that may affect mass transfer at the buffer/rock interface, as described in Section 4.7.1.

4.5.2 Piping/erosion as a hydraulic process

Overview/general description

Piping may in principle take place as long as significant hydraulic driving forces persist in the deposition drift, i.e. from the time of emplacement of the first supercontainers until the time of pressure equilibration. Physically, piping occurs when a critical hydraulic gradient is exceeded. Further requirements are i) that the hydraulic conductivity of the bentonite is so low that water flow into the bentonite is essentially stopped and ii) that there is a downstream location available for the removal of eroded materials for the pipe to stay open (some internal piping – i.e. formation of pipes that terminate within the distance blocks, has been observed experimentally, and may accelerate the saturation of the blocks). The critical hydraulic gradient depends on bentonite and fluid properties, on geometry and on hydrogeological conditions. For the sealing ability of the bentonite, the following factors seem to be the most important ones: swelling properties of bentonite, geometrical factors, water inflow rate and water pressure increase rate /Börgesson and Sandén 2006/. Initially, when the bentonite is partially saturated and partially swollen, the critical hydraulic gradient is low. It increases substantially in the course of bentonite saturation and swelling and levels off as the bentonite reaches full saturation. As long as real hydraulic gradients remain smaller than the critical value at all points in the deposition drift, piping does not occur (Figure 4-8).

Currently, there is no detailed model available for the time-dependent critical hydraulic gradient under conditions relevant for KBS-3H /Börgesson and Sandén 2006/[21]. It has been shown, however, by laboratory tests that piping at the bentonite/rock interface can be prevented in the Basic Design if all of the following conditions are fulfilled /Börgesson et al. 2005/:

- the inflow rate from the rock is below 0.1 litres min^{-1},
- the pressure increases at rates below 0.1 MPa $hour^{-1}$,
- the total applied pressure difference is below 2 MPa,
- the gap between rock surface and distance block is small.

[21] Note that there exists over one hundred years of experience in the field of soil piping in civil engineering (e.g. failure analysis for levees and dams), where criteria for soil piping have been developed for various conditions. These criteria cannot, however, directly be transferred to the case of a KBS-3H repository because the conditions and materials used are significantly different.

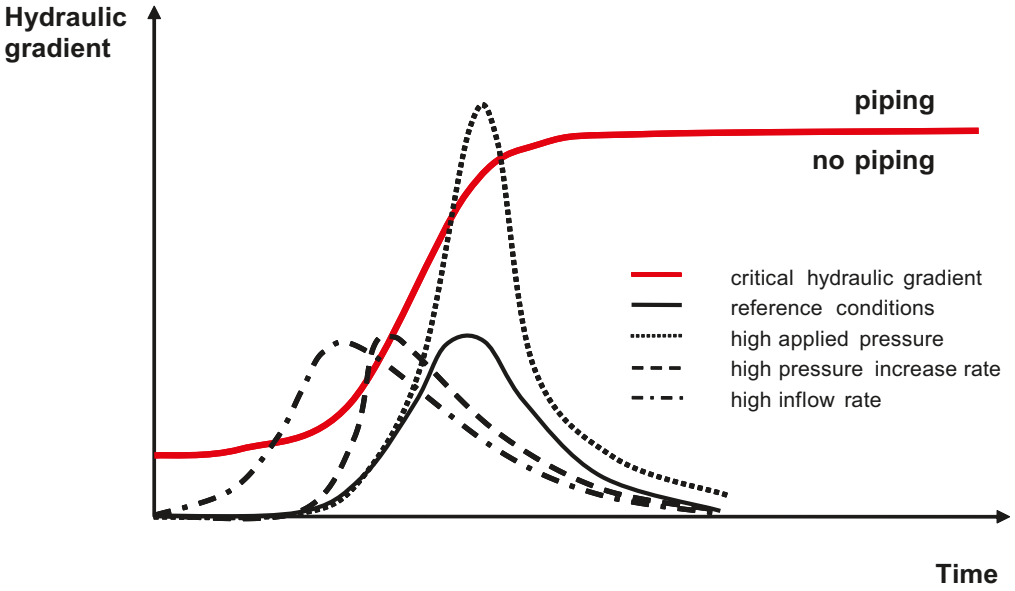

Figure 4-8. *Schematic evolution of the critical hydraulic gradient for piping and comparison with various conceivable situations under which piping will or will not occur. The bell-shaped curves represent the hydraulic gradient that may be established within a deposition drift due to heterogeneous saturation (e.g. between adjacent "less tight" and "tight" drift sections). Under reference conditions, the critical hydraulic gradient is not exceeded. Various situations are sketched where the hydraulic gradient exceeds the critical value (by the presence of high applied pressure, high pressure increase rates or high inflow rates) and where, as a consequence, piping is occurring.*

Assuming that saturation in a drift section occurs principally due to radial inflow from the rock (rather than water migration parallel to the drift), a relationship between fracture transmissivity and the rate at which a drift section saturates with water in the early phase may be obtained from Darcy's law in a radial configuration (Thiem's equation). Assuming that n fractures intersect the section:

$$Q = 2\pi nT \frac{\Delta P}{\rho_w g \ln\left(l_h / r_t\right)} \qquad \text{(Eq. 4-16)}$$

with:

Q inflow from the n intersecting fractures [$m^3\ s^{-1}$]

T fracture transmissivity [$m^2\ s^{-1}$]

ΔP magnitude of the maximum hydraulic pressure difference between the drift and the undisturbed rock during saturation [Pa]

l_h hydraulic length (from drift to nearest major fracture zone) [m]

r_t drift radius [m]

According to this equation, a single fracture with a transmissivity 3×10^{-9} $m^2\ s^{-1}$ will deliver an initial inflow of about 0.1 litres per minute, which is currently taken to be the maximum allowable value if the possibility of piping and erosion is to be avoided.

Currently, these conditions are termed "reference conditions", but the values may be changed in the future if new experimental evidence is available. 0.1 litres per minute is set as the maximum inflow rate to a drift section to be used for supercontainer and distance block emplacement. This estimate of post-closure inflow and resaturation based on the transmissivity of fractures intersecting the drift and assumed hydrostatic recovery should provide a reasonably conservative guide to the likely behaviour. The effects of grouting, ongoing changes in drawdown around

the drift due to operation of the repository, connectivity of the fracture network and unsaturated conditions will all affect the actual inflow.

If the reference conditions are not met due to unfavourable hydraulic conditions at specific locations in the deposition drift (with e.g. large heterogeneities in the water inflow rates between adjacent supercontainer units), it is difficult to show the impact of piping/erosion on long-term safety. In particular, the rate of hydraulic pressure increase once the gaps are filled with water appears to be difficult to determine and requires further investigation. A loss of swelling pressure in some supercontainer sections due to piping and erosion could lead to enhanced thermal spalling due to reduction in confining pressure associated with time-dependent degradation of rock strength. These issues, as well as the uncertainties involved, are discussed in Section 4.6.1.

The reference design has been shown to behave favourably with respect to piping and erosion in reference conditions as well as in more extreme conditions. However, recent modelling calculations concerning the effect of the hydraulic pressure on the fixing ring raise some doubts related to the overall performance of the Basic Design.

Figure 4-8 also shows situations where piping may actually occur as a result of less favourable hydraulic conditions. For example, if the inflow rate in some specific drift section is much higher than the reference value, the hydraulic gradient between this section and an adjacent "tight" drift section may rise much faster than the critical gradient, leading to piping.

Once piping has occurred, the open pipes persist as long as the erosion rate of bentonite at the pipe surfaces exceeds the bentonite swelling rate. Erosion will take place if the drag force on clay particles exerted by the flowing water is higher than the sum of the friction and attraction forces between the particles and the clay structure. While pipes remain open, significant water flow (conveying some suspended bentonite) may take place through the pipes. When all open voids in the sink (e.g. a "tight" drift section down gradient) are filled with the water/bentonite suspension, there will be no hydraulic gradient along the pipes, the flow through the pipes will stop and the pipes will be closed by bentonite swelling. The impact of the redistribution of bentonite within a deposition drift by piping/erosion is discussed in Section 4.6.1. As discussed above, the Basic Design seems to perform well with respect to the piping and erosion issue. The alternative design option DAWE is more sensitive to piping/erosion, as discussed in Appendix D, and this issue needs to be further studied.

Boundary conditions

The piping and erosion processes that are discussed here take place only at the interface between the buffer material (in particular the distance block) and the rock.

Model studies/experimental studies

The functioning of the distance block in KBS-3H, and, in particular, the conditions under which piping/erosion occurs, have been investigated by a series of laboratory tests in small and large scale /Börgesson et al. 2005, Sandén et al. 2007, Autio et al. 2007/. In the following, the relevant studies and main results are briefly discussed.

Tests in scale 1:10 of the functioning of the distance block

The complexity of processes and system geometry called for laboratory tests in scale 1:10, with the objective to improve the understanding of the relevant processes and to develop the techniques for making the distance block function properly. For the tests, the following *reference conditions* were defined: Inflow takes place in one point above and in the centre of the package with the perforated steel container with an inflow rate equivalent, in terms of filling time, to an inflow rate of 0.1 litre min^{-1} in the KBS-3H drift When the inflow is stopped by bentonite sealing, the water pressure is built up at a rate of 0.1 MPa h^{-1} up to a maximum of 2 MPa. An example of a test apparatus used is shown in Figure 4-9.

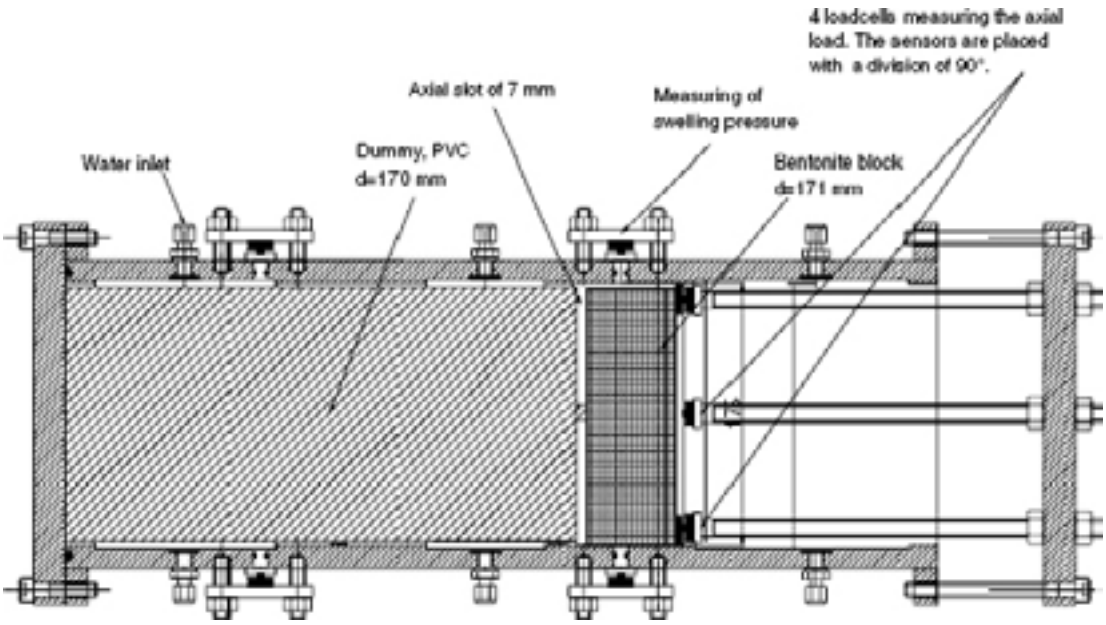

Figure 4-9. *Cross-section through one of the apparatuses used for the sealing/piping/ erosion tests in scale 1:10. From Figure 7-5 in /Börgesson et al. 2005/. The perforated supercontainer has been replaced by a PVC dummy. The slot between the bentonite block and the steel shell of the apparatus is 4 mm. Water is filled in one point above the PVC dummy at controlled rates (for details see /Börgesson et al. 2005/). Axial displacements of the distance block are monitored and axial forces are measured by load cells.*

The following main conclusions were drawn from tests of the distance block in scale 1:10 /Autio et al. 2007/:

- The filling rate and the water pressure increase rate are very important for the sealing ability. For reference conditions, the distance block seems to seal in the scale 1:10 if the annular gap between the rock and the distance block is not larger than 2–20 mm or if a pellets filled annular gap is not larger than about 15 mm.
- If the distance block seals and prevents leakage, the water pressure built up behind the distance block must be counteracted by a supporting ring. With this suggested solution, the sealing of the distance block works very well for reference conditions.
- The sealing did not work for higher water pressures.
- A gap between the supercontainer and distance block should be avoided as far as possible because it increases the force on the fixing ring.

Further scale tests have been performed to explore the impact of more unfavourable conditions with respect to the reference conditions /Sandén et al. 2007/, in particular, an inflow rate of 1 litre min^{-1}, a pressure increase rate of 1 MPa h^{-1} and a maximum water pressure of 5 MPa. The tests performed are listed in Table 4-10 and Figure 4-10 shows results for the case III-1 (large radial gap of 35/35 mm, where sealing was not successful) and for the case III-2 (small radial gap of 2/0 mm, where sealing was successful). The preliminary conclusions of these recent tests can be summarised as follows /Sandén et al. 2007/:

- For extreme conditions, the distance block seems to seal in the scale 1:10 if the annular gap between the rock and the distance block is not larger than 2.5–5 mm. It does not seal in the case of a pellet-filled annular gap.

Table 4-10. Tests performed at scale 1:10 for various unfavourable hydraulic conditions with respect to the reference conditions /Sandén et al. 2007/.

Test	Arrangement	Slot top/bottom mm	Test length m	Filling time days	Filling rate scale 1:1 l/min	Water pressure increase rate kPa/h	Maxiamal pressure kPa	Water type	Comments
III-1	35 mm slot filled with pellets	35/35	0.94	1.6	0.63		350	Tap water	After filling, a constant flow of 5 l/24h was applied. **The system did not seal**.
III-2	D bentonite 173 mm	2/0	0.94	1.9	0.53	1,000	5,000	Tap water	Some "internal piping" during the pressure ramp. **The system seals.** Water penetration 71cm in bottom.
III-3	D bentonite 170 mm	5/0	0.94	1.9	0.53	1,000	820	Tap water	"Internal piping" continued with piping. **The system did not seal.** The outer surface completely wet.
III-4	D bentonite 170 mm Pre wetted bentonite	5/0	0.94	1	1	1,000	5,000	Tap water	Some "internal piping" during the pressure ramp. **The system seals.**
III-5	D bentonite 165 mm Pre wetted bentonite	10/0	0.94	1	1	1,000 / 100	4,200	Tap water	The system can not stand the fast pressure build up. The bentonite can withstand 4.2 MPa after 2 weeks
III-6	15 mm slot filled with pellets Pre wetted bentonite	15/15	0.94	1	1	1,000 / 100	1,800	Tap water	The system can not stand the pressure build up. The bentonite can withstand 1.8 MPa after 2 weeks
III-7	D bentonite 170 mm	5/0	0.94	1	1	1,000	5,000	3.5 % salt	The salty water increases the swelling rate and by that also the sealing effect. **The system seals.**
III-8	D bentonite 165 mm Pre wetted bentonite	10/0	0.94	1	1	1,000	1,600/3,600	3.5 % salt	Piping at 1600 kPa. After 12 h resttime new pressure ramp. Clay pressed out at 3600 kPa.
III-9	D bentonite 165 mm Pre wetted bentonite	5/5	0.94	1	1	1,000	5,000	3.5 % salt	Some "internal piping" during the pressure ramp. **The system seals.**
III-10	D bentonite 165 mm Pre wetted bentonite	5/5	0.94	1	1	1,000	4,600	3.5 % salt	Repeating test III-9 "Internal piping" during the pressure ramp. **The system could not take 5 MPa.**
III-11	D bentonite 165 mm Pre wetted bentonite	5/5	0.94	1	1	1,000	5,000	3.5 % salt	Repeating test III-9 "Internal piping" during the pressure ramp. **The system seals.**
III-12	Drainage tube under block Pre wetted bentonite	10/10	0.94	Controlled (7days)	Controlled	1,000	1,700/800	3.5 % salt	Pre test with drainage tube. The system can not stand the fast pressure build up. Max 800 kPa after 20 days.
III-13	Pre wetted bentonite	10/10	0.94	-	-	1,000	5,000	3.5 % salt	After pre wetting of the slot, sample had no access to additional water. Water pressure was increased after 3 months
III-14	Drainage tube, 5mm axial slot Pre wetted bentonite	4/0	0.94	Controlled	Controlled	Controlled	5,000	3.5 % salt	Sr block=94% The bentonite can withstand 5 MPa after 20 d

Large-scale tests of the functioning of the distance block

With the objective of investigating scale effects, several tests were performed at large scale (about 1:2 scale) in the test equipment designed for the Big Bertha experiment /Börgesson et al. 2005/.

The conclusions drawn from the large scale sealing tests are the following:

- The scale effects are strong.
- Sealing is feasible for the reference conditions if a supporting ring and a very small gap of a few mm are used.
- The measured total force caused by a high water pressure inside the distance block does not correspond to the full circular area of the distance block. In fact, the hydraulic pressure is exerted only on a ring-shaped surface with an outer radius corresponding to the drift radius and a radial thickness of 10–15 mm.
- It is important, however, to avoid a slot between the bentonite blocks and between a bentonite block and the container (although a slot of 7 mm could be handled as shown in the scale tests). In the test there was, however, no steel plate, which may have an impact on the behaviour.
- The results of the large-scale tests confirm the results obtained in the 1:10 scale tests.

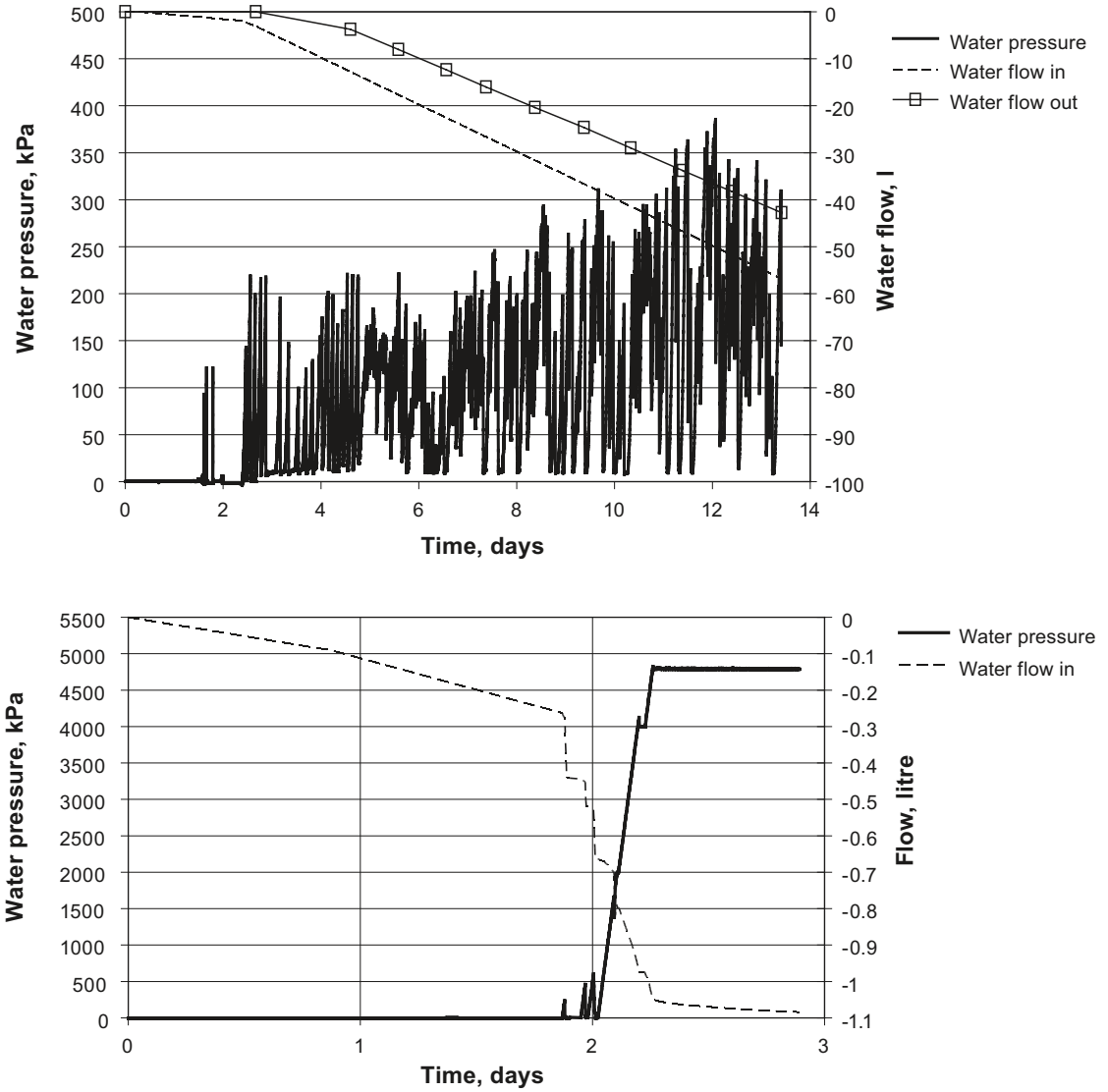

Figure 4-10. *Results from 1:10 scale tests on sealing/piping/erosion. Upper figure: Large gap of 35/35 mm (above /below) between distance block and wall, where sealing failed. Lower figure: Small gap of 2/0 mm (above /below) between distance block and wall, where sealing was successful /Sandén et al. 2007/.*

Additional finite-element modelling results on the Basic Design performance showed that the elastic deformations of the blocks when exposed to a high water pressure would be rather large (Appendix D). The deformations will lead to widening of the gap between the supercontainer and the distance block, which will give the water access to larger surfaces and full hydraulic pressure will be exposed on the whole end surface area of the distance block. This effect is due to the lower elastic modulus of the buffer blocks in light of the low water content (10%wt). Furthermore, the water intrusion in the gap will increase the gap even more in a progressive and self-sustaining fashion.

The demanding hydraulic conditions make it impossible for the distance block sections to withstand 5 MPa water pressure without a strong full plug. The design must thus allow piping and erosion between supercontainer sections before all sections are filled with water. One way to solve the problem is to use the DAWE technique where the drift is kept open and free drainage allowed. A problem with this design is that it is difficult to guarantee that there will be no bentonite slurry flowing along the drift floor out to the part of the drift where the emplacement takes place, since both water dripping on the blocks and humidity induced cracking of the blocks may take place and cause erosion of bentonite.

Recent modelling results may therefore suggest that the Basic Design will not perform as expected unless a steel compartment plug (more resistant than a fixing ring) is inserted to withstand the full hydraulic pressure. New design options are currently being developed to address this issue.

Tests on bentonite erosion

/Börgesson and Sanden 2006/ reported test results on erosion and transport of bentonite for various conditions. In laboratory tests, a suspended solids ratio of 1–10 g litre^{-1} (0.1–1%w) was measured. The measured values decreased with time and are affected by the salt content, flow rate and geometry. In the LASGIT field test, it was found that the suspended solids ratio stabilised at 1 g litre^{-1}, for flow rates in the order of 0.1 litres min^{-1}. The erosion seems to be higher for saline water than for non-saline water. The consequences of piping/erosion on the density of saturated bentonite have been evaluated by scoping calculations for a range of different conditions. For a discussion of the results, see Section 4.6.1.

Prototype repository (Äspö)

The piping phenomena have been observed in two field tests at Äspö (projects LOT and LASGIT). In LASGIT, the flow rate was in the order of 0.1 l/min, yielding an erosion rate of about 1 g litre^{-1} that remained for 2 months before the leakage was stopped artificially /Börgesson and Sandén 2006/.

Natural analogues/observations in nature

Not applicable.

Time perspective

Piping/erosion may take place as long as significant hydraulic driving forces persist in the deposition drift, i.e. from the time of emplacement of the first supercontainers until the time of pressure equilibration.

Handling in the safety assessment for KBS-3H

Under reference conditions and with the Basic Design, limited or no piping/erosion takes place and the process can be neglected in the radionuclide transport calculations. If, however, unfavourable hydraulic conditions exist at specific locations in the deposition drift (with e.g. large heterogeneities in the water inflow rates between adjacent supercontainer units), it must be shown that piping/erosion has no unacceptable impact on long-term safety**.** In particular, the rate of hydraulic pressure increase once the gaps are filled with water appears to be difficult to determine and requires further investigation. More specifically, it must be shown that piping/erosion does not lead to a violation of any of the safety function indicator criteria defined for the buffer. These issues, as well as the uncertainties involved, are discussed in Section 4.6.1.

4.6 Mechanical processes

Swelling/mass redistribution and liquefaction are the only mechanical processes relevant to the buffer. The inter-dependence between these processes and the variables in the buffer is shown in Table 4-11.

The basic processes and the boundary conditions at the canister surface are identical in KBS-3V and 3H. Differences arise, however, due to the specific geometry and boundary conditions outside the buffer, particularly due to the presence of the supercontainer and distance block and due to the properties of the interfaces (gaps) between bentonite and rock. For example, axial displacement of distance blocks/supercontainers by differential saturation and swelling and the effects of piping/erosion and volume expansion by corrosion are qualitatively different in KBS-3V and 3H. While the buffer in KBS-3V may expand by creep into the space above the canister (backfilled deposition tunnel), the buffer in KBS-3H may be axially displaced as whole blocks, involving compaction of adjacent supercontainer units. These and other processes will affect the density of the saturated bentonite (see Section 4.6.1). The effect of buffer density variations on the pressure exerted on the canister is discussed in Section 3.6.1.

The fundamental processes leading to swelling of bentonite are discussed in detail in the Process Reports for KBS-3V /Rasilainen 2004, SKB 2006d/. These discussions are, therefore, not repeated here.

Liquefaction is a mechanical process involving a transition of a stiff material (soil) into a liquid due to an effect with short duration /SKB 2006d/. It may take place in loose sand when the pore water pressure is increased due to vibration that cause the sand particles to float, or by a strong upward water flow leading to a vanishing effective stress (quick sand). A similar phenomenon has been observed during uniaxial compaction of bentonite at very high water ratios and stresses /SKB 2006d/. When the bentonite reaches a state of full saturation by compression, all further increases in stress will be taken by the water and the bentonite will behave like a liquid (vanishing effective stress). Based on current understanding, the actual transition of bentonite to a liquid phase is, however, considered highly unlikely under the expected repository conditions. Moreover, the boundary conditions involved in KBS-3H are more favourable than in KBS-3V, due to the larger canister surface area to be supported by the buffer, requiring lower effective stresses to prevent canister sinking (see also Section 4.6.1). Buffer liquefaction is thus neglected in the safety assessment for KBS-3H. There are no additional comments to the discussion of liquefaction presented for KBS-3V in /SKB 2006d/.

Table 4-11. The interdependence of hydraulic processes and identified variables in the buffer.

Mechanical processes	Variables for the buffer											
	Geometry	Pore geometry	Radiation intensity	Temperature	Water content	Gas content	Hydrovariables	Stress state	Bentonite composition	Montmorillonite composition	Porewater composition	Structural and residual materials
Swelling/mass redistribution	×	×		×	×	×	×	×	×	×	×	×
Liquefaction	×	×			×	×	×	×				

4.6.1 Swelling/mass redistribution

Overview/general description

The mechanical behaviour of the buffer in a KBS-3H deposition drift is affected by a large number of processes. Among these, swelling of bentonite is the most important process for ensuring its safety functions. Other relevant processes that affect the mechanical behaviour of bentonite are:

- Mass redistribution
  - axial displacement of distance blocks and supercontainer by differential saturation and swelling
  - vertical displacement of supercontainer by off-centred swelling pressure
  - piping/erosion
  - bentonite erosion into fractures
  - convergence of deposition drift
  - creep
  - shear displacements
  - humidity-induced swelling/cracking in the initial phase
- Chemical processes
  - volume increase by steel corrosion products
  - iron/bentonite interaction
  - interaction with high-pH leachates from cementitious materials
  - other geochemical processes (e.g. effects of Ca/Na exchange, saline groundwater, dissolution/precipitation of impurities in bentonite due to temperature gradients, etc)
- Thermal processes
  - thermal expansion of buffer porewater

In previous Process Reports for KBS-3V /SKB 1999, Rasilainen 2004, SKB 2006d/, the description of the swelling process in bentonite and the various processes affecting it are presented in great detail, together with other processes that may cause bentonite mass redistribution within the engineered barrier system, namely thermal expansion, creep and a number of interactions with the canister, near-field rock and the backfill. In general, the description of these processes relevant to swelling of bentonite and mass redistribution given in /SKB 1999, Rasilainen 2004/ and /SKB 2006d/ presents a comprehensive state-of-the-art review of current scientific knowledge. Most of these processes are similar or even identical in KBS-3H and KBS-3V and are thus not repeated here. Specific chemical processes related to the presence of steel in KBS-3H deposition drifts are addressed in Section 4.7.

Furthermore, special attention has been paid to the issue of vertical displacements of the canister within the buffer in KBS-3V (canister sinking/heaving). It has been shown in a number of consolidation and creep calculations using the finite element program ABAQUS, that the vertical displacements of the canister are very small even in the case of low bentonite densities and swelling pressures, in the order of 0.35 mm for base case assumptions and up to 23 mm for extreme conditions /Börgesson and Hernelind 2006a/. In /SKB 2006a/, a safety function indicator criterion for the minimum swelling pressure has been set to 0.2 MPa, aiming at avoiding canister sinking in KBS-3V. In KBS-3H, the extent to which canister sinking occurs is even smaller, due to the fact that the weight of the canister is distributed over a greater area than in KBS-3V. Canister sinking is discussed in Section 3.6.1. Irrespective of this difference in orientation, the same safety function indicator and criterion as for KBS-3V is used also in KBS-3H (see Table 4-5). This issue is, therefore, not further discussed in the present report.

The present chapter focuses on processes related to redistribution of bentonite that have a different significance for, or potential impact on, KBS-3H compared with KBS-3V:

- Axial displacements of distance blocks and supercontainers are of particular relevance in KBS-3H and may be caused by differential saturation and swelling along the deposition drift. Depending on the nature and rates of changes of the mechanical stresses, displacements may occur concurrent with the relatively slow swelling process, or in a more abrupt manner due to hydraulic forces leading to the abrupt sliding of entire supercontainer units.
- Vertical displacement of the supercontainer due to extrusion of bentonite in the lower part of the drift, leading to regions with slightly different swelling pressure (although there will be at least partial homogenisation over time).
- Erosion and redistribution of bentonite could take place if piping were to occur (the conditions that could give rise to piping and erosion are discussed in Section 4.5.2).
- Bentonite erosion into fractures may be of concern during the operational phase, namely if a sealed compartment is hydraulically connected to some nearby open rock excavation, and, in the much longer term, during glacial conditions when groundwater with low ionic strength comes into contact with bentonite extruding into fractures.
- Bentonite compaction due to volume changes by formation of steel corrosion products (mainly magnetite, but also some iron sulphide and siderite).
- Impact of rock shear displacements (greater than 0.1 m) on distance block or on filling blocks between compartment plugs.

Note that the redistribution of bentonite may both decrease and increase the saturated density of bentonite and affects thus the safety function indicators for the buffer and distance block. Additional scoping calculations are presented in this chapter that aim at quantifying the effects of various processes on the variations of bentonite density in KBS-3H deposition drifts, especially in the early phases of repository evolution including the operational phase (see Figure 4-11).

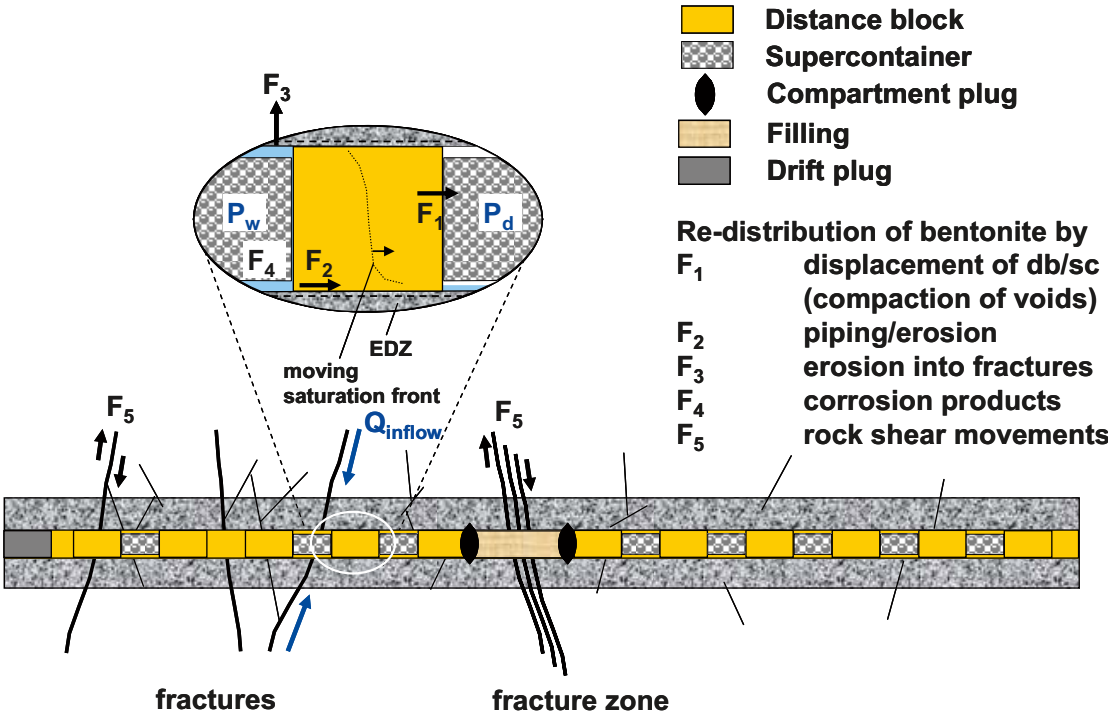

Figure 4-11. *Processes relevant for the redistribution of bentonite in a KBS-3H deposition drift.*

Model studies

Scoping calculations have been performed to estimate the effects of bentonite redistribution in KBS-3H deposition drifts. The relevant processes are sketched in Figure 4-11.

In the case of processes assumed principally to affect a distance block, the resulting change in saturated buffer density, $\Delta\rho$ [kg m^{-3}], is given by:

$$\Delta\rho = \frac{\rho_0 V_0 + \Delta m}{V_0 + \Delta V} - \rho_0 \qquad \text{(Eq. 4-17)}$$

with:

ρ_0 the density of the saturated buffer [kg m^{-3}]

and

$$V_0 = \pi r_t^2 p \qquad \text{(Eq. 4-18)}$$

with:

r_t the drift diameter [m]
p the distance block length [m]

In the case of processes assumed to affect principally the buffer originally inside a supercontainer:

$$\Delta\rho = \frac{\rho_0 V_{B,0} + \Delta m}{V_{B,0} + \Delta V} - \rho_0 \qquad \text{(Eq. 4-19)}$$

$$V_{B,0} = \pi\left(r_t^2 l_s - r_c^2 l_c - \left(1 - \frac{Z}{100}\right)\left(r_{s,o}^2 - r_{s,i}^2\right)\left(l_s - 2t_s\right) - 2r_{s,o}^2 t_s \right) \qquad \text{(Eq. 4-20)}$$

with:

l_s the length of a supercontainer [m]
l_c the length of a canister [m]
r_c the canister radius [m]
Z the degree of perforation of the supercontainer walls [%]
$r_{s,o}$ the outer radius of the supercontainer [m]
$r_{s,i}$ the inner radius of the supercontainer [m]
t_s the thickness of the supercontainer end plates [m]

Displacement of distance blocks and supercontainers

Differential saturation and swelling along the deposition drift due to the heterogeneous rate of water inflow from the host rock could potentially give rise to either (1), gradual or (2), more abrupt displacement of distance blocks and supercontainers.

Case 1: Gradual displacement could occur as a result of the development of differential swelling pressures along the drift. Upon contact with water entering through permeable fractures in a “less tight” drift section, the exposed face of the distance block starts to take up water by suction and

swells, while the remaining part of the distance block is still in its initial (partially saturated) state. In the course of time, the saturation front moves axially through the distance block. This may result in an axial volume expansion of the swelling distance block, while the part closest to the "less tight" drift section is kept in place by the high swelling pressure exerted on the rock surface. As a consequence, the bentonite density of the distance block would be decreased and the buffer density in the adjacent "tight" section(s) would be increased due to axial compaction of vertical open slots. The slots affected may be both outside and inside the supercontainer, because the steel shell may be deformed or ruptured due to the stresses exerted by the swelling distance block. The density of the buffer in the "less tight" drift section remains unchanged in this situation.

Case 2: More abrupt displacement could occur due to a large hydraulic pressure difference between "less tight" and "tight" drift sections. This is particularly of concern if there is a slot between the distance block and the supercontainer in a "less tight" drift section, increasing the surface of the distance block exposed to the hydraulic pressure and thus resulting in a higher total force on the distance block (and on any supporting rings, if used). As a consequence of the displacement, the buffer density in the "less tight" drift section is decreased and the buffer density in the adjacent "tight" section(s) is increased due to the compaction of voids, while the density of the distance block remains unchanged.

These two possibilities of mass redistribution by displacement are similar in their effects on the final saturated bentonite density, but differ in their evolutionary pathway from emplacement until full saturation. In both cases, the saturated bentonite density variation of the distance block adjacent to the "less tight" drift section (Case 1) and of the buffer in the "less tight" drift section (Case 2) can be estimated based from Equation 4-17 with:

$$\Delta V = \pi r_t^2 \, f \, n; \quad \Delta m = 0 \qquad \text{(Eq. 4-21)}$$

and with:

ΔV	total change of bentonite volume in distance block (Case 1) and in buffer (Case 2) [m^3]
f	total linear compaction[22] by reduction of void space (per "tight" supercontainer unit) [m]
n	number of "tight" supercontainer units compacted by the displacement process [–]

Similarly, the bentonite density variation in the buffer of each compacted supercontainer unit can be calculated from:

$$\Delta V = -\pi r_t^2 \, f \; ; \quad \Delta m = 0 \qquad \text{(Eq. 4-22)}$$

For Case 1, assuming f = 2 (and f=10 for sensitivity analysis purposes) cm per supercontainer unit, the change of volume of the swelling distance block is 0.054 (0.27) m^3 if only one supercontainer unit is compacted (n = 1). For each additional supercontainer (n > 1) the bentonite volume gained by compaction increases accordingly. The corresponding saturated densities of the distance block next to the "less tight" drift section (and values for f=10) are:

- 1,993 (1,964) kg m^{-3}, if only 1 supercontainer unit is compacted
- 1,985 (1,930) kg m^{-3}, if 2 supercontainer units are compacted
- 1,971 (1,864) kg m^{-3}, if 4 supercontainer units are compacted
- 1,957 (1,802) kg m^{-3}, if 6 supercontainer units are compacted.

[22] The total linear compaction f is a measure of the extent to which a supercontainer unit may be axially compacted. It sums contributions from inside the supercontainer (gaps between individual bentonite blocks as well as gaps between blocks and steel wall) and from outside the supercontainer (gaps between steel wall and distance block).

Similarly, for case 2, again assuming f = 2 (10) cm per supercontainer unit, the corresponding saturated buffer densities in the "less tight" drift section are:

- 1,990 (1,950) kg m^{-3}, if only 1 supercontainer unit is compacted
- 1,980 (1,903) kg m^{-3}, if 2 supercontainer units are compacted
- 1,960 (1,815) kg m^{-3}, if 4 supercontainer units are compacted
- 1,941 (1,735) kg m^{-3}, if 6 supercontainer units are compacted

Thus, the scoping calculations indicate that the displacement of distance blocks and supercontainers in a KBS-3H deposition drift has no significant effect on the density of bentonite (i.e. buffer density remains within the range 1,890 to 2,050 kg m^{-3} discussed in Section 4.1.3), only if:

- the total linear compaction per supercontainer unit is not too large; and/or
- the number of supercontainer units affected is also not too large.

Note, however, that, under the assumption that f = 2 cm, the saturated buffer densities of the compacted supercontainer units fulfil the criterion that density < 2,050 kg m^{-3}, irrespective of the case considered and of the number of compacted sections. If f = 10 cm, the buffer density of the compacted supercontainer units marginally exceeds the criterion (2,052 kg m^{-3}).

The number of units affected by the displacement process depends on various factors, including the resistance of the supercontainer against compaction, the distance to the next "less tight" drift section (where full counterforces are developed), the distance to the next steel ring/steel plug and friction forces opposing any displacements. It can be shown by the force balance considerations that the friction force of "tight" drift sections is not sufficient to counteract the force exerted by the swelling pressure of the wetted distance block. Furthermore, the axial stiffness of the supercontainer in a "tight" drift section is not expected to be able to withstand the swelling pressure of a nearby distance block. It will thus be deformed or ruptured and any voids within it will be compacted. There is the possibility that the broken parts of the supercontainer are pressed against the drift walls and block any further displacement. It is, however, difficult to demonstrate that this mechanism actually occurs (for this reason, no credit is taken for this process in the scoping calculations). These considerations suggest that the displacement can only be stopped by the counterforce of a wetted/nearly fully swollen supercontainer unit or by design measures such as the installation of strong fixing rings and/or compartment plugs. The fixing rings and compartment plugs are not designed to withstand significant swelling pressure gradients, and so cannot be relied upon to prevent axial movements due to heterogeneous swelling. Any development of significant swelling pressure gradients will, however, proceed in parallel to the development of high swelling pressures at the drift walls in more rapidly saturated drift sections.

If the total linear compaction per supercontainer is assumed to take the more conservative value of 10 cm, then the maximal distance to the next fully water-saturated unit or reinforced (i.e. fixed as a result of a technical feature such as a fixing ring) unit must be shown not to exceed about 2–3 supercontainer units to keep the bentonite density above a lower bound of 1,890 kg m^{-3}.

Vertical displacement (lifting) of supercontainer by off-centred swelling pressure

Water accumulating in the lower part of the drift can lead to bentonite extruding through the holes in the lower part of the supercontainer, whereas bentonite extrusion in the upper part would occur more slowly due to a somewhat later contact with liquid water. Buffer material extruded through the supercontainer perforations will be of lower density than the bulk of the buffer, and may initially and very locally take the form of a gel. If, during uneven saturation as described above, this material were to flow from the lower to the upper part of the gap around the supercontainer, then an overall higher buffer density in the upper part of the drift could occur

following saturation. Buffer homogenisation could then result in a downward displacement of the canister. A significant effect can, however, be excluded, since internal friction, and friction between the extruded material and the drift wall, will prevent significant flow of extruded material around the gap.

There may, however, be some transient upward vertical displacement of the canister during the saturation process. This could occur if the lower part of the buffer inside a supercontainer is saturated more rapidly than the upper part. In this case, the wetted bentonite in the lower part of the buffer will have a higher thermal conductivity than the drier buffer above, further accentuating the asymmetry of the saturation process. The swelling pressure of the buffer material extruded through the perforations on the lower side of the supercontainer could lift the supercontainer, together with the canister, until the supercontainer contacts the top of the drift. The resulting difference in buffer density above and below the canister is considered in a scoping calculation in Appendix B.4 of the Evolution Report /Smith et al. 2007c/. As the remaining buffer saturates, the initially higher density in the upper part of the drift will tend to homogenise and the canister will return to a more central position in the drift, although some small eccentricity may remain.

The resultant buffer densities in the upper and lower regions are expected to remain within the bounds specified by the safety function indicator criteria for the minimal and maximal buffer densities specified in Table 4-5.

Piping/erosion as a mechanical process

If piping were to occur along the bentonite/rock interface then, as long as the pipes persisted, significant water flow (conveying some suspended bentonite) could take place through the pipes from a "less tight" drift section to a "tight" drift section. The redistribution of bentonite mass in this way would persist until all open voids in the "tight" section (excluding unsaturated bentonite pores) are filled with the water/bentonite suspension. At that point, the pressure gradient along the pipes will vanish, the flow through the pipes will stop and the pipes will close due to bentonite swelling (see Section 4.5.2). The time needed to fill all open voids within and around a supercontainer (about 1.5 m^3) is estimated to be several days to weeks.

The average bentonite density decrease in the distance block adjacent to the "less tight" drift section is calculated based on Equation 4-17 with:

$$\Delta V = 0; \quad \Delta m = -V_{void}\, C_{max}\, n \qquad \text{(Eq. 4-23)}$$

and with

Δm total change of bentonite mass in distance block [kg]
V_{void} void volume around a supercontainer [m^3]
C_{max} maximum bentonite mass assumed to be carried as particles by flowing water [kg m^{-3}]
n number of supercontainer units filled with water/bentonite suspension [–]

Similarly, the average bentonite density increase due to accumulation of bentonite in each affected supercontainer unit can be calculated from:

$$\Delta V = 0; \quad \Delta m = V_{void}\, C_{max} \qquad \text{(Eq. 4-24)}$$

Local density changes in the distance blocks are initially likely to be greater in parts of the distance blocks where erosion has occurred compared with the average. Due to the plasticity of bentonite, it is considered possible that large local density reductions would homogenise over long periods of time, although the timescale is uncertain. Two cases are thus considered:

Case 1: the situation after full homogenisation has taken place; and

Case 2: the situation of an extremely localised density reduction, in which the loss of bentonite affects only 10% of the designed volume and mass of the distance block.

Using the values given in Appendix A, Δm = 75 kg. For each additional supercontainer ($n > 1$) the bentonite mass lost by piping/erosion increases accordingly. The average saturated densities of the distance block next to the "less tight" drift section (i.e. Case 1) are thus:

- 1,995 kg m^{-3}, if only 1 supercontainer unit is filled with a water/bentonite suspension
- 1,990 kg m^{-3}, if 2 supercontainer units are filled
- 1,985 kg m^{-3}, if 3 supercontainer units are filled
- 1,898 kg m^{-3}, if 20 supercontainer units are filled

In the supercontainer units that become filled with the water/bentonite suspension, the average saturated densities of the buffer originally inside the supercontainers are changed to 2,007 kg m^{-3}, irrespective of the number of filled units.

In Case 2, the local density changes of the distance block next to the "less tight" drift section are:

- 1,949 kg m^{-3}, if only 1 supercontainer unit is filled with a water/bentonite suspension
- 1,896 kg m^{-3}, if 2 supercontainer units are filled
- 1,847 kg m^{-3}, if 3 supercontainer units are filled
- 981 kg m^{-3}, if 20 supercontainer units are filled

The above considerations seem to indicate that the redistribution of bentonite by piping/erosion in a KBS-3H deposition drift has no significant effect on the density of bentonite (i.e. buffer density remains within the range 1,890 to 2,050 kg m^{-3} discussed in Section 4.1.3), provided that (i), the total suspended solids ratio is not too large (in the order of a few weight% (note that the 5% weight ratio of bentonite/suspension assumed in these calculations is a pessimistic, high value), (ii) the volume available to be filled with suspension is not too high – i.e. only a few supercontainer units are filled, and (iii), local density changes are quickly homogenised by the plasticity of bentonite. Moreover, the increase in bentonite density in each of the filled supercontainer units is marginal, i.e. to a value 2,007 kg m^{-3}, irrespective of the number of filled units.

Redistribution of bentonite by erosion into fractures during the operational phase

Plugs and compartments will be positioned in such a way that no highly transmissive fracture pathways exist from a sealed drift section into any open rock excavations. There may, however, be some less transmissive fractures that provide a hydraulic connection between a sealed drift compartment and:

- an open central tunnel via a fracture bypassing the plug at the end of the drift;
- an open neighbouring drift via a fracture through the near-field rock; or
- an open compartment in the same drift, by-passing the compartment plug.

These fractures could convey significant amounts of water and suspended bentonite if the sealed compartment is quickly saturated and pressurised so that large hydraulic gradients are established between the sealed compartment and any nearby open rock excavations. Thus the relevant process during the operational phase is mechanical erosion of bentonite (particle entrainment by flowing water). Although it seems likely that such fractures would be self-sealed by accumulation and swelling of the intruded bentonite, there is a risk of ongoing bentonite erosion if the fracture aperture is too large. In the following calculations no credit is taken for the possible sealing of fractures.

If the breakthrough of any significant flows of water, possibly conveying some suspended bentonite, were observed in the open rock excavations, measures would be taken to stop the flow (grouting, etc). In the following calculations, it is therefore assumed (though in practice it cannot be taken for granted) that the flow of water could be stopped in due time, e.g. within less than a year.

As in the case of erosion by piping, local density changes in the distance blocks are initially likely to be greater in parts of the distance blocks where erosion has occurred compared with the average; two limiting cases are considered:

Case 1: the situation after full bentonite homogenisation has taken place; and

Case 2: the situation of an extremely localised density reduction, in which the loss of bentonite affects only 10% of the designed volume and mass of the distance block.

The average bentonite density variation in the buffer adjacent to a transmissive fracture conveying water/bentonite suspension is calculated based on Equation 4-25 with:

$$\Delta V = 0; \quad \Delta m = -Q\tau\, C_{max} \qquad \text{(Eq. 4-25)}$$

Δm total change of bentonite mass in buffer next to the fracture [kg]

Q flow rate through fracture from sealed drift into open excavation [$m^3\ a^{-1}$]

C_{max} maximum bentonite mass assumed to be carried as particles by flowing water [kg m^{-3}]

τ time needed to stop the flow of water through the fracture [a]

In Equation 4-25 it is pessimistically assumed that any bentonite lost into the fracture stems from the buffer originally contained within a single supercontainer. In reality, neighbouring supercontainer buffer sections and distance blocks may also be affected, which would mitigate the effects of erosion on the saturated bentonite density.

If a fracture intersecting an open drift also intersects a sealed compartment in a parallel drift, and this sealed compartment contains water-filled void space with a high hydraulic conductivity, then the proportion of the total inflow to the open drift that passes through this void space may be approximated as:

$$\frac{r_f C}{\pi s} = 0.024 \qquad \text{(Eq. 4-26)}$$

with

s drift separation [m]

C is a flow concentration factor accounting for the convergence of the streamlines towards the sealed compartment, set to 2.

Assuming a high inflow rate via the fracture to the drift of 0.1 litres per minute, the corresponding flow rate conveying suspended buffer material from the sealed compartment is 2.4×10^{-3} litres per minute[23]. The average saturated densities of the buffer next to the permeable fracture connecting the sealed section with any open excavation (i.e. Case 1) are:

- virtually unchanged, if the flow of water is stopped within 1 month
- 1,996 kg m^{-3}, if the flow of water is stopped within 1 year.

[23] Lower rates are calculated on the basis of the DFN modelling reported in /Lanyon and Marschall 2006/. In particular, using the model of two adjacent drifts W01T22 and W01T23, net steady-state fluxes through a supercontainer section are calculated as having a mean value of 3×10^{-4} litres per minute and a maximum of 10^{-3} litres per minute.

In Case 2, the local density changes are:

- 1,997 kg m^{-3}, if the flow of water is stopped within 1 month
- 1,958 kg m^{-3}, if the flow of water is stopped within 1 year

These results indicate that the redistribution of bentonite by erosion into a permeable fracture connecting a sealed KBS-3H deposition drift with any open rock excavation is unlikely to have a detrimental effect on the capacity of the eroded buffer to perform its safety functions (i.e. buffer density remains within the range 1,890 to 2,050 kg m^{-3} discussed in Section 4.1.3).

As discussed in the KBS-3H Evolution Report /Smith et al. 2007c/, bentonite gel that has intruded into fractures intersecting the drift could potentially break up and disperse in the form of colloids if the concentration of cations in solution at the gel/water interface falls below the Critical Coagulation Concentration (CCC). The CCC is uncertain but, according to Appendix A of /SKB 2006d/, is around 1 mmol per litre. Prior to the period of large-scale climatic changes, surface waters that penetrate to repository depth will be subject to chemical interactions with the rock, increasing their ionic strength to values higher than the CCC. Therefore, chemical erosion of buffer during the temperate period is not a concern. In fact, bentonite intrusion into fractures may even be beneficial as clay transported out into fractures will tend to become consolidated and attached to fracture coatings (e.g. chlorite) and hence clog the fractures limiting or preventing flow and advective transport. Furthermore, compared with water-filled fractures, clay filling up fractures would increase the resistance to diffusion of radionuclides by approximately one to two orders of magnitude, given the smaller effective diffusion coefficient of species in saturated bentonite compared with that in water.

Compaction of bentonite by formation of corrosion products

Corrosion of steel components affects the final density of the buffer due to the greater volume of the corrosion products compared with uncorroded steel. The dominant corrosion product is magnetite, although depending on solution conditions some iron sulphide and siderite may also form. The formation of a protective magnetite layer leads to a strong decrease in the corrosion rate to a long-term value of about 1 μm a^{-1}, with a range of 0.1–2 μm a^{-1} (see Chapter 5). This implies complete conversion of the 8 mm thick steel plate of the supercontainer within 4,000 years. In the case of corrosion of a canister insert following canister failure, the duration of complete conversion to corrosion products takes much longer (several hundreds of thousands of years).

In the case of the corrosion of the supercontainer, the change in average bentonite density in the buffer is calculated based on Equation 4-17 with:

$$\Delta V = \frac{M_{sc}}{\rho_{Fe}}(1-\delta); \quad \Delta m = 0 \qquad \text{(Eq. 4-27)}$$

and with

ΔV total change of bentonite volume in buffer due to formation of corrosion products [m^3]
M_{sc} mass of supercontainer iron (including feet) [kg]
ρ_{Fe} density of iron/steel [kg m^{-3}]
δ volume increase factor relative to iron [–]

The resulting saturated bentonite densities for the buffer are given in Table 4-12, based on the volume increase factors also given in the table.

Table 4-12. Summary of steel corrosion processes and corresponding changes in saturated density of the buffer.

Corrosion product	Process	Volume increase factor (relative to iron) [–]	Resulting saturated density of buffer [kg m^{-3}]
Magnetite	$3Fe + 4H_2O \rightarrow Fe_3O_4 + 4H_2$	2	2,026
Iron sulphide	$Fe + HS^- + H^+ \rightarrow FeS + H_2$	2.5	2,040
Siderite	$Fe + HCO_3^- + H^+ \rightarrow FeCO_3 + H_2$	4.7	2,101

These results indicate that the volume increase due to corrosion of the supercontainer will not have a detrimental effect on the capacity of the eroded buffer to perform its safety functions (i.e. buffer density remains within the range 1,890 to 2,050 kg m^{-3} discussed in Section 4.1.3), except if it is assumed that the corrosion product is siderite. The production of siderite is, however limited by the availability of carbonate from bentonite (in the form of calcite) or from the host rock. The buffer contains only very limited amounts of calcite, which may release some carbonate upon dissolution (0.1% for siderite and calcite combined – /SKB 2006a/). Moreover, the molar volumes of calcite and siderite are similar. This means that even if some carbonate could be provided by the bentonite enabling siderite formation, no significant volume increase would be involved with this process. At Olkiluoto, the present carbonate content of groundwaters at a depth of 400–500 m is below 1 mmol per litre (/Andersson et al. 2007/ Site Report 2006). During the operational phase, carbonate-rich groundwaters from above may flow towards the drift.

In the brackish groundwaters at depths down to 300 m, the carbonate content is up to 4–5 mmoles per litre. As noted in Section 4.5.1, during saturation, about 2.7 m^3 of groundwater (containing maximally about 10–15 moles of carbonate) are needed to fill all voids and pores within and around supercontainer. After saturation and pressure equilibration, some 0.0035 m^3 a^{-1} of groundwater may flow through a supercontainer unit, assuming that there is a permeable fracture intersecting the drift (transmissivity 3×10^{-9} m^2 s^{-1}, hydraulic gradient 0.01 m m^{-1}, flow convergence factor of 2), conveying some 0.02 moles of carbonate per year. An additional 0.5 moles of carbonate per year may be provided by diffusion through the intact host rock (effective diffusion constant 10^{-10} m^2 s^{-1}, carbonate concentration gradient 5 mol m^{-4}). At such transport rates, the complete conversion of the supercontainer (1,071 kg – or 19,000 moles of iron) to siderite would take some tens of thousands of years, compared with an expected corrosion time of a few thousand years. This is a clear indication that the transformation of iron to siderite is limited by the availability of carbonate. The value given in Table 4-12 for siderite is therefore likely to overestimate the buffer density increase under the expected repository conditions.

In the case of corrosion of the insert following canister failure the change in average bentonite density in the buffer around a supercontainer is calculated based on Equation 4-27 with:

$$\Delta V = \frac{M_{insert}}{\rho_{Fe}}(1-\delta) + V_{canvoid}; \quad \Delta m = 0 \qquad \text{(Eq. 4-28)}$$

and with

M_{insert} mass of iron and steel inside the canister [kg]

$V_{canvoid}$ void space inside the canister [m^3]

Here, it is assumed that the corrosion products will preferentially fill the void space inside the canister; only once this is filled is the buffer compacted.

The resulting change in volume (ΔV) to be taken up by the buffer is 0.77 m^3 and the resulting density is 2,160 kg m^{-3}, assuming the corrosion product to be magnetite. This does not satisfy the criteria for the safety function indicators for the buffer, which give a maximum buffer density of 2,050 kg m^{-3}. The calculation is, however, conservative. In particular, it is assumed that the only part of the buffer to be compacted is that originally inside the supercontainer. In reality, there is likely to be some relaxation of the increased density by buffer creep along the drift, although internal friction will mean that some locally increased density around the failed canister is likely to remain.

Impact of rock shear displacements

In Section 3.4, it is described how shear movement on fractures intersecting the deposition drifts may arise from a number of causes, including, most significantly, post-glacial earthquakes. Drift sections intersected by fractures having the possibility of shear displacements greater than 0.1 m will be avoided as locations for canister emplacement, since shear displacements of this magnitude have the potential to damage canister integrity, but it may not be possible to avoid such fractures throughout an entire drift. Thus, the impact of rock shear on the distance blocks, or on the backfill in sealed sections between drift compartments (which may be intersected by larger fractures capable of undergoing larger shear displacements), needs to be considered (Figure 4-12).

The main concern is redistribution and mechanical erosion of bentonite during the shear movement. It is instructive to estimate how much bentonite would have to be lost by mechanical erosion of a distance block in order, say, for an initial buffer density of 2,000 kg m^{-3} to be reduced to 1,890 kg m^{-3}, which, as discussed in Section 4.1.3, is the lower bounding value for density that ensures that relevant buffer safety function criteria are met, taking into account variability in groundwater salinity over time.

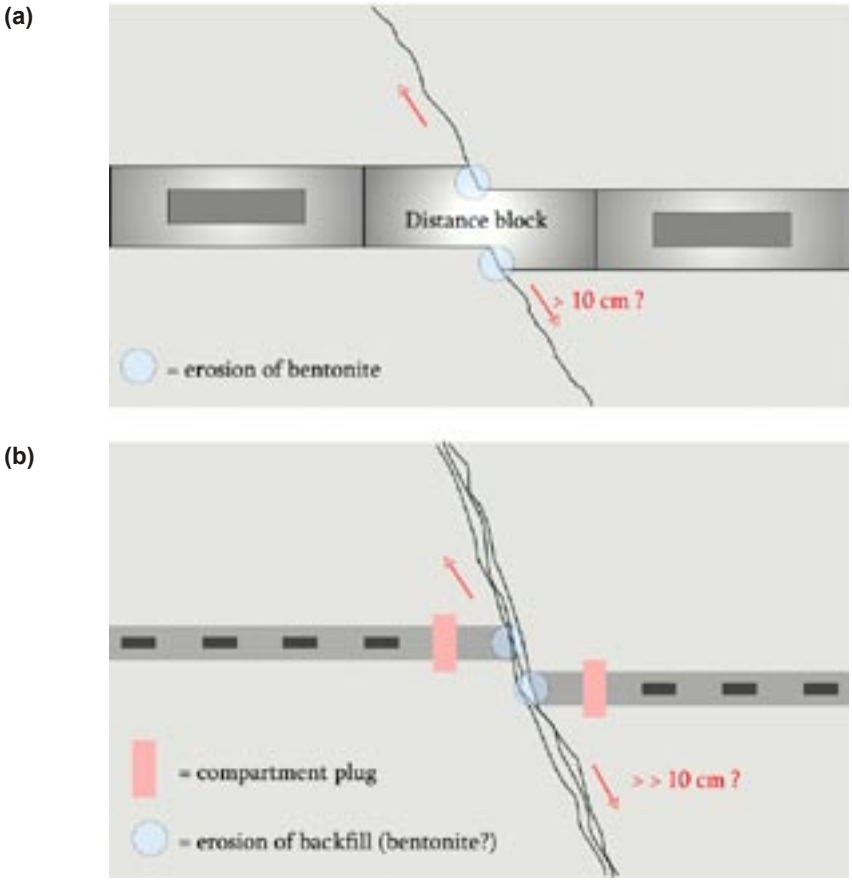

Figure 4-12. *Rock shear affecting (a), the distance blocks and (b), the backfill in sealed sections between drift compartments.*

The change in mass, Δm [kg], required to achieve a change in density $\Delta\rho$ [kg m^{-3}] is, from Equation 4-28:

$$\Delta m = (\rho_0 + \Delta\rho)(V_0 + \Delta V) \qquad \text{(Eq. 4-29)}$$

Masses and volumes of bentonite in a saturated distance block and in the buffer around a canister in the absence of any mass redistribution are given in Appendix A. From this data, and taking:

$\rho_0 = 2{,}000$ kg m^{-3};
$\Delta\rho = -110$ kg m^{-3};
$V_0 = 14.7$ m^3 (saturated distance block)
$\Delta V = 0$;
$m_0 = 29{,}400$ kg (saturated distance block)

a change of mass of about 1,600 kg is required, corresponding to a volume of eroded bentonite of about a cubic metre at a density of 1,890 kg m^{-3}.

Considering the buffer around the canisters /Börgesson and Hernelind 2006c/, have calculated the buffer swelling pressure for cases where, in KBS-3V, one, two and three entire bentonite rings have been omitted, to illustrate the effects of a local loss of large amounts of bentonite. The conclusion was that a mass loss of 1,200 kg to a fracture intersecting the deposition hole would lead to conditions where advective conditions in the buffer must be considered. Due to the similarity between the deposition hole diameter in KBS-3V (1.75 m) and the deposition drift diameter of in KBS-3H (1.85 m), this conclusion can be taken to apply to both alternatives. Although no specific studies have been conducted, mass losses from the buffer of this magnitude due to shear movements are considered unlikely.

In order to accommodate 1,200–1,600 kg of eroded bentonite, the shear movement would have to create new volume of about a cubic metre or more in the host rock along the shear plane. As an illustration, if the shear plane had an average porosity similar to the crushed zone of the EDZ (0.064% /Johnson et al. 2005/), all voids in a bulk rock volume of 140 m^3 (corresponding to a disk with a radius of about 7 m and a thickness of 1 m) would have to be filled with bentonite, which seems to be highly unlikely. In reality, it is more likely that shear displacements as depicted in Figure 4-12 will create little or no new volume, and so significant erosion of bentonite will probably not occur.

Summary and time perspective

In the present chapter, scoping calculations have been presented for various mechanisms leading to bentonite mass redistribution in a KBS-3H deposition drift. The preliminary results can be summarised as follows:

Redistribution of bentonite by axial displacement of distance block and supercontainer

- Axial displacements of distance blocks and supercontainers may be caused by differential saturation and swelling along the deposition drift and may occur in the form of a slow axial expansion by swelling or by a more abrupt axial displacement due to high hydraulic forces.
- The results of scoping calculations suggest that the displacements can only be stopped by the counterforce of a wetted/nearly fully swollen supercontainer unit.
- The fixing rings and compartment plugs are not designed to withstand significant swelling pressure gradients, and so cannot be relied upon to prevent axial movements due to heterogeneous swelling. Any development of significant swelling pressure gradients will, however, proceed in parallel to the development of high swelling pressures at the drift walls in more rapidly saturated drift sections.

- Displacements have no significant effect on the density of bentonite (i.e. buffer density remains within the range 1,890 to 2,050 kg m^{-3} discussed in Section 4.1.3) provided that neither the total linear compaction per supercontainer unit, nor the number of supercontainer units affected, are too large.
- If the total linear compaction per supercontainer is assumed to take a conservative value of 10 cm, then the maximum distance to the next fully water-saturated unit or reinforced (i.e. fixed as a result of a technical feature such as a fixing ring) unit must not exceed about 2–3 supercontainer units to keep the bentonite density above a lower bound of 1,890 kg m^{-3}.
- The relevant time frames of the processes discussed above are related to the time needed to establish homogeneous saturation and swelling. The slow expansion of the distance block by swelling (with compaction of nearby "tight" supercontainer units) may take one hundred to several thousand years, depending mainly on the hydraulic transmissivity of fractures present in the "tight" drift sections (Section 4.5.1). Abrupt displacements due to high hydraulic forces may occur within time periods of days to weeks, depending on how fast the hydraulic pressure in the "less tight" drift section is built up.
- Based on these preliminary considerations and limitations, there is no need for a specific treatment of this process in radionuclide release and transport assessment cases.

Redistribution of bentonite by lifting of supercontainer due to off-centred swelling pressure

- Off-centred saturation and swelling of the buffer may cause slight lifting of the supercontainer and a reduction of bentonite density in the lower part of the drift. As the remaining buffer saturates, the initially higher density and swelling pressure in the upper part of the drift will tend to homogenise and return the canister to a more central position in the drift, although some small eccentricity may remain. This is not expected to lead to density changes outside the bounds specified by the safety function indicator criteria for the buffer. There is thus no need for a specific treatment of this process in radionuclide release and transport assessment cases.

Redistribution of bentonite by piping/erosion

- The maximum inflow rate to a drift section to be used for supercontainer and distance block emplacement is set as 0.1 litres per minute to minimise the possibility of piping and erosion during the early phase of evolution while the drift is saturating. The reference design has also been shown to behave favourably with respect to piping/erosion for more extreme conditions. Piping, if it were to occur, could lead to significant water flows between "less tight" and "tight" supercontainer units that cause erosion and redistribution of bentonite. Scoping calculations indicate that the redistribution of bentonite by piping/erosion in a KBS-3H deposition drift has no significant effect on the density of bentonite (i.e. buffer density remains within the range 1,890 to 2,050 kg m^{-3} discussed in Section 4.1.3), provided that (i), the total suspended solids ratio is not too large (in the order of a few weight% – note that the 5% weight ratio of bentonite/suspension assumed in these calculations is a pessimistic, high value), (ii) the volume available to be filled with suspension is not too high – i.e. only a few supercontainer units are filled, and (iii), local density changes are quickly homogenised by the plasticity of bentonite. Moreover, the increase in bentonite density in each of the filled supercontainer units is marginal, i.e. to a value 2,007 kg m^{-3}, irrespective of the number of filled units. However, it is unclear whether all possibilities regarding piping and erosion can be addressed in such calculations, because of uncertainties associated with some of the assumptions. Therefore, these results are not sufficient to give guidance on the design requirements regarding the avoidance of piping and erosion.

- The relevant time frames of the processes discussed above are determined by the time during which piping/erosion can take place. As discussed in Section 4.5, piping/erosion occurs within days to weeks.
- At the current design stage, however, the possibility of some degree of piping and erosion during buffer saturation cannot be completely eliminated. Therefore, a calculation case is included in the Radionuclide Transport Report /Smith et al. 2007a/ addressing the loss of a limited amount of bentonite due to this process.

Redistribution of bentonite by erosion into fractures

- Bentonite erosion into fractures may be of concern during the operational phase, namely if a sealed compartment is hydraulically connected to some nearby open rock excavation.
- The results on buffer erosion during the operational phase seem to indicate that redistribution of bentonite by erosion into a permeable fracture connecting a sealed KBS-3H deposition drift with any open rock excavation is unlikely to have a detrimental effect on the capacity of the eroded buffer to perform its safety functions (i.e. buffer density remains within the range 1,890 to 2,050 kg m^{-3} discussed in Section 4.1.3). There is thus no need for a specific treatment of this process in radionuclide release and transport assessment cases.

Compaction of bentonite by formation of corrosion products

- Corrosion of the steel components affects the final density of the buffer due to the greater volume of the corrosion products compared with uncorroded steel. The dominant corrosion product is magnetite, although depending on solution conditions some iron sulphide and siderite may also form.
- Scoping calculations of the corrosion of the insert lead to a density that does not satisfy the criteria for the safety function indicators for the buffer, which give a maximum buffer density of 2,050 kg m^{-3}. The calculations are, however, conservative. In particular, it is assumed that the only part of the buffer to be compacted is that originally inside the supercontainer. In reality, there is likely to be some relaxation of the increased density by buffer creep along the drift, although internal friction will mean that some locally increased density around the failed canister is likely to remain.
- The relevant time frame for conversion of iron into corrosion products such as magnetite is a few thousand years for the supercontainer to several hundreds of thousands of years for the canister insert (assuming a steel corrosion rate of 1 μm a–1, see Section 5.7.1).
- Buffer with a density above 2,050 kg m^{-3} may give reduced protection of the canister against rock shear (although a corroded insert implies that the canister has already failed). Furthermore, the increased buffer swelling pressure could cause some damage to the adjacent rock, although the extent of such damage is likely to be limited to a small region adjacent to the drift wall. TM-modelling by /Lönnqvist and Hökmark 2007/ has found that pressures of the order of 10 MPa are required in the deposition drift to cause opening of intersecting rock fractures. To open these sufficiently to bring them into tension at distances between 0 m and 0.2 m from the drift periphery requires about 20 to 25 MPa. Furthermore, the aperture increases were found to be modest.
- Based on these preliminary considerations and limitations, there is thus no need for a specific treatment of this process in radionuclide release and transport assessment cases.

Impact of rock shear displacements

- It may not be possible to exclude larger rock shear displacements (greater than 0.1 m) through distance blocks or through filling blocks located between compartment plugs. In the position of supercontainer/canisters, such large rock shear displacements must, however, be avoided (safety function indicator). The main concern is redistribution and mechanical erosion of bentonite during the shear movement.
- It is likely that shear displacements will create little or no new volume, and so significant erosion of bentonite will probably not occur. Scoping calculations for displacements across filling blocks indicate that even under very pessimistic conditions regarding the created void space in the shear zone, the safety function indicator criteria for the buffer can be fulfilled.
- The relevant time frame for post-glacial earthquakes shear displacements to take place is several tens to one hundred thousand years.
- Based on these preliminary considerations and limitations, the impact of rock shear displacements on bentonite density does not lead to a violation of the safety function indicator criteria for bentonite. There is thus no need for a specific treatment of damaged bentonite due to rock shear movement in the KBS-3H Radionuclide Transport Report /Smith et al. 2007a/. However, the case of canister failure due to rock shear movement is treated in that report.

Handling in the safety assessment for KBS-3H

Under reference conditions, some limited piping and erosion may occur during the saturation of the KBS-3H buffer, but it is not expected to be sufficiently extensive to result in loss or significant degradation of the buffer safety functions (see scoping calculations in Evolution Report Appendix B.4). In particular, although it may result in some local increase the diffusion coefficient of the buffer, transport within the buffer is expected to remain diffusion-dominated. The impact of a higher buffer diffusion coefficient on sulphide transport and canister lifetime has been evaluated in scoping calculations in Appendix B.7 of the Evolution Report, and shown to be minor. Piping and erosion does not, therefore, give rise to any specific scenarios in the Radionuclide Transport Report /Smith et al. 2007a/, although an assessment case is calculated (PD-HIDIFF) in which an increased buffer diffusion coefficient is used to model radionuclide transport through the buffer in the event of radionuclide release from a canister with an initial penetrating defect.

In summary, the radiological consequences of a buffer with reduced density caused by mass redistribution but still satisfying the safety function indicator criteria are evaluated in a variant radionuclide release and transport case with increased diffusivity for radionuclides in the buffer (PD-HIDIFF).

4.7 Chemical processes

An overview of chemical processes in the subsystem “buffer” is shown in Table 4-13. The majority of these processes and the acquired information are considered not to depend significantly on the specific conditions in KBS-3H (exceptions see below). This is because the material properties, basic processes and the boundary conditions at the canister surface are identical in KBS-3V and KBS-3H. The large amount of information on these common processes is, therefore, not reproduced in the present report. For a detailed discussion of these processes, see the relevant Process Reports for KBS-3V /Rasilainen 2004, SKB 2006d/.

Table 4-13. The interdependence of chemical processes and identified variables in the buffer.

Chemical processes	Variables for the buffer											
	Geometry	Pore geometry	Radiation intensity	Temperature	Water content	Gas content	Hydrovariables	Stress state	Bentonite composition	Montmorillonite composition	Porewater composition	Structural and residual materials
Advection	×	×		×	×	×	×	×			×	×
Diffusion		×		×		×			×	×	×	×
Colloid transport		×		×	×	×	×	×		×	×	
Sorption (including ion-exchange)				×					×	×	×	×
Alterations of impurities	×	×		×	×			×	×	×	×	×
Aqueous speciation and reactions			×	×			×	×		×	×	
Osmosis	×	×		×	×		×	×		×	×	
Montmorillonite transformation	×	×		×	×			×	×	×	×	
Iron/bentonite interaction	×	×		×	×		×	×	×	×	×	×
Colloid release/erosion	×	×		×	×		×	×	×	×	×	
Radiation-induced transformation			×									
Radiolysis of porewater	×		×		×	×					×	
Microbial processes		×	×	×	×	×		×	×		×	×
Speciation of radionuclides			×	×					×	×	×	×
Cement/bentonite interaction	×	×		×	×		×	×	×	×	×	×

Differences in the chemical processes between KBS-3V and 3H arise due to the boundary conditions outside the buffer, particularly the presence of the supercontainer and of other structural materials (e.g. cement) and the properties of the interfaces (gaps) to the rock surface and to the adjacent distance blocks.

The only newly introduced chemical processes in Table 4-13 are “Iron/bentonite interactions” and “Cement/bentonite interactions”. Section 4.7.1 discusses the consequences of iron/bentonite interactions in terms of the safety-relevant properties of the buffer, including swelling pressure, sorption capacity and hydraulic conductivity. Section 4.7.2 deals with the impact of cement/bentonite interactions on these properties. “Colloid release/erosion” is relevant to both KBS-3V and KBS-3H, but is discussed in Section 4.7.3 in view of its significant potential consequences to either type of repository.

4.7.1 Iron/bentonite interaction

Overview/general description

A large amount of reactive iron is introduced by the steel components within KBS-3H. Looking at the design of the engineered barrier, it appears reasonable to assume that the largest impact on geochemical conditions in the near field comes from the supercontainer. Its mass is significantly larger than that of other iron components outside the canister, such as fixing rings or spray and drip/moisture shields. The amount of iron in the supercontainer also far exceeds the amount of reduced iron in buffer minerals, as illustrated in Table 4-14.

The status of current knowledge of iron/bentonite interaction and its potential impact on bentonite properties has been reported in /Marcos 2003, Johnson et al. 2005, Carlson et al. 2006, Wersin et al. 2007/. Experimental studies have also been performed to support the KBS-3H safety studies /Carlson et al. 2006/. Furthermore, a workshop on iron/bentonite interaction related to spent nuclear fuel disposal was held in Basel/Switzerland in May 2006, which provided valuable information on most recent R&D on this topic /Wersin and Mettler 2006/. The objectives of this section are:

- to summarise current knowledge based on these sources of information;
- to assess the effects on iron/bentonite interactions on physical properties of the buffer in contact with a reduced iron source;
- to evaluate implications for long-term safety with particular focus on KBS-3H.

Boundary conditions

The relevant boundary conditions for the iron/bentonite interaction are the amounts of iron present in the deposition drifts, the expected conditions in the host rock and the chemical properties of the buffer (in the absence of any steel components). These are discussed below, under "mineral transformations", as well as in Section 7.1 (properties of the host rock) and Section 4.1 (properties of the buffer).

Table 4-14. Iron fractions of different components in the near field. From /Wersin et al. 2007/; not all values correspond to the numbers given in Appendix A of this report as the analysis predates the final data set for the KBS-3H Project.

	Mass [kg]	kmol keq	Comments
Buffer initially inside supercontainer			
Total bentonite material [a]	16,129		Dry density = 1.56 Mg m^{-3} ε = 0.44, Engineered barrier systems' dimensions given in Appendix A
Montmorillonite [b]	12,097	29.8	75wt%
Siderite, pyrite [b]	164	1.4	Assumption: 0.5% $FeCO_3$ and 0.5 FeS_2
Fe(III) oxide [c]	16.4	0.2	0.1% FeOOH
Structural Fe^{3+} [b]	338	6.0	
Structural Fe^{2+} [b]	16.9	0.3	
Cation exchange capacity [c]		3.4	75 meq/100g
Edge sites [c]		0.5	15% of CEC
Steel supercontainer [d]	869	15.6	length = 5,546 mm, thickness = 8 mm, perforation 62%

[a] Derived from Appendix A.

[b] /Müller-Vonmoos and Kahr 1983/ for Na-sat form: $Na_{0.30}(Al_{1.55}Fe^{3+}_{0.20}Fe^{2+}_{0.01}Mg_{0.24})(Si_{3.96}Al_{0.04})O_{10}(OH)_2$.

[c] /Bradbury and Baeyens 1997/.

[d] Dimensions of supercontainer from /Johnson et al. 2005/. The present design includes non-perforated end-plates and a total mass of 1,071 kg (see Appendix A).

Model studies/experimental studies

Iron/smectite interaction

Under repository conditions, steel will corrode and produce hydrogen gas and corrosion products, such as magnetite. Moreover, the corroding iron may react with the clay fraction of the buffer. Although the corrosion and the clay reaction processes are linked, it is useful first to discuss these processes separately.

Steel corrosion (for more details, see also Section 5.7.1)

There have been a number of corrosion studies under anaerobic conditions in water and bentonite lasting several years. All these studies indicate a strong decrease in corrosion rates to a few µm per year /see e.g. Andra 2005/ due to the build-up of a protective layer (e.g. magnetite, siderite) and, in the case of compacted clay media, possibly also due to diffusional limitations. The results of these studies are corroborated by investigations on archaeological analogues /David 2001/.

In most experimental studies, magnetite was identified as the main corrosion product /e.g. Grauer 1984, Smart et al. 2001, 2004/. However, in case of high pCO_2, siderite formation occurred /Bataillon 2006/. The observed corrosion products are in agreement with thermodynamic predictions. Long-term corrosion rates (e.g. several years) in compacted bentonite were found to be rather similar to those in water although certain differences between the studies can be noted. For example, in the experiments of /Bataillon 2006/, a slight decrease in corrosion rates in compacted bentonite relative to those in water was noted, whereas the opposite was observed in the experiments of /Smart et al. 2004, Smart 2006/. In the latter study, an increase in iron content in the adjacent bentonite resulting from the diffusion of corroded iron and interaction with the clay was determined. A rather low apparent diffusivity, Da, of ~10^{-15} m^2/s for Fe(II) was estimated. No new iron phase in the iron-enriched clay could be identified.

Since compacted bentonite acts as an effective filter, virtually no significant microbial activity is expected in the inner the part of the buffer. Near to the buffer/rock interface, however, it is possible that the density of any buffer extruded through the perforations in the supercontainer wall will be lower than that of the bulk of the buffer. Furthermore, the supercontainer may rupture due to the swelling pressure of the saturating buffer inside it, which could bring steel in direct contact with the drift wall. The fixing rings will also be in direct contact with the drift wall, as well as partly embedded in the buffer. In these cases, it is conceivable that sulphate-reducing or perhaps Fe(III)-reducing bacteria adhering to the steel surface may affect corrosion. This could result in increased pitting and/or in the precipitation of iron sulphide phases. However, the effect on overall corrosion rates is not expected to be large, as suggested from natural analogue observations.

Corrosion-derived iron may also form Fe(II) silicate phases, which in principle may compete with the formation of oxides or carbonates. The thermodynamics and kinetics of this iron/clay interaction process are still not well known, as outlined below.

Sorption and redox reactions

Fe(II) released via the corrosion process will strongly interact with the clay surface via sorption. Sorption has been shown to occur by cation exchange to interlayer sites and by some type of surface complexation process to the so-called edge sites. This latter process was shown to be dominant under non-acidic conditions and to involve a complex redox/precipitation reaction at pH values above 7. /Charlet 2006/ hypothesised that the iron precipitation reaction represents the initial stage of a clay neo-formation. In the test by /Carlson et al. 2006/ with iron coupons or wires in MX-80 at different temperatures and time spans, an obvious effect of the incorporation of iron into the bentonite was a significant decrease of cation exchange capacity. This suggests that iron was adsorbed onto exchange sites by a less reversible mechanism than regular cation exchange, possibly onto favoured sites on sheet surfaces or at mineral discontinuities in the montmorillonite.

Structural iron in smectites occurs mainly as Fe(III), which, under strongly reducing conditions, may be reduced to Fe(II). This, in turn has consequences for the stability and to some extent also on the hydraulic properties of the swelling clay /e.g. Foster 1953, Stucki et al. 1984/. The mechanism of this redox process is still controversial. The relevance of this effect for the buffer is not clear, since available experimental data are not representative of repository conditions.

Mineral transformation

Recently, progress has been made regarding smectite transformation in contact with zero-valent iron. Most of the experimental work has been performed in France /e.g. Cathelineau et al. 2005, Lanson 2006/. Process understanding is, however, still limited. Since reaction rates are slow and reaction products are difficult to analyse, high temperatures and/or low solid/liquid ratios are necessary to obtain reliable experimental information on smectite transformation. This introduces further uncertainties in extrapolation to repository conditions. A summary of the recent experimental work is presented in Table 4-15.

The oxidation reaction Fe(s) to Fe_3O_4(s) is treated kinetically and thus the uncertainty in the equilibrium constant of this reaction has no effect on the rate of generation of H_2 and Fe_3O_4 build-up. Moreover, it has been experimentally shown that the reaction is not sensitive to H_2 concentrations up to 10 MPa in H_2 equilibrium pressure /Smart et al. 2001/.

The uncertainty in Fe_3O_4 solubility data will have some consequences on the relative proportions of Fe_3O_4 and other Fe minerals formed as result of the corrosion and Fe-clay interaction process. This uncertainty however is small compared with uncertainty in kinetic data of these phases and has been entirely covered in the bounding cases considered in the reactive transport calculations.

In spite of the existing shortcomings, the available data suggest two general reaction pathways:

1. Fe-poor smectite + Fe → berthierine and/or chlorite
2. Fe-poor smectite + Fe → Fe-rich smectite

The first transformation has the greatest potential to impair the performance of the buffer, since berthierine and chlorite, unlike Fe-rich smectitite, are non-swelling clays.

Table 4-15. Experimental data on transformation of smectite in contact with reduced iron. From /Wersin et al. 2007/. S/L = solid/liquid ratio.

Reference	Experimental conditions	Neo-formed iron phases
/Madsen 1998/	MX-80 bentonite + Fe/Fe_3O_4 powder Clay/Fe^0 = 1, S/L = 0.1, t = 180 d, T = 80°, water vapour	none
/Lantenois 2003/	Various pure smectite minerals + Fe powder Clay/Fe^0 = 1, S/L = 0.04, t = 45 d, T = 80°	Magnetite*, cronstedtite (“berthierine”)
/Guillaume et al. 2003, 2004/	MX-80 bentonite + Fe/Fe_3O_4 powders clay/Fe = 10, S/L = 0.1, t ≤ 9 months, T = 300°C	chlorite, saponite
	same, T = 80°C	nontronite
/Cathelineau et al. 2005/	MX-80 bentonite + Fe/Fe_3O_4 powders S/L varied, T = 80°C, t ~ 1 a	berthierine
/Carlson et al. 2006/	Compacted MX-80 bentonite + Fe coupons or wires clay/Fe ~ 1, S/L = 3.6, t ≤ 900 d, T = 30 and 50°C	Magnetite*, goethite- no Fe silicate
/Wilson et al. 2006a/	Na-montmorillonite, Fe and Fe_3O_4 powders, calcite, S/L = 0.01, t ~ 100 d, T = 250°C	Fe-rich smectite (from solute conc. Fe-saponite proposed)
	Na-montmorillonite + Fe powder $FeCl_2$ solution, S/L = 0.01, t ~ 90 d, T = 80–250°C	Magnetite*, hematite*, at 250°C: 1:1 clay (from solute conc. berthierine proposed)

* Corrosion products formed.

The experimentally observed reaction products are generally in agreement with thermodynamic predictions, as indicated in the recent study by /Wilson et al. 2006b/ (cf. also /Savage and Wilson 2006/). This is illustrated in chemical stability diagrams, such as that shown in Figure 4-13. It should however be kept in mind that uncertainties in equilibrium data for iron phyllosilicates are still rather large.

Very few attempts have been made to model the impact of iron/bentonite interactions on the stability of the bentonite buffer in repository environments. One modelling exercise involved the reaction of the steel canister with MX-80 bentonite in the French repository concept for high-level waste /Fritz et al. 2006/ based on a coupled diffusion-reaction model. The data indicated a spatially very restricted zone of transformation after 50,000 years, which was explained by diffusional limitation and clogging effects. A similar result was obtained in another study in which a quite different reactive transport model was applied /Bildstein et al. 2006/.

Case study for the Olkiluoto site

A preliminary modelling study was performed for KBS-3H using Olkiluoto as case study /Wersin et al. 2007/. The first approach involved simple mass balance calculations to estimate the maximum amount of swelling clay (montmorillonite) transformed to a non-swelling iron silicate by interaction with the steel from the supercontainer. These estimates indicate that, from a mass balance perspective, about 10–30% could be converted, depending on which reaction product was assumed (berthierine or chamosite). This would lead to significant reduction of swelling pressure (from 8 MPa to 2–4 MPa). It is important to note that this simple mass balance calculation overestimates the amount of montmorillonite transformed, because (1) corrosion reaction products such as magnetite will compete for dissolved Fe(II), and (2) mass transfer constraints are neglected in these estimates.

This simple mass balance estimate highlights the need for a more sophisticated modelling approach. Thus, a second modelling exercise was performed to simulate the migration of Fe(II) emanating from the supercontainer and reacting with the buffer /Wersin et al. 2007/. For this purpose, 1D reactive transport calculations based on PHREEQC and CrunchFlow were performed.

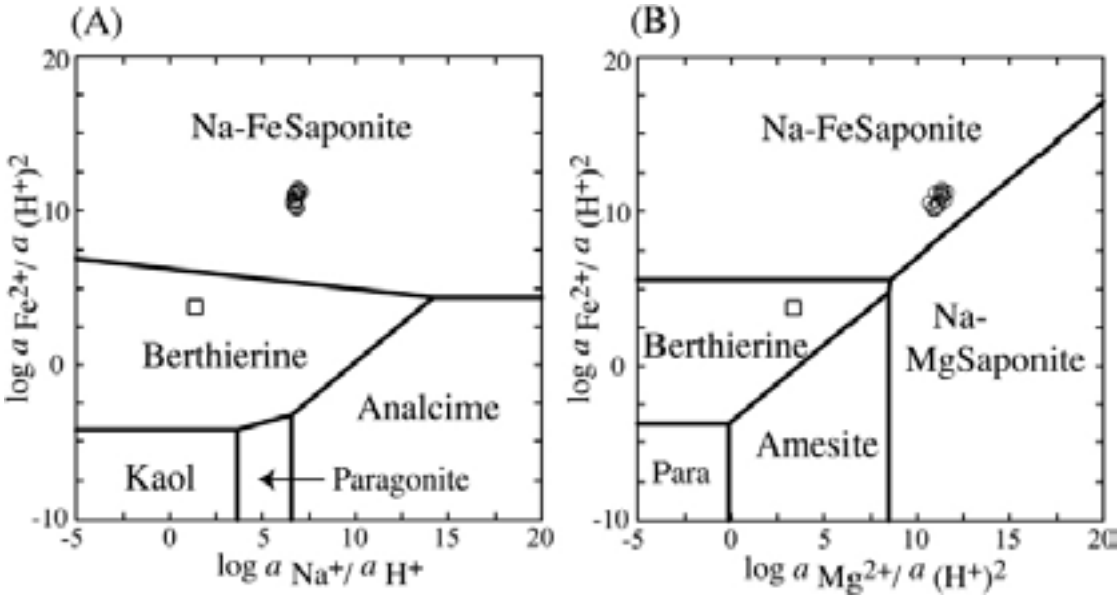

Figure 4-13. *Chemical stability diagrams for smectite. At (T = 250°C, $\log a_{SiO2(aq)}$ = –3). Points denote experimental data. Figure taken from /Wilson et al. 2006a/.*

Site-specific information from Olkiluoto, such as groundwater and mineralogical data, reported microbially mediated redox processes, and expected geochemical evolution was considered. Iron(II) released from the supercontainer was assumed to react via cation exchange and surface complexation. In the first variant of calculations with PHREEQC, the movement of the Fe(II) was described without considering Fe transformation reactions. Two cases were considered therein: In case A, Fe(II) release is controlled by a rather insoluble FeS source (4 µmole l^{-1}). The outcome of this result is illustrated in Figure 4-14. The movement of the iron front is very slow and would take several hundreds of thousands of years to extend across the buffer.

In case B, Fe(II) concentration is controlled by siderite solubility, a concentration about ten times higher than Case A. The diffusive flux is higher because of the steeper concentration gradient. Moreover, pH conditions are less alkaline, thus leading to less strong sorption. The estimated time for the Fe(II) front to extend 15 cm into the buffer is 30,000 years. A much longer time, 150,000 years, is required for the front to penetrate 30 cm (Figure 4-15). Nevertheless, the results indicate effective retardation of iron even for this less favourable case.

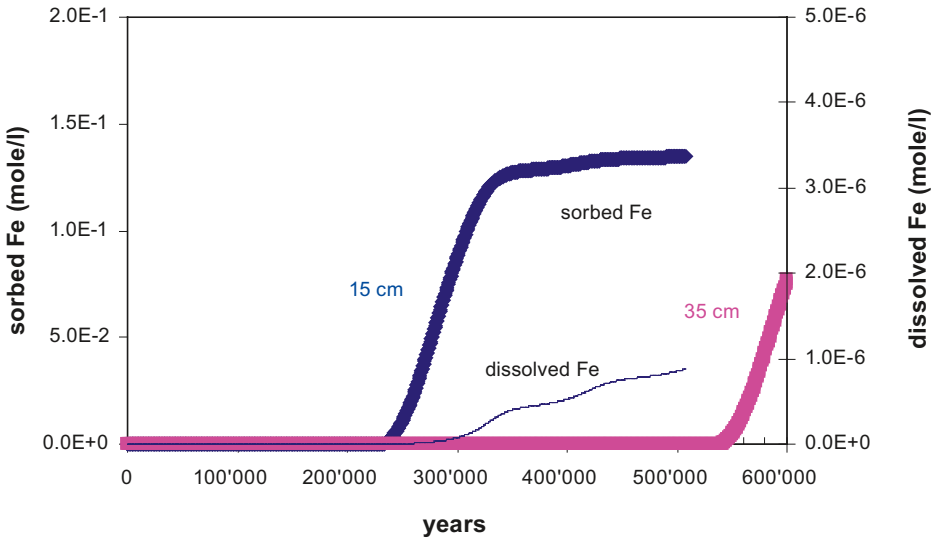

Figure 4-14. *Breakthrough curves of Fe(II) in bentonite. Case A (FeS source) at 15 cm and 35 cm distance from the supercontainer; only sorption considered; from /Wersin et al.2007/.*

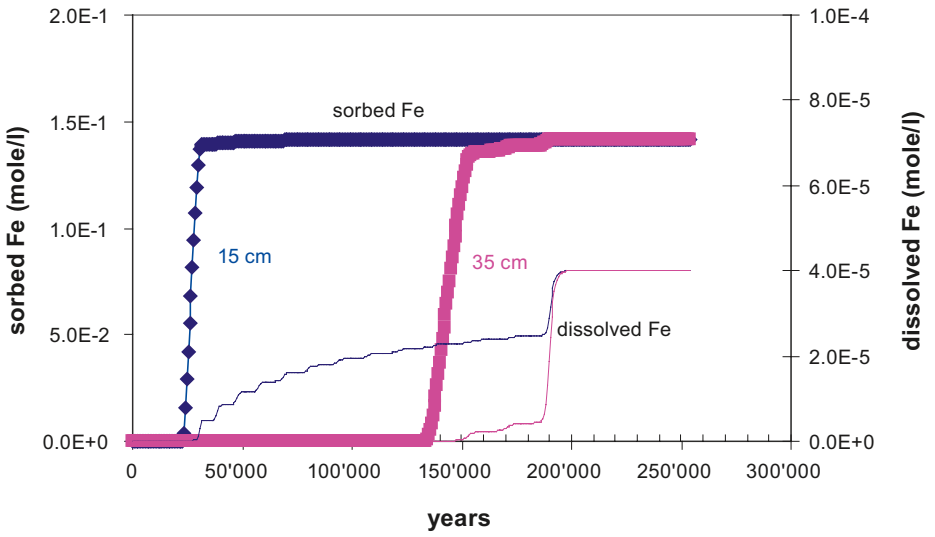

Figure 4-15. *Breakthrough curves of Fe(II) for* ***test case B*** *at 15 cm and 35 cm distance from the supercontainer; only sorption considered.*

In the second variant, additional reactive transport calculations were performed with the CrunchFlow code. In this approach, equilibrium and kinetic reactions of Fe species and clay minerals were specifically included, bearing in mind the large uncertainty involved in some of these reactions.

The outcome of the Crunchflow can be summarised as follows:

- The results of the PHREEQC calculations were confirmed with this different reactive transport code.
- The extent of the altered montmorillonite zone remained with a few cm, even for very unfavourable bounding assumptions. This is illustrated for example in Figure 4-16, for a case for which released Fe(II) was assumed to react with the clay (no magnetite formed). The zone of altered montmorillonite for this case extends to about 5 cm into the buffer after 500,000 years.

In summary, the reactive transport calculations indicate (1) limited migration of the Fe(II) front and (2) an even more limited zone of clay alteration even after time periods >100,000 years. This is mainly due to the low Fe(II) gradient between the iron source and the buffer, the strong sorption of Fe(II) to the clay, and iron precipitation reaction leading to partial clogging. The adverse effects on the swelling buffer material are thus spatially limited to the outermost few cm near the buffer-rock interface for very long periods /Wersin et al. 2007/.

Impact on physical properties

Iron/bentonite interaction may, by various mechanisms, lead to an alteration of the physical properties of the buffer, i.e. swelling pressure, swelling capacity, hydraulic conductivity and rheology. For example, in many of the transformed minerals resulting from iron/smectite interaction, water no longer has access to interlayer spaces, and the swelling ability is lost or strongly reduced. Moreover, the growth of iron corrosion products will vary along the container length, which can cause axial movement of the buffer that is outside the supercontainers.

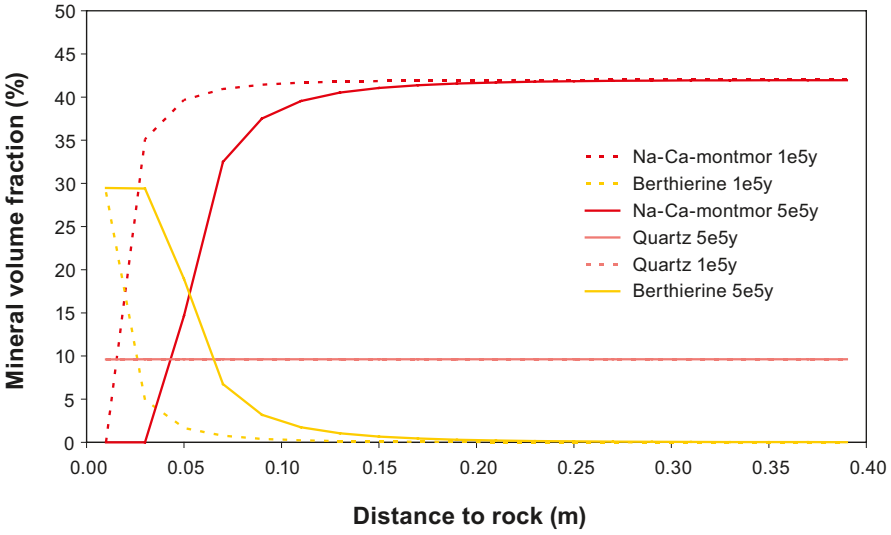

Figure 4-16. *Mineral distribution case for $5{\cdot}10^5$ (solid line) and 10^5 years (dashed line). Magnetite precipitation excluded. For details see /Wersin et al. 2007/.*

Swelling pressure and swelling capacity

Buffer swelling pressure is related to the (mean) interlayer distance of separate montmorillonite clay platelets /Karnland and Birgersson 2006/. The impact of a mineral transformation will therefore depend on the density change induced by the transformation in the remaining (untransformed) montmorillonite system. The effect is illustrated in Figure 4-17 in the case of chloritisation. Picture A shows an unaltered, water saturated Na-montmorillonite buffer (density 2,000 kg m^{-3}). The thickness of the interlamellar layers at this density is approximately 8 Å with a corresponding swelling pressure of ~7 MPa (for salinities up to ~1 mole l^{-1}, see Figure 4-18). The effect of chloritisation is exclusion of water from interlayer pores and reduction of interlayer thickness to approximately 4 Å in the transformed system, thus increasing the mean layer distance for the remaining unaltered montmorillonite (picture B) and lowering the swelling pressure. The rightmost picture shows the result of a complete chloritisation; the swelling pressure is lost and the pore structure is completely changed with larger voids appearing.

Figure 4-18 shows calculated and measured swelling pressures as a function of density for MX-80 bentonite in contact with solutions of various salinities. The expected dry density of the saturated buffer (~1,570 kg m^{-3}) is indicated by the green arrow. The red arrow shows the effective density reduction due to 50% chloritisation. The swelling pressure reduction is substantial, but the residual swelling pressure nevertheless remains above 1 MPa, even in the case of a highly saline porewater (0.3 M NaCl-solution).

The impact of iron/bentonite interaction on swelling pressure has been investigated experimentally in only a few cases known to the authors. /Stucki et al. 2000/ found a minor reduction of the swelling pressure of iron-rich Na-montmorillonite when structural iron is reduced. They explain this by layer collapse (see above) but present their data relative to unaltered samples and no comparison to Figure 4-18 can be made.

Dots show measured values. The green arrow (right) indicates the swelling pressure of unaltered buffer material at KBS-3 target density whereas the red arrow (left) illustrates the pressure at a 50% chloritisation. From /Wersin et al. 2007/.

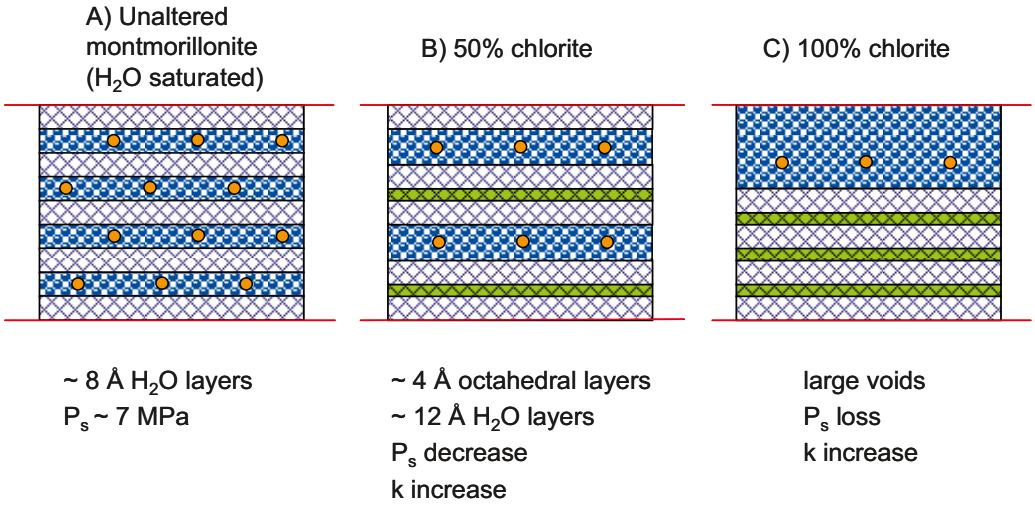

Figure 4-17. *Stylised illustration of water conditions in the montmorillonite interlayers. P_s indicates swelling pressure and k indicates hydraulic conductivity. Picture A shows the maximum cation hydration of unaltered montmorillonite in a limited space. The chequered, uncoloured areas represent the tetrahedral-octahedral-tetrahedral platelets, while water and cations are represented by circles. 50% chlorite (B) shows the collapsed interlayers and non-collapsed layers further hydrated. The additional octahedral hydroxide layers of chlorite, replacing water in the collapsed layers, are represented by green-chequered areas. 100% chlorite (C) shows the totally collapsed interlayers and large voids over which no force interaction with the surroundings particles exist. From /Wersin et al. 2007/.*

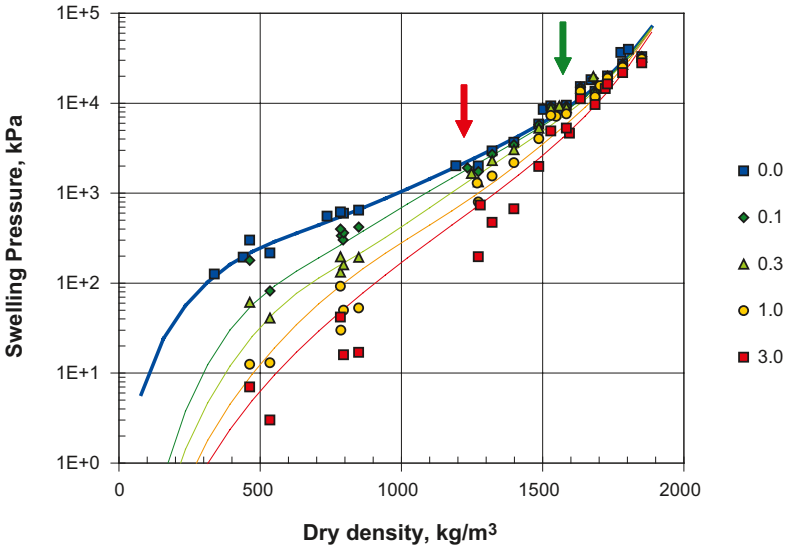

Figure 4-18. *Swelling pressure of MX-80 material in contact with pure water and NaCl solutions.*

/Carlson et al. 2006/ found small or no changes in swelling pressure in a test where iron coupons or wires were mixed with MX-80 and allowed to react at different temperatures and during different time spans. These results are presented in Figure 4-19.

Even if the swelling pressure is sustained following significant buffer alteration, it is important to distinguish between swelling pressure and swelling capacity. In the hypothetical case where the volume of the alteration products is large enough not to change the montmorillonite/water ratio, the swelling pressure will remain constant even though montmorillonite is consumed in the process. The swelling capacity, however, always lowers as montmorillonite is being consumed.

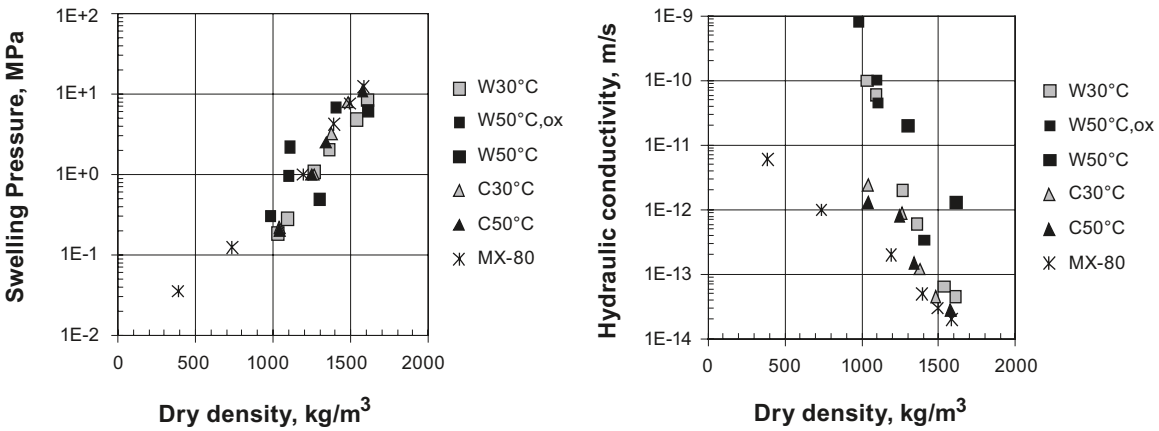

Figure 4-19. *Measured swelling pressure (left) and hydraulic conductivity (right) as a function of reduced clay dry density. From the study of /Carlson et al. 2006/. C indicates coupon samples, W indicates wire samples, W50°C, ox indicates a slightly oxidized wire 50°C material.*

Hydraulic conductivity

The discussion above on swelling pressure could also be applied to the impact on hydraulic conductivity. As the effective density of the montmorillonite part of the system decreases, the hydraulic conductivity increases as shown in Figure 4-19 (reference points for MX-80). In this case, however, the macroscopic structures of the alteration products are probably more permeable than the remaining montmorillonite, and will function as preferential paths. Thus, the hydraulic conductivity in an altered system is likely to be larger than expected from only considering the effective density of the remaining montmorillonite.

It is also important to note that hydraulic conductivity is not directly related to average porosity. A complete chloritisation, for example, will result in a system with lower average porosity than the original buffer (picture C in Figure 4-17). However, the hydraulic conductivity in such a system will be substantially larger than in the original montmorillonite.

In the study by /Carlson et al. 2006/ a substantial increase in hydraulic conductivity was found in some of the treated samples as shown in Figure 4-19. As the swelling pressure, on the other hand, was rather unaffected in these systems, this indicates an inhomogeneous system with localised high density/low hydraulic conductivity volumes and low density/high hydraulic conductivity volumes. Similar results were also found in bentonite material exposed to corroding iron in laboratory tests performed to simulate the conditions in a KBS-3H repository /Börgesson et al. 2005/. These experiments were, however, not performed under oxygen-free conditions.

The investigations of physical properties due to Fe(III)-reduction in smectites performed by Stucki and co-workers give somewhat ambiguous results as no correlation with iron content on the effects is shown. For example, /Stucki et al. 2000/ found a small and similar reduction in swelling pressure on reduced Na-exchanged smectites with very different iron content. Also /Shen et al. 1992/ showed only minor changes in hydraulic conductivity as an effect of reduction of structural iron in two smectites with a large difference in iron content.

Rheology

The term “cementation” has often been used in a broad sense to describe effects of chemical and mineralogical processes that can lead to various changes in the rheological properties of the buffer material, such as increased mechanical strength, brittleness or reduced swelling capacity. A number of completely different processes could conceivably cause similar effects, and the underlying reactions can occur directly in the montmorillonite, in the interlayer space or in accessory minerals.

Available data on the effects of cementation on the rheological properties of the buffer is by no means conclusive on this issue. The effect on the canister due to changes on buffer plasticity induced by chemical alteration is discussed in Section 3.6.1. The cementation effect is still not well understood and is an issue for further investigation.

While the effect of gas and its penetration of intact buffer is relatively well known, there is little or no understanding of how Fe-saturated or otherwise chemically altered smectite clay lets gas through. It is known, however, that the microstructural constitution of Fe-saturated MX-80 is characterized by channels, meaning that gas can get through at lower pressures. This is an issue that is relevant also for KBS-3V because of the iron in the insert.

Natural analogues/observations in nature

Data on relevant natural analogues is very limited /Marcos 2003/. Low-charge and iron-poor smectites are rarely associated with potential reaction products, such as berthierine, chlorite, nontronite or iron-rich saponite. Berthierine is often encountered in ironstones and may form mixed layers with chlorite. It can act as diagenetic precursor of chlorite. Chloritisation of

smectites is common in sediments, but occurs at rather elevated temperatures (150–200°C). Moreover, this transformation involves high-charge smectites (e.g. saponite), which often form mixed layers with iron-rich chlorite (chamosite). The formation of berthierine as an intermediate phase may also be involved in the transition of saponite to chlorite /Mata et al. 2001/. Interesting natural analogues are altered meteorites rich in metallic iron. Reported alteration products are sulphides, and these are depleted, cronstedtite, berthierine, chlorites and iron-rich smectites. Archaeological analogues such as clays altered by contact with iron and steel artefacts have not yet been investigated. Examples from natural systems reported refer to cementation effects induced by iron oxide precipitation under oxic, but not anoxic conditions. There is no natural analogue known to us which would indicate significant cementation effects in swelling clays under anoxic conditions.

Time perspective

The corrosion of the supercontainer will be fairly rapid. Complete conversion of Fe^0 to oxidised Fe^{2+}/Fe^{3+} species may occur within a few thousands of years. Fe(II) derived from the corrosion process has a high affinity for the clay which will lead to sorption and precipitation (perhaps with simultaneous oxidation) of Fe(II). The movement of the iron front is, however, very slow and would, according to preliminary calculations, take more than 150,000 years to extend across the thickness of the buffer (see discussion of the Olkiluoto case above).

Handling in the safety assessment for KBS-3H

Based on the reported long-term corrosion rates, complete corrosion of the supercontainer will take in the order of four thousand years. Corrosion of this material may be affected by microbial attack, which may increase localised corrosion, but probably not significantly increase average corrosion rates. The space between the supercontainer and the drift wall is likely to become filled with bentonite as the buffer saturates, although the possibility that the ruptured supercontainer will be pressed against the drift wall cannot be excluded. In either case, the bentonite in the vicinity of the drift wall will be chemically altered by interaction with the corroding iron.

Chemical alteration may adversely affect swelling, hydraulic and rheological properties of the buffer in the outer region. Because of large uncertainties in current knowledge of iron/smectite interaction processes it is difficult to describe these effects in quantitative terms. Nevertheless, a bounding analysis can be made with the help of available literature, design and site-specific information. A preliminary assessment for the Olkiluoto case indicates that the iron/bentonite interactions will remain spatially restricted for very long times, because of diffusional limitations and the strong affinity of the clay for Fe(II) released from the corroding supercontainer.

In the alteration zone, significant increase in hydraulic conductivity is expected based on available experimental data, although swelling pressure will probably only be affected to a minor extent.

In the KBS-3H Radionuclide Transport Report /Smith et al. 2007a/, the impact of iron/bentonite interaction is treated in a simplified and conservative manner. In specific radionuclide release and transport variant cases dealing with this and other potential perturbations to the buffer/rock interface, two different buffer domains are modelled: an inner part of the buffer that is not affected by iron/bentonite interactions; and an outer part of the buffer treated as a mixing tank. The extent of bentonite alteration zone in the calculation cases is 0% (but with altered transfer coefficients), 10% and 50% of bentonite thickness (corresponding to variant cases FEBENT-1, FEBENT-2, FEBENT-3). This approach, in which the altered buffer has essentially an infinite hydraulic conductivity, is highly conservative. The impact of alteration is more likely to give rise to a hydraulic conductivity that is higher than that of unaltered bentonite by one or two orders of magnitude, but the simplified and conservative approach is adopted in the present assessment due to lack of more specific information and for modelling simplicity.

Handling of uncertainties

Large uncertainties exist with regard to process understanding of the iron/bentonite interactions and their impacts on the physical properties of the buffer. Uncertainties concerning the occurrence of a perturbed buffer/rock interface, the physical extent of such an interface and the flow through the perturbed region are handled in the Radionuclide Transport Report as discussed above /Smith et al. 2007a/. It would be useful to perform long-term experiments to gain a better level of knowledge on iron/bentonite interaction. As pointed out by /Wersin et al. 2007/, further experimental work should include measurements of swelling pressure and hydraulic properties, including gas transport properties of altered bentonite. Furthermore, the potential effect of H_2 on Fe-clay interactions and on reduction of structural iron in smectite should be experimentally investigated. Finally, the impact of H_2 on porewater chemistry should be considered in future studies (see Section 4.7.4). The processes related to the interaction of iron on the buffer are complex and the consequent impact on the required properties of bentonite is far from being completely understood.

From the modelling side, it would be useful to include reaction kinetics for smectite transformation in the KBS-3H conceptual model to obtain a more realistic description of the evolution of iron front.

4.7.2 Cement/bentonite interaction

Overview/general description

Cementitious materials are being used in the construction of ONKALO and will be used in the construction and operation of the repository, whether KBS-3V or KBS-3H. The purposes of cementitious materials are to limit the groundwater inflow (grouting), to stabilise the rock (shotcrete, castings of rock bolts), to construct plugs and seals (e.g. drift end plugs, compartment plugs), to enhance operational safety (e.g. to fill anchoring holes). Concrete will also be used for temporary construction elements (walls, intermediate floors, doors). Most of the cementitious materials will be removed before the final closure of the repository but, according to the estimates of residual materials in the KBS-3H repository, between 1,200,000 and 1,800,000 kg[24] of cement will be left in the entire repository (including ONKALO). Of these, an average of 2,600 to 3,900 kg of cement will be located in each drift /Hagros 2007a/. The details are discussed in Section 6.1.

The highly reactive high-pH fluids from cementitious materials could in principle constitute a threat to the long-term stability of the buffer and other bentonite components. The reaction of the cement-conditioned alkaline water with the buffer will result in mineral dissolution and formation of new phases. Consequently, it is likely that the hydraulic and chemical properties of both the cementitious materials themselves and any bentonite that comes into contact with high-pH fluids will change (the impact of such fluids on the geosphere is discussed in Section 7.7). The main concerns are:

- montmorillonite dissolution leading to changes in swelling pressure, porosity and hydraulic conductivity,
- bentonite cementation by secondary phases leading to fracturing, with the possibility of advective transport,
- formation of alteration products, and their consequences for the properties of altered clay

It is currently foreseen that limited amounts of low-pH cement and colloidal silica grouts will be used inside a KBS-3H drift. These may have reduced detrimental effects on the buffer compared with Ordinary Portland Cement (OPC) because of the reduced alkalinity of their porewater leachates, although the long-term durability and evolution of such materials is not as well understood as in the case of OPC. In this section, the potential impacts of cementitious materials on bentonite are discussed. Further details are presented in Appendix F.

[24] Estimates depend on the alternatives for design, rock support, grouting, backfill and drift end plug /Hagros 2007a/.

Experimental/modelling studies

Cement degradation

In the case of OPC, porewater evolution is relatively well understood in controlled conditions (see Appendix F). The porewater is initially (up to 1,000 years approximately) hyperalkaline with an initial pH of 13.4 (KOH/NaOH buffered); between one thousand and ten thousand years the pH decreases to pH 12.5 ($Ca(OH)_2$ buffered) where it stays relatively stable up to a few hundred thousand years; finally, after a few hundred thousand years it decreases to 11 and below (calcium-silica-hydrate (CSH) phases). The timeframe during which high-pH conditions are likely to be encountered could be over 100,000 years. Low-pH cement is manufactured by adding silica fume as a microsilica slurry to the cement blend and reducing the cement content. Experimental studies suggest that amorphous silica reacts with $Ca(OH)_2$ during hydration and forms C-S-H phases so that almost no "free" $Ca(OH)_2$ remains /Vuorinen et al. 2005/. As a result, the pore fluid chemistry is controlled by the C-S-H phases causing lower pH values, and the incongruent dissolution of the C-S-H phases is likely to be the dominant leaching process. However, degradation mechanisms for low-pH cement are still under investigation.

Bentonite alteration in presence of cementitious porewater

There are two situations to be considered in regards to bentonite alteration by cementitious porewater. The most important in relation to buffer function is that due to porewater from grout or the end plug reaching the buffer via fractures intersecting the drift. Any cementitious porewater transported by groundwater to the drift from a distance should first interact with the host rock before it reaches the bentonite in the drift. The cement-host rock interaction could include both the reactions with the fracture surface minerals and with any fault infill or gouge plus the accessible porosity in the rock matrix behind the fractures (as long as this is not sealed by reaction). The interaction with the host rock could result in the formation of CSH phases, calcium-aluminum-silica hydrates (CASH) and zeolites in the fracture fillings. This interaction would reduce the pH of the cementitious alkaline plume. However, no experimental data on the host rock buffering capacity are available. Modelling studies suggest that the host rock buffering capacity at Olkiluoto is rather low /Montori et al. 2008/. The second situation to be considered is the direct contact at the drift end plug/bentonite distance block interface at the end of the drift (see Figure 6-1). This is less safety relevant, as the distance block is likely to be >5 m long and a significant alteration zone would have no impact on buffer function.

Few experimental studies are available involving compacted MX-80 bentonite and cementitious material (see Appendix F) and even fewer of compacted bentonite in presence of low-pH cement. While the detailed mechanism is still unclear, the current consensus is that the main effect of alkaline cementitious porewater on bentonite is montmorillonite dissolution due to OH^- ions. Bentonite undergoes the following mineral transformations as a function of time and distance from the cement/bentonite interface:

Cement/bentonite interface→ Montmorillonite dissolution (pH buffering) → CSH precipitation → CASH precipitation → Illite precipitation → Zeolite precipitation

The transformation begins with an illitisation of the montmorillonite. The illite then dissolves as zeolites phases are precipitated. These are finally dissolved to produce cement phases near the cement or concrete interface (e.g. at the interface between a drift end plug and a bentonite distance block) as a result of an increase in the Ca/Si ratio in the solid phases. This transformation sequence causes a decrease in the total volume of the clay as illitisation of the montmorillonite progresses and a strong increase in the total volume of zeolite as phases precipitate, which would lead to a decrease in porosity near the cement/clay interface.

The pH in the bentonite porewater is also expected to increase: this increase influences both the chemical and physical properties of the buffer, significantly decreasing swelling pressure and increasing hydraulic conductivity. However, the exact nature and properties of the secondary minerals that are dissolved and/or precipitated as well as sorption properties of altered bentonite are still affected by significant uncertainties (see Appendix F).

/Metcalfe and Walker 2004/ summarised the main modelling approaches of cement/ bentonite interaction. Modelling efforts are also affected by significant uncertainties due to shortcomings in:

1. appropriate mineral representation, especially the secondary minerals;
2. formulation of key underlying models/laws/functions, such as solid solution models, activity coefficient models, dissolution and precipitation rate laws of relevant phases in the system, hydrological constraints;
3. differences between actual and modelled phases, notably the chemical differences and the degree of crystallinity;

Moreover, the most advanced modelling studies (see Appendix F) mostly focus on the effect of an alkaline plume on clay rocks and are therefore not directly applicable to the effects on compacted bentonite. These uncertainties greatly affect the modelling results so that no quantitative conclusions from these studies can be drawn thus far.

Mass balance calculations on bentonite alteration in the presence of cement

The dissolution of montmorillonite in a hyperalkaline solution (pH >10) can be formulated as follows /Metcalfe and Walker 2004/:

$$Na_{0.33}Si_4Al_{1.67}Mg_{0.33}O_{10}(OH)_2 + 2\,H_2O + 4.68\,OH^- \rightarrow 0.33\,Na^+ + 0.33\,Mg^{2+} + 1.67\,Al(OH)_4^- + 4\,HSiO_3^- \quad \text{(Eq. 4-30)}$$

It thus takes 4.68 moles of OH^- to dissolve one mole of montmorillonite. The molar mass of montmorillonite is M=0.367 kg/mol.

Based on its composition, low pH cement can potentially release 5.7 moles OH^- per kg of cement (Appendix F). The current estimate of the amount of cement in the drift (approximately 2,600 to 3,900 kg) suggests that there could be up to 15,100–22,700 moles of OH^- released in the vicinity of the drift from the various cementitious sources. The amount of OH^- ions is likely to be much less if low-pH cement is used because calcium ions are mainly bound in a CSH ($CaO\text{-}SiO_2\text{-}H_2O$) phase rather than being released as portlandite ($Ca(OH)_2$), as shown by experimental evidence /Vuorinen et al. 2005/.

Comparing the amount of bentonite susceptible to dissolution by the entire OH^- inventory (1,185–1,780 kg of montmorillonite or 1,481–2,224 kg of bentonite, assuming 80w% montmorillonite content for bentonite) to the approximately 1,095,000 kg of buffer bentonite in a single 300 m-drift (see Table F-5 in Appendix F) the mass of altered bentonite due to cement is well below 1 w% (1 to 2 w‰).

Localised effects of the cementitious porewater on the buffer surrounding the supercontainer, rather than on all bentonite-bearing components in a KBS-3H drift, are of higher concern. According to the current drift design, no cement-bearing component will be in direct contact with the bentonite in the supercontainer and distance block unit. The minimum distance between each cementitious component in the drift and the supercontainer is 5 metres, which is the length of a block of compacted bentonite (19,000 to 23,000 kg). Therefore, even though some of the bentonite can be altered in direct contact with the cement-bearing components no direct threat is posed to the buffer surrounding the supercontainers.

However, cement could interact indirectly with the buffer if the alkaline cement porewater plume spreads through the network of fractures on the drift wallrock to a section of the drift containing a supercontainer. The minimum buffer thickness between the wallrock and the canisters is 40 cm (including space occupied by the supercontainer and its corrosion products).

According to the calculations in Appendix F, any high-pH leachate from the cement used to grout a fracture that migrates through the wallrock fracture network to the buffer/rock interface could potentially alter a 4 cm wide layer of bentonite around the drift, assuming that all OH^- eventually find their way to the buffer.

These mass balance calculations do not represent the physical or chemical reality. Firstly, the current reference design emphasises the use of Silica Sol rather than low-pH cement for grouting. Secondly, the amount of OH^- in low pH cement is likely to be lower than that inferred from in Equation 4-30 because the alkaline plume is reduced due to restricted formation of $Ca(OH)_2$. OH^- will be released at the time of CSH degradation, which occurs much later. Thirdly /Vieno et al. 2003/ calculated that only approximately 1% of OH^- released from the grouted fracture finds its way into the buffer based on fracture transmissivity considerations. Additional mitigating factors that were not taken into account in the mass balance calculations are the following:

- dissolution of accessory minerals in bentonite
- extent, rate and timing of OH^- release by low pH cement
- effect of compaction on OH^- diffusion in the bentonite rings
- potential interaction with corrosion products from the supercontainer.

Boundary conditions

The relevant boundary conditions for the cement/bentonite interaction are the expected conditions in the host rock, the chemical properties of buffer (in the absence of any cementitious materials) and the types and amounts of cementitious materials introduced. These are discussed in Section 7.1 (properties of the host rock), Section 4.1 (properties of the buffer) and above (types and quantities of cement).

Natural analogues/observations in nature

Two natural analogue sites have been identified in Jordan (Maqarin and Khushaym Matruk) featuring a clayey rock in contact with highly alkaline groundwater. Sealing of fractures by CSH phases as well as similar distribution patterns of zeolites/CSH and CASH mixtures as those predicted by modelling studies have been observed in the host rock at these sites. Although these natural analogues provide some information on the long-term effects of hyperalkaline waters on natural clay they are not fully relevant to the case of compacted bentonite exposed to low-pH cement porewater.

Time perspective

The duration of the high alkaline conditions due to cementitious leachates (pH>11) is uncertain, in particular with respect to low-pH cement. In the case of OPC, however, it has been estimated to last over 100,000 years (Appendix F).

Handling in the safety assessment for KBS-3H

In the KBS-3H Radionuclide Transport Report /Smith et al. 2007a/, three calculation cases (PD-FEBENT-1, PD-FEBENT-2, PD-FEBENT-3) are introduced in which the buffer and the buffer/rock interface are perturbed by various possible mechanisms, including bentonite alteration by interaction with high-pH cement leachates. The extent of bentonite alteration zone in the calculation cases is 0% (but with altered transfer coefficients), 10% and 50% of bentonite thickness to take into account the uncertainties in the actual mass and flow rate of OH^- penetrating into the buffer from the host rock. The same assessment case is used to address uncertainties due to the iron/bentonite interaction.

Handling of uncertainties

Even if mass balance calculations show only a minor effect on the bentonite inventory, considering the uncertainties in the cement/bentonite interaction and the potential effects on local bentonite performance, it is prudent to minimise the amount of cement (even low–pH cement) in the vicinity of the repository. For example, the use of colloidal silica for grouting in the drift is being considered /Autio et al. 2007/. However, the use of colloidal silica introduces additional uncertainties, such as (see Appendix F):

- long-term basic mechanical properties of colloidal silica, such as drying shrinkage, flexural strength, compressive strength, and shear strength;
- penetration ability of grouting material in the fractures;
- eventual release of colloids;
- long-term effect of salt accelerators in Silica Sol on bentonite;
- long-term effect of biocide agents such as isothiazols and bromo-nitropropandiols (<1%) present in the Silica Sol mixture to extend its shelf life.

4.7.3 Colloid release/erosion

Overview/general description

Bentonite gel that has intruded into fractures intersecting the drift could potentially break up and disperse in the form of colloids if the concentration of cations in solution at the gel/water interface falls below the Critical Coagulation Concentration (CCC), as discussed in some detail in Appendix A of /SKB 2006d/. The cation concentration at the interface is determined by the cation concentration in the groundwater, and also by the supply of cations to the interface through the dissolution of Ca and Mg minerals in the bentonite and subsequent diffusion of these ions to the interface. The CCC is uncertain but, according to Appendix A of /SKB 2006d/, is around 1 mmol per litre.

Currently, the ionic strength of Olkiluoto groundwater at repository depth exceeds the CCC by a significant margin (the sum of Ca^{2+} and Mg^{2+} concentrations at repository depth at Olkiluoto is in the range 50–80 mmol per litre). The ionic strength is expected to increase further during the transient period due to the upconing of deeper, more saline waters. In the longer term, continuing isostatic uplift will result in a replacement of the saline water at repository depth with more brackish water of lower ionic strength. Nevertheless, surface waters that penetrate to repository depth will be subject to chemical interactions within the overburden and the rock, increasing their ionic strength, thus the CCC is still expected to be exceeded. At present, very dilute groundwaters occur in Olkiluoto practically only in the overburden. The stability of the gel/water interface is therefore expected to be maintained, and no significant erosion of the buffer will occur prior to any major climate change affecting groundwater ionic strength. Penetration of dilute water to repository depth in association with glacial retreat cannot, however, be ruled out.

Time perspective

The timing of any future penetration of dilute glacial meltwater to repository depth is uncertain, being affected, for example, by the impact of greenhouse gas emissions on future climate change. According to the Weichselian-R climate scenario, the next glacial retreat, and hence the next possibility for penetration of glacial meltwater to repository depth, will be in 70,000 years time, as discussed in the KBS-3H Evolution Report /Smith et al. 2007c/.

Experimental/modelling studies

In SR-Can, it is concluded on the basis of tentative model calculations that the possibility of buffer mass loss due to chemical erosion sufficient for advective conditions to become established in the buffer cannot currently be excluded, and that this may occur as early as the

next period of glaciation in the least favourably located deposition holes. On the other hand, the model on which the conclusion is based is subject to significant uncertainties. It should be noted that, for KBS-3H, the loss of buffer around one canister due to exposure to glacial meltwater may affect the corrosion rate of neighbouring canisters, since the the buffer density along the drift will tend to homogenise over time. This also means, however, that the impact on buffer density and on the corrosion rate of the first canister will diminish with time. This is in contrast to the case of KBS-3V, where buffer loss around one canister will not affect the state of the buffer around the other canisters.

Handling in the safety assessment for KBS-3H

It is cautiously assumed in the safety assessment for KBS-3H that the tentative finding in SR-Can that advective conditions in the buffer could arise during the next period of glaciation also applies to a KBS-3H repository at Olkiluoto. The impact of a single canister failure due to dilute glacial meltwater penetrating to repository depth, leading to chemical erosion of the buffer and to advective conditions becoming established in the buffer is considered in the radionuclide release and transport calculations (cases CC-GMW, CC-LOGEORG). Even in the case of severely damaged buffer, the canister is expected to remain unbreached for at least 100,000 years.

Handling of uncertainties

It is acknowledged in SR-Can that better understanding of the erosion process could lead to models that yield either lower or higher bentonite loss rates. A new model is currently under development by SKB and the Royal Institute of Technology (KTH).

4.7.4 Effect of hydrogen gas on porewater chemistry

The presence of high hydrogen partial pressures due to the corrosion of the supercontainer shells and the other steel components of a KBS-3H repository, may have an effect on the bentonite porewater chemistry. The impact of hydrogen gas on the bentonite porewater chemistry has not yet been fully evaluated. Various factors need to be considered, including acid-base equilibria and the pH buffering capacity of bentonite, as well as the limited timeframe of hydrogen production of several thousand years. The overall impacts, in particular any effects on the buffer, should be taken into account in future studies.

4.8 Radionuclide transport processes

An overview of processes relevant to radionuclide transport in the buffer is shown in Table 4-16. For radionuclide transport in the water phase, the following processes are relevant:

- advection, but only if the hydraulic conductivity of the buffer is increased, or high gas pressures inside the canister result in the expulsion of water from the canister interior;
- diffusion, which will be the dominant transport mechanism through the buffer;
- sorption, which will have a strong effect on the transport of certain radionuclides;
- speciation, which will determine how the radioelements are sorbed (or precipitated if solubility limits are exceeded, for example because of radioactive ingrowth during transport);
- colloid transport, which could enhance the transport of radionuclides, but only if buffer density is significantly reduced;
- radioactive decay.

Radionuclide solubilities were calculated by /Grivé et al. 2007/ for the near-field groundwater conditions at Olkiluoto. All of these processes are not specifically dependent on the conditions in KBS-3H, except for effects related to the issues discussed in previous chapters (e.g. iron/bentonite interactions). For a detailed discussion of these processes, see the relevant Process Reports for KBS-3V /Rasilainen 2004, SKB 2006d/. In addition, a pulse of hydrogen gas may be released from a defective canister, conveying some volatile radionuclides (mainly C-14). In such a situation, volatile radionuclides could be transported to the surface much more rapidly than in the case of a release in the aqueous phase.

The possible transport pathways for radionuclides are depicted in Figure 4-20 for the case of a canister with an initial penetrating defect. After release from a defective canister and diffusive transport through the buffer (pathway R_1), radionuclides may migrate

- into a nearby fracture (pathways R_2)
- along the rock/drift interface (R_3) to some more distant fracture (R_4) or via a compartment plug to the next transmissive fracture zone (R_5)
- along the rock/drift interface via the drift end plug into the access tunnels (R_6).

The most unfavourable situation is represented by pathways R_1/R_2 in the case of a transmissive fracture that intersects the deposition drift right next to the defect in the canister. All other transport pathways involve longer path lengths and higher transport resistances in the near field.

Differences between KBS-3V and 3H arise due to the presence of the corroded supercontainer, the absence of backfill immediately in contact with the buffer, and the smaller and less transmissive EDZ in the KBS-3H deposition drift compared with the KBS-3V tunnel. The cementation of the buffer next to the corroded supercontainer may lead to a zone of increased porosity and hydraulic conductivity, reducing the transport resistance of the buffer/rock interface).

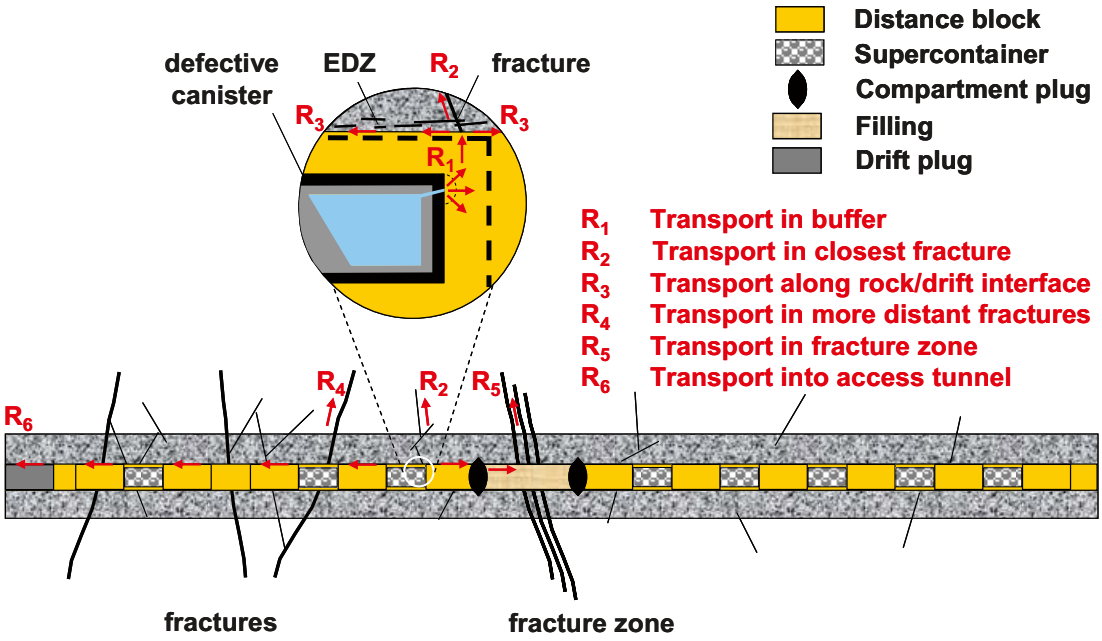

Figure 4-20. *Illustration of possible radionuclide transport pathways in the KBS-3H near field.*

Table 4-16. The interdependence of processes relevant to radionuclide transport and identified variables in the buffer.

Radionuclide processes	Variables for the buffer											
	Geometry	Pore geometry	Radiation intensity	Temperature	Water content	Gas content	Hydrovariables	Stress state	Bentonite composition	Montmorillonite composition	Porewater composition	Structural and residual materials
Transport of radionuclides in water phase	×	×		×			×		×	×	×	
Transport of radionuclides in gas phase	×						×	×				

Handling in the safety assessment for KBS-3H

Transport calculations for dissolved radionuclides that are released from a failed canister into the buffer are performed in the current safety assessment using the code REPCOM /Vieno and Nordman 2000/.

Buffer transport and retention processes are modelled using REPCOM with the following assumptions:

- advection is assumed to be negligible;
- diffusion is treated with diffusivities and porosities that are specific for anions, cations and neutral species;
- sorption is treated with element-specific linear sorption coefficients (K_d);
- colloids are assumed to be immobile in the fine pore structure of the buffer;
- precipitation of radionuclides is treated by element-specific solubility limits (with the computer code REPCOM used for near-field release calculations solubility limits are applied only in the canister interior and at the buffer/rock interface);
- speciation is considered in the determination of solubility limits and sorption coefficients, as discussed in /Smith et al. 2007a/ and in /Grivé et al. 2007/;
- radioactive decay and ingrowth are considered in the calculations.

These model assumptions are applicable in the majority of assessment cases considered in the safety assessment for KBS-3H.

The migration of volatile C-14 with repository-generated gas is considered in two separate release and transport assessment cases (PD-VOL-1 and PD-VOL-2), which consider high and low rates of repository gas generation, respectively. C-14 in the form of methane is assumed to mix with gas generated in the interior of the canister and be transported with this gas through the buffer to the geosphere at a rate determined by the rate of gas generation. Radionuclides dissolved in water expelled from the canister interior by repository-generated gas are also considered in a separate release and transport assessment case, and modelled assuming instantaneous transfer of expelled water through the buffer to the geosphere once the gas inside the canister interior reaches a critical pressure (PD-EXPELL).

5 Supercontainer shell and other steel structural materials

5.1 Description of supercontainer shell and other steel structural materials

5.1.1 General

Structural materials made of steel used in the KBS-3H drift include the supercontainer shell, fixing rings, compartment plugs and spray and drip shields (see Sections 1.6.4 and 1.6.6). Two design options are currently under consideration – the Basic Design (BD) and the Drainage, Artificial Watering and air Evacuation (DAWE) design. The analysis of processes presented in this chapter (and elsewhere in the present report) focuses on the chosen reference design for safety studies, referred to as Basic Design. The DAWE design option is discussed in Appendix D. The total quantities of steel used in the repository for the Basic Design are given in Table 5-1.

5.1.2 Overview of variables

The geometry of the supercontainer and of other structural materials is described in Section 1.6.4. Other variables that are relevant to the subsystem are radiation intensity, temperature, stress state, material composition, and water composition (Table 5-2).

Table 5-1. Steel components and masses in all 171 drifts of a KBS-3H repository at Olkiluoto (data from Appendix A).

Steel component	Mass (whole repository) [kg]
Supercontainers (incl. feet)	3,041,640 (1,071 kg per supercontainer)
Compartment plugs	872,100 (5,100 kg per set of 2 plugs)
Steel plug (adjacent to drift end plug)	360,810 (2,110 kg per plug)
Fixing rings (4.5 per drift in average)	461,700 (600 kg per ring)
Spray and drip shields (4–5 per drift in average)	462

Table 5-2. Variables in the supercontainer shell and other steel structural materials.

Variable	Explanation
Geometry	Geometric dimensions for supercontainer and other structural materials (fixing rings, steel feet, compartment plugs, drip shields, rock bolts, etc).
Radiation intensity	Intensity of α-, β-, γ-, and neutron radiation as a function of time and space in supercontainer and other structural materials.
Temperature	Temperature as a function of time and space in supercontainer and other structural materials.
Stress state	Stress conditions as a function of time and space in supercontainer and other structural materials.
Material composition	Material composition of the supercontainer and other structural materials.
Water composition	Composition of water in contact with the supercontainer.

5.1.3 Safety function indicators

There are no safety function indicators for the supercontainer shell and other steel structural materials.

5.1.4 Summary of handling in safety assessment

Table 5-3 summarises the handling of processes for the supercontainer shell and other steel structural materials in the safety assessment for KBS-3H, as suggested in the following sections of Chapter 5. In the table, the process is either "mapped" to a model by which it will be quantified or associated with a brief verbal description of how it will be handled.

Since the early evolution, characterised by unsaturated conditions and elevated temperatures, is in many respects different from the long-term, saturated phase, the description in the table has been divided accordingly. The period covered by "early evolution" is defined in Section 4.1.4.

5.2 Overview of processes

Based on the FEP analysis for the KBS-3H deposition drift /Johnson et al. 2005/, a list of processes for the supercontainer shell and other steel structural materials has been derived following the methodology in Appendix B. No equivalent list of processes for KBS-3V is available.

The processes are structured into radiation-related, thermal, hydraulic, mechanical and chemical process categories. In addition, radionuclide transport is discussed separately. In the introductory part of each of the following chapters, the processes pertinent to the process category are tabulated.

5.3 Radiation-related processes

Radiation attenuation/heat generation is the only radiation-related process relevant to the supercontainer shell and other steel structural materials in the deposition drift. The inter-dependence between this process and the variables in the subsystem is shown in Table 5-4.

5.3.1 Radiation attenuation/heat generation

Overview/general description

Radiation attenuation/heat generation within the supercontainer shell is considered to be insignificant because the canister will retain its integrity and its shielding function for a very long time. Even in the case of an early failure of the canister, no safety-relevant effects of radiation on the supercontainer are expected because of the attenuation of radiation within the bentonite buffer. Furthermore, no safety function is attributed to the supercontainer. Radiation effects on other structural materials (e.g. spray and drip shields, fixing rings, compartment plugs, etc) in the deposition drift are even less significant due to the greater distance and more efficient shielding compared with the supercontainer.

These issues are thus not discussed any further.

Table 5-3. Process table for the supercontainer shell and other steel structural materials describing how processes are handled in different time periods. Green fields denote processes that are omitted or irrelevant for the time period of concern. Red fields denote processes that are quantified by modelling in the safety assessment. Orange fields denote processes that are omitted subject to a specified condition. Motives for handling are given in the relevant sections of Chapter 5.

Process Type	Internal process	Early evolution of the repository	The longer term	Notes/*Section in KBS-3H Process Report*
Radiation-related processes	Sc1. Radiation attenuation/heat generation	Omitted since dose rate is too low to be of importance.	Omitted since dose rate is too low to be of importance.	*Section 5.3 The handling of the process in the safety assessment for KBS-3H is also discussed.*
Thermal processes	Sc2. Heat transport	Thermal process model /Ikonen 2003, 2005/	Thermal process model /Ikonen 2003, 2005/	Heat transport is not significantly affected by the presence of the supercontainer and other structural materials. *The handling of the process in the safety assessment for KBS-3H is also discussed* (the process is neglected in radionuclide transport calculations). *Section 5.4*
Hydraulic processes	Sc3. Gas generation	Gas Model (process model)	Gas Model (process model)	*The handling of the process in the safety assessment for KBS-3H is also discussed, see Ge4.* *Section 5.5*
Mechanical processes	Sc4. Deformation of supercon-tainer and other structural materials	Mechanical design calculations (compartment plugs, fixing rings)	These components have no long-term safety function; however, they may influence safety-related functions of other components; see Sections 5.6 and 4.7.1, which address the issue of corrosion following deformation of the supercontainer that brings it into contact with the rock wall. The porous corrosion products could subsequently affect radionuclide transport (modelled in Appendix B of Evolution Report).	Issues related to changes in bentonite density as a result of volume changes or displacements of the supercontainer and other structural materials are addressed in Bu8. *Sections 4.7.1 and 5.6*
Chemical processes	Sc5. Steel corrosion	Gas Model (process model)	Gas Model (process model)	Steel corrosion is the main source for the generation of hydrogen gas. For handling in safety assessment, see Ge4. For the handling of iron/bentonite interactions and the corroded supercontainer in the safety assessment, see Bu17. *Section 5.7*
Radionuclide transport-related processes	Sc6. Transport of radionuclides	Not relevant	Not relevant since supercontainer and other structural materials have no long-term safety function.	Supercontainer and other structural materials neither contribute to isolation nor retardation. Radionuclide sorption on corrosion products is not taken into account. For the effects of corrosion products on radionuclide transport (reduction of transport resistance at the buffer/rock interface), see Bu17. *Section 5.8*

Table 5-4. The interdependence of radiation-related processes and identified variables in supercontainer shell and in other steel structural materials.

Radiation-related processes	Variables in supercontainer shell and in other steel structural materials					
	Geometry	Radiation intensity	Temperature	Stress state	Material composition	Water composition
Radiation attenuation/ heat generation	×	×	×		×	

Handling in the safety assessment for KBS-3H

The effects of radiation on the supercontainer shell and other steel structural materials in the deposition drift are considered to be insignificant to long-term safety and may thus be neglected in the safety assessment for KBS-3H.

5.4 Thermal processes

The only relevant thermal process is heat transport. The inter-dependence between this process and the variables in the subsystem is shown in Table 5-5. The specifics of thermal processes and the evolution of temperature within the deposition drifts and in the near-field rock are discussed in the context of the buffer and distance block (see Section 4.4). The radiation intensity at the supercontainer is negligible and is decoupled from the heat transport, as in the case of the canister thermal processes (see Section 3.4).

Handling in the safety assessment for KBS-3H

Heat transport is not significantly affected by the presence of the supercontainer shell and other steel structural materials. The process is thus neglected in the radionuclide transport calculations.

Table 5-5. The inter-dependence of thermal processes and identified variables in supercontainer shell and in other steel structural materials.

Thermal processes	Variables in supercontainer shell and in other steel structural materials					
	Geometry	Radiation intensity	Temperature	Stress state	Material composition	Water composition
Heat transport	×		×	×	×	

5.5 Hydraulic processes

Gas generation is the only process related to the presence of the supercontainer shell and other steel structural materials in the deposition drift that is relevant to hydraulic conditions within and around the repository. The inter-dependence between this process and the variables in the subsystem is shown in Table 5-6.

5.5.1 Gas generation

Overview/general description

Gas generation in a deep geological repository may take place by various processes, including anaerobic metal corrosion, microbial degradation of organic compounds, radiolysis, radioactive decay (helium) and formation of volatile fission products.

In KBS-3H, steel corrosion is expected to be the only relevant process for gas generation in the time period before canister breaching[25]. This is because no significant amounts of organics and gas-generating metals other than steel are present and because the intact canister provides a complete containment and shields the environment against radiation. Any air initially trapped in the deposition drifts at the time of closure will be either dissolved in groundwater or compressed in the course of time.

The masses of steel per supercontainer unit are given in Table 5-7 for the Basic Design option for KBS-3H. Included in Table 5-7 are the total masses of steel for the supercontainer, the feet, the fixing ring (including rock bolts), the spray and drip shields and the steel plugs. 10 steel feet (each weighing 4 kg) are envisaged for the supercontainer. For the average steel thickness of the feet, a value of 6 mm is assumed. Note that fixing rings and compartment plugs are used only when needed, and an average number of 4–5 fixing rings and 2 compartments (being separated by pairs of steel plugs) per drift is envisaged (Appendix A, and /Autio et al. 2007/). The average steel thickness for the fixing rings and compartment plugs is 10 mm.

The anaerobic corrosion reaction for pure iron and carbon steel can be written as (Section 5.7.1):

$$3Fe + 4H_2O \rightarrow Fe_3O_4 + 4H_2 \qquad \text{(Eq. 5-1)}$$

Table 5-6. The inter-dependence of hydraulic processes and identified variables in supercontainer shell and in other steel structural materials.

Hydraulic processes	Variables in supercontainer shell and in other steel structural materials					
	Geometry	Radiation intensity	Temperature	Stress state	Material composition	Water composition
Gas generation		×		×	×	

[25] Some decay gases will, however, be generated within intact canisters. This issue is addressed in Sections 2.5 and 2.7.

Table 5-7. Steel components and masses per supercontainer + distance block unit used in the Basic Design (for references see Appendix A).

Steel component	Average steel thickness [mm]	Steel mass per supercontainer unit [kg]
Supercontainer	8	1,031
Feet beneath supercontainer	6	40.2
Feet beneath distance block	6	–[1]
Spray and drip shields	1	0.600[2]
Total mass	–	ca 1,072
		Steel mass per structural element [kg]
Fixing ring	10	600
Compartment plug[3] (two double-sided caps plus bolts)	10	2,550

[1] According to the reference design, there will be feet beneath the loose distance blocks.

[2] The thickness of spray and drip shields is not specified in the Design Description 2006 /Autio et al. 2007/ but here it is assumed to be 1 mm. One shield is conservatively included in a supercontainer unit for gas generation estimates; in reality only 4–5 such shields are expected to be used in the entire drift.

[3] Similar plugs (single-sided, weighing 2,110 kg with bolts) may also be used as one component of the drift end plugs.

Given that one mole of iron produces 4/3 moles of hydrogen gas (H_2), the total amount of H_2 produced per supercontainer unit, n_{tot} [mol], is calculated as follows:

$$n_{tot} = \frac{4}{3}\frac{m}{M} \qquad \text{(Eq. 5-2)}$$

where

m total mass of steel per supercontainer unit [kg]
M molar mass of iron [55.85×10^{-3} kg mol^{-1}]

The rate of H_2 production per supercontainer unit, $\dot{n}$ [mol a^{-1}], is calculated as follows:

$$\dot{n} = \frac{n_{tot}}{t_c} \qquad \text{(Eq. 5-3)}$$

where t_c [a] is the corrosion time (time needed for complete corrosion of steel):

$$t_c = \frac{d}{2R} \qquad \text{(Eq. 5-4)}$$

d average steel thickness [m]
R steel corrosion rate [m a^{-1}]

A reference corrosion rate value of 1 μm a^{-1} is used. In the framework of sensitivity analysis, rates in the range of 0.1–2 μm a^{-1} are also considered. The rationale for using a different range of corrosion rates of the steel supercontainer than that used for the insert corrosion rates (see Section 2.5.1) for the sensitivity analysis is discussed in Section 5.7.1.

Model studies/experimental studies

The generation of hydrogen due to steel corrosion has been studied both experimentally and theoretically by several authors (see Section 5.7.1). The reaction responsible for H_2 generation is shown in Equation 5-1. The total amount of gas generated per supercontainer unit and the contributions of the various steel components for the different design options are calculated based on the amounts of steel and listed in Table 5-8. According to the reference design (Basic Design), there will be feet beneath the loose distance blocks. These feet have not yet been included in the gas calculations, but they will contribute only around 1% to the total gas volume and the effect on the results will be small.

The estimated gas generation rates are shown in Figure 5-1 for a steel corrosion rate of 1 μm a^{-1}. Apart from the compartment plugs, the largest contribution to the gas generation rate stems from the supercontainer. After 5,000 years, the corrosion and the gas production cease. The feet of the supercontainer and distance block (the latter are not included in the calculations) and the spray and drip shields add only marginally to the overall gas production rates. Note that the amount of initially trapped gas (a few m^3 STP per supercontainer) is small compared with the amount produced by steel corrosion (several hundred m^3 STP per supercontainer).

Table 5-8. Total amounts of gas generated per supercontainer unit (calculated with Equation 5-2) and corrosion times based on a corrosion rate of 1 μm a^{-1} (calculated with Equation 5-4) for the Basic Design. Steel mass and thicknesses are from Table 5-7.

Steel component	Total amount of gas generated per supercontainer unit [mol]	Corrosion time [a]
Supercontainer	2.5×10^4	4,000
Feet beneath supercontainer	9.6×10^2	3,000
Spray and drip shield	1.4×10^1	500
Total amount	2.6×10^4	
	Amount of gas generated per structural element [mol]	
Fixing ring	1.4×10^4	5,000
Compartment plugs	6.1×10^4	5,000

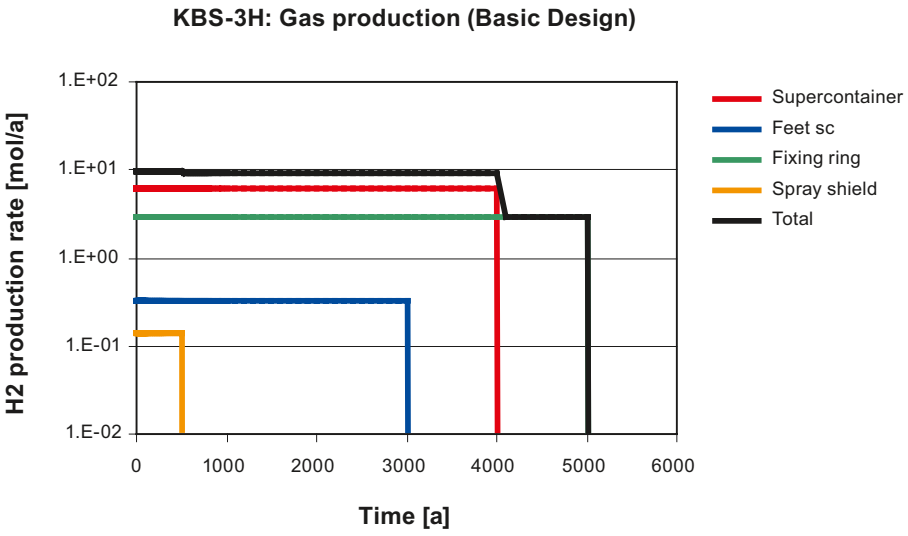

Figure 5-1. *Hydrogen gas generation rates for the Basic Design (steel corrosion rate 1 μm a^{-1}).*

In Table 5-9, the maximum total gas generation rates per supercontainer unit are listed for the Basic Design as a function of the steel corrosion rate, namely 1 μm a^{-1} (base case) and 0.1–2 μm a^{-1} (values for sensitivity analysis). Note that the values given in Table 5-9 per supercontainer unit include the contribution of a fixing ring, but no contribution from the compartment plugs, because these are located in the vicinity of permeable fractures and do not significantly contribute to gas pressure build-up (see Section 7.5.2). The total gas production rates are proportional to the steel corrosion rate, whereas the duration of the gas production (corrosion time) is inversely proportional to the steel corrosion rate.

There is the possibility that some of this hydrogen will be consumed by microbially mediated reduction of sulphate to sulphide, or of carbonate to acetic acid or methane. However, this is likely to have a negligible impact on the total amount of hydrogen in the repository system so this process is conservatively neglected in the calculations of gas pressure evolution. As noted in Section 5.7, the consumption of hydrogen by bacteria would not be expected to increase the corrosion rate.

As discussed in Section 4.5, gas generation compress the bentonite causing a delay and non-uniformity (in case of gas bubbles) of the saturation of the buffer. However, the extent of this non-uniformity and its long-term safety consequences are unclear at this time.

Handling in the safety assessment for KBS-3H

The effects of gas generation on the performance of the repository, their handling in the safety assessment and the uncertainties involved are discussed in the context of gas transport through the geosphere (Section 7.5).

5.6 Mechanical processes

Deformation is the only relevant mechanical process in the supercontainer and in other structural materials in the deposition drift. The inter-dependence between this process and the variables in the subsystem is shown in Table 5-10.

5.6.1 Deformation of supercontainer and other structural materials

Overview/general description

The expected difference of swelling pressure inside and outside the supercontainer may lead to considerable forces acting on the perforated steel shell and to elasto-plastic deformations. Rupturing of the steel shell may occur, most likely at or near the circular edges of the supercontainer (end-plates) where the stresses are expected to be highest, and as result of the ongoing corrosion and weakening of the steel.

Table 5-9. Maximum total gas production rates per supercontainer unit (one supercontainer, feet, spray and drip shield, and one fixing ring) for the Basic Design as a function of the steel corrosion rate (see Table 5-7 and Table 5-8).

Steel corrosion rate [μm a^{-1}]	Basic Design [mol a^{-1}]	[m^3 STP a^{-1}]
0.1	0.95	0.021
1	9.5	0.21
2	19	0.42

Table 5-10. The inter-dependence of mechanical processes and identified variables in supercontainer and in structural materials.

Mechanical processes	Variables in supercontainer and in structural materials					
	Geometry	Radiation intensity	Temperature	Stress state	Material composition	Water composition
Deformation of supercontainer and other structural materials	×		×	×	×	

A quasi-stationary state of stress equilibrium is reached when all forces acting in the system (including the force caused by volume expansion of corrosion products, by gas pressure build-up, hydrostatic pressure and rock stress) are balanced, resulting in a homogenisation of bentonite swelling pressures inside and outside the supercontainer.

The time to reach this equilibrium depends on a number of rates and factors, including the steel corrosion rate and the various mechanisms affecting gas pressure build-up and bentonite swelling. The formation of steel corrosion products involves a volume increase (about a factor of 2 for magnetite, which is the dominant corrosion product for the expected repository conditions). This leads to a slight increase in bentonite density and swelling pressure (see Section 4.6.1).

Axial displacements of supercontainers/distance blocks may give rise to bentonite density variations along the deposition drift (Section 4.6.1). Under normal conditions, such movements are avoided by the friction between the swollen distance blocks and the rock surface. Fixing rings are foreseen in the Basic Design to counteract the large axial forces such as those occurring between drift sections that are relatively quickly saturated/pressurised and drift sections that stay under pressure for longer periods of time (up to roughly hundred years). These fixing rings will be positioned on one side of the distance block to prevent a one-way movement (/Autio 2007/ p. 29). Massive steel rings would be required to counteract the full hydrostatic pressure exerted on the entire circular surface area of the distance block. This has been assessed as being technically and economically unfeasible. An important technical constraint of the Basic Design is that massive steel rings would add significant amounts of steel in the deposition drifts, leading to increased hydrogen generation and gas pressure buildup. The amount of steel in the fixing rings can be reduced significantly and the rings can be made lighter if the hydrostatic pressure is exerted on only on part of the surface of the distance block, i.e. on a ring-shaped surface. At emplacement, the supercontainer and distance block will have to be positioned in such a way that good contact is ensured in all parts of the interface (see discussions below). This constraint does not apply to the DAWE alternative (see Appendix D), which significantly simplifies the implementation of the KBS-3H design.

Steel plugs are foreseen to seal off compartments from highly conductive fractures intersecting the deposition drifts. These plugs are thus used to isolate suitable from unsuitable drift sections. Such plugs locally add substantial amounts of steel to the overall steel inventory.

Due to the transient temperature increase and subsequent decrease, the supercontainer experiences thermal expansion/contraction and possibly some structural alterations. These effects may be enhanced by increased temperatures due to a reduction of the heat transport capacity by gaps initially present around the canister, buffer and supercontainer. In permeable drift sections, these gaps are expected to close relatively rapidly due to the swelling of bentonite.

In tight drift sections, they may remain partially open for longer periods of time (several hundreds to thousands of years). Given that the maximal temperatures within bentonite remain below 90°C (10°C below the design basis maximum of 100°C), thermal expansion/contraction of the supercontainer and of other structural materials in the deposition drift are not expected to be of any significance. Likewise, structural alterations induced by thermal gradients are not significant under the expected thermal conditions in the repository.

Boundary conditions

The relevant boundary conditions for mechanical deformations of the supercontainer and other structural materials are determined by the stresses exerted by bentonite and by the surface of the rock, by hydraulic forces acting in the system, by temperature gradients and by processes leading to volume changes (bentonite swelling, corrosion).

Model studies/experimental studies

Swelling of bentonite through the holes of the supercontainer has been analysed both theoretically and experimentally /Börgesson et al. 2005/. The theoretical analysis showed that the maximal swelling pressure is reduced when bentonite swells through the holes and further when it swells into the void space between supercontainer and rock. The swelling pressure difference within and outside the supercontainer was estimated to be several MPa. This difference in swelling pressure results in considerable forces acting outwards on the steel shell of the supercontainer. The mechanical resistance of the thin steel shell (thickness 8 mm) is limited and elasto-plastic deformations as well as rupturing of the steel shell are likely to take place. The various strain mechanisms that are involved in the early evolution of the supercontainer shells could have a detrimental effect on the outer part of the buffer depending on how the shells deform and they may generate heterogeneities in the buffer. This is an issue for further study.

Laboratory tests in scale 1:10 have demonstrated that bentonite swelling through the holes and behind the steel shell does occur and that the measured swelling pressure inside and outside the steel shell are similar to the swelling pressure expected in the absence of the supercontainer. This is explained by the observed expansion (and partial rupturing) of the perforated steel shell, leading to stress equilibration. The axial hydraulic conductivity of the buffer in the slot outside the supercontainer was measured (about 10^{-12} m s^{-1}) and found to be higher than expected based on measured density and swelling pressure, but still low enough for fulfilling the safety function indicator for the buffer. The increase is likely to be caused by the uneven swelling behind the container, as shown by the theoretical calculations.

Further laboratory tests on the Basic Design in scale 1:10 have been performed to determine the required dimensions of steel rings that counteract axial hydraulic forces on the distance block /Börgesson et al. 2005/. In a series of tests, the axial hydraulic forces acting on the distance block were measured. It was concluded that a fixing ring was required for proper sealing of the distance block and to prevent piping. Furthermore, the results indicated that if the gap between distance block and supercontainer is narrow (not more than 7 mm), the pressure is exerted on a ring shaped surface area only, located at the outer part of the distance block and excluding the major part of the circular footprint of the supercontainer. The measured thickness of the ring was in the order of a few (up to 10) centimetres radially inwards from the rock surface (see Appendix L of /Autio et al. 2007/). No experimental investigations have been performed so far on the steel plugs used to seal off compartments from highly conductive fractures intersecting the deposition drifts.

Handling in the safety assessment for KBS-3H

Deformations of the supercontainers are relevant to the safety assessment for KBS-3H, although the supercontainers have no long-term safety function (see Section 1.7), because they and their corrosion products may affect the safety functions of other components. There is the possibility

that deformation of the supercontainer will cause contact with the drift wall and the presence of the supercontainers and their potentially porous or fractured corrosion products may perturb mass transfer across the buffer-rock interface. The impact of this and other processes that could perturb the buffer-rock interface and therefore affect the canister lifetime is assessed in scoping calculations in Appendix B of the KBS-3H Evolution Report /Smith et al. 2007c/. The impact on radionuclide transport of a higher permeability zone of very limited thickness at the buffer-rock interface in the case of a canister with an initial penetrating defect is assessed in variant assessment cases called PD-SPALL (because it also addresses the issue of thermally-induced rock spalling) and PD-FEBENT (because it also addresses the issue of iron-bentonite interaction) in the KBS-3H Radionuclide Transport Report /Smith et al. 2007a/. Issues related to changes in bentonite density as a result of volume changes or displacements of the supercontainer and other structural materials are addressed in Section 4.6.1.

5.7 Chemical processes

Steel corrosion is the only relevant chemical process for the supercontainer shell and other structural materials in the deposition drift. The inter-dependence between this process and the variables in the subsystem is shown in Table 5-11.

5.7.1 Steel corrosion

Overview/general description

The corrosion of the steel components present in the deposition drifts (supercontainer and structural materials such as rings and supporting feets) will be fairly rapid. For the expected steel corrosion rate of 1 μm a^{-1}, complete conversion of Fe^0 to oxidised Fe^{2+}/ Fe^{3+} species may occur within a few thousand years. The main corrosion product will be magnetite. Depending on the groundwater composition, some iron sulphide and siderite may also be formed.

In the major part of the deposition drifts, there will likely be sufficient water available in the vicinity of the steel surfaces to maintain anaerobic corrosion at a rate of 1 μm a^{-1}. In very tight drift sections with hydraulic transmissivities of 10^{-11}–10^{-12} m^2 s^{-1}, steel corrosion may be limited by the supply of liquid water and water vapour and the corrosion rate may decrease to 0.1 μm a^{-1}.

In the KBS-3H design, the supercontainer shell and the copper canister are separated by the bentonite buffer and galvanic coupling would not be expected to occur. In relation to the cast iron canister, galvanic corrosion of copper-cast iron couples has been studied by SKB /Smart et al. 2005/. Although galvanic corrosion was initially higher, deareation led to a pronounced decrease in the corrosion rates of iron. The corrosion rates of iron in deareated environments were not significantly different from those measured in the absence of galvanic couplings.

Table 5-11. The interdependence of chemical processes and identified variables in supercontainer and in structural materials.

Chemical processes	Variables in supercontainer and in structural materials					
	Geometry	Radiation intensity	Temperature	Stress state	Material composition	Water composition
Steel corrosion	×	×	×	×	×	×

The galvanic corrosion rates of iron coupled to copper at low O_2 concentration were measured as < 0.1 um/year at 30°C and < 1 um/year at 50°C. The presence of bentonite (bentonite slurry) appeared to increase the galvanic corrosion current compared to aqueous solutions. No tests with compacted bentonite have been reported.

Thus, even if galvanic coupling of the supercontainer shell and the copper canister occurred, there would be a negligible impact on the supercontainer shell corrosion rate. The corrosion rate of steel in this report has been varied from 0.1–2 μm/year in the gas generation calculations.

Boundary conditions

The relevant boundary conditions for anaerobic corrosion of steel are the supply of water and other species with the inflowing groundwater.

Model studies/experimental studies

Influence on depletion of residual oxygen

Oxygen present in the gap between the supercontainer and rock will be consumed rapidly (months to a few years) by microbial processes and corrosion of steel. However, for consumption of oxygen in the buffer, considering that during the initial stage the heat from the canister will move the water front towards the outer side of the buffer, the cathodic reaction may be limited by slow diffusion, especially in case of a low hydraulic conductivity of the host rock. Calculations performed for the Swiss design concept (initial bentonite dry density = 1.5 Mg/m^3; initial moisture content = 2%) under the assumption that O_2 is consumed entirely by steel corrosion at fully saturated conditions indicate timescales for oxygen depletion of about 20–50 years /Wersin et al. 2003/. This estimation is based on the assumption that the O_2 depletion occurs entirely by inorganic reaction processes.

Studies have also been carried out for the KBS-3V alternative (/Pastina and Hellä 2006/ and references therein) which suggest oxygen depletion in a few years to a few hundred years, associated with copper corrosion and consumption by Fe(II)-bearing minerals in the buffer (see Section 4.1.1).

From these considerations, it is likely that the consumption of oxygen will be at least as rapid for KBS-3H and may be faster due to the large amount of steel present, but the differences are presently not quantifiable.

Corrosion rates and corrosion products

Iron is unstable in water and corrodes by forming an oxide-type surface layer. The corrosion of carbon steel under aerated conditions in the initial aerobic stage is relatively rapid, as has been pointed out in the previous section. Under anoxic conditions iron corrodes by the reaction with water according to the overall reaction:

$$3Fe + 4H_2O \rightarrow Fe_3O_4 + 4H_2 \qquad \text{(Eq. 5-5)}$$

The reaction is shown for the corrosion of Fe to magnetite, which is the corrosion product formed under relevant conditions. As discussed in Section 4.7.1, dissolution of this film may subsequently transport Fe(II) into the buffer and form other Fe(II)-rich phases. Early resaturation phase oxic corrosion is neglected in gas calculations (Section 5.5.1), as no gas is evolved under these conditions. The formation of a protective oxide layer leads to a strong decrease in the corrosion rate. This is shown by a number of corrosion experiments under a variety of solution conditions in which a significant decrease of the corrosion rates with time is noted. Thus, corrosion rates determined from weight loss and hydrogen production measurements show a decrease from

20 µm a^{-1} to less than 5 µm a^{-1}. As noted by /Johnson and King 2003/, weight loss measurements frequently lead to overestimates of the long-term instantaneous rate, which can be measured with high accuracy and reproducibility by direct measurement of the H_2 evolved. This is illustrated in Figure 5-2 for the specific case of corrosion of steel in compacted bentonite /Smart et al. 2006/. Other results in /Smart et al. 2001, 2006/ illustrate the rather low sensitivity of the rate to changes in chemistry, provided corrosion occurs under conditions above pH 7.

Experiments performed in compacted bentonite /Smart et al. 2004, 2006/ revealed higher rates in compacted bentonite compared with those obtained in water media. The corrosion rates obtained in compacted bentonite after a period of about 1 year were 1–2 µm a^{-1}. The use of a corrosion rate of 1–2 µm a^{-1} for the supercontainer is considered justifiable based on the high reproducibility of the measurements that have been done under directly relevant conditions. The rate is further supported by various natural analogue studies, as discussed in SR-Can's Fuel and Canister Process report /SKB 2006c/. The possibility that the downward trend continues is considered in gas production rate calculations for the supercontainer (Section 5.5.1) and for associated gas pressure build-up calculations (Section 7.5.2). The higher rate was explained by the slower build-up of a protective magnetite film because of incorporation of released iron in the clay. This aspect is addressed in more detail below.

Pitting

Pitting and crevice corrosion are favoured when the cathodic and anodic reaction are physically separated, which in turn results from heterogeneities within the material or gradients within the solution. For example, attack of the passivating oxide layer by chloride or sulphate leads to localised corrosion under oxic conditions.

The effect of pitting decreases with corrosion depth. This is evident from a compilation of pitting factors taken from laboratory studies and iron samples buried in soils for periods up to 15 years /JNC 2000/. This shows that pitting factors strongly decrease with corrosion depth. At a corrosion depth of 1 mm, the maximum pitting factors drop below 5 /Johnson and King 2003/. Anaerobic corrosion of steel is much more uniform than that under aerated conditions and pitting factors are very low. Some pitting may occur in the presence of sulphide and/or the presence of microbes (see sections below).

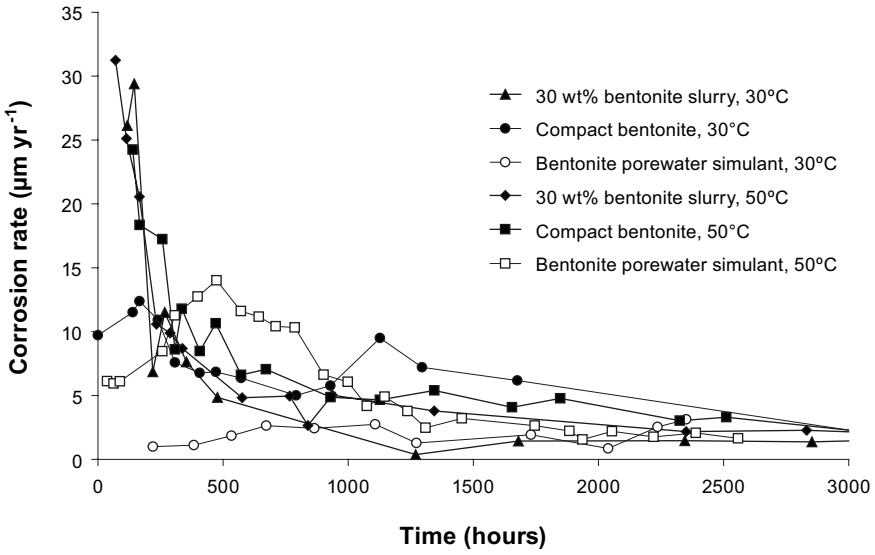

Figure 5-2. *Corrosion rate of steel in bentonite porewater, bentonite slurry and compacted bentonite at 30°C and 50°C /Smart et al. 2006/.*

Nature of corrosion products

The dominant anaerobic corrosion product that is experimentally observed under near-neutral and alkaline conditions is magnetite, which is a very stable and insoluble solid phase. The stability of magnetite increases with increasing temperature /Hermansson 2004/. Results obtained from /Smart et al. 2001/ indicate that magnetite occurs as a thin (< 100 nm) uniform inner layer and a porous outer layer.

Depending on solution conditions other iron corrosion products may also form. Thus, at high concentrations of sulphide or carbonate, iron sulphide or siderite formation is expected:

$$Fe + HS^- + H^+ \rightarrow FeS + H_2 \qquad \text{(Eq. 5-6)}$$

$$Fe + HCO_3^- + H^+ \rightarrow FeCO_3 + H_2 \qquad \text{(Eq. 5-7)}$$

In addition, green rust type phases (double layer mixed Fe(III)/Fe(II) hydroxides) may form, which are expected to be metastable under conditions of interest with respect to magnetite and siderite /Génin et al. 1998/.

The stability fields of the different iron corrosion products under conditions representative of deep groundwater at Olkiluoto are presented in classical Eh-pH diagrams calculated for 25°C (Figure 5-3). They illustrate the stability field of magnetite at pH values higher than 8. FeS (Figure 5-3A) is also thermodynamically stable under conditions of the repository.

On the other hand, pyrite (not shown here) has a much larger stability field; its formation however may be limited by slow kinetics. An indication that pyrite formation may not be relevant under repository conditions stems from the observed groundwater composition in the host rock, which indicate equilibrium with FeS rather than with FeS_2, although pyrite has been observed in all boreholes studied so far at the site. Although the temperature conditions in the near field of

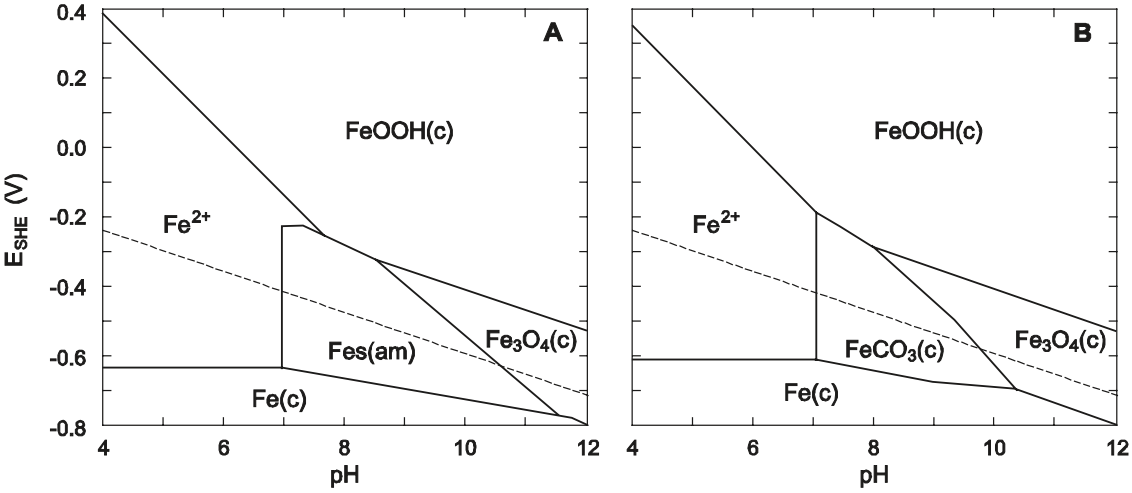

Figure 5-3. *pH-Eh diagram showing stability fields of potential corrosion products. A: Conditions representing sulphate reduction zone ($Fe_{tot} = 10^{-5}$ M, $HS_{tot} = 10^{-5}$ M, DIC = 5 × 10^{-4} M, I = 0.1 M); B: Conditions representing iron reduction zone with low sulphide ($Fe_{tot} = 5 \times 10^{-5}$ M, $HS_{tot} = 10^{-6}$ M, DIC = 5 mM, I = 0.1 M). The dashed line is the H_2/H_2O boundary.The pH is 7.5 to 8.5 and Eh about –300 to –200 mV at repository depth at Olkiluoto (see Chapter7).*

the repository will be somewhat higher than 25°C, the stability relationships of the iron phases are not expected to be significantly different. Siderite formation is in principle also possible (Figure 5-3B) but requires high carbonate and low sulphide activities in the groundwater, as discussed in Sections 4.6.1 and 4.7.1.

Observations from archaeological objects buried in sediments /David 2001/ show the presence of magnetite and iron sulphides and to a lesser extent of siderite, on iron surfaces.

Besides hydroxide, sulphide and carbonate, Fe^{2+} from the corrosion reaction may also react with dissolved silicate and the solid clay fraction. The reaction with silicate can schematically be written as:

$$Fe + H_4SiO_4 \rightarrow FeSiO_3 + H_2 + H_2O \qquad \text{(Eq. 5-8)}$$

Little is known about the details of this process, such as the nature of the iron silicate phases and the thermodynamic and kinetic constraints. This aspect is discussed in Section 4.7.

Effect of microbial activity

Microbial activity is known to influence iron corrosion. For example, the presence of sulphate-reducing bacteria (SRB) on the surface of steel may lead to increased attack by sulphide and thus affect the formation of the protective oxide layer. Moreover, iron-reducing bacteria (IRB) might be active by adhering to the magnetite layer and promoting reductive dissolution of the Fe(III) component /Kostka and Nealson 1995, Dong et al. 2000/. In addition, autotrophic methanogenic bacteria promoting degradation of inorganic carbon by using the hydrogen source could be envisioned to be active in the buffer region close to the host rock.

These three bacterially-mediated processes are probably occurring within the deep groundwaters at Olkiluoto (see Chapter 7). Hence, in principle, it is conceivable that these occur also in the supercontainer-rock interface region. The distance from the supercontainer to the rock wall is small (≈ 4 cm) and some reduction in swelling of the bentonite separating the supercontainer and host rock is expected from degradation of the swelling component (smectite) (Section 4.7). Thus, microbial activity cannot be excluded, although the clay buffer does not provide a favourable environment at full swelling pressure.

The microbial effects on corrosion rates are not expected to be very large, as suggested from observation from archaeological analogues. If, for example, SRB were active at the supercontainer surface, this would favour a sulphide surface layer, which would also be protective against high corrosion rates. However, in this case increased pitting may occur /Johnson and King 2003/. Similarly, the build-up of Fe^{2+} by IRB on magnetite-coated steel is limited by sulphide and siderite precipitation as well as by the slow dissolution kinetics /Dong et al. 2000/.

The impact of thriving methanogenic bacteria on corrosion is uncertain. Consumption of H_2 by methanogens may reduce the hydrogen pressure build-up, although there is no quantitative evidence for this. The impact of thriving methanogenic bacteria that might consume H_2 on the corrosion rate would be negligible. Firstly, the H_2 pressures that might be reached in a repository are far below equilibrium values (the equilibrium pressure for the corrosion process, Equation 5-1, is approximately 40 MPa /Neretnieks 1985/. Secondly, the corrosion rate measurements by /Smart et al. 2006/ which give values of 1–2 μm/a, are performed at near zero hydrogen pressure, thus any process that consumes some of the H_2 that builds up in the repository could not increase the rate. Reduction of inorganic carbon would limit siderite precipitation and, in the case of simultaneous sulphate reduction, counteract alkalinity increase. However, SRB that utilise H_2 could increase the amount of sulphide available for steel corrosion; this process should be evaluated in future microbial studies.

Significance for the supercontainer environment

From the extensive corrosion data available, corrosion rates under anaerobic conditions are expected to be 1–2 μm a^{-1} in the compacted bentonite environment (see Figure 5-2). The contribution of aerobic corrosion will not be significant. The lifetime of the steel under these conditions will be rather short. For a rate of 1 μm a^{-1} (R), the time for complete corrosion (t_c) can be calculated:

$$t_c = \frac{d}{2R} = 4000\,a \qquad \text{(Eq. 5-9)}$$

where d is the thickness of the supercontainer shell (8 mm).

Due to the attack by sulphide, possibly enhanced by microbial activity, significant pitting cannot be ruled out. Localised corrosion is also favoured by the geometric configuration of the perforated supercontainer (i.e. large number of machined holes). This, however, will not lead to a significant enhancement of the consumption rate of steel. On the other hand, the formation of a protective corrosion layer might also considerably slow down corrosion rates leading to an extended life-time of uncorroded steel.

The nature of the corrosion products will depend on the composition of groundwater. Because of the slightly alkaline conditions expected in all scenarios (pH = 7.5–8.5), an inner magnetite-type oxide layer will build up. The thickness of this layer, however, depends on the concentrations of other anions (sulphide, carbonate), the reactivity of the clay and the impact of microbial action. Under conditions of elevated sulphide concentrations, as expected for the reference water scenario, iron sulphide precipitation will be favoured (Equation 5-6). In the case of upconing of saline waters (saline water scenario), less sulphide is available for competing for the corroded iron, thus less FeS will form relative to magnetite. In the dilute water scenario (zone of Fe(III) reduction), corroded Fe^{2+} may react to form siderite, although carbonate levels will probably not be very high. In all scenarios the clay may react with iron to form iron-rich clay. However, from a thermodynamic perspective, the extent will probably be less important when significant sulphide concentrations arising from sulphate reduction are available to bind Fe(II).

The thickness of the corroded layer, and thus the increase in supercontainer volume, depends on the molar volume of the corrosion phases. In case of magnetite the increase of volume is about a factor of two. For FeS and $FeCO_3$ the increase is 2.5 and 4.7 respectively (see Table 4-12). A much higher volume increase for corroded iron incorporated in a silicate phase is calculated. Thus assuming the formation of berthierine the volume increase is a factor of 8. This increase will, however, be largely compensated by the break down of the reacting clay. Under the assumption that all steel is converted to magnetite a decrease in porosity of about 2% would arise. This would lead to a slight increase in swelling pressure from 7 to about 8 MPa.

Because the area between the supercontainer and the drift wall is small (≈ 4 cm thickness) a significant fraction may be filled with iron corrosion products and Fe-altered clay (Section 4.7). Due to volume expansion the total porosity in this area is likely to be decreased relative to the unaffected buffer. On the other hand, the corrosion may adversely affect swelling properties. The mechanical and hydraulic properties in the drift periphery are briefly discussed in Sections 5.5 and 5.6.

The effects of radiation on corrosion will be negligible, since the canister will retain its integrity for a long time. Even in case of an early failure of the canister, no safety-relevant effect of radiation on the supercontainer is expected because of the attenuation of radiation within bentonite (e.g. preventing radiolysis) and because no safety function is attributed to the supercontainer.

The question has been raised whether the corroded supercontainer and the mineralogyically altered bentonite outside the supercontainer could – in the long run – lead to increased water flow along the periphery of the deposition drift. Such a situation would lower the concentration

of dissolved radionuclides at the outer boundary of the buffer and would thus enhance diffusive radionuclide flux through the buffer. As noted in Chapter 4, there is substantial residual swelling pressure of the buffer even under very pessimistic assumptions on iron/bentonite interaction. Moreover, when quasi-stationary stress equilibrium is achieved, significant pressures are exerted on all parts of the engineered barrier system. Under such conditions, larger voids are unlikely to exist. Nonetheless, cementation of altered clay with corrosion products may result in a more permeable material and increase the stiffness of the buffer, making the canisters more vulnerable to post-glacial earthquakes (Section 3.6.1). The impact of buffer permeability changes in this region on the corrosion rate of the canister is addressed in detail in Appendix B.7 of the KBS-3H Evolution Report /Smith et al. 2007c/ and the effects on radionuclide transport in the case of a failed canister are discussed in Section 5.8.

Limitation of steel corrosion by hydrogen pressure

From a thermodynamic point of view, magnetite formation by anaerobic corrosion of steel stops at hydrogen partial pressures of about 40 MPa /Neretnieks 1985/. This is far beyond any significant gas pressure at which hydrogen gas could be confined in the host rock. Steel corrosion is thus not limited by the pressure of hydrogen under repository conditions.

Limitation of steel corrosion by the availability of water

Water flowing into the deposition drift is slowly consumed by the corrosion of iron. Based on the corrosion reaction producing hydrogen and magnetite (Equation 5-5), the rate of water consumption is calculated from:

$$\dot{n}_w = \begin{cases} \dot{n}_{w,\max} & V_w > 0 \\ \min(-Q_w \dfrac{\rho_w}{M_w}, \dot{n}_{w,\max}) & V_w = 0 \end{cases} \qquad n_w(t_0) = n_0 \qquad \text{(Eq. 5-10)}$$

$$\dot{n}_{w,\max} = \frac{4}{3} R F_0 \frac{\rho_{Fe}}{M_{Fe}} \qquad \text{(Eq. 5-11)}$$

where

$\dot{n}_w$ water consumption rate (the dot signifies time derivative) [mol a^{-1}]
$\dot{n}_{w,max}$ maximal water consumption rate (for unlimited water supply) [mol a^{-1}]
Q_w water flow rate (note that for inflow: $Q_w < 0$) [m^3 a^{-1}]
V_w volume of liquid water in deposition drift contacting the steel surfaces [m^3]
R steel corrosion rate [m a^{-1}]
F_0 total steel surface (supercontainer and feet) [m^2]
ρ_w, ρ_{Fe} density of water and iron [kg m^{-3}]
N_w, N_{Fe} molar weight of water and iron [kg mol^{-1}]

Equation 5-10 means that the water consumption rate is at its maximal value if either one of the following conditions is satisfied: i) there is some liquid water available near to the supercontainer, or ii) the inflow rate of liquid water is sufficient to maintain corrosion. Note that the supply of water vapour is not included in Equation 5-10 (for an estimate of the vapour supply rate from the near-field rock and from the bentonite, see discussion below). Based on the corrosion process involving magnetite as the dominant corrosion product, 0.75 moles of iron are consumed per mole of water, i.e. 2.3 kg of iron can be corroded by 1 litre of water. In other words, in order to sustain a corrosion rate of 1 μm a^{-1} over the total steel surface of 28.3 m^2 per supercontainer (including feet), about 0.1 litres a^{-1} of water are needed.

The conversion of the total mass of steel (about 1,071 kg per supercontainer including feet) would require 460 litres of water. This is to be compared with the initial water content in the buffer in the supercontainer of about 1,650 litres, based on the Basic Design with a buffer volume of about 7.2 m^3 and a dry density of 1,885 kg m^{-3} for ring blocks and a volume of about 1.7 m^3 and 1,753 kg m^{-3} for end blocks, assuming an initial water content of 10% w for both ring and end blocks. This means that the amount of water initially available for corrosion is about 3 to 4 times higher than the amount required for conversion of all steel. The question arises, however, whether this water can be withdrawn from the buffer by evaporation/vapour diffusion at a sufficient rate to maintain corrosion (see discussion below).

i) Supply of water by advective inflow from the near-field rock

The inflow rate of liquid water from the near-field rock depends on the hydraulic transmissivity of fractures intersecting the deposition drift and on the hydraulic gradient. As discussed in Section 4.5.1, drift sections in permeable rock ("less tight" drift sections) are quickly saturated (within about 10 years), whereas typical inflow rates to tighter drift sections with hydraulic conductivities in the range 10^{-13} to 10^{-12} m s^{-1} are 11–100 litres a^{-1}. This is 2 to 3 orders of magnitude more than the 0.1 litres per year needed to sustain corrosion at a rate of 1 μm a^{-1}, meaning that corrosion is not limited by the water availability as long as a significant hydraulic gradient towards the drift persists.

However, due to hydrogen gas generation by anaerobic corrosion of steel, gas pressure build-up takes place. The gas pressure reaches the hydrostatic pressure within roughly hundred years and any inflows of liquid water from the rock and from wetter sections through the distance blocks, along the drift/rock interface and through the EDZ will thus be stopped. For hydraulic transmissivities of 10^{-10}–10^{-12} m^2 s^{-1}, several thousand litres of water will have entered the drift within 100 years. This water will only be partially consumed by corrosion during this time period. The remaining water will be taken up by bentonite and may be available for steel corrosion at a later stage. On the other hand, if the gas pressure rises further, gas-induced water displacement into the rock or along the EDZ may occur (see Section 5.5), reducing the amount of water available for corrosion.

ii) Supply of water by vapour diffusion from the near-field rock and from bentonite

Even in the absence of any hydraulic gradient, there may be some supply of water by transport of vapour, which further maintains steel corrosion. Both the near-field rock and the unsaturated bentonite may act as sources of water. The dominant driving force for vapour transport is the vapour pressure gradient that is established by a gradient in the relative humidity (which in turn is a function of the total suction potential) and by a temperature gradient. Other gradients such as the osmotic gradient, density gradient or gravity are less important for vapour transport in bentonite (/SKB 2006d/ Section 2.3) and in the near-field rock. Note that vapour transport by a temperature gradient (thermal diffusion) can be viewed as being part of vapour transport driven by a gradient in the relative humidity. This is because a temperature difference causes a vapour pressure difference, which drives vapour from the warmer part to the cooler part.

Both steel corrosion and suction/condensation in bentonite take up moisture from the gas phase and tend thus to maintain a vapour pressure gradient from the rock into to drift (Figure 5-4). This is opposed by the temperature gradient which, by thermal diffusion, tends to evaporate water near the heat source (canister) and to drive water vapour outwards to cooler areas where condensation takes place. The importance of thermal diffusion, however, decreases with time due to the gradual decrease of temperature at the canister surface. After some transient phase, a steady-state vapour flux is likely to be established, where the consumption of water at the steel surface (the sink) is balanced by transport of vapour towards the sink. It is important to note that the conversion of water to corrosion products is an irreversible process and is thus a true sink, whereas the uptake/condensation of moisture in bentonite may be reversed by evaporation/removal (drying of bentonite).

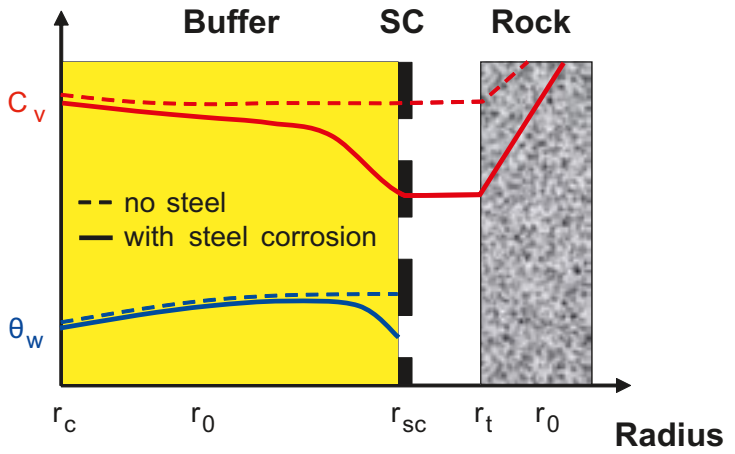

Figure 5-4. *Schematic radial profile of water content (θ_w) and vapour concentration (C_v) in bentonite and at the interface supercontainer/near-field rock, with and without the effect of steel corrosion (vapour sink). Note that the figure represents a situation where a thermal gradient exists from the canister towards the rock. In this situation, water in bentonite pores is driven outwards by vapour diffusion.*

The steady-state transport rate of vapour from a source of water, located at some radial distance r_0, to the sink (supercontainer shell), located at the radius r_{sc}, may be estimated as follows:

$$Q_v = 2\pi\, D_v S_g l_{sc} \frac{C_v(r_0) - C_v(r_{sc})}{\ln(r_0 / r_{sc})} \qquad \text{(Eq. 5-12)}$$

where

Q_v vapour transport rate [kg a^{-1}]
D_v effective vapour diffusion constant of porous medium [m^2 a^{-1}]
S_g average saturation of the porous medium [–]
C_v vapour concentration in gas phase [kg m^{-3}]
l_{sc} length of supercontainer [m]
r_{sc} radius of supercontainer [m]
r_o radial location of water source [m]

The concentration of vapour in the gas phase is given by:

$$C_v = \frac{M_w P_{v,sat} r_H}{R_0 T} \qquad \text{(Eq. 5-13)}$$

where

$P_{v,sat}$ saturated vapour pressure [Pa]
r_H relative humidity [–]
M_w molar weight of water [kg mol^{-1}]
R_0 universal gas constant [J K^{-1} mol^{-1}]
T temperature [K]

In the case of vapour diffusion from the near-field rock into the drift, the vapour pressure gradient is spanned by a relative humidity of 1 within the rock, assumed to be saturated at a radial distance of 0.1 m from the rock surface, and by a relative humidity of 0.6 near to the steel surface of the supercontainer. Note that corrosion is strongly reduced for relative humidities below

the "critical relative humidity", which for metals is generally in the range 0.5–0.7 /King et al. 2001/2002/. In the presence of hygroscopic salts on the steel surface, the threshold value for the relative humidity above which significant corrosion can occur may be even lower (in the order of 0.4). In the present calculations a reference value of 0.6 and an alternative value of 0.4 are assumed. The saturated vapour pressure at an assumed temperature of 60°C at the steel surface is about 2×10^4 Pa. Based on these values and on an average gas saturation in the pores of the rock matrix of 0.1, an effective gas diffusion constant of the rock matrix D_v of 2.6×10^{-10} m^2 s^{-1} (for fully gas saturated conditions, see /Johnson et al. 2005/ p. 149), a supercontainer radius and length of 0.88 m and 5.56 m (this value was subsequently revised to 5.525 m, Figure 1-4, which has little effect on the calculations below, thus they were not revised), respectively, one obtains:

$$Q_v = \begin{cases} 0.010\ kg\,a^{-1} & (r_H = 0.6) \\ 0.015\ kg\,a^{-1} & (r_H = 0.4) \end{cases} \qquad \text{(Eq. 5-14)}$$

This is about an order of magnitude lower than the minimal rate of water supply (0.1 kg a^{-1}) required to maintain corrosion at a rate of 1 µm a^{-1}.

In the case of vapour diffusion within the pores of the bentonite buffer, an additional equation is needed to relate the relative humidity within the bentonite pores with the total suction potential, ψ [Pa]. Neglecting osmotic effects, this relationship reduces to Kelvin's equation:

$$\psi = \frac{\rho_w R_0 T}{M_w} \ln(r_H) \qquad \text{(Eq. 5-15)}$$

For a water content of 10%, corresponding to the initial water content of the buffer in KBS-3H, a total suction potential of –70 MPa (/SKB 2006d/ p. 39) to –100 MPa (/JNC 2000/ Figure B5-13) is reported. The total suction potential does not show a strong dependence on temperature (/JNC 2000/ Figure B5-11). From Equation 5-15, the relative humidity within bentonite pores can be calculated (Table 5-12).

Table 5-12. Relative humidity within bentonite pores as a function of the water content and temperature, calculated with Equation 5-15.

Water content [%w]	Total suction potential [MPa]	Temperature [°C]	Relative humidity [–]
10	–70	10[1]	0.58
	–100	10	0.46
20	–20	10	0.86
10	–70	60[2]	0.63
	–100	60	0.52
20	–20	60	0.87
10	–70	80[3]	0.65
	–100	80	0.54
20	–20	80	0.88

[1] Ambient rock temperature at 400 m depth.

[2] Average temperature of supercontainer during early thermal phase.

[3] Average temperature of inner bentonite during early thermal phase.

From the values in Table 5-12 and using Equations 5-12 and 5-13, the rate of vapour transport from the inner part of the buffer to the steel surface of the supercontainer (where a constant relative humidity of 0.6 or 0.4 is assumed) can be calculated. The resulting vapour transport rates are presented in Figure 5-5 as a function of the average water content and of the relative humidity at the steel surface. The effective vapour diffusion constant in unsaturated bentonite is assumed to be 10^{-9} m^2 s^{-1} (see Section 4.5.1). Two sets of curves are shown:

- Thermal phase (upper curves): Temperature of 80°C and a saturated vapour pressure of about 5×10^4 Pa in the inner part of the bentonite buffer (halfway between the canister and the supercontainer); temperature of 60°C and a saturated vapour pressure of about 2×10^4 Pa near the supercontainer shell.
- Isothermal conditions (lower curves): Uniform temperature of 10°C throughout the near field, saturated vapour pressure of about 1.2×10^3 Pa.

The vapour transport rate during the transient thermal phase is a factor of 1–3 higher than the minimal rate of water supply (0.1 kg a^{-1}) required to maintain corrosion at a rate of 1 µm a^{-1}. After roughly 100 years of cooling, the heat flux from the canister is reduced to about half its initial value. By then, the supply of water vapour has dropped to values below 0.1 kg a^{-1}. In the course of further cooling, the temperature gradient gradually decreases until – after a few thousand years – the temperature returns to ambient conditions (about 10°C). For these conditions, the vapour transport rate is below 0.01 kg a^{-1}. Some additional water vapour is provided by the rock (see above) and from the two adjacent distance blocks towards the supercontainer. The latter contribution has not been quantified, but is considered to be smaller than the water vapour supply from the buffer due to geometrical reasons.

Natural analogues/observations in nature

Since experimental studies can assess only a limited time frame, natural and archaeological analogues data can yield valuable information. A comprehensive review on archaeological analogues and corrosion by /David 2001/ and in SR-Can's fuel and canister process report /SKB 2006c/ demonstrates that the majority of iron objects experienced corrosion of 0.1–10 µm a^{-1}. This suggests low and relatively uniform long-term corrosion rates in very different geochemical environments.

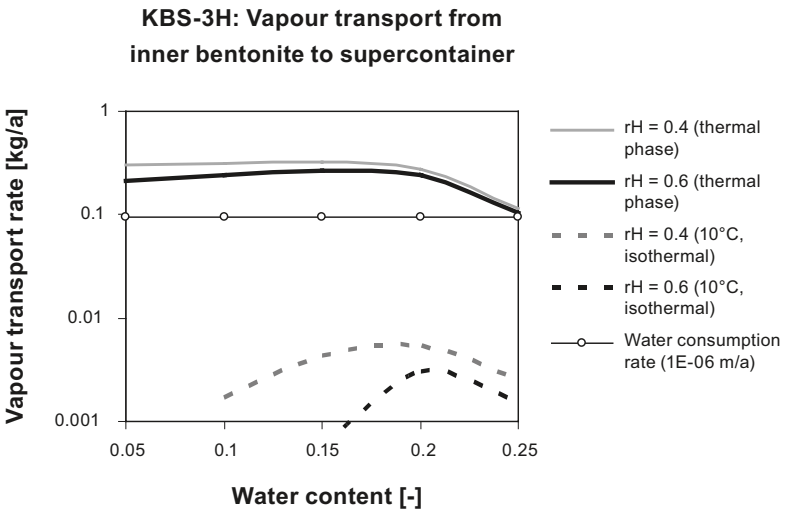

Figure 5-5. *Vapour transport from inner part of bentonite to supercontainer shell as a function of the water content in bentonite (by weight) for the transient thermal phase (upper curves) and for isothermal conditions after the transient thermal phase. Note that the initial water content of bentonite inside the supercontainer is 10% by weight*

Summary and time perspective

Table 5-13 summarises the estimated water supply rates from the near-field rock and from the inner part of bentonite to the supercontainer shell for various conditions and transport processes.

Handling in the safety assessment for KBS-3H

In the major part of the deposition drifts, there will likely be sufficient water available in the vicinity of the steel surfaces to maintain anaerobic corrosion at a rate of 1 μm a^{-1}. In very tight drift sections where water from the rock and from the buffer is transported to the corroding surfaces predominantly by vapour diffusion, steel corrosion may be limited by the supply of water and the corrosion rate may decrease to 0.1 μm a^{-1} (Table 5-13). This does not, however, have any significant impact on the safety functions of the repository system in the longer term, provided that the pressure transient up to gas/water pressure equilibration does not lead to significant redistribution of bentonite within the deposition drifts (for a discussion of bentonite redistribution, see Section 4.6.1).

The effects of iron/bentonite interactions, the uncertainties involved and the treatment in the KBS-3H Radionuclide Transport Report are discussed in Section 4.7.1.

Handling of uncertainties

There is significant uncertainty in mechanistic understanding of and data relevant for transport of liquid water and vapour within and around the buffer in KBS-3H. The inflow rates of water through the near-field rock primarily depend on the hydraulic transmissivity of fractures intersecting the deposition drifts and on the hydraulic gradient. Inflow rates are expected to be very heterogeneous. Quickly saturated drift sections are expected to alternate with sections embedded in tight rock, where inflow rates are small. The saturation state after gas/water pressure equilibration in the near field affects the subsequent supply of water to maintain steel corrosion. In drift sections that are saturated before any significant amount of gas has been generated, there will be sufficient water for the full conversion of steel to corrosion products, irrespective of the design and of the detailed hydraulic conditions. In tight drift sections that remain unsaturated for longer periods of time, the dominant mechanism for water supply after pressure equilibration is vapour diffusion from the rock and from the inner parts of the bentonite buffer adjacent to the supercontainer. Both transport processes depend on a number of uncertain parameters, among which the vapour pressure gradient affected by temperature is the most important. Uncertainties in steel corrosion rates are discussed in Sections 2.5.1 and 5.7.1.

Table 5-13. Water supply rates from the near-field rock and from the inner part of bentonite to the supercontainer shell.

Situation	Critical parameter	Water supply	Time period
Drift sections in permeable and moderately tight rock	Hydraulic conductivity above about 10^{-11} m s^{-1}	unlimited[1]	0 to 5,000 years (steel corrosion rate 1 μm a^{-1})
Drift sections in very tight rock			
- advective inflow	Hydraulic gradient	unlimited[1]	0 to a few 100 years (up to gas/water pressure equilibration)
- vapour transport	Vapour pressure gradient	limited[2]	From a few 100 years until the end of steel corrosion (several 1,000 to several 10,000 years, depending on the effective corrosion rate)

[1] Water supply is sufficient to maintain corrosion at a rate of 1 μm a^{-1}.

[2] Water supply is, however, likely sufficient to maintain corrosion at a rate of 0.1 μm a^{-1}.

5.8 Radionuclide transport processes

Overview/general description

The presence of iron within the deposition drift may affect various properties of bentonite that are relevant for radionuclide transport. Theses issues are addressed in the context of the processes in the buffer and distance block (Chapter 4).

Direct effects of the supercontainer and other structural elements (be it in the uncorroded or corroded state) on the transport of radionuclides is considered to be small in the overall evaluation of repository performance. Sorption of many radionuclides on corrosion product is expected to take place under repository conditions /Nagra 2002/, contributing to the effectiveness of the engineered barriers. On the other hand, Fe(II) from the corroding steel components could compete for sorption sites with some migrating radionuclides, such as isotopes of Ni(II) and Sr(II). The contribution of these processes to overall safety is difficult to quantify and is not discussed further in this report.

Handling in the safety assessment for KBS-3H

The supercontainer and other structural materials do not contribute to the long-term safety functions (long-term isolation and containment; retention, retardation and dilution of radionuclides). The supercontainers could, however, perturb these functions, as in the case of the mass transfer properties of the buffer/rock interface, and the impact of this possibility is evaluated in scoping calculations of canister lifetime (Appendix B of the KBS-3H Evolution Report by /Smith et al. 2007c/ and in the KBS-3H Radionuclide Transport Report /Smith et al. 2007a/.

A number of chemical consequences of the formation of corrosion products, both positive and negative, in terms of possible impacts on safety functions, are discussed in Section 4.8. The presence of corrosion products and of iron silicates formed by Fe-bentonite interaction will considerably enhance the reducing capacity of the buffer adjacent to the supercontainer. However, the corrosion-derived hydrogen may also aid in the microbial reduction of sulphate to sulphide. Furthermore, the corrosion products themselves display good sorption properties for some radionuclides. Such sorption is considered to be a reserve FEP and is conservatively neglected in the safety assessment for KBS-3H. On the other hand, Fe(II) generated by the corrosion process sorbs strongly to clay mineral surfaces. This Fe(II) sorption may compete with that of other radionuclides, such as Ni(II), and thus weaken the barrier function of the buffer. However, the relevance of competitive sorption of Fe(II) is presently not yet understood because of lack of experimental data. Further studies are needed to understand the overall effect of sorption on iron corrosion products of certain radionuclides as these can both act initially as a scavenger but as geochemical conditions evolve, these sorbed radionuclides can be released into the geosphere.

6 Sealing and backfilling

6.1 Description of sealing and backfilling materials

6.1.1 General

In KBS-3H, it will be necessary to seal the smaller diameter part of the drift with a drift end plug after emplacement of the supercontainers (Figure 6-1). Because the adjacent transport tunnel may be open for some time, high hydraulic pressure gradients and gradients in buffer swelling pressure may develop along the deposition drifts, and between deposition drifts and transport tunnels. The drift end plugs must withstand these pressures until final sealing of transport tunnels. Drift end plugs will incorporate cementitious materials, which will also be used elsewhere in the drifts, possibly as grouting material, and further cementitious materials will be used in association with steel plugs and fixing rings (see Figures 1-10 and 1-11). In the adjacent transport tunnels, cementitious materials will be used in the form of shotcrete, tunnel floors and temporary construction elements. Clay-based backfill material will be used to fill the transport tunnels, in a similar fashion as in KBS-3V. This chapter discusses mostly the processes associated with the function of the drift end plug and how they are handled in the context of safety assessment.

The drift end plugs have no long-term safety functions in themselves, but support the long-term safety functions of the buffer by preventing hydraulic and swelling pressure gradients leading either to significant water flows that could cause erosion and redistribution of buffer mass, or to significant displacement of the distance blocks and supercontainers. As a result, these potential impacts must be evaluated. Similarly, the cementitious materials used in other parts of the repository have no long-term safety functions, but their impacts on safety functions, particularly of the buffer, need to be considered. Important requirements on the compartment plugs and drift end plugs are that they should not give rise to stresses that could lead to damage of canisters or host rock and should not undergo volume changes that that could lead to significant changes in density of the buffer (see the KBS-3H Evolution Report by /Smith et al. 2007c/).

The present chapter provides design and materials inventory information for the end plug and other backfilling and sealing materials. This information is relevant to the assessment of the safety functions of KBS-3H components. The potential impacts of the plug and cementitious materials on buffer function are discussed in Section 4.7.2. The gas-related processes associated with steel compartment plugs are discussed in Chapter 5. The filling material within compartment plugs has not yet been designed. The only other processes associated with sealing materials are related to the cementitious materials used to fix the plug. These aspects are covered by Section 4.7.2.

The plugs can be composed of steel, low-pH concrete, or both. Steel plugs can be installed in a relatively short time whereas concrete structures will require a minimum hardening time of two weeks until the structure can be loaded. Steel or a steel/concrete combination is favoured

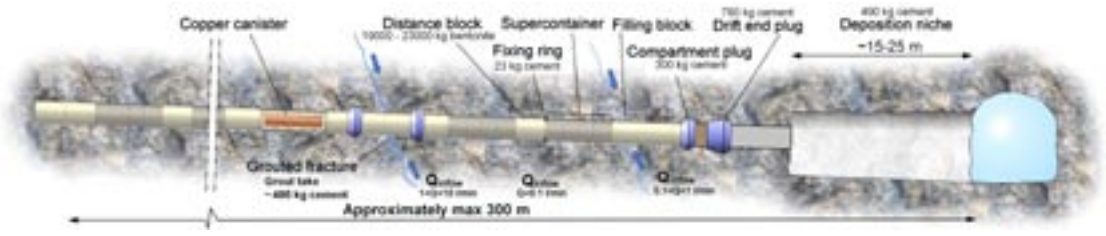

Figure 6-1. *Average locations and amounts of cement in a KBS-3H drift according to /Hagros 2007a, Autio et al. 2007/.*

over concrete as a material because the short plugging and sealing time of a steel plug reduces the risks of buffer erosion and distance block/supercontainer displacement during saturation and increases the emplacement efficiency. Only the steel-reinforced low-pH concrete plug is described below; alternative designs for drift end plugs are described in Appendix E of the present report and in Appendix G of /Autio et al. 2007/.

(i) Cement inventories in a KBS-3H drift

Low-pH cementitious materials are foreseen in the KBS-3H deposition drift as part of various system components, as shown in Table 6-1 and in Figure 6-1. Detailed breakdown of cement masses in a KBS-3H drift are presented in Appendix F.

(ii) Drift end plug design

The drift end plug reference design is a steel-reinforced concrete plug positioned in a notch, see Figure 6-2. It is selected on the basis of minimising the amount of concrete and maximising technical feasibility. A steel plug is positioned adjacent to the concrete plug when necessary for rapid sealing during the hardening of concrete /Autio et al. 2007/.

Table 6-1. Quantities of low-pH cementitious materials in one deposition drift. Cement-bearing components and weight (in average) per drift (including the 15 m long emplacement section, see Appendix F). Only low-pH cement is considered (dry density=1,354 kg/m^3). Dimensions are from Appendix F.

Cement-bearing component	Cement mass per drift
Drift end plug (plus steel plug)	1,080 kg (steel/LHHP[1] cement) or 1,900 kg (rock kernel)
Compartment plugs	600 kg
Fixing rings	Up to 460 kg
Grouting material for transmissive fractures	0 (Silica Sol) – 500 kg (low-pH cement)
Other components (deposition niche)	490 kg
Total	2,630–3,950 kg

[1] The composition of Low Heat High Performance (LHHP) cement is in Appendix A.

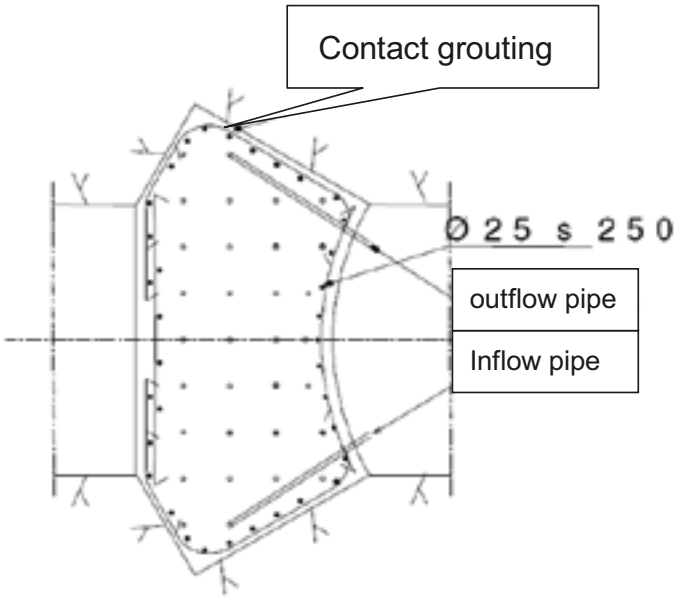

Figure 6-2. *The steel-reinforced plug positioned in a notch (see /Autio et al. 2007/ for details).*

The low-heat high-performance (LHHP) concrete plug, based on low-pH cement developed by AECL is under consideration for use with this design /Martino et al. 2002/. If this type of plug is used, 3.2 times less cement will be required compared with the case of "traditional" low-pH cement because of the low ratio cement/aggregate materials.

Several filling blocks of bentonite are installed in the drift adjacent to the drift end plugs, to isolate the canisters and their surrounding buffer from any leachates from the concrete bulkhead. Alternatives to the reference design are different types of concrete plugs, including a low-pH shotcrete plug type, and a cement-grouted rock plug, as detailed in Appendix E. A cement-grouted rock plug, in particular, could provide a promising alternative to the reference design because of the small quantity of concrete, but the design is novel and needs to be properly verified.

(iii) Compartment plugs and fixing rings

Low-pH cementitious material is foreseen in the design for compartmentalising the drifts (Figure 6-1). It will be used at the interface of the steel compartment plugs and the rock, with the main purpose of limiting the water flow past the plugs. Fixing rings seated using cementitious materials are used at intervals along the drift to keep the supercontainers and the distance blocks in place.

(iv) Grouting material for transmissive fractures

Transmissive fractures intersecting the deposition drift are likely to be grouted by Silica Sol or low-pH cement, depending on the aperture of the fractures. The amount of grouting material introduced depends on the number and transmissivity of intersected fractures. The reference material for groundwater control is Silica Sol because the fracture physical apertures expected in various parts of the drift are small, as noted in the Design Description 2006 /Autio et al. 2007/. If low-pH cement were used for groundwater control (assuming it could penetrate the fractures to be grouted) an average 500 kg of cement grout per drift could be used, based on the average physical apertures of the KBS-3H drift (see Appendix A).

(v) Cementitious materials in the deposition niche

Cement is also used in the 15 m long deposition niche (used for canister deposition equipment) as support bolts, anchor bolts, shotcrete, floors and miscellaneous engineering structures. Most of these sources will be removed to the maximum extent practical. Remaining quantities of cement in these emplacement sections are in Table A-1 of Appendix A.

(vi) Backfill materials

Backfill material is used to fill the deposition niche behind the drift end plug and to fill transport tunnels, shafts and other repository cavities. The material is assumed to be a mixture of crushed rock and bentonite (70 wt% and 30 wt%, respectively) but Friedland clay is also being considered as a potential backfill material /Pastina and Hellä 2006/. The backfill in a KBS-3H repository is not different from backfill of repository areas beyond the deposition tunnels in a KBS-3V repository, thus processes associated with backfill are not evaluated and are not considered in the assessment cases (see Section 6.8).

Only the processes associated with the drift end plugs are discussed in the rest of this chapter.

6.1.2 Overview of variables

Table 6-2. System variables for the drift end plug.

Variable	Explanation
Geometry	Geometric dimensions of drift end plug.
Pore geometry	Pore geometry as a function of time and space in drift end plug. The porosity, i.e. the fraction of the volume that is not occupied by solid material is given.
Temperature	Temperature as a function of time and space in drift end plug.
Water content	Water content as a function of time and space in drift end plug.
Gas content	Gas contents (including any radionuclides in volatile or gaseous form) as a function of time and space in the drift end plug.
Hydrovariables	Flows and pressures of water and gas as a function of time and space in drift end plug.
Stress state	Stress conditions as a function of time and space in drift end plug.
Material composition	Mineralogical/chemical composition of the plug in time and space (e.g. low-pH concrete).
Porewater composition	Composition of porewater (including any radionuclides and dissolved gases) in time and space in drift end plug.
Structural and residual materials	Chemical composition and quantity of structural and residual materials.

6.1.3 Safety function indicators

There are no safety function indicators for the sealing and backfilling materials.

6.1.4 Summary of handling in safety assessment

Table 6-3 summarises the handling of processes in the drift end plug in the safety assessment for KBS-3H, as suggested in the following sections of Chapter 6. In the table, the process is either "mapped" to a model by which it will be quantified or associated with a brief verbal description of how it will be handled. Since the early evolution, characterised by unsaturated conditions and elevated temperatures, is in many respects different from the long-term, saturated phase, the description in the table has been divided accordingly. The period covered by "early evolution" is defined in Section 4.1.4.

6.2 Overview of processes

Based on the FEP analysis for KBS-3V /SKB 2006b/, a list of processes for the drift end plug has been derived for SR-Can. Following the methodology in Appendix B, this list of processes is considered appropriate for KBS-3H.

The processes are structured into radiation-related, thermal, hydraulic, mechanical and chemical process categories, see Figure 1-3. In addition, radionuclide transport is discussed separately. In the introductory part of each of the following chapters, the processes pertinent to the process category are tabulated.

Processes related to the drift end plug are KBS-3H specific and therefore have not been addressed in other reports. There is, however, some relevant information presented in SR-Can in the context of the discussion of backfill processes (e.g. project "Backfill and Plug Test" /SKB 2006d/).

Table 6-3. Process table for the drift end plugs describing how processes are handled in different time periods. Green fields denote processes that are omitted or irrelevant for the time period of concern. Red fields denote processes that are quantified by modelling in the safety assessment. Orange fields denote processes that are neglected subject to a specified condition. Motives for handling are given in the relevant sections of Chapter 6. The handling of processes in the KBS-3H safety assessment and the handling of uncertainties are discussed only in certain cases specific to KBS-3H (as noted in the table). If not mentioned, the handling of other processes and uncertainties are assumed to be handled in the same way as for KBS-3V and are not discussed in this report.

Process Type	Internal process	Early evolution of the repository	The longer term	*Notes/Section in KBS-3H Process Report*
Thermal processes	Dp1. Heat transport	Thermal process model /Ikonen 2003, 2005/	Thermal process model /Ikonen 2003, 2005/	KBS-3H specific heat transport calculations show similar results as for KBS-3V. *Section 6.4 / 4.4*
Hydraulic processes	Dp2. Water transport	DFN-modelling assuming saturated flow conditions /Lanyon and Marschall 2006/	DFN-modelling /Lanyon and Marschall 2006/	*Section 6.5 / 7.5. The handling of the process in the safety assessment for KBS-3H is also discussed.*
	Dp3. Gas transport/dissolution	Gas Model (process model)	Gas Model (process model)	Gas Model assumes impermeable drift end plugs. *Section 6.5 / 7.5*
Mechanical processes	Dp4. Mechanical degradation of inorganic engineering materials	Currently omitted	Currently omitted	At a later stage, modelling and/or experimental investigations will be needed. *Section 6.6*
Chemical processes	Dp5. Decomposition of inorganic engineering materials	Chemical model for cement dissolution	Chemical model for cement dissolution	Discussed in the context of interactions with bentonite in Section 4.7.2. *Section 6.7 / 4.7*
	Dp6. Diffusion	Negligible	Negligible	*Section 6.7. The handling of the process in the safety assessment for KBS-3H is also discussed.*
	Dp7. Sorption (including ion-exchange)	Negligible	Negligible	*Section 6.7. The handling of the process in the safety assessment for KBS-3H is also discussed.*
	Dp8. Microbial processes	Currently omitted	Currently omitted	See also Dp5. *Section 6.7*
Radionuclide transport-related processes	Dp9. Transport of radionuclides	Negligible	Negligible	*Section 6.8. The handling of the process in the safety assessment for KBS-3H is also discussed.*

6.3 Radiation-related processes

No radiation-related processes of importance have been identified for the drift end plug, because of the large distance between the plugs at the end of the deposition drifts and the source of radiation (the nearest copper canister).

6.4 Thermal processes

The specifics of thermal processes and the evolution of temperature within the deposition drifts and in the near-field rock are discussed in the context of the buffer and distance block (see Section 4.4).

6.5 Hydraulic processes

Overview/general description

Water transport and gas transport/dissolution are the only hydraulic processes relevant to the drift end plug. The interdependence between these processes and the variables in the drift end plug is shown in Table 6-4.

The basic hydraulic processes for the drift end plug are identical in KBS-3V and KBS-3H. Differences arise, however, due to the specific geometry, materials and boundary conditions, particularly the drift size and the type and properties of materials present in the deposition drift. For example, due to the presence of the distance blocks and supercontainers the hydraulic boundary conditions are qualitatively different in KBS-3V and -3H. This is mainly due to the presence of buffer rather than backfill material on one side of the plug in the case of KBS-3H (the transport tunnel is similarly backfilled in both alternatives) and to the presence of large amounts of gas-generating materials in KBS-3H. On the one hand, the more permeable backfill tends to rapidly homogenise the hydraulic conditions along a deposition tunnel in KBS-3V. On the other hand, the generation of hydrogen by anaerobic corrosion of steel in the KBS-3H deposition drift may induce high gas pressures. As a consequence, there may be a hydraulic gradient across the drift end plug for as long as unsaturated conditions prevail on either side of it. The hydraulic gradient may be directed into the drift, if the transport tunnel is fully saturated and the supercontainer units closest to the plug are unsaturated, due to low inflow rates from the rock. Alternatively, the hydraulic gradient may be oriented from the deposition drift outwards to the transport tunnel, if a gas overpressure exists inside the deposition drift.

Table 6-4. The interdependence of hydraulic processes and identified variables for the drift end plug.

Hydraulic processes	Variables in drift end plug									
	Geometry	Pore geometry	Temperature	Water content	Gas content	Hydrovariables	Stress state	Material composition	Porewater composition	Structural and residual materials
Water transport	×	×		×	×	×		×		
Gas transport/ dissolution	×	×		×	×	×	×	×	×	×

Boundary conditions

The relevant boundary conditions for the hydraulic behaviour of the drift end plug are determined by the prevailing conditions in the closest supercontainer units inside the deposition drift, in the transport tunnel and by the plug/rock interface.

Model studies/experimental studies

In the Äspö HRL there are three full-scale projects that will provide information relevant to the hydraulic behaviour of the drift end plug. Two of them (projects "Backfill and Plug Test" and "Prototype Repository") address a KBS-3V type repository, whereas the third (project "ESDRED") is specifically designed to test the performance of a KBS-3H type repository (Appendix E). In addition, a discrete fracture network model has been created for a KBS-3H repository at Olkiluoto, which represents the plugs as hydraulic resistor elements at the ends of the deposition drifts (for a detailed discussion of the DFN model, see Section 7.5.1). A detailed discussion of the fate of gas generated in KBS-3H deposition drifts is given in Section 7.5.2, but no detailed studies have been performed on the behaviour of drift end plugs with respect to gas transport/dissolution.

Backfill and Plug Test

Besides tests of backfill materials and emplacement methods, the "Backfill and Plug Test" includes a test of the hydromechanical functioning of a full-scale plug /SKB 2005/. The entire test set-up with backfilling and casting of the final part of the plug was finished in 1999. The plug has been grouted and tested and in January 2002 the water pressure was increased to 500 kPa.

The amount of water passing through the plug and the surrounding rock has been measured by collecting the water outside the plug. Figure 6-3 shows the results with a direct response of each pressure increase and then a successive reduction in flow until steady state is reached. The measured leakage past the plug has been slowly decreasing to about 0.02 l min^{-1} in the course of the last few years.

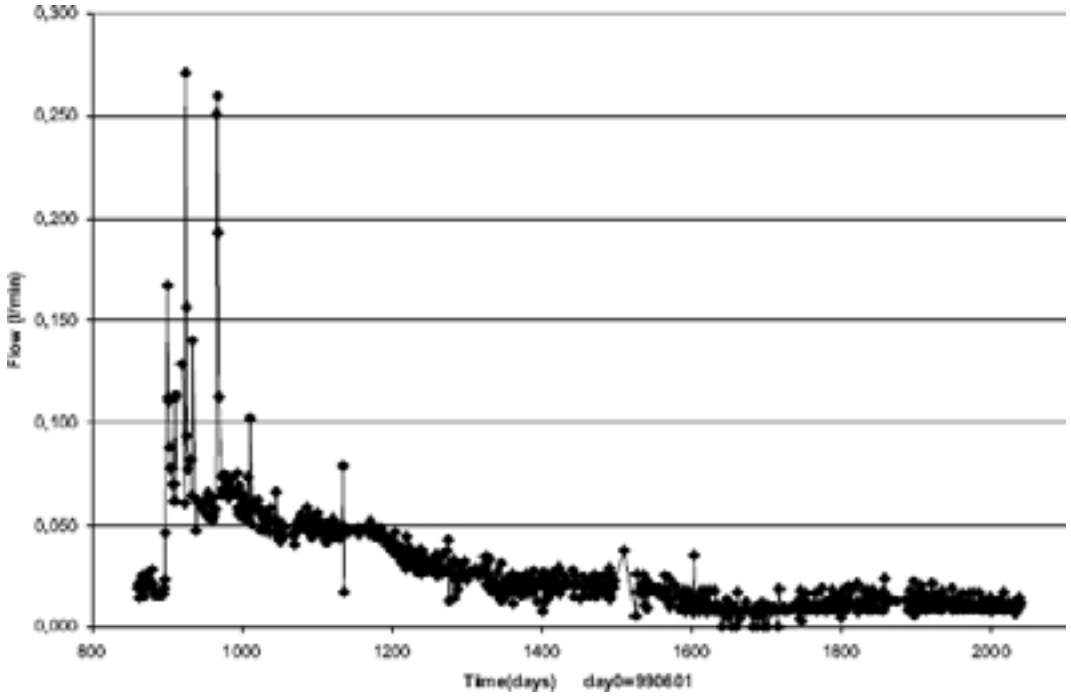

Figure 6-3. *Measured water flow past the plug and its surroundings.*

Prototype Repository

The Prototype Repository is a demonstration of the integrated function of a KBS-3V type repository and provides a full-scale reference for testing predictive models concerning individual components as well as the complete repository system. The layout involves altogether six deposition holes, four in an inner section and two in an outer. The tunnels are backfilled with a mixture of bentonite and crushed rock (30/70).

500 kPa has been kept inside the plug from day 965 to day ~ 1,320, when the pressure was reduced to 400 kPa; Project "Backfill and Plug Test" at Äspö HRL; figure taken from /SKB 2005/.

A massive concrete plug designed to withstand full water and swelling pressures separates the test area from the open tunnel system and a second plug separates the two sections. The two plugs were installed and grouted in 2001 and in 2004, respectively. The plugs are equipped with sensors measuring compressive and tensile stresses, movements, deformations, strains and temperatures.

The evolution of the Prototype Repository is planned to be monitored over a long period, possibly up to 20 years. This is to provide long-term experience of repository performance, which can subsequently be used in the evaluation that will be made after the initial operational stage in the deep repository.

Natural analogues/observations in nature

No relevant natural analogues or observations in nature are available.

Time perspective

The relevant time scales for the hydraulic processes range from the operational period, where relatively large hydraulic gradients across the plugs may exist, up to long periods of time, when the hydraulic properties of the plugs may change due to geochemical processes.

Handling in the safety assessment for KBS-3H

From a hydraulic point of view, the purpose of the drift end plugs is to prevent significant water flows that could cause erosion of the buffer during repository saturation, and thus compromise the ability of the buffer and distance block to fulfil its purpose with respect to long-term safety.

No explicit modelling of hydraulic processes, other than the more general modelling performed in the framework of the DFN modelling and gas modelling discussed in Chapter 7, is thus considered necessary at the current stage of repository development to quantify the long-term hydraulic behaviour of the drift end plugs.

6.6 Mechanical processes

Overview/general description

Mechanical degradation of engineering materials seems to be the only mechanical process of relevance for the drift end plug. The inter-dependence between this process and the variables in the drift end plug is shown in Table 6-5.

The basic mechanical behaviour of the drift end plug is considered to be identical in KBS-3V and 3H. Differences arise, however, due to the specific geometry, materials and boundary conditions, particularly the drift size, the type and properties of materials present in the deposition drift and the mechanical boundary conditions set by the host rock.

Currently, there is little specific information available on the mechanical behaviour of the drift end plug itself, mainly because the plug design is still in an early development stage.

Table 6-5. The interdependence of mechanical processes and identified variables for the drift end plug.

Mechanical processes	Variables in drift end plug									
	Geometry	Pore geometry	Temperature	Water content	Gas content	Hydrovariables	Stress state	Material composition	Porewater composition	Structural and residual materials
Mechanical degradation of inorganic engineering materials	×			×	×	×	×	×		

Model studies/experimental studies

In the Äspö HRL there are three full-scale projects that will provide some information relevant to the hydromechanical behaviour of the drift end plug: “Backfill and Plug Test”, “Prototype Repository“ and “ESDRED”. A short discussion of these projects can be found in Section 6.5. Currently, there is little information available on specific hydromechanical processes related to the drift end plugs.

Handling in the safety assessment for KBS-3H

From a mechanical point of view, the purpose of the drift end plugs is to prevent significant displacement of the distance blocks and supercontainers, which would compromise the ability of the buffer and distance block to fulfil its purpose with respect to long-term safety. The fulfilment of this design requirement will be demonstrated by modelling and/or experimental investigations in the course of repository development.

6.7 Chemical processes

Overview/general description

An overview of chemical processes relevant to the drift end plug is shown in Table 6-6. These processes have been identified in the buffer process report of SR-Can /SKB 2006b/ to be relevant for the “drift end plugs” in KBS-3V. The basic chemical behaviour for the drift end plug is considered to be similar in KBS-3V and 3H. Differences arise, however, due to the specific geometry, materials and boundary conditions, particularly the type and properties of materials present in the deposition drift and the chemical boundary conditions set by the host rock.

Alteration of engineering materials is particularly relevant for the low-pH shotcrete drift end plug, but also for the alternative concept based on a rigid rock cylinder as a kernel of the drift end plug. This is because all design options include significant amounts of cementitious materials, which are not stable under repository conditions. The dissolution/precipitation of cement in the presence of flowing porewater and the impact of cement/bentonite interactions are discussed in detail in the context of the buffer (see Section 4.7).

Diffusion, sorption and microbial processes are not considered to depend significantly on the specific conditions in KBS-3H. This is because the material properties, basic processes and the boundary conditions set by the host rock are very similar in KBS-3V and 3H. There exists a large amount of information on the basic mechanisms involved (e.g. for the buffer and the geosphere). For a detailed discussion of these processes, see the relevant Process Reports for KBS-3V /Rasilainen 2004, SKB 2006d/.

Table 6-6. The interdependence of chemical processes and identified variables for the drift end plug.

Chemical processes	Variables in drift end plug									
	Geometry	Pore geometry	Temperature	Water content	Gas content	Hydrovariables	Stress state	Material composition	Porewater composition	Structural and residual materials
Alteration of inorganic engineering materials	×	×		×		×		×	×	×
Diffusion	×	×		×				×	×	×
Sorption (including ion-exchange)		×		×				×	×	×
Microbial processes		×		×			×	×	×	×

Handling in the safety assessment for KBS-3H

Diffusion and sorption of radionuclides on cementitious materials are omitted in the safety assessment, because the main transport path for radionuclides is considered to be via buffer into a nearby fracture (see Section 6.8).

The impact of other chemical processes, in particular the alteration of cementitious materials, on the long-term chemical stability of the drift end plugs is currently assumed not to be relevant to radionuclide release and transport calculations. Although alteration will slowly occur, little will take place during the time during which transient water flows exist. Once pressures are equalised, transport past the plug is likely to occur by diffusion.

6.8 Radionuclide transport

Overview/general description

The drift end plugs have no long-term safety functions in themselves, but support the long-term safety functions of the buffer by preventing hydraulic and swelling pressure gradients leading either to significant water flows that could cause erosion and redistribution of buffer mass, or to significant displacement of the distance blocks and supercontainers. They are not required to provide a barrier to radionuclides in the long-term. This is because in KBS-3H, the main transport resistance along the axis of the deposition drifts is provided by the buffer.

Handling in the safety assessment for KBS-3H

In the radionuclide release and transport calculations, the main release path for radionuclides is from a defect in the canister through the buffer into a nearby fracture, and, ultimately, through a major fracture zone into the biosphere (transport path R_1/R_2 in Figure 4-20). Transport along the axis of the deposition drift past the drift end plug into the access tunnel (transport path R_6 in Figure 4-20) and further into the biosphere is considered to be a far less important release path. This path would involve transport through the buffer immediately surrounding a failed canister and through or past one (or several) distance blocks and filling blocks before reaching the drift end plug. The corresponding transfer resistance is expected to be significantly higher than the transfer resistance provided by the buffer between a failed canister and rock fractures intersecting the deposition drift. The transport path past the drift end plug is, therefore, not explicitly considered in the radionuclide release and transport calculations.

7 Geosphere

7.1 Description of the geosphere at Olkiluoto

7.1.1 General

This chapter describes geosphere-related processes at Olkiluoto. Data from the most recent Olkiluoto Site Description 2006 /Andersson et al. 2007/ have been used in this report whenever possible as they became available in the later phase of writing the present report. Geological, geochemical, thermal, hydrological and rock mechanics studies are ongoing at the Olkiluoto site, supported by data from new investigation trenches, boreholes, several pilot holes for modelling and prediction purposes that have been realized during the construction of ONKALO, tunnel mapping and monitoring activities. Data used in this report are presented in Appendix A along with their origin.

Due to the schedule of the KBS-3H project, an older version of the bedrock model, called Bedrock model 2003/1 /Vaittinen et al. 2003/, was used for the DFN-based flow modelling /Lanyon and Marschall 2006/. However, the most important hydraulic zones according to Bedrock model 2003/1 /Vaittinen et al. 2003/ and the recent hydrostructural model presented in Site Description 2006 /Andersson et al. 2007/ do not differ much.

7.1.2 Surface conditions, overburden and bedrock geology

Olkiluoto is a relatively flat island with an average height of 5 m above sea level and with the highest point at 18 m above sea level. The island is covered by forest and shoreline vegetation. The sea around the island is shallow, with a depth mainly less than 12 m within 2 km of the current shoreline. The elevations relative to sea level are continuously changing, since the apparent rate of uplift is significant at 6 mm per year, mainly due to isostatic adjustment of the bedrock.

The overburden, both onshore and offshore is mostly till. The other terrestrial sediment types are, in order of abundance, fine sand, sand and silt, with the thickness of the overburden mostly being between 2 and 4 m, although deposits up to 12 to 16 m in thickness have been observed in rock surface depressions /Lahdenperä et al. 2005, Posiva 2005/. The groundwater table follows the surface topography and is mainly 0 to 2 m below surface, with some exceptions. Olkiluoto Island forms its own hydrological unit; the surface waters flow directly into the sea /Lahdenperä et al. 2005, Posiva 2005/. Infiltration of surface water is currently being investigated. Current (and provisional) estimates are approximately 1–2% of the annual precipitation. The evolution of surface conditions and local ecosystem has been described in more detail in the Terrain and Ecosystems Development Model Report /Ikonen et al. 2007/.

The bedrock at Olkiluoto belongs to the Svecofennian domain of Southern Finland and comprises a range of high-grade metamorphic and igneous rocks. The metamorphic rocks include various migmatitic gneisses and homogeneous, banded or only weakly migmatised gneisses, such as mica gneisses, quartz gneisses, mafic gneisses and tonalitic-granodioritic-granitic gneisses. The igneous rocks comprise abundant pegmatitic gneisses and sporadic narrow diabase dykes /Paulamäki et al. 2006/.

Three different alteration episodes can be identified at Olkiluoto, which have affected the chemical composition and mineralogical character of the altered rocks and, as a consequence, the physical properties of the bedrock /Andersson et al. 2007/:

- a *retrograde phase of metamorphism*, which affected the bedrock during the Svecofennian Orogeny about 1,900 to 1,800 million years ago;
- *hydrothermal alteration processes*, which are estimated to have taken place at temperatures from 50°C to slightly over 300°C and are thought to be related to the late stages of metamorphism, to the emplacement of rapakivi granites 1,580 to 1,570 million years ago and to the intrusion of olivine diabase dykes 1,270 to 1,250 million years ago; and
- *surface weathering*, which probably dates back some tens of millions of years and is currently still active.

The bedrock was deformed in a ductile manner during the Svecofennian Orogeny and was subsequently affected by several tectonic events that resulted in brittle deformation.

Modelling of brittle deformation zones and hydraulically important zones is still evolving at Olkiluoto and the most recent description is found in Site Report 2006 /Andersson et al. 2007/. However, at the time of writing this report, the Bedrock model 2003/1 /Vaittinen et al. 2003/, an older version of the current site model was used for the DFN modelling. The most important hydraulic zones in the older version do not differ much from the recent hydrostructural model presented in Site Description 2006 /Andersson et al. 2007/. In the Bedrock model 2003/1, the modelling of structures is based on their identification in the boreholes /Vaittinen et al. 2003/. Objective criteria for the identification of fracture zones, which are based on fracture frequency and hydraulic conductivity, are used in each borehole. Considering only the directly-observed structures, the structural model consists of 92 fractured structures and the hydrogeological model of 75 hydraulically-significant features. There are 22 common structures, included in both models. The total number of directly-observed structures is 145. The bedrock model version 2003/1 /Vaittinen et al. 2003/ is shown in Figure 7-1, together with the interpreted locations of the major fracture zones. An example layout adaptation of the KBS-3H repository at Olkiluoto based on the hydrostructural model presented in Site Description 2006 /Andersson et al. 2007/ is illustrated in Figure 7-2.

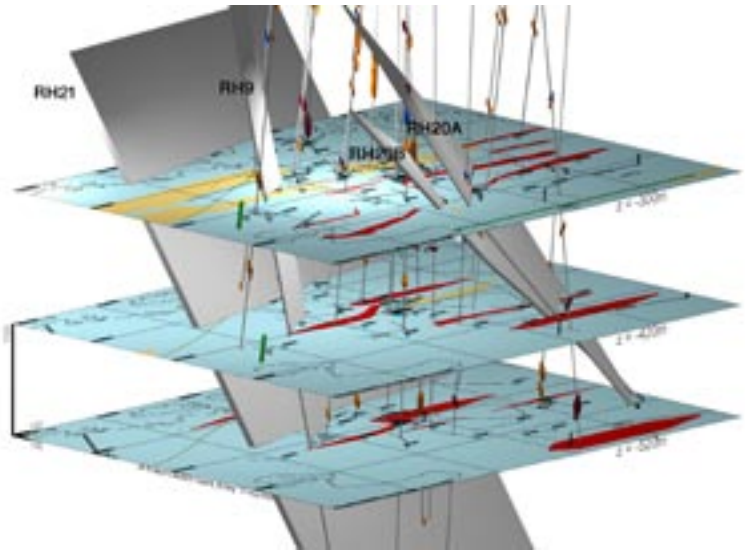

Figure 7-1. *The bedrock model 2003/1 (figure from /Vaittinen et al. 2003/). The horizontal cross-sections of the bedrock model are located at the depths of –300 m, –420 m, and –520 m. Structures RH9, RH20A, RH20B and RH21 are major fracture zones. Structure intersections with boreholes are shown along boreholes. The vertical scale is five times the horizontal scale.*

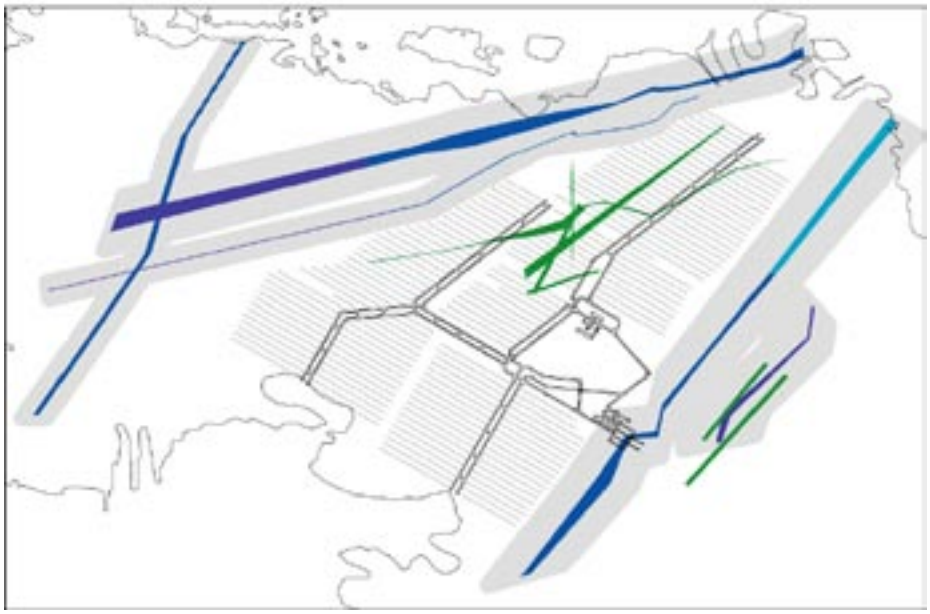

Figure 7-2. *Example layout adaptation of a KBS-3H repository at Olkiluoto /after Johansson et al. 2007/. Hydraulically conductive zones, termed "hydrogeological zones" in the Site Description 2006, are shown in blue. Grey areas indicate the area that the layout is not allowed to intersect due to the proximity of these hydraulically conductive zones. Features shown in green are not considered to be layout determining, and may thus intersect the deposition drifts. The layout is based on the most recent bedrock model, presented in the Site Description 2006, in which the hydrogeological zones and their extensions are taken into account.*

Seismic activity in the Olkiluoto region is currently low (see, e.g. /La Pointe and Hermanson 2002, Enescu et al. 2003, Saari 2006/). Seismic studies at Olkiluoto show rock movements of less than 0.1 mm per year /Posiva 2003/. Concerning past seismic movements, in particular those related to post-glacial earthquakes, no signs of rock displacements were found in a recent mapping campaign on outcrops in the islands surrounding Olkiluoto /Lindberg 2007/. However, seismic activity in the future cannot be excluded. Major seismic activity is likely to occur with the greatest frequency following glaciations, although infrequent but significant seismic events during inter-glacial periods are also possible.

7.1.3 Rock fracturing and groundwater flow

Polyphase deformation has resulted in a network of fractures and fracture zones with different scales within the Olkiluoto bedrock. The frequency, spatial distribution, size distribution, shape and orientation of these structures affect both the hydraulic and mechanical properties of the rock. The fracture zones often constitute dominant paths for groundwater flow and their size also determines the size of rock shear movements taking place in the zone. As noted above, hydrothermal alteration has occurred in certain domains in the rock mass, and this also affects its strength and transport properties.

Information has been gathered on the occurrence, frequency and orientation of transmissive fractures at Olkiluoto. Up till now, the focus of the hydrogeological modelling has been on identifying and characterising the major hydraulically active deformation zones, whereas the rock masses between these zones have been given average hydraulic properties. However, for assessing the evolution of the engineered barrier systems and for modelling the performance of the geosphere transport barrier, it is also necessary to describe the flow system at the scale of individual fractures. Detailed data on the fractures exist, but so far the analyses of these data have focused on those fractures reflecting likely conditions in the deposition drifts /Hellä et al. 2006/.

Groundwater flow at Olkiluoto is concentrated in the upper part of the rock and in the few fracture zones that are likely to intersect the deposition drifts at various locations, and will lead to water inflow and saturation of gas-filled voids during the early transient period. Transmissive fractures at relevant depths, especially those with transmissivities higher than 10^{-8} m^2 s^{-1}, are concentrated mainly in local zones of abundant fracturing. Fractures with lower transmissivities occur outside these zones, but also tend to form clusters /Hellä et al. 2006/. The rock matrix between fractures has an average porosity of 0.14% /Autio et al. 2003/ and a low hydraulic conductivity so that water fluxes through it are negligible compared to that through fractures.

Based on the analysis of available geohydrological (borehole) data in /Hellä et al. 2006/, flow conditions in a deposition drift have been estimated as shown in Section 1.7. The estimates of /Hellä et al. 2006/ may be revised as a result of the ongoing detailed site characterisation work at ONKALO and associated modelling.

Calcite and a range of clay minerals (illite, smectite, kaolinite, vermiculite and chlorite) make up most of the fracture filling. Pyrite coatings in fractures are abundant, mainly as coatings on calcite grains. Pyrite has been observed in all boreholes studied so far at the site. These fracture fillings play an important role in the hydrogeochemical conditions at Olkiluoto and their evolution. Locally, rock matrix minerals may also be exposed on fracture surfaces /Luukkonen et al. 2004, Pitkänen et al. 2004/. Trace element data of fracture fillings is scarce. Some results are presented in the fracture calcite study of /Gehör et al. 2002/ during the EQUIP project, however, this study did not analyse when trace elements were precipitated in calcites. A qualitative estimate of heavy metal concentrations within gouge minerals was carried out by /Gehör 2007/. Trace elemental monitoring (in addition to U) to establish the elemental cycling baseline is currently under planning as part of the site characterization activities.

7.1.4 Groundwater composition

The geochemistry of the Olkiluoto site has been extensively investigated by geochemical and mineralogical analysis of a number of deep boreholes. /Posiva 2003, 2005, Andersson et al. 2007, Pitkänen et al. 2004/ give a comprehensive picture of the hydrogeochemical conditions at Olkiluoto. Generally, chemical conditions in the groundwater are stable at depth at Olkiluoto and reactions and transport processes proceed slowly, but may be perturbed by the presence of the repository and by external events occurring in the far future, such as major climate change.

The groundwater composition over the depth range 0 to 1,000 m at Olkiluoto is characterised by a significant range in salinity (see, e.g. Figure 11-8 in /Andersson et al. 2007/). Fresh groundwater with low total dissolved solids (TDS less than about 1 g/l) is found only at shallow depths, in the uppermost tens of metres. Brackish groundwater, with TDS up to 10 g/l dominates at depths between 30 m and about 400 m. Saline groundwaters (TDS > 10 g/l) dominate at still greater depths. The current salinity of groundwater at repository depth (400 to 500 m below ground) ranges from 10 to 20 g per litre TDS /Andersson et al. 2007/. Chloride is normally the dominant anion in all bedrock groundwaters. Near-surface groundwater is also rich in dissolved carbonate and groundwater at depths between about 100 and 300 m is characterised by high sulphate concentrations. Both carbonate and sulphate concentrations decrease significantly at greater depths. Sodium and calcium dominate as main cations in all groundwaters, and magnesium is also notably enriched in sulphate-rich waters.

The ions dominating in different groundwater types reflect the origins of their salinity. In crystalline rocks, high dissolved carbonate content is typical of meteoric groundwaters that have infiltrated through organic soil layers. High sulphate content indicates a marine origin in crystalline rocks without sulphate mineral phases. More generally, the wide groundwater salinity variations at Olkiluoto can be interpreted in terms of varying degrees of mixing of certain reference water types, together with a range of water/rock interactions that buffer pH and redox conditions and stabilise groundwater composition. The reference water types are present-day *Baltic seawater* and four different groundwater types, termed, in order of decreasing age, *brine reference*, *glacial reference*, *Littorina (Sea) reference* and *meteoric water*. The groundwater

flow and composition near to the surface is characterised by a dynamic hydraulic regime and a significant imprint of young meteoric waters. Below about 300 m depth, studies of methane and of isotopic composition indicate that the deep stable groundwater system has not been disturbed by glacial and post-glacial transients and that neither oxidising glacial meltwater nor marine water have mixed in this deeper system.

The redox conditions are illustrated in Figure 7-3 (taken from /Pitkänen et al. 2004/). Microbially-driven sulphate reduction is the dominant redox reaction between 100 and 400 m depth, whereas methanogenesis, accompanied by high hydrogen levels predominates at greater depths. Isotopic data suggest that at around 400 m concomitant sulphate reduction and methane oxidation occurs. In this zone sulphide is enriched (a few mg l^{-1} but up to 12 mg/L has been measured), whereas Fe concentrations are low. The sulphate content in the sulphate-rich brackish groundwater is at maximum about 500 mg/l. Below 400 m, sulphide concentrations drop to insignificant levels in the methane-rich saline groundwater , whereas Fe concentrations show an increase with depth, reaching several mg l^{-1} in the brine-type waters.

Formation and accumulation of CH_4 in groundwater are evaluated in /Pitkänen and Partamies 2007/. Methane in the groundwater is thought to have two primary sources. Thermal abiogenic hydrocarbons (a crustal inorganic carbon source without biogenic processes) dominate at greater depth where the highest CH_4 contents are observed and are near saturation. At repository level, biogenic CH_4 seems to dominate, total contents are smaller and far from saturation but the CH_4 mass is clearly higher than mass of sulphate in sea water.

Relative (in addition to absolute) decrease of CH_4 upwards in methanic groundwater layer indicates that mixing and dilution of saline groundwater may have been more rapid than the accumulation of CH_4 (either diffusion of abiogenic methane or biogenic production) at repository depths. Chemical and isotopic data of saline groundwater however indicate that mixing of groundwater has been a slow process, predating the last glaciation. Abiogenic CH_4 is not believed to derive from the Earth's mantle. More probably CH_4 was generated in the bedrock in hydrothermal conditions (at least 200 –300°C). Fluid inclusions in quartz grains have very high CH_4 contents, possibly indicating a very slow diffusion from the rock /Pitkänen and Partamies 2007/. Methane concentration is lower at repository depth than at greater depths and is far from saturation, but the role of methane in the reduction of sulphate to sulphide, its evolution over time and its impact on canister lifetime are issues requiring further investigation.

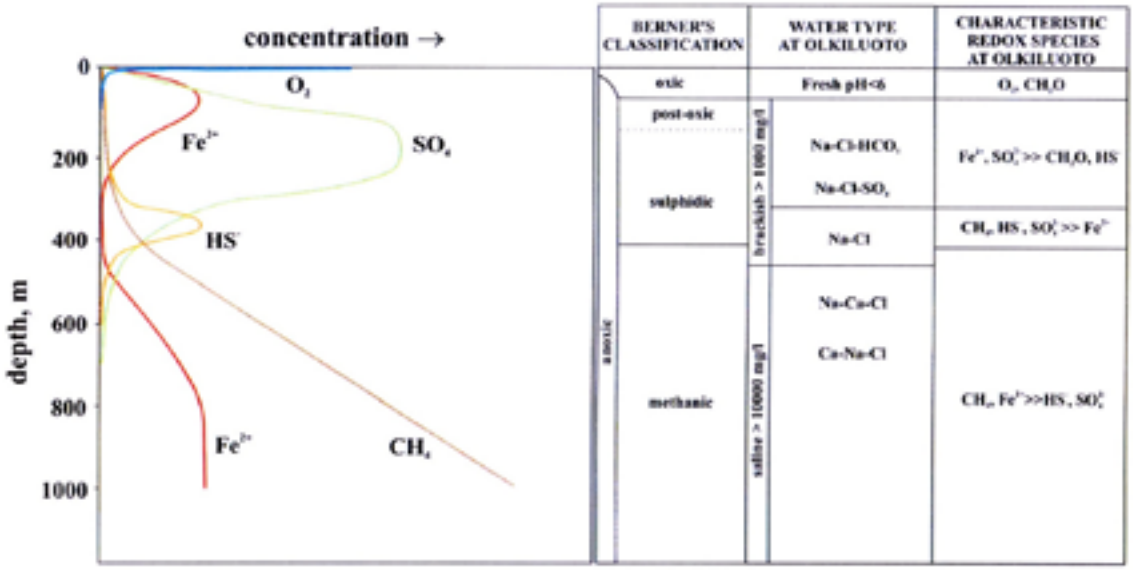

Figure 7-3. *Redox zones at Olkiluoto as function of depth /from Pitkänen et al. 2004/.*

Microbial studies on a few samples have been carried out from deep boreholes /Haveman et al. 1998, 2000/ and recently from the shallow parts and overburden /Pedersen 2006, 2007/. Microbial activity was found to be low, which is typical for nutrient-poor deep crystalline environments. Sulphate-reducing bacteria were generally the most abundant species, but iron reducers were also detected. The presence of methanogens and acetogens was noted, but, because of the low amount of cultivatable cells, interpretation of these data is hampered. The presence of autotrophic methanogens (which use inorganic carbon together with hydrogen) in deep saline samples, together with high amounts of dissolved hydrogen and methane gases, indicate that carbonate reduction is an important process at great depths. Deep waters are rich in both CH_4 and H_2 but low in bicarbonate (i.e. CO_2 and dissolved inorganic carbon). According to carbon isotopic analyses results, reduced carbon species (i.e. methane) in deeper layers of groundwater is of old origin and was formed via an abiogenic pathway. Nowadays, biogenic production in deeper water layers is hindered by the lack of dissolved bicarbonate /Pitkänen and Partamies 2007/.

The pH conditions in the deep aquifer system at Olkiluoto are well buffered by the presence of abundant carbonate and clay minerals found in fracture fillings. The pH values at relevant depths are generally in the range 7.5–8.5 /Pitkänen et al. 2004/. Also the redox conditions are well buffered at Olkiluoto by the presence of iron sulphides and microbially-mediated redox processes. The estimated Eh values in the sulphidic zone are in the range of –200 to –250 mV (vs. SHE, Standard Hydrogen Electrode). In the methanogenic (carbonate reduction) zone, the Eh is estimated to be about –300 mV.

As noted above, there are indications at Olkiluoto that glacial meltwater is present at repository depth and at present the glacial component is less than 20% of the groundwater at repository level /Andersson et al. 2007/. Glacial meltwater may be from the latest glaciation but may also come from earlier episodes. These glacial meltwater intrusions are thought to be the result of slow mixing of water layers rather than from the direct intrusion from the surface.

Oxygen intrusion at the repository depth could happen either by extensive flushing of the groundwater system at the repository depth or by slow dilution and mixing of glacial meltwater with existing groundwater layers. Interpreted data and observations at Olkiluoto support the latter hypothesis /Andersson et al. 2007/. Even though the glacial meltwater component is not presently very large, it may have been larger in the past and the possibility of future infiltration of glacial meltwater cannot be ruled out. The migration of oxygen dissolved in glacial meltwater to repository depth is unlikely due to its interaction with minerals in the rock and microbial activity. The recent interpretation of the hydrogeochemical site data in the Site Description 2006 report /Andersson et al. 2007/ and especially gas data from Olkiluoto by /Pitkänen and Partamies 2007/ show no evidence of oxidising meltwater intrusion into the deeper groundwater system at Olkiluoto although more information to support this tentative finding will be required in future studies.

Isotopic results suggest that no oxidation of methane, anaerobic or aerobic, has occurred in the deeper groundwater system below SO_4-rich groundwater (i.e. –300 m and deeper). For example, calcites with very low, methane based C-13 values have not been observed in fracture mineral studies, which can be expected if O_2 bearing water had infiltrated and mixed in methanic groundwater system. The presence of abundant sulphide minerals and lack of iron oxyhydroxides on fracture coatings are also indicators of the lack of a continuous infiltration of oxygenated water, as oxygen would dissolve sulphides and precipitate oxyhydroxides into bedrock fractures. This indicates that neither oxidising glacial meltwater nor marine water, which can cause either aerobic or anaerobic oxidation of CH_4, respectively, have affected the composition of this deeper system despite the potential to do so during the periodic glacial cycles of the Quaternary. A transient reduction in salinity in association with glacial retreat is, however, possible. Ongoing site characterisation work is exploring whether such events have happened in the past.

Reference groundwaters

Based on the available data from deep boreholes /Pitkänen et al. 2004, 2007/, reference groundwaters representative of repository conditions at Olkiluoto have been defined in Table 7-1. The first two waters (brackish/saline and saline) reflect the expected range of compositions at repository depth (465 m and 498 m) reasonably well for the present site conditions and the conditions once the site is constructed and natural conditions have been restored based on the discussion presented in the KBS-3V Evolution report /Pastina and Hellä 2006/. The third (brine) and fourth (dilute/brackish) types reflect brine-type water conditions (represented by a sample at 740 m depth from borehole KR12) and dilute/brackish water conditions (represented by a sample taken at 58 m depth from borehole KR6) as limiting compositions of the expected possible variations in future chemical conditions.

Table 7-1. Compositions of groundwaters at Olkiluoto. From /Wersin et al. 2007/. Calculated values obtained with PHREEQC assuming T = 15°C. Concentrations in mmole l^{-1} unless otherwise indicated. SI: saturation index. Compositions of groundwaters taken from selected measurements /Pitkänen et al. 2007/. Calculated values obtained with PHREEQC assuming T = 15°C. Concentrations in mmol l^{-1} unless otherwise indicated. SI: saturation index. (After Table 3.2.2 of /Wersin et al. 2007/, but with the addition of phosphate (PO_4) and fluoride (F)).

	Saline waters		Brine type water	Dilute/brackish water
Sample	**KR20/465/1**	**KR10/498/1**	**KR12/741/1**	**KR6/58/1**
Depth (m)	465	498	741	58
TDS (mg/l)	10,544	22,099	49,483	1,026
Ionic strength (meq/l)	218	478	1,180	20
pH	7.4	8.0	8.2	7.6
Alkalinity	0.66	0.11	0.12	2.79
DIC	0.55	0.11	0.04	2.72
SO_4	0.21	0.01	0.05	1.31
Cl	180.5	380.8	863.2	10.4
Na	114.8	210.0	360.9	9.8
K	0.28	0.36	0.49	0.20
Ca	32.4	89.1	254.5	2.1
Mg	2.6	1.6	1.5	1.1
Sr	0.16	0.37	1.14	0.01
SiO_2	0.36	0.28	0.21	0.41
Mn	5.8E–03	7.3E–03	9.3E–03	
Fe	2.5E–03	2.0E–03	3.8E–04	0.024
S^{2-}tot	5.61E–03	<3.12E–04	1.25E–03	6.24E–04
F	1E–05	9.8E–05	6.3E–05	3.2E–05
PO_4	<3E–07	1E–07	2.6E–06	5E–06
Calculated data				
Eh (mV)	–217 S(6)/S(–2)	–258 S(6)/S(–2)	–299 C(4)/C(–4)	–35 $Fe(OH)_3$/Fe(2)
SI(calcite)	0.03	0.06	0.57	0.00
SI(FeS_{am})	–0.34	–1.06	–0.11	0.00
SI(pyrite)	8.80	6.05	6.40	16.2
SI(siderite)	–1.72	–2.16	–2.11	0.34

7.1.5 Rock stress

The natural in situ rock stress is due to the gravitational component (the weight of the rock) and the tectonic component (the stress due to the mid-Atlantic ridge push). The stress state at the Olkiluoto site has been determined for different depths /Johansson et al. 2002, Posiva 2005, Andersson et al. 2007/.

The main mechanical properties of the host rock are summarised in Appendix A. The repository drifts will be aligned as much as possible with the direction of the maximal horizontal stress for reasons of mechanical stability. Regional data indicate that the mean orientation of the maximum horizontal stress is roughly E-W, but the data display a large scatter, so that it is currently uncertain whether the stress orientation at the site differs from the mean regional orientation. At 500 m, the maximal horizontal stress is estimated to be between 15 and 31 MPa and the minimum horizontal stress is estimated to be in the range 10 to 18 MPa. The vertical stress is estimated to be between 7 and 15 MPa at 500 m. The major principal stress is subhorizontally orientated, and is thus slightly larger in magnitude than the maximum horizontal stress. The other two principal stress components vary significantly in magnitude and orientation between the different measurement locations, indicating the need to relate the stress field to geological structure and to conduct associated numerical analyses. The minimal principal rock stress is also relevant to the early evolution of the buffer, for example in that it affects the maximum gas pressures that can develop around the repository as a result of gas generation by the corrosion of steel components.

7.1.6 Ambient rock temperature

Ambient rock temperature is relevant to the early evolution of the buffer in that it provides a boundary condition in the evaluation of repository temperature evolution, temperature being a parameter influencing many transient near-field processes. At the time of emplacement of the first canister, the ambient rock temperature at depths of 400 m and 500 m are 10.5°C and 12°C, respectively /Anttila et al. 1999/.

7.1.7 Impact of repository excavation

The effect of the ONKALO and repository construction on the hydrologic and geochemical groundwater regime is subject to considerable uncertainty. These effects were assessed by /Vieno et al. 2003, Löfman and Mészáros 2005, Ahokas et al. 2006, Alexander and Neall 2007/. In the Site Description 2006 (see Chapter 9 of /Andersson et al. 2007/) these effects were recently re-evaluated using the most up-to-date hydrogeological model, as well as knowledge of baseline conditions, data from monitoring during the excavation of ONKALO (which is still on-going) and numerical flow modelling. These flow modelling results indicate that ONKALO and repository construction will have a pronounced effect on the flow and salinity at repository depth. Thus, water inflow into the tunnel system is expected to lead to a drawdown of the water table and to induce upconing of saline waters into the repository area. This hydraulic disturbance can be significantly reduced by grouting of fractures in the rock. Groundwater monitoring will be performed during the construction of ONKALO (see summary of ongoing and planned activities in /Ahokas et al. 2006/).

Recent calculations (presented in /Pastina and Hellä 2006/) based on the assumption that tunnels are grouted to 1×10^{-7} m^2/s, suggest that salinity (Total Dissolved Solids, TDS) may rise up to 30–45 gL^{-1} at the lowest point of the tunnel system in ONKALO at depth of –550 m, whereas at the repository level (–420 m) the maximum salinity may rise from 4–12 gL^{-1} at emplacement to 10–25 gL^{-1} TDS during the operational phase /Pastina and Hellä 2006/.

The mixing of the waters from closer to the surface may induce some changes in pH and Eh of the groundwaters, although buffering by the host rock should prevent significant Eh and pH changes. Preliminary calculations have been carried out based on the estimation of the lifetime of fracture mineral buffers, such as calcite and pyrite in the fractures, against acid pH and oxygen containing infiltrating waters from the surface /Andersson et al. 2007/. Further field studies and more advanced modelling are planned.

7.1.8 Overview of variables

The system variables relevant to the geosphere are listed in Table 7-2.

7.1.9 Safety function indicators

The host rock safety function indicators and associated criteria, as presented in SR-Can for KBS-3V, are summarised in Table 7-3.

Table 7-2. Variables in the geosphere.

Variable	Explanation
Temperature	Temperature as a function of time and space in the geosphere.
Groundwater flow	Groundwater flow as a function of time and space in the geosphere fracture system.
Groundwater pressure	Groundwater pressure as a function of time and space in the geosphere fracture system.
Gas flow	Gas flow as a function of time and space in the geosphere fracture system.
Repository geometry	Geometric description of deposition drifts, transport drifts, ramps, shafts, boreholes, etc i.e. of all excavated volumes.
Fracture geometry	All geosphere cavities, from fracture zones to micropores in the rock matrix. Also included here are the excavation-disturbed zone (EDZ) and any other geometric changes in the fracture structure induced by construction.
Stress state	Stress conditions as a function of time and space in the geosphere.
Rock strength	Compressive and tensile strength of the rock as a function of space and time.
Matrix minerals	Chemical composition of the rock matrix as a function of (time and) space, i.e. a description of the various minerals that occur. Also the amount and composition of fracture minerals in existing fractures.
Fracture minerals	Chemical composition of the fracture minerals as a function of (time and) space, i.e. a description of the various fracture minerals that occur. Also the amount and composition of fracture minerals in existing fractures.
Groundwater composition	Chemical composition of the groundwater as a function of time and space in the geosphere, i.e. concentrations of relevant components in the groundwater, especially the salinity of groundwater at Olkiluoto is an important issue to be considered. This variable also includes quantities such as Eh and pH, as well as any radionuclides and dissolved gases. The high amount of methane gas in the saline groundwater is a specific issue to be considered for Olkiluoto.
Gas composition	Chemical description of gases in geosphere cavities including any radionuclides.
Structural and residual materials	Chemical composition and quantities of grouts and other structural and residual materials injected/located in fractures in the rock.
Saturation	Degree of saturation of the geosphere.

Table 7-3. Safety function indicators and criteria for the host rock (adapted for KBS-3H from Figure 7-2 of /SKB 2006a/).

Safety function indicator	Criterion	Rationale
Redox conditions	No dissolved oxygen	The presence of measurable O_2 would imply oxidising conditions
Minimum ionic strength	Total divalent cation concentration > 10^{-3} M	Avoid buffer erosion
Maximum chloride concentration or minimum pH	pH^{GW} > 4 or $[Cl^-]^{GW}$ < 3 M	Avoid chloride corrosion of canister
Limited alkalinity	pH^{GW} < 11	Avoid dissolution of buffer smectite
Limited salinity (expressed in total dissolved solids, TDS)	[NaCl] < 100 g/l (or other compositions of equivalent ionic strength)	Avoid detrimental effects, in particular on swelling pressure of buffer and distance block
Limited concentration of detrimental agents for buffer, distance block and canister	Applies to HS^-, K^+ and Fe(II)/Fe(III). The lower the better (no quantitative criterion)	Avoid canister corrosion by sulphide, avoid illitisation (K^+) and chloritisation (Fe) of buffer and distance block
Limited rock shear at canister/distance block locations in deposition drift	< 10 cm	Avoid canister failure due to rock shear in deposition drift

Loss or degradation of the isolation function of the host rock would occur if erosion of the Precambrian Shield were to erode the repository horizon (this situation, which concerns the farthest future, is discussed in Chapter 9 of the KBS-3H Evolution Report /Smith et al. 2007c/. Loss or degradation of the protective function of the host rock could occur if chemical conditions in the groundwater become unfavourable to buffer and canister longevity, or if a fracture intersecting the deposition drifts near a canister location were to slip sufficiently to cause rupturing of the canister. Finally, there are several rock properties that can favour its performance as a radionuclide transport barrier (for example, absence or low frequency of highly transmissive fractures, low hydraulic gradient, mineralogical and geochemical characteristics giving high retention by sorption). Some of these may vary over time (especially geochemical characteristics), potentially leading to some degradation of the host rock as a transport barrier.

In this report (and other reports of the safety studies), it is generally assumed in scoping calculations and assessment cases for radionuclide release and transport that drift sections having intersecting fractures with transmissivities above about 3×10^{-9} $m^2 s^{-1}$ will be excluded as distance block or supercontainer emplacement locations. It is further assumed that radionuclides released to water-conducting fractures at the drift wall will have to migrate at least 10 m before encountering fractures with transmissivities above about 3×10^{-9} $m^2 s^{-1}$. Such assumptions correspond to moderately favourable hydrogeological conditions in terms of the geosphere transport barrier function, where the host rock provides an effective barrier to the transport of most radionuclides released in the event of canister failure, as shown in the scoping calculations in Appendix B.2 of the Evolution Report /Smith et al. 2007c/.

As also discussed in the Evolution Report, the assumed hydrogeological conditions also limit the rate at which corrosive agents (principally sulphide) can be transferred from the groundwater to the canister surface via the buffer, protect the buffer from the possibility of mechanical erosion by flowing groundwater following saturation, and limit the rate of chemical erosion of the buffer at distance block and supercontainer positions should dilute glacial meltwater penetrate to repository depth. However, further study is needed to assess whether these conditions can be identified in practice when categorising drift sections as suitable or unsuitable for distance block and supercontainer emplacement.

The transmissivity of intersecting fractures is related to the initial rate of inflow to the drift observed at the drift wall prior to distance block or supercontainer emplacement. Applying Darcy's law in a radial configuration (Thiem's equation; see Section 4.5.1, Equation 4-15), and assuming a 4 MPa pressure difference between the drift and the undisturbed rock during saturation and a distance of 50 m between the drift wall and the nearest major fracture zone, a fracture with a transmissivity of 3×10^{-9} m^2 s^{-1} will give an inflow of about 0.1 litres per minute in each supercontainer section. As discussed in Appendix B.2 of the Evolution Report /Smith et al. 2007c/, the 0.1 litres per minute inflow rate to a drift section containing a supercontainer and a distance block is also consistent with inflow rates estimated from the discrete fracture network (DFN) modelling results of /Lanyon and Marschall 2006/ presented in Section 7.5.1, in which a maximum transmissivity of 3×10^{-9} m^2 s^{-1} for fractures intersecting the drift at supercontainer/distance block locations is assumed. This implies that transmissive fractures that could give rise to relatively high flows around the repository drift in the longer term, once the drift is saturated, will also be avoided.

The relationship between initial inflow and longer-term flow is, however, complicated by a number of factors. On the one hand, grouting may reduce the observed inflow of some larger aperture fractures elsewhere. On the other hand, a larger leakage elsewhere may reduce the hydrostatic pressure at the observation point and thus give a wrong interpretation of the observed inflow. Furthermore, initial inflows may also be reduced by drawdown of the water table, which will give a reduction in the hydrostatic pressure at repository depth; the impact of other open repository tunnels and drifts; and potentially by mineral precipitation and degassing in the fracture. These are generally transient effects which do not affect flow in the longer term, once the drifts are saturated. Finally, inflow is determined not only by the hydraulic properties of fractures intersecting the drift, but also by those of other connected fractures in the wider fracture network.

The grout is likely to become degraded and ineffective in reducing flow in the longer term. In view of current uncertainties in the performance of any grout, an inflow of less than 0.1 litres per minute *prior* to grouting is used as a criterion for a drift section to be suitable for the emplacement of canisters and buffer in deriving a preliminary repository layout.

Initial inflows may be reduced by transient drawdown of the water table, which will give a reduction in the hydrostatic pressure at repository depth. Furthermore, the properties of other fractures connected to a fracture intersecting the drift wall may also modify the initial rate of inflow. It must further be kept in mind that the inflow assumption refers to flow before any grouting is implemented, and that the impact of repository excavation on the hydrostatic pressure around the drift (hence on inflow) requires further investigation.

In the current reference design, drift sections with initial inflows higher than 0.1 L/min will be excluded as distance block or supercontainer emplacement locations in order to reduce the possibility of piping and erosion during buffer saturation (Section 5.5.6 and Appendix L of /Autio et al. 2007/. Fractures with transmissivities higher than 3×10^{-9} m^2 s^{-1} may, however, intersect such sections if, for example, inflows can be reduced or prevented for sufficient time by control measures and, in particular, by grouting potentially problematic fractures.

In many of the scoping calculations and radionuclide release and transport calculations carried out for the KBS-3H safety studies, it is tentatively assumed that the highest transmissivity of any fracture intersecting a drift at locations where canisters and buffer are emplaced is 3×10^{-9} m^2 s^{-1}. This assumption (which is discussed further in Appendix B.2 of the Evolution report /Smith et al. 2007c/, is based on an application of Darcy's law in a radial configuration (Thiem's equation; Equation B.2-1) to a single fracture giving an inflow of 0.1 litres per minute, assuming a 4 MPa pressure difference between the drift and the undisturbed rock during saturation and a distance of 50 m between the drift wall and the nearest major fracture zone. In view of the factors mentioned above, higher transmissivities cannot currently be

excluded (radionuclide release and transport calculations include the possibility that a higher transmissivity fracture intersects the drift at the location of a failed canister in a variant case /see Smith et al. 2007a/), but a transmissivity of 3×10^{-9} $m^2 s^{-1}$ at a canister and buffer emplacement location is nevertheless considered to be towards the high end of the expected distribution.

The possibility that higher transmissivity fractures are present is, therefore, acknowledged, and cases addressing higher transmissivity features are considered in the Radionuclide Transport Report /Smith et al. 2007a/.

7.1.10 Summary of handling in safety assessment

Table 7-4 summarises the handling of processes in the geosphere in the safety assessment for KBS-3H, as suggested in the following sections of Chapter 7. In the table, the process is either "mapped" to a model by which it will be quantified or associated with a brief verbal description of how it will be handled. Since the early evolution, characterised by unsaturated conditions and elevated temperatures, is in many respects different from the long-term, saturated phase, the description in the table has been divided accordingly. The period covered by "early evolution" is defined in Section 4.1.4. In addition, the handling of processes in the excavation/operation period is discussed separately.

7.2 Overview of processes

Based on the FEP analysis for KBS-3V, a list of processes for the geosphere has been derived in /SKB 2006a/. The list of processes discussed in the SR-Can Geosphere Process Report /SKB 2006e/ differs, however, slightly from the list given in SR-Can interim report /SKB 2004b/. For consistency between Process Reports, the present report adopts the list of processes given in /SKB 2006e/, which is considered appropriate for KBS-3H.

The processes are structured into radiation-related, thermal, hydraulic, mechanical and chemical process categories (see Figure 1-3). In addition, radionuclide transport is discussed separately. In the introductory part of each of the following chapters, the processes pertinent to the process category are tabulated.

7.3 Radiation-related processes

No radiation-related processes of importance have been identified for the geosphere. Naturally occurring radioactive decay chains (mainly decay chain 4N+2 starting from U-238) have been studied in water, fracture coating and rock matrix samples to track past geochemical changes in bedrock, see Section 5.7.4 in /Rasilainen 2004/.

Table 7-4. Process table for the geosphere describing how processes are handled in different time periods. Green fields denote processes that are neglected or irrelevant for the time period of concern. Red fields denote processes that are quantified by modelling in the safety assessment. Orange fields denote processes that are omitted subject to a specified condition. Motives for handling are given in the relevant sections of Chapter 7. The handling of processes in the KBS-3H safety assessment and the handling of uncertainties are discussed only in certain cases specific to KBS-3H (as noted in the table). If not mentioned, the handling of other processes and uncertainties are assumed to be handled in the same way as for KBS-3V and are not discussed in this report.

Process type	Internal process	Excavation/ operation	Early evolution of the repository after completion of operations	The longer term	Notes/*Section in KBS-3H Process Report*
Thermal processes	Ge1. Heat transport	Omitted since sensitivity studies show that evolution of heating is not sensitive to detailed pattern of deposition (as in SR-Can).	Thermal process model /Ikonen 2003, 2005/.	Thermal process model /Ikonen 2003, 2005/.	KBS-3H specific heat transport calculations show similar results as for KBS-3V. *Section 7.4*
	Ge2. Freezing	Not relevant.	Not relevant.	Omitted as temperature at repository depth > 0°C. (SR-Can: Site-specific 1-D estimations of permafrost depth.)	Permafrost will occur at Olkiluoto before and during next glaciation but is not expected to reach repository depths /Hartikainen 2006, Cedercreutz 2004/. *Section 7.4*
Hydraulic processes	Ge3. Groundwater flow	DFN-modelling assuming saturated flow conditions /Lanyon and Marschall 2006/.	DFN-modelling assuming saturated flow conditions /Lanyon and Marschall 2006/.	DFN-modelling /Lanyon and Marschall 2006/.	Transport paths, times and transport resistances are also calculated by DFN model. *Section 7.5* *The handling of the process in the safety assessment for KBS-3H and handling of uncertainties are also discussed*. Groundwater flow is included implicitly in radionuclide transport calculations for the geospher.
	Ge4. Gas flow/ dissolution	Omitted based on arguments supporting the assumption of small effects of unsaturated regions on inflows to tunnels (as in SR-Can).	Gas Model (process model).	Gas Model (process model).	Storage and transport of gas by diffusion/ advection and capillary leakage in fracture network within host rock and EDZ. *Section 7.5.* *The handling of the process in the safety assessment for KBS-3 and handling of uncertainties are also discussed.* Gas flow is included implicitly in radionuclide transport calculations dealing with volatile C-14.
Mechanical processes	Ge5. Displacements in intact rock	3DEC modelling of near-field effects of excavation of deposition drifts.	3DEC modelling of thermal stresses and deformations.	3DEC modelling of thermal stresses and deformations.	*Section 7.6* *The handling of the process in the safety assessment for KBS-3H is also discussed.*

Process type	Internal process	Excavation/ operation	Early evolution of the repository after completion of operations	The longer term	Notes/*Section in KBS-3H Process Report*
	Ge6. Reactivation displacement along existing discontinuities	3DEC modelling of construction-induced reactivation.	3DEC modelling of reactivation induced by gas and bentonite swelling.	Estimate of probability of intersection of canisters and shear displacements due to post-glacial faulting. 3DEC modelling of reactivation induced by gas and bentonite swelling.	*Section 7.6* *The handling of the process in the safety assessment for KBS-3H and the handling of uncertainties are also discussed*. Included implicitly in radionuclide transport calculations of canister failure by rock shear, by reducing the transport resistance of the geosphere.
	Ge7. Fracturing	Assessment of EDZ. Modelling (3DEC) and observations of fracturing around deposition drifts (spalling).	THMC process modelling of rock fracturing induced by thermal stresses, gas and bentonite swelling (3DEC).	THMC process modelling of rock fracturing induced by thermal stresses, gas and bentonite swelling (3DEC).	*Section 7.6* *The handling of the process in the safety assessment for KBS-3H and the handling of uncertainties are also discussed.*
	Ge8. Creep	Not relevant. Covered by construction-induced reactivation (as in SR-Can).	Omitted because of insignificant convergence of deposition drifts at expected rock stresses (as in SR-Can).	Omitted because of insignificant convergence of deposition drifts at expected rock stresses (as in SR-Can).	*Section 7.6.* *The handling of the process in the safety assessment for KBS-3H is also discussed.*
	Ge9. Surface weathering and erosion	Outside scope. (SR-Can: Not relevant.)	Outside scope. (SR-Can: Omitted because of low erosion rates.)	Outside scope. (SR-Can: Omitted because of low erosion rates.)	*Section 7.6* Discussed in the KBS-3H Evolution Report /Smith et al. 2007c/ in the context of the "farthest future". *The handling of the process in the safety assessment for KBS-3H is also discussed.*
	Ge10. Erosion/ sedimentation in fractures	Omitted because of flow rates in non-grouted fractures are so low.	Omitted because of very limited significance.	Omitted because of very limited significance.	For bentonite erosion into fractures, see Bu18. *Section 7.6*
Chemical processes	Ge11. Advection/mixing	DFN-modelling /Lanyon and Marschall 2006/. (SR-Can: Advection of salt included in hydro-geological modelling. Composition of mixtures assessed from hydrogeological modelling and site understanding.)	DFN-modelling /Lanyon and Marschall 2006/. (SR-Can: Advection of salt included in hydro-geological modelling. Composition of mixtures assessed from hydrogeological modelling and site understanding.)	DFN-modelling /Lanyon and Marschall 2006/. (SR-Can: Advection of salt included in hydro-geological modelling. Composition of mixtures assessed from hydrogeological modelling and site understanding.)	*Section 7.7* Also included in radionuclide transport calculations for the geosphere.
	Ge12. Diffusion and matrix diffusion	No specific process analysis in KBS-3H. (SR-Can: Diffusion of salt between mobile and immobile groundwater included in hydrogeological modelling.)	No specific process analysis in KBS-3H. (SR-Can: Diffusion of salt between mobile and immobile groundwater included in hydrogeological modelling.)	No specific process analysis in KBS-3H. (SR-Can: Diffusion of salt between mobile and immobile groundwater included in hydrogeological modelling.)	*Section 7.7* Also included in radionuclide transport calculations for the geosphere (cases MD-1, MD-2, MD-3 addressing uncertainties in matrix diffusion depth).

Process type	Internal process	Excavation/ operation	Early evolution of the repository after completion of operations	The longer term	Notes/*Section in KBS-3H Process Report*
	Ge13. Speciation and sorption	Not relevant.	Not relevant.	Simplified K_d-approach for modelling sorption of radionuclides. Speciation considered in the selection of K_d (as in SR-Can).	*Section 7.7*
	Ge14. Reactions groundwater/rock matrix	Omitted since reactions are considered to take place at fracture surfaces only.	Omitted because of expected insignificant impact on groundwater composition and matrix porosity (as in SR-Can).	Omitted because of expected insignificant impact on groundwater composition and matrix porosity (as in SR-Can).	*Section 7.7*
	Ge15. Dissolution/ precipitation of fracture-filling minerals	No specific analysis in KBS-3H. (SR-Can: Modelling of reactions using PHREEQC.)	No specific analysis in KBS-3H. (SR-Can: Modelling of reactions using PHREEQC.)	No specific analysis in KBS-3H. (SR-Can: Modelling of reactions using PHREEQC.)	*Section 7.7*
	Ge16. Microbial processes	No specific analysis in KBS-3H (SR-Can: Mass balance calculations of organic matter and modelling of microbial processes coupled with solute transport and hydrochemical equilibrium calculations.)	No specific analysis in KBS-3H. (SR-Can: Mass balance calculations of organic matter and modelling of microbial processes coupled with solute transport and hydrochemical equilibrium calculations.)	Microbial processes controlling the redox conditions in the groundwater at Olkiluoto are included in the definition of the redox states of the groundwaters in hydrochemical equilibrium calculations. (SR-Can: Mass balance calculations of organic matter and modelling of microbial processes coupled with solute transport and hydrochemical equilibrium calculations.)	*Section 7.7*
	Ge17. Degradation of grout	Omitted since expected effects will not occur during this period.	No specific analysis in KBS-3H. (SR-Can: Modelling of effects on chemistry of fractures.)	No specific analysis in KBS-3H. (SR-Can: Modelling of effects on chemistry of fractures.)	Analysis of cement/bentonite interactions discussed in Chapter 6, see Bu22. *Section 7.7*
	Ge18. Colloid formation and transport	Omitted because of insignificant impact on geochemical conditions.	Omitted because of insignificant impact on geochemical conditions (as in SR-Can).	No specific analysis in KBS-3H. (SR-Can: Included in modelling of radionuclide transport.)	*Section 7.7*
	Ge19. Formation/ dissolution/ reaction of gaseous species	Natural gases omitted since concentrations are expected to remain substantially unchanged (as in SR-Can).	Natural gases neglected since concentrations are expected to remain substantially unchanged (as in SR-Can). High concentrations of methane are noted as a potential source for sulphate reduction. Corrosion-derived drogengas are also a source for SRB.	Natural gases neglected since concentrations are expected to remain substantially unchanged (as in SR-Can). High concentrations of methane are noted as a potential source for sulphate reduction. Corrosion-derived hydrogen gas is also a source for SRB.	*Section 7.7* Transport of volatile species of C-14 and Rn-222 in geosphere included implicitly in RN transport calculations.
				Gas formed in the canister by corrosion of the insert in the case of a defective canister is handled in the safety assessment (Section 2.1.4).	See F-16, Table 2.2

Process type	Internal process	Excavation/ operation	Early evolution of the repository after completion of operations	The longer term	Notes/*Section in KBS-3H Process Report*
	Ge20. Methane hydrate formation	Not relevant.	Not relevant.	Omitted provided that permafrost does not reach repository depth (as in SR-Can).	See Ge2. *Section 7.7*
	Ge21. Salt exclusion	Not relevant.	Not relevant.	Neglected provided that permafrost does not reach repository depth. (SR-Can: Modelling of transport of out frozen salt.)	See Ge2. *Section 7.7*
	Ge22. Radiation effects (rock and grout)	Omitted because radiation fluxes are very low.	Omitted because radiation fluxes are very low.	Omitted because radiation fluxes are very low.	*Section 7.7*
	Ge23. Earth currents	Omitted since expected electrical potential fields are too small to affect groundwater flow or solute transport.	Omitted since expected electrical potential fields are too small to affect groundwater flow or solute transport.	Omitted since expected electrical potential fields are too small to affect groundwater flow or solute transport.	*Section 7.7*
Radio-nuclide transport-related processes	Ge24. Transport of radionuclides in the water phase	Omitted, because no failures are expected during this period.	Omitted, because no failures are expected during this period. A postulated initially penetrated defect is considered in the Radionuclide Transport Report.	Advection, dispersion, matrix diffusion, sorption, radioactive decay included in integrated radionuclide release and transport modelling (FTRANS). (SR-Can: Additionally, modelling of colloid transport and transport in EDZ.)	*The handling of the process in the safety assessment for KBS-3H is also discussed.* Included in radionuclide transport calculations, but limited uncertainty analysis because focus is mainly on near field. *Section 7.8*
	Ge25. Transport of radionuclides in the gas phase	Omitted, because no failures are expected during this period.	Omitted, because no failures are expected during this period.	Radionuclide transport in the gas phase (e.g. C-14) is handled by bounding calculations. (SR-Can: Assessed neglecting the geosphere as a barrier.)	*The handling of the process in the safety assessment for KBS-3H is also discussed.* Fate of volatile radionuclides in gas phase somewhat different in KBS-3V/3H due to gas generation by supercontainer in the case of 3H (see F16). Transport of volatile species of C-14 and Rn-222 in geosphere included implicitly in RN transport calculations (see Ge 19, F16). *Section 7.8*

7.4 Thermal processes

Heat transport and freezing are the only relevant thermal processes in the subsystem geosphere (Table 7-5). Heat transport controls the dissipation of heat from fuel through the engineered and geological barriers into the biosphere, the latter being the ultimate heat sink of the system. As concluded by /Ikonen 2003, 2005/ based on model studies, the overall thermal evolution in KBS-3V and 3H are very similar. The details of these model studies and the handling in the safety assessment for KBS-3H are discussed in the context of the buffer and distance block, see Section 4.4. The thermal characteristics of the rock at Olkiluoto are discussed in Section 5.4 in /Rasilainen 2004/ and in Section 5.4.4 in /Posiva 2005/, based on investigations reported by /Kukkonen 2000/. Coupled thermohydraulic calculations show that the decay heat of spent nuclear fuel rises the temperature of the repository and the surrounding bedrock several tens of degrees for many centuries /Löfman 2005/. For the one-storey repository the maximum temperature rise of 54°C is achieved at 180 years after the construction of the repository, while the two-storey repository resulted in the maximum temperature rise of 70°C at 280 years.

A recent report by /Ikonen 2007/ analysed the far-field thermo-mechanical response for a KBS-3V repository at Olkiluoto. The objective of the study was to determine the extent of the tensile stressed bedrock near the ground surface. Tensile stress may open fractures in the rock and groundwater flow may become faster, if suitable pressure differences exist, with the negative consequences on radionuclide and mass transport that this entails. /Ikonen 2007/ estimated that the thickness in tensioned rock volume at the ground surface is about 100 m after 300 years and the maximum tensile strain on the ground surface is about 0.00024 after about 600 years. Ground uplift would reach a maximum of 6.9 cm in about 1,230 years. The decrease of thermal power with time is taken into account in this study. The local average power density used in the analyses was 7.3 W m^{-2} at the time of individual canister disposal based on the KBS-3V layout /Ikonen 2007/. The results are expected to apply to KBS-3H as well because the orientation of the canisters has a negligible effect on the far field.

Future climate scenarios for the Olkiluoto site with emphasis on permafrost were investigated in /Cedercreutz 2004/. The aim of the study was to search the literature for the most recent research results concerning future climate scenarios to estimate the range of climate evolutions for Olkiluoto as far as possible into the future (up to 125–225 ka after present). The focus was on identifying relevant climate scenarios and on examining permafrost occurrence and shoreline displacement during a glacial cycle. Two relevant climate scenarios were identified: Scenario B (now referred to as "Weichselian-R" scenario) and Scenario D (now referred to as "Emissions-M scenario"). The conditions in Scenario B (Weichselian-R) are based on the repetition of the conditions reconstructed for the last (Weichselian) glacial cycle whereas the conditions in Scenario D (Emissions-M) are the consequence of moderate emissions of anthropogenic CO_2 causing climate warming (the greenhouse gas effect) and a delay of ice sheet formation.

Table 7-5. The inter-dependence of thermal processes and identified variables in the geosphere.

Thermal processes	Variables in geosphere												
	Repository geometry	Fracture geometry	Temperature	Groundwater flow	Groundwater pressure	Gas flow	Stress state	Matrix minerals	Fracture minerals	Groundwater composition	Gas composition	Structural and residual materials	Saturation
Heat transport	×		×	×				×					×
Freezing		×	×	×	×	×			×	×	×		×

It was concluded that the current interglacial will last for at least a further 50,000 years, but that future climate development depends much on atmospheric CO_2 concentration. Permafrost will occur at Olkiluoto before glaciations but will not reach repository depths.

/Hartikainen 2006/ numerically estimated the development of permafrost at Olkiluoto during the next 125,000–200,000 years, based on a 1D subsurface model reaching to a depth of 10 km. The Weichselian-R climate scenario is illustrated in Figure 7-4a and the Emissions-M scenario is illustrated in Figure 7-4b. The calculated temperatures are shown in Figure 7-5 as a function of time and depth.

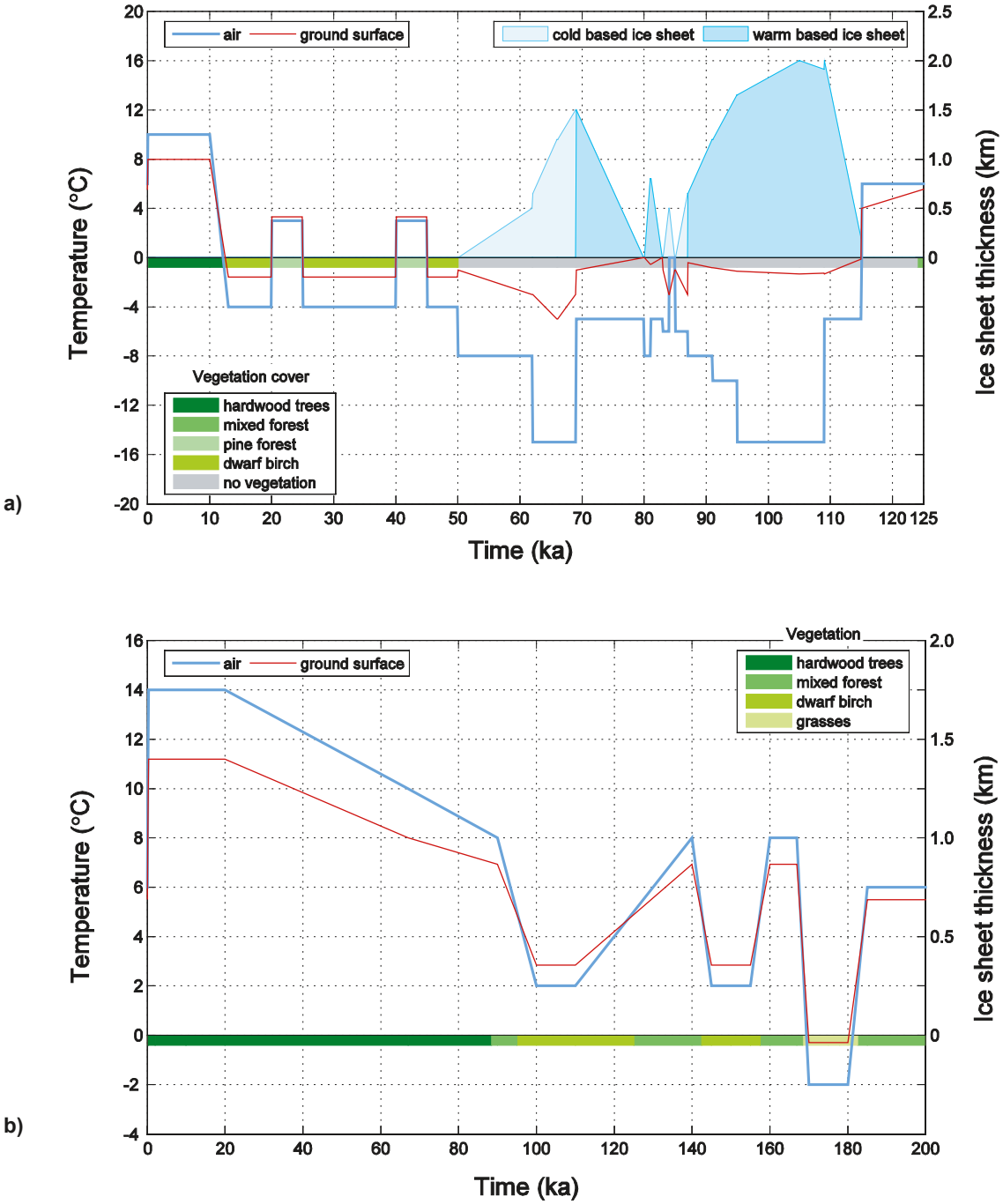

Figure 7-4. *Evolution of air temperature, ice sheet thickness and vegetation cover and modelled ground surface temperature at Olkiluoto. a) Scenario B, b) Scenario D /from Hartikainen 2006/.*

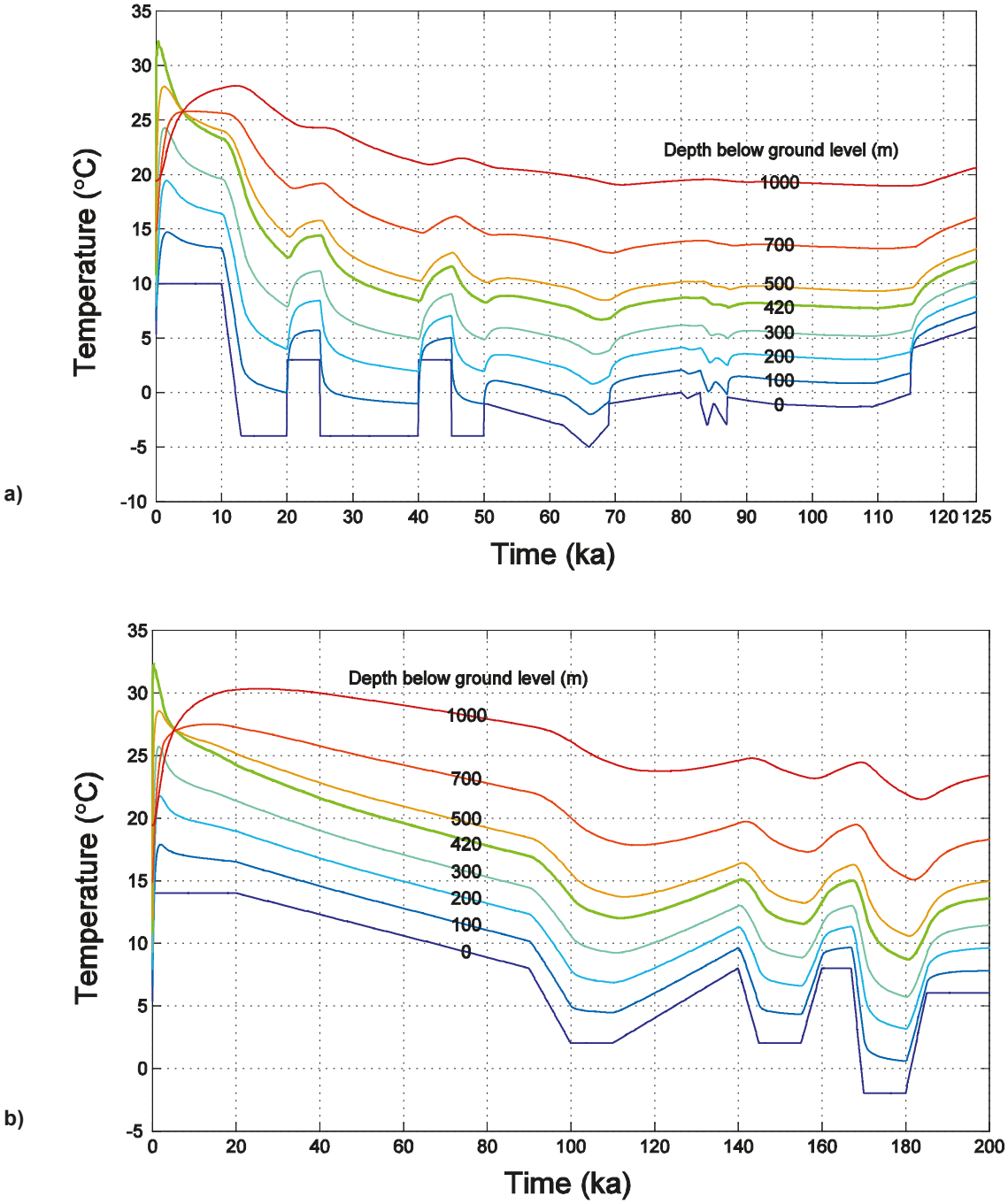

Figure 7-5. *Evolution of subsurface temperature at Olkiluoto as a function of depth below ground level. a) Scenario B, b) Scenario D /from Hartikainen 2006/; in both cases it is pessimistically assumed that no vegetation cover exists at the surface.*

This model includes the decay heat from spent fuel assumed to be disposed of at a depth of 420 m. The site specific surface conditions at Olkiluoto are based on time histories of ground level temperature, ice sheet thickness, shoreline migration and vegetation cover of the climate scenarios B and D as described in /Cedercreutz 2004/. From these results, it is concluded that repository at Olkiluoto seems to remain well outside the range of permafrost development in all investigated cases and the temperature in the near-field of the repository remains above the freezing point (which is slightly lower than 0°C due to the hydraulic pressure and salinity at repository depth) for times beyond several hundred thousand Based on these results, freezing can be neglected in the safety assessment for KBS-3H.

A state-of-the-art description of thermal processes (heat transport and freezing) is given in /SKB 2006e/. No other issue has been identified for KBS-3H, in addition to those presented in the relevant Process Reports for KBS-3V /Rasilainen 2004, SKB 2006e/.

7.5 Hydraulic processes

Groundwater flow and gas flow/dissolution are the most relevant hydraulic process in the geosphere. The inter-dependence between these processes and the variables is shown in Table 7-6.

7.5.1 Groundwater flow

Overview/general description

The characterisation of deep groundwater flow based on numerical modelling has been an essential part of the site investigations at Olkiluoto from the early 1990's. The main objectives for characterising groundwater flow at the repository site are to improve understanding on how groundwater interacts with the chemical environment of the repository and on radionuclide transport. The characterisation of past and present groundwater conditions forms the basis, by predictive modelling, of the understanding of the future evolution of groundwater flow at the site over time-scales relevant to the safety assessment.

In crystalline hard rocks, groundwater flow takes place predominantly in a fracture network. The properties of the fracture network at Olkiluoto have been investigated in great detail /Posiva 2005, Hellä et al. 2006/. Although the spatial occurrence of fractures is highly variable (as is typical for the Finnish bedrock in general), it exhibits certain patterns. For example, fractures may occur in clusters with similar orientations, the size of fractures and their hydraulic transmissivities may be correlated and transmissive fractures may be spatially clustered.

During the construction and operation of ONKALO and of the repository, the open excavations dominate the flow conditions in the vicinity of the repository and draw groundwater from all directions in the bedrock towards the open excavations. As a consequence, the water table and the associated hydraulic heads are lowered. The hydraulic disturbances in the host rock can be significantly reduced by grouting of fractures /Löfman and Mészáros 2005, Ahokas et al. 2006/.

After closure of the tunnels, the flow conditions and the salinity distribution start to recover towards the natural state, except in the vicinity of the repository, where the decay heat increases the temperature, which in turn results in an upward groundwater flow /Löfman 2005/. The thermally induced upward flow delays the recovery of the flow conditions towards the natural state for several hundred years.

Table 7-6. The interdependence of hydraulic processes and identified variables in the geosphere.

Hydraulic processes	Variables in geosphere												
	Repository geometry	Fracture geometry	Temperature	Groundwater flow	Groundwater pressure	Gas flow	Stress state	Matrix minerals	Fracture minerals	Groundwater composition	Gas composition	Structural and residual materials	Saturation
Groundwater flow	×	×	×	×	×	×	×			×	×	×	×
Gas flow/ dissolution	×	×	×	×	×	×	×			×	×		×

The principles and approaches used in groundwater flow modelling in the geosphere are well known and have been documented in many reports. /SKB 1999, Rasilainen 2004/ and /SKB 2006e/ contain a state-of-the-art discussion of hydraulic processes, and modelling thereof at various scales (regional scale, site scale, repository scale, canister scale), occurring in and around of a KBS-3V repository for spent fuel sited in a granitic environment. These discussions are not reproduced here.

The focus of the present chapter is on a new repository-scale discrete fracture network model (DFN model) that has recently been developed for the Olkiluoto site /Lanyon and Marschall 2006/.

Boundary conditions

The boundary conditions for hydrodynamic modelling depend on the envisaged scale. For the repository-scale DFN model, the relevant external boundary conditions are either set at the locations of major geological features (where fixed hydraulic heads can be prescribed) or by the results of a higher-scale hydrodynamic model (where hydraulic heads or water flows can be prescribed). In addition, internal boundary conditions are needed at the walls and ends of deposition drifts during the operational phase. Salinity effects on boundary conditions are not accounted for in the DFN modelling.

Model studies/experimental studies

A DFN modelling study was performed in the framework of the KBS-3H Safety Case project /Lanyon and Marschall 2006/. The main motivation for initiating the DFN model has been to look for the discrete inflows for layout adaptation. For the hydraulic conditions and groundwater flow including radionuclide transport, the TILA-99 approach was used in order to have comparable far-field conditions. The focus of the KBS-3H study was on the near field where the differences between the KBS-3H and -3V are of most relevance (see Section 1.5.2). The DFN study is based on existing descriptive structural and hydrogeological models of the site in 2005 /Hellä et al. 2006, Vaittinen et al. 2003/. There now are more up-to-date descriptions, as described in the Site Description 2006 /Andersson et al. 2007/, but these – due to time constraints – were not available for the DFN model used in this report /Lanyon and Marschall 2006/. However, the most important hydraulic zones according to the Bedrock model 2003/1 /Vaittinen et al. 2003/ and the recent hydrostructural model presented in the Site Description 2006 /Andersson et al. 2007/ do not differ much. The DFN modelling study is set up to investigate expected behaviour of the disposal system and deviations from that behaviour. The objectives related to expected system behaviour are: i) justification of conceptual assumptions (key processes, relevant scenarios, system parameterisation, boundary conditions), ii) provision of input values for performance assessment calculations (geometric simulations, transient inflows), and iii) assessment of robustness of conceptual assumptions. An additional objective is to identify relevant processes and parameters related to possible deviations from the expected behaviour. All simulations were performed using the CONNECTFLOW hybrid continuum porous medium/DFN model (Version 9.1).

Geometrical DFN modelling

The types of hydrogeological features considered within the model are:

- Major Fracture Zones (MFZ)
- Local Fracture Zones (LFZ) and associated water conducting features (LFZ-WCF)
- Water Conducting Features in the background rock (BR-WCF)
- The background rock itself.

The geosphere description is mainly based on that given in the analysis of geohydrological data performed by /Hellä et al. 2006/ and on the Olkiluoto bedrock model /Vaittinen et al. 2003/. The DFN concepts (model variants) investigated in the geometrical studies are listed in Table 7-7. The model variants differ only in their treatment of the water-conducting features (WCFs).

For the Reference Case, the data are based on flow log data from /Hellä et al. 2006/. Results from constant head injection tests with double-packers using the Hydraulic Testing Unit (HTU) (HTU data from 1991–1997) and from difference flow meter measurements in normal mode have been used for checking the results. An extended version of the reference case is also developed to include lower transmissivity features using a compilation of 2 m packer test data.[26] The Extended Reference Case uses all the available HTU data (1991–2005), including a distribution of hydraulic transmissivity of WCF that extends to below 10^{-12} m^2 s^{-1}, but reliable data is probably only available to a transmissivity of 10^{-10} m^2 s^{-1} (equivalent to a hydraulic conductivity of 5×10^{-11} m s^{-1} over a 2 m interval). The simulations use two versions of the model with transmissivity cut-offs of 10^{-10} and 10^{-11} m^2 s^{-1}. The use of the lower cut-off variant is to check that no significant changes in output measures occurred when including the additional low transmissivity features.

The Channel variant again includes lower transmissivity features and has a consequently higher density of features. It is fitted to the observed inflow data assuming that only a fraction of the features below the 10^{-9} m^2 s^{-1} detection limit will be identified.

The LT Correlation transmissivity distribution is also fitted to the same data as the Reference Case from the data in /Hellä et al. 2006/, but is corrected for the borehole bias due to longer fractures being more transmissive and more likely to be intersected by a borehole.

Table 7-7. The DFN concepts (model variants) investigated in the geometrical studies. Legend: Water-conducting feature (WCF), localized fracture zone (LFZ), major fracture zone (MFZ).

Concept	Reference Case	Extended Reference Case	LT Correlation variant	Channel variant
Description/ motivation	Model based on flow logging data in /Hellä et al. 2006/.	Model based on input from all the available Hydraulic Testing Unit data (1997–2005), including data from /Hellä et al. 2006/. Model extended to address lower transmissivity range.	WCF length and transmissivity are correlated.	WCFs assumed to be channelled; only a fraction of WCFs identified during flow logging.
Number of realisations	100	100	100	50
Treatment of background rock WCFs	Density based on borehole data. Orientation from outcrop mapping. Power law length distribution. Transmissivity uniform across feature.	Increased density log normal distribution fitted to 2 m packer test data (references in Table 2-2 of /Lanyon and Marschall 2006/) two variants with cut-off at T=10^{-10} and T=10^{-11} m^2/s.	Length and transmissivity are highly correlated. The longest WCFs are also the most transmissive. Density, size and orientation are the same as reference case. Transmissivity distribution adjusted to compensate for size-biased sampling.	Same as reference case apart from channelling. Five times as many WCFs but only 20% of WCF area greater than flow logging detection limit. WCFs split into 10 × 10 subplanes. Transmissivity varies across WCF.
Treatment of LFZs	Average spacing of 150 m in borehole. Orientation uses same sets as WCFs. LFZ associated WCFs cluster around LFZ plane.	As reference case	As reference case	As reference case
MFZ Treatment	Deterministic structures Transmissivity =1×10^{-5} m^2/s	As reference case	As reference case	As reference case

[26] This type of packer test may show in some cases artificial flow path connections because of the over-pressure used in the tests. In sparsely fractured rock this risk is minor /Ahokas 2003/.

All geometrical calculations are performed on a 2,400 m × 1,600 m × 100 m block at 400 m depth corresponding to the repository layout depicted in /Johansson et al. 2002/ (note that the updated repository layout presented in Figure 7-2 in /Johansson et al. 2007/ was not available for the DFN study). The domain for the generation of the fracture network is chosen much larger to avoid boundary effects. An example realisation of the fracture network for the Reference Case is shown in Figure 7-6. The number of WCFs in a model range from about 20,000 for the Reference Case to 110,000 for the Extended Reference Case model variant with a cut-off at 10^{-11} m^2 s^{-1}. In the Channel model variant there are approximately 30,000 WCFs, each being represented by up to 100 sub-fractures resulting in over 1,500,000 sub-fractures.

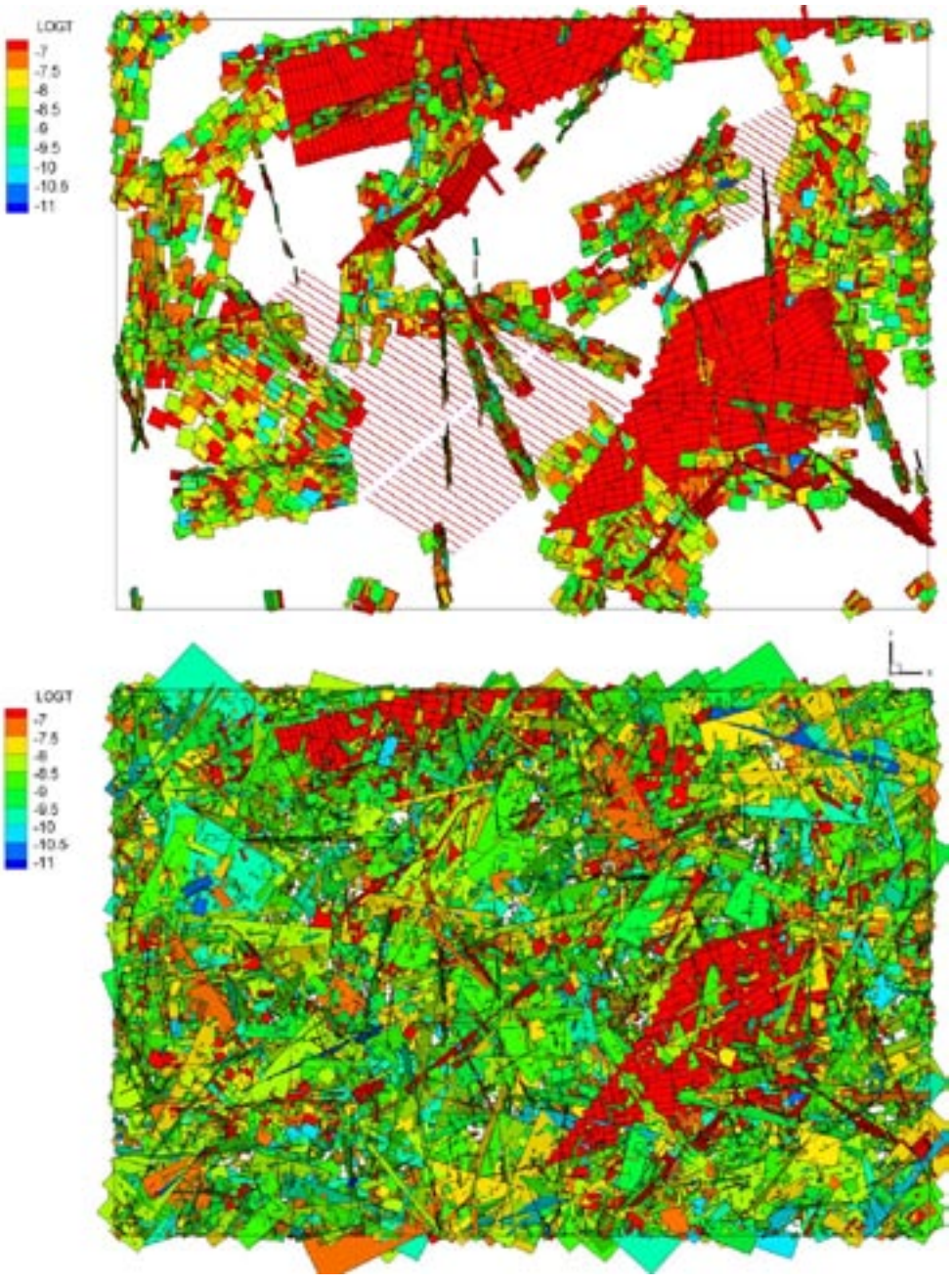

Figure 7-6. *Plan view of an example realisation of the fracture network in the Reference Case. Upper figure: MFZs, WCF associated with LFZs and deposition drifts (common to all model variants). Lower figure: WCFs in the Reference Case. WCFs are coloured by log_{10} transmissivity [m^2 s^{-1}]. From /Lanyon and Marschall 2006/. a) FZs (red) and WCFs associated with LFZs (representation common to all models) and deposition drifts. b) Reference case DFN model realisation. WCFs coloured by log_{10} transmissivity (m^2/s).*

The DFN model is used as a tool for the layout adaptation of deposition drifts, within the framework of the repository layout depicted in Figure 7-2. The terminology used within the DFN study is illustrated in Figure 7-7, which also gives the values for transmissivity thresholds (based on the inflow classes in Table 7-8) used to make the layout adaptation.

The layout adaptation in the DFN model was based on DFN model transmissivity values. However, the layout adaptation for a real repository will be based on the available data, and is therefore likely to be based on inflows at the drift walls and other quantities that can be observed directly, rather than on transmissivities, which must be inferred from a model and are therefore subject to greater uncertainty.

Table 7-8. Inflow classes for layout adaptation. From /Lanyon and Marschall 2006/.

Inflow Q* (l min^{-1})	Transmissivity T** (m^2 s^{-1})*	Hydraulic aperture e*** (µm)	Compartment/ Isolated	Treatment of inflow in deposition drift
Q < 0.004	T < 1 × 10^{-10}	e < 5	Supercontainer Compartment	Tight section where gas build-up possible.
0.004 ≤ Q < 0.1	1 × 10^{-10} ≤ T < 2.65 × 10^{-9}	5 ≤ e < 15	Supercontainer Compartment	Acceptable.
0.1 ≤ Q < 1	2.65 × 10^{-9} ≤ T<2.65 × 10^{-8}	15 ≤ e < 32	Compartment or isolation (in compartment but no supercontainer, only filling)	Sealing by using extra fine low pH grout. Limit for sealing by cementitious grout is likely at the level of 1.0 × 10^{-8} m^2 s^{-1} (the same limit is probably also applicable for non-cementitious grout).
1 ≤ Q < 10	2.65 × 10^{-8} ≤ T < 2.65 × 10^{-7}	32 ≤ e < 69	Isolated	Defines compartment – inflow reduced by grouting or optional structural sealing.
10 ≤ Q < 30	2.65 × 10^{-7} ≤ T	69 ≤ e	Isolated	As above, optional structural sealing. Abandon drift if flow after sealing above 30 litres min^{-1}.

* Assuming one inflowing fracture.

** Into one supercontainer section from fractures without sealing.

*** Hydraulic apertures have been calculated assuming a water density ρ of 1,000 kg m^{-3} and viscosity µ of 1 × 10^{-3} Pa·s using the cubic law

$$T = \frac{\rho g e^3}{12\mu}$$

where T is the transmissivity in m^2 s^{-1} and e the hydraulic aperture in metres.

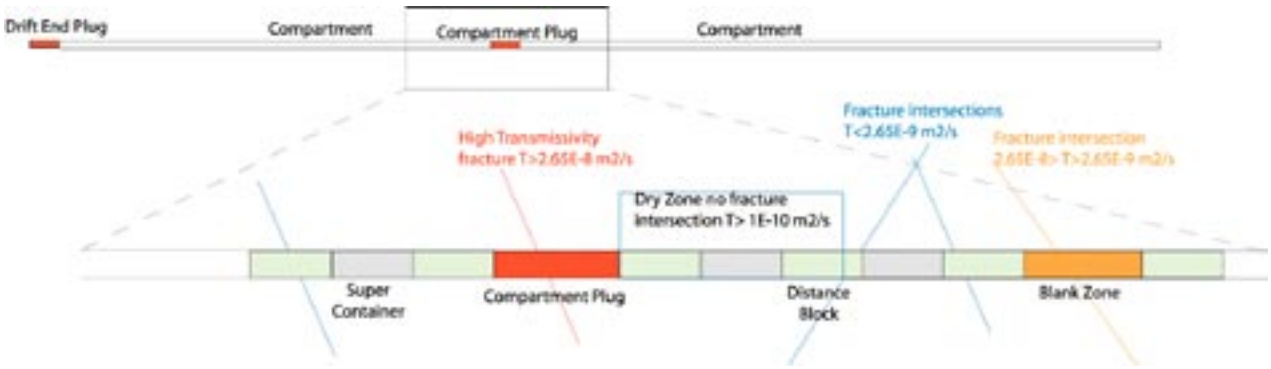

Figure 7-7. *Illustration of terminology and threshold values used in layout adaptation. From /Lanyon and Marschall 2006/.*

The layout adaptation in the DFN models has been based on the "within model" transmissivity values (see an example in Figure 7-8 for the Reference Extended Model) equivalent to assuming a robust characterisation of the local fracture transmissivity. No attempt has been made to simulate any detection or characterisation process. The models have therefore focussed on the feasibility (in terms of utilisation) of such a layout adaptation rather than any demonstration of how the post-closure inflow can be robustly estimated from characterisation work performed in pilot boreholes or in the open tunnel. Transient flow simulations of the interactions between drifts show that significant interactions are possible and that local changes in boundary conditions (due to opening and closure of adjacent drifts) are likely to significantly affect inflows. In addition the effects of unsaturated conditions and grouting together with changes in drawdown will need to be considered in any robust estimate of inflow after emplacement based on geological and hydraulic characterisation in borehole or the open tunnel.

Figure 7-8 shows a detailed view of one realisation of a single panel that illustrates the use of the DFN model in the layout adaptation using the Reference Extended Model. The results of the DFN modelling are presented in terms of simulated trace maps, histograms and tables of selected measures at various scales (drift scale, compartment scale, WCF scale), for details see /Lanyon and Marschall 2006/. As an example, Figure 7-9 shows a histogram of various measures at the drift scale.

The simulations indicate a very consistent picture across all the model variants and realisations. Typically, each 300 m drift is divided into 2 compartments by a single seal zone. Each drift contains on average 23 supercontainers with 3–4 blank sections. Total inflows to the compartments (prior to grouting) are on average about 1.5 litres min^{-1}. Inflows to a single compartment are below 1.0 litres min^{-1}.

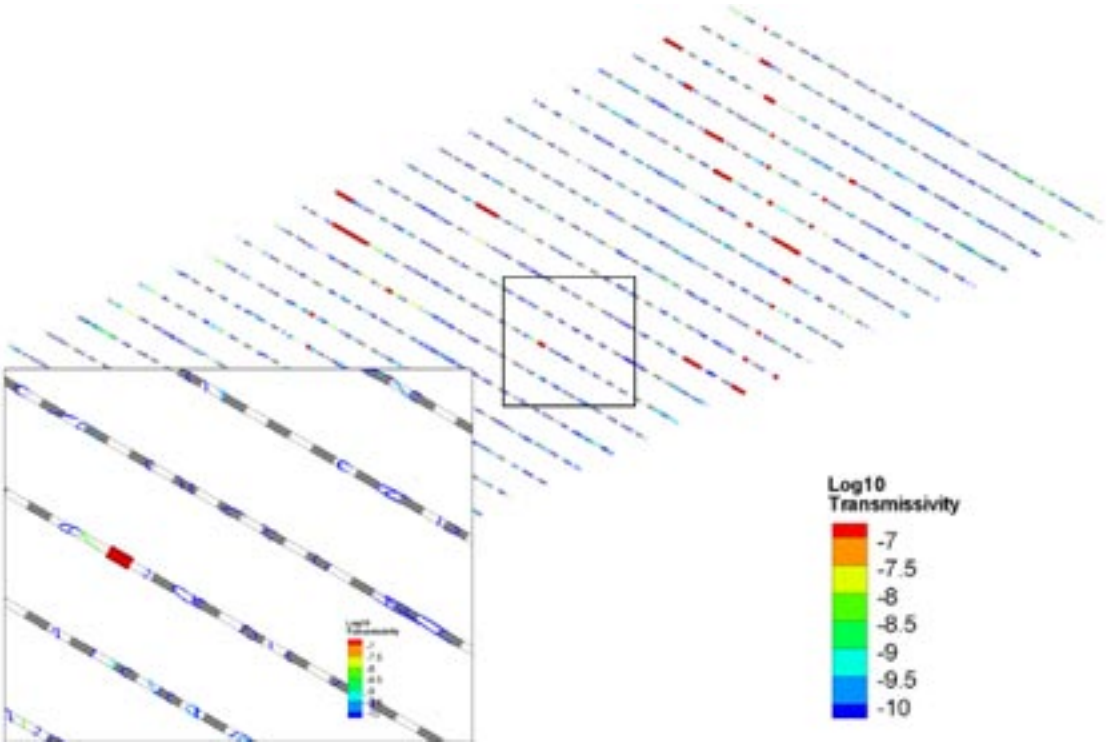

Figure 7-8. *Detailed plan view of an example realisation of the Reference Extended model, showing compartment plugs (in red) and supercontainer positions (in dark grey). WCF traces are also shown coloured by log_{10} transmissivity [m^2 s^{-1}]. From /Lanyon and Marschall 2006/.*

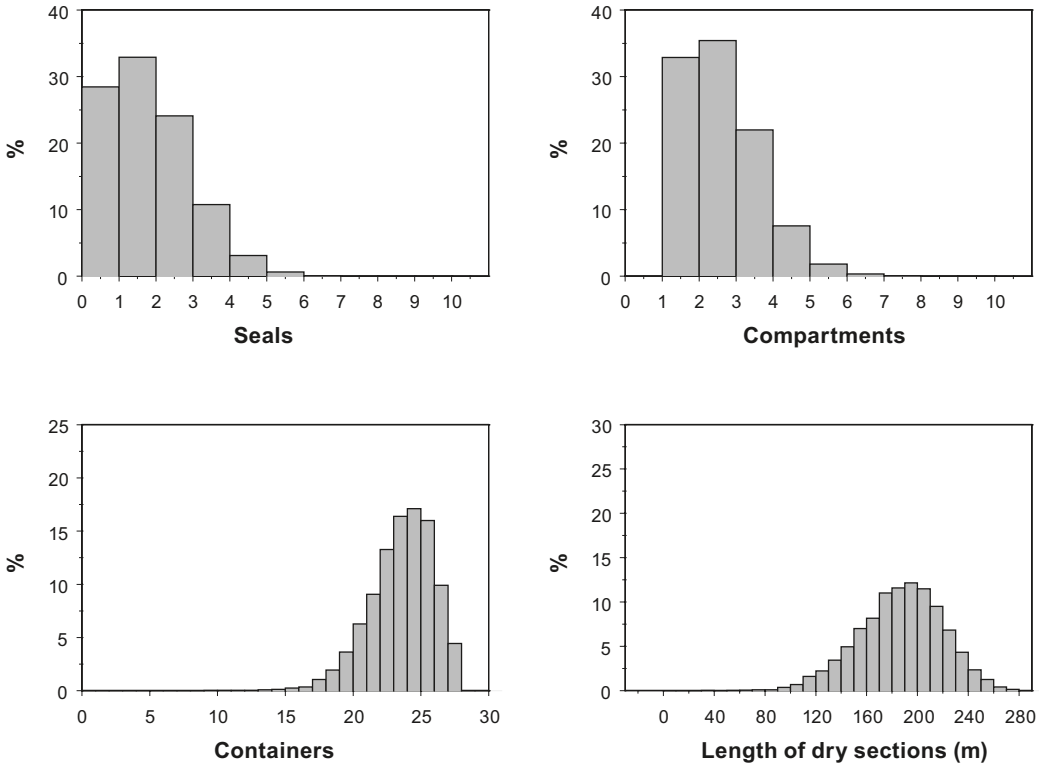

Figure 7-9. *Summary histograms of selected drift measures for the Reference Extended model. The drift length was 300 m and the number of realisation was 100. Legend: Seals (number of seal zones per drift), Compartments (number of compartments per drift), Containers (number of supercontainers per drift), length of "tight" sections (summed length of "tight" zones per drift). From /Lanyon and Marschall 2006/.*

The different measures are generally insensitive to the differences in the model variants. This is because, for the most part, the measures focus on the probability of intersection with transmissive features with transmissivity > 10^{-9} m^2 s^{-1}. As all the model variants are well calibrated to the flow logging data there is very little difference in the results. The only significant differences arise from the treatment of lower transmissivity features and prediction of "tight" zones (drift intervals with transmissivity below 10^{-10} m^2 s^{-1}). For the two model variants with additional transmissive features in the range 10^{-10} to 10^{-9} m^2 s^{-1} (Reference Extended and Channel variant) the lengths of "tight" sections are reduced as would be expected.

Transient hydrodynamic DFN calculations

The drift scale models described in /Lanyon and Marschall 2006/ consider transient flow (i.e. during excavation and pressure recovery after emplacement) around either one or two deposition drifts. The models are based on the Extended Reference case model variant as this variant is consistent with both inflow and 2 m packer test data and includes low transmissivity features. Four sample drifts are selected from one realisation of the Extended Reference case. All four drifts are located in Panel 1 of the western section of the repository. Figure 7-10 shows the DFN model volumes used for three selected drifts. The individual features are split up into 10 m × 10 m sub-fractures, which are each in turn discretised as a grid of 1,000 or more linear finite elements for flow calculations.

The DFN flow model features are summarised in Table 7-9. It is acknowledged that by applying a fixed head on all model surfaces some overestimation of the inflows may occur /Svensson 2006/. For more details on the representation of the various elements of the repository, see /Lanyon and Marschall 2006/.

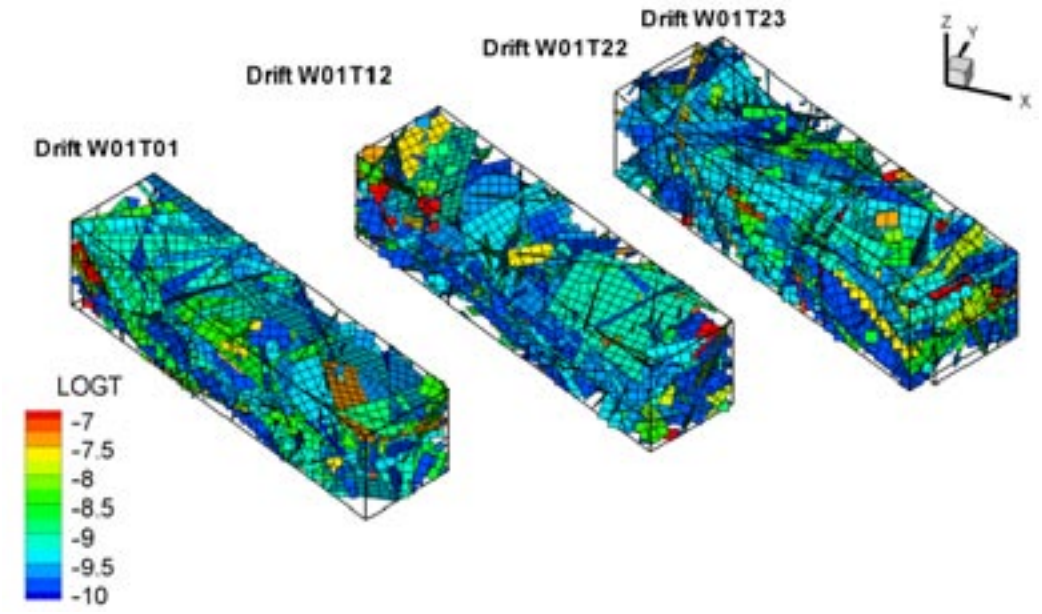

Figure 7-10. *DFN model volumes around selected deposition drifts. Reference Extended model for fractures with transmissivity > 10^{-10} m^2 s^{-1}. From /Lanyon and Marschall 2006/.*

Table 7-9. DFN flow model features. From /Lanyon and Marschall 2006/.

Feature	Representation in DFN flow models
Model region	Single drift models: 400 m long, 100 m×100 m cross-section rectangular block around deposition drift.
	Two drift models: 400 m long, 125 m×100 m cross-section rectangular block around deposition drift.
Geosphere representation	Selected realisations from Extended Reference Case geosphere representation. Only features with transmissivity > 10^{-10} m^2/s included (variant cases where features with transmissivity > 10^{-11} m^2/s included).
Deposition drift	1-D elements representing 300 m drift with super-containers, distance blocks, blank zones and compartment plugs.
Transport tunnels and other excavations	Not included.
Outer boundary condition	Fixed 400 m (relative to drift centre line) head on all model outer surfaces.
Drift boundary conditions	a) Fixed zero head (relative to drift centre line) to represent open drift.
	b) Closed zero net flow condition to represent closure of drift section after emplacement.

The outputs calculated by the transient flow models are:

- pressure at fracture intersections with drift elements
- pressure derivative (kPa per hour) at fracture intersections with drift elements
- net in/outflow to each intersection on a drift element
- net in/outflow to each drift element
- integrated net inflow to each drift element.

Note that water flows through the EDZ, rock matrix and distance block along the drift axis are not included in the models, as these are small compared with the inflows conveyed by individual fractures.

The calculated water inflows are shown in Figure 7-11 for the two adjacent drifts W01T22/23. The timing of the inflows relate to the positions of the fractures along the drift assuming a 10 m per day advance rate during drift excavation. Inflows reach steady state levels quickly after the end of excavation. Lower transmissivity fractures are likely to be of lower diffusivity resulting in longer transients, while pressure changes within the matrix are likely to be very slow indeed.

The dominant factor in pressure recovery in the supercontainer sections is the length of time required to fill up the gap volume prior to the start of pressure recovery. Pressure responses are heterogeneous with the majority of supercontainers not intersecting transmissive fractures. Within these sections no significant pressure rise is predicted within the first years as any water inflow is taken up by the bentonite. Significant differential forces will develop across the distance blocks separating a pressurised supercontainer section where the bentonite is likely to have swollen from the adjacent potentially "tight" super container section, as also illustrated in Figure 7-11.

The rate of pressure rise (pressure derivative in kPa per hour) is largely controlled by the geosphere inflow and the assumptions concerning the storage term associated with the super-containers and distance blocks. In models where no storage is associated with the drift sections, the pressure rises very quickly with derivatives greater than 1 MPa per hour. In the models containing greater storage (as in storage model E) the highest gradients are only associated with high transmissivity features located in blank or seal sections. The most significant elements in the storage term are likely to be the uptake of water into the bentonite and the presence of any trapped air in the gap volume.

The models further suggest that pressure disturbances due to the excavation of adjacent drifts may be quite significant (in the order of 2 MPa) and fast (depending on the storage). Typically the most transmissive features react most quickly, but drawdowns are seen in almost all intervals intersected by transmissive features.

Steady-state DFN calculations

Particle tracking calculations were performed based on steady-state DFN calculations and using the Extended Reference case model with a transmissivity cut-off of 10^{-11} m^2/s. The transport aperture b is assumed to be a simple function of the feature transmissivity T (m^2/s) such that $b = \sqrt{T}/2$ (for details, see /Lanyon and Marschall 2006/). Note that the models do not currently consider small-scale heterogeneity within flowing features as there is only very limited information available on channel properties for the repository volume. A unit vertical pressure gradient of 0.01 m m^{-1} is applied to the outer model boundaries, resulting in an overall downward flow.

Particles are released at the intersection of fracture sub-planes with the 1D super-container drift elements and are then tracked within the detailed pressure field from the steady-state solution. The advective travel time and the F-quotient[27] are calculated for each particle. Figure 7-12 shows sample particle tracks for drift W01T01 and corresponding F-quotients. Figure 7-13 shows the cumulative distribution of flow for the two methods and transmissivity cut-offs. Where transmissive features exist close to the drift, particles are typically diverted into them (see for example the path along edge of steep vertical feature in the centre of the model).

[27] In numerical codes where transport calculations are based on particle tracking, like e.g. ConnectFlow, F is calculated as the sum of advective travel time, t, divided by half-aperture, b, in individual transport segments along the path (in the most general sense an integral). This definition and concept used by SKB is described in /Andersson et al. 1998/ and used in /Hartley et al. 2006a, 2006b/. Regarding flow rates the F-quotient (or F-factor) for a single planar fracture can be defined as F=2WL/Q (= t/b), where W(m) is the channel width over which Q has been determined.

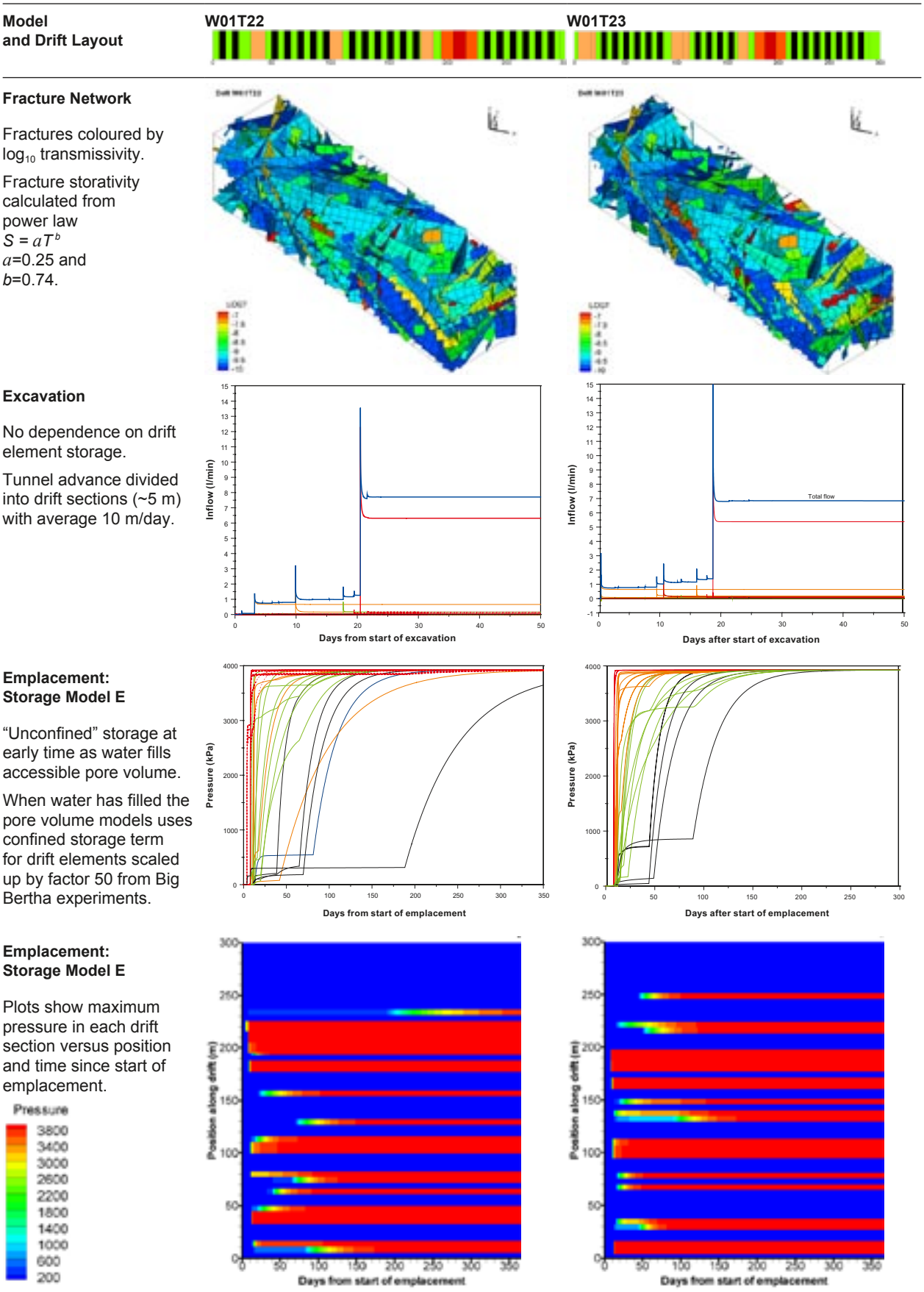

Figure 7-11. *Inflow rates during excavation and pressure recovery after emplacement as a function of the position along two example drifts. Reference Extended model for fractures with transmissivity > 10^{-10} m^2 s^{-1}; storage model E. From /Lanyon and Marschall 2006/.*

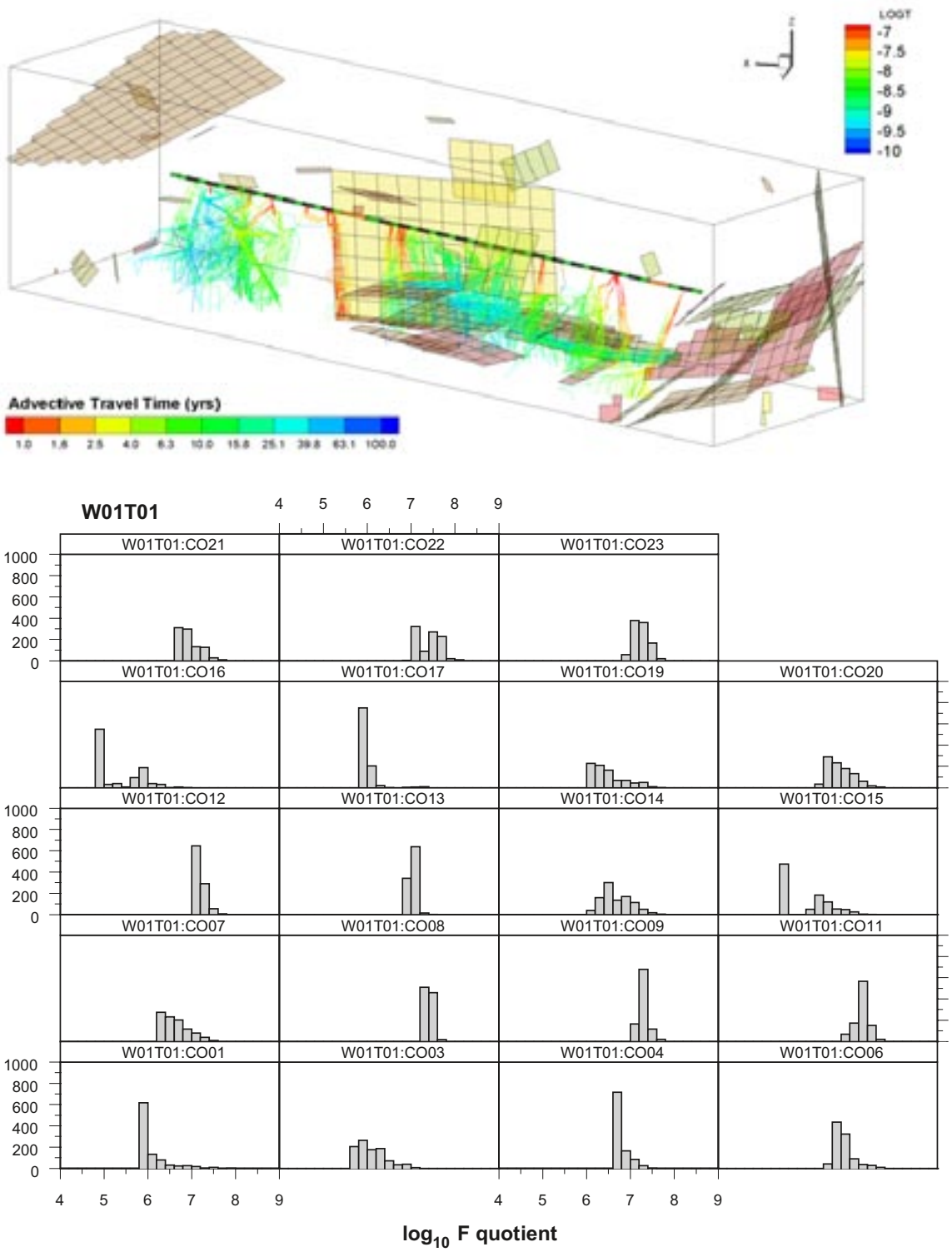

Figure 7-12. *Particle tracks from supercontainer elements for a selected deposition drift (W01T01). Upper figure: Tracks are coloured by travel time. Fractures are coloured by log transmissivity, only features with transmissivity greater than 10^{-8} m^2 s^{-1} are shown. Lower figure: F-quotients in log (a m^{-1}). In addition to the particle tracking outputs, the water flow past a supercontainer is calculated based on geometric estimates based on the trace-map analyses, using two methods of estimating the flow rate: Method 1 only considers the fraction of the trace within the length of the supercontainer, while in method 2 the trace-length of any feature intersecting the supercontainer section is assumed to contribute to flow. Calculations are performed for 10 realisations of the repository layout for the Extended Reference Case model with transmissivity cut-offs at 10^{-10} and 10^{-11} m^2/s. Figure 7-13 shows the cumulative distribution of flow for the two methods and transmissivity cut-offs.*

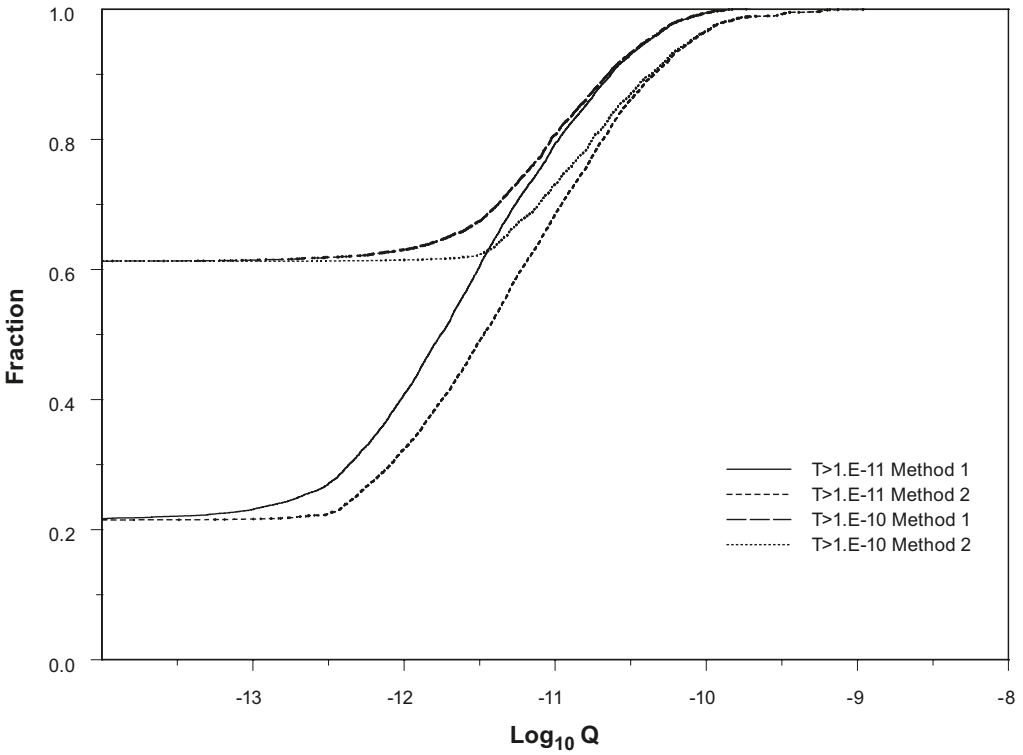

Figure 7-13. *Cumulative distribution of the steady-state flow rate past a supercontainer section. For Extended Reference Case with transmissivity cut-offs at 10^{-10} and 10^{-11} m^2/s. Results derived from geometric estimates based on the trace-map analyses for two slightly different methods (see text).*

A number of tests of the DFN model for model verification and confidence building have been performed:

- comparison of measured and simulated intersection statistics for selected borehole sections;
- simulated borehole test for one selected borehole interval (upper interval of KRI1, from 325.0 to 590.3 m);
- consistency check of DFN model with continuum site-scale models developed by VTT for Posiva (effective hydraulic conductivity of discrete fracture network).

The results of these tests are reported in detail in /Lanyon and Marschall 2006/. As an example, a comparison of the overall transmissivity distribution of intersections for the various DFN model variants is shown in Figure 7-14. For all the considered model variants the calibration is considered successful for transmissivities above the detection limit (10^{-9} m^2 s^{-1}). The fracture detection limit of 10^{-9} m^2/s is the limit above which the experimentalists felt that detection was near certain. Transmissive features below 10^{-9} m^2/s are only detected in favourable circumstances. Thus the mismatch below 10^{-9} m^2/s in Figure 7-14 illustrates the range of different assumptions about the presence of low transmissivity features affected by the assumed detection limit. Layout adaptation issues are, however, not sensitive to such low transmissivity features.

The only significant differences between model variants arise from the treatment of lower transmissivity features and prediction of "tight" zones (drift intervals with transmissivity below 10^{-10} m^2 s^{-1}). For the two model variants with additional transmissive features in the range 10^{-10} to 10^{-9} m^2 s^{-1} (Reference Extended and Channel variant), the lengths of "tight" sections are reduced as would be expected.

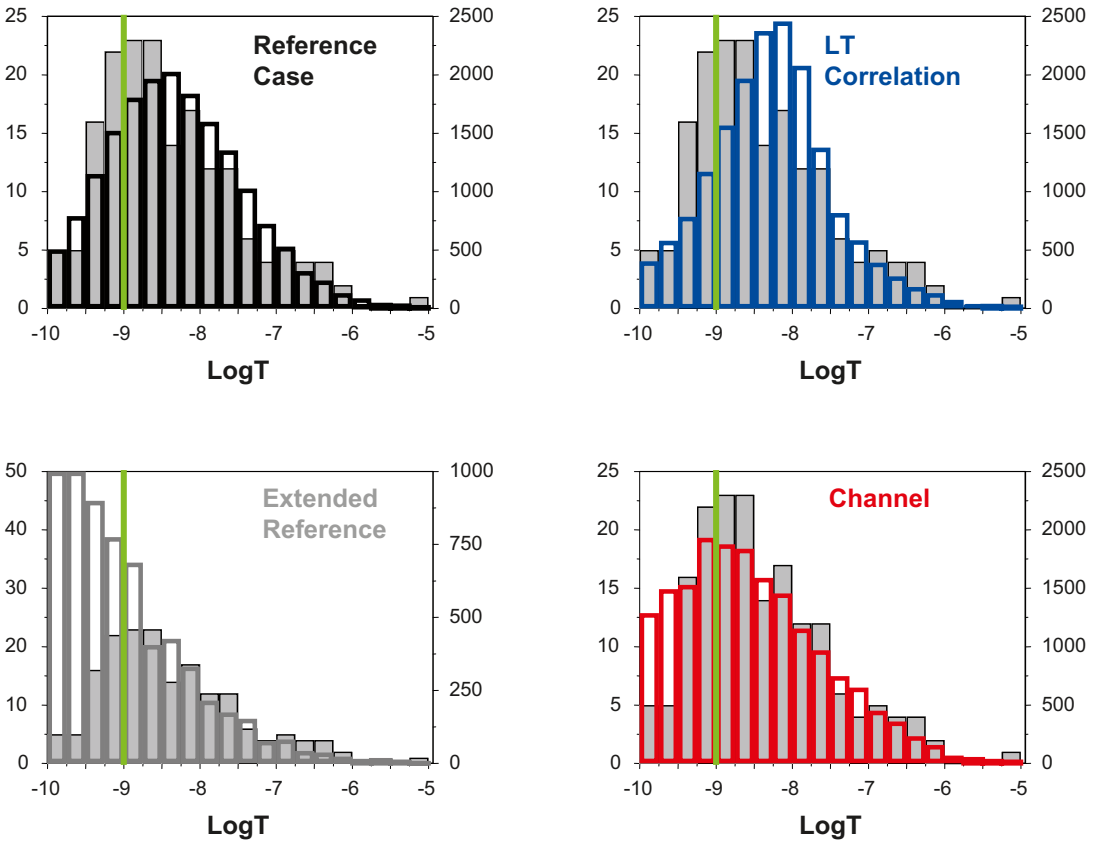

Figure 7-14. *Comparison of simulated (empty bars) and measured (filled bars) intersection transmissivity distribution for the different model variants. Flow logging detection limit shown in green. From /Lanyon and Marschall 2006/.*

Generally, a good match is found in most cases between the data and the DFN simulations showing that the DFN model is reasonably well calibrated to the average hydraulic behaviour of the host rock at the Olkiluoto site.

Natural analogues/observations in nature

No natural analogues or observatios in nature havebeen idetife.

Time perspective

The total water inflow rate is expected to quickly reach a steady-state level after the end of excavation, i.e. within a few weeks, given that the bulk of the inflows will be associated with the more permeable fracture intersections. However, they may decrease with time. Changes to water inflow during the construction/operational period are possible due to precipitation of solids in the fractures, as observed in Äspö and in the interim storage facilities for low-level waste (called VLJ-repositories) in Loviisa and Olkiluoto. For example, in the VLJ-repository of Olkiluoto the inflow has decreased from 45 L/min to about 37 L/min from 1992 to 2006 /Hagros and Öhberg 2007/.

After canister emplacement, times for saturation and pressure recovery are expected to greatly vary along the axis of individual deposition drifts. While in permeable drift sections the saturation rates are mainly determined by the hydraulic resistance of the bentonite (resulting in saturation times of roughly 10 years), in tighter drift sections the saturation rates are much smaller and saturation may be further retarded by gas generation due to anaerobic corrosion of steel (resulting in saturation times of several thousand years for the tightest drift sections, see also Sections 4.5.1 and 7.5.2).

Handling in the safety assessment for KBS-3H

In the safety assessment for KBS-3H, the DFN modelling results are used for repository layout and adaptation purposes, based on the available statistical information on fracture intersections in the deposition drifts (locations of compartment plugs, supercontainers and filling blocks, e.g. see Figure 7-7), on water inflow rates and pressure increase rates for the post-emplacement phase (see e.g. Figure 7-11); this includes process model calculations and scoping calculations performed to improve system understanding with respect to various safety-relevant processes (e.g. impact of rock shear, bentonite erosion through fractures, bentonite redistribution within deposition drifts, gas migration calculations). The results are also used to provide additional support for hydrogeological parameter selection in radionuclide release and transport calculations, although the hydrogeological parameters used are taken, in the first place, from TILA-99.

In the majority of radionuclide transport calculations in the safety assessment /Smith et al. 2007a/, the flow around a deposition drift is calculated based on the assumption that a drift section with a supercontainer is intersected by a fracture of transmissivity 3×10^{-9} $m^2 s^{-1}$. The possibility that, in reality, some higher transmissivity fractures are present is also acknowledged (and is considered in two variant cases in radionuclide transport calculations, PD-LOGEOR and PD-LOGEORS, see Appendix G). This can affect not only flow around the deposition drift, but also the geosphere transport resistance (WL/Q). Higher flow and/or geosphere transport resistance is considered in the following cases (see Appendix G):

- PD-HIFLOW (increased flow at buffer/rock interface);
- PD-LOGEOR, CC-LOGEOR, CC-LOGEORG, CC-LOGEORS (reduced geosphere transport resistance, different canister failure modes and groundwater compositions); and
- PD-HIFLOWR (increased flow at buffer/rock interface and reduced geosphere transport resistance).

The case of a more favourable, increased geosphere transport resistance with respect to the Base Case (PD-BC) is considered in case PD-LOGEOR.

For further information about assessment cases calculated in the Radionuclide Transport Report, see Appendix G.

Handling of uncertainties

The transient and steady state flow models described above aim to provide input to the safety assessment for KBS-3H. While they are quite detailed in their representation of the fractured rock and the excavation and emplacement sequence, they are necessarily idealisations of the real system. In particular, the discussed models do not include the following processes:

- gas generation due to corrosion of metal waste and packaging and two phase flow within the engineered barrier system;
- coupled thermo-mechanical (T-M) processes, such as those associated with the swelling and redistribution of bentonite, rock spalling and rock shear deformations;
- coupled hydraulic-chemical (H-C) processes, such as density-driven flow in temperature and salinity fields;
- coupled hydraulic-chemical processes, such as bentonite erosion, mineralogical transformations, upconing of saline water, intrusion of oxidising water, etc.

Setting aside these fundamental limitations, the main uncertainties related to the DFN models can be summarised as follows.

With respect to the geometrical representation of the fault and fracture network, relatively little variation in the statistics of fracture intersections and inflows between the different model variants is found. The choice of model variants, however, is concentrated on the interpretation of the transmissivity and frequency of the water-conducting features (WCFs) in the background

rock. The following features of the fault and fracture system could have a significant impact on the prediction of likely inflows and pressure responses to excavation and drift closure:

- clustering of WCFs and Local Fracture Zones (LFZs), creating zones of more intense fracturing and large unfractured regions;
- depth trends in the fracture system such that the properties derived by averaging over the 300–750 m depth horizon are not representative of 400 m depth (e.g. a significant drop in fracture density below 500 m);
- different interpretations of LFZ orientation and distributions (currently assumed to mimic the orientation distribution derived from outcrop maps);
- very small scale channelling at sub-metre scales. The channel variant includes transmissivity variation across WCFs at 1/10 the size of the WCF i.e. from 1 to 50 m. Given that most intersections are with the largest structures, there is little difference between the intersection statistics of a 100 mm diameter borehole and a 1.85 m drift. If channels occur at small scales e.g. cm or dm, however, then intersection statistics for drifts might be significantly different than for boreholes;
- flow concentrated in small fractures. The models have only considered fractures >10 m in length as contributing to significant flow;
- any bias in the measurement of transmissivity during flow logging; and
- action of near drift-wall processes in changing inflows (e.g. ventilation, EDZ, two-phase flow).

With respect to the engineered barrier system, the major uncertainty relates to the representation of the "storage" associated with supercontainers and distance blocks. In this context storage is a "lumped term" incorporating multiple effects (e.g. inflow into the compacted bentonite; compressibility of gel/water mix in the gap volume, effect of trapped air and compressibility of the rock and compacted bentonite), which will change with time as the bentonite swells and homogenises.

7.5.2 Gas flow/dissolution

Overview/general description

Introduction

Gas is generated within the repository, predominantly through the corrosion of steel components. There will also be some trapped air, which will be compressed, dissolve and migrate into the geosphere as the repository saturates. There are indications that deep saline groundwaters contain gases, and in particular methane, at near-saturation concentrations (see Section 7.3.3 of /Pastina and Hellä 2006, Pitkänen and Partamies 2007/. The convective cell created by the thermal gradients around the repository will draw up dissolved gases from depth, and elevated temperatures will promote degassing. Furthermore, as gas rises through the fracture network within the host rock, it may carry water with it, and perturb groundwater flow to a degree not currently fully understood.

The following discussion concerns the fate of repository-generated gas. Although this concerns the engineered barrier system as well as the geosphere, the discussion is included here since the bulk of the gas will eventually reach the geosphere, and migrate there either in solution or as a separate gas phase.

Gas generation in the deposition drifts starts immediately upon contact of water with steel surfaces, where gas is predominantly produced by anaerobic steel corrosion. The quantities of steel present in the deposition drifts are moderate, about 1.1 tons per supercontainer unit for the Basic Design (Section 5.5.1, Table 5-7). In addition, any compartment plugs present in the deposition drift will contribute to the overall amount of generated gas (about 2,550 kg per plug). These gas sources are, however, located in the vicinity of permeable fractures and thus do not significantly contribute to gas pressure buildup.

Other gas-generating materials are either absent or exist in quantities too small to contribute significantly to gas production.

The overall gas production is in the order of 2.6×10^4 moles of H_2 or 580 m^3 H_2 (STP) per supercontainer unit (see Table 5-8). These gas volumes are relatively low, particularly in the case of initially intact copper-iron canisters. The case of initially defective canisters is discussed in Section 2.5.1.

The gas production *rates* are, however, significant, mainly because the supercontainer and other structural materials provide relatively large surface areas for steel corrosion. The time needed for complete corrosion of the entire steel inventory (excluding the cast iron insert inside the canister) is comparatively short (about 5,000 years for the reference steel corrosion rate of 1 μm a^{-1}, see Section 5.7.1).

The pressure build-up caused by gas generation in the repository is mitigated by gas dissolution, gas diffusion[28], gas-induced porewater displacement (incl. gas advection[29]) and capillary leakage[30] from the deposition drifts into the host rock (fractures, matrix) or along the EDZ. Gas transported through the fractures in the background host rock will eventually reach higher-permeability geological features, from which gas release takes place into the surface environment. These processes are discussed in more detail in the following.

Capacity for dissolution and storage and gas

In the following, a comparison is made between the total amount of generated gas, n_{tot} [mol] (Table 5-8), with the overall capacity for storing and dissolving gas in the repository system (Figure 7-15). The objective of this analysis is to show that even for optimistic gas storage and dissolution capacities the generated gas cannot be stored/dissolved in the repository system. In this sense, the upper bound of the amounts of gas that can be dissolved, $n_{diss,I}$ [mol], and stored, $n_{stor,I}$ [mol], in the various parts of the repository system is estimated by:

$$n_{diss,i} = V_i \frac{C(P_0)}{P_0} P_i \qquad \text{(Eq. 7-1)}$$

$$n_{stor,i} = \frac{V_i^* P_i}{R T_0} \qquad \text{(Eq. 7-2)}$$

where

V_i	saturated pore volume available for dissolution of gas in repository part *i* [m^3 per supercontainer unit]
V_i*	gas accessible pore volume available for storage of gas in repository part *i* [m^3 per supercontainer unit]
$C(P_0)$	gas solubility at ambient pressure P_0 [mol m^{-3}]
P_i	average pressure in repository part *i* [Pa]
R	universal gas constant [J K^{-1} mol^{-1}]
T_0	temperature during thermal transient (30°C, assumed constant) [K].

[28] G*as diffusion* is an abbreviation for diffusive transport of dissolved gas in the aqueous phase.

[29] *Gas advection* is an abbreviation for advective transport of dissolved gas in the aqueous phase.

[30] C*apillary leakage* is an abbreviation for advective transport of gas in the gas phase under two-phase conditions (no structural changes in pore space involved).

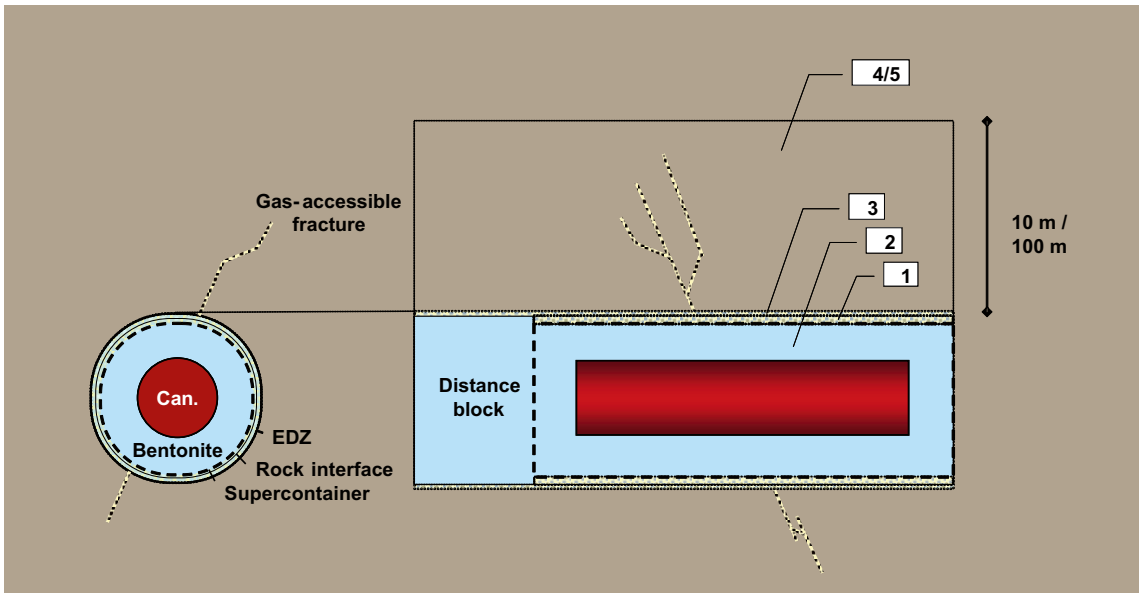

Figure 7-15. *Sketch of the various repository domains (i = 1–5) considered in the estimation of the capacities for gas dissolution and gas storage. Domain 1 corresponds to 4 cm of bentonite at the buffer/rock interface, Domain 2 corresponds to the bulk of the buffer, Domain 3 to the EDZ, Domain 4 to the first 10 m of host rock, and Domain 5 to 100 m of host rock. Gas dissolution takes place in various parts of the system (see Table 7-10), but is not shown in the figure.*

The volumes available for dissolution and storage of gas and the corresponding estimate capacities are summarised in Table 7-10. These calculations are based on emplacement of BWR spent fuel canisters (Posiva) and do not depend on a particular design option. The parameter values are taken from Appendix A (Table A-1). For the bentonite outside the shell of the supercontainer (assumed thickness of 4 cm) and for the EDZ, it is hypothetically assumed that the entire pore space is available for gas storage, i.e. all porewater would be displaced from these domains by the generated gas. This is considered to set an upper bound to the storage capacity around the supercontainer.

Table 7-10. Estimated capacities for gas dissolution and gas storage per supercontainer unit in the various repository domains. The calculations are based on Posiva BWR spent fuel; the parameter values are taken from Table A-1 and the symbols are explained in Appendix C. All values refer to one supercontainer unit.

Repository domain	Volume for gas dissolution V_i		Volume for gas storage V^*_i		Amount of dissolved gas	Amount of stored gas
	[m³]		[m³]		[mol]	[mol]
i	Formula		Formula			
1 4 cm of bentonite outside container shell	–	0	$\pi\,(r_t^2 - (r_t - \Delta r_t)^2)\,\varepsilon_b\,l_{sc}$	0.55	0	920
2 Remaining bentonite (incl. distance block)	$\pi\,(r_t^2\,p_c - r_c^2\,l_c)\,\varepsilon_b - V_1^*$ (where $V_1^* = V_{i=1}^*$)	10.6	–	0	340	0
3 EDZ	–	0	$\pi\,(r_{EDZ}^2 - r_t^2)\,p_c\,\varepsilon_{EDZ}$	0.005	0	8
4 10 m of host rock	$p_c\,dh\varepsilon_m$	3.9	$p_c\,dhP_{32}a$	0.011	120	18
5 100 m of host rock	$p_c\,dh\varepsilon_m$	39	$p_c\,dhP_{32}a$	0.11	1,100	160

For the remaining bentonite including the distance block, it is likely that the gas saturation is very low, because of the fine bentonite pore structure and the corresponding high gas entry pressure. Therefore, all pore space is assumed to be available for gas dissolution only. In the host rock, it is assumed that gas can readily be stored in fractures, whereas the matrix pore space is accessible for gas only in dissolved form. The storage volume in fractures is calculated based on a total fracture intensity of $P_{32} = 2\ m^{-1}$ (Table C-1) and on a mean hydraulic aperture of 2 μm. Note that using the mean hydraulic aperture (derived from the cubic law, see Equation C-10 in Appendix C) instead of the mean arithmetic aperture leads to an underestimation of the gas storage volume in fractures.

Table 7-10 shows that the largest contribution to gas storage is from the bentonite outside the shell of the supercontainer, whereas the porosity in the remaining bentonite and in the host rock matrix provides significant dissolution capacities.

In Figure 7-16, these estimated capacities for gas dissolution and gas storage are compared with the total amount of generated gas in the repository (Table 5-8). Clearly, neither gas dissolution nor gas storage (nor the sum of the two) are sufficient to accommodate all generated gases in the repository. In fact, the total amounts of generated gases are more than one order of magnitude higher than the (upper bounds of the) capability of the repository system to dissolve and store gases. For this reason, more detailed calculations are needed to show that the generated gases are sufficiently mobile so that excessively high gas pressures in the repository system can be avoided (see below).

Saturation of drifts

While the gas pressure in the repository is below the hydrostatic pressure of 4 MPa, slow inflow of water from the host rock occurs and water saturation in the deposition drifts increases. Any residual air in the void space between the supercontainer and rock as well as between the distance block and rock will be trapped. This concerns both the Basic Design and the DAWE design, because in the DAWE design, despite the fact that a significant part of the air is evacuated during watering, the large quantity of air trapped within the fine pore structure of the bentonite cannot be removed by this technique. Full saturation is, therefore, not likely to be reached before the start of gas generation and a residual free gas phase will remain in both design options considered.

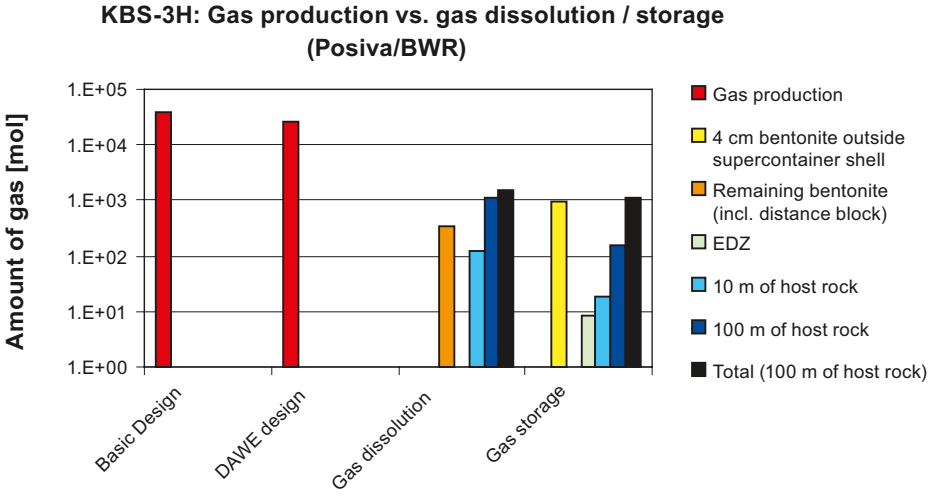

Figure 7-16. *Estimated capacity for gas storage and gas dissolution in one supercontainer unit in comparison with the total amount of generated gas. All values refer to one supercontainer unit.*

Gas generation

Gas generation is caused by anaerobic corrosion of supercontainers and structural materials. The gas generation rate is determined by the steel corrosion rate, for which different values are considered: 1 μm a^{-1} (Base Case) and 0.1–2 μm a^{-1} (range of values for sensitivity analysis). As discussed in Section 5.7.1, in the major part of the deposition drifts there will likely be sufficient water available in the vicinity of the steel surfaces to maintain anaerobic corrosion at a rate of 1 μm a^{-1}. In very tight drift sections with hydraulic transmissivities of 10^{-11}–10^{-12} m^2 s^{-1}, steel corrosion may be limited by the supply of water and the corrosion rate may decrease to 0.1 μm a^{-1}.

There is the possibility that some hydrogen is consumed by microbially-mediated reduction of sulphate to sulphide or carbonate to acetic acid or methane by microbial activity. This would lead to a reduction in the total amount of hydrogen in the repository system, but this process is conservatively neglected in the calculations.

Gas dissolution and diffusion

Hydrogen gas generated by anaerobic steel corrosion, as well as gas entrapped at the time of closure, will dissolve in the near field pore water until the solubility limit at the governing pressure and temperature at repository depth is reached. Note that in the temperature range of interest during the thermal phase, i.e. 30–60°C, the solubility of hydrogen is not strongly dependent on the temperature /Himmelblau 1960/. Dissolved gas diffuses through the drift walls into the host rock. The natural hydrogen concentration is far from its solubility limit under repository conditions /Rasilainen 2004/ and is not taken into account in the model calculations. Although the natural methane concentration is relatively close to its solubility limit, this is not expected to affect the hydrogen solubility. The effect of dissolved hydrogen (redox conditions) on solubility limits has been taken into account in the solubility limits used in the Radionuclide Transport Report /Smith et al. 2007a/.

The formation of bubbles from either natural dissolved gas or from repository-generated hydrogen gas formation is only likely to occur during the first few thousand years of repository evolution (during the period of elevated temperatures in the case of natural dissolved gas and during the period of steel corrosion in the case of repository-generated gas), and any perturbation to groundwater flow will have largely ceased by the time any radionuclides are released from failed canisters. The effects of gas rising through the fracture on groundwater flow are not, however, currently fully understood.

Pressure build-up and porewater displacement in the near field

The pressure of the free gas phase increases as a result of the ongoing generation of gas. In the near field, the pressure increases until gas pathways from the steel surfaces through the bentonite are created. This results in gas-induced displacement of porewater and advection of dissolved gas, although there is evidence that little water is expelled from dense saturated bentonite /Harrington and Horseman 2003/. Gas storage volumes are created, mainly within bentonite in the vicinity of the steel surfaces, but also in the EDZ. If the gas generation rate exceeds the rate of gas removal (by dissolution/diffusion) and gas volume increase (by porewater displacement), then the gas pressure further rises until capillary leakage into the host rock or along the EDZ occurs (see next two headings).

Capillary leakage and porewater displacement (incl. advection of dissolved gas) into host rock

When the gas pressure exceeds the threshold for capillary leakage (hydrostatic pressure of 4 MPa plus gas entry pressure of up to a few MPa[31] depending on the fracture transmissivity), leakage of gas into existing fractures takes place. This involves porewater displacement (moving gas front) and advection of dissolved gas within the fractures as well as diffusion of dissolved gas from the fractures into the rock matrix. The latter process quickly leads to partial saturation of the rock matrix with dissolved hydrogen gas. At higher pressures (gas entry pressure of up to 10 MPa depending on the permeability of the matrix), gas leakage also takes place into the host rock matrix. Gas leakage is assumed to be proportional to the product of the fracture transmissivity (case of fractures) or gas permeability (case of matrix) times the hydraulic gradient (Darcy's law). A conceptual model for gas transport in the repository system illustrating the various processes is shown in Figure 7-17.

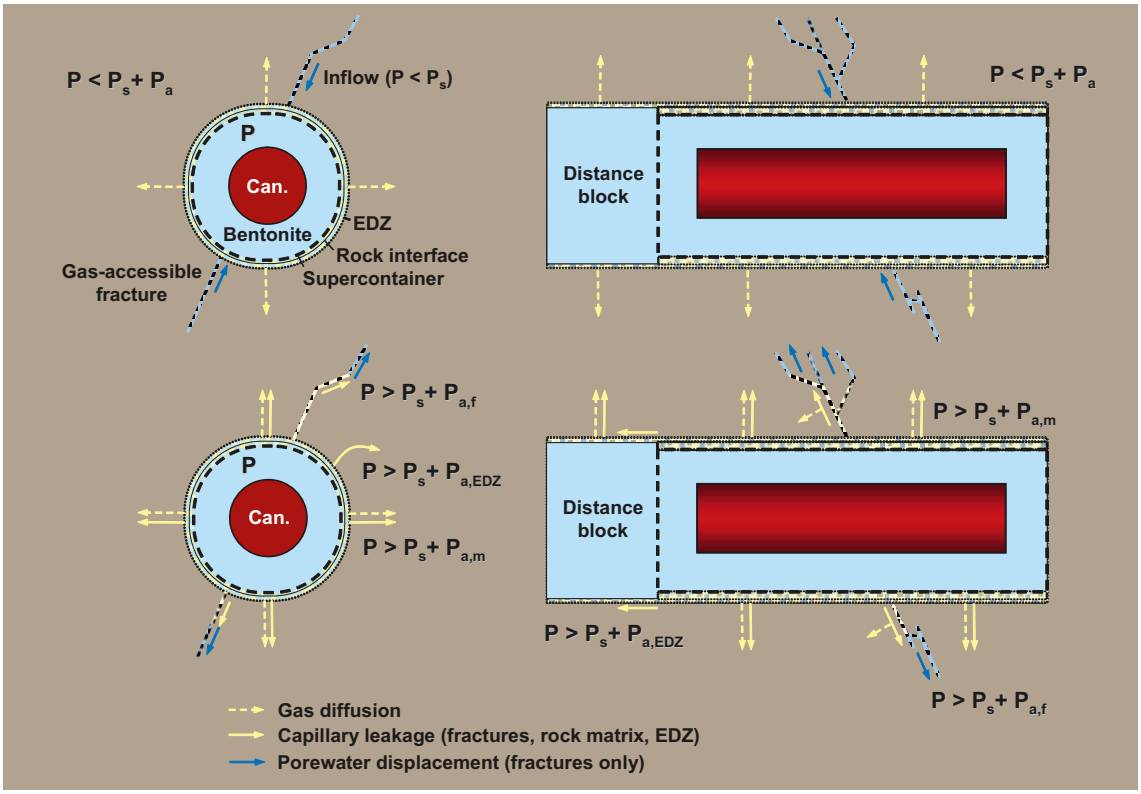

Figure 7-17. *Conceptual model for gas transport in the repository system for spent fuel at the Olkiluoto site. P_s is the groundwater pressure, $P_{a,EDZ}$ is the air entry pressure in the EDZ, $P_{a,f}$ is the air entry pressure in the fractures, $P_{a,m}$ is the air entry pressure for the rock matrix. Gas dissolution takes place in various parts of the system (see Table 7-10), but is not shown in the figure.*

[31] Because of the very complicated relationship between capillary pressure and heterogeneities and fracture transmissivity, the uncertainty on the gas entry pressure of a few MPa cannot be specified more accurately. There is still a significant margin for uncertainties between 4 MPa and the pressure at which new fractures may form or existing fractures may open, which happens around the lithostatic pressure, approximately 11 MPa.

Formation of gas pathways along the deposition drift

Pressure may further increase until the threshold pressure for the formation of gas pathways through or around the distance blocks (EDZ) is reached (gas piping). This is likely to occur from drift sections with extremely tight rock to the next drift sections where fractures of sufficient transmissivity and connectivity are present, thus allowing gas to migrate through the host rock. In the model calculations, gas leakage is assumed to occur within the fracture network of the EDZ, as soon as the gas pressure exceeds the hydrostatic pressure (4 MPa) plus the gas entry pressure within the EDZ. Gas migration along the deposition drift may be hindered or completely stopped by swelling of distance blocks. This situation is addressed by considering a separate calculational case with an impermeable EDZ. Bentonite erosion by gas piping in the post-operational phase is not likely to have any significant effect on the long-term properties of bentonite and is not considered in the model calculations. Gas escape along the axis of the deposition drift to the access tunnel system, where significant pore volumes are provided for additional gas storage, is pessimistically neglected in the model calculations.

Gas breakthrough to major geological features of enhanced transmissivity

Gas transported through the host rock will eventually reach major geological features with enhanced transmissivity, through which gas will migrate to the surface. After breakthrouh, the gas pressure in the deposiion drifts will lowly dereae.

Gas breakthrough is taken into account in the model calculations by assuming a maximum travel distance for the moving gas front in fractures, whereas gas breakthrough from the matrix is not accounted for (long-distance transport through the matrix is unlikely to occur). The detailed transport processes after breakthrough are not modelled explicitly, because they have no influence on the maximal pressure in the system. The possibility of reactivation of fractures in the near-field rock as a consequence of gas pressure build-up is discussed in Section 7.6.

Boundary conditions

One important boundary condition is provided by the gas generation rate by anaerobic corrosion of steel (supercontainer and other structural materials). The gas generation rate is mainly determined by the steel corrosion rate and by the total steel surface exposed to corrosion, but is not limited by the availability of water, except in very tight drift sections (see discussion in Section 5.7.1). The outer boundary is provided by the transport capacity of gas pathways in the near-field rock.

If the gas generation rate exceeds the rate of gas removal (by dissolution/diffusion and gas leakage) and gas volume increase (by porewater displacement) then a build-up of gas pressures will take place in the deposition drift.

Model studies/experimental studies

Simplified gas transport calculations have been performed for a KBS-3H repository at Olkiluoto, based on the processes shown in Figure 7-17 and described above. The mathematical model, input data and the results are discussed in detail in Appendix C. Here only a summary of the main findings is given.

The hydrogen gas generated by anaerobic corrosion of the supercontainer and other structural material, as well as gas entrapped at the time of closure, will dissolve in the near field pore water until the solubility limit at repository pressure is reached. Dissolved gas diffuses through the drift walls into the host rock. The pressure of the free gas phase increases as a result of the ongoing generation of gas. In the near field, the pressure increases until gas pathways from the steel surfaces through the bentonite are created. This results in gas storage volumes being created, mainly within bentonite in the vicinity of the steel surfaces, but also in the EDZ. If the gas generation rate exceeds the rate of gas removal (by dissolution/diffusion) and gas volume increase (by porewater displacement), then the gas pressure rises further.

When the gas pressure exceeds the threshold for capillary leakage (hydrostatic pressure of 4 MPa plus gas entry pressure of fractures), leakage of gas into existing fractures takes place. This involves porewater displacement and advection of dissolved gas within the fractures as well as diffusion of dissolved gas from the fractures into the rock matrix. The magnitude of the gas pressures reached in the drifts strongly depends on the gas transport capacity of fractures and may thus vary considerably along a deposition drift. Of particular importance is the hydraulic transmissivity T_{max} of the most conductive gas pathway in each supercontainer unit, because this feature is expected to dominate the supply of water and the transport of gas away from the deposition drifts. For $T_{max} \geq 10^{-10}$ m^2 s^{-1}, the supply of water is unlimited and the expected steel corrosion rate is 1 µm a^{-1}. For $T_{max} < 10^{-10}$ m^2 s^{-1}, steel corrosion may be limited by the availability of water and the steel corrosion rate may be as low as 0.1 µm a^{-1} (Section 5.7.1). In the gas model calculations, this possible reduction in the steel corrosion rate is not considered and the calculated gas overpressures may thus be somewhat overestimated.

The results of the simplified gas transport calculations indicate that:

- for $T_{max} \geq 10^{-10}$ m^2 s^{-1}, the near field is relatively quickly saturated (within roughly 10 years). Subsequently, small amounts of gas may be accumulated in the near field for as long as gas generation is ongoing, but the maximal gas pressure stays close to the hydrostatic pressure (about 4 MPa at a depth of 400 m), because the generated gas is sufficiently rapidly transported through the fractures intersecting the deposition drift.
- For $T_{max} < 10^{-10}$ m^2 s^{-1}, the near field may remain in an unsaturated state for as long as gas is being produced and the maximal gas pressure is in the order of a few MPa above hydrostatic pressure, but still below the minimal principal stress (about 9 MPa at a depth of 400 m).

In drift sections surrounded by tight host rock (characterized by hydraulic transmissivity of the most conductive pathway of the order of 10^{-12} m^2 s^{-1} in the supercontainer unit) the transport through the EDZ dominates and the gas pressure development becomes sensitive to EDZ permeability. If the EDZ permeability in tight drift sections is of the order of 10% of the measured intrinsic permeability, the pressure may rise to values near the minimum principal rock stress, as shown in Figure C-2. However, if the permeability is of the order of the measured intrinsic EDZ permeability (fully gas saturated EDZ), the gas pressure will rise only slightly above hydrostatic pressure, as discussed by /Autio et al. 2005/. In the absence of an EDZ (i.e. assuming an impermeable EDZ) the pressure will rise slightly above the minimum principal stress (Figure C-6).

In extremely tight supercontainer units, considerable pressures may thus be reached and gas pathways may be formed by reactivation of low-permeability fractures in the host rock or by penetration through or around the distance blocks. This point is further discussed in Section 7.6.

Any steel compartment plugs present in the deposition drift will contribute to the overall amount of generated gas. By definition, these gas sources are located in the vicinity of permeable fractures and thus do not significantly contribute to gas pressure build-up.

Gas transported through the host rock will eventually reach major geological features with enhanced transmissivity, through which gas will migrate to the surface. After breakthrough, the gas pressure in the deposition drifts will reach an equilibrium state. After gas generation ceases, the pressure returns to ambient pressure at repository depth at a rate determined mainly by the fracture transmissivities in each supercontainer unit.

Natural analogues/observations in nature

Not applicable.

Time perspective

The relevant time scales for gas flow/dissolution mainly depend on the hydraulic transmissivity of the most conductive gas pathway in each supercontainer unit, T_{max}. For $T_{max} \geq 10^{-10}$ m^2 s^{-1}, the relevant time frame for saturation is in the order of 10 years, followed by a phase in which small

amounts of gas may still be present. For tight drift sections with $T_{max} < 10^{-10}$ m^2 s^{-1}, the near field will remain in an unsaturated state for periods of up to several thousand years and overpressures may persist, until the generation of hydrogen gas ceases.

Handling in the safety assessment for KBS-3H

The results of the gas analysis illustrate that there is – for the purpose of the present stage of repository development – sufficiently detailed scientific understanding of gas production in and release from a repository sited in fractured host rock at Olkiluoto to make a provisional assessment of the impacts of gas on the KBS-3H disposal system. The envisaged system is considered to be robust with regard to gas build-up and release, i.e. gas pressures increase slowly and various mechanisms of transport are capable of transporting the gas gradually through the host rock or through the tunnel system without significantly disturbing the isolation characteristics of the repository system. Under extreme conditions (very tight drift sections, impermeable EDZ, corrosion not limited by water availability), reactivation of very low-permeability fractures intersecting the drift cannot be ruled out (see Figure C-6).

Given the overall large-scale permeability of the fracture network, however, gas effects are unlikely to significantly alter the hydraulic properties of the host rock and the transport of dissolved radionuclides subsequent to the migration of gas. Moreover, the release rates of radionuclides are expected to be highest in situations where a permeable fracture intersects the drift in the vicinity of a supercontainer with a defective canister. In such a situation, the gas generated by the corrosion of the supercontainer will be quickly transported away through the permeable fracture and no gas overpressures develop. The release rates of dissolved radionuclides may even be lowered should a gas phase be present at the same time as radionuclide transport occurs, due to the reduction in relative permeability for water.

On the other hand, radionuclide release rates from very tight drift sections are expected to be lower than in more permeable drift sections, even though some potential reactivation of tight fractures by gas overpressurisation may have previously taken place, allowing gas escape and subsequent radionuclide release to a more permeable fracture intersecting the drift at some distance.

In the KBS-3H Radionuclide Transport Report /Smith et al. 2007a/, the release of dissolved radionuclides is evaluated for the case of a permeable fracture intersecting the deposition drift in the vicinity of a defect in the canister (assessment case PD-BC). For such a situation, the effects of gas need not be taken into consideration, for the reasons discussed above.

During the phase of gas generation by anaerobic corrosion of the supercontainer and other structural materials, transport of volatile radionuclides in the gas phase may, however, be facilitated/accelerated. In the radionuclide release and transport calculations for KBS-3H, this is handled in two variant assessment cases for a canister with an initial penetrating defect (PD-VOL-1 and PD-VOL-2). A case addressing expulsion of contaminated water from the canister by repository-generated gas is also evaluated (PD-EXPELL, see also 2.8).

Handling of uncertainties

More detailed analyses are needed in future stages of repository development, to address the characteristics and performance of fracture network systems both in the EDZ and in the background rock with respect to gas transport. In particular, the EDZ properties at repository depth at Olkiluoto (permeability, porosity and depth of fracturing) remain somewhat uncertain. In the evaluation it is assumed that the effective permeability of the EDZ is 10% of the measured intrinsic permeability, i.e. after sealing of the drifts the EDZ may be partially sealed and the effective permeability of the EDZ may be reduced to 10% of the intrinsic permeability by various processes (e.g. bentonite swelling, mineral precipitation). However, there is not sufficient evidence to fully support the selection of this value. The properties of the EDZ are subject to a variety of rock-specific and site-specific conditions as well as to the repository layout and engineering techniques applied (rock strength, rock stress at repository level, orientation and size of the drifts, excavation method).

If the EDZ were more permeable or would extend to greater depths, as observed in the Grimsel rock laboratory /Marschall et al. 1999/, then transport of gas bypassing the distance blocks would be enhanced, leading to lower gas pressures in very tight drift sections. On the other hand, if self-sealing processes (drift convergence, bentonite swelling, calcite precipitation, bentonite intrusion) would lead to a reduction of the gas transport capacity of the EDZ, the hydraulic separation of individual supercontainer units would be more pronounced and, as a consequence, increased gas pressures in tight sections would be expected. Thus it seems necessary to further investigate the properties of the EDZ under repository-like conditions and, where possible, to include results from other studies on EDZ properties relevant to gas transport.

More detailed analysis of the properties of the fracture network in the background rock seems also necessary. In particular, there remains significant uncertainty, under which conditions the percolation threshold for gas migration is exceeded. Further analyses are needed to clarify this point. In particular, the fracture connectivity relevant for gas migration could be tested by calculating the percolation threshold for gas migration using a fracture network model along the lines of the DFN model presented in Section 7.5.1. Such an analysis would provide more reliable information on the hydraulic transmissivity of gas pathways that are to be expected at the Olkiluoto site.

7.6 Mechanical processes

An overview of mechanical processes in the geosphere is shown in Table 7-11. These processes have been identified in /SKB 1999, Rasilainen 2004/ and /SKB 2006e/ to be relevant for the subsystem "geosphere" in KBS-3V. The majority of these processes does not depend on the specific conditions in KBS-3H, because the origin of the relevant driving forces is within the geosphere or because they do not affect/are not affected by the geometry and properties of the near field. For these processes, no additions or comments to the discussions in the relevant Process Reports for KBS-3V /Rasilainen 2004, SKB 2006e/ are made.

Table 7-11. The inter-dependence of mechanical processes and identified variables in the geosphere.

Mechanical processes	Variables in geosphere												
	Repository geometry	Fracture geometry	Temperature	Groundwater flow	Groundwater pressure	Gas flow	Stress state	Matrix minerals	Fracture minerals	Groundwater composition	Gas composition	Structural and residual materials	Saturation
Displacements in intact rock			×				×	×					
Reactivation – displacements along existing discontinuities		×			×		×	×	×				
Fracturing		×	×		×	×	×	×	×				×
Creep		×	×		×		×	×	×				
Surface weathering and erosion		×	×				×	×	×	×			×
Erosion/ sedimentation in fractures		×		×	×	×			×	×		×	×

Mechanical processes in the geosphere are the same for the KBS-3H and 3V but the consequences to the near field are different. The following processes thus need to be discussed (sections where the issues are addressed are indicated in brackets):

- shear displacements along discontinuities (Section 7.6.2)
- rock spalling (Section 7.6.3)
- EDZ around deposition drifts (Section 7.6.3)
- gas-induced fracturing of the near-field rock (Section 7.6.3)
- bentonite erosion into fractures (Section 7.6.6)

7.6.1 Displacements in intact rock

Overview/general description

A discussion of displacements in intact rock at Olkiluoto is given in SR-Can Geosphere Process report /SKB 2006e/ and in /Rasilainen 2004/. There is no relevant difference in processes related to displacements in intact rock between KBS-3V and 3H.

Handling in the safety assessment for KBS-3H

As proposed in the Geosphere Process Report of SR-Can /SKB 2006e/, the displacements in intact rock do not have *per se* any direct impact on the safety assessment unless they are accompanied by fracturing and fracture displacement. However, all rock mechanics phenomena start with displacements of the intact rock that then manifest themselves as more macro-scale phenomena where existing fractures play a major role.

7.6.2 Reactivation – displacements along existing discontinuities

Overview/general description

The general processes and conditions affecting displacements along existing fractures and fracture zones at Olkiluoto are discussed in /Rasilainen 2004/ (see pp. 105–107 for displacements during the construction and operation phase and pp. 109–110 for the post-closure phase). This general process description is not repeated here. The impact of rock shear displacements on the buffer and the canister are discussed in Section 4.6.1 and Section 3.6.1, respectively.

The focus of the present section is on processes and conditions that are specific to KBS-3H, namely shear displacements on fractures or fracture zones intersecting the deposition drift that may give rise to mechanical forces on the horizontally emplaced canisters. Although the process for shear movement is the same, different sets of fractures are of relevance as the canister orientation and the orientation of rock stresses are different.

Among all potential causes for shear displacements, post-glacial earthquakes, which are expected to occur during or shortly after any future deglaciation, have the potential to give rise to the largest displacements and so are of greatest concern. Major deformation zones capable of accommodating significant slip should be readily identified and KBS-3H drifts will not be constructed within, or in the immediate vicinity of such zones. An earthquake occurring on a major deformation zone may, however, give rise to stress changes in the rock that trigger the reactivation of smaller-scale fractures that cannot be avoided when constructing the drifts. Efforts will be made to avoid fractures at canister emplacement locations that could undergo shear movements that could damage the canisters in the event of a large post-glacial earthquake. The extent to which it will be possible to identify and avoid fractures capable of undergoing potentially damaging displacements is currently under investigation for both the KBS-3V and KBS-3H. The amount of shear movement that will occur as a result of future post-glacial earthquakes is uncertain, but is related to fracture size. The size of fractures will, to some (uncertain) extent, be correlated to their transmissivity, and the more transmissive fractures (and fractures with the highest initial inflow) will be avoided for reasons outlined below and in Appendix B.2 of the Evolution Report /Smith et al. 2007c/.

Due to the higher stiffness of canisters in the longitudinal direction, shear displacements on reactivated flat (subhorizontal) fractures across the deposition holes are most relevant for KBS-3V, whereas in KBS-3H canisters are likely to be more vulnerable to shear displacements on steep (subvertical) fractures perpendicular to the axis of the deposition drift. Subhorizontal fractures are predominant at the Olkiluoto site /Andersson et al. 2007/. /La Pointe and Hermanson 2002/ discuss rock shears and secondary rock movements at the site and estimate the probability of various types of fracture movements (see below). In principle, if its size and the shear movement it underwent were sufficiently large, a single subhorizontal fracture could affect multiple KBS-3H canisters (see Figure 3-3). It is, however, considered likely that any such fracture would be readily detected and that portion of the drift affected by it would be excluded for canister emplacement. Thus, the main concern for KBS-3H remains movement on subvertical fractures. There are also potentially significant coupled hydro-mechanical effects due to glaciations that could possibly open fractures, including hydraulic jacking as well as highly anistropic stress field in relation to deglaciation, as discussed in Section 9.4.5 of SR-Can Main report /SKB 2006a/.

The amount of movement on such fractures is a function of a number of factors including:

- the change of shear stress acting on the plane of the deformation zone on which the earthquake occurs;
- the distance of the reactivated fracture from the epicentre of the earthquake;
- size and orientation of the reactivated fractures;
- the density of reactivated fractures; and
- friction on the fracture surfaces.

These factors are discussed in more detail in the following sections, with particular emphasis on aspects with a different significance for, or potential impact on, KBS-3H compared with KBS-3V.

Boundary conditions

The boundary conditions are determined by the mechanical properties of the rock surrounding the deposition drift, in particular the properties of fractures that may undergo shear displacements in the future, and by the mechanical properties of the engineered barriers (mainly the buffer).

Model studies/experimental studies

Modelling studies investigating the relationship between the factors above, including orientation, and the amount of shear movement on fractures, have been carried out by /La Pointe et al. 1997/ and /Munier and Hökmark 2004/. The latter authors have extended the earlier work by /La Pointe et al. 1997/ and addressed some of the issues of model simplification pointed out in /La Pointe et al. 2000/. In these various studies, the rock is modelled as a linearly elastic fractured medium. The earthquake is represented either by enforcing a movement along the deformation zone (the primary fault) or by letting the movement on the primary fault occur as a result of stresses and primary fault properties. The resulting movement on reactivated ("target") fractures is then evaluated. The analyses are not site specific; the parameter values and model assumptions used are applicable to a range of locations in Sweden and Finland, including Olkiluoto.

Although the orientation of major deformation zones with respect to the major horizontal stress affects their likelihood of undergoing shear displacements caused by post-glacial earthquakes, the results of these studies indicate that there is no simple and generic functional relationship between the orientation of fractures reactivated by these earthquakes and the amount of shear

movement that they undergo[32]. It appears, in any case, that orientation is a much less sensitive parameter than, say, the change on shear stress acting on the plane of the deformation zone on which the earthquake occurs or the size of the reactivated fracture, and orientation effects are likely to be small compared with the uncertainties in other factors such as these (see, e.g. Figure 2-2 in /La Pointe et al. 2000/.

Modelling studies, together with other more qualitative arguments such as empirical knowledge of earthquake-induced damage on tunnels summarised in /Bäckblom and Munier 2002/, have been used by /Munier and Hökmark 2004/ to propose conservative respect distances to major deformation zones that can be used to determine whether fractures above a certain size (i.e. the minimum size that can be assumed to be detected during construction) can intersect a KBS-3V deposition hole used for canister emplacement. The respect distances are based on the 0.1 m failure criterion, and take account of the width of the "transition zones" that typically lie on either side of the core of a deformation zone. Given the insensitivity of modelled displacements to fracture orientation, and the conservativeness of the chosen respect distances, the distances should be equally applicable to fractures intersecting a KBS-3H drift at a canister emplacement location.

A methodology for calculating the probability of a KBS-3V canister location being intersected by a fracture exceeding a prescribed size, assuming that such fractures are not detected and avoided when the canisters are deposited, is given in /Hedin 2005/. Hedin applied the method using data from the Forsmark site in Sweden. The method has also been applied to KBS-3H canister locations at Olkiluoto, and it can be easily extended to evaluate the special case of several adjacent KBS-3H canisters in a deposition drift being affected by the same fracture (see Appendix B in the KBS-3H Evolution Report by /Smith et al. 2007c/).

The calculations show that about 1 out of 190 (or 16 out of 3,000) horizontally emplaced canisters will be affected by a potentially damaging fracture, compared with about 1 out of 150 (or 20 out of 3,000) vertically emplaced canisters. The difference is largely due a lower sensitivity of KBS-3H on sub-horizontal fractures. The possibility of several adjacent horizontally deposited canisters being affected by displacement on the same fracture or fractures is indicated to be very low (about 1 in 2,800 for canister pairs and about 1 in 8,300 for canister triples). In these calculations, the key properties are the density and length scale of fractures that may potentially shear rather than the hydraulically active fractures used in the hydro-DFN model.

The marginal probability of encountering an earthquake of sufficient magnitude to induce damaging movements on these fractures at Olkiluoto in a 100,000 year time frame has been estimated at 0.02 (Table 5-8 in /La Pointe and Hermanson 2002/). The expectation value of the number of canisters damaged by rock shear in a 100,000 year period is thus $16 \times 0.02 = 0.32$ (or 1 canister in 300,000 years).

Scoping calculations presented in Appendix B of the KBS-3H Evolution Report by /Smith et al. 2007c/ show the sensitivity of the expectation values of the total number of canister positions that are intersected by potentially damaging fractures, to:

r_{max} – the maximum radius of fractures that are assumed to escape detection (a base case value of 500 m is assumed)

d_{crit} – the critical shear displacement at a canister position, above which damage is assumed to occur (a base case value of 0.1 m is assumed).

The calculations show how the expectation values of the total number of intersected canister positions increases with the threshold size for fracture detection, and decreases with the threshold shear displacement (note that, for d_{crit} – 0.1 m, fractures of radii less than 100 m are assumed not to have the potential to cause damage).

[32] /La Pointe et al. 2000/ note, however, that, consistent with linear elastic theory, their model indicates that the "worst" orientation for a fracture (i.e. that tending to undergo the largest shear movements) is to make a solid angle of 45° with the deformation zone rupture direction.

The expected number of canisters that could potentially be damaged by rock shear in the event of a large earthquake (16 out of 3,000) is a preliminary result since there are some significant uncertainties associated with these values that could lead to them giving either an underestimate or an overestimate of the actual likelihood of damage. Key assumptions and sources of uncertainties are detailed in Section 7.4.5 of the Evolution report /Smith et al. 2007c/.

Natural analogues/observations in nature

A compilation of natural analogues/observations in nature is given in the Geosphere Process report for SR-Can /SKB 2006e/. From this compilation it is concluded, that clear correlations exist between the measured shear displacement and the lengths of the structures where these displacements have taken place.

Time perspective

Shear displacements induced by post-glacial earthquakes are expected to occur during or shortly after any future deglaciation, i.e. not before about 75–100 ka after present, depending on the climate scenario envisaged /Cedercreutz 2004/.

Handling in the safety assessment for KBS-3H

According to the methodology proposed in the context of a KBS-3V repository in Sweden in /SKB 2004b/ and in more detail in /Munier and Hökmark 2004/, canisters should not be placed in the vicinity of major deformation zones. Additionally, canister deposition positions should not be intersected by fractures above a certain size to avoid the possibility of secondary shear displacements larger than typically 0.1 m, which has been demonstrated to provide a reasonable margin for canister failure /Börgesson et al. 2004/. Given the insensitivity of modelled displacements to fracture orientation, and the conservativeness of the chosen respect distances for KBS-3V, the distances should be equally applicable to fractures intersecting a KBS-3H drift at a canister emplacement location.

In the KBS-3H Radionuclide Transport Report /Smith et al. 2007a/, large shear displacements are considered to be one of the most important causes for canister failure. The number of failed canisters due to post-glacial faulting depends on the capability of detecting fractures possibly leading to large shear displacements, ranging from zero canisters (if all fractures can be detected and respect distances are properly taken into account) to about 16 canisters (ignoring fractures prone to large shear displacements). Two assessment cases concerning canister rupture due to rock shear are calculated in the Radionuclide Transport Report /Smith et al. 2007a/:

- Base case for canister failure due to rock shear (RS-BC)
- Glacial meltwater present at repository depth at the time of rock shear (RS-GMW).

The potentially significant hydromechanical effects due to glaciation, including hydraulic jacking as well as highly anistropic stress field in relation to deglaciation that could possibly open fractures are addressed by variants to the base case (PD-LOGEOR and CC-LOGEOR), in which the geosphere resistance is lowered by a factor of 10 (WL/Q=5,000 a m^{-1} instead of 50,000 a m^{-1}).

Handling of uncertainties

As discussed in the conclusions of /Hedin 2005/, there are several uncertainties that are not treated in the approach used to estimate canister/fracture intersection frequencies, or are treated conservatively. These include the likelihood of occurrence of faulting in the vicinity of a repository, which needs to be considered in a post-glacial climate phase. Furthermore, it is assumed that all fractures reactivate as if their location and angular orientation relative to the primary earthquake were unfavourable. All fractures distant from the earthquake-generating

fault are pessimistically assumed to slip by an amount determined only by the secondary fracture size. In the radionuclide release and transport calculations addressing this scenario, it is also pessimistically assumed that there are fractures capable of slipping more than 0.1 m that are not detected and avoided. It should also be noted that the criterion that the canister may fail if slips are greater than 0.1 m is conservative, particularly if slip occurs in a plane approximately parallel to, rather than normal to, the canister axis.

Uncertainties in the calculation of the number of canisters potentially affected by a rock shear movement are discussed in Section 7.4.5 of the Evolution report /Smith et al. 2007c/.

7.6.3 Fracturing and spalling

Overview/general description

The mechanisms of fracturing of the intact rock at Olkiluoto upon loading and the mechanical properties of created fractures are discussed in /Posiva 2005/ and /Rasilainen 2004/. These issues are not specific to KBS-3H, and the discussion is not repeated here.

In contrast, rock spalling, the excavation-induced fracturing (formation of excavation damaged zone or EDZ) and the gas-induced fracturing around cavities depend on the repository layout (geometry, materials, thermal load, mechanical properties), on the excavation technique and on bedrock properties (in situ stress, intact rock mechanical strength). These types of deformations are irreversible.

High-stress induced brittle failure (rock spalling) can be caused by high initial rock stresses. In cases where the initial rock stress is not sufficient to cause spalling, there is the possibility that spalling occurs at a later stage due to the additional thermal load (radiogenic heat). This type of fracturing may occur in cases where slow water supply delays the development of a supporting bentonite swelling pressure. Experimentally, it has been observed that very small confining stresses, e.g. by partial development of bentonite swelling pressure, are sufficient to suppress initiation and propagation of brittle failures /SKB 2006e/.

A conservative scoping calculation in Appendix B.4 of the Evolution Report indicates that corrosion of the insert could lead to an increase in buffer density around the canister to about 2,160 kg m^{-3}, which could give swelling pressures of around 10 MPa or greater, depending on the salinity of the groundwater (see Figure 4-7 in /SKB 2006a/). A modelling study by /Lönnqvist and Hökmark 2007/ found that, for a KBS-3H repository at Olkiluoto, a pressure on the drift wall of 10 MPa or more might open a pre-existing horizontal fractures intersecting the drift at mid-height, although the effects are expected to be small in terms of increase in fracture aperture and distance from the drift wall to which such effects extend, even at pressures of 20 to 25 MPa.

The EDZ around a KBS-3H deposition drift results from the impact of excavation and subsequent stress relaxation. The rock around the deposition drifts undergoes deformation caused by stress relaxation, which includes elastic deformations of rock and displacements of fractures intersecting the deposition drifts.

The stress state at the Olkiluoto site has been determined for different depths (see Appendix A). The principle of the layout adaptation is to align the drifts as much as possible with the direction of the maximal principal stress to enhance mechanical stability. Some low stress areas may be present at the entrance of the KBS-3H deposition drifts (niche), especially if fractures exist in these areas, and more extensive rock support may be required in such cases.

In the framework of the analyses of coupled hydro-mechanical processes affected by gas, the relevant mechanical quantity is the minimal principal stress (σ_3). At a depth of 400 m, σ_3 is about 9 MPa, with a dip of about 55° towards NW (320°). Fracture planes oriented perpendicular to σ_3 (i.e. sub-horizontal planes dipping from NW to SE) experience thus the lowest normal effective stress and are prone to be reactivated first by gas pressure build-up.

Boundary conditions

The EDZ is comprised of two components: an inevitable component and an additional component. The inevitable component is that caused by alteration of the rock stress state and reducing the internal drift pressure to atmospheric (i.e. any damage to pre-existing fractures, any spalling and damage caused by water inflow). The additional component is that caused by the excavation method, i.e. blasting or the use of a tunnel boring machine. The extent and properties of the EDZ depend on bedrock properties and boring technique, especially cutter head design. The cutter heads used in deposition hole boring can be modified in several ways to produce different types of damage if desired. Rock spalling can occur due to high initial stresses or thermal loads (heat generation by radioactive waste).

The boundary conditions for gas pressure build-up are the rate of gas generation by anaerobic corrosion of steel (Section 5.5.1) and the properties of the engineered barriers and near-field rock (gas storage/dissolution capacity, gas transport capacity, see Section 7.5.1).

Model studies/experimental studies

Rock spalling

In /SKB 2006ae/ a number of studies on rock spalling are discussed, including observations from the isothermal phase of the APSE experiment and thermomechanical elastic 3D model calculations (code 3DEC) of the stress state around a KBS-3V deposition hole. A seminal report on the underground stability with respect to wedge and spalling at Forsmark, Simpevarp and Laxemar sites by /Martin 2005/ utilised a probability-based method taking into account the in situ rock mass spalling strength to assess the risk of spalling. A number of these studies suggest that rock spalling may occur in KBS-3V deposition holes at a depth of 500 m as a result of the initial stress conditions and/or as a result of the expected heat load, provided that there is no support from swollen bentonite. Recordings of acoustic emission data as well as the visual inspection of the rock walls during the APSE experiment supported the hypothesis that very small confining pressures (in the order of 150 to 200 kPa) are sufficient to suppress initiation and propagation of brittle failures.

The most recent 3DEC model calculations for KBS-3V deposition holes indicate that rock spalling during the operational phase is unlikely to occur, if the stresses remain below the spalling threshold, which is assumed to be 120 MPa or 55% of the uniaxial compressive strength in the case of Forsmark /Hökmark et al. 2006/. After emplacement, and provided that bentonite swelling pressure is at least partially developed, rock spalling is also not likely to occur. Without the support of the swollen bentonite, however, thermally-induced spalling is very likely to occur after some time of heat production (within years to decades or even centuries). Such situations may be encountered in very tight drift sections, where water saturation of the buffer is significantly retarded. Currently, there is no way of directly quantifying the actual shape and depth of the zone with thermally induced failures.

For KBS-3H, thermomechanical model calculations using 3DEC have been performed /Lönnqvist and Hökmark 2007/. Due to alignment of the deposition drifts with the major stress component and thanks to the smaller diameter and simpler geometry of the deposition, KBS-3H is less prone to thermally induced spalling compared with KBS-3V. The provisional results show, however, that in “tight” drift sections, rock spalling will most likely take place after some time of heating. It turns out that the relative orientation of the stress tensor with respect to the drift axis is one of the key parameters determining the mechanical behaviour of the bentonite/rock interface.

Boundary element modeling results of two KBS-3H drifts, niches and a transport tunnel (see Figure 7-18) show that stress values in the drifts are moderate and below the spalling strength of 65 MPa /Hakala et al. 2008/. Compared with KBS-3V in which stress concentrates not only around the horizontal access tunnel but also around the deposition hole and these interact to produce stresses in the vicinity of the lip of the deposition hole, KBS-3H drift is thought to be mechanically more stable because of the absence of vertical deposition holes. However, the

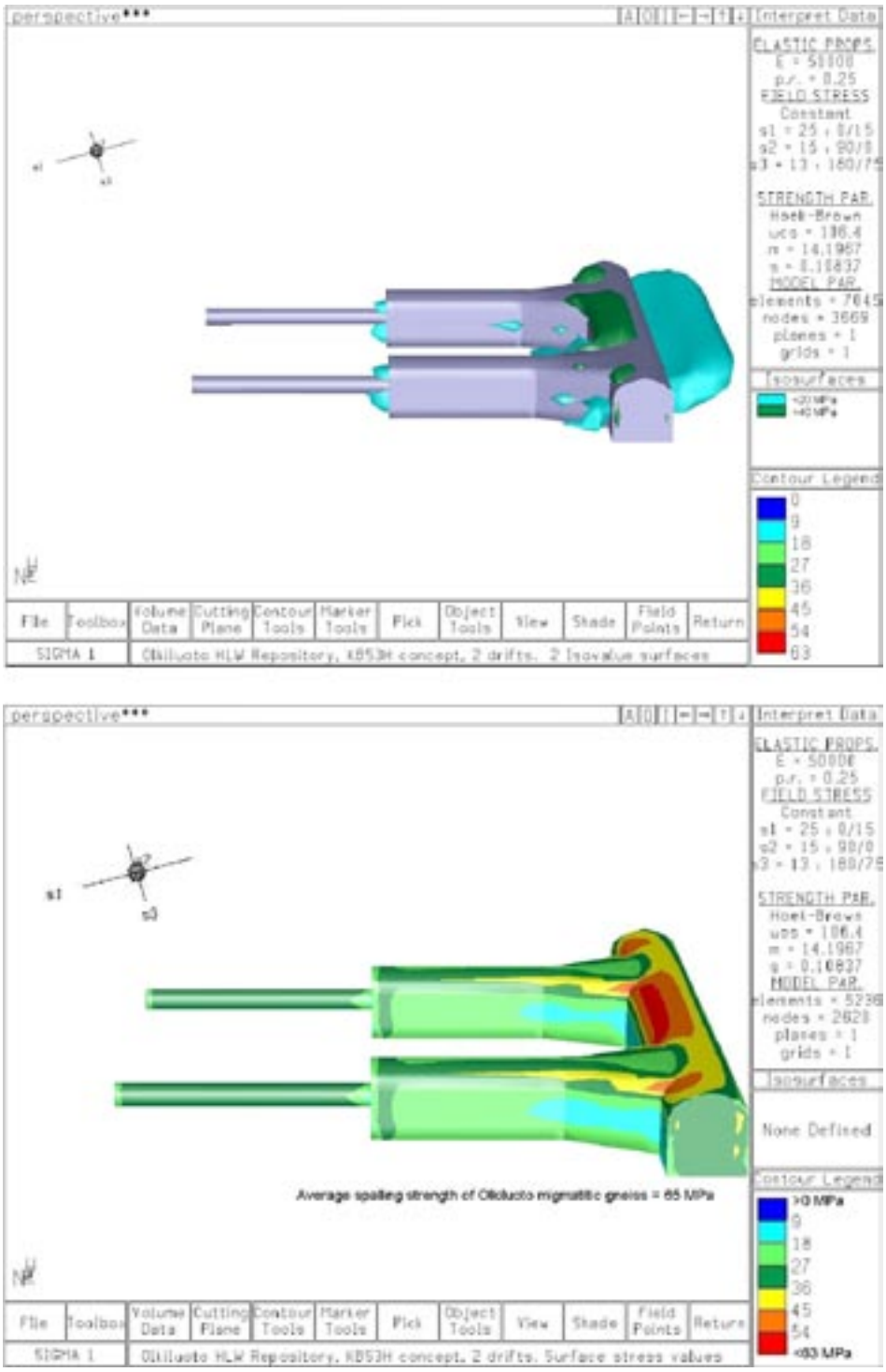

Figure 7-18. *Top: Illustration of two isovalue surfaces (<20 MPa and >40 MPa) of the major principal stress component. Bottom: stress values on the excavation surfaces, along the transport tunnel and two drifts, preceded by their deposition niches (niche dimensions are according to the latest design information to be presented in the Design Description 2007). All values in the figure are in MPa. The underlying assumption of the layout adaptation is that the drifts are planned subparallel to* σ_1*. The figure shows the rock stress is moderate along the drift and is somewhat higher along the transport tunnel. Stress values in the drift are below the average spalling strength of 65 MPa /Hakala et al. 2008/. Figure provided by A.Lehtonen (Saanio & Riekkola Oy).*

access tunnels for KBS-3V can still be suitably aligned (parallel or sub-parallel) to the major principal stress component (σ_1) to minimise this lip stress concentration (even though nothing can be done in this regard with the vertical deposition hole with its fixed orientation). In KBS-3H, some lower stress areas may be present at the interface between the deposition niche with larger radius and the part of the deposition drift with a smaller radius, see Figure 7-18. Higher stresses are present in the diagonally opposite top and lower corners of the transport tunnels, which are planned to be sub-perpendicular to σ_1. More extensive rock support (rock bolts, shotcrete, wire mesh) may be required in these areas, especially if they intersect existing fractures or lower strength rock types, to prevent possible damage/failures. These tunnels are farther away from the canisters but will also be subjected to thermal stresses to some extent. However, the function of the transport tunnels is different than that of the supercontainer-bearing sections of the drifts.

Transport tunnels will also be open for longer times, thus they also require rock support and more operational safety features. Design solutions to minimize spalling are currently under development.

Formation and properties of excavation damaged zone (EDZ)

The results presented in this report are based on deposition hole boring in the VLJ Research Tunnel at Olkiluoto and Äspö Hard Rock Laboratory where rotary crushing type boring was used. If other boring techniques or cutter head designs are used, the damage may differ from that seen at Äspö and Olkiluoto. The same applies to boring in different type of bedrock although the differences might not be significant. Cluster boring based on using water hydraulic hammers was tested in Oslo and the damage was studied in laboratory. The study indicated that the porosity of the damaged rock was similar to that caused by rotary crushing at Äspö although there were some qualitative differences in larger aperture microfracturing. The results were considered merely indicative because of large heterogeneity of samples and low state of stress at site.

The micro fracturing of samples taken from the experimental deposition holes in the VLJ Research Tunnel at Olkiluoto and in the underground Hard Rock Laboratory at Äspö were investigated by using the ^{14}C-polymethylmethacrylate (^{14}C-PMMA) method and scanning electron microscopy (SEM). The porosity, diffusivity and permeability of samples taken from the experimental deposition holes in the VLJ Research Tunnel at Olkiluoto were also measured by using He-gas method.

The boring techniques used at Olkiluoto and Äspö have been described in /Autio and Kirkkomäki 1996, Andersson and Johansson 2002/, respectively. The results of previous studies on the properties of EDZ have been presented in /Autio et al. 2003, Autio 1996/. The properties of the most damaged thin zone close to the surface of deposition holes at Olkiluoto have been studied in more detail by /Montoto et al. 2003/.

Porosity, microfracturing, fracture apertures

A total of 12 samples were taken from the experimental deposition holes in Prototype Repository Tunnel in Äspö HRL. The samples representing Äspö diorite were taken from different depths and orientations with respect to the stress field. The extent and structure of the EDZ was also very similar to that found in the experimental deposition holes in the VLJ Research Tunnel at Olkiluoto. For reference, the porosity of the undamaged rock at Äspö determined by using ^{14}C-PMMA method was 0.2–0.3% and in the VLJ Research Tunnel 0.1–0.2%.

The porosity was determined from autoradiographs (Figures 7-19, 7-20 and 7-21) by using the ^{14}C-PMMA method. The depth of the damaged zone was determined by using porosity profiles (Figure 7-22). According to the results the EDZ adjacent to the walls of the experimental deposition holes can be divided into three different zones, starting from the excavated surface as follows:

- Crushed zone (adjacent to the excavated surface, thickness 4 mm)
- Microfractured zone (beneath the crushed zone, thickness 5 mm)
- Zone of minor damage (beneath the microfractured zone, thickness 14 mm).

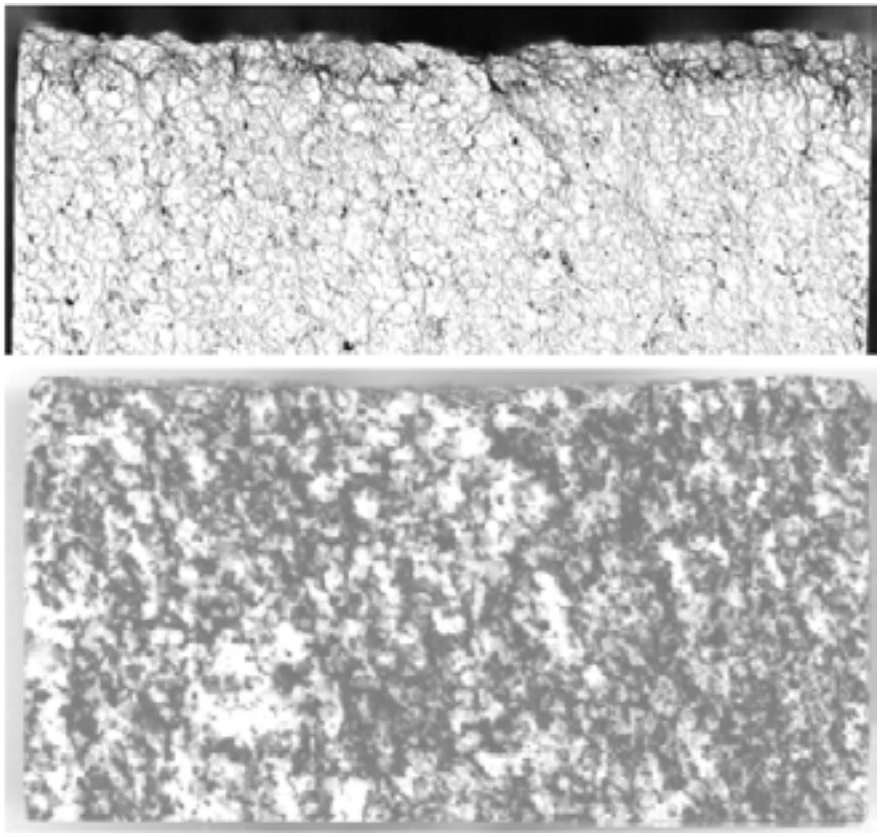

Figure 7-19. *Photo image of rock sample from the VLJ Research Tunnel at Olkiluoto (below) and corresponding autoradiograph (above). The section is perpendicular to the axis of the experimental deposition hole, the excavated surface being on top. The width of the sample is 94 mm. Different shades of gray on the autoradiograph correspond to different porosities: the darker the shade, the higher the porosity. From /Johnson et al. 2005/.*

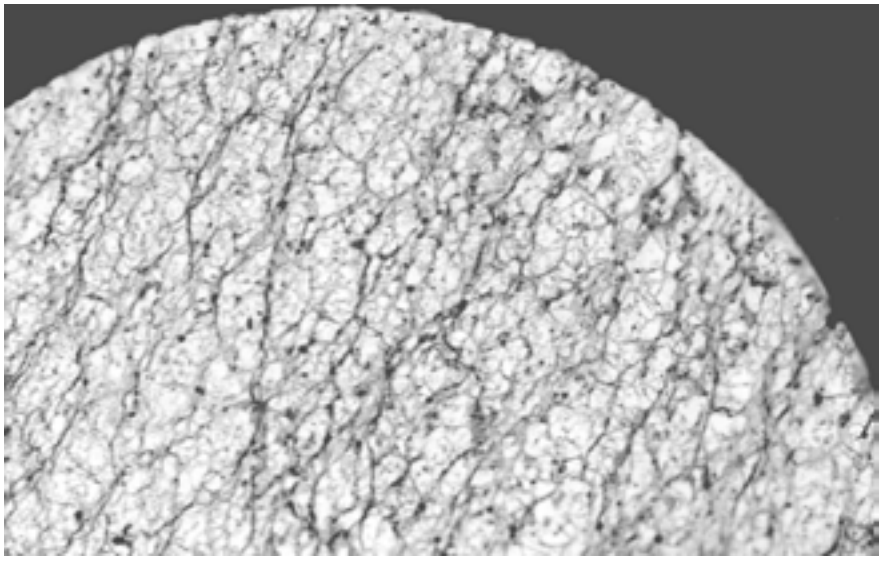

Figure 7-20. *Autoradiograph of rock sample from the VLJ Research Tunnel at Olkiluoto. The section is parallel to the surface of deposition at depth of 7 mm from the surface. The height of the sample is 47 mm. From /Johnson et al. 2005/.*

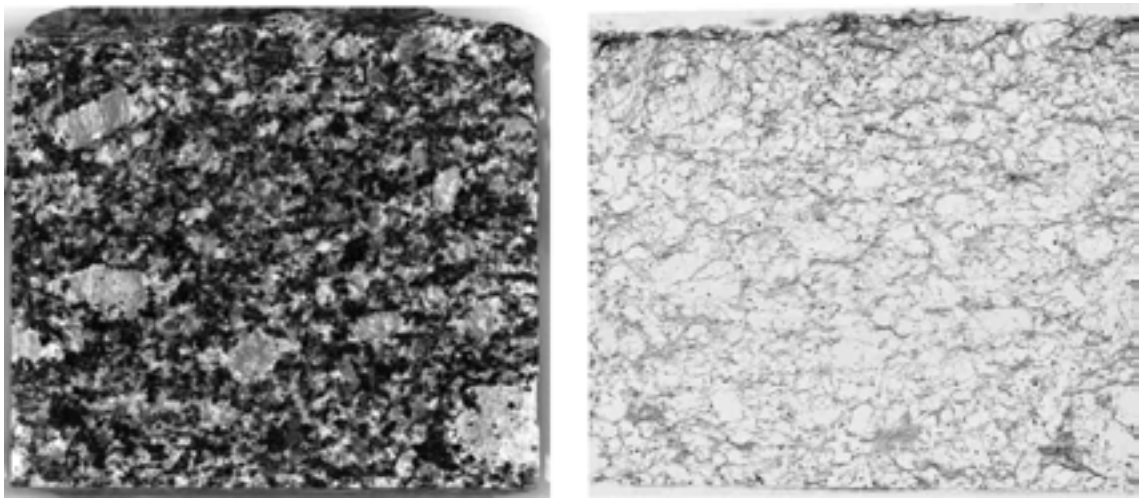

Figure 7-21. *Photo image of rock surface (left) and corresponding autoradiograph (right) from Äspö HRL. The section is perpendicular to the axis of experimental deposition hole the excavated surface being on top. The width of sample is 94 mm. From /Johnson et al. 2005/.*

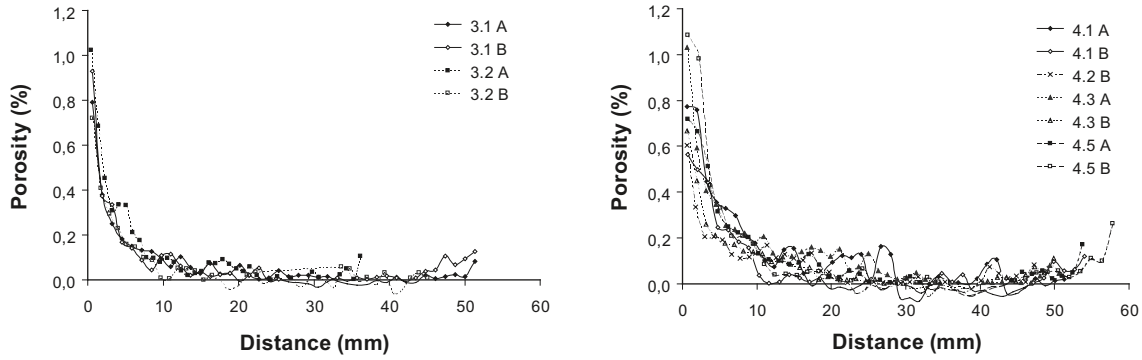

Figure 7-22. *Additional porosity in rock determined by using ^{14}C-PMMA-method with respect to the distance from the surface of the experimental deposition holes 3 and 4 in the Prototype Repository tunnel at Äspö Hard Rock Laboratory. The porosity of undamaged rock was 0.26%. From /Johnson et al. 2005/.*

- Crushed zone

The thickness of the crushed rock zone is 4 mm and the mean **additional** porosity in the crushed zone is 0.5% (0.55% ± 0.17). The porosity of the crushed zone immediately adjacent to the surface of deposition holes cannot be determined accurately by using ^{14}C-PMMA method and porosities shown in profiles (e.g. in Figure 7-22) in the first few millimetres of the crushed zone are lower than true porosities. Therefore complementary characterization of this zone was carried out fractographically by using image analysis /Montoto et al. 1999, 2003/. According to fractographic characterization of five samples from the VLJ Research Tunnel, the porosity of the first two millimetres is in order of 2–4%.

According to fractographic characterization of five samples from the VLJ Research Tunnel /Montoto et al. 1999, 2003/ the aperture of 90% of the fracture population is less than 5.4 µm. The over 5.4 µm aperture microfractures, which form 10% of the fracture population in the crushed zone, are located randomly in the crushed zone. Fractures with apertures larger than 10 µm are mainly parallel to the excavated surface. These over 10 µm aperture fractures are not directly connected to each other and do not form a continuous network of microfractures.

However, these larger aperture fractures are connected by under 5 μm aperture fractures as seen in Figures 7-23 and 7-24. Microfractures with apertures larger than 5.4 μm are mainly located from the excavated surface to a depth of 2 millimetres.

The mean fracture aperture in the crushed zone is approx. 2 μm and the quantity of microfractures with aperture from 2.17 to 5.4 μm is about 35% of the fracture population, whereas the quantity of microfractures with aperture from 5.5 to 10.8 μm is only few percent of the population (see Figure 7-26 for example). Over 90% of the microfracturing appears as intragranular fracturing in felsic minerals.

The mean crack specific surface S_v /Montoto et al. 2003/ ranges from 0.06 adjacent to the surface of the deposition hole to 0.02 μm^{-1} at the depth of few millimetres from the surface**.**

In the crushed zone from hole wall to a depth of 4 mm all the mineral grains were fractured according to qualitative evaluation /Autio et al. 2003/ and both intra- and intergranular fracturing was abundant. The most prominent fracturing in the crushed zone was oriented parallel to the hole surface at depth from 1 to 5 mm as seen in Figures 7-23, 7-24 and 7-25. However the parallel orientation was not quantified with confidence by using the fractographic characterization, although some results implied it as shown in Figures 7-26 and 7-27. The apertures of these fractures varied between 10 and 30 micrometers. Brittle quartz grains were crushed in the vicinity of the hole wall and lamellaes of biotites were opened and bended.

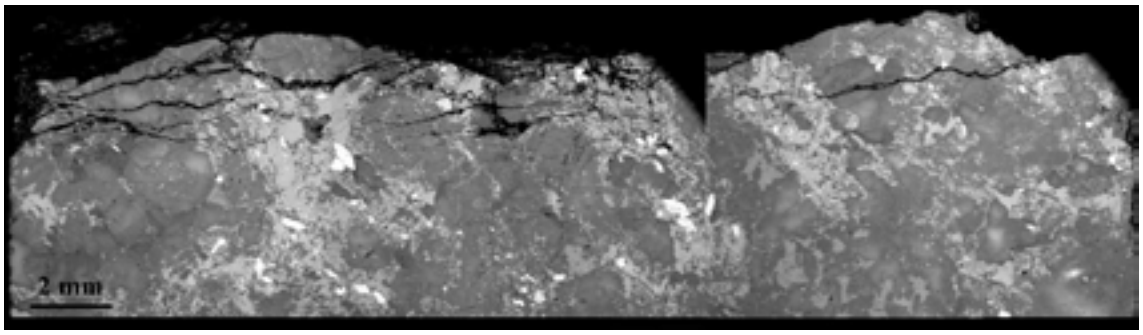

Figure 7-23. *Overview of crushed area. BSE images of Sample 4.3A showing fractures extending parallel to hole wall surface. The fracture apertures were detected to be tens of micrometers. Magnification is 10x. From /Johnson et al. 2005/.*

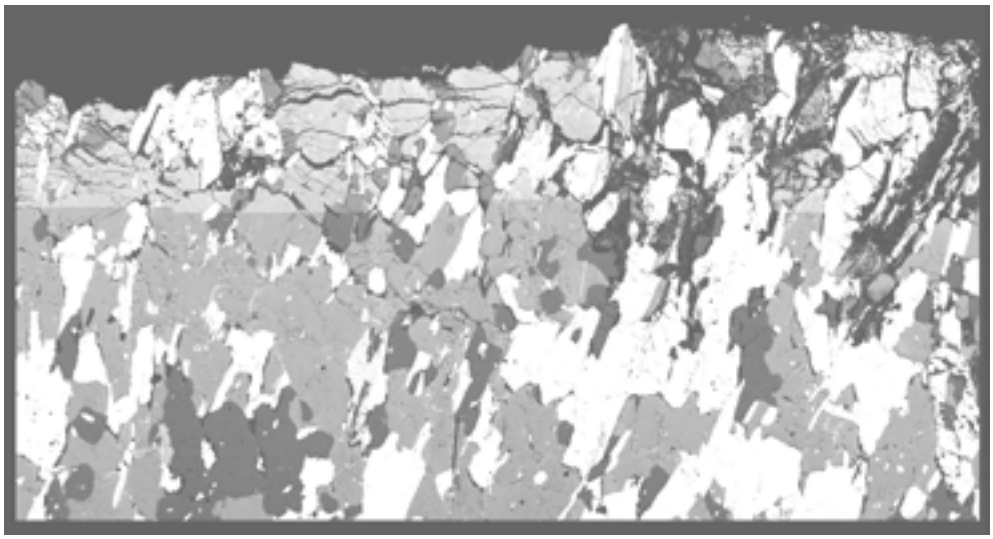

Figure 7-24. *Scanning electron microscope image of a section taken perpendicular to the disturbed surface (disturbed surface at top). The width of the image is approx. 7 mm. From /Johnson et al. 2005/.*

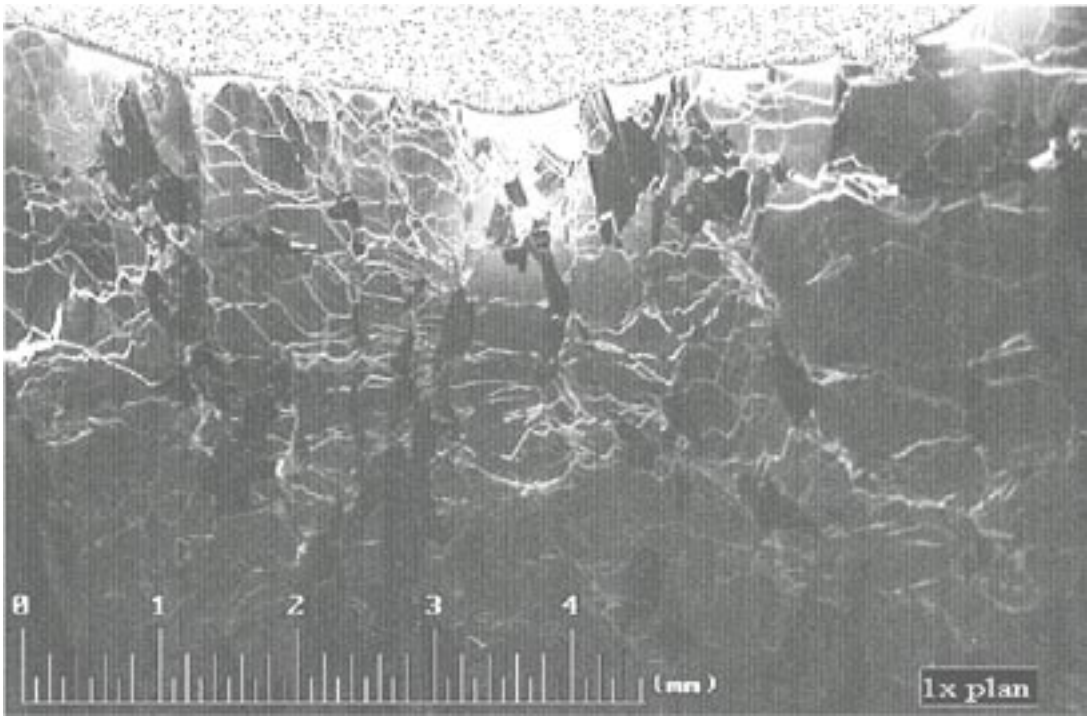

Figure 7-25. *Fluorescent thin section image taken perpendicular to the disturbed surface (disturbed surface at top). From /Johnson et al. 2005/.*

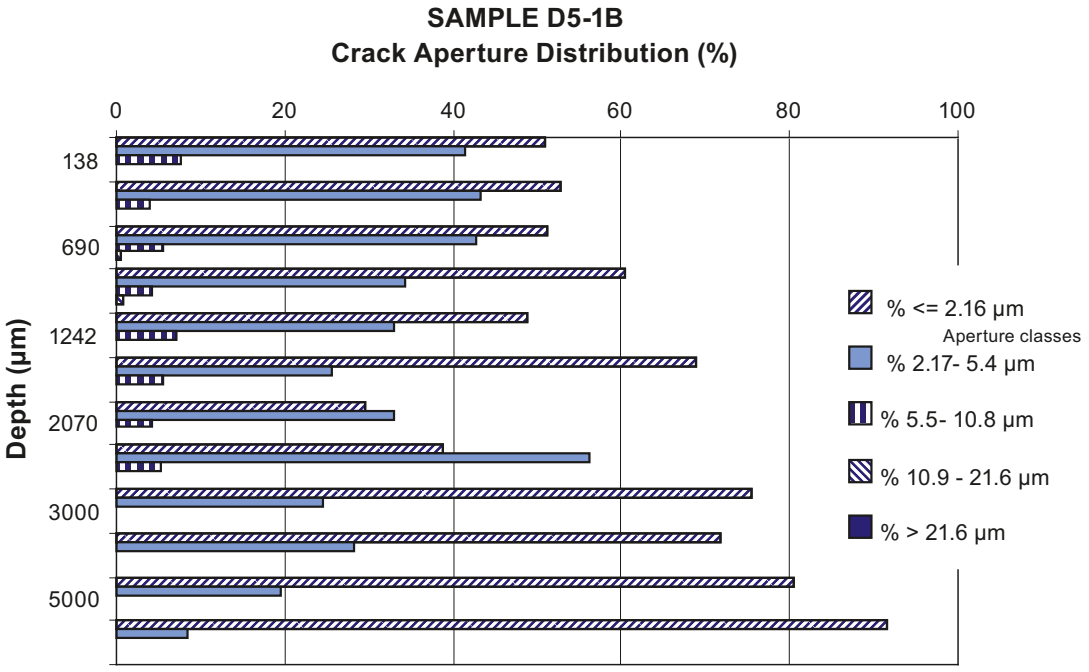

Figure 7-26. *Fracture aperture distribution at the Olkiluoto Research Tunnel on the basis of microscopy and image analysis /Montoto et al. 1999/.*

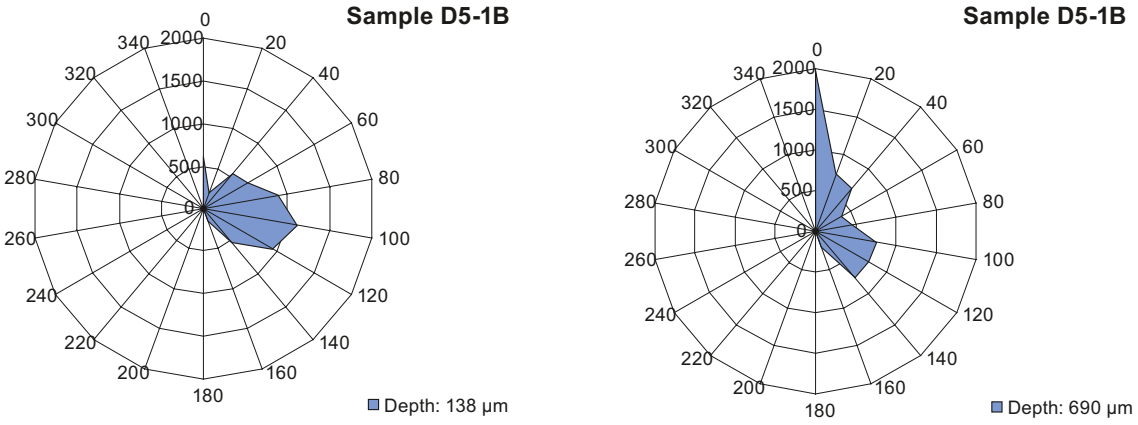

Figure 7-27. *Examples of fracture orientation at the Olkiluoto Research Tunnel with respect to sum of fracture traces in µm at two different depths (0.138 and 0.690 mm). Fracture orientation is calculated with respect to the direction of the excavated surface (0° is parallel to surface) /Montoto et al. 1999/.*

The difference between the structure of minerals in the crushed zone and undisturbed rock is clear. The apertures of a few intrafissures of potassium feldspar grains were from 5 to 20 µm in size also in the undisturbed rock, but the apertures of grain boundaries and pores and fissures were not detectable in the undisturbed zone because the apertures were less than a micrometer.

- Microfractured zone

The thickness of the microfractured zone starting from the crushed zone is 5 mm and the mean **additional** porosity in the fractured zone is approx. 0.2% (0.18% ± 0.10) /Autio et al. 2003/.

The aperture of over 60% of fracture population is less than 2.16 µm. The crack specific surface is in the range of 0.004 μm^{-1}, being about one order of magnitude lower than in crushed zone /Montoto et al. 2003/.

- Zone of minor damage

The porosity in the zone of minor damage zone is not significantly higher than the porosity of the undisturbed rock although slight differences can be seen in the porosity profiles (see Figure 7-22). The thickness of the zone of minor damage starting from the microfractured zone is about 14 mm. Damage can be observed qualitatively in the form of increased fracture apertures, but no significant quantitative differences can be measured.

Permeability and diffusivity

Diffusivity and permeability of seven different granitic rock types were measured using He-gas method and the porosity was determined by using several other techniques including water immersion techniques and ^{14}C-PMMA method /Autio et al. 2003/. Results represented seven different crystalline rock types (gneissic tonalite, rapakivi granite, muscovite granite, porphyritic granodiorite, tonalite, migmatitic gneiss and Palmottu granite).

The average values of the EDZ and undamaged rock in full-scale experimental deposition holes at Olkiluoto VLJ Research Tunnel in Finland are shown separately in Figure 7-28. The diffusivity and permeability of samples taken from the experimental deposition holes at Äspö was estimated using two empirical relationships: one between porosity and permeability and another between porosity and diffusivity. These were derived from the abovementioned set of results using Darcy's law type relationship between porosity and permeability and Archie's law type relationship between porosity and diffusivity.

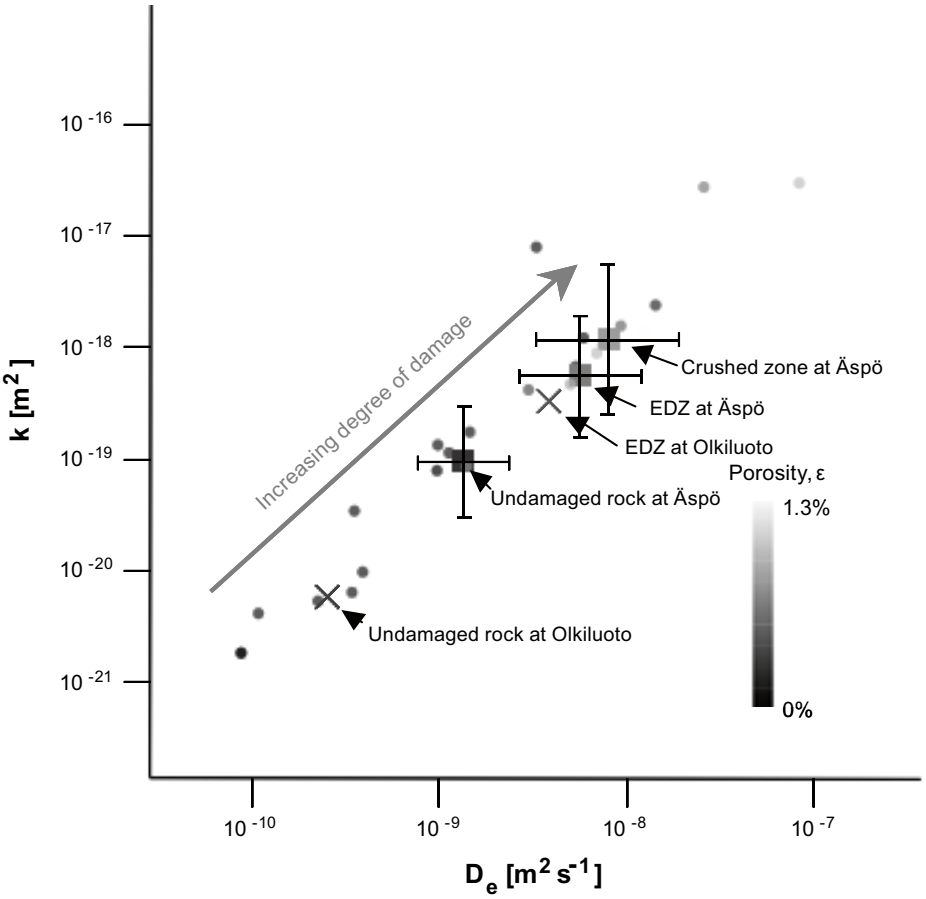

Figure 7-28. *Results of effective diffusion coefficient (D_e) of helium in pore space filled with nitrogen, permeability (k) and porosity (ε, in grey scale) measurements representing eight different crystalline rock types (gneissic tonalite, rapakivi granite, muscovite granite, porphyritic granodiorite, tonalite, migmatitic gneiss and Palmottu granite), shown as dots. The average values of the EDZ and Undamaged rock in full-scale experimental deposition holes at Olkiluoto VLJ Research Tunnel in Finland are shown as crosses (ε = 0.34%, $D_e = 3.97 \times 10^{-9}$ m^2s^{-1}, $k = 2.96 \times 10^{-19}$ m^2, and ε = 0.14%, $D_e = 2.63 \times 10^{-10}$ m^2s^{-1}, $k = 5.16 \times 10^{-21}$ m^2, respectively). The estimated values of undamaged rock, EDZ, and the crushed zone, which is part of the EDZ, in samples taken from the experimental deposition holes at Äspö (ε = 0.26%, $D_e = 1.4 \times 10^{-9}$ m^2s^{-1}, $k = 8.4 \times 10^{-20}$ m^2; ε = 0.64%, $D_e = 6.0 \times 10^{-9}$ m^2s^{-1}, $k = 4.9 \times 10^{-19}$ m^2 and ε = 0.80%, $D_e = 8.5 \times 10^{-9}$ m^2s^{-1}, $k = 1.0 \times 10^{-18}$ m^2 respectively) are shown as squares with error bars representing the 95% confidence intervals. From /Johnson et al. 2005/.*

Gas-induced fracturing of near-field rock

As discussed in Chapter 5, considerable amounts of hydrogen gas are generated by anaerobic corrosion of steel. Because the generated gas cannot be stored and/or dissolved in sufficient quantities within the near-field and surrounding rock, a free gas phase is sustained and gas pressure rises until the losses of gas into the surrounding rock and along the deposition drifts balances the generation of gas. In very tight drift sections, gas pressures are expected to rise considerably above the hydrostatic pressure at repository depth. When the gas pressure is near or above the minimal principal stress σ_3, reactivation of sub-horizontal fractures in the near-field rock may occur. Because these fracture planes are most likely oriented in the same direction as the planned deposition drifts (NW-SE, see above), it is possible that continuous gas pathways are formed along the drifts. These pathways may hydraulically connect neighbouring supercontainer units located in very tight rock and contribute thus to the gas transport capacity of the near-field rock. From these considerations, it seems likely that the maximum gas pressure in the near field does not significantly exceed the minimal principal stress (about 9 MPa at a depth of 400 m).

This is consistent with modelling by /Lönnqvist and Hökmark 2007/. The study found that pressures of the order of 10 MPa are required in the deposition drift to cause opening of intersecting rock fractures. The study also showed that to open these fractures sufficiently to bring them into tension at distances between 0 m and 0.2 m from the drift periphery requires about 20 to 25 MPa. Furthermore, the effects were found to be modest in terms of fracture aperture increase and distance from the drift wall to which such effects extend.

Gas-induced fracturing of larger blocks of the bedrock, involving the formation of direct pathways from the engineered barriers to higher permeable geological features, is not likely to occur. Fractures are expected to propagate along the steepest stress gradients, i.e. axially along the deposition drift from very tight to more permeable drift sections, where stress gradients up to 0.05–0.5 MPa may occur (corresponding to 5 MPa of gas overpressure relieved over 10–100 m). In contrast, the vertical stress gradient at Olkiluoto is about 0.024 MPa m^{-1} (/Posiva 2005/ p. 130), and the vertical distance to the next major fracture zone is about 100 m.

Continuous gas pathways in the near-field rock between neighbouring supercontainer units may form preferential pathways for the subsequent transport of radionuclides, even though gas generation may have stopped long before the onset of radionuclide release from the canisters. Such preferential pathways are expected to be limited to initially very tight drift sections, where they increase the transport capacity for radionuclides parallel to the axis of the deposition drift.

Natural analogues/observations in nature

Not applicable.

Time perspective

The EDZ around a KBS-3H deposition drift is created during the operational period (mainly during and just after construction). After sealing of the drifts, the excavation-damaged zone may be partially sealed by various processes (e.g. creep, bentonite swelling, mineral precipitation).

Rock spalling induced by high initial stresses and heat loads may occur as long as high temperatures prevail and while no significant swelling pressure is exerted on the rock surface, i.e. within the first years to decades (or even centuries) after canister emplacement. Thermally induced rock spalling is particularly significant for those drift sections where limited groundwater inflow means that significant buffer swelling pressure on the drift wall takes longer time to develop.

The relevant time scales for gas-induced fracturing in very tight drift sections is up to several thousand years. This is the time needed for the gas pressures to rise close to the minimal principal stress.

Handling in the safety assessment for KBS-3H

Rock spalling is unlikely to occur during the operational phase except for some limited spalling in the interface between the deposition niche with larger radius and the deposition drift with a smaller radius. Even if it were to occur, detached rock fragments could be removed and repair measures could be taken to avoid detrimental effects on long-term safety. Thermally induced rock spalling, should it occur after canister emplacement and closure of deposition drifts (e.g. in very tight drift sections where buffer saturation is significantly retarded), has a significant impact on the properties of the interface between buffer and rock. As a consequence, the transfer resistance to an intersecting fracture could be significantly reduced, resulting in:

- an increase of the transport rate for sulphide from the rock towards the canister surface, an increase in the copper corrosion rate and a decrease in the canister lifetime; and
- enhanced radionuclide transport from a defective canister towards an intersecting fracture.

By analogy with calculations performed to scope the impact of iron/bentonite interactions on the buffer/rock interface, the canister lifetime is not expected to be significantly reduced should rock spalling occur. A combination of pessimistic assumptions concerning the buffer/rock interface must be made before the canister lifetime drops to one million years or less (Appendix B of the KBS-3H Evolution Report by /Smith et al. 2007c/).

Nevertheless, uncertainties remain concerning the occurrence of a perturbed interface due to spalling, the physical extent of the perturbed buffer/rock interface region into the buffer, and the flow through the perturbed region. Results in SR-Can indicate that earlier, and in some cases higher, radionuclide release maxima are calculated. The impact on doses depends on a number of parameters, including properties of the canister defect, sorption properties in the buffer, water flow rate in the fracture, etc. For less favourable parameter combinations, the increase in doses can be an order of magnitude or more. Calculations reported in /SKB 2006a/, Figures 9-36 and 9-37, indicate that spalling may increase equivalent flow rates at the buffer/rock interface by more than an order of magnitude.

In the KBS-3H Radionuclide Transport Report /Smith et al. 2007a/, the uncertainties due to rock spalling are addressed in specific variant cases (PD-FEBENT 1, PD-FEBENT-2, PD-FEBENT-3 and PD-SPALL) that illustrate the impact of a loss of the transfer resistance to an intersecting fracture. A mixing tank boundary condition that pessimistically treats the impact of a more conductive buffer/rock interface on radionuclide transport is adopted.

The EDZ and the near-field rock play an important role in the migration of gas and radionuclides present as volatile species. As discussed above, continuous gas pathways in the EDZ and near-field rock between neighbouring supercontainer units may form preferential pathways for the subsequent transport of radionuclides. It is worthwhile noting that this would seem to lead to the establishment of a minimal transport capacity (for gas and radionuclides) along the drifts between very tight drift sections (where gas pathways are likely to be formed) and more permeable drift sections (where gas can dissipate through existing fractures. In the KBS-3H Radionuclide Transport Report /Smith et al. 2007a/, the EDZ is assumed not to be hydraulically significant, and therefore does not affect the transport of radionuclides migrating in solution. It is, however, implicitly taken into account in cases addressing the release of volatile C-14 with repository-generated gases (PD-VOL-1 and PD-VOL-2).

Gas-induced fracturing of the near-field rock is not expected to detrimentally affect safety. This is because the relevant transport pathways through the geosphere are provided by transmissive fractures, which are, by definition, absent in very tight drift sections. The transport resistance for radionuclides released from very tight drift sections is thus expected to be higher than for those released from permeable drift sections, due to the significant transport resistance of gas-induced fractures, should they form. Thus, there is no need to quantify the impact of gas-induced fracturing on safety.

For a more detailed discussion of radionuclide transport pathways, see Section 7.8. For additional information on assessment cases in the Radionuclide Transport report /Smith et al. 2007a/, see Appendix G.

Handling of uncertainties

The impact of rock spalling on safety is subject to uncertainties mainly related to the conditions under which rock spalling occurs (initial stresses, thermomechanical coupling parameters, timing of buffer saturation) and to the properties of the buffer/rock interface once spalling should have occurred (physical properties of interface: porosity, hydraulic conductivity, etc). Furthermore, uncertainties remain concerning the elastic heterogeneity. Local inclusions of stiff rock can concentrate stress and be preferred locations of spalling, even in relatively moderately stressed rock. Excavation-induced spalling is being studied via the Prediction-Outcome studies currently underway in Posiva's ONKALO tunnel. These studies include specific locational predictions of the potential for spalling at various depths and azimuths of the ONKALO tunnel. In this way, the potential for spalling will be calibrated, thus providing the capability of better predictions of thermal spalling.

The properties of the EDZ are also subject to considerable uncertainties, being dependent on a variety of rock-specific and site-specific factors as well as on the repository layout and engineering techniques applied. Furthermore, the data used in analyses so far are based on measurements made on a limited number of samples taken from the VLJ Research Tunnel at Olkiluoto and these may not correspond fully to the properties at repository depth. In particular,

measurements of intrinsic gas permeability were based on unfractured samples. Samples containing fractures or microfractures were rejected. Thus, the EDZ is likely on average to have a higher intrinsic permeability than suggested by the measured values.

There is also significant uncertainty in the processes leading to gas-induced fracturing of the near-field rock (threshold stress, direction of fracture propagation, propagation depth, etc). Experience from hydraulic jacking in pressure tunnels suggests that any gas pressure over the minimum stress will open fractures. Specific investigations of large-scale gas-induced fracture propagation may considerably improve the mechanistic understanding of the processes involved.

7.6.4 Creep

Overview/general description

A discussion of creep in the bedrock at Olkiluoto is given in /SKB 2006e/ and /Rasilainen 2004/. Creep is the specific case where the stress is constant and strain occurs with time. The complementary case where the strain is constant and the stress reduces with time is stress relaxation. In all real cases, time-dependent deformations will be somewhere between these two extremes because they will be a function of the unloading stiffness of the adjacent components. There is no relevant difference in processes related to creep between KBS-3V and 3H. As proposed by /Rasilainen 2004/ and by /SKB 2006e/, creep deformations are not considered to be a significant factor regarding the intact crystalline rock. Deformations along fractures are more significant, but it is stated that it probably takes very long time periods to cause significant canister deformation, see Section 7.6.2.

Handling in the safety assessment for KBS-3H

Creep deformations are not further considered in the safety assessment for KBS-3H, in accordance with the handling in the SR-Can safety assessment for KBS-3V.

7.6.5 Surface weathering and erosion

This is part of the biosphere description, which is outside the scope of the present report. For details, see Section 4.6 in /SKB 2006e/.

7.6.6 Erosion/sedimentation in fractures

Overview/general description

During and after the operational phase, the water inflows to the deposition drifts may be increased significantly. This may lead to erosion, transport and sedimentation of fault gouge material and to buffer erosion, possibly changing the hydraulic properties of fractures intersecting the deposition drifts.

Based on the discussions in /SKB 2006a/, erosion, transport and sedimentation of fault gouge material is not expected to lead to significant changes in the hydraulic properties of fractures. This is because highly conductive fractures will be grouted, to avoid upconing of saline water, and the residual transmissivity will not be sufficient to cause significant erosion, transport and sedimentation of fault gouge material during construction, operation and post-closure saturation.

Buffer erosion into fractures during glacial conditions, where groundwater with low ionic strength will come into contact with bentonite extruding into fractures, is a major concern in the safety assessment. This issue is discussed in Section 4.6.1 and in the KBS-3H Evolution Report /Smith et al. 2007c/.

Handling in the safety assessment for KBS-3H

Erosion, transport and sedimentation of fault gouge material in fractures are not included in radionuclide release and transport calculations for KBS-3H, because the expected flow rates in fractures are not expected to lead to significant changes in the hydraulic properties of fractures.

Long-term chemical erosion of bentonite into transmissive fractures may detrimentally affect the performance of the buffer, in accordance with the provisional conclusions in /SKB 2006a/. The radiological consequences of buffer erosion are evaluated by a separate variant case, assuming a significantly increased hydraulic conductivity of the buffer, causing reduced transport resistances in the buffer and at the buffer/rock interface (see Section 4.6.1).

7.7 Chemical processes

An overview of chemical processes in the geosphere is shown in Table 7-12. These processes have been identified in /SKB 1999, Rasilainen 2004/ and /SKB 2006e/ to be relevant for the subsystem "geosphere" in KBS-3V. The majority of these processes do not depend on the specific conditions in KBS-3H, because the origin of the relevant driving forces is within the geosphere or because they do not affect/are not affected by the geometry, properties and evolution of the near field. For these processes, /SKB 1999, 2006e/ provides a comprehensive description of relevant processes and interactions, whereas /Rasilainen 2004/ provides site-specific information for Olkiluoto (present-day conditions, hydrogeochemical evolution) and most recently, the KBS-3V Evolution Report by /Pastina and Hellä 2006/ provides the information on the hydrological and hydrogeochemical evolution of the site from the start of construction until the far future.

Table 7-12. The inter-dependence of chemical processes and identified variables in the geosphere.

Chemical processes	Variables in geosphere												
	Repository geometry	Fracture geometry	Temperature	Groundwater flow	Groundwater pressure	Gas flow	Stress state	Matrix minerals	Fracture minerals	Groundwater composition	Gas composition	Structural and residual materials	Saturation
Advection/mixing	×	×	×	×						×	×		
Diffusion and matrix diffusion		×	×						×	×			×
Speciation and sorption		×	×	×	×			×	×	×		×	
Reactions groundwater/rock matrix		×	×					×		×		×	×
Dissolution/precipitation of fracture-filling materials		×	×		×				×	×			×
Microbial processes			×		×				×	×		×	×
Degradation of grout		×	×	×	×	×	×		×	×		×	×
Colloid formation and transport			×	×					×	×		×	×
Formation/dissolution/ reaction of gaseous species		×	×	×	×	×	×			×	×	×	×
Methane hydrate formation		×	×		×		×			×	×		×
Salt exclusion		×	×	×	×				×	×		×	×
Radiation effects (rock and grout)	×							×	×	×		×	×
Earth currents		×	×	×						×			×

During the operation of ONKALO and of the repository, the open excavations dominate the flow conditions in the vicinity of the repository and draw groundwater from all directions in the bedrock towards the open excavations. Geochemical changes induced by such transients in groundwater flow include upconing of deep saline waters and introduction of fresh and sulphate-rich waters into greater depths. The mixing of the waters from closer to the surface may induce some changes in pH and Eh of the groundwaters, although buffering by the host rock should prevent significant Eh and pH changes. Preliminary calculations have been carried out based on the estimation of the lifetime of fracture mineral buffers, such as calcite and pyrite in the fractures, against low-pH and oxygen-containing infiltrating waters from the surface /Andersson et al. 2007/. Further field studies and more advanced modelling are planned. As a consequence of these changes in groundwater composition, the normal geochemical evolution driven by density differences of groundwater is disturbed such that conditions in bedrock that were initially considered as favourable for disposal, may appear as unfavourable as a consequence.

Therefore, the control of water inflows into ONKALO and other open excavations is needed, as confirmed by recent studies /Vieno et al. 2003, Löfman and Mészáros 2005, Ahokas et al. 2006/. When water inflow into open excavations is limited, the above-described hydrological and geochemical disturbances with respect to normal evolution can be mitigated.

After closure of the tunnels, the flow conditions and the salinity distribution start to recover towards the natural state, although calculations performed for a KBS-3V repository at Olkiluoto indicate that the thermal output from the spent fuel may cause an increased upward groundwater flow and increased salinity compared with undisturbed conditions for a period of up to several hundreds of years /Löfman 2005/. In the longer term, the salinity is expected to increase even further due to post-glacial (isostatic) uplift. The salinity of groundwater (expressed as TDS, total dissolved solids) will reach a maximum of 25 g per litre at repository level (–420 m) and about 55 g per litre at a depth of –520 m during the operational phase /Pastina and Hellä 2006/.

This complex behaviour of water, salt and heat during the operational and post-closure phase is, however, not specific to KBS-3H. For this reason, there are no additions or comments to these discussions in the present report.

Differences between KBS-3V and 3H may arise if the chemical processes in the geosphere are triggered by factors specific to KBS-3H. Generally, the impacts of chemical interactions between engineered barriers and the rock are expected to be less significant in KBS-3H compared with KBS-3V, because:

- the total excavated volume in KBS-3H is smaller (smaller interface area, smaller amount of engineering materials, smaller hydraulic draw-down cones),
- the deposition drifts will be excavated using boring techniques (smaller and tighter EDZ); there is no drilling/blasting within deposition drifts (with the exception of the deposition niche),
- the time period between excavation and sealing of a deposition drift is shorter in KBS-3H, due to design requirements; the duration of chemical and hydraulic interactions between engineered barriers and the rock will thus be shorter in KBS-3H (oxidation, microbiology, detrimental agents, saltwater intrusion, pH plume, smaller hydraulic draw-down cones, etc).

On the other hand, there may be differences in the chemical interactions between engineering barriers and rock due to the different types and amounts of structural/residual materials present in KBS-3V and 3H. The presence of residual materials (e.g. sulphur compounds and other nutrients such as N, P, organics; surfactants originating from degreasing agents and detergents; compounds deriving from cellulose, etc) may affect the geochemical conditions, microbial growth and radionuclide transport in the geosphere. For example, organic substances or their degradation products could form complexes with radionuclides that would lower radionuclide sorption and thus increase radionuclide release and transport rates in the event

of canister failure. However, the impact of these substances is the same as in a KBS-3V repository. An overall assessment of the disturbances caused by cement and other engineering and residual materials has been performed by /Vieno et al. 2003/; the key issues identified in this study are related to the to alkaline cementitious leachates that interact with the bentonite buffer. The main results and the conclusions are summarised in Section 5.7.6 in /Rasilainen 2004/. The interaction of cement with bentonite has been summarised in Sedction 4.7 and Appendix F. The long-term impact of residual materials will likely be similar in KBS-3V and 3H. /Ahokas et al. 2006/ have studied the use of cement for control of groundwater inflow to ONKALO.

In the case of KBS-3V, numerical simulations of oxygen depletion have been carried out that account for oxidation of copper, microbially-induced oxygen consumption and oxidation of Fe(II)-bearing mineral impurities in the bentonite (Chapter 11 of /Pastina and Hellä 2006/). The presence of large amounts of steel contributes to depletion of oxygen that is trapped in the deposition drifts after sealing, provides a large redox buffering capacity and through anaerobic corrosion causes relatively large amounts of hydrogen gas to be stored/dissolved in the rock pores. Natural gases present in the bedrock at Olkiluoto may interact with hydrogen gas generated within the repository. The natural hydrogen concentration is far from its solubility limit under repository conditions /Rasilainen 2004/ and can be neglected in the evaluation of gas effects (Section 5.5.2). Although the natural methane concentration is relatively close to its solubility limit in the deeper parts of the bedrock, it need not be taken into account either, because there is no significant interaction with hydrogen gas.

Methane and hydrogen gases migrating upwards may also participate in diverse redox processes in the groundwater, such as reduction of sulphate to sulphide as a consequence of always viable bacterial activity. The presence of microbes and the concentration of CH_4 dissolved in groundwater are the key factors that control the reduction of sulphate in the brackish sulphate-rich groundwater. Either methane enters into upper brackish water layer by diffusion or brackish sulphate waters enter into methane-containing waters as a result of slow downward percolation (mixing). The concentration of CH_4 significantly exceeds that of sulphate in potential source water if methane and sulphate-rich waters are mixed. Therefore, the availability of sulphate may be the rate-limiting factor for this reaction /Pitkänen and Partamies 2007/.

Currently, the various geochemical differences between KBS-3V and 3H are considered to be relatively insignificant, and no detailed discussion of these issues seems to be needed for KBS-3H. This provisional conclusion will have to be revisited when the final design for KBS-3H is fixed and all the engineering materials (types, amounts) are known. On the other hand, although microbial activity in the geosphere is unlikely to be affected by differences between KBS-3V and 3H, the presence of iron corrosion products, including hydrogen gas, in contact with the drift wall in KBS-3H and chemical interaction of the buffer with these corrosion products could lead to a perturbed buffer/rock interface and to the possibility of microbial reduction of sulphide to sulphate (using hydrogen gas) in the outer-most part of the buffer. The potential impact on canister corrosion is discussed in Appendix B.7 of the KBS-3H Evolution Report /Smith et al. 2007c/. The handling of these processes in the KBS-3H safety studies is summarized in Table 7-4.

7.8 Radionuclide transport processes

An overview of radionuclide transport processes in the geosphere is shown in Table 7-13. These processes have been identified in /SKB 1999, Rasilainen 2004/ and /SKB 2006e/ to be relevant for the subsystem “geosphere” in KBS-3V. The basic radionuclide transport processes in the geosphere are identical in KBS-3V and 3H. /SKB 1999, Rasilainen 2004/ and /SKB 2006e/ provide a comprehensive description of the basic processes and interactions. There are no additions or comments to these discussions in the present report. The handling of these processes in the KBS-3H safety studies is summarized in Table 7-4.

Table 7-13. The inter-dependence of radionuclide transport processes and identified variables in the geosphere.

Radionuclide transport	Variables in geosphere												
	Repository geometry	Fracture geometry	Temperature	Groundwater flow	Groundwater pressure	Gas flow	Stress state	Matrix minerals	Fracture minerals	Groundwater composition	Gas composition	Structural and residual materials	Saturation
Transport of radionuclides in water phase	×	×	×	×				×	×	×	×	×	×
Transport of radionuclides in gas phase	×	×	×			×		×	×	×	×	×	×

Handling in the safety assessment for KBS-3H

Some differences in transport conditions may arise due to the presence of steel supercontainers and other structural materials in KBS-3H. Due to anaerobic corrosion of steel, large amounts of hydrogen gas are produced. In tight drift sections, a free gas phase is formed which may persist for several thousand years.

For the great majority of the emplaced canisters, the formation of a free gas phase is largely decoupled from radionuclide transport. This is because the relevant time frame for gas-related effects due to the presence of supercontainers and other structural materials is up to several thousand years, whereas the release of radionuclides can only occur after canister failure, i.e. at least hundred thousand years after canister emplacement.

The situation is different in the case of initially defective canisters. Here, the relevant periods for radionuclide transport and gas generation may overlap, affecting the transport conditions for radionuclides both in the water phase and gas phase. Depending on the specific conditions, the presence of a free gas phase may increase or decrease the release of radionuclides into the geosphere and it may accelerate or retard the transport of radionuclides in the geosphere. The following situations are considered in the KBS-3H Radionuclide Transport Report /Smith et al. 2007a/:

- gas-induced release of dissolved radionuclides from the cavity of the iron insert through the hole into the saturated bentonite, and release into the geosphere (separate variant case PD-EXPELL addressing near-field performance, see Section 2.8),
- release of volatile radionuclides in the gas phase through a hole in the canister into bentonite, and direct release into the biosphere PD-VOL-1 and PD-VOL-2 (bounding calculations, see Section 2.8).

It is assumed that the impact of repository-generated gas on groundwater flow is small on the scale of the overall geosphere transport path. Thus, transport of dissolved radionuclides in the geosphere under two-phase conditions is not addressed in radionuclide release and transport calculations.

Several assessment cases in the Radionuclide Transport report /Smith et al. 2007a/ address uncertainties in the groundwater salinity conditions at different locations and times during repository evolution:

- brackish saline water (PD-SAL, CC-LOGEORS),
- saline water (PD-HISAL),
- glacial meltwater with a reference composition (PD-GMW, CC-GMW, CC-LOGEORG, RS-GMW) and an alternative composition (PD-GMWV), and
- change from reference water to glacial meltwater at 70,000 years (PD-GMWC).

Uncertainties in chemical speciation, redox conditions and solubility are reflected in the speciation of C-14 being present in the geosphere in anionic form (carbonate) for the different types of fuel:

- BWR (PD-BCC),
- VVER (PD-VVERC), and
- EPR (PD-EPRC).

Case PD-BCN also considers the case of niobium being present in both the near field and geosphere in anionic form. In case PD-NFSLV near-field solubilities for redox-sensitive elements such as U and Mo are varied according to uncertainties in redox conditions.

For additional information on assessment cases calculated in the Radionuclide Transport Report, see Appendix G.

8 Summary of main differences between KBS-3V and KBS-3H and issues for further consideration

In this chapter, differences in processes occurring in KBS-3V and KBS-3H repositories for spent fuel in crystalline rock are summarised. The analysis is based on the Olkiluoto site, although the main outcomes may be applicable to other repository sites for spent fuel in crystalline rock as well. This chapter is structured according to the subsystems fuel/cavity in the canister, canister, buffer/distance block, supercontainer and other steel structural materials, drift end plugs and backfill, and geosphere. The approximate timescales of key near-field processes and changes in key characteristics of the near field that take place during the early evolution of the repository are illustrated in Figure 8-1 (note that changes occurring within this period affect the characteristics and performance of the repository at later times, which is why the time-axis in Figure 8-1 extends to 10^6 years).

The main uncertainties associated with processes occurring in each of these systems for KBS-3H are also briefly summarised below. Several other uncertainties that are common to KBS-3H and KBS-3V (e.g. uncertainties related to the evolution of the site and climatic conditions) are not discussed here.

The issues are not prioritised and are to be considered in the context of the development of the KBS-3H design, taking into account programmatic objectives and constraints, such as schedules and resources both in Posiva and SKB.

8.1 Fuel/cavity in the canister

Water ingress to a defective canister and subsequent expulsion of water and dissolved radionuclides by gas generated and trapped inside the canister is a possibility for both KBS-3H and KBS-3V. It is, however, more likely in the case of a KBS-3H repository compared with KBS-3V if it can be assumed that penetrating defects are a possibility primarily in the welding region, which is located at the top of the canister. If this is the case then, in KBS-3V, gas can escape from a vertically orientated defective canister without the development of pressures that could expel water and radionuclides. In KBS-3H, the defect may be located at the underside of the canister and gas may be trapped inside the canister. This could possibly lead to an enhanced release of dissolved radionuclides through the buffer into the geosphere.

Calculations indicate that only a combination of rather conservative assumptions (e.g. high bentonite hydraulic conductivity and low cast iron corrosion rate which would allow a higher amount of water inside the penetrated canister) would lead to a situation in which water is expelled from the canister. Nonetheless, some significant uncertainties are acknowledged in the detailed modelling of hydraulic and gas-related processes associated with a canister with a small defect. Thus, it is considered prudent to consider several assessment cases associated with this scenario. Considering the low probability of an initial penetrating defect assessed in SR-Can, this is not a significant difference in safety between the two cases.

8.2 Canister

The effects of shear deformations (by tectonic movements, earthquakes, post-glacial faulting) depend on the relative orientation of canister and rock shear deformations at the repository depth. Shear deformations perpendicular to the canister axis have more severe effects than longitudinal deformations due to the higher canister stiffness in longitudinal direction.

Therefore, KBS-3V canisters are more vulnerable to flat (subhorizontal) shear displacements across the deposition hole. In contrast, KBS-3H canisters are considered to be more vulnerable to steep (subvertical) shear displacements perpendicular to the deposition drift.

In both the KBS-3H and KBS-3V cases, the major uncertainties are fundamentally the same, including the magnitudes and rates of shear displacements occurring at Olkiluoto in the far future, the location and orientation of the shear plane with respect to the canister, the factors affecting the density and plasticity of the buffer and whether or not potentially damaging fractures can be detected and avoided. Of these phenomena, the greatest differences between the two emplacement alternatives involve the potential changes in plasticity of the bentonite region adjacent to the supercontainer for KBS-3H, which requires further investigation. The possibility of a large rock shear movement is considered in two assessment cases.

8.3 Buffer

The early, transient phase is the most critical phase for the evolution of the bentonite buffer in the supercontainer and distance block in KBS-3H. In an early phase, water uptake and transport under two-phase conditions occur (including gas transport and dissolution). In KBS-3H, heterogeneous saturation is expected to occur along the axis of deposition drifts. This is because the individual supercontainer units are isolated from each other by massive distance blocks. In the vicinity of permeable fractures, the supercontainer units are saturated within about one decade, whereas saturation times may be much longer in tight drift sections. Due to the generation of hydrogen by anaerobic corrosion of supercontainer steel shell (and other structural steel components), full saturation of tight drift sections may even be retarded until the generation of gas ceases (several thousand years). In the KBS-3V case, there is no hydrogen generation in the early evolution phase so the saturation is expected to occur faster than in the KBS-3H case.

In KBS-3H, various processes are identified that may lead to a detrimental change in bentonite density. In the operational phase, the most important process is considered to be piping and erosion. Although the basics of this process, which may lead to some bentonite redistribution, are similar in KBS-3V, the impact on safety is qualitatively different due to the different design and it may affect the buffer around neighbouring canisters in KBS-3H, since the buffer density tends to homogenise over time, while in KBS-3V loss of buffer around one canister does not affect other canisters. On the basis of laboratory studies, it is concluded that piping and erosion are unlikely to occur for KBS-3H in the Basic Design given the current criterion on the maximum inflow rate to a supercontainer drift section of 0.1 litres per minute. However, piping and erosion could be an issue for the DAWE design option (see Appendix D). There remain, however, major uncertainties in assessing the maximum rate of hydraulic pressure increase and the maximum hydraulic pressure across a distance block, and how distance blocks can withstand the pressure conditions and the consequences of eventual axial displacement of distance block and supercontainer. Even if piping and erosion were to occur, the impact on buffer density due to bentonite redistribution is expected to be small, due to the limited duration of the phenomenon at any given location. Despite this observation, this is recognised to be a critical issue for further development of the KBS-3H design.

Axial displacement of distance blocks/supercontainers (in the BD only) by differential saturation and swelling are also qualitatively different in KBS-3H and KBS-3V. While the buffer in KBS-3V may expand by creep into the backfilled tunnel, the buffer and distance blocks in KBS-3H may be axially displaced as whole blocks, involving compaction of the adjacent supercontainer units. This process may affect the density of the saturated bentonite. Significant uncertainties are still present regarding the pressure increase rate and its coupling to other parameters, such as the water inflow rate, the effect of saline groundwater, the distance block length and design.

Besides the processes leading to redistribution of bentonite, a number of further transport and reaction processes affect the behaviour of bentonite. These processes depend on the physicochemical conditions and on the composition of bentonite and groundwater as well as

on the presence of structural and residual materials. A major difference between KBS-3V and KBS-3H arises from the iron/bentonite interaction that takes place due to the presence of the supercontainer with the perforated steel shell in KBS-3H. Chemical alteration may adversely affect swelling, hydraulic and rheological properties of the buffer in the outer region. In particular, enhanced hydraulic conductivity of the outer region of the bentonite may result, which could increase the transport of detrimental solutes to the canister or increase the rate of transport of radionuclides from the canister in case of a release. Significant uncertainties remain in the understanding of the overall impact on the affected region of the buffer, including the extent and nature of neo-mineral formation and the degree of changes in hydraulic conductivity, plasticity and swelling pressure of the affected zone. In addition, a possibly lower density in this region could permit more significant microbial activity, a process that is expected to be of little relevance in denser buffer material. The present treatment of the transport properties of the outer buffer region in safety assessment calculations (represented as a mixing tank rather than a zone of somewhat increased hydraulic conductivity) to deal with these various impacts is very conservative, as explained in the KBS-3H Radionuclide Transport Report /Smith et al. 2007a/.

An additional potential consequence of the iron/bentonite interaction is the high occupation by Fe(II) of sorption sites in the outer part of the buffer, which could reduce sorption of some radionuclides. However, the reduced sorption capacity of bentonite surface is largely compensated by that resulting from the formation of iron corrosion products (mainly Fe_3O_4) which would act as a sink. The long-term evolution of such corrosion products and the fate of the sorbed radionuclides are unclear. What can be noted at this point is that radionuclides will not come into contact with the supercontainer shell in the early stages of the repository (except for extreme early canister failure scenarios) but rather, if at all, during the very late stages (>> 100,000 years) after having travelled through the canister and bentonite buffer. The role of iron corrosion products on the fate of sorbed radionuclides is an issue for further work.

The eventual impact of the high hydrogen partial pressures generated in the corrosion of the supercontainer shells and the other steel components on the bentonite porewater chemistry is an additional issue for KBS-3H. Various factors need to be considered, including acid-base equilibria and the pH buffering capacity of bentonite, as well as the limited timeframe of hydrogen production of several thousand years. The overall impacts, in particular any effects on the buffer, are to be considered in future studies.

In the current KBS-3H drift design, no cement-bearing component will be in direct contact with the bentonite in the supercontainer and distance block unit. Nonetheless, potential effects on buffer may arise through indirect contact of alkaline cementitious porewater transported from a grouted fracture by groundwater to the supercontainer area through the fracture network. In such a case, on a mass-balance basis, an outer zone of buffer of 4 cm thickness could be altered over a period of 100,000 years. Such estimates do not take into account mitigating processes such as the reaction of the alkaline plume with minerals in the host rock; nonetheless, they emphasise the need to minimise the quantities of cement used in the repository. Assessment cases considering various thicknesses of altered bentonite around the canister are considered in the radionuclide transport report.

Both KBS-3H and KBS-3V are affected by uncertainties regarding the possibility of dilute water penetrating to repository depth in a future post-glacial period, which may lead to some chemical erosion of the buffer. If the density of the buffer were to be reduced by erosion to such an extent that advective transport could take place within the buffer region, this could increase the rate at which sulphide migrates to the copper surface, and hence increase the copper corrosion rate, reduce canister lifetime and increase radionuclide migration rates subsequent to canister failure. Currently, the possibility of advective conditions developing in parts of the buffer as early as the next period of glaciation cannot be excluded and this is treated in assessment cases in the radionuclide transport report. The effect of buffer freezing also warrants further research. In contrast with KBS-3V, where only single canisters are affected, loss of buffer around one canister due to chemical erosion by glacial meltwater may affect the buffer around neighbouring canisters, since the the buffer density along the drift will tend to homogenise over time.

8.4 Supercontainer and other structural materials

In KBS-3H, the canister and the surrounding buffer are mechanically confined within a perforated steel shell. The entire unit is called a supercontainer. These units are emplaced in one piece and separated axially by distance blocks. Due to the expected hydraulic heterogeneity, the deposition drifts may be divided into several compartments by means of compartment steel plugs. Currently, there are no equivalent design elements foreseen in KBS-3V.

Although the supercontainer shell and steel compartment plugs have no safety function, they may influence safety functions of other components. The most relevant processes related to the supercontainer steel shell and to other steel structural materials are hydrogen generation by anaerobic corrosion and iron/bentonite interactions (see discussions above). As long as the copper canisters remain intact (i.e. no contact of the cast iron insert with porewater from buffer) there is no direct equivalent to these processes in KBS-3V. The durations of the gas production periods resulting from supercontainer and compartment plug corrosion are short (several thousand years) and no significant safety-related consequences are foreseen. The deformation of a supercontainer (possible rupture and contact with the rock) and, as noted above, the iron/bentonite interaction, may have impacts on transport phenomena at the bentonite/tunnel interface. Also, volume expansion by corrosion may affect the saturated density of the buffer.

The physical properties of the corroded supercontainer have not been evaluated. Although the porosity and hydraulic conductivity of the corrosion products may be low, the possibility that fracturing could lead to the formation of pathways for water flow and advective transport cannot currently be excluded. Selected radionuclide transport calculation cases cover the case of a disturbed buffer/rock interface due to the presence of iron corrosion products in contact with bentonite.

8.5 Drift end plugs

From a mechanical point of view, the purpose of the drift end plugs in KBS-3H is to prevent significant displacement of the distance blocks and supercontainers, which would compromise the ability of the buffer and distance block to fulfil their purposes with respect to long-term safety. The basic hydraulic processes for the drift end plug are the same as those for the deposition tunnel plug in KBS-3V (although the design is different). However, due to the absence of backfill in the supercontainer-bearing part of the drift and the presence of large amounts of gas-generating materials in KBS-3H, the hydraulic boundary conditions between the drift end plug and the deposition tunnel plug in KBS-3V are considerably different. The demonstration of the performance of such a plug needs further effort in both KBS-3H and 3V.

8.6 Deposition drifts, access and central tunnels, shaft, boreholes

A major difference is in the geometry and backfilling of the KBS-3H deposition drifts compared with the KBS-3V deposition tunnels. In KBS-3H, supercontainers are emplaced along relatively narrow deposition drifts, separated by compacted bentonite distance blocks. In KBS-3V, deposition holes are bored from relatively large diameter deposition tunnels, backfilled with swelling clay or clay/crushed rock mixture. For other underground openings (access and central tunnels, shaft, boreholes) no major differences have been identified.

8.7 Geosphere

Groundwater flow and gas flow/dissolution are the most relevant hydraulic processes in the geosphere. These depend to some extent on the repository design (geometry, excavation technique, materials). KBS-3H is considered to be more sensitive to localised water inflows, which may cause piping and erosion of bentonite. In both KBS-3H and -3V , inflow is likely to be very localised and the effects of geometry do not play a major role on the inflow criterion of 0.1 litres per minute. Also, the presence of large amounts of steel in KBS-3H is expected to lead to changes in the hydrodynamic behaviour of the system. While drift sections intersected by permeable fractures are expected to show a similar behaviour in KBS-3V and 3H, tight drift sections in KBS-3H are prone to remain in an unsaturated state for prolonged periods of time due to the generation of gas and the possible gas pressure build-up.

KBS-3H is, from a rock mechanics point of view, more stable than KBS-3V. This is due to the absence in KBS-3H of the vertical deposition boreholes used in KBS-3V. Some low stress areas may be present at the entrance of the KBS-3H deposition drifts (niche), especially if fractures exist in these areas, and more extensive rock support may be required in such cases. Rock spalling around the periphery of deposition drift is unlikely to occur in permeable drift sections in KBS-3H due to swelling stresses generated by the buffer. In tight drift sections, however, thermally induced rock spalling cannot be excluded. Design solutions to minimize spalling are currently under development. Thanks to the envisaged excavation technique (boring), the excavation-damaged zone in KBS-3H has a small spatial extent and its transport capacity is relatively modest. However, the hydraulic properties of the EDZ are not well known and need to be addressed in further studies. It is expected that equivalent flow rates at the bentonite/rock interface could increase due to spalling, but the effects would be smaller for KBS-3H than for KBS-3V. In the KBS-3H radionuclide transport calculations, a mixing tank boundary condition is adopted that pessimistically treats the impact of a more conductive buffer/rock interface on radionuclide transport. In very tight drift sections in KBS-3H, gas pressure may increase to several MPa above the hydrostatic pressure, but is not expected to exceed the minimum principal stress, thus gas-induced reactivation of fractures in the near-field rock is unlikely.

Concerning the KBS-3H repository layout, the selection of deposition hole locations is more flexible than in KBS-3H because rock sections with larger inflows can be rejected. In KBS-3H, local variations in groundwater flow conditions along the drift may lead to variable saturation time for the buffer along the drift (see Figure 8-1). With respect to the effect of earthquakes and rock shear on canister integrity, KBS-3H is more sensitive to sub-vertical fractures with respect to potential damage to the engineered barrier system by rock shear, while KBS-3V is more sensitive to sub-horizontal fractures.

The heterogeneity of the host rock and the consequent spatial variability of groundwater inflow along the deposition drifts affect the timescales of several important processes. Figure 8-1 therefore distinguishes between processes with timescales that apply (i), at all locations within the drifts, irrespective of local groundwater inflow, (ii), in “less tight” drift sections, defined as drift sections in which the average hydraulic conductivity of the adjoining wallrock is about 10^{-12} m s^{-1} or more, (iii), in “tighter” drift sections, defined as drift sections in which the average hydraulic conductivity of the rock is in the range 10^{-13} to 10^{-12} m s^{-1}, and (iv), in “tightest” drift sections, defined as drift sections in which the average hydraulic conductivity of the rock is in less than 10^{-13} m s^{-1}.

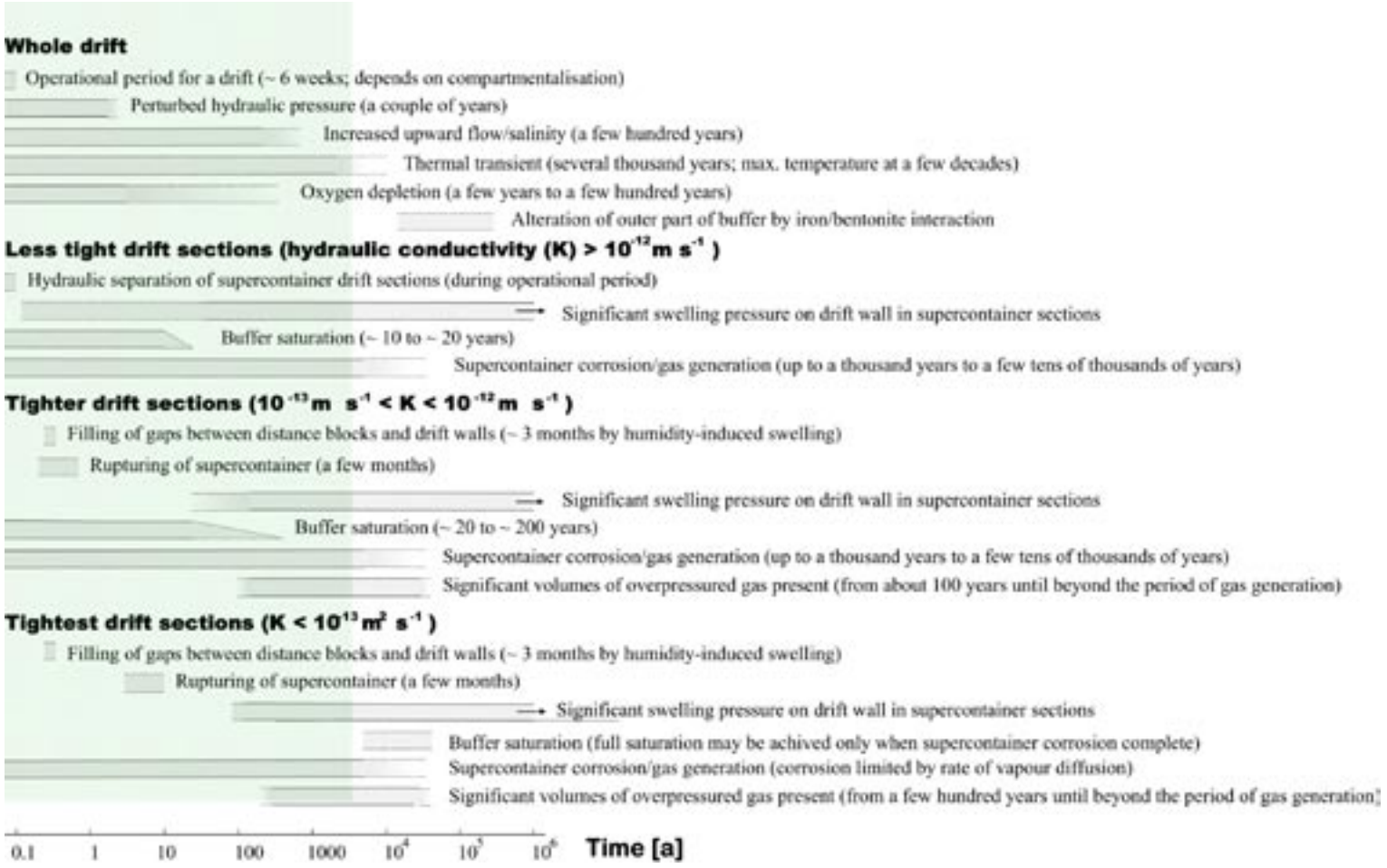

Figure 8-1. *Approximate timescales of various aspects of system evolution for a KBS-3H repository at Olkiluoto. Uncertainties are indicated by dotted lines. Tapering of the bars is used to indicate spatial variability of process timescales along the length of a deposition drift (e.g. as a result of geological heterogeneity). Background shading indicates the approximate duration of the transient phase (although some of the slowest transient processes may extend beyond this period). Right arrows indicate expected continuation beyond the million-year period covered by figure.*

9 References

Agrenius L, 2002. Criticality safety calculations of storage canisters. SKB TR-02-17, Svensk Kärnbränslehantering AB.

Ahokas H, 2003. Summary of hydraulic conductivity measurements and differences between different methods in boreholes KR1-KR10 at Olkiluoto, Finland. Proc. of the International Conference on Groundwater in Fractured Rocks, Prague, Czech Republic. IHP-VI, Series on Groundwater No. 7. ISBN 02-9220-002-X.

Ahokas H, Hellä P, Ahokas T, Hansen J, Koskinen K, Lehtinen A, Koskinen L, Löfman J, Mészáros F, Partamies S, Pitkänen P, Sievänen U, Marcos N, Snellman M, Vieno T, 2006. Control of water inflow and use of cement in ONKALO after penetration of fracture zone R19. Posiva Oy, Olkiluoto, Finland. Posiva Working Report 2006-45.

Alexander W R, Neall F B, 2007. Assessment of potential perturbations to Posiva's SF repository at Olkiluoto. Posiva Working Report 2007-35. Posiva Oy, Olkiluoto, Finland.

Andersson J, Hermansson J, Elert M, Gylling B, Moreno L, Selroos J-O, 1998. Derivation and treatment of the flow wetted surface and other geosphere parameters in the transport models FARF31 and COMP23 for use in safety assessment. SKB R-98-60, Svensk Kärnbränslehantering AB.

Andersson C, Johansson Å, 2002. Boring of full-scale deposition holes at the Äspö Hard Rock Laboratory, Operational experiences including boring performance and a work time analysis. SKB TR-02-26, Svensk Kärnbränslehantering AB.

Andersson C-G, Eriksson P, Westman M, Emilsson G, 2004. Status report, canister fabrication. SKB TR-04-03, Svensk Kärnbränslehantering AB.

Andersson J, Ahokas H, Hudson J A, Koskinen L, Luukkonen A, Löfman J, Keto V, Pitkänen P, Mattila J, Ikonen A I T, Ylä-Mella M, 2007. Olkiluoto Site Description 2006, POSIVA 2007-03. Posiva Oy, Olkiluoto, Finland.

Andra, 2005. Dossier 2005: Référentiel des matériaux d'un stockage de déchets à haute activité et a vie longue. Tome 1: Matériaux à base d'argiles gonflantes. Andra report C.RP. ASCM.04.0015.A, Châtenay-Malabry, France.

Anttila M, 1998. Radiation protection calculations for an encapsulation plant. Posiva Working Report 98-81. Posiva Oy, Olkiluoto, Finland.

Anttila M, 1999. Criticality safety calculations for the nuclear waste disposal canisters for twelve spent fuel assemblies. Posiva Working Report 99-03. Posiva Oy, Olkiluoto, Finland.

Anttila P, Ahokas H, Front K, Heikkinen E, Hinkkanen H, Johansson E, Paulamäki S, Riekkola R, Saari J, Saksa P, Snellman M, Wikström L, Öhberg A, 1999. Final disposal of spent nuclear fuel in Finnish bedrock – Olkiluoto site report. POSIVA 99-10. Posiva Oy, Helsinki, Finland.

Anttila M, 2005a. Radioactive characteristics of the spent fuel of the Finnish nuclear power plants. Posiva Working Report 2005-71. Posiva Oy, Olkiluoto, Finland.

Anttila M, 2005b. Criticality safety calculations for three types of final disposal canisters. Posiva Working Report 2005-13. Posiva Oy, Olkiluoto, Finland.

Autio J, 1996. Characterization of the excavation disturbance caused by boring of the experimental full scale deposition holes at TVO-Research Tunnel, POSIVA 96-09, Posiva Oy, Olkiluoto, Finland.

Autio J, Kirkkomäki T, 1996. Boring of full-scale deposition holes using a novel dry blind boring method. POSIVA 96-07, Posiva Oy, Olkiluoto, Finland.

Autio J, Hjerpe T, Siitari-Kauppi M, 2003. Porosity, Diffusivity and Permeability of EDZ in Crystalline Rock and Effect on the Migration in a KBS-3 Type Repository. Proceedings of a European Commission CLUSTER conference and workshop on Impact of the excavation disturbed or damaged zone (EDZ) on the performance of radioactive waste geological repositories. Luxembourgh 3–5 November 2003. EUR 21028 EN. p. 149–155

Autio J, Gribi P, Johnson L, Marschall P, 2005. Effect of Excavation Damaged Zone on Gas Migration in a KBS-3H Type Repository at Olkiluoto. Proc. of the 10th Int. Conf. on Chemistry and Migration Behaviour of Actinides and Fission Products in the Geosphere, Migration'05. Avignon, France, Sept. 18–23, 2005. Special issue of Radiochimica Acta, International Journal for Chemical Aspects of Nuclear Science and Technology. Oldenburg Verlag, Munchen, 2006.

Autio J, 2007. KBS-3H design description 2005. December 2006. Posiva Working report 2007-11 and SKB report R-08-29. Posiva Oy, Olkiluoto, Finland and SKB, Svensk Kärnbränslehantering AB.

Autio J, Börgesson L, Sandén T, Rönnqvist P-E, Johansson E, Hagros A, Eriksson M, Berghäll J, Kotola R, Parkkinen I, 2007. KBS-3H Design Description 2006. Posiva working report 2007-105 and SKB report R-08-32. Posiva Oy, Olkiluoto, Finland and SKB, Svensk Kärnbränslehantering AB.

Autio J, Anttila P, Börgesson L, Sandén T, Rönnqvist P-E, Johansson E, Hagros A, Eriksson M, Halvarsson B, Berghäll J, Kotola R, Parkkinen I, 2008. KBS-3H Design Description 2007. POSIVA Report 2008-01 and SKB report R-08-44. Posiva Oy, Olkiluoto, Finland and SKB, Svensk Kärnbränslehantering AB.

Baeyens B, Bradbury M H, 1997. A mechanistic description of Ni and Zn sorption on Na-montmorillonite. Part I: Titration and sorption measurements. J. Contam. Hydrology 27, 199–222.

Battaillon C, 2006. Corrosion products in compacted bentonite and argillite, in Wersin P, Mettler S. (2006). Workshop on Fe-clay interactions in repository environments, a joint initiative by Andra, SKB and Nagra. Basel 9–10 May 2006. Nagra NAB 06-15.

Bildstein O, Trotignon L, Hairapetian T, Jullien M, 2006. Modelling iron corrosion in clayey environments: implications for the near field geochemistry in HLW repositories. in Wersin P, Mettler S. (2006). Workshop on Fe-clay interactions in repository environments, a joint initiative by Andra, SKB and Nagra. Basel 9–10 May 2006. Nagra NAB 06-15.

Behrenz P, Hannerz K, 1978. Criticality in a spent fuel repository in wet crystalline rock. KBS Teknisk Rapport 108. SKB, Svensk Kärnbränslehantering AB.

Bond A E, Hoch A R, Jones G D, Tomczyk A J, Wiggin R W, Worraker W J, 1997. Assessment of a spent fuel disposal canister. Assessment studies for a copper canister with cast steel inner component. SKB TR 97-19, Svensk Kärnbränslehantering AB.

Bradbury M H, Baeyens B, 1997. A mechanistic description of Ni and Zn sorption on Na-montmorillonite. J. Contam. Hydrol. 27, 223–248.

Broed R, Avila R, Hjerpe T, Ikonen A T K, 2007. Biosphere analysis for selected cases in TILA-99 and in the KBS-3H safety evaluation, 2007-109. Posiva Working report. Posiva Oy, Olkiluoto, Finland.

Bruno J, Arcos D, Duro L, 1999. Processes and features affecting the near field chemistry. Groundwater-bentonite interaction. SKB TR-99-29, Svensk Kärnbränslehantering AB.

Bäckblom G, Munier R, 2002. Effects of earthquakes on the deep repository for spent nuclear fuel in Sweden based on case studies and preliminary model results. SKB TR-02-04, Svensk Kärnbränslehantering AB.

Börgesson L, 1985. Water flow and swelling pressure in non-saturated bentonite-based clay barriers. Eng. Geology, Vol. 21 (pp. 229–237).

Börgesson L, 1992. Interaction between rock, bentonite , buffer and canister. FEM calculations of some mechanical effects on the canister in different disposal concepts. SKB TR 92-30, Svensk Kärnbränslehantering AB.

Börgesson L, Hernelind J, 1999. Coupled thermo-hydro-mechanical calculations of the water saturation phase of a KBS-3 deposition hole. Influence of hydraulic rock properties on the water saturation phase. SKB TR-99-41, Svensk Kärnbränslehantering AB.

Börgesson L, Johannesson L-E, Hernelind J, 2004. Earthquake induced rock shear through a deposition hole. Effect on the Canister and the Buffer. SKB TR-04-02, Svensk Kärnbränslehantering AB.

Börgesson L, Sandén T, Fälth B, Åkesson M, Lindgren E, 2005. Studies of buffers behaviour in KBS-3H concept; Work during 2002–2004. SKB R-05-50, Svensk Kärnbränslehantering AB.

Börgesson L, Hernelind J, 2006a. Canister displacement in KBS-3V repository – A theoretical study. SKB TR-06-04, Svensk Kärnbränslehantering AB.

Börgesson L, Hernelind J, 2006b. Earthquake induced rock shear through a deposition hole – Influence of shear plane inclination and location as well as buffer properties on the damage caused to the canister. SKB TR 06-43, Svensk Kärnbränslehantering AB.

Börgesson L, Hernelind J, 2006c. Consequences of loss or missing bentonite in a deposition hole. SKB TR 06-13, Svensk Kärnbränslehantering AB.

Börgesson L, Sandén T, 2006. Piping and erosion in buffer and backfill materials – Current knowledge. SKB R-06-80, Svensk Kärnbränslehantering AB.

Carlson L, Karnland O, Olsson S, Rance A, Smart N, 2006. Experimental studies on the interactions between anaerobically corroding iron and bentonite. Posiva Working Report 2006-60 and SKB report R-08-28. Posiva Oy, Olkiluoto, Finland and SKB, Svensk Kärnbränslehantering AB.

Cathelinau M, Guillaume D, Mosser-Ruck R, Dubessy J, Charpentier D, Villiéras F, Michau N, 2005. Dissolution-crystallization processes affecting dioctahedral smectite in the presence of iron: implication on mineral distribution in clay barriers, ANDRA International Conference, 14–18 March 2005, Tours, France.

Cedercreutz J, 2004. Future climate scenarios for Olkiluoto with emphasis on permafrost. POSIVA 2004-06. Posiva Oy, Olkiluoto, Finland.

Charlet L, 2006. Transfers through the reactive clay barriers in radioactive waste repositories. Surface reactions between Fe2+ and smectites, in Wersin P, Mettler S. (2006). Workshop on Fe-clay interactions in repository environments, a joint initiative by Andra, SKB and Nagra. Basel 9–10 May 2006. Nagra NAB 06-15.

Curti E, Wersin P, 2002. Assessment of porewater chemistry in the bentonite backfill for the Swiss SF/HLW repository. Nagra Technical Report NTB 02-09. Nagra, Wettingen, Switzerland.

David D, 2001. Analogues archéologiques et corrosion. Andra Report 2001-192, Chatenay-Malabry, France.

Dillström P, 2005. Probabilistic analysis of canister inserts for spent nuclear fuel. SKB TR-05-19, Svensk Kärnbränslehantering AB.

Dong H, Fredrickson J K, Kennedy D W, Zachara J M, Kukkadapu R K, Onstott T C, 2000. Mineral transformation associated with the microbial reduction of magnetite. Chem. Geol. 169, 299–318.

Enescu N, Cosma C, Balu L, 2003. Seismic VSP and crosshole investigations in Olkiluoto, 2002. Posiva Working Report 2003-13. Posiva Oy, Olkiluoto, Finland.

Foster M D, 1953. Geochemical studies of clay minerals: II. Relation between ionic substitution and swelling in montmorillonites. Amer. Mineral. 38, 994–1006.

Fritz B, Marty N, Clément A, Michau N, 2006. Geochemical modelling of the influence of iron corrosion on bentonite stability, in Wersin P, Mettler S. (2006). Workshop on Fe-clay interactions in repository environments, a joint initiative by Andra, SKB and Nagra. Basel 9–10 May 2006. Nagra NAB 06-15.

Fälth B, Hökmark H, 2006. Seismically induced shear displacement on repository host rock fractures. Results of new dynamic discrete fracture modelling. SKB R-06-48, Svensk Kärnbränslehantering AB.

Génin J-M R, Bourrié G, Trolard F, Abdelmoula M, Jafreciz A, Refait P, Maitre V, Humbert B, Herbillon A, 1998. Thermodynamic equilibria in aqueous suspensions of synthetic and natural Fe(II)-Fe(III) green rusts: Occurences of the mineral in hydromorphic soils. Environ. Sci. Technol. 32, 1058–1068.

Gehör S, Karhu J, Kärki A, Löfman J, Pitkänen P, Ruotsalainen P, Taikina-aho O, 2002. Fracture calcites at Olkiluoto. Evidence from Quaternary Infills for Palaeohydrogeology. POSIVA 2002-03. Posiva Oy, Helsinki, Finland.

Gehör S, 2007. Mineralogical Characterization of Gouge Fillings in ONKALO Facility at Olkiluoto. Posiva working report 2007-33. Posiva Oy, Olkiluoto, Finland.

Grauer R, 1984. Behältermaterialien für die Endlagerung hochradioaktiver Abfälle: Korrosionschemische Aspekte. Nagra Technical Report NTB 84-19. Nagra, Wettingen, Switzerland.

Grivé M, Montoya V, Duro L, 2007. Assessment of the concentration limits for radionuclides for Posiva. Posiva Working Report 2007-103. Posiva Oy, Olkiluoto, Finland.

Guillaume D, Neaman A, Cathelineau M, Mosser-Ruck R, Pfeiffert C, Abdeloula M, Dubessy J, Villéras F, Baronnet A, Michau N, 2003. Experimental synthesis of chlorite from smectite at 300°C in the presence of metallic Fe.– Clay Minerals 38, 281–302.

Guillaume D, Neaman A, Cathelineau M, Mosser-Ruck R, Pfeiffert C, Abdelmoula M, Dubessy J, Villiéras F, Michau N, 2004. Experimental study of the transformation of smectite at 80 and 300°C in the presence of Fe oxides. Clay Minerals 39, 17–34.

Hagros A, 2007a. Estimated quantities of residual materials in a KBS-3H repository at Olkiluoto. Posiva working report 2007-104 and SKB report R-08-33. Posiva Oy, Olkiluoto, Finland and SKB, Svensk Kärnbränslehantering AB.

Hagros A, 2007b. Foreign materials in the repository: Update of estimated quantities. Posiva Working Report 2007-17. Posiva Oy, Olkiluoto, Finland.

Hagros A, Öhberg A, 2007. Hydrological monitoring in the VLJ repository at Olkiluoto during 2006. TVO VLJ Working report VLJ-5/07. (In Finnish with an English abstract). Posiva Oy, Olkiluoto, Finland.

Hakala M, Hudson J A, Harrison J P, Johansson E, 2008. Assessment of the Potential for Rock Spalling at the Olkiluoto Site. Working Report 2008-xx (in preparation). Posiva Oy, Olkiluoto, Finland.

Harrington J F, Horseman S T, 2003. Gas migration in KBS-3 buffer bentonite: sensitivity of test parameters to experimental boundary conditions. SKB TR-03-02, Svensk Kärnbränslehantering AB.

Hartikainen J, 2006. Numerical simulation of permafrost depth at Olkiluoto. Posiva Working Report 2006-52. Posiva Oy, Olkiluoto, Finland.

Hartley L, Hoch A, Jackson P, Joyce S, Mc Carthy R, Rodwell W, Swift B, Marsic N, 2006a. Groundwater flow and transport modelling during the temperate period for the SR-Can assessment Forsmark area – version 1.2. SKB R-06-98, Svensk Kärnbränslehantering AB.

Hartley L, Hoch A, Jackson P, Joyce S, Mc Carthy R, Swift B, Gylling B, Marsic N, 2006b. Groundwater flow and transport modelling during the temperate period for the SR-Can assessment. Laxemar subarea – version 1.2. SKB R-06-99, Svensk Kärnbränslehantering AB.

Haveman S A, Pedersen K, Ruotsalainen P, 1998. Geomicrobial investigations of groundwaters from Olkiluoto, Hästholmen, Kivetty and Rumuvaara, Finland. POSIVA 98-09. Posiva Oy, Helsinki, Finland.

Haveman S A, Larsdotter Nilsson E, Pedersen K, 2000. Regional distribution of microbes in groundwater from Olkiluoto, Hästholmen, Kivetty and Rumuvaara, Finland. POSIVA 2000-06. Posiva Oy, Helsinki, Finland.

Hedin A, 2005. An Analytic Method for Estimating the Probability of Canister/fracture intersections in a KBS-3 Repository. SKB R-05-29, Svensk Kärnbränslehantering AB.

Hellä P, Ahokas H, Palmén J, Tammisto E, 2006. Analysis of geohydrological data for design of KBS-3H repository layout. Posiva Working Report 2006-16 and SKB report R-08-27. Posiva Oy, Olkiluoto, Finland and SKB, Svensk Kärnbränslehantering AB.

Hermansson H-P, 2004. The stability of magnetite and its significance as a passivating film in the repository environment. SKI Report 2004:07, Stockholm, Sweden.

Himmelblau D M, 1960. Solubilities of inert gases in water. J. Chem. Eng, Vol. 5/1, January 1960.

Hökmark H, Fälth B, Wallroth T, 2006. T-H-M couplings in rock: Overview of numerical simulation results of importance to the SR-Can safety assessment. SKB report (draft May 2006), SKB, Svensk Kärnbränslehantering AB.

Ikonen K, 2003. Thermal analyses of KBS-3H type repository. POSIVA 2003-11. Posiva Oy, Olkiluoto, Finland.

Ikonen K, 2005. Thermal condition of open KBS-3H tunnel. POSIVA 2005-04 and SKB report R-08-24. Posiva Oy, Olkiluoto, Finland and SKB, Svensk Kärnbränslehantering AB.

Ikonen K, 2007. Far-field thermal-mechanical response of one- and two-storey repositories in Olkiluoto. Posiva Working report 2007-29. Posiva Oy, Olkiluoto, Finland.

Ikonen A T K, Hjerpe T, Aro L, Leppänen V, 2007. Terrain and ecosystems development model of Olkiluoto site, version 2006. Posiva Working Report 2007-110. Posiva Oy, Olkiluoto, Finland.

JNC, 2000. H12: Project to establish the scientific and technical basis for HLW disposal in Japan. Supporting Report 2. Repository design and engineering technology. JNC TN1410 2000-003, Japan Nuclear Cycle Development Institute, Tokai, Japan.

Johansson E, Äikäs K, Autio J, Hagros A, Malmlund H, Rautakorpi J, Sievänen U, Wanne T, Anttila P, Raiko H, 2002. Preliminary KBS-3H layout adaptation for the Olkiluoto site – Analysis of rock factors affecting the orientation of a KBS-3H deposition hole. Posiva Working Report 2002-57. Posiva Oy, Olkiluoto, Finland.

Johansson E, Hagros A, Autio J, Kirkkomäki T, 2007. KBS-3H layout adaptation 2007 for the Olkiluoto site. Posiva Working Report 2007-77 and SKB report R-08-31. Posiva Oy, Olkiluoto, Finland and SKB, Svensk Kärnbränslehantering AB.

Johnson L H, McGinnes D F, 2002. Partitioning of Radionuclides in Swiss Power Reactor Fuels. Nagra Technical Report NTB 02-07. Nagra, Wettingen, Switzerland.

Johnson L H, King F, 2003. Canister options for the disposal of spent fuel. Nagra Technical Report NTB 02-11, Wettingen, Switzerland.

Johnson L, Marschall P, Wersin P, Gribi P, 2005. HMCBG processes related to the steel components in the KBS-3H disposal concept. Posiva Working Report 2005-09 and SKB report R-08-25. Posiva Oy, Olkiluoto, Finland and SKB, Svensk Kärnbränslehantering AB.

Kalbantner P, Sjöblom R, 2000. Techniques for freeing deposited canisters Final report. SKB TR-00-15, Svensk Kärnbränslehantering AB.

Karnland O, Birgersson M, 2006. Montmorillonite stability. With special respect to KBS-3 conditions. SKB TR-06-11, Svensk Kärnbränslehantering AB.

King F, Ahonen L, Taxén C, Vuorinen U, Werme L, 2001/2002. Copper corrosion under expected conditions in a deep repository. SKB Technical Report TR-01-23, Stockholm, Sweden, and POSIVA 2002-01, Posiva Oy, Olkiluoto, Finland.

Kostka J E, Nealson K H, 1995. Dissolution and reduction of magnetite by bacteria.– Environ. Sci. Technol. 29, 2535–2540.

Kukkonen I, 2000. Thermal properties of the Olkiluoto mica gneiss: Results of laboratory measurements. Posiva Working Report 2000-40. Posiva Oy, Olkiluoto, Finland.

Lahdenperä A-M, Palmén J, Hellä P, 2005. Summary of overburden studies at Olkiluoto with an emphasis on geosphere-biosphere interface. Posiva Working Report 2005-11, Posiva Oy, Olkiluoto, Finland.

Lambeck K, Smither C, Johnston P, 1998. Sea-level change, glacial rebound and mantle viscosity for northern Europe. Geophys. J. Int, 134, 102–144.

Lanson B, 2006. Transformation processes of smectite in contact with metal iron: Mechanisms of smectite destabilization and characterization of the newly-formed phases. in Wersin P, Mettler S. (2006). Workshop on Fe-clay interactions in repository environments, a joint initiative by Andra, SKB and Nagra. Basel 9–10 May 2006. Nagra NAB 06-15.

Lantenois S, 2003. Réactivité fer métal/smectites en milieu hydraté à 80°C. PhD thesis, University of Orléans, France.

Lanyon G W, Marschall P, 2006. Discrete fracture network modelling of a KBS-3H repository at Olkiluoto. POSIVA 2006-06 and SKB report R-08-26. Posiva Oy, Olkiluoto, Finland and SKB, Svensk Kärnbränslehantering AB.

La Pointe P, Wallmann P, Thomas A, Follin S, 1997. A methodology to estimate earthquake effects on fractures intersecting canister holes. SKB TR-97-07, Svensk Kärnbränslehantering AB.

La Pointe P, Cladouhos T T, Outters N, Follin S, 2000. Evaluation of the conservativeness of the methodology for estimating earthquake-induced movements of fractures intersecting canisters, SKB TR-00-08, Svensk Kärnbränslehantering AB.

La Pointe P, Hermanson J, 2002. Estimation of rock movements due to future earthquakes at four Finnish candidate repository sites. Posiva report POSIVA 2002-02. Posiva Oy, Helsinki, Finland.

Lindberg A, 2007. Search for glacio-isostatic faults in the vicinity of Olkiluoto. Posiva Working Report 2007-05. Posiva Oy, Helsinki, Finland.

Luukkonen A, Pitkänen P, Partamies S, 2004. Significance and estimations of lifetime of natural fracture mineral buffers in the Olkiluoto bedrock. Posiva working report 2004-08. Posiva Oy, Olkiluoto, Finland.

Löfman J, 2005. Simulation of hydraulic disturbances caused by decay heat of the repository in Olkiluoto. POSIVA 2005-07. Posiva Oy, Helsinki, Finland.

Löfman J, Mészáros F, 2005. Simulation of hydraulic disturbances caused by the underground rock characterisation facility in Olkiluoto. POSIVA 2005-08. Posiva Oy, Helsinki, Finland.

Lönnqvist M, Hökmark H, 2007. Thermo-mechanical analyses of a KBS-3H deposition drift at the Olkiluoto site. Posiva Working Report 2007-66 and SKB report R-08-30. Posiva Oy, Olkiluoto, Finland and SKB, Svensk Kärnbränslehantering AB.

Madsen F T, 1998. Clay mineralogical investigations related to nuclear waste disposal. Clay Minerals 33, 109–129.

Marcos N, 2003. Bentonite-iron interactions in natural occurrences and in laboratory – the effects of the interaction on the properties of bentonite: a literature survey. Posiva Working Report 2003-55, Posiva Oy, Olkiluoto, Finland.

Marschall P, Fein E, Kull H, Lanyon W, Liedtke L, Müller-Lyda I, Shao H, 1999. Conclusions of the Tunnel Near-Field Programme. Nagra Technical Report NTB 99-07, Wettingen, Switzerland.

Martin D, 2005. Preliminary assessment of potential underground stability (wedge and spalling) at Forsmark, Simpevarp and Laxemar sites. SKB R-05-71, Svensk Kärnbränslehantering AB.

Martino J B, Chandler N A, Read R S, Baker C, 2002. Response of the tunnel sealing experiment concrete bulkhead to pressurization. Report No: 06819-REP-01200-10085-R00. Ontario Power Generation, Toronto, Canada.

Masurat P, 2006. Potential for corrosion in disposal systems for high-level radioactive waste by *Meiothermus and Desulfovibrio*. Doctoral thesis. Göteborg University, Sweden.

Mata M P, Giorgetti G, Árkai P, Peacor D R, 2001. Comparison of evolution of trioctahedral chlorite/berthierine/smectite in coeval metabasites and metapelites from diagenetic to epizonal grades. Clays and Clay Minerals 49, 318–332.

Metcalfe R, Walker C, (eds) 2004. Proceedings of a the International Workshop on Bentonite-Cement Interaction in Repository Environments, 14–16 April 2004, Tokyo, Japan. Posiva Working Report 2004-25 (NUMO-TR-04-05), Posiva Oy, Olkiluoto, Finland.

Miller B, Marcos N, 2007. Process report- FEPs and scenarios for a spent fuel repository at Olkiluoto. POSIVA 2007-12. Posiva Oy, Eurajoki, Finland.

Montori J, Soler J M, Saaltink M W, 2008. Reactive transport modeling of the effect of hyperalkaline solutions along a fracture at the Onkalo site. Posiva Working Report 2008-18. Posiva Oy, Eurajoki, Finland.

Montoto M, Rodriguez-Rey A, Martinez-Nistal A, Diez-sarriá I, 1999. Fractographic characterization by quantitative microscopy of the excavation disturbance caused by boring of the experimental full scale deposition holes in the Research Tunnel at Olkiluoto. Posiva Working Report 99-69. Posiva Oy, Olkiluoto, Finland.

Montoto M, Rodriguez-Rey A, Autio J, 2003. Microfractographic characterization of the excavation damage caused by boring of the experimental full scale deposition holes in the Research Tunnel at Olkiluoto. CLUSTER conference on "Impact of the EDZ on the performance of radioactive waste geological repositories", Luxembourgh 3–5 November 2003.

Munier R, Hökmark H, 2004. Respect distances; rationale and means of computation. SKB R-04-17, Svensk Kärnbränslehantering AB.

Muurinen A, Lehikonen J, 1999. Porewater chemistry in compacted bentonite. POSIVA 99-20. Posiva Oy, Olkiluoto, Finland.

Muurinen A, 2006. Chemical Conditions in the A2 Parcel of the long-term test of buffer material in Äspö (LOT). Posiva Working Report 2006-83. Posiva Oy, Olkiluoto, Finland.

Müller-Vonmoos M, Kahr G, 1983. Mineralogische Untersuchungen von Wyoming Bentonit MX-80 und Montigel. Nagra Technical Report NTB 83-12. Nagra, Wettingen, Switzerland.

Müller Ch, Elagin M, Scharmach M, Bellon C, Jaenisch G-R, Bär S, Redmer B, Goebbels J, Ewert U, Zscherpel U, Boehm R, Brekow G, Erhard A, Heckel T, Tessaro U, Tscharntke D, Ronneteg U, 2006. Reliability of nondestructive testing (NDT) of the copper canister seal weld. SKB R-06-08, Svensk Kärnbränslehantering AB.

Nagra, 2002. Project Opalinus Clay: Safety report. Demonstration of disposal feasibility for spent fuel, vitrified high-level waste and long-lived intermediate-level waste (Entsorgungsnachweis). Nagra Technical Report NTB 02-05. Nagra, Wettingen, Switzerland.

Neall F, Pastina B, Smith P, Gribi P, Snellman M, Johnson L, 2007. Safety assessment for a KBS-3H spent nuclear fuel repository at Olkiluoto – Complementary evaluations of safety report. POSIVA 2007-10 and SKB report R-08-35. Posiva Oy, Olkiluoto, Finland and SKB, Svensk Kärnbränslehantering AB.

Neretnieks I, 1985. Some aspects of the use of iron canisters in deep lying repositories for nuclear waste. Nagra Technical report NTB 85-35. Nagra, Wettingen, Switzerland.

Neretnieks I, 2006. Flow and transport through a damaged buffer – exploration of the impact of a cemented and an eroded buffer. SKB TR-06-33, Svensk Kärnbränslehantering AB.

Oversby V M, 1996. Criticality in a high level waste repository. A review of some important factors and an assessment of the lessons learned from the Oklo reactors. SKB TR-96-07, Svensk Kärnbränslehantering AB.

Oversby V M, 1998. Criticality in a repository for spent fuel: lessons from Oklo. Mat. Res. Soc. Symp. Proc. Vol. 506, p 781.

Pastina B, Hellä P, 2006. Expected evolution of a spent fuel repository at Olkiluoto. POSIVA 2006-05. Posiva Oy, Olkiluoto, Finland.

Paulamäki S, Paananen M, Gehör S, Kärki A, Front K, Aaltonen I, Ahokas T, Kemppainen K, Mattila J, Wikström L, 2006. Geological model of the Olkiluoto site v.0. Posiva Working Report 2006-37. Posiva Oy, Olkiluoto, Finland.

Pedersen K, 2000. Microbial processes in radioactive waste disposal. SKB TR-00-04, Svensk Kärnbränslehantering AB.

Pedersen K, 2006. Microbiology of Transitional Groundwater of the Porous Overburden and Underlying Fractured Bedrock Aquifers in Olkiluoto 2004, Finland. Posiva Working Report 2006-09. Posiva Oy, Olkiluoto, Finland.

Pedersen K, 2007. Microbiology of Transitional Groundwater of the Porous Overburden and Underlying Shallow Fractured Bedrock Aquifers in Olkiluoto, Finland, October 2005– January 2006, Finland. Posiva Working Report 2007-20. Posiva Oy, Olkiluoto, Finland.

Pitkänen P, Partamies S, Luukkonen A, 2004. Hydrogeochemical interpretation of baseline groundwater conditions at the Olkiluoto site. POSIVA 2003-07. Posiva Oy, Olkiluoto, Finland.

Pitkänen P, Partamies S, 2007. Origin and Implications of Dissolved Gases in Groundwater at Olkiluoto, POSIVA 2007-04. Posiva Oy, Olkiluoto, Finland.

Pitkänen P, Ahokas H, Ylä-Mella M, Partamies S, Snellman M, Hellä P, 2007. Quality Review of Hydrochemical Baseline Data from the Olkiluoto Site, POSIVA 2007-05. Posiva Oy, Olkiluoto, Finland.

Posiva, 2003. Baseline conditions at Olkiluoto. POSIVA 2003-02. Posiva Oy, Olkiluoto, Finland.

Posiva, 2005. Olkiluoto Site Description 2004. POSIVA 2005-03. Posiva Oy, Olkiluoto, Finland.

Posiva, 2006. Nuclear Waste Management of the Olkiluoto and Loviisa Power Plants: Programme for Research, Development and Technical Design for 2007–2009. TKS-2006. Posiva Oy, Olkiluoto, Finland.

Pusch R, Karnland O, 1990. Preliminary report on longevity of montmorillonite clay under repository-related conditions, SKB TR-90-44, Svensk Kärnbränslehantering AB.

Pusch R, 1999. Mobility and survival of sulphate-reducing bacteria in compacted and fully water saturated bentonite – microstructural aspects. SKB TR-99-30, Svensk Kärnbränslehantering AB.

Pusch R, 2000. On the effect of hot water vapor on MX-80 clay. SKB TR-00-16, Svensk Kärnbränslehantering AB.

Raiko H, Salo J-P, 1999. Design report of the disposal canister for twelve fuel assemblies. POSIVA 99-18. Posiva Oy, Helsinki, Finland.

Raiko H, 2005. Disposal canister for spent nuclear fuel – Design report. POSIVA 2005-02. Posiva Oy, Olkiluoto, Finland.

Rasilainen K, 2004. Localisation of the SR-97 process report for Posiva's spent fuel repository at Olkiluoto. POSIVA 2004-05, Posiva Oy, Olkiluoto, Finland.

Ronneteg U, Cederqvist L, Rydén H, Öberg T, Müller C, 2006. Reliability in sealing of canister for spent nuclear fuel. SKB R-06-26, Svensk Kärnbränslehantering AB.

Saari J, 2006. Local seismic network at the Olkiluoto Site – Annual Report for 2005. Posiva Working Report 2006-57, Posiva Oy, Olkiluoto, Finland.

Saanio T, Kirkkomäki T, Sacklén N, Autio J, Kukkola T, Raiko H, 2004. Spent nuclear fuel repository at Olkiluoto – Preliminary design – Stage 1. Posiva Working Report 2003-74. Posiva Oy, Olkiluoto, Finland.

Sandén T, Börgesson L, Dueck A, Goudarzi R, Lönnqvist M, Nilsson U, Åkesson M, 2007. KBS-3H Buffer tests 2005–2007. SKB R-08-40 and Posiva working report 2008-10 (in preparation). SKB, Svensk Kärnbränslehantering AB, Sweden and Posiva, Olkiluoto, Finland.

Savage D, Wilson J, 2006. Iron-bentonite Interaction: the role of secondary minerals on long-term behaviour, in Wersin P, Mettler S. (2006). Workshop on Fe-clay interactions in repository environments, a joint initiative by Andra, SKB and Nagra. Basel 9–10 May 2006. Nagra NAB 06-15.

Shen S, Stucki J W, Boast C W, 1992. Effects of structural iron reduction on the hydraulic conductivity of Na-smectite.– Clays and Clay Minerals 40, 381–386.

SKB, 1999. SR 97 Processes in the repository evolution. SKB TR-99-07, Svensk Kärnbränslehantering AB.

SKB, 2004a. RD&D-Programme 2004 – Programme for research, development and demonstration of methods for the management and disposal nuclear waste, including social science research. SKB, Svensk Kärnbränslehantering AB.

SKB, 2004b. Interim main report of the safety assessment SR-Can. SKB TR-04-11, Svensk Kärnbränslehantering AB.

SKB, 2005. Äspö Hard Rock Laboratory – Annual Report 2004. SKB TR-05-10, Svensk Kärnbränslehantering AB.

SKB, 2006a. Long-term safety for KBS-3 repositories at Forsmark and Laxemar – a first evaluation. Main report of the SR-Can project. SKB TR-06-09, Svensk Kärnbränslehantering AB.

SKB, 2006b. FEP report for the safety assessment SR-Can. SKB TR-06-20, Svensk Kärnbränslehantering AB.

SKB, 2006c. Fuel and canister process report for the safety assessment SR-Can. SKB TR-06-22, Svensk Kärnbränslehantering AB.

SKB, 2006d. Buffer and backfill process report for the safety assessment SR-Can. SKB TR-06-18, Svensk Kärnbränslehantering AB.

SKB, 2006e. Geosphere process report for the safety assessment SR-Can. SKB TR-06-19, Svensk Kärnbränslehantering AB.

SKB, 2006f. Data report for the safety assessment SR-Can. SKB TR-06-25, Svensk Kärnbränslehantering AB.

SKB, 2007. FUD-program 2007. Program för forskning, utveckling och demonstration av metoder för hantering och slutförvaring av kärnavfall. SKB AB, pages 173–176. Svensk Kärnbränslehantering AB.

SKB/Posiva, 2008. Horizontal deposition of canisters for spent nuclear fuel – Summary of the KBS-3H Project 2004–2007. SKB TR-08-03. POSIVA 2008-03 (in preparation). SKB, Svensk Kärnbränslehantering AB, Sweden and Posiva Oy, Olkiluoto, Finland.

Smart N R, Blackwood D J, Werme L, 2001. The anaerobic corrosion of carbon steel and cast iron in artificial groundwaters. SKB TR-01-22, Svensk Kärnbränslehantering AB.

Smart N R, Blackwood D J, Werme L, 2002a. Anaerobic Corrosion of Carbon Steel and Cast Iron in Artificial Groundwaters: Part 1–Electrochemical Aspects, Corrosion Vol. 58, 547.

Smart N R, Blackwood D J, Werme L, 2002b. Anaerobic Corrosion of Carbon Steel and Cast Iron in Artificial Groundwaters: Part 2–Gas Generation, Corrosion Vol. 58, 627.

Smart N R, Rance A P, Werme L O, 2004. Anaerobic corrosion of steel in bentonite.– Mat. Res. Soc. Symp. Proc. 807, 441–446.

Smart N R, Rance A P, Fennell P A H, 2005. Galvanic corrosion of copper-cast iorn couples. SKB TR-05-06, Svensk Kärnbränslehantering AB.

Smart N R, 2006. Interaction between iron corrosion products and bentonite, in Wersin P, Mettler S. (2006). Workshop on Fe-clay interactions in repository environments, a joint initiative by Andra, SKB and Nagra. Basel 9–10 May 2006. Nagra NAB 06-15.

Smart N R, Rance A P, Carlson L, Werme L O, 2006. Further Studies of the Anaerobic Corrosion of Steel in Bentonite, Mat. Res. Soc. Symp. Proc. 813–820, Vol. 932, Materials Research Society.

Smith P, Nordman H, Pastina B, Snellman M, Hjerpe T, Johnson L, 2007a. Safety assessment for a KBS-3H spent nuclear fuel repository at Olkiluoto – Radionuclide transport report. POSIVA 2007-07 and SKB R-08-38. Posiva Oy, Olkiluoto, Finland and SKB, Svensk Kärnbränslehantering AB, Sweden.

Smith P, Neall F, Snellman M, Pastina B, Nordman H, Johnson L, 2007b. Safety assessment for a KBS-3H spent nuclear fuel repository at Olkiluoto – Summary Report. POSIVA 2007-06 and SKB R-08-39. Posiva Oy, Olkiluoto, Finland and SKB, Svensk Kärnbränslehantering AB.

Smith P, Johnson L, Snellman M, Pastina B, Gribi P, 2007c. Safety assessment for a KBS-3H spent nuclear fuel repository at Olkiluoto – Evolution report. POSIVA 2007-08 and SKB R-08-37. Posiva Oy, Olkiluoto, Finland and SKB, Svensk Kärnbränslehantering AB, Sweden.

Stroes-Gascoyne S, Hamon C J, Kohle C, Dixon D A, 2006. The effects of dry density and porewater salinity on the physical and microbiological characteristics of highly compacted bentonite. Ontario Power Generation Report No: 06819-REP-01200-10016-R00.

Stucki J W, Golden D C, Roth C B, 1984. Effects of reduction and reoxidation of structural iron on the surface charge and dissolution of diochtahedral smectites.– Clays and Clay Minerals 32, 350–356.

Stucki J W, Wu J, Gan H, Komadel P, Banin A, 2000. Effects of iron oxidation state and organic cations on dioctahedral smectite hydration.– Clays and Clay Minerals 48, 290–298.

STUK, 1999. Government decision on the safety of disposal of spent nuclear fuel (478/1999). Report STUK-B-YTO 195. Radiation and Nuclear Safety Authority (STUK), Helsinki, Finland.

STUK, 2001. Long-term safety of disposal of spent nuclear fuel. Guide YVL 8.4. Radiation and Nuclear Safety Authority (STUK), Helsinki, Finland.

Svensson U, 2006. The Laxemar and Forsmark repositories. An analysis of the water inflow distribution. SKB R-06-102, Svensk Kärnbränslehantering AB.

Vaittinen T, Ahokas H, Heikkinen E, Hellä P, Nummela J, Saksa P, Tammisto E, Paulamäki S, Paananen M, Front K, Kärki A, 2003. Bedrock model of the Olkiluoto site, version 2003/1. Posiva Working report 2003-43. Posiva Oy, Olkiluoto, Finland.

Vieno T, Hautojärvi A, Koskinen L, Nordman H, 1992. TVO-92 Safety Analysis of Spent Fuel Disposal. Report YJT-92-33E, Nuclear Waste Commission of Finnish Power Companies, Helsinki, Finland.

Vieno T, Nordman H, 1999. Safety assessment of spent fuel disposal in Hästholmen, Kivetty, Olkiluoto and Romuvaara TILA-99. Posiva Report 99-07, Posiva Oy, Olkiluoto, Finland.

Vieno T, Nordman H, 2000. Updated compartment model in near-field transport in KBS-3 type repository. Posiva Working Report 2000-41. Posiva Oy, Olkiluoto, Finland.

Vieno T, Lehikoinen J, Löfman J, Nordman H, Mészáros F, 2003. Assessment of disturbances caused by construction and operation of ONKALO. POSIVA 2003-06. Posiva Oy, Olkiluoto, Finland.

Vieno T, Ikonen A T K, 2005. Plan for Safety Case of spent fuel repository at Olkiluoto. POSIVA 2005-01. Posiva Oy, Olkiluoto, Finland.

Vogt K, Köster H M, 1978. Zur Mineralogie, Kristallchemie und Geochemie einiger Montmorillonite aus Bentoniten.– Clay Minerals 13, pp.25–43.

Vuorinen U, Lehikoinen J, Imoto H, Yamamoto T, Cruz Alonso M, 2005. Injection grout for deep repositories, Subproject 1: low-pH cementitious grout for larger fractures, leach testing of grout mixes and evaluation of the long-term safety. Posiva working report 2004-46. Posiva Oy, Olkiluoto, Finland

Wanner H, Wersin P, Sierro N, 1992. Thermodynamic modelling of bentonite-groundwater interaction and implications for near field chemistry in a repository for spent fuel. SKB TR-92-37, Svensk Kärnbränslehantering AB.

Wanner H, Albinsson Y, Karnland O, Wieland E, Wersin P, Charlet L, 1994. The acid/base chemistry of montmorillonite.– Radiochim. Acta 66/67, pp.157–162.

Wersin P, 2003. Geochemical modelling of bentonite porewater in high-level waste repositories. J. Contam. Hydrol. 61, 405–422.

Wersin P, Johnson, L H, Schwyn B, Berner U, Curti E, 2003. Redox Conditions in the Near Field of a Repository for SF/HLW and ILW in Opalinus Clay. Nagra Technical Report NTB 02-13. Nagra, Wettingen, Switzerland.

Wersin P, Mettler S, 2006. Workshop on Fe-clay interactions in repository environments, a joint initiative by Andra, SKB and Nagra. Basel 9–10 May 2006. Nagra NAB 06-15.

Wersin P, Birgersson M, Olsson S, Karnland O, Snellman M, 2007. Impact of corrosion-derived iron on the bentonite buffer within the KBS-3H disposal concept. The Olkiluoto site as case study. POSIVA 2007-11 and SKB R-08-34. Posiva Oy, Olkiluoto, Finland and SKB, Svensk Kärnbränslehantering AB, Sweden.

Wikramaratna R S, Goodfield M, Rodwell W R, Nash P J, Agg P J, 1993. A preliminary assessment of gas migration from the copper/steel canister. SKB TR-93-31, Svensk Kärnbränslehantering AB.

Wilson J, Cressey G, Cressey B, Cuadros J, Ragnarsdottir K V, Savage D, Shibata M, 2006a. The effect of iron on montmorillonite stability: (II) Experimental investigation. Geochim. Cosmochim. Acta 70, 323–336.

Wilson J, Savage D, Cuadros J, Shibata M, Ragnarsdottir K V, 2006b. The effect of iron on montmorillonite stability. (I) Background and thermodynamic considerations. Geochim. Cosmochim. Acta 70, 306–322.

Appendix A

List of input parameters

The purpose of this appendix is to list the input data used in this report and in the other KBS-3H long-term safety study reports. Data used in this report are based on the preliminary information available at the time of report writing (2006–2007). Design data are to be considered preliminary as the KBS-3H design work is still in progress. The information for design provided in this table is mostly based on the Design Description 2006 (DD 2006). A generic report on data, models, codes, and databases that would apply both to the KBS-3V and KBS-3H will be produced at a later time.

A.1 Origin of input data

The data in Table A-1 is based on different origins, as discussed below. The references are in the table next to the data. Design data are to be considered as preliminary as the design work is still in progress.

- Repository depth: the values are from the preliminary design for a KBS-3V repository in Olkiluoto.
- Deposition drift: the drift diameter is from the buffer design studies and design descriptions 2006 and 2007 (the latter for tolerances). Drift length and separation between drifts are from the Layout Adaptation report. The drift dip appeared first in the KBS-3H summary report 2004. The drift orientation is from the Layout adaptation report and the main principal stress is from the Olkiluoto Site Description 2004.
- Canister and insert: dimensions are from the canister design report for all fuel types. The 2006 spent fuel inventories for Posiva's fuel types are from the 3V Evolution Report.
- Supercontainer shell: supercontainer shell material, dimensions and surface areas (including hole edges and feet) are from the DD 2006. Carbon steel composition is from the European Structural Steel Standard EN 10025. Shell diameter and steel thickness as well as perforation hole diameter and degree of perforation are from KBS-3H buffer studies. Alternative values for other fuel types (VVER and EPR) are from the Layout Adaptation report and the Canister Design report.
- Buffer rings and end blocks: Initial water content of the buffer ring is 10% after KBS-3H buffer studies (Buffer study report 2002–2004). Buffer block length and gap to canister are also from the same studies. Other buffer dimensions are from the DD 2006. The saturated porosity of the buffer is from SKB's SR-97 Process report and the swelling pressure is from SR-Can Main report. The reference value of buffer porosity is used in scoping calculation in this report and in the Evolution Report. The alternative value was used in the radionuclide transport calculations, according to SR-Can.
- Distance blocks: all data concerning the Basic Design is from the DD 2006 and references therein. Data concerning the DAWE design is partly from KBS-3H buffer studies.
- Fixing rings: Data is from the DD 2006, the *assumption* on the number of fixing rings in a drift (4–5) is from the Residual Materials report.
- Filling blocks: all data is from the DD 2006. Filling blocks have not yet been designed in detail so the information is very preliminary at this stage.
- Plugs: all data is from the DD 2006. The composition of the low-heat high performance cement is from AECL (Canada) but this type of plug has not been tested yet in the Olkiluoto conditions.
- Spray and drip shields: the description is from the DD 2006, the *assumption* on the inventory is from the Residual Materials report. In these reports, the thickness of these shields is not reported. In the present report, the *assumption* on the thickness (1 mm) was made to calculate the amount of gas generated per shield (see Section 5.5.1).

- Backfill: the *assumptions* on backfill inventories for the deposition niches and the access and central tunnels are from the Residual Materials report. The backfill material has not yet been selected.
- Cement and colloidal silica: the *assumptions* on cement inventory for the deposition niches and the access tunnels are from the Residual Materials report. Grouting estimates are based on ONKALO grouting experience, scaled to the relevant drift size. Grouting cement composition is *measured* on samples from ongoing cement tests in ONKALO. The composition of colloidal silica used for grouting is *measured* and comes from the Silica Sol supplier (BASF via EKA Chemicals).
- Bentonite: MX-80 bentonite composition is from SR-Can Main report.
- Steel: steel corrosion rate for the supercontainer shell and the cast iron insert is from *experimental work* on steel corrosion rates in presence of bentonite. *Expert judgment* has been exercised in selecting the long-term steel corrosion rate based on experimental studies and natural analogues information available in the literature. The rationale for rate selection is described in Section 2.5.1 and Section 5.7.1 of the present report.
- Rock properties:
  - Geochemical properties: TDS (Total dissolved solids) data in present day conditions is from the Olkiluoto Site Description 2006 and is a sum of concentrations of cations and anions *measured* at the repository depth (400–500 m). Hydrochemical data are from the OIVA database. This database is continuously updated along with the new data collected from Olkiluoto, as described in /Pitkänen et al. 2007/. The data table used for this report was from the file called "uusiOIVA_10032006.xls". Future evolution of the TDS is from the 3V Evolution Report and they are the result of *modelling* work and *expert judgment*. pH, redox potential, dissolved metals, dissolved gases are *measured* data. Solubilities of gases were taken from the literature.
  - Geological properties: Fractures are from the geological *model* presented in the Site Description 2006. Fracture density and transmissivity are *calculated/assumed* statistical analyses of vertical borehole data from depths of 300–700 m at Olkiluoto /Hellä et al. 2006/. The hydraulic conductivity range of mica gneiss and gneiss is *estimated (expert judgement)* from a range of rock conditions. Rock porosity, gas effective diffusion constant and gas intrinsic permeability are *measured* on Gneissic tonalite in the Research Tunnel at Olkiluoto. Hydraulic conductivity was *calculated* from the gas permeability values using a scaling factor to convert to diffusivity of heavier molecules in water- saturated samples by 1/35,000 /Autio et al. 1999/. EDZ properties are from *observations and measurements* in the Research Tunnel at Olkiluoto. EDZ properties at repository depth are still highly uncertain at present.
  - Hydraulic properties: leakage rates in a drift without sealing are *estimated* based on statistical analyses of borehole data. The leakage after grouting in a drift is from the KBS-3H DFN model /Lanyon and Marschall 2006/. The maximum inflow *calculated* in all realisations is about 15 L/min with less than 1% of drifts exceeding 10 L/min. The saturation time for the drift is *calculated* from buffer studies. The hydraulic gradient is based on site-scale groundwater flow modeling results /Löfman 1999/.
  - Mechanical properties: stress state is from in situ borehole measurements at relevant depths, as reported in the Olkiluoto Site Description 2006. Rock strength values (including spalling strength) are *estimated* based on laboratory tests on core samples from Olkiluoto and in situ observations from the Äspö Pillar Stability Experiment. Some *expert judgment* was applied in deriving the Olkiluoto in situ rock strength from laboratory results and Äspö observations.
  - Thermal properties: the temperature of the Olkiluoto rock at repository depth has been *measured.*

Table A-1. Input parameter values for the KBS-3H Process Report and in other KBS-3H long-term safety reports.

PARAMETER	Unit	Symbol	Reference value	Alternative values	Reference
REPOSITORY DEPTH					
one-storey	m		400–420		/Saanio et al 2004/
two-storeys	m			420 and 500–520	/Saanio et al 2004/
DEPOSITION DRIFT					
Diameter	mm	$2\,r_t$	1,850 0/–10 mm	1,840	/Börgesson et al. 2005, Autio et al. 2007/ tolerances are from /Autio et al. 2008/
Length	m		300 (272 mean)	100–300	/Johansson et al. 2007/ The total length includes the deposition niche.
separation between drifts	m	d	25	40	/Johansson et al. 2007/
Drift dip	°		2 +/–1		/Thorsager and Lindgren 2004/
Drift orientation	°		120 +/–10, parallel to main principal stress		/Johansson et al. 2007, Posiva 2005/
CANISTER					
Reference case					
Posiva, BWR 1700 W					
outer diameter	mm	$2\,r_c$	$1{,}050\ ^{+2,35}/_{-2,35}$		/Raiko 2005/ tolerances are from /Autio et al. 2008/
Length	mm	l_c	4,800	$4835\ ^{+2,85}/_{-2,35}$	/Raiko 2005/ tolerances are from /Autio et al. 2008/
thickness	m		0.05		/Raiko 2005/
total number of canisters			1,210		/Pastina and Hellä 2006/
total amount of spent fuel	tU		2,530		/Pastina and Hellä 2006/
Cast iron insert					
dimensions of fuel channels	m		4.45 * 0.16 * 0.16		/Raiko 2005/
number of fuel channels per insert	–		12		/Raiko 2005/
mass of iron and steel	kg		13,400		/Raiko 2005/
void space	m^3		0.95		/Raiko 2005/
Alternative cases					
Posiva VVER 1,370 W					
outer diameter	m	$2\,r_c$		1.05	/Raiko 2005/
length	m	l_c		3.60	/Raiko 2005/
thickness	m			0.05	
total number of canisters				700	/Pastina and Hellä 2006/
total amount of spent fuel	tU			1,020	/Pastina and Hellä 2006/
Posiva EPR 1830 W					
outer diameter	m	$2\,r_c$		1.05	/Raiko 2005/
length	m	l_c		5.25	/Raiko 2005/
thickness	m			0.05	
total number of canisters				930	/Pastina and Hellä 2006/
total amount of spent fuel	tU			1,980	/Pastina and Hellä 2006/
Overall Posiva inventory					
Total number of canisters			2,840	3,000	/Pastina and Hellä 2006/ A rounded up value of 3,000 canisters was used in scoping calculations in the Evolution Report /Smith et al. 2007/.
Total amount of spent fuel	tU		5,530		/Pastina and Hellä 2006/

PARAMETER	Unit	Symbol	Reference value	Alternative values	Reference
COPPER PROPERTIES					
density	kg m^{-3}	ρcu	8,900		/CRC 2007/
molar weight	g mol^{-1}		64		/CRC 2007/
SUPERCONTAINER SHELL, SC					
A SC + distance block unit can be placed in the drift in sections with water inflow rate					
< 0.1L/min					
Container materials and dimensions					
Reference case – Posiva, BWR 1700 W					
Shell material			carbon steel S235JRG2		/Autio et al. 2007/
Fraction of total mass of elements	%				/EN 10025/
C			<0.17		
Si – Mn			<0.14		
P			<0.045		
S			<0.045		
Cr,Ni,Al,Cu			–		
Shell, total mass	kg		1,031, with feet 1,071	890	/Autio et al. 2007/ the alternative value corresponds to an older shell design.
Shell, length	mm	l_{sc}	5,525	$5{,}556^{+5}/_{0}$	/Autio et al. 2007/ tolerances are from /Autio et al. 2008/
feet, total mass (10 feet per SC)	kg		40.2		/Autio et al. 2007/
Shell, outer diameter	mm	$2\,r_{sc}$	$1{,}765\ ^{0}/_{-2}$		/Börgesson et al. 2005/
inner diameter	mm		1,749		/Börgesson et al. 2005/
steel, thickness	mm		8		/Börgesson et al. 2005/
Void volume to canister and around a SC before saturation	mm		5		See definition of gaps below under Bentonite blocks in the SC
SC surface area					
External+ internal surface area+ hole edges surface area+ feet	m^2		41.52	41.39 (min)	/Autio et al. 2007/
External+ internal surface area+ feet	m^2		35.73	35.6 (min)	/Autio et al. 2007/
shell, diameter of perforation holes	mm		100		/Börgesson et al. 2005/
shell, degree of perforation	%		62		/Börgesson et al. 2005/
End plate, no perforation	%		0		/Autio et al. 2007/
steel thickness	mm		8		/Autio et al. 2007/
Alternative cases					
Posiva VVER 1370 W					
Total mass	kg			880	/Autio et al. 2007/
Length	mm	l_{sc}		4,330	/Raiko 2005/
Posiva EPR 1830 W					
Total mass	kg			1,140	/Autio et al. 2007/
Length	mm	l_{sc}		5,980	/Raiko 2005/
STEEL PROPERTIES					
Steel corrosion rate for the supercontainer shell	µm a^{-1}	R	1	2	/Smart et al. 2004/ Section 7.5.1
Steel corrosion rate for the cast iron insert	µm a^{-1}	R	1	10 (only for sensitivity analysis purposes)	/Smart et al. 2004/ Section 2.5.1
Density of iron/steel	kg m^{-3}		7,800		/CRC 2007/
Molar weight of iron	g mol^{-1}		56		/CRC 2007/
Bentonite blocks in the SC					
Bentonite, MX-80					

PARAMETER	Unit	Symbol	Reference value	Alternative values	Reference
ring blocks					
initial water content	w-%		10		/Börgesson et al. 2005/
initial dry density	kg m^{-3}		1,885	1,789–1,977	/Autio et al. 2007/
saturated density after swelling	kg m^{-3}		2,000	1,950–2,050	/Autio et al. 2007/
end blocks					/Autio et al. 2007/
initial water content	w-%		10		/Autio et al. 2007/
initial dry density	kg m^{-3}		1,753	1,667–1,837	/Autio et al. 2007/
saturated density after swelling	kg m^{-3}		2,000	1,950–2,050	/Autio et al. 2007/
ring and end blocks					
saturated porosity after swelling	%	ε_b	44	43	/SKB 1999, Autio et al. 2007/
swelling pressure	MPa		7–8		/SKB 2006/
Block dimensions					
Gap to canister (radial)	mm		5		/Börgesson et al. 2005/
gap to super container (radial)	mm		5		/Autio et al. 2007/
diameter end blocks	mm		1,739	1,740 $^{+1}/_{-2}$	/Autio et al. 2007/ tolerances are from /Autio et al. 2008/
outer diameter ring blocks	mm		1,739	1,740 $^{+1}/_{-2}$	/Autio et al. 2007/ tolerances are from /Autio et al. 2008/
inner diameter ring blocks	mm		1,058 $^{+1}/_{-1}$		/Autio et al. 2008/
length end blocks	mm		700 (2*350) $^{+2}/_{-2}$		/Börgesson et al. 2005/ tolerances are from /Autio et al. 2008/
length ring blocks	mm		4,810 (4* 1,202.5)	4,844 $^{+4}/_{-4}$ (4*1,211 $^{+1}/_{-1}$)	/Autio et al. 2007/ modified to the reference length (4,844–>4,810 mm). The alternative value and tolerances are from /Autio et al. 2008/.
Bentonite,total mass in one SC	kg		16,445		
DISTANCE BLOCKS					
Reference case – Posiva, BWR 1,700 W, 25 m separation between drifts					
Basic Design, BD					
Distance block					
Total length	mm		5,475		/Autio et al. 2007/
Distance block unit is composed of “tight” and “loose” component					
“Tight” component					
Diameter	mm		1,850	1,840	/Autio et al. 2007/
Length	mm		1,000		/Autio et al. 2007/
block slices of thickness of 500 mm					
Bentonite MX-80					
initial water content	w-%		24		
initial dry density	kg m^{-3}		1,559	1,570	Alternative value is from Figure 4-8 in Sr-Can /SKB 2006/
saturated density after swelling	kg m^{-3}		2,000		
saturated porosity after swelling	%	ε_b	44		/Autio et al. 2007/
“Loose” component					
Diameter	mm		1,820		/Autio et al. 2007/
Length	mm		4,475		/Autio et al. 2007/
block slices of thickness of 500 mm					
Centred blocks					
Supporting feets, material type and design, not done	–				

PARAMETER	Unit	Symbol	Reference value	Alternative values	Reference
Bentonite MX-80					
initial water content	w-%		24	26	/Autio et al. 2007/
initial dry density	kg m^{-3}		1,610		/Autio et al. 2007/
saturated density after swelling	kg m^{-3}		2,000		
saturated porosity after swelling	%	ε_b	44		
Total amount of bentonite (dry mass)/distance block	kg		22,940		
DAWE					
Distance blocks					
Diameter	mm			1,765	/Börgesson et al. 2005/
Length	mm			5,475	/Autio et al. 2007/
void slot	mm			37.5–42.5	/Börgesson et al. 2005/
Centred blocks					
Supporting feet, material type	–			steel	
Feet, 4 feet per block	kg			13.9	/Autio et al. 2007/
Bentonite, MX-80					
initial water content	w-%			21	/Autio et al. 2007/
Dry density	kg m^{-3}			1,712	/Autio et al. 2007/
saturated density after swelling	kg m^{-3}			2,000	/Autio et al. 2007/
Total amount of bentonite (dry mass)/distance block	kg			22,940	
FIXING RINGS, BD					
to prevent movement of distance blocks, in every position where the inflow to SC+DB unit is larger than					
0.01 L/min					
material type	–		10 mm thick steel plate		
mass	kg		600		/Autio et al. 2007/
fixing material, low pH cement					
cement	kg		23		/Autio et al. 2007/
SiO2	kg		1.5		
organic material	kg		0.009		
Total number of fixing			4.5	4–5	/Hagros 2007a/
rings in a drift					
SUPERCONTAINER +DISTANCE BLOCK UNIT					
BD AND DAWE					
Reference case – Posiva, BWR 1,700 W, 25 m separation between drifts					
Length (pitch, centre to centre distance)	m	p_c	11.0		/Autio et al. 2007/
Gap between DB and SC (BD)	mm		5	max. 7	/Autio et al. 2007/
Void volume within and outside a SC and DB unit	m^3		1.5		Appendix B.3 of 3H Evolution report /Smith et al. 2007/. Void space excludes unsaturated buffer pores and spaces
Alternative cases					
Posiva VVER 1,370 W					
Length (pitch, centre to centre distance)	m	p_c		9.1	/Raiko 2005, Autio et al 2007/
Gap between DB and SC (BD)	mm			5 (max. 7)	
Posiva EPR 1,830 W					
Length (pitch, centre to centre distance)	m	p_c		10.6	/Raiko 2005, Autio et al 2007/
Gap between DB and SC	mm			5 (max. 7)	

PARAMETER	Unit	Symbol	Reference value	Alternative values	Reference
FILLING BLOCKS, BD AND DAWE					
Distance block units (defined above) placed in positions were gw inflow before sealing is >0.1 l/min and < 1L/min (after sealing)					/Autio et al. 2007/
Dimensions and properties as for corresponding distance blocks in BD/DAWE					/Autio et al. 2007/
Length per position	mm		10,000		/Autio et al. 2007/
PLUGS, BD and DAWE					
Steel compartment plugs					
Compartment plugs will be used to isolate a section of the drift with higher inflow than 1L/min					
material type, steel	–		10 mm steel plate, S355J0		
Compartment plug components:					/Autio et al. 2007/
fastening ring	kg		400		/Autio et al. 2007/
collar	kg		1,250		/Autio et al. 2007/
cap	kg		440		/Autio et al. 2007/
bolts, steel	kg		20		/Autio et al. 2007/
total mass of one single-sided plug	kg		2,110		One-sided plugs were considered in the residual material inventory /Hagros 2007a/. Double-sided plugs are used in this report.
mass of one double-sided plug	kg		2,550		/Autio et al. 2007/
fixing material, low-pH cement					
cement	kg		300		/Autio et al. 2007/
SiO2	kg		40		
organic material	kg		0.2		
Total mass, steel 2 plugs	**kg**		**5,100**		
Total mass, cement 2 plugs	**kg**		**600**		
Filling adjacent to steel plug					
Bentonite pellets, MX-80					
Dry bulk density	kg m^{-3}		950		/Autio et al. 2007/
Bulk density (for individual pellets)	kg m^{-3}		1,830		
Sand filling in steel plug	m^3		1		
Transition blocks to compensate for the density reduction in the filled open volume					
"Loose" distance block					
Diameter	mm		1,820		/Autio et al. 2007/
Length	mm		4,475		/Autio et al. 2007/
slices of thickness of 500 mm					
Centred blocks					
Supporting feet, material type and number of not designed	–				Not designed
Filling between steel compartment plugs					
Permeable filling material in the leaking fracture intersection					/Autio et al. 2007/
crushed rock with proper grading					
In other parts compacted bentonite					/Autio et al. 2007/
Total section length	mm		30,000		

PARAMETER	Unit	Symbol	Reference value	Alternative values	Reference
Drift end plug					
Steel-reinforced concrete plug (reference design)					
Length	mm		2,000		/Autio et al. 2007/
Steel mass	kg		860		
low-pH concrete	m^3		8		LHHPC, /Martino et al. 2002/
low-pH concrete (mixture: LHHP cement)	kg		19,200		/Martino et al. 2002/
cement	kg		780		
silica	kg		2,300		
coarse aggregates	kg		8,320		
sand	kg		7,160		
organics (SP)	kg		82		
cooling and grouting pipes	mm		123,000		/Autio et al. 2007/
Rock plug					/Autio et al. 2007/
Length	mm			2,000	
Steel mass	kg			200	
low-pH concrete	m^3			1	
low-pH concrete	kg			1,900	/Autio et al. 2007/
Fixing ring + steel plug included in all drift end plug options					
Steel plug					
steel mass	kg		2,110		/Autio et al.2007/ one sided plug with bolts
Fixing material, low-pH cement					
cement	kg		300		
silica, SiO2	kg		20		
organic material	kg		0.1		
Fixing ring (as defined above)					
Total length of fixing ring + steel plug	mm		1,000		
SPRAY AND DRIP SHIELDS, BD and DAWE					
Material type			steel		/Autio et al. 2007/
Weight of one drip shield	kg		0.600		/Autio et al. 2007/
Number of drips shields in one drift			5	4–6	/Hagros 2007a/
Thickness	mm		1		Assumption used for gas generation values (Section 5.5.1)
Total amount per drift	kg		3		/Hagros 2007a/
DRAINAGE, ARTIFICIAL WETTING AND AIR EVACUATION PIPES (DAWE)					These are removed from drift
Watering pipes					one pipe in each SC section
Material				steel	
Diameter	mm			17.2	
Air evacuation system					one/two pipes in the drift
Material				steel	
Diameter	mm			10	
BACKFILL PER DRIFT					
The first 10–15 m of the drift which has a wider diameter will be backfilled	m^3		750 (max)		
Backfill crushed rock/bentonite	w%		70/30		/Hagros 2007a/
Bentonite			MX-80		

PARAMETER	Unit	Symbol	Reference value	Alternative values	Reference
Density, dry (average) 85% of the volume In addition the first 5 meters of the drift with the diameter 1.85 m will be backfilled with compacted bentonite	kg/m^3		2,150		
CEMENT IN A DRIFT (excluding the first 15 m emplacement section) **Basic Design, BD**					
Cement in compartment plugs, end plug (**reference LHHP plug**), fixing rings	kg		2,140		/Hagros 2007a/
Cement in compartment plugs, end plug for the **alternative grouted rock plug**, and fixing rings				2,960	
Composition of low-pH cement (mixture: LHHP see drift end plug)			See drift end plug		/Martino et al. 2002/
Low-pH cement for grouting	kg			500	
Composition (mixture: P308B)					
cement	kg/m^3			335	/Ahokas et al. 2006/
SiO_2	w%			52.8	/Ahokas et al. 2006/
Organic materials	w%			4	/Ahokas et al. 2006/
Density	kg/m^3			1,354	/Ahokas et al. 2006/
Total amount of cement in a drift (excl. the first 15 m)	kg		2,140	3,460	/Hagros 2007a/
Reference material, Silica Sol for grouting					
Silica Sol	l		100–500		
Silica Sol	kg		130–670		
Composition (mixture: MEYCO MP320)					
SiO_2	w%		33.5		/Hagros 2007b/
Accelerators (NaCl)	w%		1.7		/Hagros 2007b/
organic materials (biocides)	w%		<0.01		/BASF 2007/
Density	kg/m^3	ρ	~1,300		/Ahokas et al. 2006/
CEMENT IN THE DRIFT (the first 15 m emplacement section)					
Support bolts, anchor bolts, shot-crete, grouting – remaining amount					/Hagros 2007a/
Low-pH shotcrete					
Cement	kg		320	320	
Other cement bearing components	kg		170	170	
Total cement for first 15 m of a drift			490	490	
TOTAL AMOUNT OF CEMENT IN A DRIFT (BD)	kg		2,630	3,950	
DAWE					
Total amount of cement in a drift	kg			3,700	/Hagros 2007a/
BENTONITE					
Bentonite MX-80			MX-80		/SKB 2006/
Montmorillonite	w%		87		
Na-			72%		
Ca-			18%		
Mg-			8%		
K-			2%		
pyrite	w%		0.07		
Gypsum	w%		0.7		
calcite+ siderite	w%		0–1		

PARAMETER	Unit	Symbol	Reference value	Alternative values	Reference
Quartz	w%		3		
Cristobalite	w%		2		
Mica	w%		4		
Albite	w%		3		
Dolomite	w%		0		
Anorthoclase	w%		0		
organic carbon	w%		0.2		
CEC	meq/ 100 g		75		
ROCK PROPERTIES					
Geochemical conditions (at 400–500 m depth)					
Salinity (TDS, Total dissolved solids)					
Present level	g l^{-1}		10–13	10–20	/Andersson et al. 2007, Pastina and Hellä 2006/
Post-emplacement	g l^{-1}		10–25 (420 m depth)	25–45 (550 m depth)	/Pastina and Hellä 2006/ max. at 100 years after disposal
pH			7.5–8.2		/Pitkänen et al. 2004/
Redox potential	mV		–300..–250	≈ –250..–200	/Pitkänen et al. 2004/
Dissolved Fe(II)	mg l^{-1}		0.1 1(median)	0.01–0.72	/OIVA database/ (file name: “uusiOIVA_ 10032006.xls”). (see text)
Dissolved sulphide	mg l^{-1}		0.25 (median)	12 (max)	ibid
Dissolved gases					
H_2	ml l^{-1}		<1	20–25 (< 800 m)	/Pitkänen and Partamies 2007/
CH_4	ml l^{-1}		< 400	920 (< 800 m)	/Pitkänen and Partamies 2007/
Solubilities of gases at 30°C (after ≈ 2000a) at 0.1 MPa					/SKB 1999/ p. 100
H_2	mol m^{-3}		0.77		/Himmelblau 1960/
	ml l^{-1}		19		/Himmelblau 1960/
CH_4	mol m^{-3}		1.3		/Himmelblau 1960/
	ml l^{-1}		33		
Geological properties					
Gneiss (migmatitic gneiss): fracture properties					
fracture type	–		fractures	vein-like	/Andersson et al. 2007/
orientation	–		several sets		
density	m^{-1}	N	1–3	3–10	/Hellä et al. 2006/
aperture	mm	a	calc. from T-distribution		
transmissivity	m^2 s^{-1}	T	10^{-14}–10^{-7}		
hydraulic conductivity	m s^{-1}		10^{-8}–10^{-15}		Estimated range of rock hydr. cond. in /Börgesson et al. 2005/
Gneiss: average matrix properties					
porosity	%	ε_m	0.14	0.1–0.2	/Autio et al. 2003/
hydraulic conductivity	m s^{-1}		10^{-14}	≈<10^{-15}	Estimated range of tightest rock hydr.cond. in /Börgesson et al. 2005/
gas effective diffusion constant	m^2 s^{-1}		2.63 10^{-10}		/Autio et al. 2003/
intrinsic gas permeability	m^2		5.16 10^{-21}		/Autio et al. 2003/
EDZ: properties of crushed zone (0–4 mm)					
thickness (radial extent)	mm		4		/Autio et al. 2003/
porosity	%		0.64	2–4	/Autio et al. 2003/
fracture type	–		open cracks		/Montoto et al. 2003/
mean fracture aperture	µm		2		/Montoto et al. 2003/

PARAMETER	Unit	Symbol	Reference value	Alternative values	Reference
small fractures (< 5.4 µm)	%		90		/Montoto et al. 2003/
larger fractures (> 5.4 µm)	%		10		/Montoto et al. 2003/
EDZ: properties of microfractured zone (4–9 mm)					
thickness (radial extent)	mm		5		/Autio et al. 2003/
porosity	%		0.34		/Autio et al. 2003/
fracture type	–		open cracks		/Autio et al. 2003/
mean crack specific surface	μm^{-1}		0.004		/Montoto et al. 2003/
small fractures (< 2.16 µm)	%		60%		/Montoto et al. 2003/
EDZ: properties of zone of minor damage (9–23 mm)					
thickness (radial extent)	mm		14		/Autio et al. 2003/
fracturation	–		similar as in undisturbed rock		/Autio et al. 2003/
EDZ: average properties (0–23 mm)					
thickness	mm		23		Combined thickness of crushed zone, micro-fractured zone and zone of minor damage
porosity	%	ε_{EDZ}	0.34		/Autio et al. 2003/
gas effective diffusion constant	$m^2\ s^{-1}$		$3.97\ 10^{-9}$		/Autio et al. 2003/
intrinsic gas permeability	m^2		$2.96\ 10^{-19}$		/Johnson et al. 2005/ Appendix C
max hydraulic conductivity	$m\ s^{-1}$	K_{EDZ}	3×10^{-12}		The maximal hydraulic conductivity of the EDZ was indirectly calculated by taking the average intrinsic gas permeability (see line above) as an upper bound for the transport of water in the EDZ.
Hydraulic properties					
Leakage rates for 300 m drift without sealing	L/min				/Hellä et al. 2006/
long dry sections			"tight"		
Zones with 1–3 local fractures			>4		one fracture per 250 m
a few fractures or fracture zones			0.4–4		one fracture per 100 m
six 5 m long sections (per 300 m)			>0.1		
four to five 10 m long sections (per 300 m)			>0.1		
total leakage into a drift			10		/Hellä et al. 2006/ the likely range of inflow into a drift
Leakage after grouting for a 300 m drift (successful grouting to a T< 10–8 m^2/s)					
Inflow	l/min		<10 (99%)	<10 (99%)	/Lanyon and Marschall 2006/ max. inflow in all realisations is about 15 l/min with less than 1% of drifts exceeding 10 l/min
Saturation time for a supercontainer section in the drift	a		10	12,000	Figure 8-14 in /Börgesson et al. 2005/
Hydraulic gradient (post-closure phase)	%		0.01	0.01–1	/Löfman 1999/

PARAMETER	Unit	Symbol	Reference value	Alternative values	Reference
Hydraulic length (from drift to the nearest major fracture zone)	m		50		/Lanyon and Marschall 2006/ Assumed distance to constant head hydrostatic boundary in discrete fracture network modelling.
Mechanical properties at repository depth					
Main horizontal stress	MPa	σ1 or σH	5+0.021z min 10+0.042z max		/Andersson et al. 2007/ 300< z < 800 m
Secondary horizontal stress	MPa	σ2 or σh	0.021z min 5+0.027z max		Ibid.
Vertical stress	MPa	σ3 or σv	0.015z min 0.030z max		Ibid.
Spalling strength	MPa		65		/Hakala et al. 2008/ Table 2.3
Thermal properties					
Ambient temperature	°C	T_0	+10.5°C (400 m)	0	/Ikonen 2003/ gradient 1.5°C/100 m
Heat output	W				
BWR canister, OL 1-2			1,700		/Raiko 2005/
PWR canister				1370	/Raiko 2005/
EPR Canister				1830	/Raiko 2005/
Thermal conductivity (gneiss)	$Wm^{-1} K^{-1}$		2.7		/Posiva 2003/ p. 114, for a temperature 22°C
Heat capacity (gneiss)	$J\ kg^{-1} K^{-1}$		797		/Posiva 2003/ p. 114
Thermal diffusivity (gneiss)	$m^2\ s^{-1}$		$1.23\ 10^{-6}$		/Posiva 2003/ p. 114
Thermal conductivity (bentonite)	$Wm^{-1} K^{-1}$		1.0		/Ikonen 2003/
Maximum temperature at canister surface (for thermal dimensioning)	°C		90		10° below the design basis max. of 100°, /Ikonen 2003/

A.2 References

Ahokas H, Hellä P, Ahokas T, Hansen J, Koskinen K, Lehtinen A, Koskinen L, Löfman J, Mészáros F, Partamies S, Pitkänen P, Sievänen U, Marcos N, Snellman M, Vieno T, 2006. Control of water inflow and use of cement in ONKALO after penetration of fracture zone R19. Posiva Working Report 2006-45. Posiva Oy, Olkiluoto, Finland.

Andersson J, Ahokas H, Hudson J A, Koskinen L, Luukkonen A, Löfman J, Keto V, Pitkänen P, Mattila J, Ikonen A I T, Ylä-Mella M, 2007. Olkiluoto Site Description 2006, POSIVA 2007-03. Posiva Oy, Olkiluoto, Finland.

Autio J, Kirkkomäki T, Siitari-Kauppi M, Timonen J, Laajalahti M, Aaltonen T, Maaranen J, 1999. Use of 14C-PMMA method and He-gas methods to characterize excavation disturbance in crystalline rock. POSIVA 99-22, Posiva Oy, Helsinki, Finland.

Autio J, Hjerpe T, Siitari-Kauppi M, 2003. Porosity, Diffusivity and Permeability of EDZ in Crystalline Rock and Effect on the Migration in a KBS-3 Type repository. Proceedings of a European Commission Cluster conference and workshop on Impact of the excavation disturbed or damaged zone (EDZ) on the performance of radioactive waste geological repositories, Luxemburg, 3 to 5 November 2003, EUR 21028 EN, p. 149–155.

Autio J, Börgesson L, Sandén T, Rönnqvist P-E, Johansson E, Hagros A, Eriksson M, Berghäll J, Kotola R, Parkkinen I, 2007. KBS-3H Design Description 2006. Posiva working report 2007-105 and SKB R-08-32. Posiva Oy, Olkiluoto, Finland and SKB, Svensk Kärnbränslehantering AB, Sweden.

Autio J, Anttila P, Börgesson L, Sandén T, Rönnqvist P-E, Johansson E, Hagros A, Eriksson M, Halvarsson B, Berghäll J, Kotola R, Parkkinen I, 2008. KBS-3H Design Description 2007. POSIVA 2008-01 and SKB R-08-44. Posiva Oy, Olkiluoto, Finland and SKB, Svensk Kärnbränslehantering AB, Sweden.

BASF, 2007. MEYCO MP320 Data sheet. Available at: http://www.basf-cc.com.au/acrobat/meymp320.pdf

Börgesson L, Sandén T, Fälth B, Åkesson M, Lidgren E, 2005. Studies of buffer behaviour in KBS-3H concept; Work during 2002–2004. SKB R-05-50, Svensk Kärnbränslehantering AB.

CRC, 2007. CRC Handbook of Chemistry and Physics, 88th Edition (CRC Handbook of Chemistry, Physics). D.R. Lide (ed.). 88th Edition. The Chemical Rubber Company (CRC), Boca Raton, USA.

EN 10025. European Structural Steel Standard 10025.

Hagros A, 2007a. Estimated quantities of residual materials in a KBS-3H repository at Olkiluoto. Posiva Working report 2007-104 and SKB R-08-33. Posiva Oy, Olkiluoto, Finland and SKB, Svensk Kärnbränslehantering AB, Sweden.

Hagros A, 2007b. Foreign materials in the repository – update of estimated quantities. Posiva Working Report 2007-17. Posiva Oy, Olkiluoto, Finland.

Hakala M, Hudson J A, Harrison J P, Johansson E, 2008. Assessment of the Potential for Rock Spalling at the Olkiluoto Site. Working Report 2008-xx (in preparation). Posiva Oy, Olkiluoto, Finland.

Hellä P, Ahokas H, Palmén J, Tammisto E, 2006. Analysis of Geohydrological Data for Designof KBS-3H Repository Layout. Posiva Working report 2006-16 and SKB R-08-27. Posiva Oy, Olkiluoto, Finland and SKB, Svensk Kärnbränslehantering AB, Sweden..

Himmelblau D M, 1960. Solubilities of inert gases in water. J. Chem. Eng, Vol. 5/1, January 1960.

Ikonen K, 2003. Thermal Analyses of KBS-3H Type repository, POSIVA 2003-11, Posiva Oy, Olkiluoto, Finland.

Johansson E, Hagros A, Autio J, Kirkkomäki T, 2007. KBS-3H layout adaptation 2007 for the Olkiluoto site. Posiva Working Report 2007-77 and SKB report R-08-31. Posiva Oy, Olkiluoto, Finland and SKB, Svensk Kärnbränslehantering AB.

Johnson L, Marschall P, Wersin P, Gribi P, 2005. HMCBG Processes Related to the Steel Components in the KBS-3H Disposal Concept. Posiva Working report 2005-09 and SKB R-08-25. Posiva Oy, Olkiluoto, Finland and SKB, Svensk Kärnbränslehantering AB, Sweden.

Lanyon G W, Marschall P, 2006. Discrete fracture network modelling of a KBS-3H repository at Olkiluoto, POSIVA 2006-06 and SKB report R-08-26. Posiva Oy, Olkiluoto, Finland and SKB, Svensk Kärnbränslehantering AB, Sweden.

Löfman J, 1999. Site Scale Groundwater Flow in Olkiluoto. POSIVA 99-03. Posiva Oy, Olkiluoto, Finland.

Martino, J.B, Chandler N A, Read R S, C Baker, 2002. Response of the tunnel sealing experiment concrete bulkhead to pressurization. Report No: 06819-REP-01200-10085-R00. Ontario Power Generation, Toronto, Canada.

Montoto M, Rodriguez-Rey A, Autio J, 2003. Microfractographic characterization of the excavation damage caused by boring of the experimental full scale deposition holes in the Research tunnel at Olkiluoto. Proceedings of a European Commission Cluster conference and workshop on Impact of the excavation disturbed or damaged zone (EDZ) on the performance of radioactive waste geological repositories, Luxemburg, 3 to 5 November 2003, EUR 21028 EN.

OIVA data file, see Pitkänen et al. 2007.

Pastina B, Hellä P, 2006. Expected evolution of a spent fuel repository at Olkiluoto, POSIVA 2006-05, Posiva Oy, Olkiluoto, Finland.

Pitkänen P, Partamies S, Luukkonen A, 2004. Hydrogeochemical Interpretation of Baseline Groundwater Conditions at the Olkiluoto site. POSIVA 2003-07 Posiva Oy, Olkiluoto, Finland.

Pitkänen P, Partamies S, 2007. Origin and Implications of Dissolved Gases in Groundwater at Olkiluoto. POSIVA 2007-04. Posiva Oy, Olkiluoto, Finland.

Pitkänen P, Ahokas H, Ylä-Mella M, Partamies S, Snellman M, Hellä P, 2007. Quality Review of Hydrochemical Baseline Data from the Olkiluoto Site, POSIVA 2007-05. Posiva Oy, Posiva, Finland.

Posiva, 2003. Baseline conditions at Olkiluoto. POSIVA 2003-02. Posiva Oy, Olkiluoto, Finland.

Posiva, 2005. Olkiluoto Site Description 2004. Olkiluoto, Finland: Posiva Oy. POSIVA 2005-03. Posiva Oy, Olkiluoto, Finland.

Raiko H, 2005. Disposal canister for spent nuclear fuel – Design report. POSIVA 2005-02. Posiva Oy, Olkiluoto, Finland.

Saanio T, Kirkkomäki T, Sacklén N, Autio J, Kukkola T, Raiko H, 2004. Spent nuclear fuel repository at Olkiluoto – Preliminary design – Stage 1. Posiva Working Report 2003-74 (In Finnish). Posiva Oy, Olkiluoto, Finland.

SKB, 1999. SR 97 – Processes in the repository evolution. SKB TR-99-07, Svensk Kärnbränslehantering AB.

SKB, 2006. Long-term safety for KBS-3 repositories at Forsmark and Laxemar – a first evaluation – Main report of the SR-Can project. SKB TR-06-09, Svensk Kärnbränslehantering AB.

Smart N R, Rance A P, Werme L O, 2004. Anaerobic corrosion of steel in bentonite. Mat. Res. Soc. Symp. Proc. 807, 441–446.

Smith P, Johnson L, Snellman M, Pastina B, Gribi P, 2007. Safety assessment for a KBS-3H spent nuclear fuel repository at Olkiluoto – Evolution report. POSIVA 2007-08 and SKB R-08-37. Posiva Oy, Olkiluoto, Finland and SKB, Svensk Kärnbränslehantering AB, Sweden.

Thorsager P, Lindgren E, 2004. KBS-3H summary report of work done during Basic Design. SKB R-04-42, Svensk Kärnbränslehantering AB.

Appendix B

FEP analysis for fuel, canister insert, canister, buffer and other bentonite components, supercontainer and near-field rock for KBS-3H

SKB's ongoing work with identification and structuring of features, events and processes (FEPs) affecting the KBS-3V disposal system is described in the SR-Can FEP report /SKB 2006a/. The work was started by implementing the content of the SR 97 Process Report for KBS-3V /SKB 1999/, which has also been used as the basis for Posiva's Process Report for KBS-3V /Rasilainen 2004/ for the spent fuel repository at Olkiluoto, into a database format suitable for import and processing of FEP information from other sources. The SR 97 version of the FEP database was then systematically audited against the International FEP database maintained by the OECD/NEA, which includes FEP databases from several repository programmes and international exercises.

Relevant FEPs from the audit were sorted into three main categories: i) FEPs related to the initial state of the repository system, ii) FEPs related to the internal processes of the repository system, and iii) FEPs related to the external impacts on the repository system. Some FEPs were also categorised as irrelevant for a spent fuel repository in crystalline bedrock or as being related to methodology on a general level. Biosphere FEPs were not included in the SR 97 Process Report. All biosphere FEPs from the audit were therefore compiled in a single category in the SR-Can database and have not been further handled so far. The results of the FEP analysis for KBS-3V have been tabulated in Appendix 4–8 of the SR-Can FEP report. The SR-Can Buffer and Backfill Process Report /SKB 2006b/ provide complete descriptions of all buffer processes for KBS-3V.

In /Johnson et al. 2005/, a FEP analysis for KBS-3H for the deposition drift has been performed. The analysis is in line with the corresponding FEP analysis for KBS-3V discussed in /SKB 1999/. The part of the repository system covered by the FEP analysis for KBS-3H contains the fuel, canister, buffer (in the supercontainer and the distance block) and other bentonite components, supercontainer, and the near-field rock. Reinforcements, in terms of plugs, rock bolts and grouts are also considered. The access drift system (shafts and adits) and the plugs of the deposition drifts are not included. The near-field rock surroundings the deposition drifts, and its outer boundary is taken to represent the distance from the drifts to which they influence the structure and behaviour of the surrounding rock. The KBS-3H/-3V interaction matrix is developed for the post-closure phase, including the saturation phase, assuming that no radionuclides have been released from the canister.

Internal processes which may take place within the components of the KBS-3H repository system are listed for each component in the section titled "Summary of handling in the safety assessment". These tables are based on the list of internal processes for KBS-3V and have been complemented with processes that have a different significance for, or potential impact on, KBS-3H compared with KBS-3V. These additional processes are derived, on the one hand, from the FEP analysis for the KBS-3H deposition drift (documented in /Johnson et al. 2005/), and on the other hand, by the difference analysis between KBS-3V and 3H (documented in /Johnson et al. 2005/)[33].

[33] The list of internal processes for KBS-3H is not based on a full-scale FEP analysis for KBS-3H (as in the case of KBS-3V) and the completeness of processes is thus not formally ensured.

B.1 References

Johnson L, Marschall P, Wersin P, Gribi P, 2005. HMCBG processes related to the steel components in the KBS-3H disposal concept. Posiva Working Report 2005-09 and SKB R-08-25. Posiva Oy, Olkiluoto, Finland and SKB, Svensk Kärnbränslehantering AB, Sweden.

Rasilainen K, 2004. Localisation of the SR-97 process report for Posiva's spent fuel repository at Olkiluoto. POSIVA 2004-05, Posiva Oy, Olkiluoto, Finland.

SKB, 1999. SR 97 Processes in the repository evolution. SKB TR-99-07, Svensk Kärnbränslehantering AB.

SKB, 2006a. FEP report for the safety assessment SR-Can. SKB TR-06-20, Svensk Kärnbränslehantering AB.

SKB, 2006b. Buffer and backfill process report for the safety assessment SR-Can. SKB TR-06-18, Svensk Kärnbränslehantering AB.

Appendix C

Mathematical model, input data and results for gas transport in the KBS-3H repository

C.1 Mass balance for gas

The following mathematical model is a simplified representation of the processes described in Section 7.5.2 and shown in Figure 7-17. It is based on a mass balance consideration for the gas generated within the repository. All input parameters, with the exception of the gas generation rates, are assumed to be constant in time. In particular, the lengths over which the gas-induced hydraulic gradient and the concentration gradient for dissolved gas in the host rock are non-zero are assumed to be time-independent. Furthermore, gas leakage in the representative pathway is assumed to occur when the gas entry pressure is exceeded and is modelled in terms of a moving gas front at a velocity determined by the hydraulic transmissivity in a representative pathway (Figure C-1). For each supercontainer unit, the fracture network in the host rock is represented by a single one-dimensional representative pathway (gas channel), characterised by its transmissivity, trace length and degree of connectivity. The hydraulic aperture and the gas entry pressure of the representative pathway are derived from its transmissivity. The pressure in the gas phase is assumed to be everywhere the same, i.e. the pressure drop within the gas-filled pore space (e.g. within fractures in the host rock) is not considered.

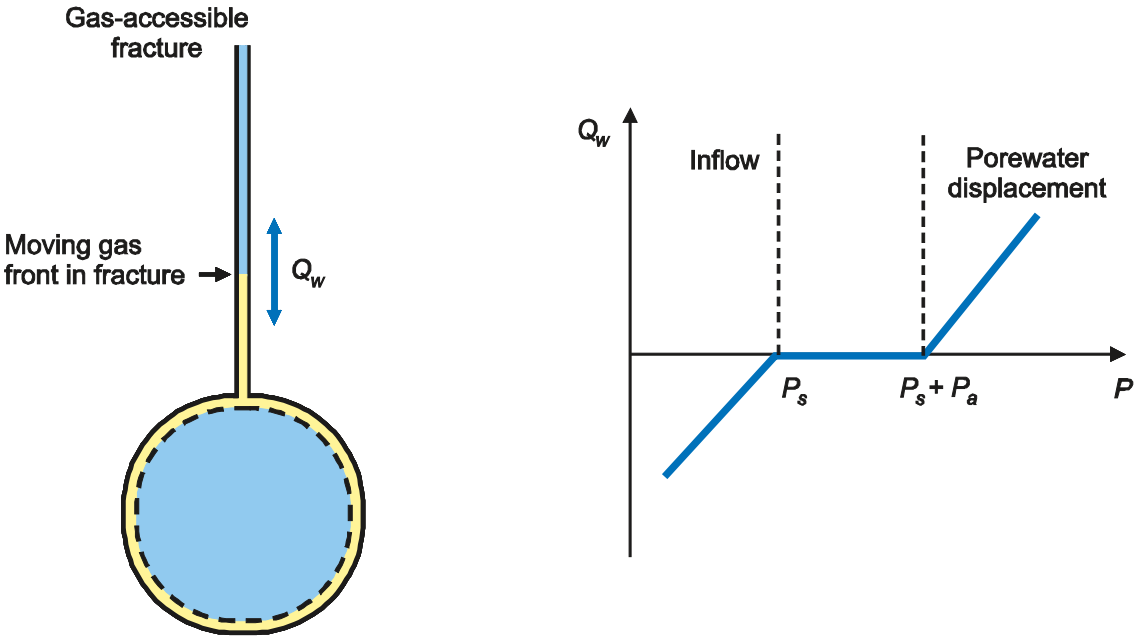

Figure C-1. *Simplified model for gas-induced water displacement from deposition drift into gas-accessible fracture allowing gas leakage and water flow.*

The gas pressure is governed by:

$$P(t) = n(t)\frac{RT_0}{V_g(t)} \qquad \text{(Eq. C-1)}$$

where the volume available for gas storage, $V_{g,}$ is equal to the initial volume within the deposition drift plus any volume change created by water displacement (see Figure C-1):

$$V_g(t) = \min\left(V_{g,\max}; V_g + \int_0^t Q_w(t')dt'\right)$$

$$\dot{V}_g(t) = Q_w(t) = \frac{TG}{\rho\ g}\frac{\Delta P(t)}{l_h} = \gamma\ \Delta P(t)$$

$$\Delta P(t) = \begin{cases} P(t) - P_s & P \le P_s \\ 0 & P_s < P \le P_s + P_a \\ P(t) - P_s - P_a & P > P_s + P_a \end{cases}$$

$$V_g(0) = V_g \qquad \text{(Eq. C-2)}$$

Symbols:

$P(t)$	gas pressure in drift at time t [Pa]
P_s	hydrostatic pressure in host rock at repository depth [Pa]
P_a	gas entry pressure of fracture [Pa]
$n(t)$	amount of gas in drift per supercontainer unit [mol can^{-1}]
R	universal gas constant [J K^{-1} mol^{-1}]
T_0	ambient temperature [K]
$V_g(t)$	volume available for gas storage per supercontainer unit [m^3 can^{-1}]
$V_{g,max}$	maximal volume available for gas storage per supercontainer unit [m^3 can^{-1}]
$Q_w(t)$	water flow rate in fractures [m^3 a^{-1} can^{-1}]
T	hydraulic transmissivity of the representative pathway [m^2 s^{-1}]
G	trace length of the representative pathway [m]
l_h	distance over which hydraulic gradient due to gas generation is non-zero [m]
ρ	density of water [kg m^{-3}]
g	gravitational acceleration [m s^{-2}]

Note that all extensive quantities correspond to a section of the deposition drift containing a single canister, its supercontainer and one distance block (supercontainer unit). The initial residual volume available for storage of gas is assumed to be equal to the pore volume of an annulus of bentonite of thickness 4 cm outside the supercontainer shell plus the pore volume in the EDZ (see Equation C-7). Note that the maximal volume available for gas storage, $V_{g,max}$, is reached when gas breakthrough to some major geological feature with enhanced transmissivity occurs. The breakthrough criterion is met when the vertical position of the moving gas front, $z(t)$, has reached the vertical position of the enhanced transmissivity feature (z_{max}):

$$z(t) = \frac{V_g(t) - V_g}{A\varepsilon_g} = z_{\max} \qquad \text{(Eq. C-3)}$$

A repository area per supercontainer unit (= pitch × drift separation = $p_c\, d$) [m^2 can^{-1}]

ε_g gas accessible porosity in host rock [–]

The gas-accessible porosity in the host rock is assumed to correspond to the cumulated fracture volume per volume of bulk host rock (see below). The contribution of the matrix porosity is pessimistically neglected, because it is accessible to gas only under extreme conditions (excessively high gas pressures).

The mass balance for gas contained in the free gas phase is expressed as (all quantities correspond to a single supercontainer unit):

$$\dot{n} = \dot{n}_p - \dot{n}_{sol} - \dot{n}_{diff} - \dot{n}_{leak,m} - \dot{n}_{leak,EDZ} \qquad \text{(Eq. C-4)}$$

where

$\dot{n}$ rate of change of gas contained in free gas phase [mol a^{-1}]

$\dot{n}_p$ gas generation rate [mol a^{-1}]

$\dot{n}_{sol}$ gas dissolution rate in near field and far field porewater [mol a^{-1}]

$\dot{n}_{diff}$ gas diffusion rate from drift walls radially into the rock matrix [mol a^{-1}]

$\dot{n}_{leak,EDZ}$ gas leakage rate to neighbouring supercontainer unit through EDZ [mol a^{-1}]

$\dot{n}_{pleak,m}$ gas leakage rate from drift walls radially into the rock matrix [mol a^{-1}]

Note that in this chapter, the time derivative of a quantity n is denoted by a dot ($\dot{n}$). In Equation C-4, loss terms due to gas migration along the drift system are assumed to take place only from one supercontainer unit to the neighbouring supercontainer unit. Long-distance gas transport through the drifts is pessimistically not taken into account, i.e. the sealing zones at the ends of deposition drifts are assumed to be impermeable. Gas advected in the displaced porewater within the fracture is absent in Equation C-4 because it does not, strictly speaking, provide a loss term for the amount of gas contained in the free gas phase.

The loss terms in Equation C-4 are calculated in a simplified fashion as follows:

$$\dot{n}_{sol} = \frac{\partial}{\partial t}\left(\frac{C(P_0)}{P_0} V_{sol}\, P \right) = \frac{C(P_0)}{P_0}\left(V_{sol}\, \dot{P} + \dot{V}_{sol}\, P \right)$$

$$\dot{n}_{diff} = 2\pi\, r_{EDZ}\, p_c \varepsilon_m D_p \frac{C(P_0)}{P_0} \frac{P}{l_d} = \delta\, P$$

$$\dot{n}_{leak,m} = 2\pi\, r_{EDZ}\, p_c \frac{k_{g,m}}{\mu_g RT_0} \frac{P^2 - (P_s + P_{a,m})^2}{2l_h} = \frac{\alpha}{RT_0}\left[P^2 - (P_s + P_{a,m})^2 \right]$$

$$\dot{n}_{leak,EDZ} = \pi (r_{EDZ}^2 - r_t^2) \frac{k_{g,EDZ}}{\mu_g RT_0} \frac{P^2 - (P_s + P_{a,EDZ})^2}{2p_c} = \frac{\beta}{RT_0}\left[P^2 - (P_s + P_{a,EDZ})^2 \right] \qquad \text{(Eq. C-5)}$$

where

$$P_{a,m} = 0.56 \times k_{g,m}^{-0.346}$$

$$P_{a,EDZ} = \frac{4\sigma}{a_{EDZ}} \qquad \text{(Eq. C-6)}$$

P_0 standard pressure [Pa]
$C(P_0)$ solubility of hydrogen gas in water [mol m^{-3}]
r_{EDZ} radius of EDZ [m]
p_c canister pitch (centre-to-centre distance) [m]
ε_m porosity of rock matrix [–]
D_p pore diffusion constant in rock matrix [m^2 s^{-1}]
$k_{g,m}$ gas permeability of rock matrix [m^2]
$k_{g,EDZ}$ gas permeability of EDZ [m^2]
$P_{a,m}$ gas entry pressure of rock matrix [Pa]
$P_{a,EDZ}$ gas entry pressure of EDZ [Pa]
σ surface tension gas/water (ca 0.073 N m^{-1} at 20°C), [N m^{-1}]
a_{EDZ} average fracture aperture of the EDZ [m]
μ_g dynamic viscosity of hydrogen gas [Pa s]
l_h distance over which hydraulic gradient due to gas generation is non-zero [m]
l_d distance over which concentration gradient of dissolved gas is non-zero [m]

Note that the gas entry pressure of the rock matrix in Equation (C-6) is calculated from the intrinsic permeability using Davies' relationship /Nagra 2004/, whereas the gas entry pressure of the EDZ is derived from the fracture apertures in the crushed zone of the EDZ using Young's equation. According to Section 7.6.3, the largest observed fractures in the EDZ have apertures over 10 μm. These features do not form a continuous network, but are connected by fractures with apertures smaller than 5 μm. In the simplified gas model calculations, the gas entry pressure is calculated based on the average aperture (2 μm). Significant uncertainty remains, however, on the effect of heterogeneity on the gas transport capacity within the EDZ.

The gas permeability of the rock matrix is assumed to be 1% of the intrinsic permeability, to take into account that only the largest matrix pores are readily accessible to gas. Similarly, for the EDZ the gas permeability is set to 10% of the intrinsic permeability, assuming that only the larger connected fractures are readily accessible to gas /Helmig 1997, Rodwell et al. 1999/. These assumed values are only very approximate and a detailed assessment based on characterisation (Section 7.6.3) and measurements would be required to evaluate the uncertainties. Smaller pores and fractures are in principle also accessible to gas but at significantly higher entry pressures.

By analogy with the formula given in Table 7-10, the volumes available for gas storage and for dissolution are calculated as follows:

$$V_g(t) = \pi \left[(r_t^2 - (r_t - \Delta r_t)^2)\varepsilon_b l_{sc} + (r_{EDZ}^2 - r_t^2) p_c \varepsilon_{EDZ} \right] + p_c d \varepsilon_g z(t)$$
$$V_{sol}(t) = \pi \left[(r_t^2 p_c - r_c^2 l_c)\varepsilon_b - (r_t^2 - (r_t - \Delta r_t)^2)\varepsilon_b l_{sc} \right] f_{sol} + p_c d \varepsilon_m f_{sol,m} z(t)$$

(Eq. C-7)

where

r_t	radius of deposition drift [m]
Δr_t	thickness of bentonite annulus (4 cm of bentonite outside the supercontainer shell) available for gas storage [m]
d	separation between deposition drifts [m]
r_c	radius of canister [m]
l_c	length of canister [m]
l_{sc}	length of supercontainer [m]
f_{sol}	volume fraction available for gas dissolution in deposition drift [–]
$f_{sol,m}$	volume fraction available for gas dissolution in rock matrix [–]
ε_b	porosity of bentonite [–]
ε_{EDZ}	porosity of EDZ [–]
ε_g	gas accessible porosity of rock matrix [–]

Combining Equation C-1 to C-7, the differential equation for the gas pressure *P(t)* reads:

$$\dot{P} = \frac{(\dot{n}_p - \delta\ P)RT_0 - \gamma\,(1 + \frac{C(P_0)}{P_0} RT_0 \frac{\varepsilon_m}{\varepsilon_g} f_{sol,m})P\Delta P - \alpha\,(P^2 - (P_s + P_{a,m})^2) - \beta\,(P^2 - (P_s + P_{a,EDZ})^2)}{V_g + \gamma \int_0^t \Delta P(t')dt' + V_{sol} \frac{C(P_0)}{P_0} RT_0}$$

(Eq. C-8)

where

$$\alpha = \pi\, r_{EDZ}\, p_c \frac{k_{g,m}}{\mu_g l_h}; \quad \beta = \pi\,(r_{EDZ}^2 - r_t^2) \frac{k_{g,EDZ}}{2\mu_g p_c}$$

$$\gamma = \frac{TG}{\rho\ g\, l_h}; \quad \delta = 2\pi\, r_{EDZ}\, p_c \varepsilon_m D_p \frac{C(P_0)}{P_0 l_d}$$

Equation C-8 is integrated numerically using a backward time-stepping procedure. The steady-state gas pressure is obtained by setting

$\dot{P} = 0$

$P > P_s + P_a$

$P > P_s + P_{a,EDZ}$

$\dot{n}_p = \dot{n}_{p,max} = \max\,[\dot{n}_p\,(t)]$

This steady-state gas pressure corresponds to the asymptotic maximal gas pressure in the deposition drift. The analytical expression is:

$$P_{\max} = \frac{\theta\,(P_s + P_a) - \delta + \sqrt{(\theta\,(P_s + P_a) - \delta)^2 + 4(\theta + \frac{\beta}{RT_0})(\frac{\beta}{RT_0}(P_s + P_{a,EDZ})^2 + \dot{n}_{p,\max})}}{2(\theta + \frac{\beta}{RT_0})}$$

(Eq. C-9)

where

$$\theta = \frac{\gamma}{RT_0}\left(1+\frac{C(P_0)}{P_0}RT_0\frac{\varepsilon_m}{\varepsilon_g}f_{sol,m}\right)$$

Note that gas leakage into the rock matrix is neglected in Equation C-9, because it takes place under excessively high pressures only.

C.2 Representation of fracture network

In the model calculations, for each supercontainer unit the fracture network in the host rock is represented by a single representative pathway. Qualitatively, the representative pathway represents those fracture(s) per supercontainer unit that will provide the dominant gas migration pathway. Because the migration of gas generally takes place within the largest pores (lowest gas entry pressures), the representative pathway corresponds to the fracture(s) with the highest hydraulic transmissivities.

As pointed out in Appendix A in /Poteri and Laitinen 1999/, it is sufficient to assume that the total transmissivity of v fractures equals that of the fracture with the highest transmissivity, if the number of fractures is small and the variance of the transmissivity distribution is large. From the DFN model calculations for the Olkiluoto site, the calculated number of water-conducting fractures intersecting deposition drifts is 0–10 fractures per supercontainer unit /Lanyon and Marschall 2006/. The calculated logarithmic standard deviation of the transmissivity of water-conducting fractures is about 1, slightly depending on the model variant envisaged (see Table A-4 in /Lanyon and Marschall 2006/). In other words, the 95% confidence interval for the transmissivity of intersecting fractures extends over roughly four orders of magnitudes (= mean ± two standard deviations). For this reason, the assumption that the representative pathway corresponds to the fracture with the highest hydraulic transmissivity within each supercontainer unit is considered to be well justified.

The representative pathway is mainly characterised by its overall transmissivity. Given the hydraulic conductivity of the background rock of roughly 10^{-9}–10^{-10} m s^{-1} (Table 2-8 in /Lanyon and Marschall 2006/), the degree of hydraulic connectivity is considered to be relatively high, i.e. the individual fractures constituting a flow path are hydraulically well connected, as also stated in /Poteri and Laitinen 1999/. There is, however, significant uncertainty in the degree of connectivity relevant for the migration of gas. In narrow sections of a flow path, the gas entry pressure may be considerably higher than in other sections and gas flow may be hindered or even stopped (bottlenecks), even though the same section may be hydraulically conductive. The connectivity relevant for gas migration could be tested by calculating the percolation threshold for gas migration using a fracture network model based on distributions of fracture transmissivity, trace length, orientation and aperture. Up to date, no such numerical calculations have been performed for gas percolation through the fractured rock at Olkiluoto. For the purpose of the present simplified model calculations, it is assumed that the fracture network is sufficiently connected, so that gas is able to percolate through the background rock. The validity of this assumption needs, however, further analysis in the future.

The hydraulic aperture and the gas entry pressure of the representative pathway are derived from its transmissivity (see below). In the framework of these simplified representations, the interaction between gas and water phases is represented by the gas entry pressure (capillary threshold pressure) only. The detailed constitutive relationships between saturation and capillary pressure/relative permeability are not taken into account in the simplified gas model calculations. The relationship between hydraulic transmissivity and hydraulic aperture of the representative pathway is approximated by the “cubic law” /De Marsily 1986/:

$$T = \frac{\rho\, g\, a^3}{12\mu} \qquad \text{(Eq. C-10)}$$

where

T	hydraulic transmissivity of representative pathway [$m^2\ s^{-1}$]
a	hydraulic aperture of representative pathway [m]
ρ	density of water [$kg\ m^{-3}$]
g	gravitational acceleration [$m\ s^{-2}$]
μ	dynamic viscosity of water [Pa s]

The relationship between radius and gas entry pressure (capillary threshold pressure) of a capillary tube is approximated by Youngs equation /De Marsily 1986/:

$$P_a = \frac{2\sigma}{r} \qquad \text{(Eq. C-11)}$$

where

Pa	gas entry pressure (capillary threshold pressure) [Pa]
σ	surface tension gas/water (ca 0.073 N m^{-1} at 20°C), [N m^{-1}]
r	pore radius of capillary tube (= a/2) [m]

A similar equation holds for flow between parallel plates when the radius *r* is substituted by the half aperture *a/2*.

The gas accessible porosity of the background rock corresponds to the volume of the most transmissive fracture and can be derived from its hydraulic aperture[34]:

$$\varepsilon_g = \frac{P_{32}}{v} a \qquad \text{(Eq. C-12)}$$

P_{32}	fracture intensity of background rock (= total surface of fractures per unit volume of bulk rock) [m^{-1}]
v	number of potentially water-conducting fractures per supercontainer unit section [–]

Because of the expected large heterogeneity of the host rock along a deposition drift, the hydraulic transmissivity of the representative pathway is varied over a broad parameter range, i.e. from 10^{-14} to 10^{-7} $m^2\ s^{-1}$ (see Section 7.5.2).

[34] Note that using the hydraulic aperture (derived from the cubic law) instead of the arithmetic aperture leads to an underestimation of the gas storage volume within the fracture.

C.3 Input data for gas transport calculations

A list of the input parameters for KBS-3H can be found in Appendix A (Table A-1). Below, some additional parameters are listed (Tables C-1 and C-2).

Table C-1. Special parameter values for the gas transport analysis.

Parameter	Unit	Symbol	Reference value	Alternative values	Comment/ Ref.
Available volume fraction for dissolution					
bentonite	–	f_{sol}	1		quickly saturated
rock matrix	–	$f_{sol,m}$	0.01	0.001	see also Table C-2
Gneiss average matrix properties					
pore diffusion const.	$m^2\ s^{-1}$	D_p	4×10^{-11}		/SKB 1999c/, p. 126
gas permeability	m^2	$k_{g,m}$	5×10^{-23}		1% of intrinsic permeability
Gneiss fracture properties					
total fracture intensity.	$m^2\ m^{-3}$	P_{32}	2		/Poteri and Laitinen 1999/ p. 63
average trace length	m	G	2.3		/Poteri 2001/ p. 12
number of potentially water-conducting fractures per supercontainer unit	m^{-1}	v	11		derived from linear fracture density ($1\ m^{-1}$) and canister pitch
fracture distribution type	–	–	log-normal		/Poteri and Laitinen 1999/ p. 64
log10-T mean	–	μ_T	–11		/Poteri and Laitinen 1999/ p. 70
log10-T std	–	σ_T	2.5		/Poteri and Laitinen 1999/ p. 70
vertical distance to closest major geological feature with enhanced permeability	m	z_{max}	large (no gas breakthrough criterion applied)	100	
EDZ average properties					
gas permeability	m^2	$k_{g,EDZ}$	3E–20	0	10% of intrinsic permeability
Special input parameters					
hydraulic length (= distance over which hydraulic gradient is non-zero)	m	l_h	100	200	vertical distance to closest major geological feature with enhanced permeability, see Table C-2
diffusive length (= distance over which hydrogen concentration in rock matrix is non-zero)	m	l_d	1	10	see Table C-2
General input parameters					
hydrodynamic viscosity water	Pa.s	μ	10^{-3}		
hydrodynamic viscosity H_2	Pa.s	μ_g	10^{-5}		
surface tension water/gas	$N\ m^{-1}$	σ	0.073		
ambient temperature	K	T_0	303		

Table C-2. Justification of chosen values for characteristic lengths of hydraulic gradient in fractures and concentration gradient of dissolved hydrogen in the rock matrix. T is the minimal hydraulic transmissivity (10^{-14} m^2 s^{-1}), a is the corresponding fracture aperture (2×10^{-7} m, calculated from cubic law), and S_s is the specific storativity (10^{-5} m^{-1}).

Time t [a]	$l_d = \sqrt{\pi D_p t}$ [m]	$l_h = \sqrt{\frac{T}{aS_s} t}$ [m]
	(hydrogen concentration gradient)	(hydraulic gradient)
10^2	0.6	> 1,000
10^3	2	> 1,000
10^4	6.0	> 1,000
Choice	**1**	**100** (= vertical distance to closest major geological feature with enhanced permeability)

These parameters are not contained in Table A-1, either because they are

- general parameters to be found in any standard data collection; or
- related to special conceptual assumptions in the gas transport calculations (examples: hydraulic length lh, diffusive length ld).

The gas transport calculations have been performed only for the Basic Design and the DAWE design alternative, presented in Appendix D.

C.4 Results

The results of the simplified gas transport calculations are presented in a deterministic manner by considering a range of fixed hydraulic transmissivities of representative pathways.

In Figures C-2 to C-6, the gas pressure is plotted against time for several different situations:

1. No gas transport and no gas dissolution (the generated gases are stored in the initial storage volume).
2. Gas dissolution in the deposition drift and EDZ and diffusion from the EDZ into the rock matrix.
3. As in 2) plus gas leakage by 2-phase flow from the EDZ into the rock matrix added
4. As in 3) plus gas leakage by 2-phase from one supercontainer unit through the EDZ around the distance block into the next supercontainer unit added (this case is relevant only for extremely tight drift sections, where gas is expected to migrate along the EDZ to a neighbouring drift sections providing sufficient gas migration capacity)
5. As in 4) plus gas leakage by 2-phase flow and porewater displacement in a representative pathway as a function of hydraulic transmissivity added.

Note that in all these situations, one single value for the steel corrosion rate is used: Either 1 μm a^{-1} (Base Case) or 0.1/2 μm a^{-1} (range of values for sensitivity analysis), despite the fact that steel corrosion may be limited by the availability for very tight rock sections.

Situations 1–4 should be viewed as hypothetical cases that visualize the individual contributions of various gas storage and transport mechanisms. Note that gas dissolution/diffusion is a considerably less efficient migration mechanism than gas leakage by 2-phase flow into the rock matrix and through the EDZ. Situation 5 presents the most realistic situation, in that all gas storage and transport mechanisms are taken into account. Gas leakage by 2-phase flow and porewater

displacement through gas pathways is found to be the most efficient gas transport mechanism for reasonably transmissive pathways (for a more detailed discussion see Section 7.5.2).

The following calculational cases are presented in this manner:

- Basic Design, with and without application of the gas breakthrough criterion to some higher transmissive geological feature, and comparison to DAWE Design, see Figure C-2.
- Alternative steel corrosion rates of 0.1 μm a^{-1} and 2 μm a^{-1}, see Figure C-3.
- Decreased initial gas storage volume in the bentonite and decreased capacity for gas dissolution in the matrix, see Figure C-4.
- Increased hydraulic length (distance over which gas-induced pressure gradient in the background rock is non-zero) and increased diffusive length (distance over which concentration gradient for dissolved gas in the background rock is non-zero), see Figure C-5.
- Impermeable EDZ (no gas transport capacity of EDZ), see Figure C-6.

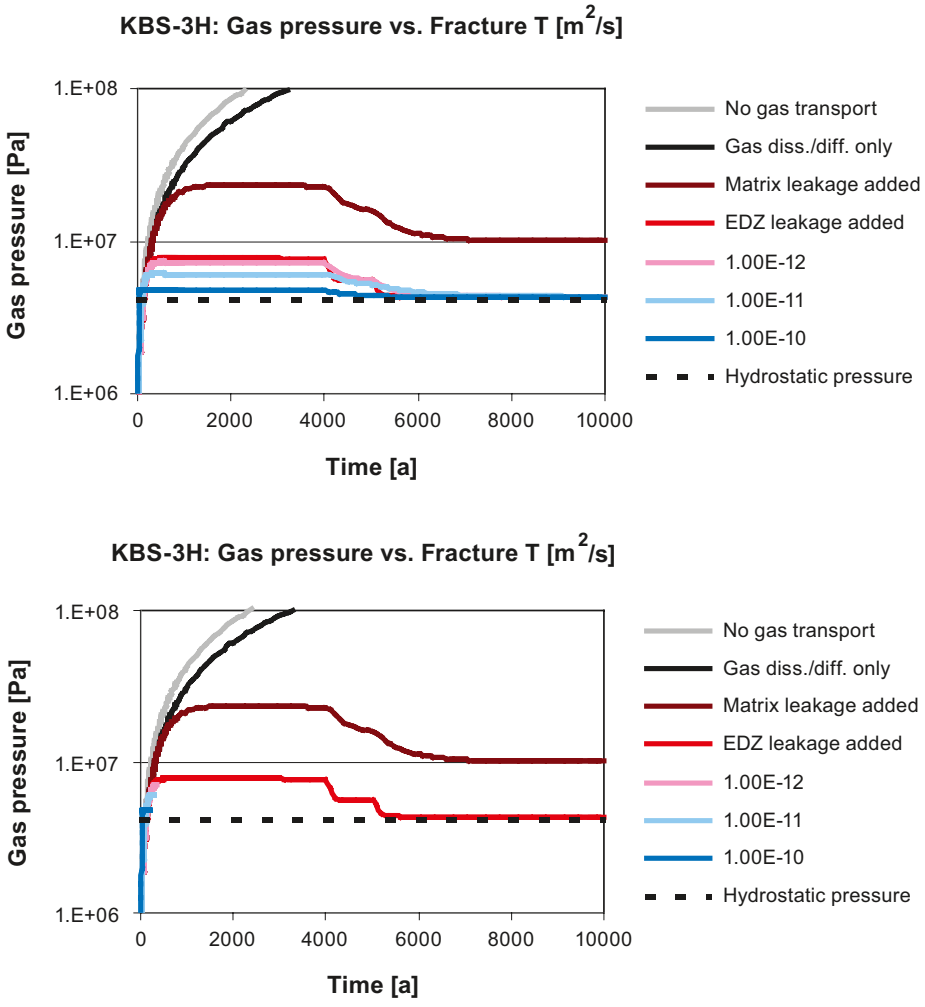

Figure C-2. *Evolution of gas pressure in the deposition drifts at Olkiluoto for the Basic Design. Upper figure: Basic Design, calculated with reference values; lower figure: Basic Design with application of breakthrough criterion to a higher transmissive geological feature (z_{max} = 100 m). The pressure evolution is shown for several different cases: i) case without gas transport and dissolution, ii) case with gas dissolution and diffusion only, iii) case with gas leakage through matrix added, iv) case with gas leakage through EDZ added and v) cases with gas leakage and porewater displacement added, as a function of the hydraulic transmissivity of the representative pathway. In all situations, a steel corrosion rate of 1 μm a^{-1} is used.*

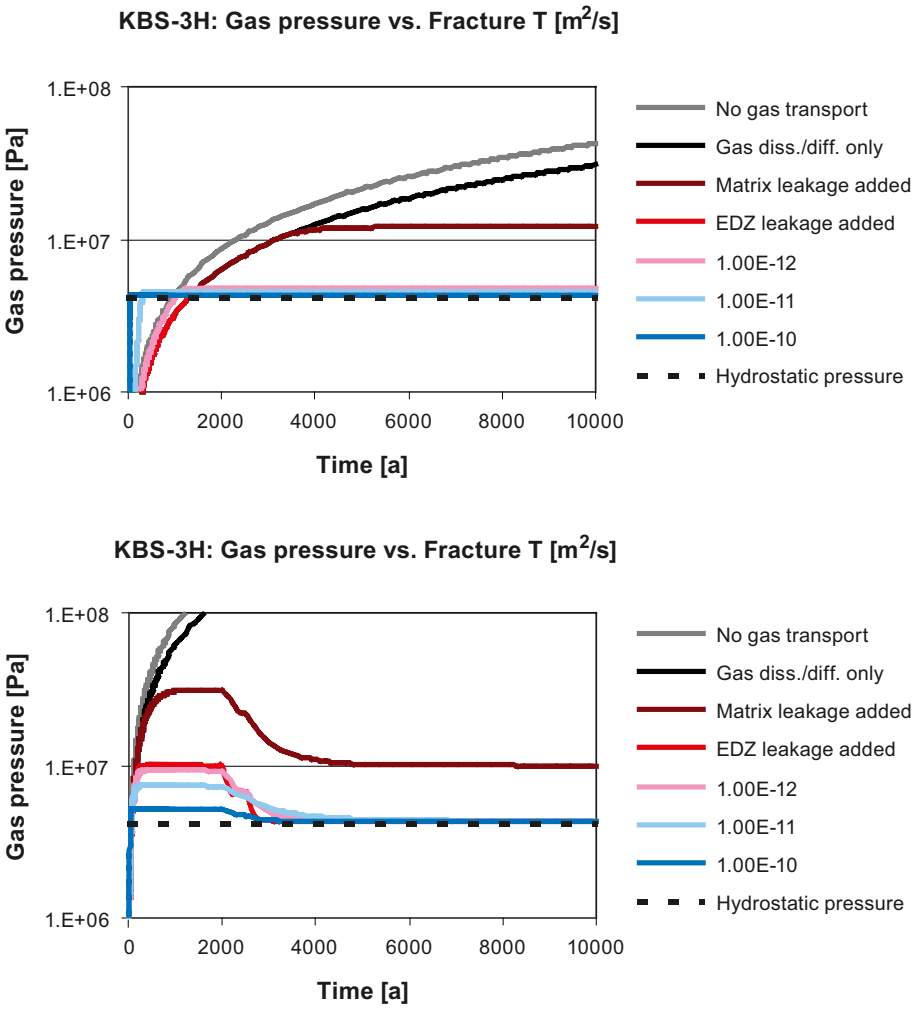

Figure C-3. *Evolution of gas pressure in the deposition drifts at Olkiluoto (Basic Design) for alternative values of the steel corrosion rates. Upper figure: R = 0.1 μm a^{-1}; lower figure: R = 2 μm a^{-1}. The pressure evolution is shown for several different cases: i) case without gas transport and dissolution, ii) case with gas dissolution and diffusion only, iii) case with gas leakage through matrix added, iv) case with gas leakage through EDZ added and v) cases with gas leakage and porewater displacement added, as a function of the hydraulic transmissivity of the representative pathway. No gas breakthrough criterion to higher transmissive geological feature is applied in these figures.*

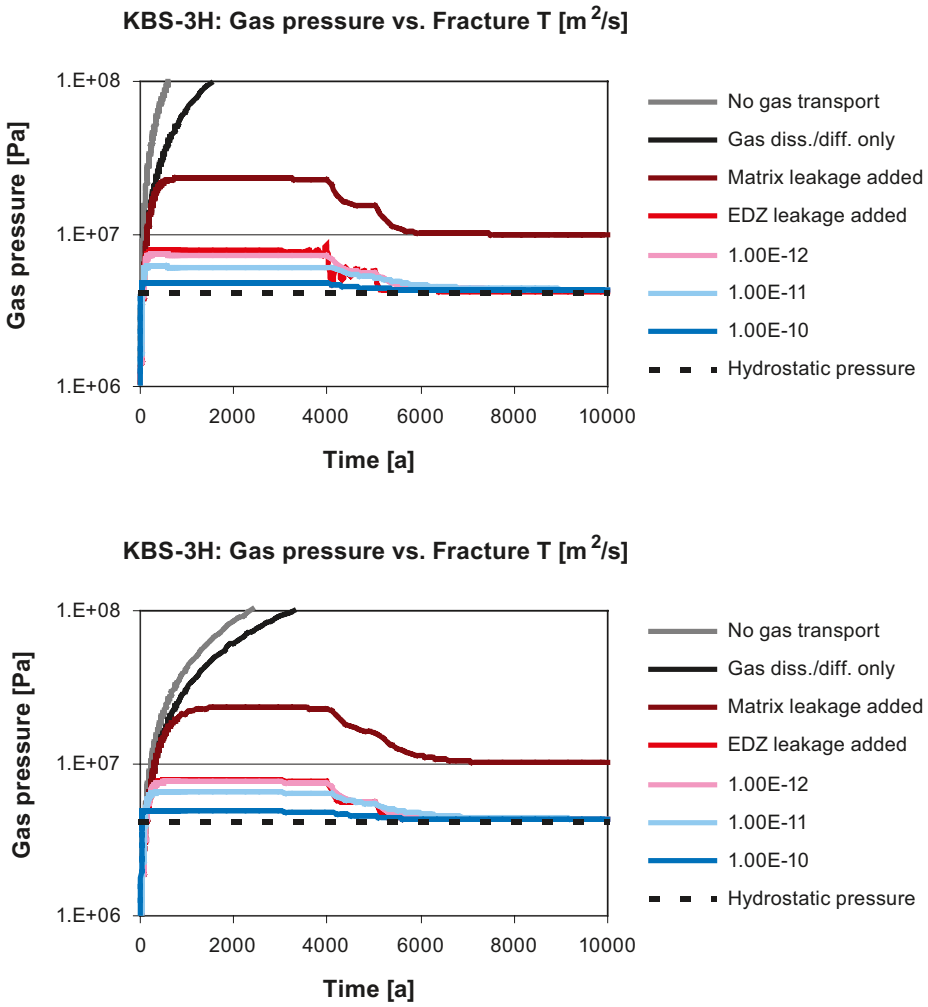

Figure C-4. *Evolution of gas pressure in the deposition drifts at Olkiluoto (Basic Design). Upper figure: decreased initial gas storage volume in the bentonite (Δr = 0.01 m instead of 0.04 m); lower figure: decreased gas dissolution volume in host rock ($f_{sol,m}$ = 0.001 instead of 0.01). The pressure evolution is shown for several different cases: i) case without gas transport and dissolution, ii) case with gas dissolution and diffusion only, iii) case with gas leakage through matrix added, iv) case with gas leakage through EDZ added and v) cases with gas leakage and porewater displacement added, as a function of the hydraulic transmissivity of the representative pathway. No gas breakthrough criterion to higher transmissive geological feature is applied in these figures. In all situations, a steel corrosion rate of 1 µm a^{-1} is used.*

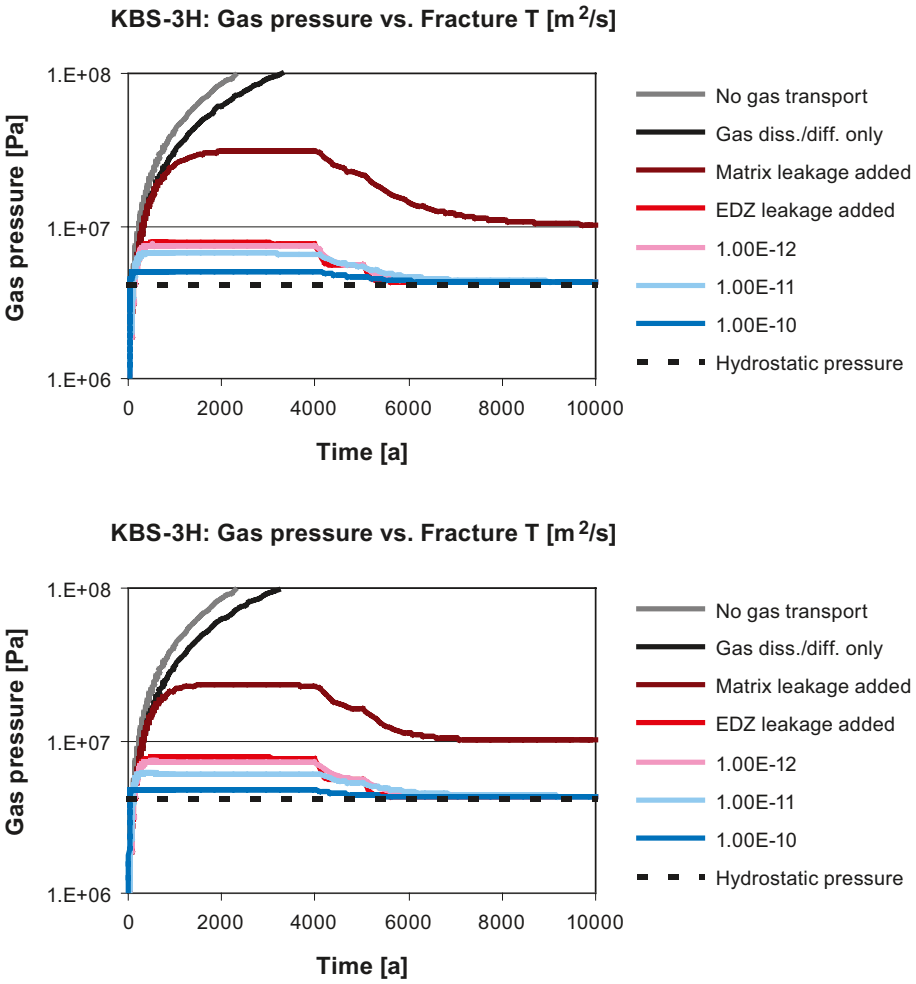

Figure C-5. *Evolution of gas pressure in the deposition drifts at Olkiluoto (Basic Design). Upper figure: increased hydraulic length (l_h = 200 m instead of 100 m); lower figure: increased diffusive length (l_d = 10 m instead of 1 m).The pressure evolution is shown for several different cases: i) case without gas transport and dissolution, ii) case with gas dissolution and diffusion only, iii) case with gas leakage through matrix added, iv) case with gas leakage through EDZ added and v) cases with gas leakage and porewater displacement added, as a function of the hydraulic transmissivity of the representative pathway. No gas breakthrough criterion to higher transmissive geological feature is applied in these figures. In all situations, a steel corrosion rate of 1 μm a^{-1} is used.*

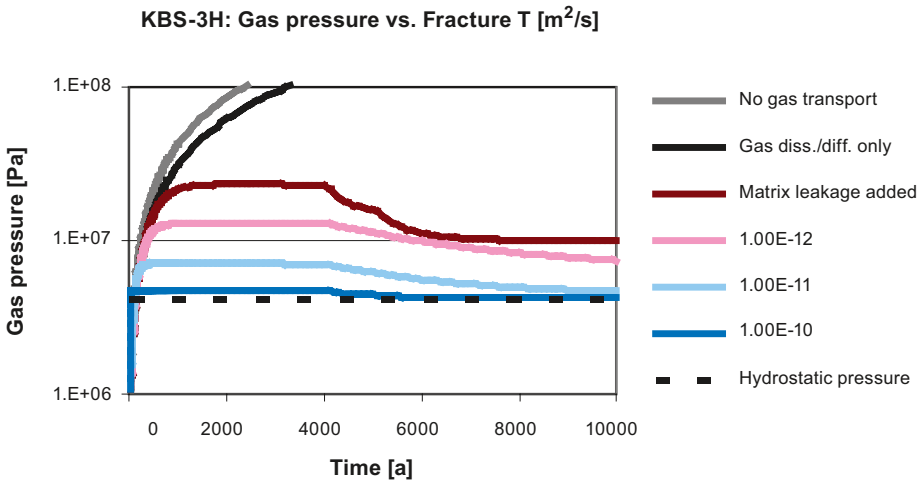

Figure C-6. *Evolution of gas pressure in the deposition drifts at Olkiluoto (Basic Design). For an impermeable EDZ (no gas transport capacity for the EDZ assumed, $k_{g,EDZ} = 0$ m^2). The pressure evolution is shown for several different cases: i) case without gas transport and dissolution, ii) case with gas dissolution and diffusion only, iii) case with gas leakage through matrix added, and iv) cases with gas leakage and porewater displacement added, as a function of the hydraulic transmissivity of the representative pathway. No gas breakthrough criterion to higher transmissive geological feature is applied in these figures. In all situations, a steel corrosion rate of 1 μm a^{-1} is used.*

C.5 References

De Marsily G, 1986. Quantitative hydrogeology. Academic Press, New York.

Helmig R, 1997. Multiphase Flow and Transport Processes in the Subsurface. Springer Verlag, Berlin.

Lanyon G W, Marschall P, 2006. Discrete fracture network modelling of a KBS-3H repository at Olkiluoto. POSIVA 2006-06 and SKB report R-08-26. Posiva Oy, Olkiluoto, Finland and SKB, Svensk Kärnbränslehantering AB, Sweden.

Nagra, 2004. Effects of post-disposal gas generation in a repository for spent fuel, high-level waste and long-lived intermediate level waste sited in Opalinus Clay. Nagra Technical Report 04-06, Nagra, Wettingen, Switzerland.

Poteri A, Laitinen M, 1999. Site-to-canister scale flow and transport in Hästholmen, Kivetty, Olkiluoto and Romuvaara. POSIVA 99-15. Posiva, Helsinki, Finland.

Poteri A, 2001. Estimation of the orientation for fractures at Hästholmen, Kivetty, Olkiluoto and Romuvaara. POSIVA 2001-10. Posiva, Helsinki, Finland.

Rodwell W R, Harris A W, Horseman S T, Lalieux P, Müller W, Amaya L O, Pruess K, 1999. Gas migration and two-phase flow through engineered and geological barriers for a deep repository for radioactive waste. European Commission Report EUR 19122 EN.

SKB, 1999c. SR 97 – Data and data uncertainties: Compilation of data and data uncertainties for radionuclide transport calculations. SKB TR-99-09, Svensk Kärnbränslehantering AB.

Appendix D

The DAWE Design

The DAWE design is being considered as a design alternative to the Basic Design. This appendix presents the main features of this design and the outstanding issues requiring further research.

D.1 DAWE design description

The DAWE design variant is intended to reduce the possibility both of erosion by water flow and of mechanical displacement of the supercontainers and distance blocks, while allowing the emplacement of supercontainers and distance blocks in drift sections that would be excluded in the Basic Design. The DAWE design variant is described in Chapter 6 of /Autio et al. 2007/ and is summarised below.

The general approach is to drain the drift of water during operations and then to use artificial watering to accelerate and make more uniform the swelling of the distance blocks and saturation of the void spaces around the supercontainers. Hydraulic pressure differences between neighbouring supercontainer drift sections that could potentially lead to buffer erosion by water flow and to mechanical displacement of the supercontainers and distance blocks thus are prevented during the operational period of a drift compartment. Furthermore, although hydraulic pressure differences may still develop between drift sections, the fact that they are water filled means that tighter drift sections do not provide sink volumes for potential water flow from drift sections intersected by transmissive fractures, at least for an initial period following artificial wetting and air evacuation.

As in the Basic Design, fractures that could give rise to significant water flows to adjacent unsaturated drifts or transport tunnels will be avoided as supercontainer emplacement locations. Nevertheless, the criteria for transmissive fractures that must be avoided are expected to be less stringent for DAWE compared with the Basic Design. Criteria will need to take account of the possibility to drain potentially large water inflows along the drift without perturbing the buffer and the possibility of internal erosion of the buffer after drift closure.

The drainage of inflowing water along the floor of the drift during operations is achieved by inclining the drift towards its entrance. There is a design gap of ca 40 mm (37.5–42.5 mm) between the distance blocks and the drift walls, which is larger than in the Basic Design and should prevent any contact with the water flowing along the bottom of the drift. Furthermore, a higher initial-water-content bentonite is used to prevent humidity-induced fracturing of the distance blocks. Drainage of inflowing water along the drift floor is expected continue until the drift or drift compartment is plugged. Following sealing of the compartment, artificial watering takes place simultaneously with evacuation of air to avoid gas pressurisation. Steel pipes along the surface of the drift are used for watering and air evacuation. The sides of the drift are the preferred position for watering pipes to avoid possible damage during operations.

Nozzles in the watering pipes are distributed along the drift in each supercontainer section to ensure uniform inflow and minimise any axial water flow in the drift that could give rise to bentonite erosion. Water is not directly injected in the sections where the distance blocks are positioned, again to avoid possible erosion.

The watering time is expected to be about 10 hours at most. The flows of water and air during the watering period are illustrated in Figure D-1. It should be noted that only about one third of the total void space (including bentonite pores) will be filled with water in this way, the remaining voids being less readily saturated. The system remains, therefore, in a partially saturated state even after artificial watering. All supercontainer sections will be filled simultaneously to avoid axial water flows that could give rise to bentonite erosion and redistribution along the drift.

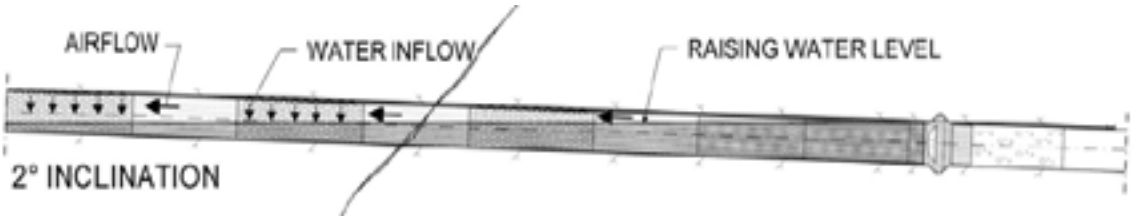

Figure D-1. *The flows of water and air during the watering period (from Figure 5.4-1 of /Autio 2007/).*

The drift design, supercontainer design, the buffer material inside the supercontainers and the length of the distance blocks are currently the same for the Basic Design and for the DAWE design variant (Table D-1).

The isolation of unsuitable drift sections by compartment plugs, the sealing of the drift using a drift end plug, and the use of filling blocks are also the same for the Basic Design and for the DAWE design variant, although the criteria for defining unsuitable drift sections may be modified. Furthermore, the compartment plugs used in the DAWE design variant will be equipped with lead-throughs, valves and collar seals for the wetting and air evacuation pipes, and also for possible drainage.

D.2 DAWE Model studies

D.2.1 Gas generation in the DAWE design

The gas generation by anaerobic corrosion of steel and the related processes are discussed in Section 5.5.1. The differences between the Basic Design and the DAWE design lead to the production of different amounts of gas. The calculation of the gas production and transport for the DAWE Design are presented in this section. The total amount of gas generated per supercontainer unit and the contributions of the various steel components are calculated based on the amounts of steel listed in Table D-2.

The amounts of gas produced by the steel components in the DAWE Design are presented in Table D-3 and the maximum gas production rates can be found in Table D-4. After 4,000 years, the corrosion and the gas production cease.

Table D-1. Initial physical properties of buffer and distance blocks in the KBS-3H DAWE Design (for references see Appendix A).

Parameter	Unit	DAWE Design
Material (buffer)	–	MX-80
Buffer dimensions:	mm	
- Ring blocks		1,739 (diameter); 5,475 (length)[a]
- End blocks		1,739 (diameter); 2 × 350 (length)[a]
Distance block dimensions	mm	1,765 (diameter); 5,475 (length)
Initial water content (w) of the distance blocks (weight of water divided by weight of dry mass)	w-%	21
Dry density	kg m^{-3}	1,712
Saturated density	kg m^{-3}	2,000
Saturated porosity (volume of water/total volume)	%	44

[a] Dimensions are for OL 1-2 reference fuel canisters.

Table D-2. Steel components and masses used in the DAWE design (for references see Appendix A).

Steel component	Average steel thickness [mm]	Steel mass per supercontainer unit [kg]
Supercontainer	8	1,031
Feet beneath supercontainer	6	40.2
Feet beneath distance block	6	13.9
Spray and drip shields	thin	0.600
Total mass	–	ca 1,086
		Steel mass per structural element [kg]
Fixing ring	–	–
Double-sided steel compartment plug[a]	10	2,550

[a] Similar plugs (one-sided caps, weighing 2,110 kg with bolts) may also be used as one component of the drift end plugs.

Table D-3. Total amounts of generated gas by the steel components of a supercontainer unit and the structural elements for the DAWE Design.

Steel component	Total amount of generated gas per supercontainer unit [mol]
Supercontainer	2.5×10^4
Feet beneath supercontainer	9.6×10^2
Feet beneath distance blocks	3.3×10^2
Spray and drip shields	7.2×10^1
Total amount	2.6×10^4
	Amount of generated gas per structural element [mol]
Fixing ring	–
Compartment plugs	6.1×10^4

Table D-4. Maximal total gas production rates per supercontainer unit for the DAWE Design as a function of the steel corrosion rate.

Steel corrosion rate [µm a^{-1}]	Gas production [mol a^{-1}]	[m^3 STP a^{-1}]
0.1	0.67	0.015
1	6.7	0.15
2	13.5	0.30

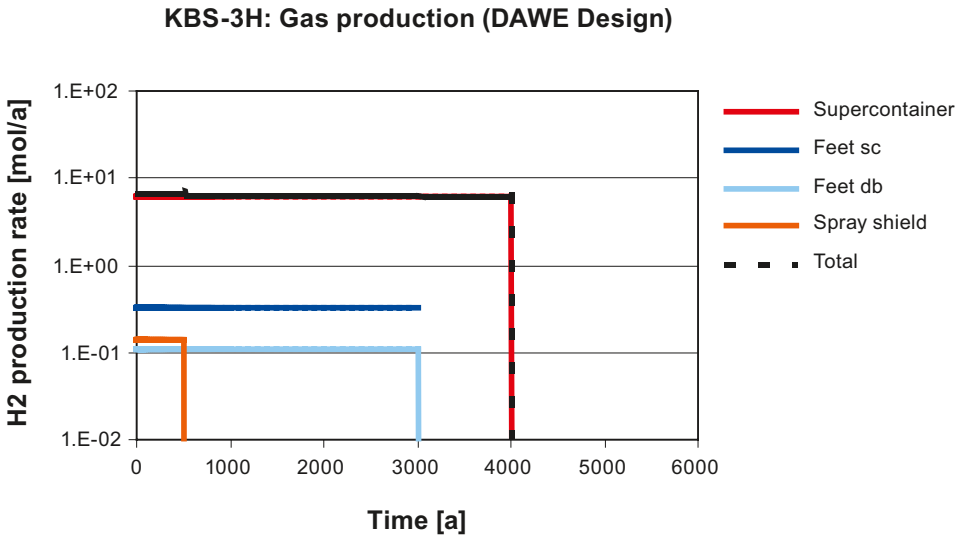

Figure D-2. *Hydrogen gas generation rates for the DAWE Design (steel corrosion rate 1 μm a^{-1}).*

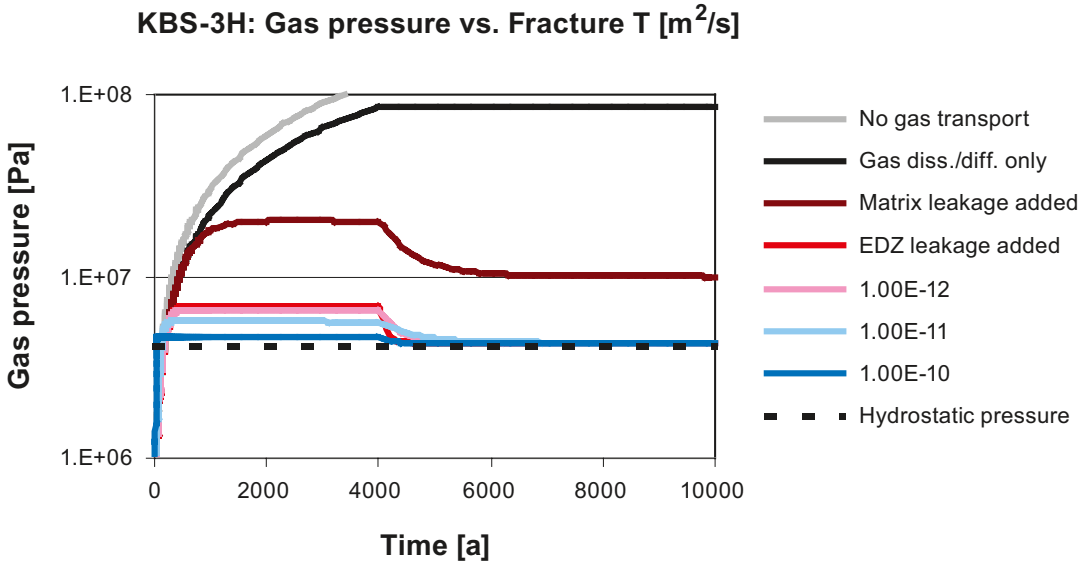

Figure D-3. *Evolution of gas pressure in the deposition drifts at Olkiluoto for the DAWE Design. For details of the model, see Appendix C. The pressure evolution is shown for several different cases: i) case without gas transport and dissolution, ii) case with gas dissolution and diffusion only, iii) case with gas leakage through matrix added, iv) case with gas leakage through EDZ added and v) cases with gas leakage and porewater displacement added, as a function of the hydraulic transmissivity of the representative pathway. In all situations, a steel corrosion rate of 1 μm a^{-1} is used.*

D.2.2 Piping and erosion in the DAWE design

In principle, the DAWE design is not affected by piping/erosion during:

- Installation: no erosion should occur since all inflowing water will be led down to the floor and run on the floor out of the drift without bentonite swelling or falling down on the floor.
- Water filling: the water filling can be done simultaneously at each section without water flowing between sections and thus no erosion should take place.
- After water filling: the situation depends on the inflow rate. If all inflow takes place in one section there will be piping and erosion when water saturates the other sections since all water must be taken from that inflow. On the other hand this situation is not realistic since there is always water flowing in the matrix of the rock. Erosion after water filling will only lead to internal redistribution of bentonite and will be limited to the amount of bentonite that can be transported with the water required to fill the unfilled pore space in the buffer blocks.

A main uncertainty with DAWE is that it is difficult to guarantee that there will be no bentonite slurry flowing along the drift floor out to the part of the drift where the emplacement takes place, since both water dripping on the blocks and humidity-induced cracking of the blocks may take place and cause erosion of bentonite.

There are thus still some uncertainties regarding the behaviour of DAWE during both the installation and the water saturation phase. Tests are ongoing for investigation of theses uncertainties. Ultimately there is a need for full-scale demonstration of this design.

D.3 References

Autio J, 2007. KBS-3H Design Description 2005. December 2006. Posiva Working report 2007-11 and SKB report R-08-29. Posiva Oy, Olkiluoto, Finland and SKB, Svensk Kärnbränslehantering AB, Sweden.

Autio, J, Börgesson L, Sandén T, Rönnqvist P-E, Johansson E, Hagros A, Eriksson M, Berghäll J, Kotola R, Parkkinen I, 2007. KBS-3H Design Description 2006. Posiva working report 2007-105 and SKB report R-08-32. Posiva Oy, Olkiluoto, Finland and SKB, Svensk Kärnbränslehantering AB, Sweden.

Appendix E

Alternative design options for drift end plugs

The reference design for the drift end plug is the steel-reinforced concrete plug, as described in Chapter 6. Possible alternatives proposed in the DD 2006 are a conventional low-pH concrete plug and a cement-grouted rock plug.

E.1 Low-pH shotcrete plug

In the framework of the European Commission project ESDRED, a shotcrete drift end plug has been tested at Äspö. The principle is similar to the concrete friction plug presented in Figure E-1. From the results and interpretation of the so called "short plug" loading tests performed, it was concluded that concrete with a pH equal to or lower than 11 may be formulated and successfully used for the construction of plugs in underground small diameter galleries using the shotcrete technique and that shrinkage is negligible with the concrete formulation used. It was further stated that the feasibility of constructing shotcrete plugs in small diameter galleries has been demonstrated, although some improvements might be needed to avoid or minimize the discontinuities between concrete layers and potential heterogeneities in the bottom part of the plug caused by shotcrete rebound.

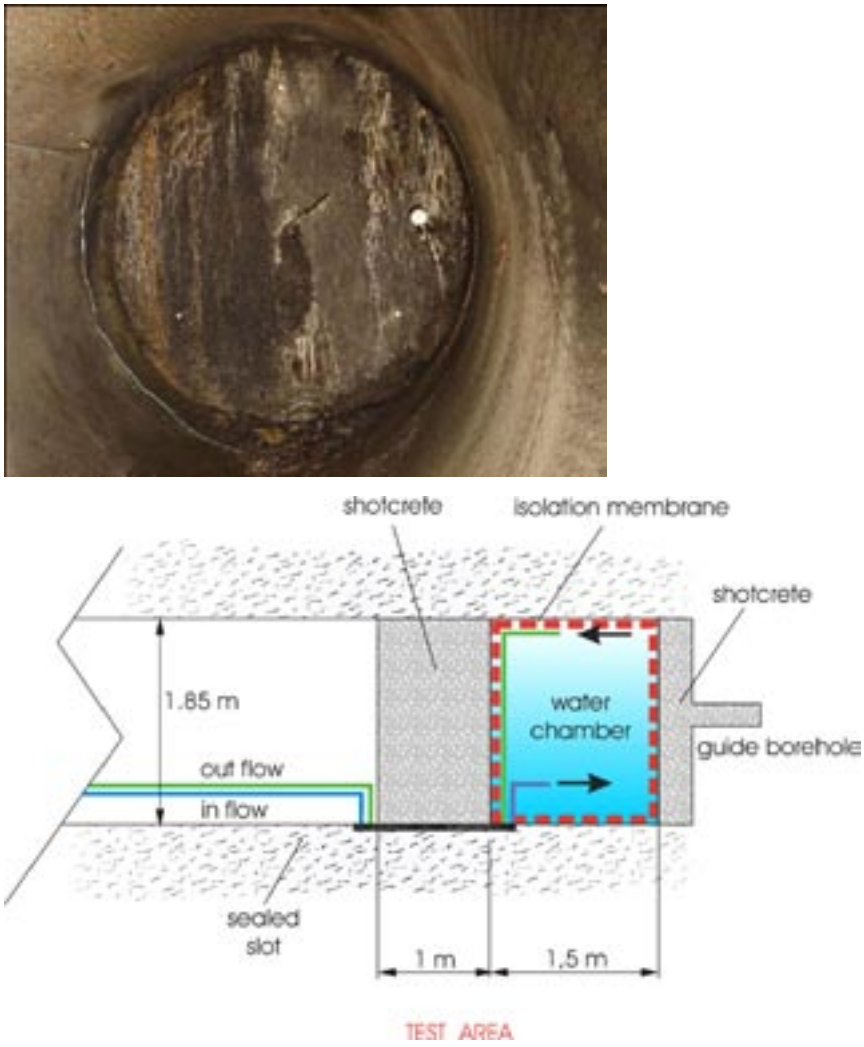

Figure E-1. *The low-pH shotcrete plug in KBS-3H demonstration drift at Äspö –220 m level (top) and principle of the test (above) (photo by J. Autio).*

E.2 Concrete plug

Conventional low-pH concrete plugs can be designed based on three different principles:

- Friction plug.
- Steel-reinforced plug positioned in a notch.
- Steel-reinforced wedge-shaped plug positioned in a notch.

These alternatives are illustrated in Figure E-2.

Cement-grouted rock plug

An alternative plug design based on using a rock kernel is illustrated in Figure E-3. The kernel is slightly wedge shaped. The amount of concrete in the design is clearly smaller than in other alternatives. Therefore the possible chemical disturbance caused by concrete is smaller than in other alternatives and the potential for volume changes caused during the long-term alteration of concrete is also smaller. The design has not been developed in detail and has not been tested.

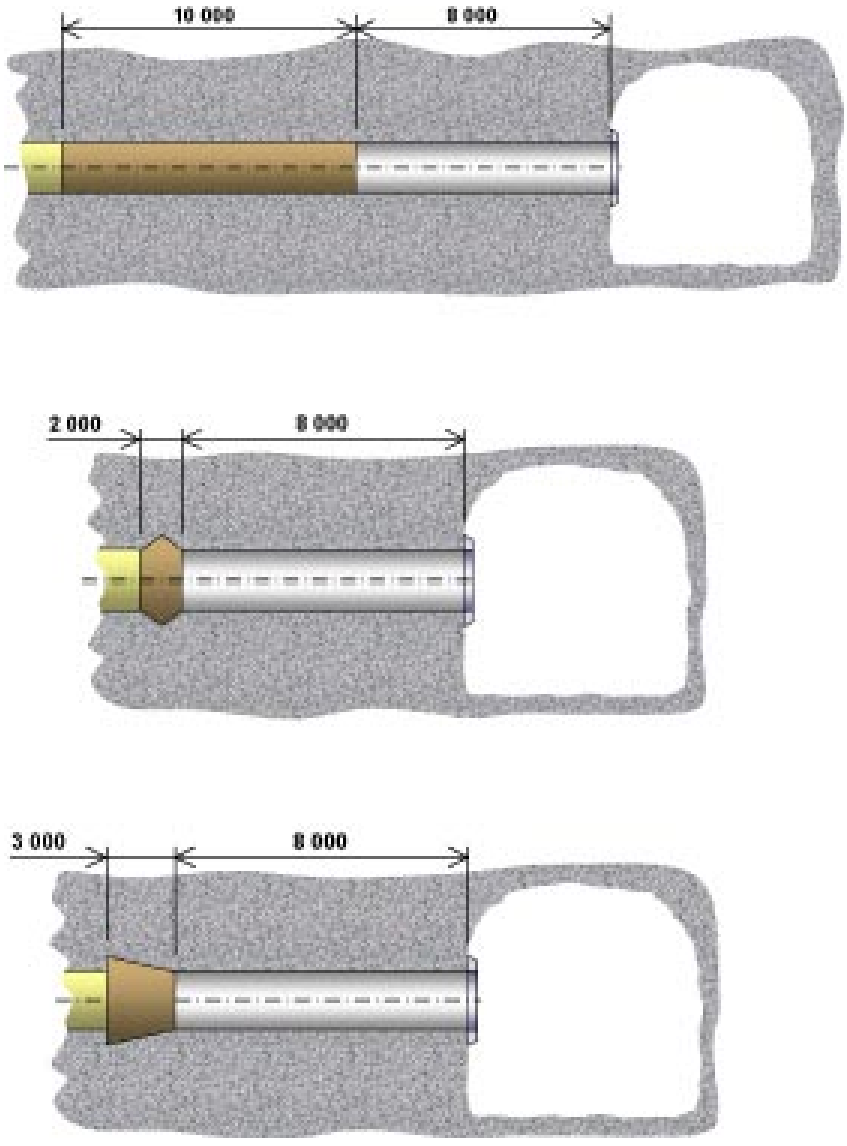

Figure E-2. *Concrete plug alternatives: Friction plug (top) similar to shotcrete plug, Steel-reinforced plug positioned in a notch (middle) and steel-reinforced plug positioned in a notch (above) /Thorsager and Lindgren, 2004/.*

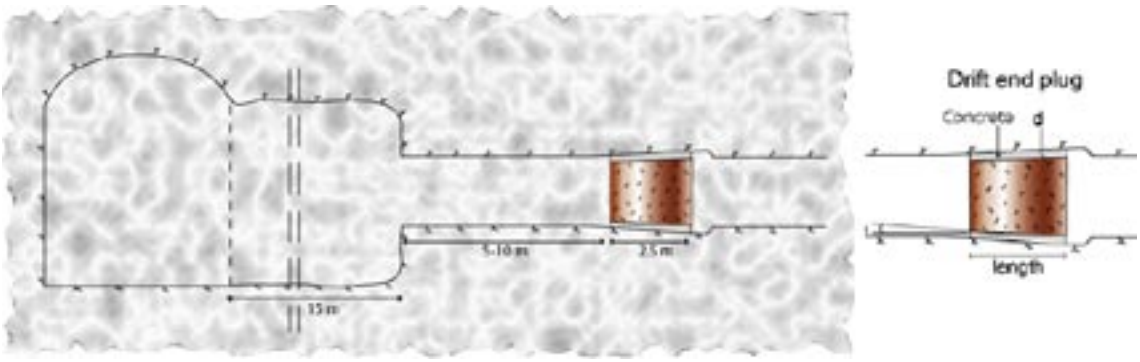

Figure E-3. *A draft of a rock plug grouted in the drift /Thorsager and Lindgren 2004/.*

E.3 References

Thorsager P, Lindgren E, 2004. Summary report of work done during Basic Design. SKB R-04-42, Svensk Kärnbränslehantering AB, Sweden.

Appendix F

Scoping calculations concerning cement/bentonite interactions

This appendix presents a qualitative discussion and a scoping calculation on the effect of cement on the bentonite in a KBS-3H drift. Further details on the current knowledge of the mechanism of cement/bentonite interaction are summarized in /Savage 2006, Ecoclay 2005, Metcalfe and Walker 2004, Alexander and Neall 2007/. Understanding the cement/bentonite interaction implies first understanding the mechanisms of cement degradation and then applying the consequences to bentonite.

F.1 Cement degradation

Because of lack of data on the degradation mechanisms of low-pH cement, the pH evolution of Ordinary Portland Cement is discussed, followed by the considerations of its applicability to low-pH cement. Consensus seems to be achieved on the evolution of Ordinary Portland Cement porewater with time producing hyperalkaline leachates with an initial pH of 13.4 (KOH/NaOH buffered), later decreasing to pH 12.5 ($CaOH_2$ buffered) as shown in Figure F-1 /Miller et al. 2000/. As the figure shows, the high alkalinity plume can last for several hundred thousands years and up to a few million years.

On the basis of geochemical first principles, /Savage 1998/ presented a simple generic conceptual model of the evolution of the host rock[35] as a hypothetical "plume" of hyperalkaline leachates migrates away from the cementitious material (Figure F-2). As summarized in /Alexander and Neall 2007/, the model assumes that the leachates are released from the cement (following mixing of groundwaters with the cement pore waters) due to the flow of groundwater into the cement further upstream[36]. At the cement/host rock interface (the proximal part of the plume), the hyperalkaline leachates have not yet reacted with the host rock and so have a high pH and high concentrations of Na, K and Ca, reflecting the cement porewater chemistry.

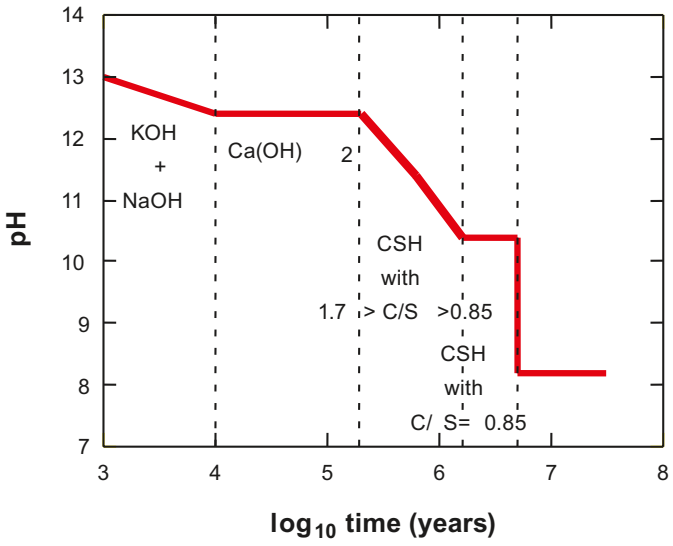

Figure F-1. *Estimated pH evolution of ordinary cement pore fluid /Miller et al. 2000/. CSH: calcium-silicate hydrate. C/S: calcium/silica ratio.*

[35] Note this model is equally applicable to interaction with bentonite.

[36] See /Neall 1994/ and /Lagerblad 2001/ for a discussion of the initial expulsion of cement pore waters from a cement mass, followed by leaching of the cement phases by the incoming groundwaters.

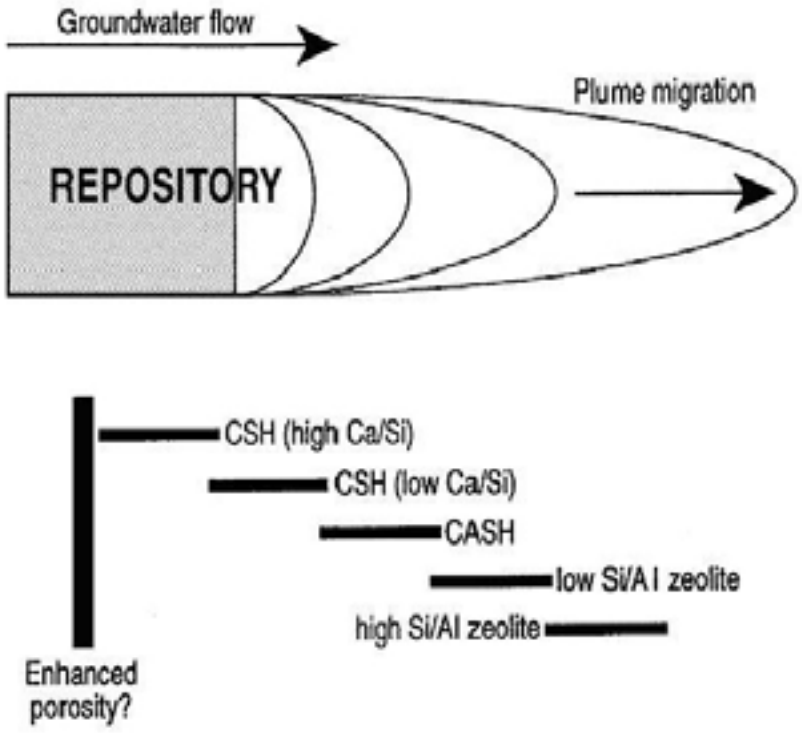

Figure F-2. *Conceptual model of the hyperalkaline plume evolution in the host rock /Savage 1998/.*

As the plume reacts with the host rock, the pH decreases, as Na, K and Ca Al and Si in groundwater equilibrate with those of the cement leachates. The extent of the cement/host rock interaction depends greatly on the groundwater composition and on the type of rock.

This pattern has consequences for the secondary mineralogy: CSH ($CaO\text{-}SiO_2\text{-}H_2O$) phases will be found in the fractured rock/porous media (through which the plume has migrated) in the proximal part of the plume, reflecting the fact that the leachate has not yet reacted with the host rock and is equilibrated with the CSH phases which make up the cement. As the leachate moves downstream and interacts with the aluminosilicates in the host rock (and the host rock groundwater and porewater), the Al concentration increases, precipitating CASH phases. At the distal edge of the plume, the leachate has reacted with an even larger volume of host rock (and the host rock groundwater and porewater) and eventually precipitates minerals such as zeolites as the Al concentration in the groundwater becomes high enough and the pH low enough /Savage 1997/[37].

If it is assumed that the plume continues to migrate, then, by analogy with the above argument, the zeolite zone produced by the distal part of the plume will later be over-run by the middle of the plume, inducing some re-dissolution of the zeolite phases and replacement by CASH phases. This mixed zeolite/CASH zone will be then over-run by the proximal part of the plume, inducing further re-dissolution of the zeolite/CASH phases and replacement by CSH phases. These complex mixtures have been observed in natural clayey formations exposed to highly alkaline groundwaters at Maqarin, Jordan in places at the advective-flow dominated fractured host rock site (see /Alexander 1992, Linklater 1998, Smellie 1998, Pitty 2007/ for details).

[37] See /Savage 1997/ for a discussion of zeolite and CSH stability fields. Briefly, in the presence of elevated Al levels in solution, zeolites will form preferentially due to the limited ability of CASH/ CSH to incorporate Al in the mineralogical structure.

Local groundwater flow and transport conditions have a major influence on the release and transport of cement and subsequently on the magnitude of the high pH plume. Important controlling factors include /Metcalfe and Walker 2004/:

1. Sub-horizontal fracture zones divide the flow pattern into layered zones. It is unlikely that a significant amount of cement above or from major subhorizontal zones would be transported into the sparsely fractured rock below the zones.
2. The water leaving a grouted rock spot will not have the pH and other properties of cement pore water, but is diluted by the groundwater flowing around/through the grouted area. This source term dilution is enhanced by the fact that grouting is carried out at fracture zones and other locations where flow rates are highest.
3. Further buffering and dilution take place during transport in the geosphere. In open fractures with a limited buffering capacity and a small WL/Q (half of the "flow wetted" surface divided by the flow rate), the leachate may, however, be transported over long distances.

Transfer of hydroxyl (OH^-) ions from water-conducting fractures intersecting a deposition hole into the buffer is limited by the boundary layer (film) resistance between the flowing groundwater and the stagnant pore water in the buffer. The fraction of OH^- ions entering the buffer decreases with an increasing flow rate of groundwater along the fractures. This applies both for the ratio of mass flow into buffer vs. advective one and for the ratio of all OH-ions transferred into buffer vs. amount of OH^- ions in a given finite source. The amount of OH^- ions transferred to the buffer (in a given time) increases as the flow rate increases but only relative to the square root of the flow rate while the overall advective transfer (during the same time) approaching the buffer increases directly proportional to the flow rate. If the source term would produce the same concentration of OH^- ions for any flow rate, the amount of OH^- ions transferred to the buffer would be the larger the higher the flow rate but the fraction of ions transferred to the buffer from the ions totally released would decrease. The release from a finite cement source would last a shorter time if the flow rate is higher (inversely proportional to the flow rate with constant concentration release). Thus the fraction of OH^- ions transferred to the buffer from the total amount of a cement source in the case of limited source would be smaller with increasing flow rate.

In summary, any cementitious porewater transported by groundwater to the drift from a distance should first interact with the host rock before it reaches the bentonite in the drift. The cement-host rock interaction could include both the reactions with the fracture surface minerals and with any fault infill or gouge plus the accessible porosity in the rock matrix behind the fractures (as long as this is not sealed by reaction). This includes any porewater held in the matrix, which can have a significant effect on preliminary mineral reactions (e.g. at Maqarin, the matrix porewater is HCO_3^--rich and so induces precipitation of calcite in/around the fracture face).

During this interaction with the host rock, the pH could be considerably lowered although no experimental data on the host rock buffering capacity are available. Modelling results suggest instead that the Olkiluoto host rock buffering capacity is quite low /Montori et al. 2008/.

F.1.1 Low-pH cement degradation studies

Low pH cement consist basically of mixtures of cement were the Ca/Si ratio and the potential for formation of $Ca(OH)_2$ (portlandite) have been reduced by replacing a large part of PC by a pozzolan.

/Ahokas et al. 2006/ summarise the current knowledge on low-pH cement degradation studies. According to experimental results, potassium and sulphate are rapidly released from the low-pH cement product, and a declining release of calcium with time was observed. Silica release continued throughout the experimental time. Distinctly higher release of the alkalis Ca, Na, K was observed for the reference Portland cement. The leached fraction of K^+ and SO_4^{2-} was calculated to be 100% for the low-pH cement mass, whereas the leaching fraction of Si and Al was low, only a few%. Based on the experimental and model results, it is conceivable that, irrespective of the mix, the whole inventory of the alkaline elements, and possibly of sulphur, is leachable.

The long-term behaviour of the product, such as phase changes and crystallization of CSH phases, which might have an effect on the long-term degradation and leaching of the product, remains to be evaluated. The long-term behaviour of the product means stability of the grout for the operation and construction period and further understanding of the degradation of the product in the longer term.

With respect to the long-term safety aspects, the relatively short-term leaching experiments performed in the laboratory revealed that the defined pH criteria could be met based on the testing procedure used measuring the maximum equilibrium pH of the leachate. The pH values measured in the saline leachates from low-pH cement were constantly lower than in the fresh leachates. Based on the analyses of the solid phase of the low-pH cementitious mix, there was no $Ca(OH)_2$ found in the hydrated paste which suggests that calcium is bound into CSH phases /Vuorinen et al. 2005/. The long-term degradation of these CSH phases and rate of calcium release is still unclear. However, the Ca/Si ratio in the low pH cement formulation planned to be used in the repository (P308B, see e.g. /Ahokas et al. 2006/) is about 0.8 and thus at the lower end of the CSH curve in Figure F-1. This indicates that the pH of the leachate should remain below 11 even if Ca is leached out as a silicate phase in the long term ($>10^5$ years). Groundwater salinity further limits the pH increase, as observed by /Vuorinen et al. 2005/, although the reason is not well understood.

F.2 Bentonite alteration in presence of cementitious porewater

While the detailed mechanism is still unclear, the current consensus is that the main effect of alkaline cementitious porewater on bentonite is montmorillonite dissolution due to the high pH conditions. The bentonite alteration pattern is similar to that presented in Figure F-2 (bottom). Bentonite undergoes the following mineral transformations as a function of time and distance from the cement/bentonite interface:

Cement/bentonite interface→ Montmorillonite dissolution (pH buffering) →
CSH precipitation → CASH precipitation →
Illite precipitation → Zeolite precipitation (Eq. F-1)

The transformation begins with an illitisation of the montmorillonite. The illite then dissolves as zeolites phases are precipitated. These are finally dissolved to produce cement phases near the concrete interface as a result of an increase in the Ca/Si ratio in the solid phases. This transformation sequence causes a decrease in the total volume of the clay as illitisation of the montmorillonite progresses and a strong increase in the total volume as cement phases precipitate, which would lead to a decrease in porosity near the concrete interface.

The pH in the bentonite porewater is also expected to increase: this increase influences significantly both the chemical and physical properties of the buffer including /Metcalfe and Walker 2004/:

1. Release of silicate (whether congruent or incongruent) from the montmorillonite structure.
2. Secondary minerals will form as a result of the interaction between cement leachate and bentonite. The types and abundances of secondary minerals will reflect the composition of the solution phase (pH, pe, cations etc). Problems still persist in predicting which of these secondary phases will be important because of the poor knowledge of possible reaction products (including some which may not yet have been identified), mineral dissolution rates and growth kinetics which are subject to considerable uncertainty /Lehikoinen 2004/.
3. Cation exchange reactions may occur at the same time as the mineral transformations Notably, Mg-exchanged sites (MgX2) in the unaltered bentonite will become Na-exchanged (NaX) in NaOH solutions, K-exchanged (KX) in KOH solutions and Ca-exchanged (CaX2) in Ca(OH)2 solutions. No information on competitivity is available.

4. Cation Exchange Capacity (CEC) is significantly increased on exposure to strong NaOH solutions (>0.3M) /Karnland et al. 2004/ and synthetic high pH Na- Ca-Cl waters (molar ratios of Na/Ca ~ 2.4, 24 and 2,330; /Vuorinen et al. 2004/). In contrast, solutions exposed only to NaCl and Ca(OH)2 saturated solutions show no significant change. Although replacement of Na in the montmorillonite by Ca was found for the experiments conducted in the Ca(OH)2 saturated solutions /Karnland et al. 2004/ and controlled replacement could be achieved using a CaCl2 solution /Ito et al. 2004/.
5. Dissolution rates of minerals in bentonite are strongly dependent on pH and temperature. The dissolution rate increases with an increase in pH and/or temperature /Sato et al. 2004/. The rate of dissolution at any time will also depend on the degree to which equilibrium is approached. Solids that are far from equilibrium with respect to a particular solution will dissolve much faster than solids that are close to equilibrium /Takase 2004/. Similar rates are obtained from Si and Al concentrations, and NaOH and KOH experiments, showing no effects of interlayer cation on dissolution rates /Sato et al. 2004/. A summary of the dissolution rate laws presented at the workshop is given in /Metcalfe and Walker 2004/.
6. The buffering capacity of bulk bentonite may be controlled by silica polymorphs in the early stages of degradation because of their faster dissolution when compared with montmorillonite /Lehikoinen 2004/. The buffering capacity of montmorillonite is the sum of two contributions: – the edge surface hydroxyl sites which undergo very fast reactions; – the montmorillonite structure itself, which tends to undergo slow reactions and will not buffer the pore fluid chemistry until the edge surface sites have been exhausted. In highly compacted bentonites, the pH buffering capacity is at a maximum because the solution migration is diffusion controlled /Lehikoinen 2004/.
7. Solution modelling predicts that with the precipitation of zeolites, associated with the mineralogical changes, the pH of the cement leachate is neutralized, which in turn may inhibit further dissolution of the bentonite /Oda et al. 2004/. Swelling pressure is reduced on exposure to high concentration NaOH and NaCl solutions (>0.3M). A major difference was that NaCl gave a rapid decrease to a new stable pressure value, while contact with the NaOH solution gave a gradual decrease /Karnland et al. 2004/. Low concentration NaOH solution and Ca(OH)2 saturated solution had no effect on the swelling pressure /Karnland et al. 2004/. Consolidation tests show that the greater the difference between the preconsolidation stress (overburden pressure) and the current overburden pressure (i.e. unloading of overburden pressure due to adjacent cement dissolution) the greater the tendency for the material to swell /Ito et al. 2004/.
8. Precipitation/cementation processes are difficult to evaluate. Depending on experimental set up (e.g. flow-through reactors), some workers found that precipitation/cementation effects were not significant. However, this may not be truly representative of a real system where secondary minerals are likely to grow in situ. Cementation may be a significant issue because of the increased chance of the bentonite barrier cracking and solution transport being advective as opposed to diffusive /McKinley et al. 2004/.
9. Porosity has been described as either increasing or decreasing as a function of dissolution and precipitation rates of the primary and secondary minerals. In the long term this will depend on the stability of these secondary phases once formed /Arthur et al. 2004/. Where only dissolution of the bentonite is considered /e.g. Kato et al. 2004/, the porosity increases. If considering the growth of alteration products they are likely to form in situ (cementation) and so decrease the porosity /e.g. Berner 2004; Gaucher 2004/.
10. Permeability and porosity are strongly dependent on each other. Similarly, permeability will increase or decrease as a function of the dissolution and precipitation of the primary and secondary minerals.
11. Hydraulic conductivity is related to the permeability and porosity of the bentonite. Predictive modelling has shown the hydraulic conductivity to generally increase with ongoing exposure to a high pH plume /Kato et al. 2004/. Similarly this is dependent on the dissolution and precipitation rates of the primary and secondary minerals.

12. Hydraulic conductivity of primary and secondary reaction products is low because of their low porosity. Therefore diffusivity in bentonite has been predicted to decrease as a function of time /Kato et al. 2004/.
13. Sorption will be important and an intact bentonite has excellent sorption capability, one of the main criteria for using it. However, assessing the sorption capability of secondary minerals is difficult and results in uncertainty as to the evolution of sorption capacity as a function of time.
14. Shear strength (the ability to resist failure by a shear stress field) is independent of sodium exchange by calcium in montmorillonite /Ito et al. 2004/.

F.2.1 Experimental studies

Few experimental studies are available with MX-80 bentonite /Vuorinen et al. 2006/ and even fewer with compacted MX-80 in presence of low-pH cement /Karnland et al. 2005/.

Batch and flow-through cell experiments (see /Alexander and Neall 2007/ for an overview) to examine the effects of hyperalkaline leachates on bentonite generally indicate the presence of secondary zeolites /e.g. ECOCLAY 2005/ and CSH gels /e.g. Vuorinen et al. 2006/, concomitant with reduced surface area and pore size increase. Presence of abundant Ca means that the bentonite is exchanged to Ca-bentonite, even if it begins as a Na-bentonite (such as MX-80), and, in saline conditions, smectite has been seen to alter to Ca-montmorillonite. NaOH solutions (pH>13) induce production of beidellite, which significantly increases the CEC /ECOCLAY 2005, Vuorinen et al. 2006/ and permanently decreases the swelling pressure by up to 60–70%, presumably due to the loss of Si /Karnland et al. 2005/. Both NaCl and NaOH solutions at concentrations of 0.3M and greater significantly decrease the swelling pressure (Section 4.2.1 and /Karnland et al. 2004, SKI 2005/) while $Ca(OH)_2$ buffered leachates make no significant difference to the swelling pressure /ECOCLAY 2005/.

The influence of compaction and high swelling pressure on smectite dissolution rates is currently not well understood and should be the target of further experimental work /Neall and Johnson 2006/. In case of compacted bentonite, the small diffusion coefficient of species in compacted bentonite should minimise interaction with the hyperalkaline leachates and the subsequent chemical reactions (i.e. production of secondary phases) appear to reduce the alteration of bentonite even more /Lehikoinen 2004, ECOCLAY 2005/. /Karnland et al. 2005/ suggest that some of the discrepancies between batch experiments and experiments with compacted bentonite may be explained by ion-equilibrium established between the hydroxide ions and the montmorillonite counter-ions in the pore fluid of compacted bentonite.

The two natural analogue sites identified in Jordan may provide some information on the long-term effects of hyperalkaline waters on natural clay but further studies could be carried out in this domain /Metcalfe and Walker 2004, Alexander and Neall 2007/.

In summary, experimental results show mainly the strong buffering power of bentonite in presence of highly alkaline water due to the dissolution of montmorillonite. Swelling pressure is also lost in contact with NaOH solutions but not in presence of $Ca(OH)_2$ (portlandite), which is the main source of OH- ions in the long term. A main source of uncertainty is the fate of $Ca(OH)_2$ in low-pH cement, which is the main source of OH- in the time scales of interest (10,000 to 100,000 years and beyond). Ongoing experimental studies (unpublished) suggest that Ca is mainly bound in a CSH phase that would decrease or inhibit the release of OH^-. If this effect were confirmed, the beneficial effect of using low-pH cement in a KBS-3H drift could be quantified. Until then, it is conservatively assumed that all CaO in the low-pH cement is transformed into OH^- ions as $Ca(OH)_2$. Other uncertainties concern the nature as well as thermodynamic and kinetics data on the secondary minerals formed or precipitated.

F.2.2 Modelling studies

/Metcalfe and Walker 2004/ summarized the main modelling approaches of cement/bentonite interaction. Several of the models were used to predict the depth of degradation as a function of time and are summarized in Table F-1.

The capability of the models to accurately predict the performance of the components in an engineered barrier system as a function of time is limited by:

1. Appropriate mineral representation, especially the secondary minerals, including:
   - CSH-phases (there is still an on-going debate concerning the nature of appropriate analogous CSH phases);
   - zeolites;
   - smectites.
2. Formulation of key underlying models/laws/functions, especially:
   - solid solution models – these have yet to be incorporated into modelling of the engineered barrier system;
   - activity coefficient models – using different methods provides different answers in terms of the activity of a species in solution;
   - rate laws – both dissolution and precipitation of relevant phases in the system;
   - hydrological constraints – including groundwater velocity, advection vs. diffusion, porosity, permeability, and hydraulic conductivity.
3. Differences between actual and modelled phases, notably:
   - chemical differences;
   - degree of crystallinity (which is very hard to determine as mineral phases may be present as gels, or be semi- or wholly- crystalline and different states of the same can have solubilities ranging over several orders of magnitude).

Figure F-3 shows the complexity of the cement-bentonite interaction in which some phenomena promote bentonite alteration while others limits it. Hence the complexity of accurately modelling the system and deriving long-term predictions.

Table F-1. Summary of predictive models described in (/Metcalfe and Walker 2004/ and references therein). These models assessed the depth of degradation of materials in the engineered barrier system as a function of time.

Worker	Material	Phenomena investigated	Time frame (years)	Depth affected (cm)	Validation against real systems?
Otsuki	OPC	Porosity increase	10 100 1000	5 10 30	Yes
Lehikoinen	Na-montmorillonite	Porosity vs. secondary minerals	1,000	Porosity lost < 10 Reaction products >35	No
Gaucher	Na-montmorillonite	Secondary minerals	100,000	65	No
Takase	Na-montmorillonite	Secondary minerals	1,000,000	50 - 200	No

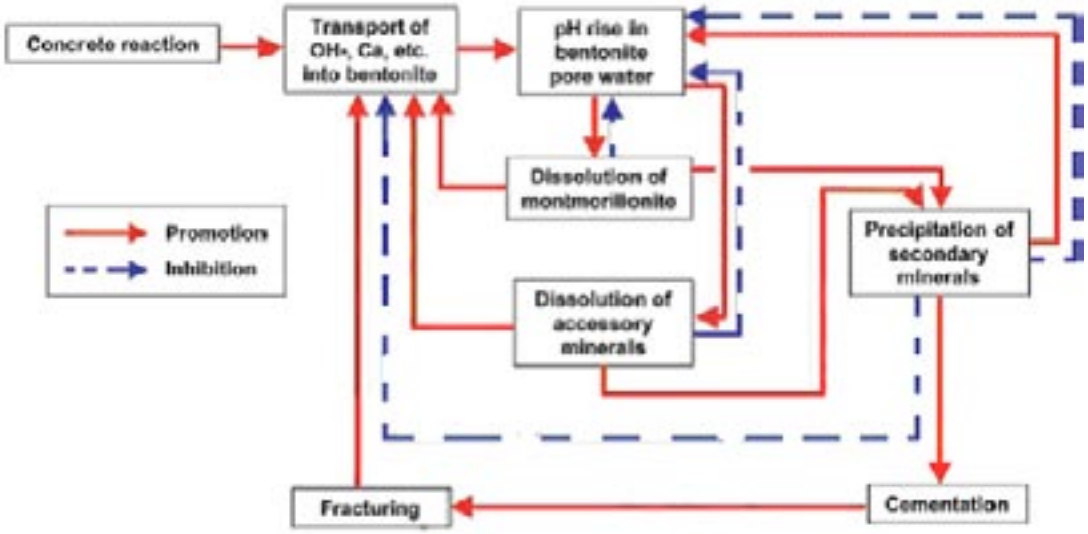

Figure F-3. *Cement/Bentonite interaction as a coupled non-linear dynamical system /Takase 2004/.*

Although the codes for modelling leachate/bentonite interaction have improved markedly over the last couple of decades, the basic mineralogical thermodynamic databases are still very weak and are probably the limiting factor to any detailed modelling of leachate/bentonite interaction. Indeed, when recently discussing the status of modelling studies, /Savage 2006/ noted that:

- the (modeller's) choice of secondary minerals influences the chemical environment by consuming or generating hydroxyl ions, even before their effects on the physical environment, such as porosity or permeability, are considered;
- it is essential to consider kinetics due to the presence of metastable secondary phases;[38]
- there remains a basic lack of thermodynamic and kinetic data for the phases of interest.

These uncertainties greatly affect the modelling results so that no quantitative conclusions from these studies can be drawn thus far. Therefore, the following discussion of the cement/bentonite interaction is only qualitative and the mass balance calculations are not representative of the physical and chemical phenomena at play.

F.3 Cement and bentonite inventories in a KBS-3H drift

Table F-2 gives the main assumptions used in the mass balance calculations. Table F-3 shows the breakdown of cement sources per drift, according to the various design options. Only low-pH cement is considered in the drift to limit the long-term alkalinity effects compared with those of Ordinary Portland Cement. Low-pH cement formulations are currently being studied as promising alternatives to Ordinary Portland Cement although they too leach considerable amounts of hydroxyl (OH^-) ions in groundwater (see Table F-4). The low-heat high-performance cement (LHHP) developed by AECL /Martino et al. 2002/ is considered the reference cement type for the drift end plug in the KBS-3H Design Description 2006 /Autio et al. 2007/. This type of plug contains roughly 2.5 times less cement than the rock kernel plug and the 3.2 times less cement than the "traditional" low-pH cement alternative materials for the drift end plug listed in /Hagros 2007/.

Other sources of cement in the KBS-3H deposition drift are in the 15 m-long emplacement section (used for canister deposition equipment) are support bolts, anchor bolts, shotcrete, floors and miscellaneous engineering structures. Most of these sources will be removed to the maximum extent practical. Remaining quantities of cement in these emplacement sections are in Table F-4.

[38] Some so-called metastable secondary phases observed at the Maqarin site in Jordan have been noted to be very long-lasting /e.g. Milodowski et al. 1998ab/. It is believed that, as long as the phases are protected against solution and further reaction (e.g. by fracture sealing), they can survive for geological timescales.

Table F-2. Assumptions used in mass balance calculations /from Hagros 2007/.

Type of cement	low-pH cement
Number of drifts	171
Average number of supercontainer per drift	18.5 (17–21 canisters depending on fuel type)
Total length of the drift	300 m
Length of the canister-bearing section	285 m
Length of the emplacement section	15 m
Volume of the canister-bearing section	800 m^3
Volume of the 15-m deposition niche	750 m^3
Density (dry) of low-pH cement	1,354 kg/m^3
Density (dry) of Silica Sol	1,250 kg/m^3
Dry density of backfill (Friedland clay or MX-80/crushed rock mixture)	1,950 kg/m^3
Type of drift end plug	Steel-reinforced cement plug using the Canadian LHHPC concrete mixture (780 kg cement) (reference plug for design)
	Or cement-grouted rock kernel plug (1,600 kg cement)

Table F-3. Cement-bearing components and weight (in average) per drift (including the 15-m long emplacement section, see Table F-4). Only low-pH cement is considered (dry density = 1,354 kg/m^3). Dimensions and assumptions are from Table F-2.

Cement-bearing component	Number of components per drift (average)	Amount of cement in each component	Total per drift
Drift end plug + steel plug	1	780 kg (steel-reinforced LHHP cement plug) or	1,080 kg
		1,600 kg (grouted rock plug)	or
		+ 300 kg in steel plug in front of the plug	1,900 kg
Compartment plugs (steel plugs)	2	300 kg	600 kg
Fixing rings for distance blocks	up to 20[c]	23 kg	up to 460 kg
Grouted areas	10% of the drift grouted[a]	0.6 kg cement/m^3 (average over the entire drift)[a]	0–500 kg[b]
	or	or	
	5.2 areas needing grouting[a]	0.07 m^3 grout take per area needing grouting[a]	
Cement in 15-m emplacement section	See Table F-4	See Table F-4	490 kg
Total cement in one drift (range)			2,630–3,950 kg (depending on plug design)

[a] Estimates from /Hagros 2007/.

[b] See Appendix A of this report. The mass of cement is 0 kg if Silica Sol is used as grouting material, 500 kg if low-pH cement is used to grout all fractures.

[c] The number of fixing rings has not been decided but there may be as many as supercontainers plus additional ones every time there is a risk of distance block displacement due to higher inflow rates /Autio et al. 2007/.

Table F-4. Other sources of cement in the emplacement section of the drift (first 15 m of the drift). Data are from /Hagros 2007/.

Cement-bearing component	Number of components per unit length (average)	Amount of cement in each component	Total (x 171 drifts)
Support bolts	1.4 bolt/m (or 21 bolts)	7.1 kg/m	106.5 kg (18,211 kg)
Anchor bolts	1 bolt/m (or 15 bolts)	0.31 kg/m	4.65 kg (795 kg)
Shotcrete	430 kg/m (prior to removal)	21.5 kg/m[a] (after removal)	322.5 kg after removal (55,147 kg)
Grouting		0.075 kg/m^3	56.25 kg (9,620 kg)
Total cement in 15-m emplacement section			490 kg (83,800 kg)

[a] Assuming a 95% removal efficiency.

Table F-5. Bentonite-bearing components in a KBS-3H drift. The type of bentonite is MX-80. Data are from /Autio et al. 2007, Johansson et al. 2007/.

Bentonite-bearing component	Number of components per drift	Amount of bentonite per component	Total amount per drift
Supercontainer	17.5	16,445 kg[a]	287,787
Ring blocks (dry density 1,885 kg/m^3) 4.810 m,			
End blocks (dry density 1,753 kg/m^3) 0.350 m			
Distance block	17.5	22,940 kg	401,450 kg
–Tight blocks (1 m long, dry density 1,559 kg/m^3)			
–Loose blocks (4.5 m long, dry density 1,610 kg/m^3)			
Compacted bentonite in the first 5 m of canister-bearing section (in contact with the drift end plug) (assumed dry density 1,600 kg/m^3)	1	19,000 kg	19,000 kg
Compartment plug	1 (incl. 2 steel plugs)	130,000 kg	130,000 kg
Filling/distance blocks in blank zones	52 m total	4,190 kg bentonite/m	217,000 kg
Filling adjacent to steel plugs (MX-80 pellets with bulk density 1,830 kg/m^3)	3	not reported	not taken into account in bentonite inventor
Total			1,055,237 kg

[a] Depending on the type of fuel (Loviisa 1-2, Olkiluoto 1,2,3), the amount of bentonite in the supercontainer varies from 13,000 to 16,000 kg. The reference spent fuel type is the BWR fuel from Olkiluoto 1-2 fuel type (17.5 canisters per drift).

Table F-3 shows the amounts of bentonite in different parts of the drift. In addition, the 15 m emplacement section will also be backfilled with a clayey compound (to be defined; the current options are Friedland Clay or a mixture of MX-80 and crushed rock, both options would have a dry density of 1,950 kg/m^3 /Hagros 2007/). From the volume of the 15-m long emplacement section (750 m^3) and the dry density of the backfill, the mass of backfill to be used is about 1,462,000 kg, the amount of clayey material susceptible to be altered by the alkaline plume depends on the choice of backfill material so the backfill buffering capacity is not taken into account in the mass balance calculations.

Grout take estimates

The largest uncertainty on the estimates of cement masses is the amount of grout (or other sealing material, such as Silica Sol) used for groundwater control. The amount of grout injected in the fracture (grout take) depends on several parameters, such as the type of fractures, grouting strategy, grouting material and grout removal efficiency.

The reference value of cement mass used to grout an average drift is 0–500 kg, depending whether Silica Sol or low-pH cement is used as grouting material (see Table F-3). These estimates are based on predictions of grout take for ONKALO at depths between 300 and 400 m (2 m^3 per 20 m grouting fan in ONKALO and scaled down to the drift and deposition niche dimensions) and on the assumption that 10% of the drift length needs grouting /Hagros 2007/.

The Design Description 2006 presents alternative grout take calculations for groundwater control, based on a statistical description of the geohydrological situation and assuming that fractures can be represented by discs completely filled with grout up to 15 m in the rock /Autio et al. 2007/. The estimated grout volume was between 0.1 and 0.5 m^3 if Silica Sol is used as grouting material /Autio et al. 2007/. Although in principle this volume could be converted into a low-pH cement grout take (135 kg and 677 kg), low-pH cement cannot penetrate as much volume as Silica Sol can and therefore this estimate is highly conservative. Given the uncertainties, however, these estimates are consistent with the reference grout take range of 0–500 kg of low-pH cement.

It should be noted that Silica Sol also contains small (<1%) amounts of biocide agents such as isothiazols and bromo-nitropropan-diols that might have an influence on long-term safety and therefore need to be evaluated.

F.4 Mass balance estimates

The dissolution of montmorillonite in a hyperalkaline solution (pH >10) can be formulated as follows /e.g. Savage et al. 2007/:

$$Na_{0.33}Si_4Al_{1.67}Mg_{0.33}O_{10}(OH)_2 + 2\,H_2O + 4.68\,OH^- \rightarrow 0.33\,Na^+ + 0.33\,Mg^{2+} + 1.67\,Al(OH)_4^- + 4\,HSiO_3^- \quad \text{(Eq. F-2)}$$

The degradation of a cementitious material with x mol of Na_2O, y mol of K_2O and z mol of CaO may produce a maximum of $n = 2(x+y+z)$ mol of OH^-,

$$x\,Na_2O + y\,K_2O + z\,CaO + n/2\,H_2O \rightarrow 2x\,Na^+ + 2y\,K^+ + z\,Ca^{2+} + n\,OH^-. \quad \text{(Eq. F-3)}$$

It thus takes 4.68 moles of OH^- to dissolve one mole of montmorillonite, assuming no hydroxide-consuming or -generating reactions (e.g. effect of constituent SiO_2 of cement, dissolution of accessory minerals in bentonite, or precipitation of secondary minerals) other than Equations F-2 and F-3 and no dilution of OH^- into the deep groundwater to take place.

The amount of dissolved bentonite is likely much less if low-pH cement is used because calcium in low-pH cement is mainly bound in a CSH ($CaO\text{-}SiO_2\text{-}H_2O$) phase. The latter ensures that the release of free hydroxide from constituent CaO is greatly suppressed or retarded, thus mitigating the threat to buffer longevity by dissolution.

The amount of moles of OH^- from the cement in the drift is calculated according to Equation F-3 and depending on the composition of low-pH cement, shown in Table F-6. For comparison purposes, the amount of OH^- generated by ordinary cement is also shown in Table F-6.

Table F-6. Initial inventory of selected constituent oxides in cement grout (in mol/kg).

Cement grout	Na_2O	K_2O	CaO	nOH^-/kg cement
Ordinary	0.009	0.032	4.900	9.841
Low-pH	0.009	0.026	2.855	5.745

If 4.68 moles of OH^- dissolve one mole of montmorillonite (Equation F-1), the mass of dissolved montmorillonite can be theoretically calculated with Equation F-4:

$$Mass\ of\ dissolved\ montmorillonite = \frac{mass\ of\ cement\ (kg)\ x\ nOH^-\ x\ M}{4.68} \qquad \text{(Eq. F-4)}$$

with nOH^- being the amount of OH^- released per kg of cement (Table F-6) and M being the molar mass of montmorillonite is M=0.367 kg/mol.

Based on Tables F-3, F-4, and F-5 the maximum amount of hydroxide a degrading grout is able to generate and the amount of montmorillonite it is subsequently able to dissolve are calculated per one drift. If the total amount of cement in a drift is 2,630–3,950 kg (Table F-3), 15,052 moles of OH^- can be generated (at most) by this amount of low pH cement. These OH^- are potentially capable to dissolve 1,185–1,780 kg of montmorillonite, which is equivalent to 1,475–2,224 kg of bentonite (assuming 80wt% of montmorillonite). According to Table F-5, the total amount of bentonite in a drift (not even taking into account the backfilled sections) is about 1,055,000 kg, so the dissolved bentonite represents 0.1–0.2% of the bentonite inventory.

It could be argued that the amount of cement in ONKALO could also interact with the bentonite in the KBS-3H drift. If the cement in ONKALO (or part of it) is included in the mass balance calculations, then the mass of bentonite in the ONKALO backfill should also be taken into account as a pH buffer. The current estimate of residual cement in ONKALO is 3,170,000 kg /Alexander and Neall 2007/. Assuming Ordinary Portland Cement is used for grouting ONKALO (unrealistic as the excavation approaches the repository level), if the 362,000 m^3 volume is backfilled using a backfill with a dry density of 1,950 kg/m^3 and a 50% montmorillonite content (353,000,000 kg of backfill montmorillonite), then 2,446,000 kg of montmorillonite would be altered, which corresponds to a ratio altered montmorillonite/backfill montmorillonite of 0.7%. Again, these mass balances do not represent the physical and chemical reality of an alkaline plume diffusing in the host rock, therefore the numbers are highly conservative estimates.

As cement is not spread uniformly along the drift, it is worth calculating the mass balance of the two largest sources of cement in a drift, the drift end plug and the grouted fractures (see Table F-3 for cement quantities). For the drift end plug (including the steel plug, a total of 1,080 kg of cement), if LHHP cement is used, the amount of montmorillonite dissolved would be 487 kg. Considering that on the canister-side of the plug there are at least two 5-m distance blocks of 22,940 kg each of bentonite (18,352 kg of montmorillonite each) and that on the emplacement section-side there is another 5 m-block of compacted bentonite, the ratio of dissolved bentonite is 1.3% if the alkaline plume migrates only in one direction toward the canisters or 0.9% if the plume spreads in two directions along the drift axis.

If the rock kernel/low pH plug design is used (1,900 kg of cement), the amount of dissolved montmorillonite would be 856 kg, which could dissolve 2% of the mass of bentonite in direct contact with the plug. Hence the advantage of using the Canadian LHHPC cement in the plug to minimize the cement quantities in the drift end plug. However, the long-term properties of this new type of high performance cement need to be assessed using Olkiluoto-specific data.

The case of a high pH plume from a grouted fracture travelling through the fracture network to the supercontainer volume is the most critical with respect to long-term safety as the thickness of bentonite around the canister is the lowest in the buffer rings surrounding the canister in the supercontainer (35–40 cm).

/Hellä et al. 2006/ estimated that in a KBS-3H drift there will be an average of 4 fractures with a transmissivity between $10^{-7}<T<10^{-8}$ m^2/s per 100 m, hence an average of 12 grouted fractures per drift. Therefore, if we divide the total amount of grouting cement (500 kg max, see Table F-3) by the number of fractures, the average mass of low-pH cement per grouted fracture is assumed to be approximately 42 kg. Using Equation F-4, these 42 kg of cement would then be theoretically capable to dissolve 19 kg of montmorillonite, corresponding to a saturated bentonite volume of 12 dm^3 (assuming 80% of montmorillonite content in bentonite and a saturated density after swelling of 2,000 kg/m^3). Assuming that a half-cylindrical volume along the circumference of the drift of 5.8 m is absorbing the OH^- ions, 12 dm^3 of bentonite would represent a thickness of less than 4 cm of altered bentonite around the drift, calculated as follows:

$$V_{affected\ bentonite} = ½\ \pi\ (r_{affected\ bent})^2\ [2\ \pi\ r_{drift}] \quad \text{(Eq. F-5)}$$

$$r_{affected\ bent} = 1/\pi\ (12\ 10^{-3}/r_{drift})^{1/2} \quad \text{(Eq. F-6)}$$

This is a highly conservative estimate because no mitigating effect on the extent of the alkaline plume (e.g. dilution) is taken into account. It is more likely that only a fraction of OH^- leached from the grout will find its way to the supercontainer, given the limited transmissivities of the fractures intersecting the supercontainer volume. In addition, the hydroxides formed/leached by the low-pH cement are conservative estimates as it is expected that a major part of calcium will be initially bound to CSH phases. If Silica Sol is used as grouting material (/as Autio et al. 2007/ suggests) only a very short lived (of the order of hours or days) alkaline plume can be developed within grouted fractures as the alkaline solution in which Silica Sol is suspended in leaches out (the pH of this suspension is around 9). The amount of OH^- released by a volume of 500 dm^3 of Silica Sol (see grout take estimates) corresponds to:

Moles of OH^- released during Silica Sol curing
= OH^- concentration × volume
= 10^{-5} mol/l × 500 l= 5×10^{-3} moles (Eq. F-7)

which is a negligible amount of OH^- compared with the amount of OH- released by a fracture grouted with low pH cement.

F.5 References

Ahokas H, Hellä P, Ahokas T, Hansen J, Koskinen K, Lehtinen A, Koskinen L, Löfman J, Mészaros F, Partamies S, Pitkänen P, Sievänen U, Marcos N, Snellman M, Vieno T, 2006. Control of water inflow and use of cement in ONKALO after penetration of fracture zone R19. Posiva Working Report 2006-45, Posiva Oy, Olkiluoto, Finland.

Alexander W R (ed), 1992. A natural analogue study of cement-buffered, hyperalkaline groundwaters and their interaction with a sedimentary host rock – I: Source-term description and geochemical code database validation; Nagra Technical Report Series NTB 91-10. Nagra, Wettingen, Switzerland.

Alexander W R, Neall F B, 2007. Assessment of potential perturbations to Posiva's spent fuel repository at Olkiluoto from the ONKALO facility. Posiva Working Report 2007-35. Posiva Oy, Olkiluoto, Finland.

Arthur R, Sasamoto H, Yui M, 2004. Potential complications in the development of a thermodynamic database for hyperalkaline argillaceous systems. *In* Metcalfe, R. and Walker, C, eds) 2004. Proceedings of the International Workshop on Bentonite-Cement Interaction in Repository Environments, 14–16 April 2004, Tokyo, Japan. Posiva Working Report 2004-25 (NUMO-TR-04-05). Posiva Oy, Olkiluoto, Finland.

Autio J, Börgesson L, Sandén T, Rönnqvist P-E, Johansson E, Hagros A, Eriksson M, Berghäll J, Kotola R, Parkkinen I, 2007. KBS-3H Design Description 2006. Posiva working report 2007-105 and SKB report R-08-32. Posiva Oy, Olkiluoto, Finland and SKB, Svensk Kärnbränslehantering AB, Sweden.

Berner U, 2004. Status of cement modelling. Future investigations in the view of cement/bentonite interactions. *In* Metcalfe, R. and Walker, C, eds). 2004. Proceedings of a the International Workshop on Bentonite-Cement Interaction in Repository Environments, 14–16 April 2004, Tokyo, Japan. Posiva Working Report 2004-25 (NUMO-TR-04-05). Posiva Oy, Olkiluoto, Finland.

ECOCLAY, 2005. ECOCLAY II: Effects of cement on clay barrier performance – Phase II, final report. ANDRA Unpubl. Internal Report, ANDRA, Paris, France.

Gaucher E, 2004. Modelling diffusion of an alkaline plume in two types of clayey systems. *In* Metcalfe, R. and Walker, C, eds), 2004. Proceedings of a the International Workshop on Bentonite-Cement Interaction in Repository Environments, 14–16 April 2004, Tokyo, Japan. Posiva Working Report 2004-25 (NUMO-TR-04-05). Posiva Oy, Olkiluoto, Finland.

Hagros A, 2007. Estimated quantities of residual materials in a KBS-3H repository at Olkiluoto. Posiva working report 2007-104 and SKB R-08-33. Posiva Oy, Olkiluoto, Finland and SKB, Svensk Kärnbränslehantering AB, Sweden.

Hellä P, Ahokas H, Palmén J, Tammisto E, 2006. Analysis of Geohydrological Data for Designof KBS-3H Repository Layout. Posiva Working report 2006-16 and SKB R-08-27. Posiva Oy, Olkiluoto, Finland and SKB, Svensk Kärnbränslehantering AB, Sweden.

Ito H, Mihara M, Ohi T, 2004. Development of MACBECE: Mechanical Analysis system considering Chemical transition of BEntonite-based and CEment-based materials. *In* Metcalfe, R. and Walker, C, eds). 2004. Proceedings of a the International Workshop on Bentonite-Cement Interaction in Repository Environments, 14–16 April 2004, Tokyo, Japan. Posiva Working Report 2004-25 (NUMO-TR-04-05), Posiva Oy, Olkiluoto, Finland.

Johansson E, Hagros A, Autio J, Kirkkomäki T, 2007. KBS-3H layout adaptation 2007 for the Olkiluoto site. Posiva Working Report 2007-77 and SKB R-08-31. Posiva Oy, Olkiluoto, Finland and SKB, Svensk Kärnbränslehantering AB, Sweden.

Karnland O, Nilsson U, Olsson S, Sellin P, 2004. Experimental study on changes of bentonite mineralogy and physical properties as a result of exposure to high pH solutions. *In* Metcalfe, R. and Walker, C, eds). 2004. Proceedings of a the International Workshop on Bentonite-Cement Interaction in Repository Environments, 14–16 April 2004, Tokyo, Japan. Posiva Working Report 2004-25 (NUMO-TR-04-05), Posiva Oy, Olkiluoto, Finland.

Karnland O, Nilsson U, Olsson S, Sellin P, 2005. Laboratory experiments with compacted bentonite in contact with highly alkaline solutions, R&D on low pH cement for a geologic repository. *In* Bäckblom, G. 2005. ESDRED: Supporting documents for the first training workshop. Proceedings of the 2nd low pH workshop, Madrid, 15–16 June, 2005. ANDRA, Paris, France.

Kato H, Asano H, Yamada N, 2004. A long-term performance assessment for engineered barriers. Study on barrier materials alteration. *In* Metcalfe, R. and Walker, C, eds). 2004. Proceedings of a the International Workshop on Bentonite-Cement Interaction in Repository Environments, 14–16 April 2004, Tokyo, Japan. Posiva Working Report 2004-25 (NUMO-TR-04-05). Posiva Oy, Olkiluoto, Finland.

Lagerblad B, 2001. Leaching performance of concrete based on studies of samples from old concrete constructions. SKB TR 01-27, Svensk Kärnbränslehantering AB.

Lehikoinen J, 2004. Cement-bentonite interaction issues, buffering capacity of bentonite. *In* Metcalfe, R. and Walker, C, eds). 2004. Proceedings of a the International Workshop on Bentonite-Cement Interaction in Repository Environments, 14–16 April 2004, Tokyo, Japan.

Linklater C M (ed), 1998. A natural analogue study of cement-buffered, hyperalkaline groundwaters and their interaction with a repository host rock. Phase II. Nirex Science Studies Report S/98/003, Nirex (now the NDA), Harwell, UK.

Martino J B, Chandler N A, Read R S, Baker C, 2002. Response of the tunnel sealing experiment concrete bulkhead to pressurization. Report No: 06819-REP-01200-10085-R00. Ontario Power Generation, Toronto, Canada.

McKinley I, Alexander R, Kickmaier W, Neall F, 2004. The bentonite/cement interaction problem: Cutting the Gordian knot. Extended abstract. *In* Metcalfe, R. and Walker, C, eds). 2004. Proceedings of a the International Workshop on Bentonite-Cement Interaction in Repository Environments, 14–16 April 2004, Tokyo, Japan. Posiva Working Report 2004-25 (NUMO-TR-04-05). Posiva Oy, Olkiluoto, Finland.

Metcalfe R, Walker C, (eds), 2004. Proceedings of a the International Workshop on Bentonite-Cement Interaction in Repository Environments, 14–16 April 2004, Tokyo, Japan. Posiva Working Report 2004-25 (NUMO-TR-04-05). Posiva Oy, Olkiluoto, Finland.

Miller W M, Alexander W R, Chapman N A, McKinley I G, Smellie J A T, 2000. Geological disposal of radioactive wastes. Pergamon, Amsterdam, The Netherlands.

Milodowski A E, Pearce J M et al. 1998a. Chapter 6 *in* Linklater, C.M, Ed.), 1998. A natural analogue study of analogue cement buffered, hyperalkaline groundwaters and their interaction with a repository host rock II Nirex Science Report, S-98-003, UK Nirex, Harwell, UK.

Milodowski A E, Hyslop E K et al. 1998b. Mineralogy and geochemistry of the Maqarin and Daba areas. Chapter 5 *in* Smellie, J.A.T, Ed.), (1998). A natural analogue study of analogue cement buffered, hyperalkaline groundwaters and their interaction with a repository host rock III. SKB TR-98-04, Svensk Kärnbränslehantering AB.

Montori J, Soler J M, Saaltink M W, 2008. Reactive transport modeling of the effect of hyperalkaline solutions along a fracture at the Onkalo site. Posiva Working Report 2008-18. Posiva Oy, Eurajoki, Finland.

Neall F B, 1994. Modelling of the near-field chemistry of the SMA repository at the Wellenberg site. PSI Technical Report 94-18, Paul Scherrer Institute, Würenlingen, Switzerland.

Neall F B, Johnson L, (eds), 2006. Proceedings of the NUMO workshop on near-field processes (Tokyo, 7–9 December, 2005). Nagra Project Report NPB 06-06, Nagra, Wettingen, Switzerland.

Oda C, Honda A, Savage D, 2004. An analysis of cement-bentonite interaction and evolution of pore water chemistry. *In* Metcalfe, R. and Walker, C, eds). 2004. Proceedings of a the International Workshop on Bentonite-Cement Interaction in Repository Environments, 14–16 April 2004, Tokyo, Japan. Posiva Working Report 2004-25 (NUMO-TR-04-05). Posiva Oy, Olkiluoto, Finland.

Pitty A (ed), 2007. A natural analogue study of cement buffered, hyperalkaline groundwaters and their interaction with a repository host rock IV: an examination of the Khushaym Matruk (central Jordan) and Maqarin (northern Jordan) sites. ANDRA Technical Report (*in press*), ANDRA, Paris, France.

Savage D, 1997. Review of the potential effects of alkaline plume migration from a cementitouus repository for radioactive waste. Implication for performance assessment. UK. Environment Agency R&D Technical Report P60, London, UK.

Savage D, 1998. Zeolite occurrence, stability and behaviour. *In* Smellie, H.A.T, ed), 1998. Maquarin Natural Analogue Study: Phase III. SKB TR 98-04, Svensk Kärnbränslehantering AB.

Savage D, 2006. Appendix B. 4. *In* Neall, F.B. and Johnson, L. 2006. Proceedings of the NUMO workshop on near-field processes (Tokyo, 7–9 December 2005). Nagra Project Report NPB 06-06, Nagra, Wettingen, Switzerland.

Savage D, Walker C, Arthur R, Rochelle C, Oda C, Takase H, 2007. Alteration of bentonite by hyperalkaline fluids: A review of the role of secondary minerals. J. Phys. Chem. Earth: 32 (1–7):287–297.

Sato T, Kuroda M, Yokohama S, Tsutsui M, Fukushi K, Tanaka T, Nakayama S, 2004. Dissolution mechanism and kinetics of smectite under alkaline conditions. *In* Metcalfe, R. and Walker, C, eds). 2004. Proceedings of a the International Workshop on Bentonite-Cement Interaction in Repository Environments, 14–16 April 2004, Tokyo, Japan. Posiva Working Report 2004-25 (NUMO-TR-04-05). Posiva Oy, Olkiluoto, Finland.

SKI, 2005. Engineered barrier system. Long-term stability of buffer and backfill. Report from a workshop in Lund, Sweden. SKI report 2005-48, SKI, Stockholm, Sweden.

Smellie J A T, 1998. Maqarin Natural Analogue Study: Phase III, vol. I and II. SKB TR 98-04, Svensk Kärnbränslehantering AB.

Takase H, 2004. Discussion on PA model development for bentonite barriers affected by chemical interaction with concrete: Do we have enough evidence to support bentonite stability? *In* Metcalfe, R. and Walker, C, eds). 2004. Proceedings of a the International Workshop on Bentonite-Cement Interaction in Repository Environments, 14–16 April 2004, Tokyo, Japan. Posiva Working Report 2004-25 (NUMO-TR-04-05). Posiva Oy, Olkiluoto, Finland.

Vuorinen U, Luukkonen A, Lehikoinen J, Ervanne H, 2004. Effects of alkaline attack on bentonite and crushed rock. Experimental and modelling studies. ECOCLAY II. *In* Metcalfe, R. and Walker, C, eds). 2004. Proceedings of a the International Workshop on Bentonite-Cement Interaction in Repository Environments, 14–16 April 2004, Tokyo, Japan. Posiva Working Report 2004-25 (NUMO-TR-04-05). Posiva Oy, Olkiluoto, Finland.

Vuorinen U, Lehikoinen J, Imoto H, Yamamoto T, Cruz Alonso M, 2005. Injection grout for deep repositories, Subproject 1: low-pH cementititous grout for larger fractures, leach testing of grout mixes and evaluation of the long-term safety. Posiva working report 2004-46. Posiva Oy, Olkiluoto, Finland.

Vuorinen U, Luukkonen A, Lehikoinen J, Ervanne H, 2006. Effects of salinity and high pH on crushed rock and bentonite – experimental work and modelling. POSIVA 2006-01. Posiva Oy, Olkiluoto, Finland.

Appendix G

Links between the process and evolution reports and assessment cases in the radionuclide transport report

Tables G-1 and G-2 in this appendix provide a link between the assessment cases calculated in the radionuclide transport report and the discussions in the present report as well as in the Evolution report.

Table G-1. Features and processes with different significance for, or potential impact on, KBS-3H compared with KBS-3V and summary descriptions of their relevance to radionuclide release and transport major uncertainties and evaluation of their implications for on canister failure modes and timing and for radionuclide transport. PR: Process Report (the present report), ER: Evolution Report /Smith et al. 2007a/, RNT: Radionuclide Transport Report /Smith et al. 2007b/.

Feature/process	Relevance to RN release and transport	Major uncertainties	Evaluation of impact Impact on canister failure mode/timing	Impact on radionuclide transport (see Table 11-2 and RNT for full lists of cases)
Piping and erosion during the operational phase and during saturation (cf. PR Section 4.5.2; ER Section 5.5.6)	May locally perturb buffer density and increase rate of diffusion of corrosive agents to canister surface and rate of radionuclide diffusion from failed canister	Likelihood of occurrence; amount of bentonite conveyed by piped water; degree of homogenisation after piping/ erosion cease	Scoping calculations in ER Appendix B.7	Illustration of impact of increased radionuclide diffusion rates in buffer in assessment case **PD-HIDIFF**
Processes due to the presence of steel components (external to canister) and their corrosion products (cf. PR Section 4.7.1; ER Sections 5.4.2; 5.6.4; 6.5.3)	May result in chemical alteration of buffer and consequent changes to physical properties; may perturb mass transfer at buffer-rock interface	Degree and spatial extent of perturbation	Scoping calculations in ER Appendix B.7 (impact on capacity of buffer to protect canister in the event of rock shear movements < 10 cm assumed to be negligible)	Illustration of impact of increased radionuclide mass transfer at buffer-rock interface and mixing in outer part of buffer in assessment cases **PD-FEBENT1; PD-FEBENT2; PD-FEBENT3**
	May provide sorbing surfaces for radio-nuclides; (which could be released following a change in groundwater chemistry) Fe(II) may compete for sorption sites on buffer; it may also act as a sink for dissolved sulphide, reducing the flux of sulphide to the canister surface.for sorption sites on buffer	Quantitative understanding of impact; possibility of release of sorbed radionuclides in the event of change in groundwater chemistry	Favourable effect of iron acting as sink for sulphides not evaluated quantitatively	Impact on sorption not assessed (remaining issue for further study); impact on buffer as a whole of change in groundwater chemistry at 70,000 years due to influx of glacial meltwater illustrated in **PD-GWMC**
H_2 from corrosion of steel components (external to canister) (cf. ER Sections 5.3.1; 5.6.4; 5.7.4)	May participate in microbial reduction of sulphate to sulphide, which may subsequently corrode canister surface	Quantitative understanding of impact	Scoping calculations in ER Appendix B.7 (minor impact)	None expected
	May perturb groundwater flow and radionuclide transport in the geosphere for the first few thousand years	Quantitative understanding of impact	Minor impact on mass transfer of corrosive agents between geosphere and buffer (not quantitatively evaluated)	Impact on radionuclide transport for an initially defective canister not assessed (remaining issue for further study)
High-pH leachates from cementitious components (cf. ER Section 5.6.5)	May result in chemical alteration of buffer and consequent changes to physical properties; may perturb mass transfer at buffer-rock interface	Degree and spatial extent of perturbation	Scoping calculations in ER Appendix B.7	Illustration of impact of increased radionuclide mass transfer at buffer-rock interface and mixing in outer part of buffer in assessment cases **PD-FEBENT1; PD-FEBENT2; PD-FEBENT3**
KBS-3H drift and surrounding EDZ/rock spalling (cf. ER Sections 4.1.2; 5.4.5)	May perturb mass transfer at buffer-rock interface	EDZ hydraulic properties; impact of buffer swelling on rock spalling; transport characteristics of spalled zone	Scoping calculations in ER Appendix B.7	Illustration of impact of rock spalling in assessment case **PD-SPALL**

Table G-2. Overview of assessment cases treated in the Radionuclide Transport (RNT) Report /Smith et al. 2007b/.

Case	Description
Cases assuming a single canister with an initial penetrating defect (PD-)	
PD-BC	Base Case for initial penetrating defect in BWR-type canister
PD-VVER	Initial penetrating defect in VVER-440 PWR type canister
PD-EPR	Initial penetrating defect in EPR type canister
PD-HIFDR	Increased fuel dissolution rate
PD-LOFDR	Reduced fuel dissolution rate
PD-IRF[a]	Evaluates transport only of radionuclides present in instant release fraction (see footnote a below this table)
PD-BIGHOLE	Increased defect size
PD-HIDELAY	Increased delay until loss of defect transport resistance
PD-LODELAY	Decreased delay until loss of defect transport resistance
PD-BHLD	Increased defect size plus decreased delay until loss of defect transport resistance
PD-HIDIFF	Increased diffusion rate in buffer
PD-FEBENT1	Perturbed buffer-rock interface – high conductivity, narrow perturbed zone
PD-FEBENT2 PD-FEBENT3	Perturbed buffer-rock interface – more extensive perturbed zone (2 different thicknesses)
PD-SPALL	Perturbed buffer-rock interface – high conductivity, narrow perturbed zone, lower flow through intersecting fractures than that assumed in cases PD-FEBENT1 , 2 and 3
PD-EXPELL	Dissolved radionuclides expelled by gas from canister interior and across buffer to geosphere
PD-VOL-1 PD-VOL-2	C-14 transported in volatile form by gas generated by corrosion (2 rates of gas generation)
PD-BCN	Initial penetrating defect in BWR-type canister; Nb present in near field and geosphere in anionic form
PD-BCC	Initial penetrating defect in BWR-type canister; C-14 present in geosphere in anionic form (carbonate)
PD-VVERC	Initial penetrating defect in VVER-440 PWR type canister; C-14 present in geosphere in anionic form (carbonate)
PD-EPRC	Initial penetrating defect in EPR type canister; C-14 present in geosphere in anionic form (carbonate)
PD-NFSLV	Near-field solubilities varied according to uncertainties in redox conditions
PD-SAL	Brackish / saline water present at repository depth (all time)
PD-HISAL	Saline water present at repository depth (all time)
PD-GMW PD-GMWV	Change from reference (dilute / brackish) water to glacial meltwater at 70,000 years (release also starts at 70,000 years – two alternative meltwater compositions)
PD-GMWC	Change from reference (dilute / brackish) water to glacial meltwater at 70,000 years (release starts at 1,000 years, as in the reference case)
PD-HIFLOW	Increased flow at buffer-rock interface
PD-LOGEOR	Reduced geosphere transport resistance
PD-HIGEOR	Increased geosphere transport resistance
PD-HIFLOWR	Increased flow at buffer-rock interface and reduced geosphere transport resistance

Table G-2. (Continued) Overview of assessment cases.

Cases assuming a single canister failing due to copper corrosion (CC-)	
CC-BC	Base Case for failure due to copper corrosion; buffer treated as mixing tank
CC-HIFDR	Increased fuel dissolution rate
CC-LOFDR	Reduced fuel dissolution rate
CC-GMW	Glacial meltwater present at repository depth (impact on near-field solubilities and geosphere retention parameters)
CC-LOGEOR	Reduced geosphere transport resistance
CC-LOGEORG	Reduced geosphere transport resistance, glacial meltwater[b]
CC-LOGEORS	Reduced geosphere transport resistance, saline groundwater[b]
Cases assuming a single canister failing due to rock shear (RS-)	
RS-BC	Base case for failure due to rock shear
RS-GMW	Glacial meltwater present at repository depth (impact on near-field solubilities and geosphere retention parameters)
Additional cases (hypothetical pulse release to geosphere) (MD-)	
MD-1	Variations in matrix diffusion depth (3 cases)
MD-2	
MD-3	

[a] Certain radionuclides are enriched at grain boundaries in the fuel, at pellet cracks and in the fuel / sheath gap as a result of thermally driven segregation during irradiation of the fuel in the reactor. These are assumed to enter solution rapidly once water contacts the fuel pellet surfaces, and are termed the instant release fraction (IRF).

[b] Glacial meltwater is a very dilute ice-melting water. Saline groundwater represents water with a TDS (Total Dissolved Solids) content of about 20 g/l. For detailed composition of the waters used in the assessment, see Appendix D of Radionuclide Transport report.

G.1 References

Smith P, Johnson L, Snellman M, Pastina B, Gribi P, 2007a. Safety assessment for a KBS-3H spent nuclear fuel repository at Olkiluoto – Evolution report. POSIVA 2007-08 and SKB R-08-37. Posiva Oy, Olkiluoto, Finland and SKB, Svensk Kärnbränslehantering AB, Sweden.

Smith P, Nordman H, Pastina B, Snellman M, Hjerpe T, Johnson L, 2007b. Safety assessment for a KBS-3H spent nuclear fuel repository at Olkiluoto – Radionuclide transport report. POSIVA 2007-07 and SKB R-08-38. Posiva Oy, Olkiluoto, Finland and SKB, Svensk Kärnbränslehantering AB, Sweden.